

INTERNATIONAL COUNCIL FOR BUILDING RESEARCH STUDIES AND DOCUMENTATION

WORKING COMMISSION W18 - TIMBER STRUCTURES

CIB - W18

MEETING THIRTY-ONE

SAVONLINNA

FINLAND

AUGUST 1998

Lehrstuhl für Ingenieurholzbau und Baukonstruktionen
Universität Karlsruhe
Germany
Compiled by Rainer Görlacher
1998

ISSN 0945-6996

CONTENTS

- 0 List of Participants
- 1 Chairman's Introduction
- 2 Co-operation With Other Organisations
- 3 Limit State Design
- 4 Timber Columns
- 5 Stress Grading
- 6 Stresses for Solid Timber
- 7 Timber Joints and Fasteners
- 8 Duration of Load
- 9 Laminated Members
- 10 Structural Stability
- 11 Fire
- 12 Test Methods
- 13 Other Business
- 14 Venue for Next Meeting
- 15 Close
- 16 List of CIB W18 Papers/Savonlinna, Finland 1998
- 17 Current List of CIB-W18 Papers

CIB-W18 Papers 31-1-1 up to 31-21-2

0 List of Participants

**INTERNATIONAL COUNCIL FOR BUILDING RESEARCH STUDIES
AND DOCUMENTATION**

WORKING COMMISSION W18 - TIMBER STRUCTURES

MEETING THIRTY-ONE

SAVONLINNA, FINLAND 12-14 AUGUST 1998

LIST OF PARTICIPANTS

AUSTRALIA

G N Boughton	Curtin University of Technology; Perth
R W Chelberg	Forest and Wood Products, Sunnybank
K Crews	University of Technology, Sydney
A Horrigan	Queensland Forestry Research Institute, Queensland
R H Leicester	CSIRO, Div. of Building, Construction and Engineering, Victoria

AUSTRIA

B Obermayr	Techn. University of Graz
G Schickhofer	Techn. University of Graz

BELGIUM

J Rathé	University of Gent, Gent
---------	--------------------------

CANADA

H G L Prion	Department of Civil Eng. UBC, Vancouver
-------------	---

DENMARK

L Damkilde	Technical University of Denmark, Lyngby
H J Larsen	Danish Building Research Institute, Hørsholm

FINLAND

H Boren	Finnish Forest Research Institute, Joensuu
M Kairi	Finnforest Oy, Lohja
J Kangas	VTT Building Technology, Espoo
A Kevarinmäki	Helsinki University of Technology
T Poutanen	Tampere University of Technology, Tampere
A Ranta-Maunus	VTT Building Technology, Espoo
U Saarelainen	VTT Building Technology, Espoo

FRANCE

L Daudeville	LMT, Cachan
F Rouger	CTBA, Bordeaux

GERMANY

P Becker	Bauhaus University, Weimar
H J Blaß	University of Karlsruhe
J Ehlbeck	University of Karlsruhe
R Görlacher	University of Karlsruhe
M Schmid	University of Karlsruhe

JAPAN

N Kawai	Building Research Institute, Tsukuba
K Komatsu	Kyoto University, Kyoto
M Yasumura	Shizuoka University, Shizuoka

NETHERLANDS

A Jorissen	TU Delft
A D Leijten	TU Delft

POLAND

B Szyperska	Building Research Institute, Warszawa
-------------	---------------------------------------

SWEDEN

L Boström	Swedish National Testing and Research Institute, Borås
M Hansson	Lund University
T Isaksson	Lund University
B Källsner	Swedish Institute for Wood Technology Research, Stockholm
J König	Swedish Institute for Wood Technology Research, Stockholm
H Petersson	Chalmers University of Technology
S Thelandersson	Lund University

SWITZERLAND

A Mischler	ETH Zürich
------------	------------

UK

T D G Canisius	Building Research Establishment, Garston
V Enjily	Building Research Establishment, Garston
R Marsh	Consultant - TRADA, London
C J Mettem	TRADA Technology LTD, Buckinghamshire
M Milner	TRADA Technology LTD, Buckinghamshire
T Reynolds	Building Research Establishment, Garston

USA

J D Dolan	Virginia Polytechnic Institute and State University, Blacksburg
-----------	---

1. **Chairman's Introduction**
2. **Co-operation With Other Organisations**
3. **Limit State Design**
4. **Timber Columns**
5. **Stress Grading**
6. **Stresses for Solid Timber**
7. **Timber Joints and Fasteners**
8. **Duration of Load**
9. **Laminated Members**
10. **Structural Stability**
11. **Fire**
12. **Test Methods**
13. **Other Business**
14. **Venue for Next Meeting**
15. **Close**

**INTERNATIONAL COUNCIL FOR BUILDING RESEARCH,
STUDIES AND DOCUMENTATION**

WORKING COMMISSION W18 - TIMBER STRUCTURES

MEETING THIRTY-ONE

SAVONLINNA, FINLAND 12 - 14 AUGUST 1998

MINUTES

1. CHAIRMAN'S INTRODUCTION

- Greetings from hosts
- Presentations: there are 28 papers, 20 minutes per presentation + 10 minutes for questions
- Authors should make concluding statement as to the impact on codes
- Registration fees to be collected during the meeting

Welcome by the host: Alpo Ranta-Maunus

A. Ranta-Maunus welcomes all attendees to Savonlinna and gives a short history of the castle, followed by a brief background on VTT:

- VTT is a technical research centre, not a University
- It has approximately 2800 employees and is centred in Helsinki

2. CO-OPERATION WITH OTHER ORGANISATIONS

(a) RILEM

S. Thelandersson:

There are 40-50 technical committees, dominated by concrete
Presently there is low activity in timber :2 active technical committees

1. Committee on Test Methods for Load Transferring Metalwork Used in Timber Engineering (i.e. hangers) (chaired by J. Ehlbeck)

- consists of 15 members
- 3 meetings so far (Cachan, Vancouver, Paris), next in Karlsruhe
- type of connectors considered : end grain to side grain, side-side, end-end
- types of connectors (metal hangers)

Notes:

Questions are prefaced with a "Q" and comments with a "C", followed by the questioner's name. Answers to questions are given in [...]

- test methods: conn. types, important parameters
- concluded not to give strict rules, rather guidelines
- 10 principles to follow when testing such connections
- document cross-sections and the intended function
- carefully decide on test configuration to avoid other failures
- carefully select appropriate secondary member
- avoid the influence of support conditions
- load transfer should be reliably measured
- use the loading procedure as outlined in EN26891
- measure the relative displacement between members
- assure gaps between members to avoid secondary interaction
- condition specimens to the proper moisture content
- record relevant specifications of the timber members, connections etc.

Q(R. Leicester) Why should certain failure methods be avoided if these could be realistic? [J. Ehlbeck: To assure a valid test method set up and not provoke unrealistic failure modes]

2. Committee on historic buildings

- would like to expand activities
- next workshop in Stockholm

3. Committee on fracture mechanics concluded its work

L. Boström announced the RILEM Symposium week in September 1999

- there would be one symposium specifically on timber engineering
- the deadline for submission of abstracts is November 1998

S. Thelandersson should be approached if anyone wants to start a new RILEM committee. There is a possibility of funding.

(b) CEN TC 124 (TIMBER STRUCTURES)

H. Larsen:

- The purpose is to produce European standards, especially for products
- Committee is working on test methods (glulam, trusses)
- So far completed ~ 30 standards
- Still have to introduce procedures for acceptance
- Expect completion in a few years (maybe 2003)
- The following are presently under discussion
- bending stiffness of timber beams (full span?)
- shear
- The next meeting is in Bordeaux in August 1998 (after ISO).

(c) CEN TC112 (Wood based panels)

M. Kairi:

- Purpose is the standardization of testing of glued laminated products (Kerto LVL)

and other)

- The initiative came from insurance companies in France. The question posed is whether the standard should be a French national standard or a European standard?
- The committee opted for a harmonized European standard. Then there would be an opportunity to develop sub standards
- The standard will open market to other producers
- The Committee opted for TC 112 because LVL is produced in panel form
- Two meetings so far (Finland, France); next in Sweden Sept 1998
- Prepare mandate for working group 10

Q(V. Enjily) This Committee should not be TC112. Who decides on the mandate?
[H. Larsen: The committee has the mandate from TC124 as long as the standard is produced along the guidelines of TC124]

(d) CEN TC250 (Eurocode 5)

H. Blaß:

- The mandate is to produce design standards
- 60 Eurocodes (23 for steel, 3 for Timber: Part 11 (buildings) 12 Fire; 2 (Bridges)
- These will be incorporated into EN
- The conversion of standards is in process
- ENV standards are out for comments which will be incorporated in the final version

(e) IUFRO S5.02

H.J. Larsen:

- Would like to expand into timber
- Questionnaire by Hoffmeyer: Should IUFRO continue and who will convene
- Need a volunteer

(f) CIB W85

R. Leicester:

- Expand activity e.g. floor vibrations
- It is planned to produce within 2 years a draft status of activities (serviceability issues)
- Next meeting tentatively in June 1999(?)

3. LIMIT STATE DESIGN

*Paper 31 - 1 - 1 A Limit States Design Approach to Timber Framed Walls -
C J Mettem, R Bainbridge and J A Gordon*

Q (K. Komatsu) Considering that the contribution of non-structural components is significant, are there product standards available for these components? It is known that the properties of these have a large variability. [Yes, but it is hard to get engineering data]

- Q(B. Källsner) Is the Eurocode less detailed than the BS code? Detailed models are required for the analysis of wall structures. In the model (p.12, sec 4.1), the panels are listed as the most important components for lateral resistance. Should it not be the connections?[Analysis methods are under discussion. They have to be kept simple for designers. To make a wall stiffer and stronger it is important to improve the connections, which includes the fasteners and the panel.]
- Q (H. Prion) Why was earthquake loading excluded from scope?[Only for the UK, but it is included in the Eurocode]
- Q (G. Boughton) Is there a cross-correlation of k-factors? [They will be interdependent and the engineer will have to make a judgment call.]
- Q(S. Thelandersson) Are there methods to calculate the resistance of complex walls? For example, the cantilever method on sections of the walls. Are any rules provided? These have to be consistent with the philosophy of wall design [This still has to be done. For the analysis one can use established engineering principles]
- Q(T. Poutanen) Are there any problems with serviceability of walls in the UK? [No indication of problems so far. For multi-party occupancy, however, this could become an issue, especially noise and vibration.]

4. TIMBER COLUMNS

Paper 31 - 2 - 1 Deformation and Stability of Columns of Viscoelastic Material Wood - P Becker and K Rautenstrauch

- Q(H. Prion) Have you done any experimental verification of your theory? [No]
- Q(H. Blaß) For beams creep deflections seem less serious since it will disappear, whereas for column it will remain. The permanent load in column is typically low, however. Where about is the critical level of axial load when creep instability becomes an issue? [For a column, a decreasing deflection rate has to be guaranteed. If it is increasing, then collapse will eventually happen. The critical level can thus be calculated.]
- C(H. Larsen) There are two sides to your theory: the philosophy and the practical application. In the past it was believed that the load would be limited to below the proportional limit. In Limit States Design, however, one can exceed the proportional limit and plastic effects may become important.
- C(R. Leicester) Should also consider previous papers, which contain experimental data that can be used for verification of the theory.
- Q(G. Canisius) For columns in a structure, load redistribution and sharing (redundancy) will reduce the creep effect. One should consider a system approach [This is taken into account since the load history of a column will be derived from the structural response]
- Q(A. Jorissen) In practical design axial loads are almost always combined with bending, therefore creep instability due to axial load only might not be important.
- C(H. Blaß) Cases of pure axial load can occur in trusses

5. STRESS GRADING

Paper 31 - 5 - 1 Influence of Varying Growth Characteristics on Stiffness Grading of Structural Timber - S Ormarsson, H Petersson, O Dahlblom and K Persson

- Q(H. Blaß) Proof load in tension, bending (flat or edge)? This might not be according to the eventual application of the wood and the cut-off of the distribution curve might not be the same for all cases. [Edgewise testing is considered the best representation]
- Q(R. Leicester) In Australia proof testing is used widely and the results could be used for comparison. How can the bending strength be used when only E is known? Correlation of the two parameters is very important. [With this new information a better idea of the bending strength will be gained. Of great importance is the issue of compression wood.]
- C(A. Mischler) When boards are used as glulam laminations, one should test in tension instead of bending since the characteristics differ in tension and bending.
- C(G. Boughton) In Australia the best correlation was found between tension strength and MOE edgewise since a corner defect often is the major factor influencing tension strength. The boards have to be tested in both directions, however.
- Q(G. Canisius) How were E values measured across the cross section of a log and how was alignment of grain considered? [Small sticks 30 cm long were cut and tested; various alignments carefully measured]
- Q(R. Marsh) Are test results using the present methods overly optimistic, considering the different strength values derived from the proposed test methods. [No, but refined test methods can identify timber with higher strength.]
- Q(R. Marsh) Can you identify advanced stress grading without proof loading? [Not for now.]

Paper 31 - 5 - 2 A Comparison of In-Grade Test Procedures - R H Leicester, H Breitingner and H Fordham

No questions

6. STRESSES FOR SOLID TIMBER

Paper 31 - 6 - 1 Length and Moment Configuration Factors - T Isaksson

- Q(H. Blaß) If there is no significant difference between 'weak' and 'strong' sections, why not use the Australian test approach, where the test methods ignore the location of the defects. [This might be reasonable since it is not easy to identify defects]
- Q(A. Ranta-Maunus) Why are the length effects so small [The statistical method is not always the same as the test procedure because of physical differences in testing, e.g. strain energy stored in longer specimens etc.]
- Q(G. Canisius) The length effect factors could be different for different parts of the distribution curve, e.g. for mean or for 5% [We used mean values for the basis of the Weibull function in statistical analysis]
- C(S. Thelandersson) Different populations will yield different distributions with different k-values. For design purposes the number of different k-factors should be reduced to a minimum
- Q(B. Källsner) In your tests you found a somewhat higher within member variation of the bending strength than in our tests. In our case all timber boards were taken closest to the pith. How were your boards sawn? [There were boards both close to the pith and boards a distance from the pith.] This may be an explanation to the higher within member variation. [It could be checked in the test data.]
- Q(B. Källsner) In your experiments you did not test all the weak sections. Since you always tried to test the weakest ones isn't there a risk that your within member variation of the bending strength becomes too low? [In some cases also not so weak sections were tested]

- Q(B. Källsner) During the CIB meeting in Vancouver last year I showed results from testing of long boards subjected to constant moment. We have evaluated the test results further and found that if we plot the bending strength as a function of the number of weak zones that the bending strength decreases about four times more than predicted by the statistical model. This indicates that the distance between the weak zones may be an important factor. The number of test data is limited, however. [I have already mentioned that the statistical model should be verified for long boards.]
- Q(A. Jorissen) Does that mean that height, length & volume effects cannot be explained statistically? [Testing of different lengths can also have other effects]
- C(H. Larsen) Results cannot be verified because testing has not been done for different lengths
- C(S. Thelandersson) This a new way of 'testing' the same board along different sections. The method serves to simulate test results. If possible, tests will be done to verify statistical results. Mechanical differences cannot always be explained statistically e.g. if crack wants to develop along long member, it will be affected by the length. Scandinavian species also seem to be relatively very uniform.
- C(G. Boughton) Intent of code is to model reality i.e longer lengths store more strain energy, thus more likely to spread cracks. Therefore these effects should be considered in the analysis
- C(S. Thelandersson) Yes, if indeed that is the case.

Paper 31 - 6 - 2 Tensile Strength Perpendicular to Grain According to EN 1193 - H J Blaß and M Schmid

- Q(A. Jorissen) Discussion about the negative correlation factor in Table 2. Surprised by comment that a correlation factor of 0.55 is considered good. [Correlation is relatively high for this study]
- Q(A. Mischler) Is there a correlation between density or grade of wood and tension perpendicular strength? [No. We used mainly clear wood in tests. Influence of knots could sometimes also be a reinforcement perpendicular to grain, especially in the radial direction.]
- C(H. Larsen) One has to distinguish between effects of different species and grades. Typically, there is a strong correlation between most properties and density. Some effects are also highly species specific and one has to be careful to generalize results since different material characteristics will be derived due to their dependency on the density.
- Q(H. Larsen) What kind of glue was used [Polyurethane]
- C(H. Blaß) Never had a failure in the glue line itself but close by.
- C(H. Larsen) The discontinuity in the vicinity of the glue line could affect the distribution of loads
- C(H. Blaß) Other tests of glulam stock showed characteristic strengths close to zero.
- Q(H. Petersson) You did not consider size effects. These should be considered in the study [We used standard testing specimens; the volume effect seems to be negligible.]
- Q(S. Thelandersson) Do the results agree with the Weibull theory or do the data distribution fit a Weibull curve? [The latter] In that case you should really consider an exponential variation of strength with size. Consider randomly distributed defects.
- Q(A. Leijten) Considering that 50% of your specimens failed along the glue line and you were testing to the European standard for which there is a limited experience, do you have any recommendations about a better test method? [One of the purposes of the project is to come up with suggestions for a better test method]

- C(G. Canisius) A previous paper shows FE results on the effect of stress concentrations along the glue line. Thus the effect of the attached plate is very important (fixed or free to rotate)
- Q(J. Ehlbeck) When discussing product standards, what is the feeling about characteristic values for designers? H. Blaß mentioned values close to zero. In standards the tension perpendicular values are increasing with higher classes.
- C(S. Thelandersson) Tension perpendicular to grain strength is often used in curved beams. However, test values are highly dependent on misalignment and moisture.
- Q(G. Schickhofer) Which grades of Glulam were tested? [All classes were tested and no correlation was observed between grade and tension perpendicular strength.]

Paper 31 - 6 - 3 Strength of Small Diameter Round Timber - A Ranta-Maunus, U Saarelainen and H Boren

- (H. Blaß) How was the bending strength of tapered pole calculated? [Use the diameter at the location of failure.]
- Q (?) Do the results apply to higher grade species too? [Yes, we have tested Douglas Fir too. Values are not as exact as for Spruce lumber]
- Q(J. Ehlbeck) Is the lumber intended to be used for structures? Has any research been done on connections? [The research also covers to some extent connections]
- C(R. Marsh) In the UK there are two examples of structures in dia-grid shells. Bob Griffiths has done some research and has developed round pole joint connections
- Q(H. Blaß) What is the expected use of small diameter timbers? [The major markets are in low cost buildings, especially for farmers & do-it-yourselfers. The major attraction is the low material cost. Other applications are for touristic buildings where architects like to use it as an expression.]
- Q(H. Petersson) How are trees selected? [The trees should be straight with a limited knot size, but nothing complicated. Should not use round poles for beams - it is not an optimal section for strength and stiffness]
- Q(A. Horigan) Were compression tests similar to bending tests? Were any tension tests done? [Length of compression specimens was 6 x diameter]

Paper 31 - 6 - 4 Compression Strength Perpendicular to Grain of Structural Timber and Glulam - L Damkilde, P Hoffmeyer and T N Pedersen

- Q(A. Jorissen) Why have you used the same regression equation for average and 5% values? [Regression equation was for correlation of 5% strength and 5% density in one case and the average strength and the average density in the other.]
- Q(C. Mettem) In FE analysis of tension perpendicular stresses, Gehri found a dependency on the configuration. One should do more tests to verify values for other configurations [In this study we only did basic tests and recommended conservative design values.]
- Q(G. Schickhofer) The case presented is not a realistic situation as in a building [In practical cases, the stress distribution needs to be accounted for, then use the basic values with modification factors]
- C(H. Blaß) One could have cases with uniform compression stresses, e.g. stress laminated bridges
- C(A. Mischler) A test project was done in Germany around 1930 on different configurations
- C(H. Larsen) Design values in code assume uniform stress situation but differed by 50% with test results. This shows importance of knowledge of stress situation. Need to consider other configurations.

Paper 31 - 6 - 5 Bearing Strength of Timber Beams- R H Leicester, H Fordham and H Breiinger

Q(H. Blaß) Is the compression perpendicular strength correlated with density? [It does not correlate exactly ;we used structural lumber ; different failure modes occurred, which were also dependent on ring orientation]

Q(H. Larsen) You should link your research with other institutions (especially Europe) so results can be compared [Standard testing methods as used in North America and Australia were used similar to case 1 (continuous support) with clear specimens. Comparisons were done to determine comparable values for structural lumber. Comparisons can be made with results from European tests.]

Q(G. Boughton) We have done tests with European standard and got values of 3 for Radiata Pine.

7. TIMBER JOINTS AND FASTENERS

Paper 31 - 7 - 1 Mechanical Properties of Dowel Type Joints under Reversed Cyclic Lateral Loading - M Yasumura

Q(H. Blaß) Were the bolts tightened? [Hand tight only]

Q(C. Mettem) Did you use washers? [Yes, large diameter washers]

Paper 31 - 7 - 2 Design of Joints with Laterally Loaded Dowels - A Mischler

Q(G. Boughton) Why do you claim a brittle failure for low slenderness dowels? The curve seems to be the same as for the slender dowels. [The ductile behaviour could be observed after the test from the dowel bent configuration. Stocky dowels were not bent.]

Q(G. Boughton) Why was there a reduction in capacity for more slender dowels? [For more slender dowels we need larger deformations to reach the plastic deformations in the dowel, thus larger elastic deformations in the timber, which leads to splitting]

C(H. Larsen) Don't agree with reduction of load with thicker specimen, i.e increase in slenderness ratio. This effect could be due to small population. Optimum slenderness should not be a consideration. Should be impossible to reduce capacity when reaching plastic deformations. The above argument is not valid based on plasticity and further investigation should be considered.

Q(H. Larsen) Are these curves from only one test? [For each configuration had 3 tests with two connections each]

Q(M. Schmid) For connections with beech, did splitting occur too? [After 6 mm displacement also saw splitting, but the dowel is severely bent at that stage. If splitting happened after reaching the plastic capacity, it was considered to have failed in a ductile mode]

C(A. Jorissen) Within normal range of hole clearances one should not have problems in connections with wood side plates, due to the deformation capacity of wood. The influence of hole clearances would be more pronounced for steel side plates.

Paper 31 - 7 - 3 Flexural Behaviour of Glulam Beams Edge-Jointed by Lagscrews with Steel Splice Plates - K Komatsu

Q(H. Larsen) The load slip curves show a considerable plastic zone. One should use the ultimate limit state using plasticity for analysis [We are interested for the time being

- in the elastic behaviour until ultimate with the intent to keep the analysis simple]
- Q(H. Blaß) In the last test series with the highest load, why is there a discontinuity in the analytical slip curve? [Up to that point program does not consider slip deformations because the compression force is still larger than the bending tension at the joint]
- C(S. Thelandersson) The jump in the load-slip curve is similar to that of cracked concrete
- Q(S. Thelandersson) What are the applications of this type of connection? [Japan imports a large amount of glulam timber with restricted length that has to be joined together]
- Q(G. Boughton) End tolerances seem to be very important [Yes]. Are there any controls on tolerances in practice to prevent secondary stresses in the timber? [Nothing in particular, but in tests initial slackness in load-slip is curve an indication of tolerance problems. We also use shear keys in Japan which will assure alignment]
- Q(A. Jorissen) Do you ever have shear failures in practice? Your tests have connection in zero shear zone.[..]
- Q(A. Jorissen) In the calculations for Fig.6 were the lag screws neglected?[Only at intersection consider effect of lag screws; not for compression side]

Paper 31 - 7 - 4 Design on Timber Capacity in Nailed Steel-to-Timber Joints - J Kangas and J Vesa

- Q(H. Blaß) Did you use a reduction of the shear strength, as a function of the shear area, as is the case for split ring connections? [No, but we had good agreement with the model. It also seemed to be a factor of the end distance]
- Q(A. Jorissen) Are the timber properties (Table 2, p.10) in the calculations using Foschi's model the same as for the tests? [Yes, as in table 1]
- Q(A. Jorissen) In eq 7, you add resistances from two types of failure, although the stiffness is different for the two failure modes. Is there indeed compatibility? [Plasticity plays an important factor in ensuring that both resistances are mobilized. Embedding is very plastic, accompanied with a lower stiffness, resulting in a relatively even tensile stresses in the timber along the last line of fasteners. Shear stresses are relatively evenly distributed. Test results verified this]

Paper 31 - 7 - 5 Timber Contact in Chord Splices of Nail Plate Structures - A Kevarinmäki

- Q(B. Källsner) One can get large rotations in joints, influenced by the moment distribution in the truss members. Was this included in the theory? [When calculating member forces, we used a nonlinear relationship. It is an Iterative procedure.]
- Q(K. Komatsu) Please clarify the definition of a tensile splice and a compression splice. [It is defined by the force in the member]
- Q(B. Källsner) How do you handle the case when a metal fastener is located in the middle of a simply supported beam? [We use a non-linear model to calculate the bending response]

Paper 31 - 7 - 6 The Fastener Yield Strength in Bending - A Jorissen and H J Blaß

- C(H. Blaß) According to the failure definition (displacement = 15mm), one should define a smaller angle to determine the plastic moment.
- Q(A. Mischler) According to EC5 (Johannsen) the yield moment is defined as the plastic resistance. This is inconsistent with EC3 (steel code) where the yield moment

has a different meaning. In the timber code, we should talk about plastic moment not yield moment. Fig 1 is confusing. [The definition of yield or plastic moment did not seem to be a problem so far. The tensile test in steel construction is well defined. Furthermore, one can incorporate strain hardening in the theoretical calculations of the plastic moment]

C(C. Mettem) I agree with A. Mischler. This is also important in the development of rules for FRP dowels

C(S. Thelandersson) It might not be safe to use the plastic capacity, which is higher than most real load cases. By reaching such high loads, one could induce a brittle failure

C(A. Mischler) In mild steel dowels one should use the real strength, not the specified (or nominal) strength, to avoid brittle failures. [In practice it is common to have a large variability in yield as well as in diameter. This is because in steel construction mild steel bolts are only used for cheap construction and quality control is minimal.]

Q(R. Leicester) When loading bolts in tests, the actual rotation angle is much higher than the residual angle (after load release).[Even if we use the full angle, we should not get a much higher moment in the hinge since the additional elastic deflection does not increase the moment]

C(JE) The same problem is experienced with nails, which are often hardened. The wire strength is typically not well controlled

Paper 31 - 7 - 7 A Proposal for Simplification of Johansen's Formulae, Dealing With the Design of Dowelled-Type Fasteners - F Rouger

C(H. Larsen) It is generally accepted that a need exists for simplification of the design formulae. It is also reasonable that the safety factor for brittle failure is increased. However, the solution presented is not the best solution as the rules should be transparent to the user. Furthermore, one should not compensate for multiple fastener effects by reducing single fastener values. The empirical 1.1 factor should be removed from the formulae.

C(H. Blaß) The 1.1 factor should not be excluded entirely but should form part of rules for different fasteners

C(H. Larsen) I have previously introduced simplifications for the embedding strength expression. (Shows slide with simplified expressions). The aim was to introduce a larger safety factor for brittle failures and a gradual change of the safety factor as one moves from brittle to ductile failure modes.

(H. Larsen) The idea of minimum length works for nails, but bolts usually fall into the intermediate range. One of the reasons for dropping simplification in Eurocode is that it does not work for gusset plates of plywood particle board (thin members) where the minimum length considerations are different.

C(H. Blaß) Regardless of simplifications, the design of joints will always be dictated by the most efficient configuration.

Paper 31 - 7 - 8 Simplified Design of Connections with Dowel-type fasteners - H J Blaß and J Ehlbeck

Q(H. Prion) The last line in the conclusions implies that splitting is not a problem when using the simplified formula. [The lower line does not imply that splitting does not occur, but the likelihood is lower] Does the use of the more accurate expressions mean that the connection has to be reinforced? [No, one can also use other materials that are less likely to fail in a brittle manner instead of reinforcement].

Q(A. Jorissen) There seems to be an inconsistency with the old code [The old code was based on allowable stress design and it was a different situation] In my own research

I have developed a lower curve based on fracture mechanics and would suggest a curved approximation. Most bolted connections fall into this intermediate range.

Q(H. Larsen) One should not disregard experience from many years and drastic changes in design practice should be avoided without compelling reason. [In nail connections a middle member slenderness of 6 or 8 is typically sufficient] A drastic reduction in capacity might be too extreme [The present more accurate calculations would still be permitted] Don't compare safety factors from allowable stress design as they include all the partial safety factors.

Q(M. Yasumura) Changes to simplify the rules should be based on rigorous theory, and should not be just an empirical simplification.

Q(A. Jorissen) It is desirable to have only one g_m for all connections. Why not use g_m for wood and steel separately in calculation model. [g_m for connections in entirety is not so simple. It will be different for dowel or other type connections]

Q(R. Leicester) Changing practices exist - Australia's code, for example, is based on the empirical US rules, which include many factors such as washer sizes etc. There are many such factors that are not considered in Johannsen's formulae [The secondary factors should be considered in a separate modification factor, not in the basic equation]

Q(G. Boughton) If one would use different g_m factors for the steel and timber parts respectively, would better safety values be obtained? [Yes, by treating timber and steel separately in the connection and applying a general k_{mod} factor for the whole connection. In a mode 3 failure, which is essentially a steel failure, a lower g_m factor could be applied] Do you have any test data to verify your model? [No, it is presently all based on the theoretical model. I would like to use more progressive g_m factors in combination with a k_{mod} factor]

Q(A. Mischler) Nails have a higher lateral resistance because of the added withdrawal resistance and it seems conservative to base nail values on the Johannsen model which is based on bending only. [Nails always fail in mode 3 and it seems feasible to add a factor that takes into account the withdrawal] It would be inconsistent, however, to increase the resistance by a multiplier to the bending resistance instead of adding the withdrawal separately. We need to develop a separate model for nails [The present model is fitted to test results and is not based on theoretical considerations]

C(A. Jorissen) A model exists by Van der Put & Kuipers for nail bending with withdrawal. [The model is too complicated and one should keep the equations as simple as possible.]

8. DURATION OF LOAD

Paper 31 - 9 - 1 Duration of Load Effect in Tension Perpendicular to Grain in Curved Glulam - A Ranta-Maunus

Q(G. Canisius) How do you get non-zero stresses perpendicular to the surface [The stresses are in the direction of the surface]

Q(M. Schmid) I also observed a higher coefficient for volume effect in short term tests, especially for small specimens. [Yes, short term experiments showed a higher volume effect. However, the long term behaviour is more important]

Q(S. Thelandersson) Did you consider the concept of an equivalent load due to moisture effects? [The values in the table are the maximum from calculations for real loads] One could calculate equivalent stresses partly for the external load and partly from moisture. Have you considered how strains would react from a fracture

mechanics approach? The situation might be less severe.[I have thought about it, but found it to be very complex. I have not done any fracture mechanics analysis. Stresses were varying over the duration of load application due to moisture histories and Weibull stresses vary quite a bit.]

Q(G. Boughton) How long after a change to 90% humidity did problems start? [The time span for maximum humidity value was about 3-4 weeks, depending on the thickness of the beam. After 1-2 weeks damage became evident and progressively got worse]

Q(G. Canisius) The loading effect on the surface is important as shear stresses can occur [On top of the beam it was local compression. In the case of tension perpendicular stresses, the external load could still have an effect. This was not taken into account in the calculations and it might be an explanation why the beams have higher stresses.]

(R. Leicester) Was the step change more important than the load duration effect? [The factor k_{mod} is partly based on experiments in a natural environment and was greatly dependent on the weather]

9. LAMINATED MEMBERS

Paper 31 - 12 - 1 Depth Factor for Glued Laminated Timber - Discussion of the Eurocode 5 Approach - B Källsner, O Carling and C J Johansson

Q(R. Leicester) How was k_h calculated from the test data? [It is the ratio between the deep beam and shallow beam bending strength]

Q(H. Larsen) I am strongly against depth factors. The depth factor in the Eurocode was meant to correct differences in prediction of strength between solid sawn and glulam beams. One should be careful to draw conclusions from limited results. The COV is misleading since all the beams were from the same batch. Should one not rather use a reference depth of 300?[No, prefer 600mm]

C(A. Ranta-Maunus) I would prefer to remove the depth factor. The sample size is too small and the results are not convincing. I would like to see larger beams, closer to more realistic structural sizes

C(G. Schickhofer) The number of specimens is too small to draw conclusions. One also needs to determine more precise material characteristics

C(F. Rouger) The factors were meant to correct various product standards, many versions of which exist. One could also use 1 as a factor if not comfortable with current adjustment factors.

C(R. Leicester) In the Australian code depth factors have been abandoned. Traditionally, depth factors were used as a punishing factor for large depths.

C(C. Mettem) I would suggest a position similar to Australia. We should analyze the existing results to verify a trend in depth effects.

C(G. Boughton) In the glulam production the bias depends on the different product standards, which can be very variable. Results might be polluted by product standards from the past.

C(G. Schickhofer) We tested 290 beams in Austria and Switzerland, and got factors between 1.1 and 1.15. The 1.07 factor does not appear to be realistic.

10. STRUCTURAL STABILITY

Paper 31 - 15 - 1 Seismic Performance Testing On Wood-Framed Shear Wall - N Kawai

- Q(G. Canisius) Is equivalent damping dependent on the response of the structure's response or is it a constant [From the static load tests, the damping was almost constant. Under actual dynamic motion damping is very difficult to obtain]
- C(D. Dolan) Your results show significant differences between results obtained using the CEN, ISTO, ASTM and Techmar cyclic testing protocols. For the latter it shows a 20% drop in response.

Paper 31 - 15 - 2 Robustness Principles in the Design of Medium-Rise Timber-Framed Buildings - C J Mettem, M W Milner, R J Bainbridge and V. Enjily

- Q(S. Thelandersson) Has this also being dealt with in other countries? Is the detailing between components replicated as in real construction? [It was proposed to design the building for disproportional collapse. It was constructed as for a two-storey building. No special considerations were taken to avoid disproportional collapse in the six-storey building, although it was formatted in a cellular shape, which helped it to survive. As to the detailing, it was built by a local construction team.]
- Q(A. Jorissen) Were the loads applied stepwise? [Yes] What would be the effect of an impact load, such as an explosion? [This was one of the criticisms, but it would have been very difficult to implement. In case of an impact load it also would have been unlikely to remove a whole panel and more localized damage would have occurred.]
- C(C. Mettem) This concept has been presented before. We carefully approached the issue of building regulations such that specialized rules would not be required. An explosion would be practically difficult to realize in addition to the difficulty of documenting the extent of the explosion and to evaluate appropriate rules.
- C(R. Leicester) In Australia we built real houses and subjected the to many load cycles. Most of the time, failure occurred due to little mistakes. Redundancy could have saved the UK building. One should be careful to extrapolate from one test of a building constructed with good quality control.
- C(G. Boughton) I recognize the importance of in grade testing, but more test results are needed before one could interpret results with confidence.

Paper 31 - 15 - 3 Numerical Simulation of Pseudo-Dynamic Tests Performed to Shear Walls - L Daudeville, L Davenne, N Richard, N Kawai and M Yasumura

no questions

Paper 31 - 15 - 4 Force Modification Factors for Braced Timber Frames - H G L Prion, M Popovski and E Karacabeyli

- Q(D. Dolan) What would be the effect of a 3-D structure on the response of the braced frame, whereas codes are based on plane frame analysis of single degree-of-freedom systems? [Multiple braced frames in a structure will add redundancy to system. Furthermore, the three dimensional response could also include torsional effects which could amplify the response. More work is planned on 3-D analysis of structures]
- Q(G. Boughton) What is the meaning of the R-factor in terms of ductility, e.g. in a ductile moment frame? [It is a measure of structure ductility, which is expressed as a multiple of the yield displacement. For example, R=4 for ductile steel frames and for wood shear walls, whereas brittle structures are assigned R=1.5.]
- Q(G. Boughton) Is there any hope of having higher R factor for braced frames? [No, not

likely because ductility of braced frame is concentrated in connections which places high displacement demand on the connections. But even with low R-factors, it is important to assure that the connection can sustain a certain amount of ductile deformation, especially in terms of capacity design, which requires the rest of the structure to be stronger than the ductile fuse (in this case the connection). Timber frames have an advantage over steel frames because of the high member strength compared to the connections.]

C(D. Dolan) Nailed plywood gusset plate portal frames, as developed in New Zealand, would probably have a higher R factor.

11. FIRE

Paper 31 - 16 - 1 Revision of ENV 1995-1-2: Charring and Degradation of Strength and Stiffness - J König

Q(H. Blaß) Is there more than one real fire? [The design of a fire is based on a real fire, from the fire code. These are temperature-time curves based on fuel load, openings and thermal properties of building materials. The curves are approximate, but better than "standard" fires.]

C(C. Mettem) It is the long term goal to have documented parametric situations, where different fire scenarios are to be considered. Real fires will be documented and used for calibration of design cases.

Q(V. Enjily) Could you explain the adjustment formula for MOE. [gmj should be 1 in fire design, but it is partly a political decision. If it is used as such, then the modification factor will not be able to replicate results as we are used to do. If gmj should be <1, then in the stiffness case it should be >1.] There is no reliability issue in a fire. Should the design values be based on the 5th percentile? Could one calibrate the existing results to obtain an appropriate safety factor for today? [For stiffness, one should have a different gm factor since the E-values will be increased.

C(H. Larsen) The E-value is used for strength purposes and should be treated as such.

C(R. Leicester) People are wary of complicated calculations [One will get different design values, which is important.]

12. TEST METHODS

Paper 31 - 21 - 1 Development of an Optimised Test Configuration to Determine Shear Strength of Glued Laminated Timber - G Schickhofer and B Obermayr

Q(R. Leicester) You have induced an artificial failure mode with the test method used, because of a non-realistic moment-shear ratio. This forced one failure mode, while a 45 degree shear failure, similar to reinforced concrete, could be possible in brittle species.[We had to decide on one particular test configuration to determine appropriate shear stress values. The next step is to test different series]

C(C. Mettem) It is difficult to believe values for cross fibre shear stress. One could devise a suitable test method and increase the load in steps. Either way it is a difficult task to find a suitable shear test and one has to agree on a compromise.

Q(H. Blaß) Did any failures happen close to glue lines? [Yes, but not in the glue line itself. It would typically fail along the annual rings]

- Q(J. Ehlbeck) Where does one find factors for impact loads? [Most codes, e.g. Eurocode or BS, have values. We also looked at work done on concrete, but it is believed that the extra resistance might be from the inertia of the specimen]
- C(K. Crews) I would caution against a general impact factor. These factors are closely related to the end use of the product. For bridges, for example, this would not be appropriate.
- C(H. Blaß) In Germany a new test has been devised in which a 100kg weight is dropped on a leather cushion.
- C(K. Crews) These tests can also be used for verification of existing planks [This series was intended to prove that planks have a higher resistance than predicted in the code]
- Q(H. Larsen) This seems to be a system problem, which indeed can be quite complicated. Since the rules should be performance based, a direct testing method could easily be devised that relates to the particular application. CEN standards exist for many products. These are well documented. Why try such a complicated method if simple solutions are available. [Test methods exist but the loads cannot be satisfied numerically. We need design equations to verify the strength of planks]
- C(G. Boughton) I believe that very little if any increase in resistance occurs under impact load. The added resistance may be due to the fact that only a small part of the board is loaded at an given time, thus relying heavily on load distribution and residual strength. Edge effects may also be very important. Different results will be achieved when using sharp boots. Furthermore, it is important to incorporate damping of the human body in the model [The model is based on the load of a body dropping on the planks]

13. OTHER BUSINESS

Authors should send the final version of their papers as a hard copy by Sept 15, 1998 if corrections are needed.

D. Dolan volunteered to create a searchable data base and abstracts for all CIB proceedings. He asked all authors to provide up to 10 key words for their papers. These should be sent via e-mail to jddolan@vt.edu

Mobile phones are to be switched off during meetings in the future.

H. Prion announced that the next World Conference on Timber Engineering (WCTE2000) would be held in Whistler (near Vancouver), July 31 - Aug 3, 2000.

14. VENUE OF THE NEXT MEETING

The next CIB-W18 meeting will be held in Graz (Austria), hosted by Gerhard Schickhofer, during the week of 23-27 Aug 1999.

The meeting venue thereafter, in 2000, has tentatively been set as Delft (Netherlands).

15. CLOSE

**16. List of CIB-W18 Papers,
Savonlinna, Finland 1998**

List of CIB-W18 Papers, Savonlinna, Finland 1998

- 31 - 1 - 1 A Limit States Design Approach to Timber Framed Walls - C J Mettem, R Bainbridge and J A Gordon
- 31 - 2 - 1 Deformation and Stability of Columns of Viscoelastic Material Wood - P Becker and K Rautenstrauch
- 31 - 5 - 1 Influence of Varying Growth Characteristics on Stiffness Grading of Structural Timber - S Ormarsson, H Petersson, O Dahlblom and K Persson
- 31 - 5 - 2 A Comparison of In-Grade Test Procedures - R H Leicester, H Breitingger and H Fordham
- 31 - 6 - 1 Length and Moment Configuration Factors - T Isaksson
- 31 - 6 - 2 Tensile Strength Perpendicular to Grain According to EN 1193 - H J Blaß and M Schmid
- 31 - 6 - 3 Strength of Small Diameter Round Timber - A Ranta-Maunus, U Saarelainen and H Boren
- 31 - 6 - 4 Compression Strength Perpendicular to Grain of Structural Timber and Glulam - L Damkilde, P Hoffmeyer and T N Pedersen
- 31 - 6 - 5 Bearing Strength of Timber Beams- R H Leicester, H Fordham and H Breitingger
- 31 - 7 - 1 Mechanical Properties of Dowel Type Joints under Reversed Cyclic Lateral Loading - M Yasumura
- 31 - 7 - 2 Design of Joints with Laterally Loaded Dowels - A Mischler
- 31 - 7 - 3 Flexural Behaviour of Glulam Beams Edge-Jointed by Lagscrews with Steel Splice Plates - K Komatsu
- 31 - 7 - 4 Design on Timber Capacity in Nailed Steel-to-Timber Joints - J Kangas and J Vesa
- 31 - 7 - 5 Timber Contact in Chord Splices of Nail Plate Structures - A Kevarinmäki

- 31 - 7 - 6 The Fastener Yield Strength in Bending - A Jorissen and H J Blaß
- 31 - 7 - 7 A Proposal for Simplification of Johansen's Formulae, Dealing With the Design of Dowelled-Type Fasteners - F Rouger
- 31 - 7 - 8 Simplified Design of Connections with Dowel-type fasteners - H J Blaß and J Ehlbeck
- 31 - 9 - 1 Duration of Load Effect in Tension Perpendicular to Grain in Curved Glulam - A Ranta-Maunus
- 31 - 12 - 1 Depth Factor for Glued Laminated Timber - Discussion of the Eurocode 5 Approach - B Källsner, O Carling and C J Johansson
- 31 - 15 - 1 Seismic Performance Testing On Wood-Framed Shear Wall - N Kawai
- 31 - 15 - 2 Robustness Principles in the Design of Medium-Rise Timber-Framed Buildings - C J Mettem, M W Milner, R J Bainbridge and V. Enjily
- 31 - 15 - 3 Numerical Simulation of Pseudo-Dynamic Tests Performed to Shear Walls - L Daudeville, L Davenne, N Richard, N Kawai and M Yasumura
- 31 - 15 - 4 Force Modification Factors for Braced Timber Frames - H G L Prion, M Popovski and E Karacabeyli
- 31 - 16 - 1 Revision of ENV 1995-1-2: Charring and Degradation of Strength and Stiffness - J König
- 31 - 21 - 1 Development of an Optimised Test Configuration to Determine Shear Strength of Glued Laminated Timber - G Schickhofer and B Obermayr
- 31 - 21 - 2 An Impact Strength Test Method for Structural Timber. The Theory and a Preliminary Study - T D G Canisius

17. Current List of CIB-W18(A) Papers

CURRENT LIST OF CIB-W18(A) PAPERS

Technical papers presented to CIB-W18(A) are identified by a code CIB-W18(A)/a-b-c, where:

a denotes the meeting at which the paper was presented.
Meetings are classified in chronological order:

- 1 Princes Risborough, England; March 1973
- 2 Copenhagen, Denmark; October 1973
- 3 Delft, Netherlands; June 1974
- 4 Paris, France; February 1975
- 5 Karlsruhe, Federal Republic of Germany; October 1975
- 6 Aalborg, Denmark; June 1976
- 7 Stockholm, Sweden; February/March 1977
- 8 Brussels, Belgium; October 1977
- 9 Perth, Scotland; June 1978
- 10 Vancouver, Canada; August 1978
- 11 Vienna, Austria; March 1979
- 12 Bordeaux, France; October 1979
- 13 Otaniemi, Finland; June 1980
- 14 Warsaw, Poland; May 1981
- 15 Karlsruhe, Federal Republic of Germany; June 1982
- 16 Lillehammer, Norway; May/June 1983
- 17 Rapperswil, Switzerland; May 1984
- 18 Beit Oren, Israel; June 1985
- 19 Florence, Italy; September 1986
- 20 Dublin, Ireland; September 1987
- 21 Parksville, Canada; September 1988
- 22 Berlin, German Democratic Republic; September 1989
- 23 Lisbon, Portugal; September 1990
- 24 Oxford, United Kingdom; September 1991
- 25 Åhus, Sweden; August 1992
- 26 Athens, USA; August 1993
- 27 Sydney, Australia; July 1994
- 28 Copenhagen, Denmark, April 1995
- 29 Bordeaux, France, August 1996
- 30 Vancouver, Canada, August 1997
- 31 Savonlinna, Finland, August 1998

b denotes the subject:

- 1 Limit State Design
- 2 Timber Columns
- 3 Symbols
- 4 Plywood
- 5 Stress Grading
- 6 Stresses for Solid Timber
- 7 Timber Joints and Fasteners
- 8 Load Sharing
- 9 Duration of Load
- 10 Timber Beams
- 11 Environmental Conditions
- 12 Laminated Members
- 13 Particle and Fibre Building Boards
- 14 Trussed Rafters
- 15 Structural Stability
- 16 Fire
- 17 Statistics and Data Analysis
- 18 Glued Joints
- 19 Fracture Mechanics
- 20 Serviceability
- 21 Test Methods
- 100 CIB Timber Code
- 101 Loading Codes
- 102 Structural Design Codes
- 103 International Standards Organisation
- 104 Joint Committee on Structural Safety
- 105 CIB Programme, Policy and Meetings
- 106 International Union of Forestry Research Organisations

c is simply a number given to the papers in the order in which they appear:

Example: CIB-W18/4-102-5 refers to paper 5 on subject 102 presented at the fourth meeting of W18.

Listed below, by subjects, are all papers that have to date been presented to W18. When appropriate some papers are listed under more than one subject heading.

LIMIT STATE DESIGN

- 1-1-1 Limit State Design - H J Larsen
- 1-1-2 The Use of Partial Safety Factors in the New Norwegian Design Code for Timber Structures - O Brynildsen
- 1-1-3 Swedish Code Revision Concerning Timber Structures - B Noren
- 1-1-4 Working Stresses Report to British Standards Institution Committee BLC/17/2
- 6-1-1 On the Application of the Uncertainty Theoretical Methods for the Definition of the Fundamental Concepts of Structural Safety - K Skov and O Ditlevsen
- 11-1-1 Safety Design of Timber Structures - H J Larsen
- 18-1-1 Notes on the Development of a UK Limit States Design Code for Timber - A R Fewell and C B Pierce
- 18-1-2 Eurocode 5, Timber Structures - H J Larsen
- 19-1-1 Duration of Load Effects and Reliability Based Design (Single Member) - R O Foschi and Z C Yao
- 21-102-1 Research Activities Towards a New GDR Timber Design Code Based on Limit States Design - W Rug and M Badstube
- 22-1-1 Reliability-Theoretical Investigation into Timber Components Proposal for a Supplement of the Design Concept - M Badstube, W Rug and R Plessow
- 23-1-1 Some Remarks about the Safety of Timber Structures - J Kuipers
- 23-1-2 Reliability of Wood Structural Elements: A Probabilistic Method to Eurocode 5 Calibration - F Rouger, N Lheritier, P Racher and M Fogli
- 31-1-1 A Limit States Design Approach to Timber Framed Walls - C J Mettem, R Bainbridge and J A Gordon

TIMBER COLUMNS

- 2-2-1 The Design of Solid Timber Columns - H J Larsen
- 3-2-1 The Design of Built-Up Timber Columns - H J Larsen
- 4-2-1 Tests with Centrally Loaded Timber Columns - H J Larsen and S S Pedersen
- 4-2-2 Lateral-Torsional Buckling of Eccentrically Loaded Timber Columns - B Johansson
- 5-9-1 Strength of a Wood Column in Combined Compression and Bending with Respect to Creep - B Källsner and B Norén
- 5-100-1 Design of Solid Timber Columns (First Draft) - H J Larsen
- 6-100-1 Comments on Document 5-100-1, Design of Solid Timber Columns - H J Larsen and E Theilgaard
- 6-2-1 Lattice Columns - H J Larsen
- 6-2-2 A Mathematical Basis for Design Aids for Timber Columns - H J Burgess
- 6-2-3 Comparison of Larsen and Perry Formulas for Solid Timber Columns - H J Burgess
- 7-2-1 Lateral Bracing of Timber Struts - J A Simon
- 8-15-1 Laterally Loaded Timber Columns: Tests and Theory - H J Larsen
- 17-2-1 Model for Timber Strength under Axial Load and Moment - T Poutanen

- 18-2-1 Column Design Methods for Timber Engineering - A H Buchanan, K C Johns, B Madsen
- 19-2-1 Creep Buckling Strength of Timber Beams and Columns - R H Leicester
- 19-12-2 Strength Model for Glulam Columns - H J Blaß
- 20-2-1 Lateral Buckling Theory for Rectangular Section Deep Beam-Columns- H J Burgess
- 20-2-2 Design of Timber Columns - H J Blaß
- 21-2-1 Format for Buckling Strength - R H Leicester
- 21-2-2 Beam-Column Formulae for Design Codes - R H Leicester
- 21-15-1 Rectangular Section Deep Beam - Columns with Continuous Lateral Restraint - H J Burgess
- 21-15-2 Buckling Modes and Permissible Axial Loads for Continuously Braced Columns - H J Burgess
- 21-15-3 Simple Approaches for Column Bracing Calculations - H J Burgess
- 21-15-4 Calculations for Discrete Column Restraints - H J Burgess
- 22-2-1 Buckling and Reliability Checking of Timber Columns - S Huang, P M Yu and J Y Hong
- 22-2-2 Proposal for the Design of Compressed Timber Members by Adopting the Second-Order Stress Theory - P Kaiser
- 30-2-1 Beam-Column Formula for Specific Truss Applications - W Lau, F Lam and J D Barrett
- 31-2-1 Deformation and Stability of Columns of Viscoelastic Material Wood - P Becker and K Rautenstrauch

SYMBOLS

- 3-3-1 Symbols for Structural Timber Design - J Kuipers and B Norén
- 4-3-1 Symbols for Timber Structure Design - J Kuipers and B Norén
- 28-3-1 Symbols for Timber and Wood-Based Materials - J Kuipers and B Noren
- 1 Symbols for Use in Structural Timber Design

PLYWOOD

- 2-4-1 The Presentation of Structural Design Data for Plywood - L G Booth
- 3-4-1 Standard Methods of Testing for the Determination of Mechanical Properties of Plywood - J Kuipers
- 3-4-2 Bending Strength and Stiffness of Multiple Species Plywood - C K A Stieda
- 4-4-4 Standard Methods of Testing for the Determination of Mechanical Properties of Plywood - Council of Forest Industries, B.C.
- 5-4-1 The Determination of Design Stresses for Plywood in the Revision of CP 112 - L G Booth
- 5-4-2 Veneer Plywood for Construction - Quality Specifications - ISO/TC 139. Plywood, Working Group 6
- 6-4-1 The Determination of the Mechanical Properties of Plywood Containing Defects - L G Booth

- 6-4-2 Comparison of the Size and Type of Specimen and Type of Test on Plywood Bending Strength and Stiffness - C R Wilson and P Eng
- 6-4-3 Buckling Strength of Plywood: Results of Tests and Recommendations for Calculations - J Kuipers and H Ploos van Amstel
- 7-4-1 Methods of Test for the Determination of Mechanical Properties of Plywood - L G Booth, J Kuipers, B Norén, C R Wilson
- 7-4-2 Comments Received on Paper 7-4-1
- 7-4-3 The Effect of Rate of Testing Speed on the Ultimate Tensile Stress of Plywood - C R Wilson and A V Parasin
- 7-4-4 Comparison of the Effect of Specimen Size on the Flexural Properties of Plywood Using the Pure Moment Test - C R Wilson and A V Parasin
- 8-4-1 Sampling Plywood and the Evaluation of Test Results - B Norén
- 9-4-1 Shear and Torsional Rigidity of Plywood - H J Larsen
- 9-4-2 The Evaluation of Test Data on the Strength Properties of Plywood - L G Booth
- 9-4-3 The Sampling of Plywood and the Derivation of Strength Values (Second Draft) - B Norén
- 9-4-4 On the Use of the CIB/RILEM Plywood Plate Twisting Test: a progress report - L G Booth
- 10-4-1 Buckling Strength of Plywood - J Dekker, J Kuipers and H Ploos van Amstel
- 11-4-1 Analysis of Plywood Stressed Skin Panels with Rigid or Semi-Rigid Connections - I Smith
- 11-4-2 A Comparison of Plywood Modulus of Rigidity Determined by the ASTM and RILEM CIB/3-TT Test Methods - C R Wilson and A V Parasin
- 11-4-3 Sampling of Plywood for Testing Strength - B Norén
- 12-4-1 Procedures for Analysis of Plywood Test Data and Determination of Characteristic Values Suitable for Code Presentation - C R Wilson
- 14-4-1 An Introduction to Performance Standards for Wood-base Panel Products - D H Brown
- 14-4-2 Proposal for Presenting Data on the Properties of Structural Panels - T Schmidt
- 16-4-1 Planar Shear Capacity of Plywood in Bending - C K A Stieda
- 17-4-1 Determination of Panel Shear Strength and Panel Shear Modulus of Beech-Plywood in Structural Sizes - J Ehlbeck and F Colling
- 17-4-2 Ultimate Strength of Plywood Webs - R H Leicester and L Pham
- 20-4-1 Considerations of Reliability - Based Design for Structural Composite Products - M R O'Halloran, J A Johnson, E G Elias and T P Cunningham
- 21-4-1 Modelling for Prediction of Strength of Veneer Having Knots - Y Hirashima
- 22-4-1 Scientific Research into Plywood and Plywood Building Constructions the Results and Findings of which are Incorporated into Construction Standard Specifications of the USSR - I M Guskov
- 22-4-2 Evaluation of Characteristic values for Wood-Based Sheet Materials - E G Elias
- 24-4-1 APA Structural-Use Design Values: An Update to Panel Design Capacities - A L Kuchar, E G Elias, B Yeh and M R O'Halloran

STRESS GRADING

- 1-5-1 Quality Specifications for Sawn Timber and Precision Timber - Norwegian Standard NS 3080
- 1-5-2 Specification for Timber Grades for Structural Use - British Standard BS 4978
- 4-5-1 Draft Proposal for an International Standard for Stress Grading Coniferous Sawn Softwood - ECE Timber Committee
- 16-5-1 Grading Errors in Practice - B Thunell
- 16-5-2 On the Effect of Measurement Errors when Grading Structural Timber- L Nordberg and B Thunell
- 19-5-1 Stress-Grading by ECE Standards of Italian-Grown Douglas-Fir Dimension Lumber from Young Thinnings - L Uzielli
- 19-5-2 Structural Softwood from Afforestation Regions in Western Norway - R Lackner
- 21-5-1 Non-Destructive Test by Frequency of Full Size Timber for Grading - T Nakai
- 22-5-1 Fundamental Vibration Frequency as a Parameter for Grading Sawn Timber - T Nakai, T Tanaka and H Nagao
- 24-5-1 Influence of Stress Grading System on Length Effect Factors for Lumber Loaded in Compression - A Campos and I Smith
- 26-5-1 Structural Properties of French Grown Timber According to Various Grading Methods - F Rouger, C De Lafond and A El Quadrani
- 28-5-1 Grading Methods for Structural Timber - Principles for Approval - S Ohlsson
- 28-5-2 Relationship of Moduli of Elasticity in Tension and in Bending of Solid Timber - N Burger and P Glos
- 29-5-1 The Effect of Edge Knots on the Strength of SPF MSR Lumber - T Courchene, F Lam and J D Barrett
- 29-5-2 Determination of Moment Configuration Factors using Grading Machine Readings - T D G Canisius and T Isaksson
- 31-5-1 Influence of Varying Growth Characteristics on Stiffness Grading of Structural Timber - S Ormarsson, H Petersson, O Dahlblom and K Persson
- 31-5-2 A Comparison of In-Grade Test Procedures - R H Leicester, H Breitingner and H Fordham

STRESSES FOR SOLID TIMBER

- 4-6-1 Derivation of Grade Stresses for Timber in the UK - W T Curry
- 5-6-1 Standard Methods of Test for Determining some Physical and Mechanical Properties of Timber in Structural Sizes - W T Curry
- 5-6-2 The Description of Timber Strength Data - J R Tory
- 5-6-3 Stresses for EC1 and EC2 Stress Grades - J R Tory
- 6-6-1 Standard Methods of Test for the Determination of some Physical and Mechanical Properties of Timber in Structural Sizes (third draft) - W T Curry
- 7-6-1 Strength and Long-term Behaviour of Lumber and Glued Laminated Timber under Torsion Loads - K Möhler
- 9-6-1 Classification of Structural Timber - H J Larsen
- 9-6-2 Code Rules for Tension Perpendicular to Grain - H J Larsen
- 9-6-3 Tension at an Angle to the Grain - K Möhler

- 9-6-4 Consideration of Combined Stresses for Lumber and Glued Laminated Timber - K Möhler
- 11-6-1 Evaluation of Lumber Properties in the United States - W L Galligan and J H Haskell
- 11-6-2 Stresses Perpendicular to Grain - K Möhler
- 11-6-3 Consideration of Combined Stresses for Lumber and Glued Laminated Timber (addition to Paper CIB-W18/9-6-4) - K Möhler
- 12-6-1 Strength Classifications for Timber Engineering Codes - R H Leicester and W G Keating
- 12-6-2 Strength Classes for British Standard BS 5268 - J R Tory
- 13-6-1 Strength Classes for the CIB Code - J R Tory
- 13-6-2 Consideration of Size Effects and Longitudinal Shear Strength for Uncracked Beams - R O Foschi and J D Barrett
- 13-6-3 Consideration of Shear Strength on End-Cracked Beams - J D Barrett and R O Foschi
- 15-6-1 Characteristic Strength Values for the ECE Standard for Timber - J G Sunley
- 16-6-1 Size Factors for Timber Bending and Tension Stresses - A R Fewell
- 16-6-2 Strength Classes for International Codes - A R Fewell and J G Sunley
- 17-6-1 The Determination of Grade Stresses from Characteristic Stresses for BS 5268: Part 2 - A R Fewell
- 17-6-2 The Determination of Softwood Strength Properties for Grades, Strength Classes and Laminated Timber for BS 5268: Part 2 - A R Fewell
- 18-6-1 Comment on Papers: 18-6-2 and 18-6-3 - R H Leicester
- 18-6-2 Configuration Factors for the Bending Strength of Timber - R H Leicester
- 18-6-3 Notes on Sampling Factors for Characteristic Values - R H Leicester
- 18-6-4 Size Effects in Timber Explained by a Modified Weakest Link Theory- B Madsen and A H Buchanan
- 18-6-5 Placement and Selection of Growth Defects in Test Specimens - H Riberholt
- 18-6-6 Partial Safety-Coefficients for the Load-Carrying Capacity of Timber Structures - B Norén and J-O Nylander
- 19-6-1 Effect of Age and/or Load on Timber Strength - J Kuipers
- 19-6-2 Confidence in Estimates of Characteristic Values - R H Leicester
- 19-6-3 Fracture Toughness of Wood - Mode I - K Wright and M Fonselius
- 19-6-4 Fracture Toughness of Pine - Mode II - K Wright
- 19-6-5 Drying Stresses in Round Timber - A Ranta-Maunus
- 19-6-6 A Dynamic Method for Determining Elastic Properties of Wood - R Görlacher
- 20-6-1 A Comparative Investigation of the Engineering Properties of "Whitewoods" Imported to Israel from Various Origins - U Korin
- 20-6-2 Effects of Yield Class, Tree Section, Forest and Size on Strength of Home Grown Sitka Spruce - V Picardo
- 20-6-3 Determination of Shear Strength and Strength Perpendicular to Grain - H J Larsen
- 21-6-1 Draft Australian Standard: Methods for Evaluation of Strength and Stiffness of Graded Timber - R H Leicester

- 21-6-2 The Determination of Characteristic Strength Values for Stress Grades of Structural Timber. Part 1 - A R Fewell and P Glos
- 21-6-3 Shear Strength in Bending of Timber - U Korin
- 22-6-1 Size Effects and Property Relationships for Canadian 2-inch Dimension Lumber - J D Barrett and H Griffin
- 22-6-2 Moisture Content Adjustments for In-Grade Data - J D Barrett and W Lau
- 22-6-3 A Discussion of Lumber Property Relationships in Eurocode 5 - D W Green and D E Kretschmann
- 22-6-4 Effect of Wood Preservatives on the Strength Properties of Wood - F Ronai
- 23-6-1 Timber in Compression Perpendicular to Grain - U Korin
- 24-6-1 Discussion of the Failure Criterion for Combined Bending and Compression - T A C M van der Put
- 24-6-3 Effect of Within Member Variability on Bending Strength of Structural Timber - I Czmocho, S Thelandersson and H J Larsen
- 24-6-4 Protection of Structural Timber Against Fungal Attack Requirements and Testing - K Jaworska, M Rylko and W Nozynski
- 24-6-5 Derivation of the Characteristic Bending Strength of Solid Timber According to CEN-Document prEN 384 - A J M Leijten
- 25-6-1 Moment Configuration Factors for Simple Beams - T D G Canisius
- 25-6-3 Bearing Capacity of Timber - U Korin
- 25-6-4 On Design Criteria for Tension Perpendicular to Grain - H Petersson
- 25-6-5 Size Effects in Visually Graded Softwood Structural Lumber - J D Barrett, F Lam and W Lau
- 26-6-1 Discussion and Proposal of a General Failure Criterion for Wood - T A C M van der Put
- 27-6-1 Development of the "Critical Bearing": Design Clause in CSA-086.1 - C Lum and E Karacabeyli
- 27-6-2 Size Effects in Timber: Novelty Never Ends - F Rouger and T Fewell
- 27-6-3 Comparison of Full-Size Sugi (*Cryptomeria japonica* D. Don) Structural Performance in Bending of Round Timber, Two Surfaces Sawn Timber and Square Sawn Timber - T Nakai, H Nagao and T Tanaka
- 28-6-1 Shear Strength of Canadian Softwood Structural Lumber - F Lam, H Yee and J D Barrett
- 28-6-2 Shear Strength of Douglas Fir Timbers - B Madsen
- 28-6-3 On the Influence of the Loading Head Profiles on Determined Bending Strength - L Muszyński and R Szukala
- 28-6-4 Effect of Test Standard, Length and Load Configuration on Bending Strength of Structural Timber - T Isaksson and S Thelandersson
- 28-6-5 Grading Machine Readings and their Use in the Calculation of Moment Configuration Factors - T Canisius, T Isaksson and S Thelandersson
- 28-6-6 End Conditions for Tension Testing of Solid Timber Perpendicular to Grain - T Canisius
- 29-6-1 Effect of Size on Tensile Strength of Timber - N Burger and P Glos
- 29-6-2 Equivalence of In-Grade Testing Standards - R H Leicester, H O Breiting and H F Fordham

- 30-6-1 Strength Relationships in Structural Timber Subjected to Bending and Tension - N Burger and P Glos
- 30-6-2 Characteristic Design Stresses in Tension for Radiata Pine Grown in Canterbury - A Tsehaye, J C F Walker and A H Buchanan
- 30-6-3 Timber as a Natural Composite: Explanation of Some Peculiarities in the Mechanical Behaviour - E Gehri
- 31-6-1 Length and Moment Configuration Factors - T Isaksson
- 31-6-2 Tensile Strength Perpendicular to Grain According to EN 1193 - H J Blaß and M Schmid
- 31-6-3 Strength of Small Diameter Round Timber - A Ranta-Maunus, U Saarelainen and H Boren
- 31-6-4 Compression Strength Perpendicular to Grain of Structural Timber and Glulam - L Damkilde, P Hoffmeyer and T N Pedersen
- 31-6-5 Bearing Strength of Timber Beams - R H Leicester, H Fordham and H Breitingner

TIMBER JOINTS AND FASTENERS

- 1-7-1 Mechanical Fasteners and Fastenings in Timber Structures - E G Stern
- 4-7-1 Proposal for a Basic Test Method for the Evaluation of Structural Timber Joints with Mechanical Fasteners and Connectors - RILEM 3TT Committee
- 4-7-2 Test Methods for Wood Fasteners - K Möhler
- 5-7-1 Influence of Loading Procedure on Strength and Slip-Behaviour in Testing Timber Joints - K Möhler
- 5-7-2 Recommendations for Testing Methods for Joints with Mechanical Fasteners and Connectors in Load-Bearing Timber Structures - RILEM 3 TT Committee
- 5-7-3 CIB-Recommendations for the Evaluation of Results of Tests on Joints with Mechanical Fasteners and Connectors used in Load-Bearing Timber Structures - J Kuipers
- 6-7-1 Recommendations for Testing Methods for Joints with Mechanical Fasteners and Connectors in Load-Bearing Timber Structures (seventh draft) - RILEM 3 TT Committee
- 6-7-2 Proposal for Testing Integral Nail Plates as Timber Joints - K Möhler
- 6-7-3 Rules for Evaluation of Values of Strength and Deformation from Test Results - Mechanical Timber Joints - M Johansen, J Kuipers, B Norén
- 6-7-4 Comments to Rules for Testing Timber Joints and Derivation of Characteristic Values for Rigidity and Strength - B Norén
- 7-7-1 Testing of Integral Nail Plates as Timber Joints - K Möhler
- 7-7-2 Long Duration Tests on Timber Joints - J Kuipers
- 7-7-3 Tests with Mechanically Jointed Beams with a Varying Spacing of Fasteners - K Möhler
- 7-100-1 CIB-Timber Code Chapter 5.3 Mechanical Fasteners; CIB-Timber Standard 06 and 07 - H J Larsen
- 9-7-1 Design of Truss Plate Joints - F J Keenan
- 9-7-2 Staples - K Möhler
- 11-7-1 A Draft Proposal for International Standard: ISO Document ISO/TC 165N 38E

- 12-7-1 Load-Carrying Capacity and Deformation Characteristics of Nailed Joints - J Ehlbeck
- 12-7-2 Design of Bolted Joints - H J Larsen
- 12-7-3 Design of Joints with Nail Plates - B Norén
- 13-7-1 Polish Standard BN-80/7159-04: Parts 00-01-02-03-04-05.
"Structures from Wood and Wood-based Materials. Methods of Test and Strength Criteria for Joints with Mechanical Fasteners"
- 13-7-2 Investigation of the Effect of Number of Nails in a Joint on its Load Carrying Ability - W Nozynski
- 13-7-3 International Acceptance of Manufacture, Marking and Control of Finger-jointed Structural Timber - B Norén
- 13-7-4 Design of Joints with Nail Plates - Calculation of Slip - B Norén
- 13-7-5 Design of Joints with Nail Plates - The Heel Joint - B Källsner
- 13-7-6 Nail Deflection Data for Design - H J Burgess
- 13-7-7 Test on Bolted Joints - P Vermeyden
- 13-7-8 Comments to paper CIB-W18/12-7-3 "Design of Joints with Nail Plates"- B Norén
- 13-7-9 Strength of Finger Joints - H J Larsen
- 13-100-4 CIB Structural Timber Design Code. Proposal for Section 6.1.5 Nail Plates - N I Bovim
- 14-7-1 Design of Joints with Nail Plates (second edition) - B Norén
- 14-7-2 Method of Testing Nails in Wood (second draft, August 1980) - B Norén
- 14-7-3 Load-Slip Relationship of Nailed Joints - J Ehlbeck and H J Larsen
- 14-7-4 Wood Failure in Joints with Nail Plates - B Norén
- 14-7-5 The Effect of Support Eccentricity on the Design of W- and WW-Trussed with Nail Plate Connectors - B Källsner
- 14-7-6 Derivation of the Allowable Load in Case of Nail Plate Joints Perpendicular to Grain - K Möhler
- 14-7-7 Comments on CIB-W18/14-7-1 - T A C M van der Put
- 15-7-1 Final Recommendation TT-1A: Testing Methods for Joints with Mechanical Fasteners in Load-Bearing Timber Structures. Annex A Punched Metal Plate Fasteners - Joint Committee RILEM/CIB-3TT
- 16-7-1 Load Carrying Capacity of Dowels - E Gehri
- 16-7-2 Bolted Timber Joints: A Literature Survey - N Harding
- 16-7-3 Bolted Timber Joints: Practical Aspects of Construction and Design; a Survey - N Harding
- 16-7-4 Bolted Timber Joints: Draft Experimental Work Plan - Building Research Association of New Zealand
- 17-7-1 Mechanical Properties of Nails and their Influence on Mechanical Properties of Nailed Timber Joints Subjected to Lateral Loads - I Smith, L R J Whale, C Anderson and L Held
- 17-7-2 Notes on the Effective Number of Dowels and Nails in Timber Joints - G Steck
- 18-7-1 Model Specification for Driven Fasteners for Assembly of Pallets and Related Structures - E G Stern and W B Wallin

- 18-7-2 The Influence of the Orientation of Mechanical Joints on their Mechanical Properties - I Smith and L R J Whale
- 18-7-3 Influence of Number of Rows of Fasteners or Connectors upon the Ultimate Capacity of Axially Loaded Timber Joints - I Smith and G Steck
- 18-7-4 A Detailed Testing Method for Nailplate Joints - J Kangas
- 18-7-5 Principles for Design Values of Nailplates in Finland - J Kangas
- 18-7-6 The Strength of Nailplates - N I Bovim and E Aasheim
- 19-7-1 Behaviour of Nailed and Bolted Joints under Short-Term Lateral Load - Conclusions from Some Recent Research - L R J Whale, I Smith and B O Hilson
- 19-7-2 Glued Bolts in Glulam - H Riberholt
- 19-7-3 Effectiveness of Multiple Fastener Joints According to National Codes and Eurocode 5 (Draft) - G Steck
- 19-7-4 The Prediction of the Long-Term Load Carrying Capacity of Joints in Wood Structures - Y M Ivanov and Y Y Slavic
- 19-7-5 Slip in Joints under Long-Term Loading - T Feldborg and M Johansen
- 19-7-6 The Derivation of Design Clauses for Nailed and Bolted Joints in Eurocode 5 - L R J Whale and I Smith
- 19-7-7 Design of Joints with Nail Plates - Principles - B Norén
- 19-7-8 Shear Tests for Nail Plates - B Norén
- 19-7-9 Advances in Technology of Joints for Laminated Timber - Analyses of the Structural Behaviour - M Piazza and G Turrini
- 19-15-1 Connections Deformability in Timber Structures: A Theoretical Evaluation of its Influence on Seismic Effects - A Ceccotti and A Vignoli
- 20-7-1 Design of Nailed and Bolted Joints-Proposals for the Revision of Existing Formulae in Draft Eurocode 5 and the CIB Code - L R J Whale, I Smith and H J Larsen
- 20-7-2 Slip in Joints under Long Term Loading - T Feldborg and M Johansen
- 20-7-3 Ultimate Properties of Bolted Joints in Glued-Laminated Timber - M Yasumura, T Murota and H Sakai
- 20-7-4 Modelling the Load-Deformation Behaviour of Connections with Pin-Type Fasteners under Combined Moment, Thrust and Shear Forces - I Smith
- 21-7-1 Nails under Long-Term Withdrawal Loading - T Feldborg and M Johansen
- 21-7-2 Glued Bolts in Glulam-Proposals for CIB Code - H Riberholt
- 21-7-3 Nail Plate Joint Behaviour under Shear Loading - T Poutanen
- 21-7-4 Design of Joints with Laterally Loaded Dowels. Proposals for Improving the Design Rules in the CIB Code and the Draft Eurocode 5 - J Ehlbeck and H Werner
- 21-7-5 Axially Loaded Nails: Proposals for a Supplement to the CIB Code - J Ehlbeck and W Siebert
- 22-7-1 End Grain Connections with Laterally Loaded Steel Bolts A draft proposal for design rules in the CIB Code - J Ehlbeck and M Gerold
- 22-7-2 Determination of Perpendicular-to-Grain Tensile Stresses in Joints with Dowel-Type Fasteners - A draft proposal for design rules - J Ehlbeck, R Görlacher and H Werner

- 22-7-3 Design of Double-Shear Joints with Non-Metallic Dowels A proposal for a supplement of the design concept - J Ehlbeck and O Eberhart
- 22-7-4 The Effect of Load on Strength of Timber Joints at high Working Load Level - A J M Leijten
- 22-7-5 Plasticity Requirements for Portal Frame Corners - R Gunnewijk and A J M Leijten
- 22-7-6 Background Information on Design of Glulam Rivet Connections in CSA/CAN3-086.1-M89 - A proposal for a supplement of the design concept - E Karacabeyli and D P Janssens
- 22-7-7 Mechanical Properties of Joints in Glued-Laminated Beams under Reversed Cyclic Loading - M Yasumura
- 22-7-8 Strength of Glued Lap Timber Joints - P Glos and H Horstmann
- 22-7-9 Toothed Rings Type Bistyp 075 at the Joints of Fir Wood - J Kerste
- 22-7-10 Calculation of Joints and Fastenings as Compared with the International State - K Zimmer and K Lissner
- 22-7-11 Joints on Glued-in Steel Bars Present Relatively New and Progressive Solution in Terms of Timber Structure Design - G N Zubarev, F A Boitemirov and V M Golovina
- 22-7-12 The Development of Design Codes for Timber Structures made of Compositive Bars with Plate Joints based on Cylindrical Nails - Y V Piskunov
- 22-7-13 Designing of Glued Wood Structures Joints on Glued-in Bars - S B Turkovsky
- 23-7-1 Proposal for a Design Code for Nail Plates - E Aasheim and K H Solli
- 23-7-2 Load Distribution in Nailed Joints - H J Blass
- 24-7-1 Theoretical and Experimental Tension and Shear Capacity of Nail Plate Connections - B Källsner and J Kangas
- 24-7-2 Testing Method and Determination of Basic Working Loads for Timber Joints with Mechanical Fasteners - Y Hirashima and F Kamiya
- 24-7-3 Anchorage Capacity of Nail Plate - J Kangas
- 25-7-2 Softwood and Hardwood Embedding Strength for Dowel type Fasteners - J Ehlbeck and H Werner
- 25-7-4 A Guide for Application of Quality Indexes for Driven Fasteners Used in Connections in Wood Structures - E G Stern
- 25-7-5 35 Years of Experience with Certain Types of Connectors and Connector Plates Used for the Assembly of Wood Structures and their Components- E G Stern
- 25-7-6 Characteristic Strength of Split-ring and Shear-plate Connections - H J Blass, J Ehlbeck and M Schlager
- 25-7-7 Characteristic Strength of Tooth-plate Connector Joints - H J Blass, J Ehlbeck and M Schlager
- 25-7-8 Extending Yield Theory to Screw Connections - T E McLain
- 25-7-9 Determination of k_{def} for Nailed Joints - J W G van de Kuilen
- 25-7-10 Characteristic Strength of UK Timber Connectors - A V Page and C J Mettem
- 25-7-11 Multiple-fastener Dowel-type Joints, a Selected Review of Research and Codes - C J Mettem and A V Page
- 25-7-12 Load Distributions in Multiple-fastener Bolted Joints in European Whitewood Glulam, with Steel Side Plates - C J Mettem and A V Page

- 26-7-1 Proposed Test Method for Dynamic Properties of Connections Assembled with Mechanical Fasteners - J D Dolan
- 26-7-2 Validatory Tests and Proposed Design Formulae for the Load-Carrying Capacity of Toothed-Plate Connected Joints - C J Mettem, A V Page and G Davis
- 26-7-3 Definitions of Terms and Multi-Language Terminology Pertaining to Metal Connector Plates - E G Stern
- 26-7-4 Design of Joints Based on in V-Shape Glued-in Rods - J Kangas
- 26-7-5 Tests on Timber Concrete Composite Structural Elements (TCCs) - A U Meierhofer
- 27-7-1 Glulam Arch Bridge and Design of it's Moment-Resisting Joints - K Komatsu and S Usuku
- 27-7-2 Characteristic Load - Carrying Capacity of Joints with Dowel - type Fasteners in Regard to the System Properties - H Werner
- 27-7-3 Steel Failure Design in Truss Plate Joints - T Poutanen
- 28-7-1 Expanded Tube Joint in Locally DP Reinforced Timber - A J M Leijten, P Ragupathy and K S Viridi
- 28-7-2 A Strength and Stiffness Model for the Expanded Tube Joint - A J M Leijten
- 28-7-3 Load-carrying Capacity of Steel-to Timber Joints with Annular Ring Shanked Nails. A Comparison with the EC5 Design Method - R Görlacher
- 28-7-4 Dynamic Effects on Metal-Plate Connected Wood Truss Joints - S Kent, R Gupta and T Miller
- 28-7-5 Failure of the Timber Bolted Joints Subjected to Lateral Load Perpendicular to Grain - M Yasumura and L Daudeville
- 28-7-6 Design Procedure for Locally Reinforced Joints with Dowel-type Fasteners - H Werner
- 28-7-7 Variability and Effects of Moisture Content on the Withdrawal Characteristics for Lumber as Opposed to Clear Wood - J D Dolan and J W Stelmokas
- 28-7-8 Nail Plate Capacity in Joint Line - A Kevarinmäki and J Kangas
- 28-7-9 Axial Strength of Glued-In Bolts - Calculation Model Based on Non-Linear Fracture Mechanics - A Preliminary Study - C J Johansson, E Serrano, P J Gustafsson and B Enquist
- 28-7-10 Cyclic Lateral Dowel Connection Tests for seismic and Wind Evaluation - J D Dolan
- 29-7-1 A Simple Method for Lateral Load-Carrying Capacity of Dowel-Type Fasteners - J Kangas and J Kurkela
- 29-7-2 Nail Plate Joint Behaviour at Low Versus High Load Level - T Poutanen
- 29-7-3 The Moment Resistance of Tee and Butt - Joint Nail Plate Test Specimens - A Comparison with Current Design Methods - A Reffold, L R J Whale and B S Choo
- 29-7-4 A Critical Review of the Moment Rotation Test Method Proposed in prEN 1075 - M Bettison, B S Choo and L R J Whale
- 29-7-5 Explanation of the Translation and Rotation Behaviour of Prestressed Moment Timber Joints - A J M Leijten
- 29-7-6 Design of Joints and Frame Corners using Dowel-Type Fasteners - E Gehri
- 29-7-7 Quasi-Static Reversed-Cyclic Testing of Nailed Joints - E Karacabeyli and A Ceccotti

- 29-7-8 Failure of Bolted Joints Loaded Parallel to the Grain: Experiment and Simulation - L Davenne, L Daudeville and M Yasumura
- 30-7-1 Flexural Behaviour of GLT Beams End-Jointed by Glued-in Hardwood Dowels - K Komatsu, A Koizumi, J Jensen, T Sasaki and Y Iijima
- 30-7-2 Modelling of the Block Tearing Failure in Nailed Steel-to-Timber Joints - J Kangas, K Aalto and A Kevarinmäki
- 30-7-3 Cyclic Testing of Joints with Dowels and Slotted-in Steel Plates - E Aasheim
- 30-7-4 A Steel-to-Timber Dowelled Joint of High Performance in Combination with a High Strength Wood Composite (Parallam) - E Gehri
- 30-7-5 Multiple Fastener Timber Connections with Dowel Type Fasteners - A Jorissen
- 30-7-6 Influence of Ductility on Load-Carrying Capacity of Joints with Dowel-Type Fasteners - A Mischler
- 31-7-1 Mechanical Properties of Dowel Type Joints under Reversed Cyclic Lateral Loading - M Yasumura
- 31-7-2 Design of Joints with Laterally Loaded Dowels - A Mischler
- 31-7-3 Flexural Behaviour of Glulam Beams Edge-Jointed by Lagscrews with Steel Splice Plates - K Komatsu
- 31-7-4 Design on Timber Capacity in Nailed Steel-to-Timber Joints - J Kangas and J Vesa
- 31-7-5 Timber Contact in Chord Splices of Nail Plate Structures - A Kevarinmäki
- 31-7-6 The Fastener Yield Strength in Bending - A Jorissen and H J Blaß
- 31-7-7 A Proposal for Simplification of Johansen's Formulae, Dealing With the Design of Dowelled-Type Fasteners - F Rouger
- 31-7-8 Simplified Design of Connections with Dowel-type fasteners - H J Blaß and J Ehlbeck

LOAD SHARING

- 3-8-1 Load Sharing - An Investigation on the State of Research and Development of Design Criteria - E Levin
- 4-8-1 A Review of Load-Sharing in Theory and Practice - E Levin
- 4-8-2 Load Sharing - B Norén
- 19-8-1 Predicting the Natural Frequencies of Light-Weight Wooden Floors - I Smith and Y H Chui
- 20-8-1 Proposed Code Requirements for Vibrational Serviceability of Timber Floors - Y H Chui and I Smith
- 21-8-1 An Addendum to Paper 20-8-1 - Proposed Code Requirements for Vibrational Serviceability of Timber Floors - Y H Chui and I Smith
- 21-8-2 Floor Vibrational Serviceability and the CIB Model Code - S Ohlsson
- 22-8-1 Reliability Analysis of Viscoelastic Floors - F Rouger, J D Barrett and R O Foschi
- 24-8-1 On the Possibility of Applying Neutral Vibrational Serviceability Criteria to Joisted Wood Floors - I Smith and Y H Chui
- 25-8-1 Analysis of Glulam Semi-rigid Portal Frames under Long-term Load - K Komatsu and N Kawamoto

DURATION OF LOAD

- 3-9-1 Definitions of Long Term Loading for the Code of Practice - B Norén
- 4-9-1 Long Term Loading of Trussed Rafters with Different Connection Systems - T Feldborg and M Johansen
- 5-9-1 Strength of a Wood Column in Combined Compression and Bending with Respect to Creep - B Källsner and B Norén
- 6-9-1 Long Term Loading for the Code of Practice (Part 2) - B Norén
- 6-9-2 Long Term Loading - K Möhler
- 6-9-3 Deflection of Trussed Rafters under Alternating Loading during a Year - T Feldborg and M Johansen
- 7-6-1 Strength and Long Term Behaviour of Lumber and Glued-Laminated Timber under Torsion Loads - K Möhler
- 7-9-1 Code Rules Concerning Strength and Loading Time - H J Larsen and E Theilgaard
- 17-9-1 On the Long-Term Carrying Capacity of Wood Structures - Y M Ivanov and Y Y Slavic
- 18-9-1 Prediction of Creep Deformations of Joints - J Kuipers
- 19-9-1 Another Look at Three Duration of Load Models - R O Foschi and Z C Yao
- 19-9-2 Duration of Load Effects for Spruce Timber with Special Reference to Moisture Influence - A Status Report - P Hoffmeyer
- 19-9-3 A Model of Deformation and Damage Processes Based on the Reaction Kinetics of Bond Exchange - T A C M van der Put
- 19-9-4 Non-Linear Creep Superposition - U Korin
- 19-9-5 Determination of Creep Data for the Component Parts of Stressed-Skin Panels - R Kliger
- 19-9-6 Creep an Lifetime of Timber Loaded in Tension and Compression - P Glos
- 19-1-1 Duration of Load Effects and Reliability Based Design (Single Member) - R O Foschi and Z C Yao
- 19-6-1 Effect of Age and/or Load on Timber Strength - J Kuipers
- 19-7-4 The Prediction of the Long-Term Load Carrying Capacity of Joints in Wood Structures - Y M Ivanov and Y Y Slavic
- 19-7-5 Slip in Joints under Long-Term Loading - T Feldborg and M Johansen
- 20-7-2 Slip in Joints under Long-Term Loading - T Feldborg and M Johansen
- 22-9-1 Long-Term Tests with Glued Laminated Timber Girders - M Badstube, W Rug and W Schöne
- 22-9-2 Strength of One-Layer solid and Lengthways Glued Elements of Wood Structures and its Alteration from Sustained Load - L M Kovaltchuk, I N Boitemirova and G B Uspenskaya
- 24-9-1 Long Term Bending Creep of Wood - T Toratti
- 24-9-2 Collection of Creep Data of Timber - A Ranta-Maunus
- 24-9-3 Deformation Modification Factors for Calculating Built-up Wood-Based Structures - I R Kliger
- 25-9-2 DVM Analysis of Wood. Lifetime, Residual Strength and Quality - L F Nielsen

- 26-9-1 Long Term Deformations in Wood Based Panels under Natural Climate Conditions. A Comparative Study - S Thelandersson, J Nordh, T Nordh and S Sandahl
- 28-9-1 Evaluation of Creep Behavior of Structural Lumber in Natural Environment - R Gupta and R Shen
- 30-9-1 DOL Effect in Tension Perpendicular to the Grain of Glulam Depending on Service Classes and Volume - S Aicher and G Dill-Langer
- 30-9-2 Damage Modelling of Glulam in Tension Perpendicular to Grain in Variable Climate - G Dill-Langer and S Aicher
- 31-9-1 Duration of Load Effect in Tension Perpendicular to Grain in Curved Glulam - A Ranta-Maunus

TIMBER BEAMS

- 4-10-1 The Design of Simple Beams - H J Burgess
- 4-10-2 Calculation of Timber Beams Subjected to Bending and Normal Force - H J Larsen
- 5-10-1 The Design of Timber Beams - H J Larsen
- 9-10-1 The Distribution of Shear Stresses in Timber Beams - F J Keenan
- 9-10-2 Beams Notched at the Ends - K Möhler
- 11-10-1 Tapered Timber Beams - H Riberholt
- 13-6-2 Consideration of Size Effects in Longitudinal Shear Strength for Uncracked Beams - R O Foschi and J D Barrett
- 13-6-3 Consideration of Shear Strength on End-Cracked Beams - J D Barrett and R O Foschi
- 18-10-1 Submission to the CIB-W18 Committee on the Design of Ply Web Beams by Consideration of the Type of Stress in the Flanges - J A Baird
- 18-10-2 Longitudinal Shear Design of Glued Laminated Beams - R O Foschi
- 19-10-1 Possible Code Approaches to Lateral Buckling in Beams - H J Burgess
- 19-2-1 Creep Buckling Strength of Timber Beams and Columns - R H Leicester
- 20-2-1 Lateral Buckling Theory for Rectangular Section Deep Beam-Columns - H J Burgess
- 20-10-1 Draft Clause for CIB Code for Beams with Initial Imperfections - H J Burgess
- 20-10-2 Space Joists in Irish Timber - W J Robinson
- 20-10-3 Composite Structure of Timber Joists and Concrete Slab - T Poutanen
- 21-10-1 A Study of Strength of Notched Beams - P J Gustafsson
- 22-10-1 Design of Endnotched Beams - H J Larsen and P J Gustafsson
- 22-10-2 Dimensions of Wooden Flexural Members under Constant Loads - A Pozgai
- 22-10-3 Thin-Walled Wood-Based Flanges in Composite Beams - J König
- 22-10-4 The Calculation of Wooden Bars with flexible Joints in Accordance with the Polish Standart Code and Strict Theoretical Methods - Z Mielczarek
- 23-10-1 Tension Perpendicular to the Grain at Notches and Joints - T A C M van der Put
- 23-10-2 Dimensioning of Beams with Cracks, Notches and Holes. An Application of Fracture Mechanics - K Riipola

- 23-10-3 Size Factors for the Bending and Tension Strength of Structural Timber - J D Barret and A R Fewell
- 23-12-1 Bending Strength of Glulam Beams, a Design Proposal - J Ehlbeck and F Colling
- 23-12-3 Glulam Beams, Bending Strength in Relation to the Bending Strength of the Finger Joints - H Riberholt
- 24-10-1 Shear Strength of Continuous Beams - R H Leicester and F G Young
- 25-10-1 The Strength of Norwegian Glued Laminated Beams - K Solli, E Aasheim and R H Falk
- 25-10-2 The Influence of the Elastic Modulus on the Simulated Bending Strength of Hyperstatic Timber Beams - T D G Canisius
- 27-10-1 Determination of Shear Modulus - R Görlacher and J Kürth
- 29-10-1 Time Dependent Lateral Buckling of Timber Beams - F Rouger
- 29-10-2 Determination of Modulus of Elasticity in Bending According to EN 408 - K H Solli
- 29-10-3 On Determination of Modulus of Elasticity in Bending - L Boström, S Ormarsson and O Dahlblom
- 29-10-4 Relation of Moduli of Elasticity in Flatwise and Edgewise Bending of Solid Timber - C J Johansson, A Steffen and E W Wormuth
- 30-10-1 Nondestructive Evaluation of Wood-based Members and Structures with the Help of Modal Analysis - P Kuklik
- 30-10-2 Measurement of Modulus of Elasticity in Bending - L Boström
- 30-10-3 A Weak Zone Model for Timber in Bending - B Källsner, K Salmela and O Ditlevsen
- 30-10-4 Load Carrying Capacity of Timber Beams with Narrow Moment Peaks - T Isaksson and J Freysoldt

ENVIRONMENTAL CONDITIONS

- 5-11-1 Climate Grading for the Code of Practice - B Norén
- 6-11-1 Climate Grading (2) - B Norén
- 9-11-1 Climate Classes for Timber Design - F J Keenan
- 19-11-1 Experimental Analysis on Ancient Downgraded Timber Structures - B Leggeri and L Paolini
- 19-6-5 Drying Stresses in Round Timber - A Ranta-Maunus
- 22-11-1 Corrosion and Adaptation Factors for Chemically Aggressive Media with Timber Structures - K Erler
- 29-11-1 Load Duration Effect on Structural Beams under Varying Climate Influence of Size and Shape - P Galimard and P Morlier
- 30-11-1 Probabilistic Design Models for the Durability of Timber Constructions - R H Leicester

LAMINATED MEMBERS

- 6-12-1 Directives for the Fabrication of Load-Bearing Structures of Glued Timber - A van der Velden and J Kuipers
- 8-12-1 Testing of Big Glulam Timber Beams - H Kolb and P Frech

- 8-12-2 Instruction for the Reinforcement of Apertures in Glulam Beams -
H Kolb and P Frech
- 8-12-3 Glulam Standard Part 1: Glued Timber Structures; Requirements for Timber
(Second Draft)
- 9-12-1 Experiments to Provide for Elevated Forces at the Supports of Wooden Beams
with Particular Regard to Shearing Stresses and Long-Term Loadings - F
Wassipaul and R Lackner
- 9-12-2 Two Laminated Timber Arch Railway Bridges Built in Perth in 1849 - L G Booth
- 9-6-4 Consideration of Combined Stresses for Lumber and Glued Laminated Timber -
K Möhler
- 11-6-3 Consideration of Combined Stresses for Lumber and Glued Laminated Timber
(addition to Paper CIB-W18/9-6-4) - K Möhler
- 12-12-1 Glulam Standard Part 2: Glued Timber Structures; Rating (3rd draft)
- 12-12-2 Glulam Standard Part 3: Glued Timber Structures; Performance (3 rd draft)
- 13-12-1 Glulam Standard Part 3: Glued Timber Structures; Performance (4th draft)
- 14-12-1 Proposals for CEI-Bois/CIB-W18 Glulam Standards - H J Larsen
- 14-12-2 Guidelines for the Manufacturing of Glued Load-Bearing Timber Structures -
Stevin Laboratory
- 14-12-3 Double Tapered Curved Glulam Beams - H Riberholt
- 14-12-4 Comment on CIB-W18/14-12-3 - E Gehri
- 18-12-1 Report on European Glulam Control and Production Standard - H Riberholt
- 18-10-2 Longitudinal Shear Design of Glued Laminated Beams - R O Foschi
- 19-12-1 Strength of Glued Laminated Timber - J Ehlbeck and F Colling
- 19-12-2 Strength Model for Glulam Columns - H J Blaß
- 19-12-3 Influence of Volume and Stress Distribution on the Shear Strength and Tensile
Strength Perpendicular to Grain - F Colling
- 19-12-4 Time-Dependent Behaviour of Glued-Laminated Beams - F Zaupa
- 21-12-1 Modulus of Rupture of Glulam Beam Composed of Arbitrary Laminae -
K Komatsu and N Kawamoto
- 21-12-2 An Appraisal of the Young's Modulus Values Specified for Glulam in
Eurocode 5- L R J Whale, B O Hilson and P D Rodd
- 21-12-3 The Strength of Glued Laminated Timber (Glulam): Influence of Lamination
Qualities and Strength of Finger Joints - J Ehlbeck and F Colling
- 21-12-4 Comparison of a Shear Strength Design Method in Eurocode 5 and a More
Traditional One - H Riberholt
- 22-12-1 The Dependence of the Bending Strength on the Glued Laminated Timber Girder
Depth - M Badstube, W Rug and W Schöne
- 22-12-2 Acid Deterioration of Glulam Beams in Buildings from the Early Half of the
1960s - Preliminary summary of the research project; Overhead pictures -
B A Hedlund
- 22-12-3 Experimental Investigation of normal Stress Distribution in Glue Laminated
Wooden Arches - Z Mielczarek and W Chanaj
- 22-12-4 Ultimate Strength of Wooden Beams with Tension Reinforcement as a Function
of Random Material Properties - R Candowicz and T Dziuba

- 23-12-1 Bending Strength of Glulam Beams, a Design Proposal - J Ehlbeck and F Colling
- 23-12-2 Probability Based Design Method for Glued Laminated Timber - M F Stone
- 23-12-3 Glulam Beams, Bending Strength in Relation to the Bending Strength of the Finger Joints - H Riberholt
- 23-12-4 Glued Laminated Timber - Strength Classes and Determination of Characteristic Properties - H Riberholt, J Ehlbeck and A Fewell
- 24-12-1 Contribution to the Determination of the Bending Strength of Glulam Beams - F Colling, J Ehlbeck and R Görlacher
- 24-12-2 Influence of Perpendicular-to-Grain Stressed Volume on the Load-Carrying Capacity of Curved and Tapered Glulam Beams - J Ehlbeck and J Kürth
- 25-12-1 Determination of Characteristic Bending Values of Glued Laminated Timber. EN-Approach and Reality - E Gehri
- 26-12-1 Norwegian Bending Tests with Glued Laminated Beams-Comparative Calculations with the "Karlsruhe Calculation Model" - E Aasheim, K Solli, F Colling, R H Falk, J Ehlbeck and R Görlacher
- 26-12-2 Simulation Analysis of Norwegian Spruce Glued-Laminated Timber - R Hernandez and R H Falk
- 26-12-3 Investigation of Laminating Effects in Glued-Laminated Timber - F Colling and R H Falk
- 26-12-4 Comparing Design Results for Glulam Beams According to Eurocode 5 and to the French Working Stress Design Code (CB71) - F Rouger
- 27-12-1 State of the Art Report: Glulam Timber Bridge Design in the U.S. - M A Ritter and T G Williamson
- 27-12-2 Common Design Practice for Timber Bridges in the United Kingdom - C J Mettem, J P Marcroft and G Davis
- 27-12-3 Influence of Weak Zones on Stress Distribution in Glulam Beams - E Serrano and H J Larsen
- 28-12-1 Determination of Characteristic Bending Strength of Glued Laminated Timber - E Gehri
- 28-12-2 Size Factor of Norwegian Glued Laminated Beams - E Aasheim and K H Solli
- 28-12-3 Design of Glulam Beams with Holes - K Riipola
- 28-12-4 Compression Resistance of Glued Laminated Timber Short Columns- U Korin
- 29-12-1 Development of Efficient Glued Laminated Timber - G Schickhofer
- 30-12-1 Experimental Investigation and Analysis of Reinforced Glulam Beams - K Oiger
- 31-12-1 Depth Factor for Glued Laminated Timber-Discussion of the Eurocode 5 Approach - B Källsner, O Carling and C J Johansson

PARTICLE AND FIBRE BUILDING BOARDS

- 7-13-1 Fibre Building Boards for CIB Timber Code (First Draft)- O Brynildsen
- 9-13-1 Determination of the Bearing Strength and the Load-Deformation Characteristics of Particleboard - K Möhler, T Budianto and J Ehlbeck
- 9-13-2 The Structural Use of Tempered Hardboard - W W L Chan
- 11-13-1 Tests on Laminated Beams from Hardboard under Short- and Longterm Load - W Nozynski

- 11-13-2 Determination of Deformation of Special Densified Hardboard under Long-term Load and Varying Temperature and Humidity Conditions - W Halfar
- 11-13-3 Determination of Deformation of Hardboard under Long-term Load in Changing Climate - W Halfar
- 14-4-1 An Introduction to Performance Standards for Wood-Base Panel Products - D H Brown
- 14-4-2 Proposal for Presenting Data on the Properties of Structural Panels - T Schmidt
- 16-13-1 Effect of Test Piece Size on Panel Bending Properties - P W Post
- 20-4-1 Considerations of Reliability - Based Design for Structural Composite Products - M R O'Halloran, J A Johnson, E G Elias and T P Cunningham
- 20-13-1 Classification Systems for Structural Wood-Based Sheet Materials - V C Kearley and A R Abbott
- 21-13-1 Design Values for Nailed Chipboard - Timber Joints - A R Abbott
- 25-13-1 Bending Strength and Stiffness of Izopanel Plates - Z Mielczarek
- 28-13-1 Background Information for "Design Rated Oriented Strand Board (OSB)" in CSA Standards - Summary of Short-term Test Results - E Karacabeyli, P Lau, C R Henderson, F V Meakes and W Deacon
- 28-13-2 Torsional Stiffness of Wood-Hardboard Composed I-Beam - P Olejniczak

TRUSSED RAFTERS

- 4-9-1 Long-term Loading of Trussed Rafters with Different Connection Systems - T Feldborg and M Johansen
- 6-9-3 Deflection of Trussed Rafters under Alternating Loading During a Year - T Feldborg and M Johansen
- 7-2-1 Lateral Bracing of Timber Struts - J A Simon
- 9-14-1 Timber Trusses - Code Related Problems - T F Williams
- 9-7-1 Design of Truss Plate Joints - F J Keenan
- 10-14-1 Design of Roof Bracing - The State of the Art in South Africa - P A V Bryant and J A Simon
- 11-14-1 Design of Metal Plate Connected Wood Trusses - A R Egerup
- 12-14-1 A Simple Design Method for Standard Trusses - A R Egerup
- 13-14-1 Truss Design Method for CIB Timber Code - A R Egerup
- 13-14-2 Trussed Rafters, Static Models - H Riberholt
- 13-14-3 Comparison of 3 Truss Models Designed by Different Assumptions for Slip and E-Modulus - K Möhler
- 14-14-1 Wood Trussed Rafter Design - T Feldborg and M Johansen
- 14-14-2 Truss-Plate Modelling in the Analysis of Trusses - R O Foschi
- 14-14-3 Cantilevered Timber Trusses - A R Egerup
- 14-7-5 The Effect of Support Eccentricity on the Design of W- and WW-Trusses with Nail Plate Connectors - B Källsner
- 15-14-1 Guidelines for Static Models of Trussed Rafters - H Riberholt
- 15-14-2 The Influence of Various Factors on the Accuracy of the Structural Analysis of Timber Roof Trusses - F R P Pienaar

- 15-14-3 Bracing Calculations for Trussed Rafter Roofs - H J Burgess
- 15-14-4 The Design of Continuous Members in Timber Trussed Rafters with Punched Metal Connector Plates - P O Reece
- 15-14-5 A Rafter Design Method Matching U.K. Test Results for Trussed Rafters - H J Burgess
- 16-14-1 Full-Scale Tests on Timber Fink Trusses Made from Irish Grown Sitka Spruce - V Picardo
- 17-14-1 Data from Full Scale Tests on Prefabricated Trussed Rafters - V Picardo
- 17-14-2 Simplified Static Analysis and Dimensioning of Trussed Rafters - H Riberholt
- 17-14-3 Simplified Calculation Method for W-Trusses - B Källsner
- 18-14-1 Simplified Calculation Method for W-Trusses (Part 2) - B Källsner
- 18-14-2 Model for Trussed Rafter Design - T Poutanen
- 19-14-1 Annex on Simplified Design of W-Trusses - H J Larsen
- 19-14-2 Simplified Static Analysis and Dimensioning of Trussed Rafters - Part 2 - H Riberholt
- 19-14-3 Joint Eccentricity in Trussed Rafters - T Poutanen
- 20-14-1 Some Notes about Testing Nail Plates Subjected to Moment Load - T Poutanen
- 20-14-2 Moment Distribution in Trussed Rafters - T Poutanen
- 20-14-3 Practical Design Methods for Trussed Rafters - A R Egerup
- 22-14-1 Guidelines for Design of Timber Trussed Rafters - H Riberholt
- 23-14-1 Analyses of Timber Trussed Rafters of the W-Type - H Riberholt
- 23-14-2 Proposal for Eurocode 5 Text on Timber Trussed Rafters - H Riberholt
- 24-14-1 Capacity of Support Areas Reinforced with Nail Plates in Trussed Rafters - A Kevarinmäki
- 25-14-1 Moment Anchorage Capacity of Nail Plates in Shear Tests - A Kevarinmaki and J. Kangas
- 25-14-2 Design Values of Anchorage Strength of Nail Plate Joints by 2-curve Method and Interpolation - J Kangas and A Kevarinmaki
- 26-14-1 Test of Nail Plates Subjected to Moment - E Aasheim
- 26-14-2 Moment Anchorage Capacity of Nail Plates - A Kevarinmäki and J Kangas
- 26-14-3 Rotational Stiffness of Nail Plates in Moment Anchorage - A Kevarinmäki and J Kangas
- 26-14-4 Solution of Plastic Moment Anchorage Stress in Nail Plates - A Kevarinmäki
- 26-14-5 Testing of Metal-Plate-Connected Wood-Truss Joints - R Gupta
- 26-14-6 Simulated Accidental Events on a Trussed Rafter Roofed Building - C J Mettem and J P Marcroft
- 30-14-1 The Stability Behaviour of Timber Trussed Rafter Roofs - Studies Based on Eurocode 5 and Full Scale Testing - R J Bainbridge, C J Mettem, A Reffold and T Studer

STRUCTURAL STABILITY

- 8-15-1 Laterally Loaded Timber Columns: Tests and Theory - H J Larsen
- 13-15-1 Timber and Wood-Based Products Structures. Panels for Roof Coverings. Methods of Testing and Strength Assessment Criteria. Polish Standard BN-78/7159-03
- 16-15-1 Determination of Bracing Structures for Compression Members and Beams - H Brüninghoff
- 17-15-1 Proposal for Chapter 7.4 Bracing - H Brüninghoff
- 17-15-2 Seismic Design of Small Wood Framed Houses - K F Hansen
- 18-15-1 Full-Scale Structures in Glued Laminated Timber, Dynamic Tests: Theoretical and Experimental Studies - A Ceccotti and A Vignoli
- 18-15-2 Stabilizing Bracings - H Brüninghoff
- 19-15-1 Connections Deformability in Timber Structures: a Theoretical Evaluation of its Influence on Seismic Effects - A Ceccotti and A Vignoli
- 19-15-2 The Bracing of Trussed Beams - M H Kessel and J Natterer
- 19-15-3 Racking Resistance of Wooden Frame Walls with Various Openings - M Yasumura
- 19-15-4 Some Experiences of Restoration of Timber Structures for Country Buildings - G Cardinale and P Spinelli
- 19-15-5 Non-Destructive Vibration Tests on Existing Wooden Dwellings - Y Hirashima
- 20-15-1 Behaviour Factor of Timber Structures in Seismic Zones. - A Ceccotti and A Vignoli
- 21-15-1 Rectangular Section Deep Beam - Columns with Continuous Lateral Restraint - H J Burgess
- 21-15-2 Buckling Modes and Permissible Axial Loads for Continuously Braced Columns- H J Burgess
- 21-15-3 Simple Approaches for Column Bracing Calculations - H J Burgess
- 21-15-4 Calculations for Discrete Column Restraints - H J Burgess
- 21-15-5 Behaviour Factor of Timber Structures in Seismic Zones (Part Two) - A Ceccotti and A Vignoli
- 22-15-1 Suggested Changes in Code Bracing Recommendations for Beams and Columns - H J Burgess
- 22-15-2 Research and Development of Timber Frame Structures for Agriculture in Poland- S Kus and J Kerste
- 22-15-3 Ensuring of Three-Dimensional Stiffness of Buildings with Wood Structures - A K Shenghelia
- 22-15-5 Seismic Behavior of Arched Frames in Timber Construction - M Yasumura
- 22-15-6 The Robustness of Timber Structures - C J Mettem and J P Marcroft
- 22-15-7 Influence of Geometrical and Structural Imperfections on the Limit Load of Wood Columns - P Dutko
- 23-15-1 Calculation of a Wind Girder Loaded also by Discretely Spaced Braces for Roof Members - H J Burgess
- 23-15-2 Stability Design and Code Rules for Straight Timber Beams - T A C M van der Put

- 23-15-3 A Brief Description of Formula of Beam-Columns in China Code - S Y Huang
- 23-15-4 Seismic Behavior of Braced Frames in Timber Construction - M Yasumura
- 23-15-5 On a Better Evaluation of the Seismic Behavior Factor of Low-Dissipative Timber Structures - A Ceccotti and A Vignoli
- 23-15-6 Disproportionate Collapse of Timber Structures - C J Mettem and J P Marcroft
- 23-15-7 Performance of Timber Frame Structures During the Loma Prieta California Earthquake - M R O'Halloran and E G Elias
- 24-15-2 Discussion About the Description of Timber Beam-Column Formula - S Y Huang
- 24-15-3 Seismic Behavior of Wood-Framed Shear Walls - M Yasumura
- 25-15-1 Structural Assessment of Timber Framed Building Systems - U Korin
- 25-15-3 Mechanical Properties of Wood-framed Shear Walls Subjected to Reversed Cyclic Lateral Loading - M Yasumura
- 26-15-1 Bracing Requirements to Prevent Lateral Buckling in Trussed Rafters - C J Mettem and P J Moss
- 26-15-2 Eurocode 8 - Part 1.3 - Chapter 5 - Specific Rules for Timber Buildings in Seismic Regions - K Becker, A Ceccotti, H Charlier, E Katsaragakis, H J Larsen and H Zeitter
- 26-15-3 Hurricane Andrew - Structural Performance of Buildings in South Florida - M R O'Halloran, E L Keith, J D Rose and T P Cunningham
- 29-15-1 Lateral Resistance of Wood Based Shear Walls with Oversized Sheathing Panels - F Lam, H G L Prion and M He
- 29-15-2 Damage of Wooden Buildings Caused by the 1995 Hyogo-Ken Nanbu Earthquake - M Yasumura, N Kawai, N Yamaguchi and S Nakajima
- 29-15-3 The Racking Resistance of Timber Frame Walls: Design by Test and Calculation - D R Griffiths, C J Mettem, V Enjily, P J Steer
- 29-15-4 Current Developments in Medium-Rise Timber Frame Buildings in the UK - C J Mettem, G C Pitts, P J Steer, V Enjily
- 29-15-5 Natural Frequency Prediction for Timber Floors - R J Bainbridge, and C J Mettem
- 30-15-1 Cyclic Performance of Perforated Wood Shear Walls with Oversize Oriented Strand Board Panels - Ming He, H Magnusson, F Lam, and H G L Prion
- 30-15-2 A Numerical Analysis of Shear Walls Structural Performances - L Davenne, L Daudeville, N Kawai and M Yasumura
- 30-15-3 Seismic Force Modification Factors for the Design of Multi-Storey Wood-Frame Platform Construction - E Karacabeyli and A Ceccotti
- 30-15-4 Evaluation of Wood Framed Shear Walls Subjected to Lateral Load - M Yasumura and N Kawai
- 31-15-1 Seismic Performance Testing On Wood-Framed Shear Wall - N Kawai
- 31-15-2 Robustness Principles in the Design of Medium-Rise Timber-Framed Buildings - C J Mettem, M W Milner, R J Bainbridge and V. Enjily
- 31-15-3 Numerical Simulation of Pseudo-Dynamic Tests Performed to Shear Walls - L Daudeville, L Davenne, N Richard, N Kawai and M Yasumura
- 31-15-4 Force Modification Factors for Braced Timber Frames - H G L Prion, M Popovski and E Karacabeyli

FIRE

- 12-16-1 British Standard BS 5268 the Structural Use of Timber: Part 4 Fire Resistance of Timber Structures
- 13-100-2 CIB Structural Timber Design Code. Chapter 9. Performance in Fire
- 19-16-1 Simulation of Fire in Tests of Axially Loaded Wood Wall Studs - J König
- 24-16-1 Modelling the Effective Cross Section of Timber Frame Members Exposed to Fire - J König
- 25-16-1 The Effect of Density on Charring and Loss of Bending Strength in Fire - J König
- 25-16-2 Tests on Glued-Laminated Beams in Bending Exposed to Natural Fires - F Bolonius Olesen and J König
- 26-16-1 Structural Fire Design According to Eurocode 5, Part 1.2 - J König
- 31-16-1 Revision of ENV 1995-1-2: Charring and Degradation of Strength and Stiffness - J König

STATISTICS AND DATA ANALYSIS

- 13-17-1 On Testing Whether a Prescribed Exclusion Limit is Attained - W G Warren
- 16-17-1 Notes on Sampling and Strength Prediction of Stress Graded Structural Timber - P Glos
- 16-17-2 Sampling to Predict by Testing the Capacity of Joints, Components and Structures - B Norén
- 16-17-3 Discussion of Sampling and Analysis Procedures - P W Post
- 17-17-1 Sampling of Wood for Joint Tests on the Basis of Density - I Smith, L R J Whale
- 17-17-2 Sampling Strategy for Physical and Mechanical Properties of Irish Grown Sitka Spruce - V Picardo
- 18-17-1 Sampling of Timber in Structural Sizes - P Glos
- 18-6-3 Notes on Sampling Factors for Characteristic Values - R H Leicester
- 19-17-1 Load Factors for Proof and Prototype Testing - R H Leicester
- 19-6-2 Confidence in Estimates of Characteristic Values - R H Leicester
- 21-6-1 Draft Australian Standard: Methods for Evaluation of Strength and Stiffness of Graded Timber - R H Leicester
- 21-6-2 The Determination of Characteristic Strength Values for Stress Grades of Structural Timber. Part 1 - A R Fewell and P Glos
- 22-17-1 Comment on the Strength Classes in Eurocode 5 by an Analysis of a Stochastic Model of Grading - A proposal for a supplement of the design concept - M Kiesel
- 24-17-1 Use of Small Samples for In-Service Strength Measurement - R H Leicester and F G Young
- 24-17-2 Equivalence of Characteristic Values - R H Leicester and F G Young
- 24-17-3 Effect of Sampling Size on Accuracy of Characteristic Values of Machine Grades - Y H Chui, R Turner and I Smith
- 24-17-4 Harmonisation of LSD Codes - R H Leicester
- 25-17-2 A Body for Confirming the Declaration of Characteristic Values - J Sunley
- 25-17-3 Moisture Content Adjustment Procedures for Engineering Standards - D W Green and J W Evans

- 27-17-1 Statistical Control of Timber Strength - R H Leicester and H O Breitingger
 30-17-1 A New Statistical Method for the Establishment of Machine Settings - F Rouger

GLUED JOINTS

- 20-18-1 Wood Materials under Combined Mechanical and Hygral Loading - A Martensson and S Thelandersson
 20-18-2 Analysis of Generalized Volkersen - Joints in Terms of Linear Fracture Mechanics - P J Gustafsson
 20-18-3 The Complete Stress-Slip Curve of Wood-Adhesives in Pure Shear - H Wernersson and P J Gustafsson
 22-18-1 Perspective Adhesives and Protective Coatings for Wood Structures - A S Freidin

FRACTURE MECHANICS

- 21-10-1 A Study of Strength of Notched Beams - P J Gustafsson
 22-10-1 Design of Endnotched Beams - H J Larsen and P J Gustafsson
 23-10-1 Tension Perpendicular to the Grain at Notches and Joints - T A C M van der Put
 23-10-2 Dimensioning of Beams with Cracks, Notches and Holes. An Application of Fracture Mechanics - K Riipola
 23-19-1 Determination of the Fracture Energie of Wood for Tension Perpendicular to the Grain - W Rug, M Badstube and W Schöne
 23-19-2 The Fracture Energy of Wood in Tension Perpendicular to the Grain. Results from a Joint Testing Project - H J Larsen and P J Gustafsson
 23-19-3 Application of Fracture Mechanics to Timber Structures - A Ranta-Maunus
 24-19-1 The Fracture Energy of Wood in Tension Perpendicular to the Grain - H J Larsen and P J Gustafsson
 28-19-1 Fracture of Wood in Tension Perpendicular to the Grain: Experiment and Numerical Simulation by Damage Mechanics - L Daudeville, M Yasumura and J D Lanvin
 28-19-2 A New Method of Determining Fracture Energy in Forward Shear along the Grain - H D Mansfield-Williams
 28-19-3 Fracture Design Analysis of Wooden Beams with Holes and Notches. Finite Element Analysis based on Energy Release Rate Approach - H Petersson
 28-19-4 Design of Timber Beams with Holes by Means of Fracture Mechanics - S Aicher, J Schmidt and S Brunold
 30-19-1 Failure Analysis of Single-Bolt Joints - L Daudeville, L Davenne and M Yasumura

SERVICEABILITY

- 27-20-1 Codification of Serviceability Criteria - R H Leicester
 27-20-2 On the Experimental Determination of Factor k_{def} and Slip Modulus k_{ser} from Short- and Long-Term Tests on a Timber-Concrete Composite (TCC) Beam - S Capretti and A Ceccotti
 27-20-3 Serviceability Limit States: A Proposal for Updating Eurocode 5 with Respect to Eurocode 1 - P Racher and F Rouger

- 27-20-4 Creep Behavior of Timber under External Conditions - C Le Govic, F Rouger, T Toratti and P Morlier
- 30-20-1 Design Principles for Timber in Compression Perpendicular to Grain - S Thelandersson and A Mårtensson
- 30-20-2 Serviceability Performance of Timber Floors - Eurocode 5 and Full Scale Testing - R J Bainbridge and C J Mettem

TEST METHODS

- 31-21-1 Development of an Optimised Test Configuration to Determine Shear Strength of Glued Laminated Timber - G Schickhofer and B Obermayr
- 31-21-2 An Impact Strength Test Method for Structural Timber. The Theory and a Preliminary Study - T D G Canisius

CIB TIMBER CODE

- 2-100-1 A Framework for the Production of an International Code of Practice for the Structural Use of Timber - W T Curry
- 5-100-1 Design of Solid Timber Columns (First Draft) - H J Larsen
- 5-100-2 A Draft Outline of a Code for Timber Structures - L G Booth
- 6-100-1 Comments on Document 5-100-1; Design of Solid Timber Columns - H J Larsen and E Theilgaard
- 6-100-2 CIB Timber Code: CIB Timber Standards - H J Larsen and E Theilgaard
- 7-100-1 CIB Timber Code Chapter 5.3 Mechanical Fasteners; CIB Timber Standard 06 and 07 - H J Larsen
- 8-100-1 CIB Timber Code - List of Contents (Second Draft) - H J Larsen
- 9-100-1 The CIB Timber Code (Second Draft)
- 11-100-1 CIB Structural Timber Design Code (Third Draft)
- 11-100-2 Comments Received on the CIB Code
 a U Saarelainen
 b Y M Ivanov
 c R H Leicester
 d W Nozynski
 e W R A Meyer
 f P Beckmann; R Marsh
 g W R A Meyer
 h W R A Meyer
- 11-100-3 CIB Structural Timber Design Code; Chapter 3 - H J Larsen
- 12-100-1 Comment on the CIB Code - Sous-Commission Glulam
- 12-100-2 Comment on the CIB Code - R H Leicester
- 12-100-3 CIB Structural Timber Design Code (Fourth Draft)
- 13-100-1 Agreed Changes to CIB Structural Timber Design Code
- 13-100-2 CIB Structural Timber Design Code. Chapter 9: Performance in Fire
- 13-100-3a Comments on CIB Structural Timber Design Code
- 13-100-3b Comments on CIB Structural Timber Design Code - W R A Meyer
- 13-100-3c Comments on CIB Structural Timber Design Code - British Standards Institution

- 13-100-4 CIB Structural Timber Design Code. Proposal for Section 6.1.5 Nail Plates - N I Bovim
- 14-103-2 Comments on the CIB Structural Timber Design Code - R H Leicester
- 15-103-1 Resolutions of TC 165-meeting in Athens 1981-10-12/13
- 21-100-1 CIB Structural Timber Design Code. Proposed Changes of Sections on Lateral Instability, Columns and Nails - H J Larsen
- 22-100-1 Proposal for Including an Updated Design Method for Bearing Stresses in CIB W18 - Structural Timber Design Code - B Madsen
- 22-100-2 Proposal for Including Size Effects in CIB W18A Timber Design Code - B Madsen
- 22-100-3 CIB Structural Timber Design Code - Proposed Changes of Section on Thin-Flanged Beams - J König
- 22-100-4 Modification Factor for "Aggressive Media" - a Proposal for a Supplement to the CIB Model Code - K Erler and W Rug
- 22-100-5 Timber Design Code in Czechoslovakia and Comparison with CIB Model Code - P Dutko and B Kozelouh

LOADING CODES

- 4-101-1 Loading Regulations - Nordic Committee for Building Regulations
- 4-101-2 Comments on the Loading Regulations - Nordic Committee for Building Regulations

STRUCTURAL DESIGN CODES

- 1-102-1 Survey of Status of Building Codes, Specifications etc., in USA - E G Stern
- 1-102-2 Australian Codes for Use of Timber in Structures - R H Leicester
- 1-102-3 Contemporary Concepts for Structural Timber Codes - R H Leicester
- 1-102-4 Revision of CP 112 - First Draft, July 1972 - British Standards Institution
- 4-102-1 Comparison of Codes and Safety Requirements for Timber Structures in EEC Countries - Timber Research and Development Association
- 4-102-2 Nordic Proposals for Safety Code for Structures and Loading Code for Design of Structures - O A Brynildsen
- 4-102-3 Proposal for Safety Codes for Load-Carrying Structures - Nordic Committee for Building Regulations
- 4-102-4 Comments to Proposal for Safety Codes for Load-Carrying Structures - Nordic Committee for Building Regulations
- 4-102-5 Extract from Norwegian Standard NS 3470 "Timber Structures"
- 4-102-6 Draft for Revision of CP 112 "The Structural Use of Timber" - W T Curry
- 8-102-1 Polish Standard PN-73/B-03150: Timber Structures; Statistical Calculations and Designing
- 8-102-2 The Russian Timber Code: Summary of Contents
- 9-102-1 Svensk Byggnorm 1975 (2nd Edition); Chapter 27: Timber Construction
- 11-102-1 Eurocodes - H J Larsen

- 13-102-1 Program of Standardisation Work Involving Timber Structures and Wood-Based Products in Poland
- 17-102-1 Safety Principles - H J Larsen and H Riberholt
- 17-102-2 Partial Coefficients Limit States Design Codes for Structural Timberwork - I Smith
- 18-102-1 Antiseismic Rules for Timber Structures: an Italian Proposal - G Augusti and A Ceccotti
- 18-1-2 Eurocode 5, Timber Structures - H J Larsen
- 19-102-1 Eurocode 5 - Requirements to Timber - Drafting Panel Eurocode 5
- 19-102-2 Eurocode 5 and CIB Structural Timber Design Code - H J Larsen
- 19-102-3 Comments on the Format of Eurocode 5 - A R Fewell
- 19-102-4 New Developments of Limit States Design for the New GDR Timber Design Code - W Rug and M Badstube
- 19-7-3 Effectiveness of Multiple Fastener Joints According to National Codes and Eurocode 5 (Draft) - G Steck
- 19-7-6 The Derivation of Design Clauses for Nailed and Bolted Joints in Eurocode5 - L R J Whale and I Smith
- 19-14-1 Annex on Simplified Design of W-Trusses - H J Larsen
- 20-102-1 Development of a GDR Limit States Design Code for Timber Structures - W Rug and M Badstube
- 21-102-1 Research Activities Towards a New GDR Timber Design Code Based on Limit States Design - W Rug and M Badstube
- 22-102-1 New GDR Timber Design Code, State and Development - W Rug, M Badstube and W Kofent
- 22-102-2 Timber Strength Parameters for the New USSR Design Code and its Comparison with International Code - Y Y Slavik, N D Denesh and E B Ryumina
- 22-102-3 Norwegian Timber Design Code - Extract from a New Version - E Aasheim and K H Solli
- 23-7-1 Proposal for a Design Code for Nail Plates - E Aasheim and K H Solli
- 24-102-2 Timber Footbridges: A Comparison Between Static and Dynamic Design Criteria - A Ceccotti and N de Robertis
- 25-102-1 Latest Development of Eurocode 5 - H J Larsen
- 25-102-1A Annex to Paper CIB-W18/25-102-1. Eurocode 5 - Design of Notched Beams - H J Larsen, H Riberholt and P J Gustafsson
- 25-102-2 Control of Deflections in Timber Structures with Reference to Eurocode 5 - A Martensson and S Thelandersson
- 28-102-1 Eurocode 5 - Design of Timber Structures - Part 2: Bridges - D Bajolet, E Gehri, J König, H Kreuzinger, H J Larsen, R Mäkipuro and C Mettem
- 28-102-2 Racking Strength of Wall Diaphragms - Discussion of the Eurocode 5 Approach - B Källsner
- 29-102-1 Model Code for the Probabilistic Design of Timber Structures - H J Larsen, T Isaksson and S Thelandersson
- 30-102-1 Concepts for Drafting International Codes and Standards for Timber Constructions - R H Leicester

INTERNATIONAL STANDARDS ORGANISATION

- 3-103-1 Method for the Preparation of Standards Concerning the Safety of Structures (ISO/DIS 3250) - International Standards Organisation ISO/TC98
- 4-103-1 A Proposal for Undertaking the Preparation of an International Standard on Timber Structures - International Standards Organisation
- 5-103-1 Comments on the Report of the Consultation with Member Bodies Concerning ISO/TC/P129 - Timber Structures - Dansk Ingeniorforening
- 7-103-1 ISO Technical Committees and Membership of ISO/TC 165
- 8-103-1 Draft Resolutions of ISO/TC 165
- 12-103-1 ISO/TC 165 Ottawa, September 1979
- 13-103-1 Report from ISO/TC 165 - A Sorensen
- 14-103-1 Comments on ISO/TC 165 N52 "Timber Structures; Solid Timber in Structural Sizes; Determination of Some Physical and Mechanical Properties"
- 14-103-2 Comments on the CIB Structural Timber Design Code - R H Leicester
- 21-103-1 Concept of a Complete Set of Standards - R H Leicester

JOINT COMMITTEE ON STRUCTURAL SAFETY

- 3-104-1 International System on Unified Standard Codes of Practice for Structures - Comité Européen du Béton (CEB)
- 7-104-1 Volume 1: Common Unified Rules for Different Types of Construction and Material - CEB

CIB PROGRAMME, POLICY AND MEETINGS

- 1-105-1 A Note on International Organisations Active in the Field of Utilisation of Timber - P Sonnemans
- 5-105-1 The Work and Objectives of CIB-W18-Timber Structures - J G Sunley
- 10-105-1 The Work of CIB-W18 Timber Structures - J G Sunley
- 15-105-1 Terms of Reference for Timber - Framed Housing Sub-Group of CIB-W18
- 19-105-1 Tropical and Hardwood Timbers Structures - R H Leicester
- 21-105-1 First Conference of CIB-W18B, Tropical and Hardwood Timber Structures Singapore, 26 - 28 October 1987 - R H Leicester

INTERNATIONAL UNION OF FORESTRY RESEARCH ORGANISATIONS

- 7-106-1 Time and Moisture Effects - CIB W18/IUFRO 55.02-03 Working Party

CIB-W18/31-1-1

**INTERNATIONAL COUNCIL FOR BUILDING RESEARCH STUDIES AND DOCUMENTATION
WORKING COMMISSION W18 - TIMBER STRUCTURES**

A LIMIT STATES DESIGN APPROACH TO TIMBER FRAMED WALLS

by

C J Mettem
R J Bainbridge
J A Gordon

TRADA Technology

UNITED KINGDOM

MEETING THIRTY-ONE

SAVONLINNA

FINLAND

AUGUST 1998

A Limit States Design Approach To Timber Framed Walls

By: C J Mettem, R J Bainbridge, J A Gordon, TRADA Technology, UK

Abstract

Lightweight platform framed walls have become established on the basis of quasi-empirical design methods, allowing interpolation, but not extrapolation. Both medium-rise building aims, & desired wall construction improvements, place limitations on furthering this approach.

This paper describes investigations carried out under a research & development project, the principal purpose of which is to produce an efficient limit-states design method for timber frame walls that is compatible with EC 5 Part 1-1 [1] & suitable for both low-rise & medium-rise buildings

DEFINITION OF SYMBOLS

ψ	=	Psi factors for serviceability actions
γ_G	=	Permanent action partial factor
γ_M	=	Material safety factor
γ_Q	=	Variable action partial factor
F_{max}	=	Maximum racking test load (kN)
FOS	=	Factor of safety (BS 5268)
h	=	Height of wall (m)
H_{wp}	=	Height of wall panel (mm)
$K_{###}$	=	Modification factors, drawn from BS 5268: Part 6
K_m	=	Material modification factors (BS 5268)
k_{mod}	=	Duration of load modification factor from EC5
K_w	=	Wall configuration modification factors (BS 5268)
L	=	Length of wall (m)
R	=	Racking stiffness (kN/mm)
R_1	=	Test racking stiffness load (kN/mm)
R_b	=	Basic racking resistance (kN/m)
R_d	=	Design racking resistance (kN)

1. INTRODUCTION

The subject of the behaviour of timber framed wall panels is not as simple as might at first be imagined, & has a long history of research & development [2]. Although most research has led to valuable information regarding the general behaviour, there is a certain degree of conflict, particularly in relation to test methods. This results in apparent discrepancies in racking capacity when designing to different design codes.

The subject is addressed in Section 5.4.3 of EC5, but this currently provides only one design principle, accompanied by a number of application rules based on a cantilever model. This constitutes only a very minor section of EC5 & is massively disproportionate to the parallel guidance provided in the current UK national code, whereby an entire section of BS 5268 is devoted to the design of domestic type timber frame walls [3], & a companion section to address non-domestic design, testing, fabrication & erection is under development. Whilst it is recognised that EC5 draws upon other supporting standards in some of these respects, there currently remains an area of strong divergence from the main body of EC5 in the UK NAD.

The continued adoption of the construction methods currently employed in the UK for timber frame walls is supported by their long established history of use, which has led to commercial confidence in the timber frame product. The BS 5268 method is in compliance with EC5 Cl 5.4.3 P(1) & there is no reason why the racking resistance assessment procedure in BS 5268: Part 6.1 cannot form a foundation for conversion to limit states, hence enabling full compatibility within the broader scope of the structural Eurocodes. Conversion however is not a straightforward exercise, the largest hurdle being the need to separate ultimate strength considerations from serviceability conditions.

The work reported herein is therefore composed of two key aspects:

- a) The development of a limit states based method in the spirit of existing BS 5268 practice
- b) Experimental work, focused upon serviceability limit states aspects & gauging the influence of boundary test conditions upon the behaviour pattern of simple wall panels of modern constructional form, thus providing pointers towards translation of component to system behaviour.

2. DEVELOPMENT OF A LIMIT STATES DESIGN METHOD

2.1 Summary of the BS 5268: 6.1 Method

A simplified overview of the permissible stress wall design method contained in BS 5268: Part 6 is presented in Figure 1.

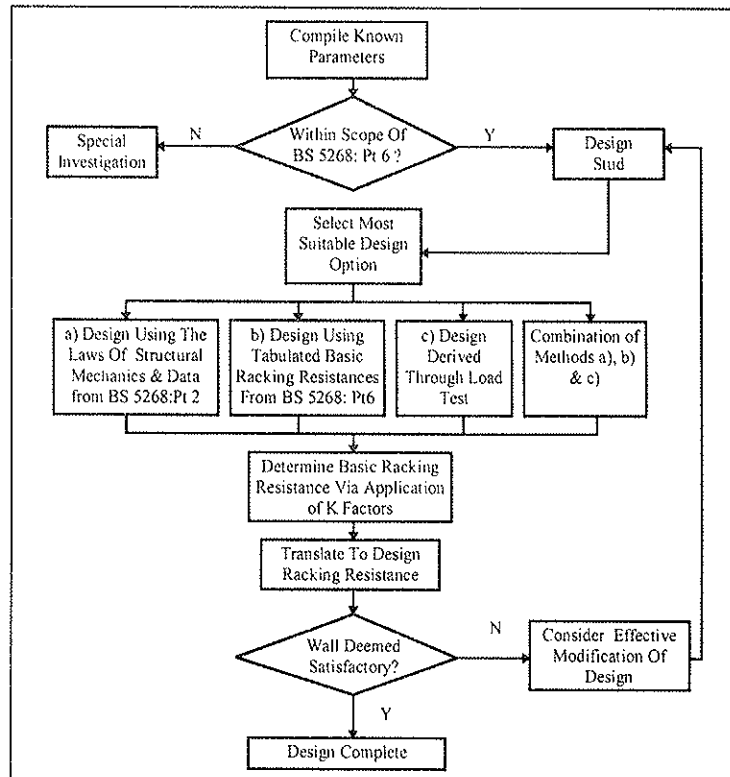


Figure 1 Overview of BS 5268 Wall Design Methodology

The method focuses on two principal functions of the wall:

- Resistance of vertical load, addressed through design of studs;
- Resistance of horizontal load, through determination of basic racking resistance, which is then translated to a design value by application of a range of modification factors. These 'K' factors address nail diameter, nail spacing, board thickness, wall height, wall length, vertical load, framed openings & interaction with the other elements of the structure.

The method is the result of continual development since the 1960's, with the latest version having been published in 1996. A recent development, proposed since publication of the latest revision, concerns a 'Shape Factor' which has been suggested to replace the Height & Length factors in BS 5268, the Shape Factor being defined thus [4]:

- $K_{shape} = L/h$ for wall length from 0 to h metres
- $K_{shape} = (L/h)^{0.4}$ for wall length from h to 2h metres
- $K_{shape} = 1.32$ for wall length equal to or greater than 2h metres

Application of such a factor would be equally justified in the Limit States Based derivation of design strength.

2.2 Overview of The EC5 Method For Wall Design

An overview of the current EC5 design method is presented in Figure 2. It is clear that the dominant consideration in this method is satisfaction of ULS criteria. The current UK NAD to EC5 states that :

"The design method for timber frame walls given in EC5: Part 1.1 lacks sufficient information with regard to the determination of racking resistance (F_R) from the test method. This NAD will be revised in due course to give the required additional information. Until that revision is published, timber frame wall panels should be designed & tested to BS 5268: Section 6.1."

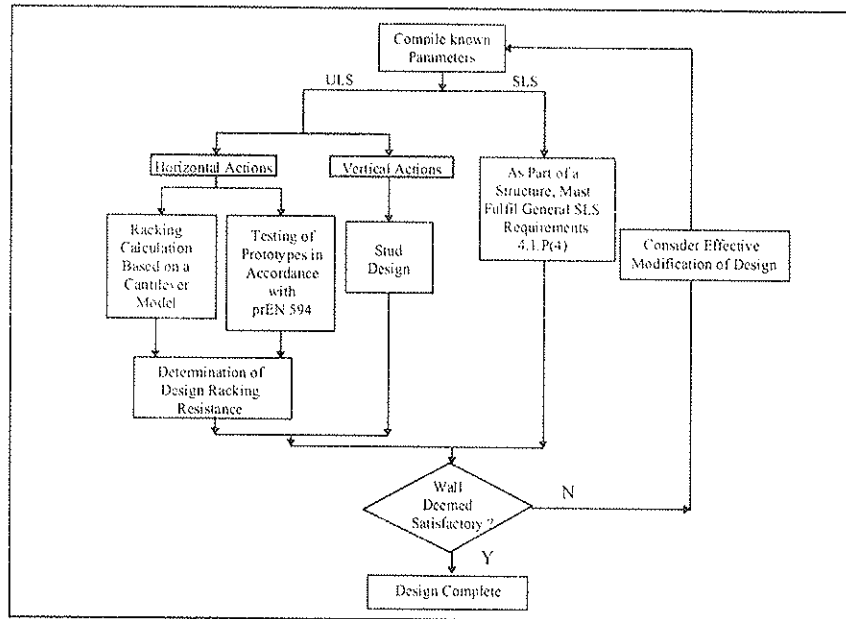


Figure 2 Overview of EC5 Wall Design Methodology

In BS 5268: Part 6.1: Section 5 the load-carrying capacity of a panel is determined by tests which measure both strength & stiffness, & in practice the test racking stiffness load (the mean load at which the racking deflection equals 0.003 x the panel height) usually determines the load-carrying capacity.

Therefore, a suitable design methodology should address at least two design principles: one concerning strength, & the other concerning stiffness, equivalent to Clause 4.1 (P) but specific to wall panels. These would be supported by a set of application rules to facilitate limit states based wall design.

At an early stage of this research it was identified that there are a number of possible mechanisms to achievement of the research objective. Of these, three principal options were considered:

- 1) suitable modification of the set of rules in the existing text in EC5;
- 2) an alternative design basis derived from the laws of structural mechanics for use in conjunction with the principles of EC5;
- 3) a limit-states methodology in the spirit of BS 5268: Part 6 & compatible with EC5.

The developments towards a limit states wall racking method have been based upon the latter, with a view to development of a basis suitable for adoption in the UK NAD as an alternative to that currently recommended in EC5.

2.3 Conversion Of BS 5268 Racking Design To Limit States Logic

Conversion to a basis fully compatible with Eurocodes requires the fundamental differentiation between ultimate limit states (ULS) & serviceability limit states (SLS) behaviour. Re-assessment of K factors & identification of load combination factors are primary requirements.

2.3.1 Modification Factors (K Factors)

A summary of the conclusions from a review of previous research concerning K factors, assessing the feasibility of identifying separate values for individual limit states, is presented in Table 1.

Since it is apparent that work beyond the intended scope of the project would be required to develop separate K factors, relating to material & connection performance, the factors from BS 5268 have been adapted for the purposes of present development. It is also likely that the scope for limit states differentiation of the K factors may need to be revised at a latter stage, since such development may necessitate incorporation of factors modified to accommodate the interaction of parameters. For example, the interaction of nail diameter, nail spacing and board thickness across the limit states may respond to different models depending upon the specific configuration, thus resulting in definition of separate factors either in addition to those presented or as a replacement, as has already been suggested in the case of K_{shape} .

K Factor	Separate ULS & SLS Values	Comment
K ₁₀₁ nail diameter	Yes	More test data will be required to finalise.
K ₁₀₂ nail spacing	Possibly	More test data required to confirm separation of ULS & SLS.
K ₁₀₃ board thickness	Unlikely	
K ₁₀₄ wall height	Unclear	Basis for current factor unclear. Future preference may be to combine K ₁₀₄ & K ₁₀₅ into a shape factor. Further work will be required to resolve this.
K ₁₀₅ wall length K ₁₀₇ wall vertical load	Yes	These values are related. More panel failure test data required to complete ULS/SLS separation.
K ₁₀₆ openings	Possibly	More panel failure test data required to confirm whether separating ULS & SLS is feasible.
K ₁₀₈ Interaction	Unclear	Whilst it is recognised that the effect of interaction is real, actual qualification let alone subdivision in respect of limit states remains un-answered, although current research may provide information that can be considered at a latter date.

Table 1 K Factor Summary

2.3.2 Load Combinations

For the majority of situations the only load combination of importance will consist of the wind action, self weight & the roof & floor loads.

Since vertical load up to a certain level enhances the panel performance, EC5 requires it to be considered as a favourable load. EC1 [5] therefore gives partial load factors for application in ultimate limit states, as described in Table 2.

Case	Equivalent Wall Failure	Action	Symbol	Persistent/ Transient Situations
A	sliding or overturning	Permanent, favourable	γ_{Ginf}	0.90
		Variable, unfavourable	γ_Q	1.50
B	failure of materials	Permanent, favourable	γ_{Ginf}	1.00
		Variable, unfavourable	γ_Q	1.50

Table 2 ULS Partial Factors For Application in Wall Racking [EC1: Part 1, Table 9.2]

Should the vertical loads to which the wall is subjected become too high, then there is a theoretical risk of reduction of racking resistance. If the vertical loads are deemed by the designer to pose a risk of reducing the panel racking capacity, then the unfavourable permanent load partial factor of 1.35 may be used to make appropriate checks.

An aspect also taken into account locally, for the present, is that the UK NAD to EC5 directs that "the wind loading should be taken as 90% of the value obtained from CP3: Chapter V: Part 2." hence producing a reduced total factor of safety. The UK is in a transient situation at the moment with regard to this issue, since this wind load code has been superseded by BS 6399: Part 2 yet is still likely to be employed by a sizeable proportion of designers for some time to come. There are many issues in relation to BS 6399: Part 2 that have not been fully resolved, but it is understood that such a reduction may not be justified for calculation under the 'new' code.

2.4 Ultimate Limit States Basis

Ultimate Limit State assessment relates directly to the existing BS 5268 strength requirements for wall panels, which directs that wall studs be designed as compression members & that racking resistance be determined.

The ULS aspects of performance addressed in the studies described herein focus upon by quantification of 'Racking Resistance'. In BS 5268, the strength based aspects are defined by way of the basic racking resistance which is either obtained from tabulated data or from test data, to which modification factors (K₁₀₁₋₁₀₈) are applied. Following EC5, a characteristic strength can be derived from test data, which can then be modified by k_{mod} & γ_M to produce a design strength. In order to achieve a compatible basis for ULS design values, an assessment is required of the relative safety factors applied in each case.

Referring to BS 5268: Part 2 [6], for sheet materials (other than plasterboard) the factor of safety to be applied to test panels is given in C1.8.5.4 which specifies that the relationship between design & test load should be 1.25 multiplied by tabulated factors reproduced in Table 3.

Duration of Loading	Timber & Plywood K_{85}	Tempered Hardboard K_{71}	Particleboard K_{79}
Very Short Term	1.30	1.23	1.25

Table 3 *Modification Factors For Strength Tests (SC1 & SC2) [BS5268:Part2:1996, Table 97]*

This is further translated & expanded to the specific application of diaphragm walls in BS 5268: Section 6.1, as described in Table 4. When the load factors from Table 3 are multiplied by 1.25, they produce modification factors in the range 1.537 - 1.625, & so although in broad agreement with the value in Table 4, there is a certain scope for further material based development. For simplification the values in Table 4 are retained for the purposes of current development.

Sheathing	Factor of Safety
a) Any of the sheet materials other than plasterboard, described in BS 5268: Section 6.1: 1996, Cl.2.3	1.6
b) Plasterboard	2.4

Table 4 *Factors of Safety (FOS) For Test Racking Load [BS5268:Section 6.1:1996, Table 8]*

It is reasonable to assume that similar values can be employed for the translation of tabulated values for basic racking strength that underline the “assessment method” in BS 5268. Drawing from EC5, for timber & wood-based materials $\gamma_M = 1.3$ & $\gamma_Q = 1.5$, which together give a “factor of safety” of 1.95. For plasterboard, no γ_M factor is given in EC5, but a value may be proposed as follows:-

$$\gamma_{M, \text{plasterboard}} = \frac{\gamma_{M, \text{timber}} \times \text{FOS}_{\text{BS 5268, plasterboard}}}{\text{FOS}_{\text{BS 5268, timber}}} = \frac{1.3 \times 2.4}{1.6} = 1.95 \quad (1)$$

$$\therefore \text{Combined factor of safety for plasterboard} = 1.95 \times 1.5 = 2.93$$

These “factors of safety” are summarised in Table 5. It is clear that for both classes of sheathing, either with or without the NAD wind load factor, EC5 results in a higher “factor of safety”.

Sheathing Material	Combined Factor Of Safety (FOS)		
	BS 5268 Derived	EC5	UK NAD / EC5*
Timber/ Wood-Based Sheathing	1.6	1.95	1.76
Plasterboard	2.4	2.93	2.63

Table 5 *Factors of Safety For ULS Application*

*Note: Incorporates wind load reduction as in UK NAD, on the basis of CP3 derived wind actions.

With a view to translation to a design code support format (application rule), the basic racking resistance could either be tabulated including or excluding the k_{mod} factors, depending on how the values are to be presented, & what the accompanying application procedures will be. For example, the equivalent tabulated form to that existing in BS 5268 for ULS design is presented in Table 6. These values are calculated on the basis of proportionality between factor of safety & basic racking strength, & incorporate k_{mod} values applicable to short-term load duration (i.e. wind) under Service Class 1.

This will then facilitate the ultimate strength prediction of the wall using an expression of the form:

$$R_d = R_b \times L \times K_m \times K_w \quad (2)$$

where

R_b is the basic racking resistance (as presented in Table 6)

L is the length of the panel

K_m is the product of the material related modification factors from BS 5268: Part 6

(K_{101} , K_{102} & K_{103})

K_w is the product of the wall geometry related modification factors from BS 5268: Part 6

(K_{104} & K_{105} (or K_{shaspe}), K_{106} , K_{107} & K_{108})

Primary Board Material	Fixing	Racking Resistance (kN/m)	Additional contribution of Secondary Board On Timber Frame Wall	
			Category 2 or 3 Materials (kN/m)	Category 1 Materials (kN/m)
Category 1 Materials: <ul style="list-style-type: none"> • 9.5mm plywood; • 9.0mm medium board; • 12.0 mm chipboard (type C3M, C4M or C5); • 6.0mm tempered hardboard; • 9.0mm OSB (type F2) 	3.00 mm diameter wire nails at least 50mm long, maximum spacing 150mm on perimeter, 300mm internal.	2.27	0.38	1.13
Category 2 Materials: <ul style="list-style-type: none"> • 12.5mm bitumen impregnated insulation board; • separating wall of minimum 30mm plasterboard (in 2 or more layers) 	3.00 mm diameter wire nails at least 50mm long, maximum spacing 75mm on perimeter, 150mm internal.	1.21	0.61	1.43
	Each layer should be individually fixed with 2.65 mm diameter plasterboard nails at 150mm spacing, nails for the outermost layer should be at least 60mm long.	1.21	0.61	1.43
Category 3 Materials: <ul style="list-style-type: none"> • 12.5mm plasterboard 	2.65 mm diameter plasterboard nails at least 40mm long, maximum spacing 150mm	1.21	0.61	1.43

Table 6 Proposed Ultimate Limit States Basic Racking Resistance R_b For A Range Of Common Materials & Combinations of Materials

2.5 Serviceability Limit States Basis

It has been identified that further component based research is needed, together with full scale structural research [7,8], because severe inadequacies & limitations in present structural design codes are restricting the development of timber-frame construction. The serviceability limit states issues of compatibility between component based test performance & that which will be delivered in the context of a complete structural system in service, is an area of particular concern in this respect.

It is of note that other than compliance with the general requirement 4.1 which is given in EC5, there is no SLS guidance directly for application to timber diaphragm wall design.

Full assessment of SLS should relate to the fundamental EC1 requirements for satisfaction under SLS design. These relate to the following criteria:-

- (i) **Functionality:** Gusts should not interfere with the functioning of plant/equipment/furnishings (china cabinets!)
- (ii) **Appearance:** Damage to finishes due to nail popping, panel rotation needs to be controlled.
- (iii) **Comfort :** The gust deflection should not unduly alarm or annoy the occupants

In terms of structural parameters in building design, these aspects can all be seen to translate to deflection & vibration control, both of which relate to the stiffness of the wall. It should be remembered that in practice the stiffness of a wall depends on the interaction of many factors, & not simply on the stiffness of an individual panel. For a design method, however, it is necessary to know the stiffness of the individual members in order to determine the stiffness of the complete structure. It is recognised that due to this fundamental misalignment of test basis and in-situ behaviour, the actual deformations likely in a wall of a building may be dramatically different to those recorded through stiffness testing of panels.

2.5.1 Deflection Control

Deflection is to some extent considered in BS 5268, & during the literature studies at the start of this research, it was noted that the original basic racking resistance values from BS 5268 translated into Table 6 relate to a deflection limit of 0.003_{HWP} . Regarding actual deflections in “real structures”, there are a number of arguments that state that the cladding can take more load, the panels are stiffer than assumed, a lot of the walls are ignored & composite action is better than $K_{108} = 1.1$. However “ignorance factors” cannot form the basis for new design proposals, especially as the industry looks to expand the timber frame horizon to multi- storey structures & large wall constructions (e.g. school halls), some of which may not use masonry cladding.

An ideal goal for longer term developments of the design basis is to make deflection criteria more realistic, whilst at the same time taking full account of “whole building” stiffness. This will provide a more adaptable design tool to tackle more innovative design situations & to address any desired enhancements of appearance or comfort-related criteria.

2.5.2 Vibration Control

The subject of vibrational performance is not addressed by BS 5268. The importance of vibration is however recognised nowadays, & work has been carried out in this area, relating to floors & footbridges. Although a considerable amount of work has been performed internationally in relation to the dynamic aspects of wall behaviour, this has focused principally upon response to seismic activity, which is not normally considered in the UK. Other dynamic actions that may require consideration in the assessment of the whole building behaviour can be attributed to either internal or external sources, as described in Table 7.

Internal Sources	External Sources
Human	Wind
Oscillating machinery	Traffic
Impact machinery	Local construction activity
Industrial lifting equipment	Heavy impact machinery in nearby buildings
Activity in adjoining parts of building	

Table 7 Normal Vibration Sources That May Affect Building and Hence Wall Panels

The stiffness assessment after panel testing in accordance with BS 5268, is based on a theoretical deformation of $0.003 \times \text{panel height} = 7.2\text{mm}$ for a 2.4m high panel. (The actual calculation takes the stiffness at a deflection of $0.002 \times \text{panel height}$ & then multiplies by a factor of 1.25, to arrive at the 0.003 “equivalent stiffness”.) Movements of this order of magnitude, resulting from a gust wind load, would certainly be sensed as a dynamic experience by occupants. Whilst it is known that timber wall panels can “recover” from deflections of this magnitude, the manner in which they would subsequently behave is unclear.

Vibration levels related to human perception & tolerance levels are indicated in relevant standards such as ISO 10137 [9]. The actual levels which it is believed can be tolerated depend upon the specific cases under consideration. Tolerance is also quantified in relation to body axes. Perceptions change with the frequency & direction of vibrations. In an actual building, the resultant vibrations may be due to a number of sources, hence multiple phenomena may need to be considered. Depending upon the structural response as a whole, the phenomena may be related to low frequency effects (sway type movements) or higher frequency situations, whereby the wall & floor diaphragms interact to some degree to produce the perceived behaviour due to whole-body vibration.

Work from the late 70’s & early 80s in relation to acceptability of motion in structures has been summarised in recent wind-induced motion studies [10]. However there is no definitive prescription as to tolerable levels, with various limits being suggested. For example, Tables 8 & 9 illustrate two sets of criteria for application to horizontal accelerations for low frequency wind induced vibration, whereas the comfort criteria base curves from ISO 10137 for a range of higher frequencies in buildings is summarised in Figure 3.

Building Motion (milli-g)	Observation at $f < 1$ Hz
< 1	most people cannot perceive motion
3	over 50% of people physically sense motion
6	people engaged in work sense motion
10-20	people begin to feel differences in walking & action
> 20	motion sickness complaints

Table 8 Occupancy Responses to Low Frequency Vibration [10]

Acceleration At $f < 1$ Hz (milli-g)	Degree of Discomfort
< 5	Imperceptible
5 - 15	Perceptible
15 - 50	Annoying
50- 150	Very Annoying
> 150	Intolerable

Table 9 Discomfort Levels for Low Frequency Vibration [11]

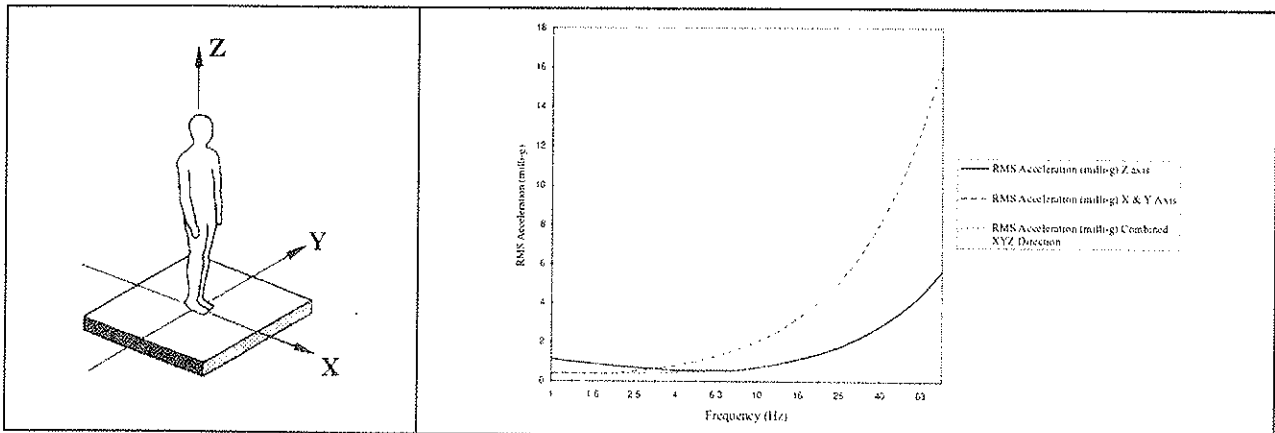


Figure 3 ISO Reference Axis & Base Curves for Quantification of Human Perception Of Vibration

It should also be noted that the control levels which have started to be considered here do not make allowance for potential building occupant complaints about “noises” within the timber frame structure, which is recognised as an important performance concept relating to movement.

Although serviceability design of walls is an area obviously requiring further development, an initial series of tests were performed, to help in establishing some of the principles.

2.5.3 Serviceability Criteria/Wind Load Relationship

To apply the correct wind actions in serviceability design, EC1 requires that the reasons for limiting the deflection are established. This then makes it possible to decide whether the loads are reversible or irreversible, & hence whether “action combination” or ψ factors are required.

For appearance considerations, it would normally be expected that damage should be avoided, leading to an “irreversible” load case. To design for this, the “characteristic” load combination should be used i.e. the full characteristic wind load should be applied.

Checks to avoid offending the functionality & comfort criteria will normally be associated with “reversible” load cases. In this instance, the “frequent” load case is considered, for which $\psi_1 = 0.5$ i.e. for this SLS, the design wind load is 0.5 x the characteristic wind load. This reduced load recognises & accepts that the chosen criterion will be exceeded on a number of occasions throughout the building life. This approach is gaining acceptance for static loading situations but it is as yet unclear as to whether it can be applied to dynamic loads, i.e. explicit description of the duration and frequency of occurrence of a dynamic loading event in relation to its magnitude of influence in a timber frame building.

The current guidance provided by ISO codes [9,12,13] and BS 6472 [14] recognise a basic difference with respect to human perception, via the employment of base curve factors to address either “transient vibration excitation with several occurrences per day” or “continuous or intermittent vibration”, but this is not as closely defined as the basis for static actions via EC1. Existing recommendations [15] for tolerable responses of buildings to vibrations for SLS, resulting in minor cracking, degradation of paint and plaster finishes, unacceptable deflection or accelerated ageing effects are largely empirical in nature and can be traced to the recommendations of Civil Engineering codes for blasting, compassion and traffic vibration.

3. EXPERIMENTAL INVESTIGATIONS

From the work carried out in converting BS 5268: Part 6 to a limit states basis, it was apparent that although deflection is considered in the original design by test procedures, the actual nature of the wall behaviour with respect to SLS parameters required clarification. Therefore a series of experimental investigations were conducted. These were focused upon a series of computer model simulations. Most importantly however, was the detailed SLS-linked testing of a wall panel of simple geometry. These were regarded as “special” tests, devised for the SLS investigation aim, & consequently differing in detail from “design by test” standard procedures.

3.1 Computer Modelling.

A 3-D model of a standard test wall panel was created, as shown in Figure 4. This consisted of a framework of members to represent the timber frame, & a mesh of rectangular elements to simulate the sheathing. The frame was joined to the sheathing elements by short members representing nails at appropriate nodes. The wall model included a central vertical discontinuity in the mesh to simulate two sheathing boards, thus reflecting a normal test specimen. The model was calibrated against test results.

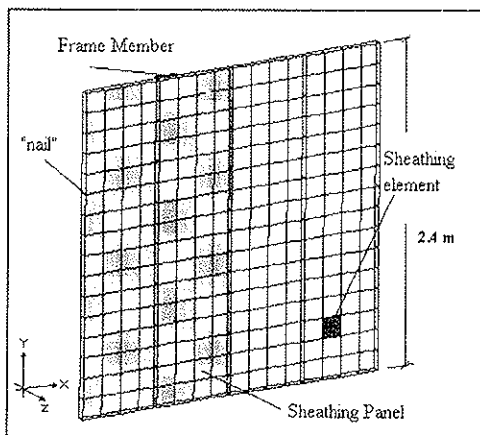


Figure 4 Schematic of Wall Model

The model was used to investigate the effect of variations in racking force, top load, sheathing stiffness, sheathing thickness & frame stiffness upon the predicted deflections, in order to identify the behaviour of the system relative to variations in actions & component properties.

3.2 Serviceability Tests on Simple Panels.

The history & development of “design by test & calculation” for timber frame walls has been presented in CIB-W18/29-15-3 [2]. In order to facilitate compatibility of test findings with existing knowledge of panels of varying dimension & form [16], these new tests were based upon the stiffness test methodology presented in BS 5268: Section 6.1: 1988 [17] rather than that defined in BS EN 594 [18]. The test specimens differed from the standard panel configuration in BS 5268, consisting of only one sheet of sheathing material, thus avoiding certain known complications in behaviour pattern. Measurements additional to those required in the standard test procedure were taken, & the panel was subjected to a higher overall deformation, to try to establish more clearly its actual mechanisms.

A series of vibration tests were also performed, fulfilling two functions - to qualify the boundary condition influences upon dynamic performance, & also to provide a means of detection of possible damage accumulated within the wall panel through the process of cyclic testing. These tests were not intended to simulate actual wind gust events, but were employed to demonstrate the principles of panel behaviour under the defined conditions.

3.2.1 Test Specimens

Four similar test specimens as described in Figure 5 were fabricated using hand-held tools, the implications of industrial-scale manufacture not being considered important for the particular aim concerned.

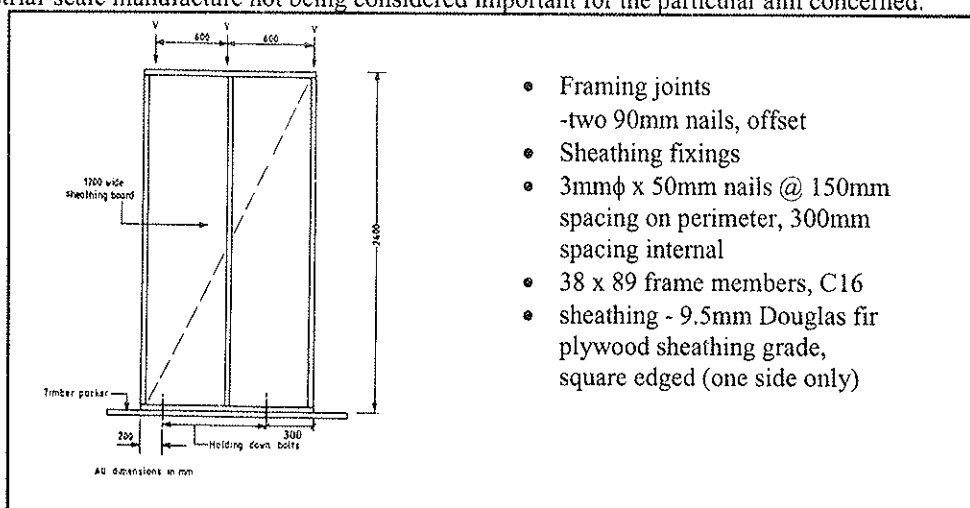


Figure 5 Test Specimen

The test specimens were fixed down to a 35mm x 90mm hardwood timber packer using two 18mm diameter bolts. The packer was in turn fixed rigidly to the test frame.

3.2.2 Instrumentation

Racking loads & vertical stud loads were applied hydraulically, with actual loads being monitored through calibrated load cells. Deflections, differential movements & closing of framing gaps were monitored using a combination of electronic transducers, DEMEC gauges & feeler gauges.

The set up of electronic transducers is shown in Figure 6. The precise locations of these were defined in relation to the component aspects of the overall behaviour to be monitored through the test:

- Transducers A & B were located across the diagonals of the sheathing, thus recording actual deformations in the sheathing only.
- Transducers C, G & H measured the horizontal frame movement, providing information about the net movement (H-C) & also deformation of the top of the frame (H-G).
- Transducers at points D, E & F measured the horizontal sheet movement,
- Transducer I measured the lift of the stud from the base plate.

DEMEC gauges were employed to monitor the local differential movement between the sheathing & frame in a selection of locations as shown in Figure 6. These readings were taken as both horizontal & vertical differentials, to quantify the movement accountable to slip at the nail fixings.

Feeler gauges were employed in the locations shown in Figure 6 to record the gaps between the studs at intersections in the frame at different points in the test cycle.

For the vibration tests, accelerometers were attached to the specimen, in the positions shown in Figure 6, to record the in-plane & out-of-plane dynamic response of the panel to a soft body impact applied in the same direction as the loads applied under static racking tests.

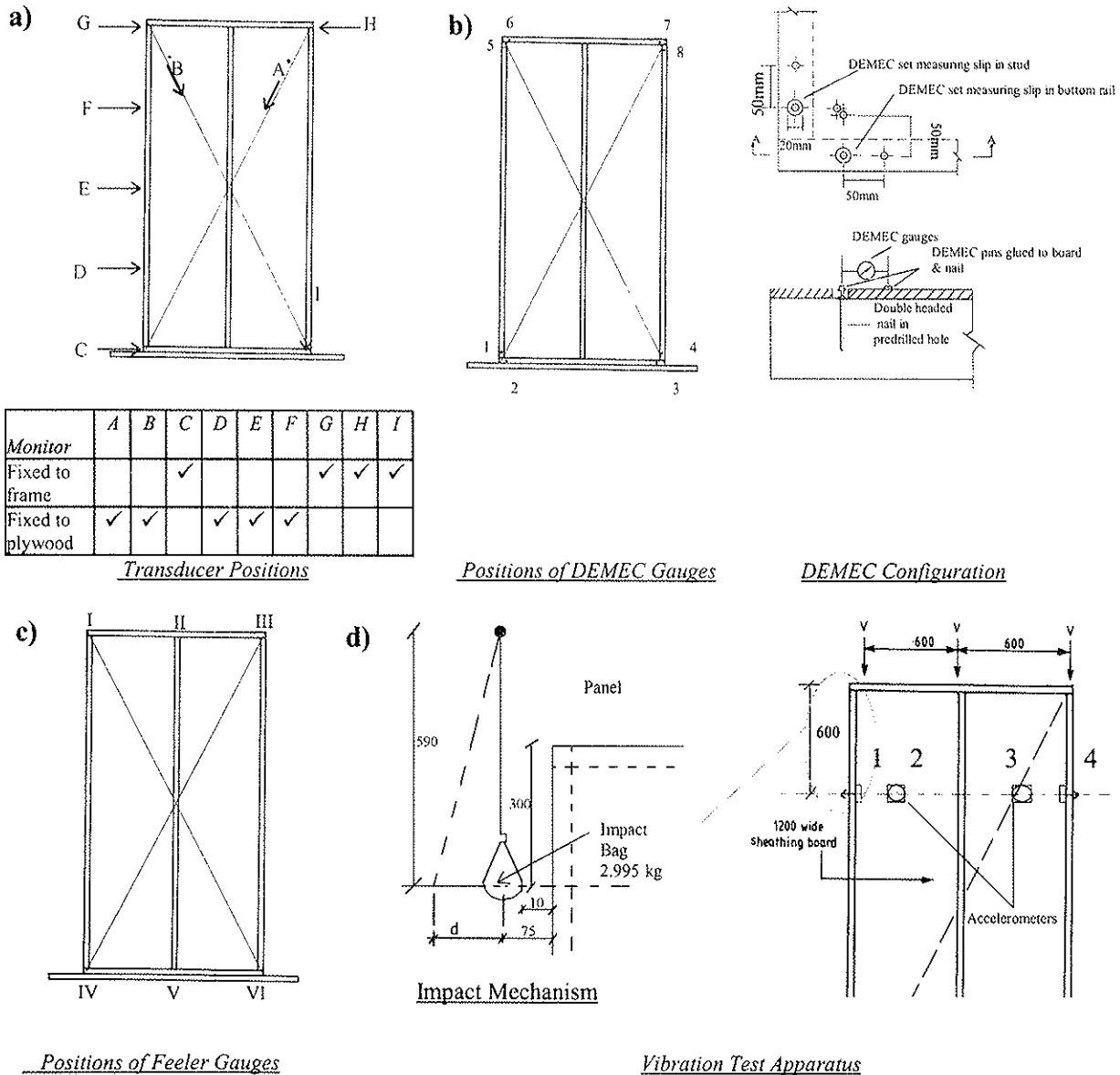


Figure 6 Monitor Locations on Test Panel

3.2.3 Test Procedures

Racking tests were performed following the principles laid down in BS 5268: Section 6.1: 1988, horizontally loading the panels to a deflection of $0.002 H_{wp}$ over 4 cycles. On the final cycle, this deflection limit was taken up to $0.003 H_{wp}$.

Vibration Tests were performed on the panels prior to & also after a static stiffness test had been performed. In each case, a single impact was induced upon the end stud via the swinging bag mechanism. Three magnitudes of impact were investigated through variation of the distance, d .

4. RESULTS

4.1 Computer Modelling

A plot of the deflected model under racking is shown in Figure 7. The behaviour of the calibrated model, confirmed certain aspects of general deflection behaviour of the panel under the racking load, such as the stabilising influence of top load, tendency for the individual panels to interact, yet rotate independently & the uplift potential in tension studs. It was found however that the scope for application to a wider set of geometries was limited due to the need for calibration against test, resulting from the simplifications incorporated in the model itself.

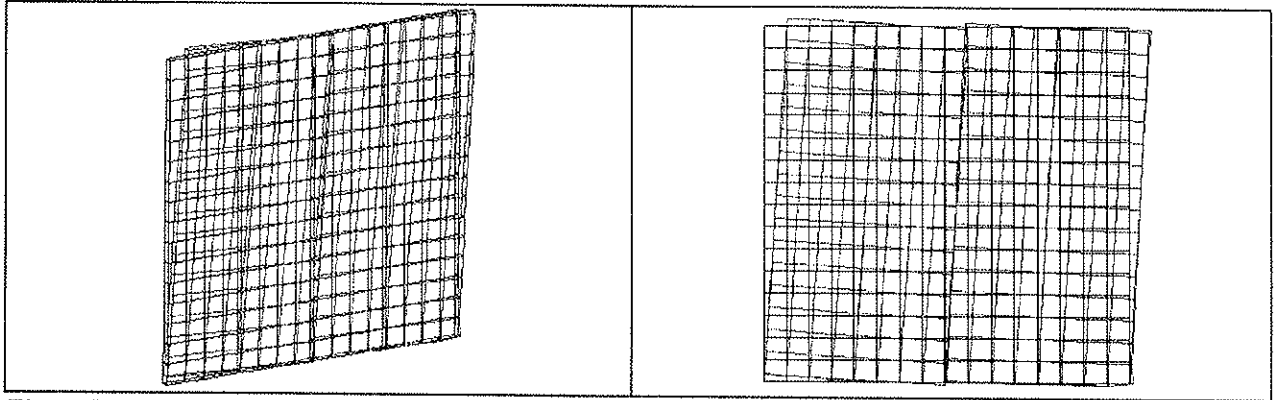


Figure 7 Racking Deflection Modelled Behaviour

A linear response to increased racking load was observed as might be expected for a system acting within its elastic range, i.e. displacement is proportional to a function of applied force.

The observed stabilising effect of top loads upon wall panels subjected to racking forces is in agreement with racking theory, however a negative stud displacement is predicted by the model at a point where the top load is of greater effect than the racking load. This indicates a deviation from the modelled behaviour of the panels & the expected behaviour in real walls.

It was found that the variation of deflection of the panels is not directly proportional to the thickness or elasticity of the sheathing material, nor to the elasticity of the frame timber.

The results all agree with the general principle that the stiffer the system, the less it will deflect when subjected to a racking load. The results also indicate that within the investigated parameter range, enhancement of the sheathing E-value is the most effective method for enhancement of performance.

4.2 Racking Tests

4.2.1 Overall Panel Behaviour

Figure 8 shows the net deflection of the panel throughout the 4 cycles of each test.

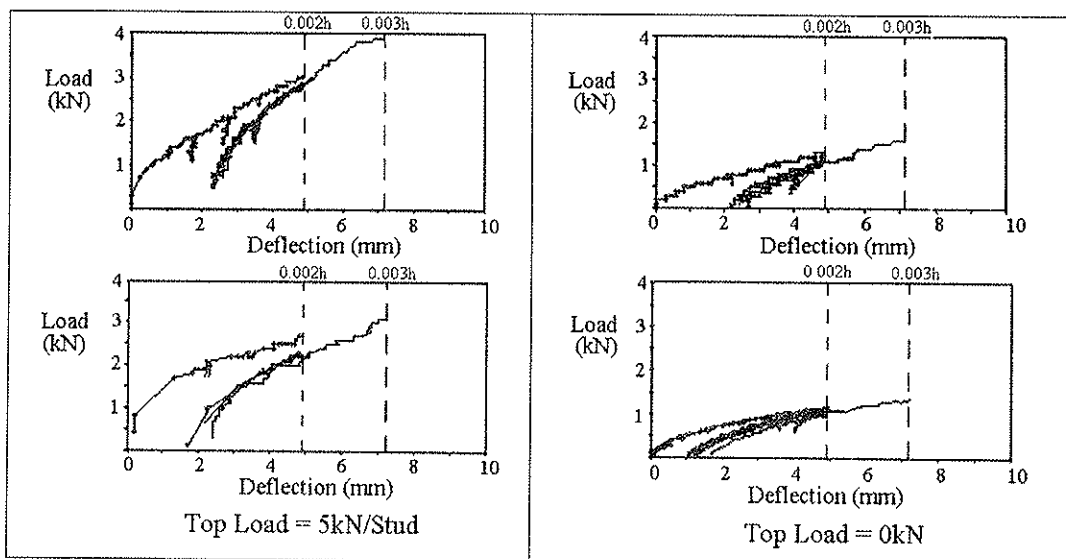


Figure 8 Load - Deflection Results Recorded in Racking Tests

From Figure 8 it can be seen that:

- The use of top load clearly improves the tested performance with regard to stiffness behaviour within the limits of this test.
- The pattern of deflection recorded up to 0.002h follows a continued curve when higher load is applied to produce a deflection of approximately 0.003h.

The recorded overall deflection in a wall panel will be composed of a number of mechanisms:

- Slippage at nails, due to embedment & nail deformation
- Deformation of sheathing
- Deformation of framing, due to uplift at joints or deformation of framing members themselves
- Lifting of frame due to framing joint failure in tension

These act in combination to produce a deflected panel shape which will depend upon the relative contribution of deflection modes associated with these phenomena & the boundary conditions such as restraints at panel base & top load. The results in this paper are discussed in terms of four conceptual modes as detailed in Table 10.

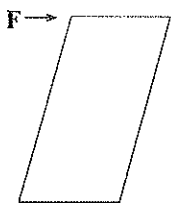
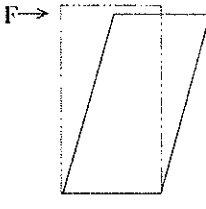
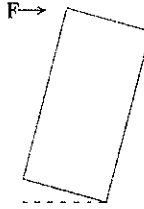
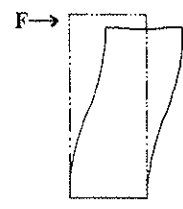
Mode Reference	1	2	3	4
Deflection Composed of				
Requires sheathing deformation	✓			
Requires frame deformation	✓	✓		✓
Requires sheathing nail slippage		✓	✓	✓
Requires frame joint slippage			✓	
Principal Assumptions	Frame pinned	Frame pinned Sheathing rigid, but may rotate	Sheathing rigid, but may rotate (Note: if uplift = zero, this will be pure rotation & requires nail slip, hence equivalent to mode 4)	Sheathing rigid, but may rotate
——— = Movement of frame (or whole panel if no movement in sheathing) - - - = Movement of sheathing = Position of footplate				

Table 10 Conceptual Deformation Modes

The actual deflection of a panel subject to racking is complex. Besides the influence of variations within the panel construction itself, the boundary conditions have an influence upon the apparent performance. This is a recognised fact, even in the recommendations for such tests developed in the 1960s prior to the existence of BS 5268 [19]. It is therefore apparent that the different test methods that have been suggested over time will influence the measured performance.

4.2.2 Sheathing Deformation (Mode 1)

The sheathing material has an equal modulus of elasticity in both compression & tension parallel to the grain, therefore any lozengeing of the panel should result in equal strain being induced upon both diagonals. However it is possible that the plywood may buckle in compression, although this is not possible under tension. Measurements were taken & it was found that the deflections were larger during compression, this was probably due to minor buckling. It was also found that the deformation of the sheathing was greatest when the top load was induced. The translation of the diagonal strain to the horizontal suggests that the approximate component of the total deflection was up to 5% when the top load was in place, but under 1% when the top load was zero.

4.2.3 Differential Frame/ Sheathing Movement (Mode 2)

The differential between the frame & the sheathing was due to nail slippage at the connections. The contribution of this to the whole panel deflection can be approximated through a spring model which considers horizontal differential movement recorded at the head of & the bottom of the panel. The contribution of this to the overall panel deflection was less than 10% when there was zero top load, but between 30-60% when the top load was 5kN.

4.2.4 Overturning Of Panel Through Rotation (Mode 3)

The overturning of the panel was caused by the rotation of the base at the compression stud, accompanied by uplift of the tension stud. The horizontal deflection due to uplift can therefore be approximated due to the translation of the panel through an angle. The geometric studies suggest that this is a considerable component of the overall panel deflection, however the top load reduces it. The approximate contribution to overall panel deflection was between 60-90% when the top load was zero, but only 30-50% when the top load was 5kN.

4.2.5 Deformation of Frame (Mode 4)

Deformation in the frame can be attributed to deformation in both framing members and the butt joints where they meet. With regard to the abutting faces of timber members in a panel frame, BS 5268 recommends a maximum of 2mm as a tolerable gap. The test specimens were found to have gaps in the range of 0-1.8mm, with one instance of a joint gap measured at a fraction over 2mm. There was recorded movement during the tests, with a maximum closure of 1.2mm & a maximum opening of 1.8mm. This is significant, compared with the overall deflection of the panel.

It is also of note that the interaction of framing gaps and components of deformation should be considered if realistic quantification of SLS related deformations are to be made from tests. Application of top load can close such gaps and at low racking loads produce a negative overall displacement in tension stud locations when compared to the initial test datum. It is not believed to be a viable option to specify a tighter tolerance on the framing gap and so cognisance of this effect is essential in transfer of test data to an estimation of stiffness and strength.

4.3 Vibration Tests

4.3.1 Overall Response

Typical responses recorded in the tests are illustrated in Figure 9. These show the acceleration traces over time at each of the sensor locations, with variation in top load & relative magnitude of impact.

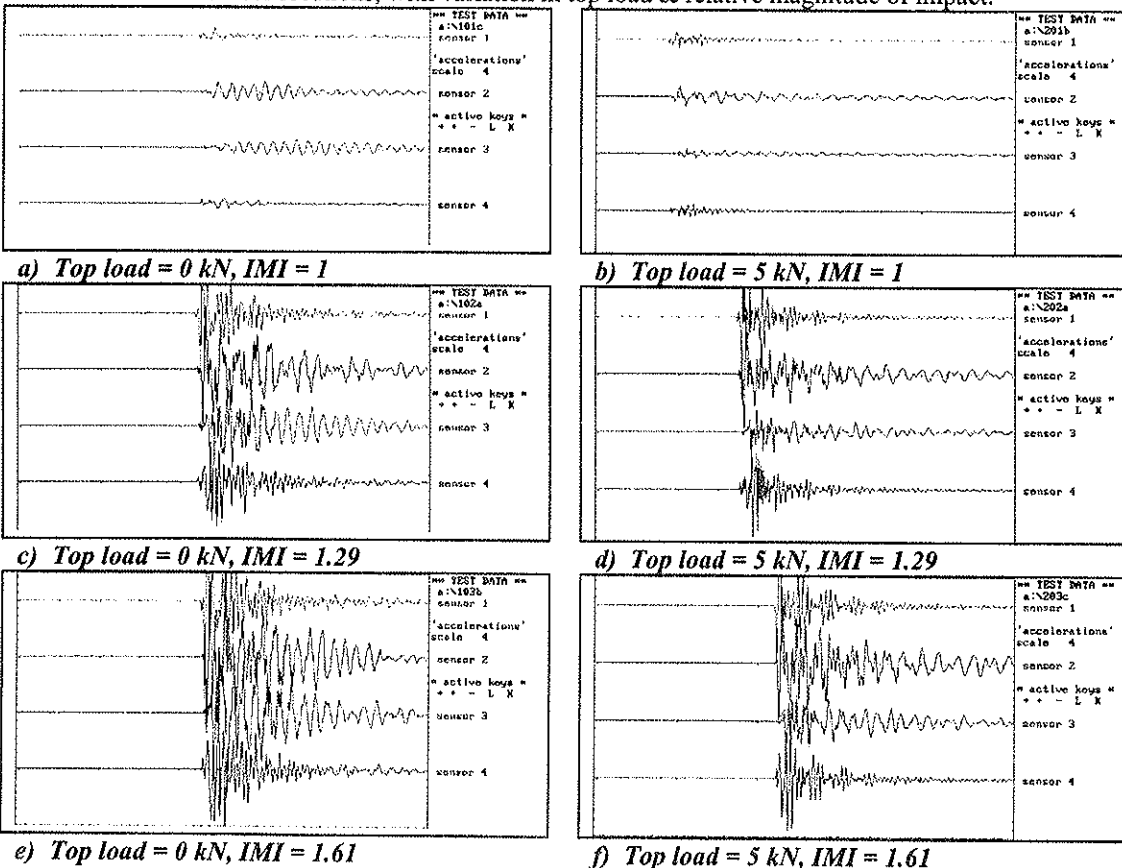


Figure 9

Acceleration Response Recorded From Test Panels

Note: IMI = Impact Magnitude Index, in relation to smallest test impact.

Analysis of the recorded data, via construction of frequency spectra, revealed that the dominant modal frequencies lie in the range of approximately 25-120 Hz. The influence of top load was again noted, changing the relative magnitude of the peaks spectra.

4.3.2 Influence of Impact Magnitude

The magnitude of maximum accelerations recorded in response to the impacts are illustrated in Table 11.

Relative Impulse Magnitude		1	1.29	1.61
Acceleration	(mm/s ²)	3.2	17.12	25.34
	milli-g	0.3	1.7	2.6

Table 11 Maximum Recorded Accelerations in Relation to Magnitude of Impulse

Comparing these values back to the base curves presented in Figure 9, at the test levels investigated, it appears that the motions recorded are of an order that may be physically perceptible, probably not cause for concern in their own right. This will obviously depend upon the magnitude of the excitation force & the translation of the behaviour into the context of the complete building.

Secondary effects may also be of notable consideration. The most obvious in the case of vibrations in walls being resultant noise from objects fixed to or located near to walls. e.g. rattling picture frames, rattling windows, etc.

Quantifying the actual magnitude of an impact type test load to represent actions likely to be experienced in a building & causing vibration requires further development, but these results show that even a relatively minor impact can produce results of significant magnitude compared to the identified perception levels.

4.3.3 Mode of Vibration

As can be seen from the responses recorded in Figures 9, the response recorded out of plane (sensors 2 & 3) was found to be of greater magnitude than those recorded in the plane of the panel. The damping of the motion (signified by the decay of the plots) in this sense is also significantly less, with oscillations of considerable magnitude persisting for some time.

The vibrational response of any system will be composed of many vibration components (or modes) acting in all directions, influenced by the associated relative stiffness & mass interactions. It can therefore be deduced that since the panel is least stiff in the horizontal direction perpendicular to sheathing & that even an impact with no component in this direction causes a dominant effect in this sense, that as far as a single panel is concerned, vibrations in this direction will be of major concern. For longer panels, this tendency has the potential to increase due to the balance of stiffness being even further weighted in the longitudinal direction of the panel.

The influence within the context of a complete structure is however less clear, since the building will act as a system, the panel itself will be connected to some form of cladding in the form of lightweight panels or single leaf masonry, the excitation may not be from a single source or direction & the occupant perception will be influenced by the combined effect of wall & floor movement & phenomena associated with their particular circumstance.

4.3.4 Influence of top load

In almost all buildings the wall panels will be subjected to some form of vertical load. This will be determined by the combination of self weight of structure & wind induced uplift. It is apparent from the test results that the presence of a top load placing the panel into compression has a measurable influence upon the dynamic response of the panel, resulting in stabilisation of the panel in this instance.

4.3.5 Comparison of Behaviour Before & After Deflection Tests

The vibration responses recorded before & after deflection tests were not found to exhibit any noticeably significant differences. This suggests that the timber & plywood materials in the test specimens do not suffer damage from the limited cyclic deflection test. This is in agreement with evidence from tests on small samples of sheathing material which also suggests that provided loads do not exceed a critical level, many thousands of cycles may occur without damage to sheathing fixings [20].

5. COMPARISON OF SLS TEST OBSERVATIONS & THEORETICAL DERIVATION OF DEFORMATIONS

As presented in BS 5268, a justified route for panel design is that of “Detailed analytical methods outside the scope” of the British Standard. Such an exercise was performed to assess the translation of nail slip, stud lift rotation & panel ‘lozenging’ to components of deformation in a panel similar to that tested. The findings, based upon a combination of graphical & theoretical models, are presented in Table 12.

	Theoretical	
	Absolute (mm)	%
Total Deflection (0.003 H_{wp})	7.20	100
Panel Lozenging	0.45	6
Stud Lift / Panel Rotation	2.00	28
Translated Nail Slip + Sheathing Rotation	1.83	26
Other Deformations	2.92	40

Table 12 Theoretical Deflection Components

From the experimental evidence, the following trends can be picked out in relation to the panels investigated through these tests:

- The introduction of top load promotes the relative magnitude of mode 1 & 2 deformations;
- In all instances, as deflection increases, the make up of the deformed wall changes with mode 2 & 3 becoming more appreciable.

Observations from previous studies in relation to BS 5268 based wall tests show that failures tend to occur as a result of fastener movement in the sheathing rather than the framing material. With low vertical loads failures generally result through 'break-out' of the nails at the bottom edge of the sheathing. With high vertical loads, failure at the joint between two sheets is more common. These observations are in agreement with the trends of relative contribution of the modes of deformation described.

It is of note that the magnitude of the theoretically derived deformation components translates reasonably to an overall deformation as observed in a panel under top load. The panel lozenging component is very close to that observed in test. The overall panel rotation due to tension stud uplift is slightly less than that observed in test.

The calculated components due to pure sheathing rotation & "other deformation" are believed to interact to such a degree that their separation may not be fully justifiable in developing a method further. Their combined effect is mirrored by that of combining modes 2 & 4. Although this exercise has shown a certain degree of consistency with test data in separation of deflection components, the evidence of computer modelling suggests its application to panels of more than one sheathing panel is a far more complex issue.

6. COMPARISON OF STIFFNESS PERFORMANCE FROM TEST & RACKING CALCULATION

The test racking stiffness load is calculated in BS 5268: Part 6.1 using the equation:

$$R_1 = R \times 0.002 \times H_{wp} \times 1.25 \times K_{109} \quad (3)$$

Where: R is the racking stiffness of the panel (expressed in kN/mm as a load per unit deflection)
 H_{wp} is the panel height (in mm)
 K_{109} is a modification factor to take account of the number of similar panels tested

The factor of 1.25 is employed as a means of converting the load prediction for a deflection of $0.002 \times H_{wp}$ to an estimate for an acceptable performance at $0.003 \times H_{wp}$. By assessment of the test results presented in Figure 8 the relative magnitude of load at the two deflection limits supports the factor of 1.25.

It is stated in BS EN 594 that F_{max} is reached either when the panel collapses or when the panel obtains a deformation of 100mm. The force needed to produce such a deformation was found, drawing upon extrapolated load / deflection graphs for each of the tests on the fourth cycle.

Theoretical basic racking resistance calculated from BS 5268: Part 6.1 & also on the limit states method were determined & are presented in Table 13. There is reasonable agreement in the figures developed from stiffness tests & BS 5268 assessment on this basis. Therefore, in relation to a serviceability related assessment by test, this may be suitable, provided similar conversion factors as previously incorporated are employed.

Specimen	Test Racking Resistance (kN)	Theoretical Wall Racking Resistance (kN)	
		BS 5268	Limit States Based
I	1.70	1.71	2.31
II	1.14	1.11	1.50
III	1.27	1.71	2.31
IV	1.07	1.11	1.50

Table 13 Packing Resistance Developed From Theory & Stiffness Tests

7. CONCLUSIONS

Drawing from the limit state basis described in the first part of this paper & incorporating the findings from the experimental investigations, the status of development of the method to date is as described in Table 14. Work is in hand to draft a series of clauses that would form a suitable basis for inclusion in a future UK NAD to EC5, thus establishing a basis for a limit states design method in the spirit of BS 5268: Part 6. This facilitates assessment of panels, primarily on a ULS basis (as does EC5), to determine a racking resistance in a manner which is reasonably simple & makes economical use of the material.

Limit States	Quantity	Status		Comment
		Resolved	Scope For Further Development	
ULS	Resistance to Vertical Load	✓		Via Column Design Basis
	Resistance to Horizontal load	✓		Development of basic racking resistance values compatible with EC5
SLS	Deflection Limitation		✓	- 'Design By Test' related issues
	Vibration		✓	- Actual Performance Issues

Table 14 *Current Status of the Component Limit States*

The work to date has facilitated development of a limit states (i.e. EC5 compatible) design method for timber frame walls. Since this has been translated from BS 5268: Section 6.1 it is directly suited to "Dwellings not exceeding four storeys", & the method employed thus far will also be applicable to the current format of the non-domestic counterpart, which is under development at the time of writing.

Further development may be necessary using this limit state method as a foundation, as witnessed by the continual development of BS 5268: Part 6. Refinement of the K factors in the limit states may also be desirable, to consider whole-wall behaviour including effects upon individual ULS & SLS considerations of panels containing partial openings & connectivity between adjacent prefabricated panels.

A more direct approach, aimed at understanding better the behaviour of walls as constituents of whole structures, may soon be possible. This will prioritise future investigations. In three dimensions, & especially within structures of four to six storeys, wall panels are unlikely to act as simple cantilevers. Influences of building mass, contributions of cladding, diaphragm actions of floors & roofs, are important aspects which must be better understood in order to improve reliability & efficiency. Combined effects of walls, roof & floor diaphragms has been investigated to a limited degree [21] & it is reported that savings can be made through modelling as a three dimensional structure as opposed to series of components. Such modelling relies on a host of assumptions relating to effects which are currently unproven for structures defined with respect to UK design codes & construction practice. Developments in this area may facilitate a holistic design alternative & may provide a basis for incorporation of similar translations in the limit states method via the 'interaction' factor.

The racking tests have demonstrated that the boundary test conditions (top load) affects both the stiffness & the mechanism of deformation. It can be seen that in the specimen test, the action of a top load will simulate the dual interaction of actual structural load upon the panel & the actual restraint at the base of the panel provided by the building construction. The interaction of the panel with other components of the buildings structural system & hence its boundary conditions in service, will obviously become more complicated for more complex geometry, as has been shown in previous studies which have led to development of guidance in this respect. In such instances it is known that top load may change the limit states dictating the design, for example strength (ULS) becoming the governing factor over stiffness (SLS) where large panels with substantial openings are considered [16].

A further point of note relates to deformation of the sheathing which was found to deform to a measurable degree when top load was applied to the panel, & not remain absolutely rigid as assumed in some models. Again the influence of boundary conditions is obviously paramount.

From the simple vibration tests, a number of principles have been confirmed with respect to the test configuration & hence the actual performance in service. Top load influences response, serving in these tests to stabilise the panels through reduction of response acceleration & enhancement of damping. It may be necessary to broaden the scope of any future investigations in relation to vibration, beyond consideration of acceleration or velocity, since 'jerk' (the differential of acceleration with time, or the rate of acceleration) is recognised as being of, potential importance.

This study has illustrated that dynamic aspects may be of importance as SLS design develops in the context of whole building behaviour. The clear influence of boundary test conditions upon both ULS & SLS reinforces the underlying principle that component testing must be viewed in the context of a whole building, as identified in the 1967 TRADA proposals for racking tests which led to the BS 5268 method:

'The panels to be tested should be set up in the manner in which they are designed to be used in the building' [19]

ACKNOWLEDGEMENT

This paper has been developed through a research project which is co-sponsored by the Department of the Environment, Transport & the Regions (DETR), TRADA, & by individual industrial partners. TRADA Technology gratefully acknowledge this sponsorship.

REFERENCES

- [1] BSI, (1994). DD ENV 1995-1-1:1994, Eurocode 5: Design Of Timber Structures Part 1.1: General Rules & Rules For Buildings. British Standards Institution, London, UK.
- [2] GRIFFITHS, D.R., METTEM, C.J., ENJILY, V. & STEER, P.J. (1996). The Racking Resistance of Timber Frame Walls: Design by Test & Calculation. Paper CIB-W18/29-15-3, Proceedings of the International Council For Building Research Studies & Documentation, Working Commission W18 - Timber Structures, Meeting Twenty-Nine, Bordeaux, France.
- [3] BSI, (1996). BS 5268: Section 6.1: 1996, Structural Use of Timber, Part 6. Code of Practice For Timber Frame Walls, Section 6.1 Dwellings Not Exceeding Four Storeys. British Standards Institution, London, UK.
- [4] ENJILY, V. & GRIFFITHS, R.D. (1996). The Racking Resistance of Large Wall Panels. Proceedings of the 1996 International Wood Engineering Conference, Volume 2, New Orleans, USA. 2-321 - 2-328.
- [5] BSI, (1996). DD ENV 1991-1:1996. Eurocode 1 - Basis of Design & Actions on Structures - Part 1 : Basis of Design. British Standards Institution, London, UK..
- [6] BSI, (1996). BS 5268 :Part 2: 1996, Structural Use Of Timber Part 2 Code Of Practice For Permissible Stress Design, Materials & Workmanship. British Standards Institution, London, UK.
- [7] METTEM, C.J., PITTS, G.C., STEER, P.J. & ENJILY, V. (1996) Current Developments in Medium-Rise Timber Frame Buildings in The UK. CIB-W18/29-15-4, CIB-W18 Meeting Twenty-Nine, Bordeaux, France.
- [8] ENJILY, V. & METTEM, C.J. (1996). The Current Status of Medium-Rise Timber Frame Buildings in the UK Proceedings of the International Wood Engineering Conference, New Orleans, Louisiana, USA 28-31 October, 1996. Vol.2. Madison, WI, USA: IWEC. 2/63-2/69.
- [9] ISO (1992). ISO 10137: 1992(E) Basis Of Design of Structures - Serviceability of Buildings Against Vibration. ISO, Geneva, Switzerland.
- [10] MELBOURNE, W.H. (1998). Comfort Criteria for Wind-Induced Motion in Structures. Structural Engineering International, 1/98, IABSE, Zurich.
- [11] SIMIU, E. & SCANLAN, R.H. (1986). Wind Effects on Structures (Second Edition). Wiley-Interscience, John Wiley & Sons, New York.
- [12] ISO, (1985). ISO 2631-1:1985 (E) Evaluation of Human Exposure To Whole Body Vibration - Part 1: General Requirements. ISO, Geneva, Switzerland.
- [13] ISO, (1989). ISO 2631-2:1989 (E) Evaluation of Human Exposure To Whole Body Vibration - Part 2: Continuous and Shock-induced Vibration in Buildings (1 To 80 Hz). ISO, Geneva, Switzerland.
- [14] BSI, (1992). BS 6472: 1992, Guide To Evaluation of Human Exposure To Vibration in Buildings. British Standards Institution, London, UK.
- [15] BUCHMANN, H. et al. (1995). Vibration Problems in Structures - Practical Guidelines. Birkhauser Verlag, Basel.
- [16] GRIFFITHS, D.R. & WICKENS, H.G. (1996). Timber Frame Walls: Design For Racking Resistance. Proceedings of the 1996 International Wood Engineering Conference, Volume 2, New Orleans, USA. 2-37 - 2-44.
- [17] BSI, (1988). BS 5268: Section 6.1: 1988, Structural Use of Timber, Part 6. Code of Practice For Timber Frame Walls, Section 6.1 Dwellings Not Exceeding Four Storeys. British Standards Institution, London, UK. *Note: Superseded by 1996 edition*
- [18] BSI, (1996). BS EN 594: 1996. Timber Structures - Test Methods - Racking Strength & Stiffness Of Timber Frame Wall Panels. British Standards Institution, London, UK.
- [19] LANTOS, G. (1967). Proposed Method of Testing Timber Wall Panels Under Lateral Load (Racking). TRADA, High Wycombe, UK.
- [20] ROBERTSON, R.A. & GRIFFITHS, D.R. (1981). Factors Affecting The Racking Resistance of Timber Framed Panels. The Structural Engineer, Volume 59B, No. 4, December 1981, IStructE, London.
- [21] LEICHTI, R.J. & KASAL, B. (1993). A Look At A Structure As A Three Dimensional System. Systems Approach To Wood Structures, Proceedings of The Wood Engineering Division, 1993 Annual Meeting of Forest Products Society, Florida. Proceedings Ref. 7312, F.P.S., Madison, WI, USA.

SUGGESTED DRAFT CLAUSE

COMMENT

DD ENV 1995-1-1

1.4.2 SPECIAL TERMS USED IN PART 1.1 OF EUROCODE 5

P(1) The following terms are used in this Part with the following meanings:

-

- Racking: Effect caused by horizontal actions in the plane of a wall. This is quantified in terms of a racking force, F_{rack} , acting at the top of a wall panel and the racking resistance, R_{rack} , that can be developed by the wall

Provides a definition of racking, thus simplifying the structure of clause under section 5.4.3 for design of walls

5.4.3 WALL DIAPHRAGMS

P(1) Timber frame walls shall be designed to resist both horizontal and vertical actions.

Fundamental definition for design of walls

P(2) The wall shall be adequately restrained to avoid overturning and sliding.

Fundamental assumption in all walls

P(3) Timber frame walls deemed to provide racking resistance shall be stiffened in plane by board materials, diagonal bracing or moment connections.

Essentially a re-phrased version of existing P(1) in 5.4.3

P(4) The racking resistance, R_{rack} , shall be determined either by test or calculations, employing appropriate analytical methods or design models.

A re-phrased version of existing (2) in 5.4.3, making use of 2.3P(4), but extending scope to cover suggested limit states method proposed for inclusion as Informative Annex of National Addendum, whilst allowing continued adoption of existing EC5 principles

P(5) The design shall take account of both the material and geometric make-up of the wall under consideration.

Recognised fact in all wall design methods

P(6) The response of walls due to applied actions shall be assessed to ensure that the construction remains within appropriate serviceability limits, related to the type of construction.

Expansion of the scope of the EC5 method to recognise SLS as well as ULS considerations, conforming with 4.1 P(1).

The legal validity of this document can be claimed only on presentation of the complete document. All pages of original copies of this document are embossed with the TTL logo.



CIB-W18/31-2-1

INTERNATIONAL COUNCIL FOR BUILDING RESEARCH STUDIES AND DOCUMENTATION

WORKING COMMISSION W18 - TIMBER STRUCTURES

**DEFORMATION AND STABILITY OF COLUMNS
OF VISCOELASTIC MATERIAL WOOD**

by

P Becker

K Rautenstrauch

Bauhaus-University Weimar

GERMANY

MEETING THIRTY-ONE

SAVONLINNA

FINLAND

AUGUST 1998

Deformation and stability of columns of viscoelastic material wood

P. Becker, K. Rautenstrauch
Bauhaus-University Weimar, Germany

1 Introduction

Assuming linear viscoelasticity, deformation calculation of bending elements turns out to be very simple using a creep factor. The increase of the determined elastic deformation corresponds to the creep factor. Deformation calculation of columns proves to be involved with much more effort. Considering the problem according to theory of second order, creep deformation leads to an increasing bending moment, which again results in further elastic deformation. Superposition of creep deflection considering different classes of loads also turns out to be problematic. The object of this paper is the derivation of simple formulars, which guarantee the reliable determination of column deformations and an easy prove of the long-term stability.

2 Definitions and assumptions

2.1 Stability of columns with linear-elastic material

The Eulerload sets up the idealistic upper boundary value for the short-term stability of a simply supported column.

$$F_{ki} = EI \frac{\pi^2}{L^2} \quad (2.1)$$

The lateral elastic deflection w_{el} of the column according to the theory of second order, which appears for a specific compression load, can be computed as follows:

$$w_{el} = w_0 \frac{F}{F_{ki} - F} \quad (2.2)$$

w_0 represents a stressless predeformation, which is assumed sinusoidal. The moment of theory II. order is then determined by the equation

$$M^{II} = F \cdot (w_0 + w_{el}) \quad (2.3)$$

2.2 Assumptions

As already mentioned in 2.1, we assume a sinusoidal curve of deflection. Further we presuppose the Bernoulli-hypothesis, the cross-section remains plane. Time-dependent considerations are based on linear viscoelasticity. According to Blaß [1] this is possible up to 40% of the short-term strength. Morlier [2] also indicates this proportional limit as 40%, Gressel [3] assumes creep, which is proportional to the load, up to 50% of the short-term strength. Rautenstrauch [4] determined a linear relation of load degree and creep deformation. His loadings ranged within the area of the design load due to the German code DIN 1052. Since the specified proportional limits will hardly be exceeded in practice, the assumption of linear viscoelasticity seems appropriate.

Even though some new results in research (i.e. [6]) indicate the existence of an upper creep limit for loads in the proportional area, this problem is not finally clarified yet. Because it is our defined objective to derive a formula, with which the creep-deformation can be simply determined, we have to assume the existence of such a final value. Possible deflections occurring after reaching the final state of deformation shall be of insignificant order of magnitude.

2.3 Creep factor

To arrange the prove of serviceability of a timber construction for the structural engineer as simple as possible, creep factors are given in the codes, which enable the determination of creep deformation from the computed elastic deformation. Among other things the creep factor depends on load duration class and service class, which is taken into account in the draft to Eurocode 5.

The considerations done here are always based on a relative creep factor φ , which is defined for a bending element under constant load without normal force as follows:

$$\varphi = \frac{w_{\varphi}}{w_{el}} \quad (2.4)$$

w_{φ} refers to the additional deflection because of creep, which results from the final state of deflection described in 2.2. The elastic deflection, which appears immediately after applying the load, is represented by w_{el} .

2.4 Basics of linear viscoelasticity

Linear viscoelastic material behaviour can be described by rheological models. These models consist of combinations of the basic elements, a linear-elastic spring (Hooke element) and a viscous dashpot (Newton element). For the spring the strain and for the dashpot the strain rate is proportional to the applied stress. Basically it is distinguished between models, which represent material behaviour of solids and fluids. The difference is, that the solid reaches a final state of strain, when the stress is kept constant, while the strain of a fluid does not have an upper limit because of a dashpot, which is arranged in series. It might be stressed explicitly, that both kind of models are suitable to describe viscoelastic material behaviour. The use of the fluid model requires a time-limit though. The most important and simple representatives are the standard solid (3-parameter-model) and the so-called Burger-model (4-parameter fluid), which are shown in figure 2.2 and 2.3. With regard to the existence of an upper creep limit, as assumed in 2.2, which is required to determine a final deformation value, the primitive standard solid model proves to be suitable. More parameter solid models could certainly describe the development of creep deformation much more precisely, but for the determination of the final deformation the standard solid proves to be totally sufficient.

A further point of discussion in present research is the reversibility of creep. A possibly irreversible proportion of creep deformation is not covered by the standard solid model.

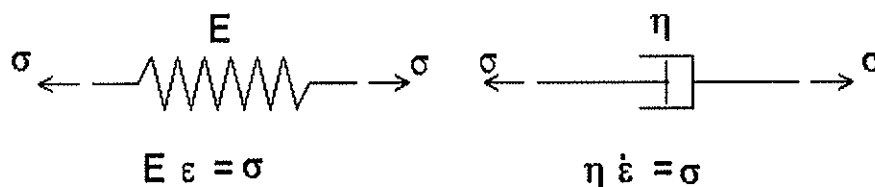


Fig. 2.1 Linear-elastic spring, viscous dashpot with material law

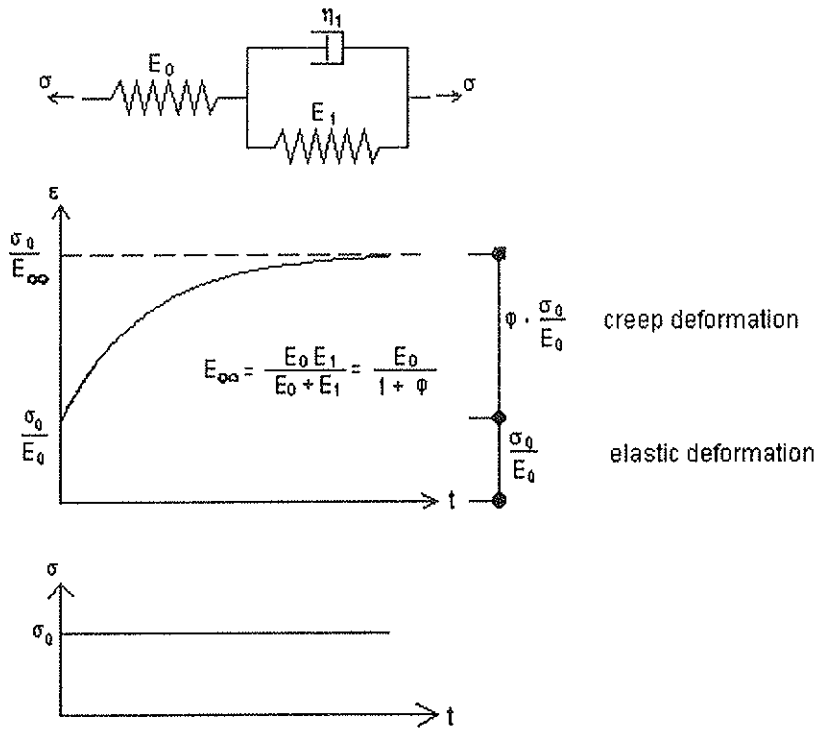


Fig. 2.2 Standard solid with time-deformation curve

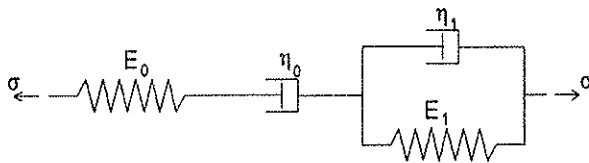


Fig. 2.3 Burger-model

2.5 Material parameter for the standard solid

The parameters E_0 and E_1 are given automatically via the Young's modulus and the creep factor (Fig. 2.2). So we are only short of the viscosity coefficient η_1 , which is not important for the final deformation. For certain approaches in chapter 4 and 5 it is of importance though, that the retardation time θ , which is defined by η_1/E_1 , is long compared to the duration time of variable loads. Considering dashpot constants, which have been published for the standard solid in earlier works (i.e. [4]), this requirement can be regarded as satisfied.

3 Application of linear viscoelasticity to columns

3.1 Solution of the standard solid differential equation for a compressive member

Material behaviour of the standard solid with the parameters given in figure 2.2 can be described by the following differential equation:

$$\sigma + \frac{\eta_1}{E_0 + E_1} \dot{\sigma} = \frac{E_0 \cdot E_1}{E_0 + E_1} \varepsilon + \frac{E_0 \eta_1}{E_0 + E_1} \dot{\varepsilon} \quad (3.1)$$

We assume, that the cross section remains plane (Bernoulli-hypothesis). So the strain ϵ can be substituted by the expression

$$\epsilon = \kappa \cdot z \approx -w'' \cdot z \quad (3.2)$$

All terms in (3.1) are now extended by z and integrated over the cross section A .

$$\int \sigma z dA + \frac{\eta_1}{E_0 + E_1} \int \dot{\sigma} z dA = -\frac{E_0 \cdot E_1}{E_0 + E_1} w'' \int z^2 dA - \frac{E_0 \eta_1}{E_0 + E_1} \dot{w}'' \int z^2 dA \quad (3.3)$$

Taking the relations

$$I = \int z^2 dA \quad , \quad M = \int \sigma z dA \quad \text{and} \quad E_\infty = \frac{E_0 \cdot E_1}{E_0 + E_1}$$

into account and expressing M by the compressive force F by

$$M = F \cdot w_0(x) + F \cdot w(x, t) \quad , \quad (3.4)$$

where w_0 represents the stress-free predeflection, we finally get the following expression:

$$E_\infty I \cdot w'' + \frac{\eta}{E_0 + E_1} E_0 I \cdot \dot{w}'' = -F(w_0 + w + \frac{\eta}{E_0 + E_1} \dot{w}) \quad (3.5)$$

As already mentioned in 2.2, the stress-free predeflection w_0 and the additional deflection w are assumed as sinusoidal.

$$w_0(x) = w_0 \sin \frac{\pi x}{L} \quad , \quad w(x, t) = w(t) \sin \frac{\pi x}{L} \quad (3.6)$$

Differentiating these expressions and substituting them into (3.5) yields

$$\frac{\eta}{E_0 + E_1} \left[E_0 I \left(\frac{\pi}{L} \right)^2 - F \right] \dot{w} + \left[E_\infty I \left(\frac{\pi}{L} \right)^2 - F \right] w = F \cdot w_0 \quad (3.7)$$

As initial condition of this differential equation the elastic solution can be used:

$$w(t=0) = \frac{F \cdot w_0}{E_0 I \left(\frac{\pi}{L} \right)^2 - F}$$

The solution of the inhomogeneous linear differential equation then results in

$$w(t) = \frac{F \cdot w_0}{E_\infty I \left(\frac{\pi}{L} \right)^2 - F} - \left(\frac{F \cdot w_0}{E_\infty I \left(\frac{\pi}{L} \right)^2 - F} - \frac{F \cdot w_0}{E_0 I \left(\frac{\pi}{L} \right)^2 - F} \right) e^{-\frac{E_\infty I \left(\frac{\pi}{L} \right)^2 - F}{E_0 I \left(\frac{\pi}{L} \right)^2 - F} \frac{E_0 + E_1}{\eta} t} \quad (3.8)$$

3.2 Interpretation and application of the result

At first the strain rate, which is obtained by differentiating with respect to time, is given by

$$\dot{w}(t) = C_1 \cdot e^{-\frac{E_\infty I \left(\frac{\pi}{L} \right)^2 - F}{E_0 I \left(\frac{\pi}{L} \right)^2 - F} C_2 \cdot t} \quad (3.9)$$

C_1 and C_2 are time-independent constants. It can be recognized, that the deformation rate decreases with deformation approaching a limit only if the exponent remains negativ, i.e. $F < E_{\infty}I (\pi/L)^2$. For $F = E_{\infty}I (\pi/L)^2$ the exponents becomes zero, so the deformation rate remains constant, for $F > E_{\infty}I (\pi/L)^2$ it increases. Considering viscoelastic material a state is practically defined as stable, if the deformation rate decreases for this reason. The unstable state is consequently characterized by an increasing deformation rate. Therefore the boundary value of long-term stability results in

$$F_{\infty} = E_{\infty}I \left(\frac{\pi}{L} \right)^2, \quad E_{\infty} = \frac{E_0}{1 + \varphi} \quad (3.10)$$

The short-term and long-term stability are therefore related as follows:

$$F_{\infty} = \frac{F_{ki}}{1 + \varphi} \quad (3.11)$$

The final deflection w_{∞} for $t = \infty$ ($F < F_{\infty}$) may be easily determined from (3.8):

$$w_{\infty} = \frac{F \cdot w_0}{F_{\infty} - F} \quad (3.12)$$

This result has to be interpreted as the sum of elastic and creep deflection.

$$w_{\infty} = w_{el} + w_{\varphi} \quad (3.13)$$

If the column is unloaded, the elastic part of the deformation vanishes immediately. The remaining deformation is then put together by the pre- and creep deformation. Therefore the elastic component of w_{∞} can also be determined by considering the creep deformation as an additional predeformation:

$$w_{el} = (w_0 + w_{\varphi}) \frac{F}{F_{ki} - F} \quad (3.14)$$

Substituting (3.14) in (3.13) an expression for w_{φ} is obtained.

$$w_{\varphi} = \frac{w_0 \cdot \varphi \cdot F}{F_{ki} - (1 + \varphi) \cdot F} \quad (3.15)$$

This creep deformation has to be understood as a final value, which is approached asymptotic for a permanent load $F < F_{\infty}$. By applying this creep deformation as an additional predeformation we are on the safe side as long as an appropriate creep factor φ is chosen. Dividing both deformation components for $t = \infty$ as it is already done by the definition of the normal force-free bending element (2.4), the quotient interestingly turns out to be φ again.

$$\frac{w_{\varphi}}{w_{el}} = \varphi \quad (3.16)$$

3.3 Determination of end-deflection considering only dead-load creep

The codes (e.g. the German code DIN 1052) are often based on the assumption, that it is sufficient to calculate the creep deformation from permanent loads only. The creep caused by variable loads is ignored. This point of view seems reasonable. The loads and deforma-

tions caused by permanent actions may now be indicated by the index g . Then the lateral creep deflection is computed using (3.15).

$$w_{g,\varphi} = \frac{w_0 \cdot \varphi \cdot F_g}{F_{ki} - (1 + \varphi) \cdot F_g} \quad (3.17)$$

For the determination of the maximum deflection the computed creep deflection is now assumed as an additional predeflection. The maximum deflection is determined by applying the maximum load F .

$$w_{\infty,\max} = (w_0 + w_{g,\varphi}) \frac{F}{F_{ki} - F} + w_{g,\varphi} \quad (3.18)$$

4 Including variable action

Even though the permanent acting loads should be mainly responsible for creep deformation, it is also influenced by snow, live and wind loads. Especially for columns this influence is increased by the effects of the theory of second order. Therefore the determination of creep deformation only because of dead loads is on the unsafe side. In literature two different suggestions can be found dealing with the computation of creep deformation of variable loads.

4.1 Replacing variable load by creep equivalent permanent load

The first method calls for the conversion of the variable load into a permanent load, which causes the same creep deformation. Carstensen [5] determined by “in-situ” deformation measurements in the region of Hannover/Germany and additional simulations, where he applied snow loads and durations in accordance to weather recordings to a building, from snow loads creep equivalent dead loads. According to Carstensen the creep deflection can be determined by assuming 1/15 of the snow load, which has to be applied according to the codes, as permanently acting. This result is probably applicable to most regions of Germany. For other regions creep equivalent dead loads could be derived in a similar way. This concept is only valid for bending beams though. The determination of creep deflections of columns yields results, which become too small because of the low dead load. It also turns out as problematic to record live loads this way. A corresponding research is not known to the authors.

4.2 Creep factors depending on the class of load duration

The concept of Eurocode 5 defines different creep factors for different actions depending on the load duration and service class. With these the determination of creep deflection for beams turns out to be very simple. During the computation of the elastic deflection it has to be distinguished between actions and multiplied with the corresponding creep factor. The deflection components can then be superpositioned.

Because we are dealing with different creep factors, the creep factor for a permanent load may be defined as φ_g . The creep factors for variable loads, which are smaller of course, shall be called φ_i for now.

If a variable load is applied for a certain time, the material behaviour corresponds to that under dead load for that time. So the creep factors for variable actions φ_i should only be seen as auxiliary values. The material law of the standard solid shall be valid regardless whether the load action is permanent or variable. The different end-deflections result from

the varying load durations. In order to determine these out of the different given creep factors, it is necessary to examine the creep deformation for a beam first.

In this matter it seems especially interesting, how long the variable load has to be applied, to cause the corresponding creep deflection. In figure 4.1 two time-periods are defined: The

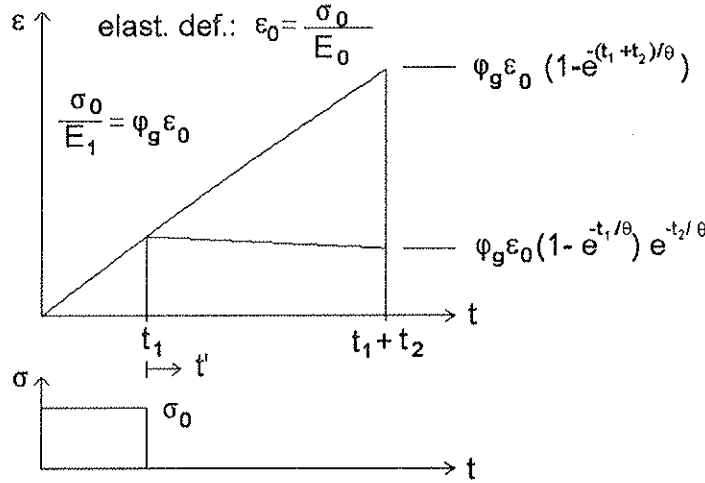


Fig. 4.1 Graph of a variable load during two time-periods

time-period $0 < t < t_1$, during which the variable load is applied, and the time-period $t_1 < t < t_1 + t_2$ with no load involved. Since we are especially interested in the creep deflection, we limit our consideration to the Kelvin-element, which represents the time-dependent behaviour in the standard solid model. The corresponding material law in the first time-period with the initial condition $\varepsilon(t=0) = 0$ reads

$$\varepsilon_1(t) = \varphi_g \varepsilon_0 (1 - e^{-t/\theta}) \quad (4.1)$$

with the elastic initial deformation ε_0 and the retardation time $\theta = \eta_1/E_1$. For the second time-period the initial condition $\varepsilon_2(t'=0) = \varepsilon_1(t_1)$ with $t' = t - t_1$ is valid. Therefore the following material law results:

$$\varepsilon_2(t') = \varphi_g \varepsilon_0 (1 - e^{-t'/\theta}) \cdot e^{-t_1/\theta} \quad (4.2)$$

For $t = t_1 + t_2$ a permanent action would cause the creep deformation $\varepsilon_1(t=t_1+t_2)$. Because of the variable action the creep deformation must become the φ_i/φ_g -time fraction of the creep deformation from dead load at the end of the second time-period. This is described by the following equation.

$$\frac{\varphi_i}{\varphi_g} \cdot \varepsilon_1(t = t_1 + t_2) = \varepsilon_2(t' = t_2) \quad (4.3)$$

Substituting (4.1) and (4.2) into (4.3) yields the relation between t_1 and t_2 .

$$t_1 = \theta \cdot \ln \left[\frac{\varphi_i}{\varphi_g} (e^{(t_1+t_2)/\theta} - 1) + 1 \right] \quad (4.4)$$

The quotient $t_1/(t_1+t_2)$ strongly depends on the accumulated duration of the characteristic action t_1+t_2 . For t_1+t_2 becoming smaller $t_1/(t_1+t_2)$ approaches the quotient φ_i/φ_g . Considering the actions snow (in regions without high snow loads for long durations) and wind in Germany the class of duration reads in the German NAD of the Eurocode as short-term, i.e. usually less than one week. According to the assumption of η_1 in 2.5 $t_1/(t_1+t_2)$ can be

approximately equated with the quotient φ_i/φ_g . Even for medium-term load durations this is also possible in a good approximation. We therefore can assume the following time-periods of load duration:

$$t_1 = \frac{\varphi_i}{\varphi_g} (t_1 + t_2) \quad , \quad t_2 = \frac{\varphi_g - \varphi_i}{\varphi_g} (t_1 + t_2) \quad (4.5)$$

The load-cycle may now be continued up to the lifetime of a building. But already few load-cycles show, that the quotient of creep deformation from variable and permanent load always results in φ_i/φ_g after each load-cycle (figure 4.2).

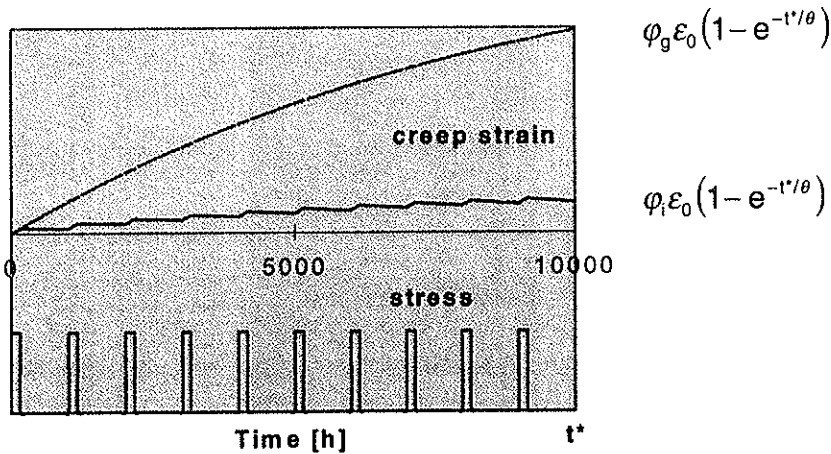


Fig. 4.2 Development of creep deformation of a beam caused by permanent and variable load

5 Creep deformation and stability considerations of columns with simultaneous action of permanent and variable loads

5.1 Lateral creep deflection for simultaneous action of permanent and variable compressive forces

The superposition of lateral creep deflection components from permanent and variable action becomes quite problematic. As an example a column may be mentioned, which receives normal forces from dead and snow load. Both create creep deflection. Even if the snow load is not acting, it leaves behind a creep deflection, which again leads to further creep deflection because of dead load. The creep deflections as a result of different actions influence each other. This results in two principle questions: What final deformation will appear and how does the limit for long-term stability F_∞ (3.11) change?

As already mentioned in 4.1 the applying of a creep equivalent dead load leads to results, which are on the unsafe side. We therefore make use of the results of the consideration in

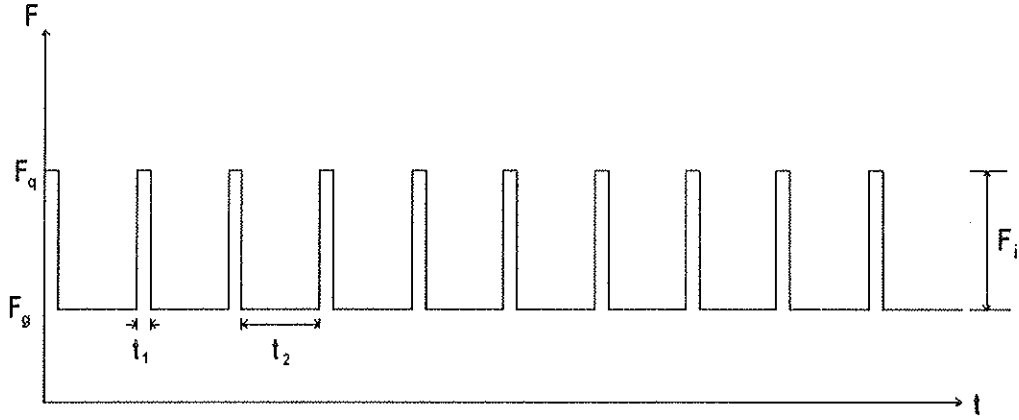


Fig. 5.1 Load history for combined acting by permanent (F_g) and variable load (F_i)

4.2 and apply the full variable load for the time period t_1 , for the other time period t_2 we apply non of it. The dead load is of course acting permanently (fig. 5.1). The creep deflection limit, which establishes under this load history, could now be determined by a computer simulation for example, in which the stress increase because of theory II. order is taken into consideration. Our objective is an analytical solution though, which puts the problem possibly into a simple formula easily useable for a structural engineer. Therefore we consider the problem stepwise as already done in 4.2. Again we are mainly interested in creep deflection, so only the deflection part of the Kelvin-element is reflected.

1. Time-period: In the first time-period the creep deflection is developing under maximum load comparable to a beam according to

$$w_{1\varphi}(t) = \varphi_g \cdot w_{el}(t) \cdot (1 - e^{-t/\theta}) \quad (5.1)$$

However the elastic deflection is not proportional to the applied load anymore, as it was for a beam. Considering theory II. order it now also depends on the creep deflection and therefore on the time in the following way.

$$w_{el}(t) = \left[w_0 + w_{1\varphi}(t) \right] \frac{F_q}{F_{ki} - F_q} \quad (5.2)$$

Substituting (5.2) in (5.1) yields the creep deflection $w_{1\varphi}$ of the time-period.

$$w_{1\varphi}(t) = \frac{w_0 \cdot \varphi_g \cdot F_q \cdot (1 - e^{-t/\theta})}{F_{ki} - F_q(1 + \varphi_g) + \varphi_g F_q e^{-t/\theta}} \quad (5.3)$$

The creep deflection at the end of the period is computed by substituting $t = t_1$ in (5.3).

2. Time-period: Now only the dead load is acting. The deflection from the end of the first time-period has to be taken over of course. So we obtain as initial condition

$$w_{2\varphi}(t' = 0) = w_{1\varphi}(t = t_1) \quad , \quad t' = t - t_1 \quad (5.4)$$

Considering the relation of creep and elastic deflection (5.2) gives us the following expression for creep deflection.

$$w_{2\varphi}(t') = \frac{w_0 \cdot \varphi_g \cdot F_q \cdot (1 - e^{-t'/\theta})}{F_{ki} - F_q(1 + \varphi_g) + \varphi_g F_q e^{-t'/\theta}} + \frac{w_0 \cdot \varphi_g \cdot F_q \cdot (1 - e^{-t_1/\theta})}{F_{ki} - F_q(1 + \varphi_g) + \varphi_g F_q e^{-t_1/\theta}} \cdot \frac{(F_{ki} - F_g) \cdot e^{-t'/\theta}}{F_{ki} - F_q(1 + \varphi_g) + \varphi_g F_q e^{-t'/\theta}}$$

(5.5)

This procedure can now be continued for an unlimited number of time-steps. Of course it is completely sufficient to continue until a constant final creep value is reached and a further load cycle doesn't lead to a deflection increase anymore.

After realization of further time-steps the following creep deflection is obtained after each unloading period (only dead load acting):

$$w_\varphi = w_0\varphi_g \left\{ \begin{aligned} & \sum_{i=1}^n F_q(1-e^{-t_1/\theta}) \cdot \frac{(F_{ki}-F_g)^i(F_{ki}-F_q)^{i-1}(e^{-t_1/\theta})^{i-1}(e^{-t_2/\theta})^i}{(F_{ki}-(1+\varphi_g)F_q+\varphi_g F_q e^{-t_1/\theta})^i(F_{ki}-(1+\varphi_g)F_g+\varphi_g F_g e^{-t_2/\theta})^i} \\ & + \sum_{i=1}^n F_g(1-e^{-t_2/\theta}) \cdot \frac{(F_{ki}-F_g)^{i-1}(F_{ki}-F_q)^{i-1}(e^{-t_1/\theta})^{i-1}(e^{-t_2/\theta})^{i-1}}{(F_{ki}-(1+\varphi_g)F_q+\varphi_g F_q e^{-t_1/\theta})^{i-1}(F_{ki}-(1+\varphi_g)F_g+\varphi_g F_g e^{-t_2/\theta})^i} \end{aligned} \right\} \quad (5.6)$$

The sum-parameter n stands for the number of load cycles. Each load cycle consists of two time-periods and is of duration t_1+t_2 . Expression (5.6) can be made more clearly, if the common expressions in both sums are factored out.

$$\frac{w_\varphi}{w_0\varphi_g} = \sum_{i=1}^n \left\{ \frac{(F_{ki}-F_q)(F_{ki}-F_g) \cdot e^{-(t_1+t_2)/\theta}}{(F_{ki}-(1+\varphi_g)F_q+\varphi_g F_q e^{-t_1/\theta})(F_{ki}-(1+\varphi_g)F_g+\varphi_g F_g e^{-t_2/\theta})} \right\}^{i-1} \cdot \left[\frac{F_q(1-e^{-t_1/\theta})(F_{ki}-F_g) \cdot e^{-t_2/\theta}}{(F_{ki}-(1+\varphi_g)F_q+\varphi_g F_q e^{-t_1/\theta})(F_{ki}-(1+\varphi_g)F_g+\varphi_g F_g e^{-t_2/\theta})} + \frac{F_g(1-e^{-t_2/\theta})}{F_{ki}-(1+\varphi_g)F_g+\varphi_g F_g e^{-t_2/\theta}} \right] \quad (5.7)$$

Let's consider this creep deflection in terms of stability first. The expression inside the braces, which we call "A" from now on, turns out to be crucial for the creep rate increasing, decreasing or remaining constant. For $A>1$ the term A^{i-1} becomes indefinite for a large number of load cycles. If A equals 1 the creep rate remains constant and only for $A<1$ the long-term stability is guaranteed. Simplification of A under consideration of the relations

$$\frac{1-e^{-t_1/\theta}}{1-e^{-(t_1+t_2)/\theta}} = \frac{t_1}{t_1+t_2} \quad \text{and} \quad \frac{1-e^{-t_2/\theta}}{1-e^{-(t_1+t_2)/\theta}} = \frac{t_2}{t_1+t_2} \quad , \quad (5.8)$$

which are valid for in comparison to lifetimes of buildings small t_1 and t_2 , simultaneous application of (4.5) und substitution of the maximum load F_q by the sum of the permanent component F_g and variable component F_i finally results in the now valid condition for the long-term stability.

$$(F_{ki}-F_g)(F_\infty-F_g)-F_i[(1+\varphi)F_\infty-F_g] > 0 \quad (5.9)$$

F_∞ still represents the limit of long-term stability for a dead load defined in (3.11).

For determination of the final creep deflection some additional simplifications are necessary concerning (5.7). The braced sum expression A in (5.7) can be replaced the following way.

$$\sum_{i=1}^n A^{i-1} = \frac{A^n - 1}{A - 1} = \frac{1}{1 - A} \quad \text{for } A < 1 \quad (5.10)$$

Applying these simplifications and using

$$e^{-t_1/\theta} \approx e^{-t_2/\theta} \approx 1 \quad (5.11)$$

the creep deflection can be finally expressed as follows:

$$w_\varphi = w_0 \cdot \frac{\varphi_g F_g + \varphi_l F_l - \varphi_g F_g (F_g + F_l) / F_{ki}}{F_{ki} - (2 + \varphi_g) F_g - (1 + \varphi_l) F_l + F_g (F_g + F_l) / F_\infty} \quad (5.12)$$

The formulas (5.9) and (5.12) seem to be simple enough to give a tool to the structural engineer, with which the deformation and stability behaviour of a timber column can be anticipated in a reliable way. If the stability criterion is satisfied, the denominator in (5.12) automatically becomes positiv.

A long-term simulation, which was done here with the same assumptions as a control of the derived formulas, yields the same results. A further possibility of control is obtained by considering the case $F_l = 0$. Only the dead load is acting then, so (5.9) and (5.12) should correspond to the formulas (3.11) and (3.15) derived in chapter 3. It can be easily certified that this is the case.

5.2 Creep deflection of columns loaded by permanent compressive force and a lateral continuous variable load in addition

As a further situation to examine we like to introduce a column, which receives a compressive force from dead load and additionally variable continuous load perpendicular to the column axxis from wind action. We again can assume, that the duration of wind load is short-term, so the problem can be based on short time-periods t_1 and t_2 according to (4.5). The creep factor for wind load is called φ_w .

1. Time-period: The wind is acting in its full size next to the dead load. At the beginning of the time period we have the initial condition $w_\varphi = 0$. The developing creep deflection can be written as (5.1):

$$w_{1\varphi}(t) = w_{1el}(t) \cdot \varphi_g \cdot (1 - e^{-t/\theta}) \quad (5.13)$$

While determining the elastic deflection under dead load F_g , the elastic part caused by wind load, which is time-independent, has to be considered.

$$w_{1el}(t) = \left[w_0 + w_{el,w} + w_{1\varphi}(t) \right] \frac{F_g}{F_{ki} - F_g} + w_{el,w} \quad (5.14)$$

Substituting (5.14) in (5.13) and solving for $w_{1\varphi}$ yields the creep deflection in the first time-period.

$$w_{1\varphi}(t) = \left[w_0 + w_{el,w} \frac{F_{ki}}{F_g} \right] \frac{\varphi_g F_g (1 - e^{-t/\theta})}{F_{ki} - F_g - \varphi_g F_g (1 - e^{-t/\theta})} \quad (5.15)$$

2. Time-period: The second time-period again starts with $t' = t - t_1 = 0$. Only the dead load F_g is acting. As initial condition the deflection at the end of the first time-period ($t = t_1$) is taken. The elastic deflection because of wind does not exist anymore. So the elastic deflection in the second time-period is calculated as follows:

$$w_{2el}(t') = (w_0 + w_{2\varphi}(t')) \frac{F_g}{F_{ki} - F_g} \quad (5.16)$$

Application of Kelvin-material, the initial condition and (5.16) gives us the creep deflection during the second time-period.

$$w_{2\varphi}(t') = w_0 \frac{\varphi_g F_g (1 - e^{-t'/\theta})}{F_{ki} - (1 + \varphi_g)F_g + \varphi_g F_g e^{-t'/\theta}} + \frac{(w_0 + w_{el,w} F_{ki} / F_g) \varphi_g F_g (F_{ki} - F_g) (1 - e^{-t_1/\theta})}{(F_{ki} - (1 + \varphi_g)F_g + \varphi_g F_g e^{-t_1/\theta}) (F_{ki} - (1 + \varphi_g)F_g + \varphi_g F_g e^{-t'/\theta})} e^{-t'/\theta} \quad (5.17)$$

Again it is possible to continue the time-steps until no further creep deflections appear and a constant creep deflection is obtained after each complete load-cycle. Continuing the time-steps the following expression is developing:

$$\frac{w_\varphi}{\varphi_g} = \sum_{i=1}^n \left\{ \frac{(F_{ki} - F_g)^2 \cdot e^{-t_1/\theta} \cdot e^{-t_2/\theta}}{(F_{ki} - (1 + \varphi_g)F_g + \varphi_g F_g e^{-t_1/\theta}) (F_{ki} - (1 + \varphi_g)F_g + \varphi_g F_g e^{-t_2/\theta})} \right\}^{i-1} \cdot F_g \left[\begin{aligned} & \left(w_0 + w_{el,w} \frac{F_{ki}}{F_g} \right) \frac{(F_{ki} - F_g) (1 - e^{-t_1/\theta}) \cdot e^{-t_2/\theta}}{(F_{ki} - (1 + \varphi_g)F_g + \varphi_g F_g e^{-t_1/\theta}) (F_{ki} - (1 + \varphi_g)F_g + \varphi_g F_g e^{-t_2/\theta})} \\ & + w_0 \frac{(1 - e^{-t_2/\theta})}{(F_{ki} - (1 + \varphi_g)F_g + \varphi_g F_g e^{-t_2/\theta})} \end{aligned} \right] \quad (5.18)$$

Again n represents the number of complete load cycles (t_1+t_2). As in (5.1) the creep deflection approaches only a limit, if the braced expression ("A") is smaller than one. Application of (4.5) and (5.8) results in the stability condition for the column.

$$(F_{ki} - F_g)(F_{ki} - (1 + \varphi_g)F_g) > 0 \quad (5.19)$$

This criterion is satisfied by $F_g < F_\infty$ and therefore corresponds to (3.10). So the lateral wind action has no influence on the long-term stability of timber columns. Additionally applying (5.10) and (5.11) to (5.18) leads to an useable expression for determining the final value of creep deflection.

$$w_\varphi = \left(w_0 + \frac{\varphi_w F_{ki}}{\varphi_g F_g} w_{el,w} \right) \frac{\varphi_g F_g}{F_{ki} - (1 + \varphi_g)F_g} \quad (5.20)$$

Again the results were confirmed by limit considerations and long-term simulations.

6 Conclusion

In this paper formulas are derived, which contribute to the determination of creep deflections of timber columns under permanent and variable loading. In addition stability aspects are considered. It has to be found out by some further discussion in which way the results should be included in the codes. A consequent application of the probabilistic design concept demands, that the conditions (5.9) and (5.19) are satisfied by the design values of material properties and actions including the creep factors. The prove according to the codes has to make sure, that not only the short-term load bearing capacity is guaranteed.

7 Literature

- (1) Blaß H.J. (1988) - Einfluß des Kriechens auf die Tragfähigkeit von Holzdruckstäben. Holz als Roh- und Werkstoff 46, 405-411.
- (2) Morlier P. (1994) - Creep in timber structures. RILEM Report 8, Chapman&Hall, 149 p.
- (3) Gressel P. (1983) - Erfassung, systematische Auswertung und Ergänzung bisheriger Untersuchungen über das rheologische Verhalten von Holzwerkstoffen - Ein Beitrag zur Verbesserung des Formänderungsnachweises. Bericht der Versuchsanstalt für Stahl, Holz und Steine, Abt. Ingenieurholzbau, Universität Karlsruhe.
- (4) Rautenstrauch K. (1989) - Untersuchungen zur Beurteilung des Kriechverhaltens von Holzbiegeträgern. Dissertation Universität Hannover.
- (5) Carstensen J. (1993) - Beiträge zum Biegekriechverhalten von Holzbauteilen unter bau-praktischen Bedingungen. Dissertation Universität Hannover.
- (6) Toratti T. (1996) - Verification of a creep limit from experiments in variable humidity subjected to five years of loading. Proceedings of the Int. Conf. on Wood Mechanics, Stuttgart, Germany.

INTERNATIONAL COUNCIL FOR BUILDING RESEARCH STUDIES AND DOCUMENTATION
WORKING COMMISSION W18 - TIMBER STRUCTURES

INFLUENCE OF VARYING GROWTH CHARACTERISTICS
ON STIFFNESS GRADING OF STRUCTURAL TIMBER

by

S Ormarsson

O Dahlblom

K Persson

Division of Structural Mechanics

Lund University, Lund

H Petersson

Department of Structural Mechanics,

Chalmers University of Technology, Göteborg,

SWEDEN

MEETING THIRTY-ONE

SAVONLINNA

FINLAND

AUGUST 1998

Influence of Varying Growth Characteristics on Stiffness Grading of Structural Timber

Ormarsson S.¹, Petersson, H.², Dahlblom O.¹, and Persson K.¹

¹ Division of Structural Mechanics, Lund University, Lund, Sweden

² Department of Structural Mechanics, Chalmers University of Technology, Göteborg, Sweden.

1 Introduction

The common practice in investigating stiffness and strength properties of sawn timber is to load the specimens and measure the deflection. The longitudinal modulus of elasticity (MOE) is obtained as some kind of average value, determined on the basis of elementary beam theory. This value is correlated to the strength of the board. The results obtained from measurements are strongly influenced by grain deviations with respect to the longitudinal direction and variation of material properties with the position in the log (often explained by juvenile wood and influence of compression wood). The value obtained from a measurement may therefore be regarded as an "effective modulus of elasticity". In addition to influence from fibre misalignment and property variation, the grading procedure is often disturbed by twist deformations of the board caused by spiral grain.

To improve the stiffness and strength grading process for sawn timber, it is important to clarify how the material properties and the internal structure affect the stiffness properties. In the prediction of timber stiffness, the fibre orientation, growth ring width distribution, juvenile wood and compression wood are of considerable importance. Because of the complex growth characteristics of wood and of various imperfections, the stiffness prediction may require computer simulations based on experimental data.

In the present study, finite element simulations have been performed to investigate how a number of basic parameters primarily affect the stiffness properties and indirectly the strength properties. Some preliminary results are also presented from an experimental investigation of basic material properties of spruce. The properties studied are stiffness and shrinkage parameters and grain deviations. The measurements have been carried out for stems from different stands. The specimens have been sawn at different distances from the pith and at different heights in the stem. The aim is to gain information about the variation of properties with the distance from the pith and with the height in the stem, and also about the influence from growth conditions on the properties examined.

2 Stiffness parameters to be determined

In Boström et al. 1996 and Johansson et al. 1996, different aspects of the determination of the longitudinal modulus of elasticity in bending are treated. The starting point is the

bending stiffness defined as $\int_{\Lambda} E_1(x,y)y^2 dA$ and the moment of inertia $I = \int_{\Lambda} y^2 dA$. The modulus $E_1 = E_1(x,y)$ is assumed to vary over the cross section, and the loading occurs in the y-z-plane with z as the longitudinal direction. An equivalent or apparent modulus of elasticity is defined as

$$E^* = \frac{1}{I} \int_{\Lambda} E_1(x,y)y^2 dA \quad (1)$$

The same type of definition was used both for edgewise and flatwise bending. Determination first at the E_1 -distribution over the cross section of the board followed by a calculation of E^* according to Eq. (1) gave almost the same values as bending tests for edgewise bending, while the calculated value was too large for flatwise bending, see Johansson et al. 1996. A somewhat more general discussion of the concept of apparent modulus of elasticity for bending may be needed when the modulus E_1 varies strongly over the cross section without one symmetric distribution. Let us study the cantilever beam in Figure 1, loaded in such a way that sectional forces N , M_x , M_y and T are constant over the length L . The associated displacement and rotations are denoted by n , m_x , m_y and φ . All properties are assumed to be constant in the longitudinal direction z , while the longitudinal modulus $E = E_1(x,y)$ varies over the cross section.

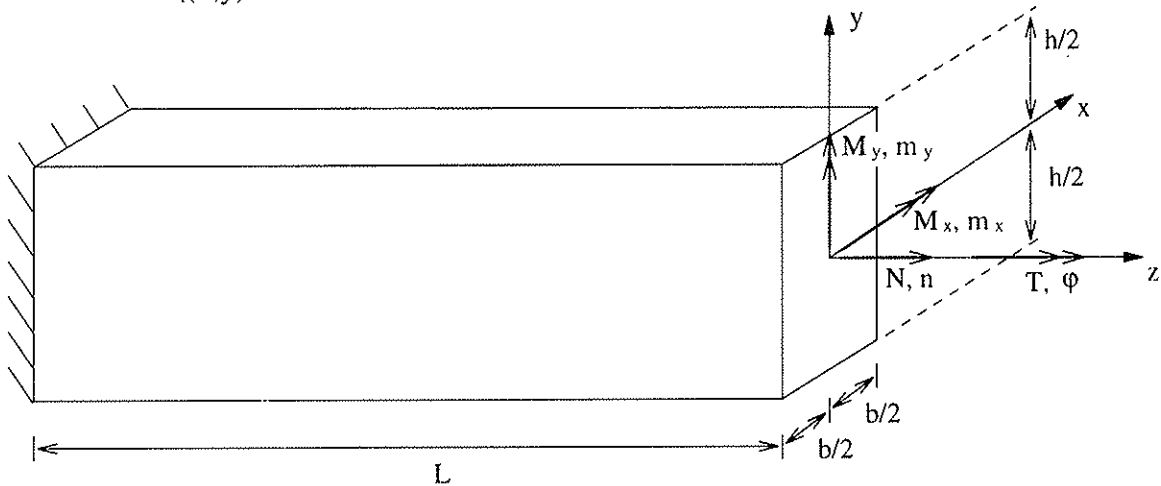


Figure 1. Cantilever beam with constant sectional forces N , M_x , M_y and T (and thus no shear forces V_x and V_y). The associated displacement variables are n , m_x , m_y and φ .

With reference to a longitudinal axis in the center of the cross section a stiffness formulation might be written in the form

$$\begin{bmatrix} \frac{\tilde{E}A}{L} & \bullet & \bullet & \bullet \\ \bullet & \frac{\tilde{E}I_y}{L} & \bullet & \bullet \\ \text{SYM} & \bullet & \frac{\tilde{E}I_x}{L} & \bullet \\ \bullet & \bullet & \bullet & \frac{\tilde{G}K_v}{L} \end{bmatrix} \begin{bmatrix} n \\ m_x \\ m_y \\ \varphi \end{bmatrix} = \begin{bmatrix} N \\ M_x \\ M_y \\ T \end{bmatrix} \quad (2)$$

with ten stiffness parameters to be defined. If for simplicity we neglect all coupling terms between the twisting moment T and the other sectional forces we may write

$$\begin{bmatrix} \frac{\bar{E}A}{L} & \bullet & \bullet & 0 \\ & \frac{\bar{E}I_y}{L} & \bullet & 0 \\ \text{SYM} & & \frac{\bar{E}I_x}{L} & 0 \\ & & & \frac{\bar{G}K_v}{L} \end{bmatrix} \begin{bmatrix} n \\ m_x \\ m_y \\ \varphi \end{bmatrix} = \begin{bmatrix} N \\ M_x \\ M_y \\ T \end{bmatrix} \quad (3)$$

The three first equations of Eq (3) may be written as

$$\left(\frac{1}{L} \int_A E_1(x, y) \begin{bmatrix} 1 & y & x \\ y & y^2 & xy \\ x & xy & x^2 \end{bmatrix} dA\right) \begin{bmatrix} n \\ m_x \\ m_y \end{bmatrix} = \begin{bmatrix} N \\ M_x \\ M_y \end{bmatrix} \quad (4)$$

where E_1 is the longitudinal modulus at elasticity and A is the area of the cross section. By choosing another location (x_0, y_0) of the reference axis and referring to the principal directions \bar{x} and \bar{y} instead of x and y we get the uncoupled relations

$$\left(\frac{1}{L} \int_A E_1 \begin{bmatrix} 1 & 0 & 0 \\ 0 & \bar{y}^2 & 0 \\ 0 & 0 & \bar{x}^2 \end{bmatrix} dA\right) \begin{bmatrix} \bar{n} \\ \bar{m}_x \\ \bar{m}_y \end{bmatrix} = \begin{bmatrix} \bar{N} \\ \bar{M}_x \\ \bar{M}_y \end{bmatrix} \quad (5)$$

The new reference system is illustrated in Figure 2.

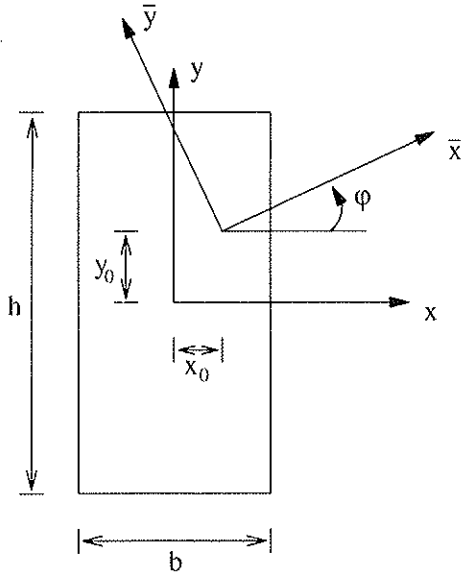


Figure 2. Reference system for uncoupled relations.

In cases where bending only occurs in the y-direction and there is no twist, we may write according to Eq. (4)

$$\left(\frac{1}{L} \int_{\Lambda} E_1(x, y) \begin{bmatrix} 1 & y \\ y & y^2 \end{bmatrix} dA\right) \begin{bmatrix} n \\ m_x \end{bmatrix} = \begin{bmatrix} N \\ M_x \end{bmatrix} \quad (6)$$

If we instead refer to a reference axis located at $\bar{y} = y - y_0$ we get the uncoupled relation ($n = \bar{n} - y_0 m_x$)

$$\left(\frac{1}{L} \int_{\Lambda} E_1 \begin{bmatrix} 1 & 0 \\ 0 & \bar{y}^2 \end{bmatrix} dA\right) \begin{bmatrix} \bar{n} \\ m_x \end{bmatrix} = \frac{1}{L} \begin{bmatrix} \overline{EA} & 0 \\ 0 & \overline{EI} \end{bmatrix} \begin{bmatrix} \bar{n} \\ m_x \end{bmatrix} = \begin{bmatrix} N \\ M_x - y_0 N \end{bmatrix} \quad (7)$$

where

$$y_0 = \frac{\int_{\Lambda} E_1 y dA}{\int_{\Lambda} E_1 dA} \quad (8)$$

$$\overline{EA} = \int_{\Lambda} E_1 dA \quad (9)$$

and

$$\overline{EI} = \int_{\Lambda} E_1 y^2 dA - y_0^2 \overline{EA} \quad (10)$$

For the uncoupled system of equations in Eq. (7) the concept of a single apparent modulus may conveniently be applied for tension and bending, respectively, but not for the more general case. We may for a case of plane bending without any twist write

$$E_{\text{tension}}^* = \frac{\overline{EA}}{bh} \quad (11)$$

according to Eq. (9) and

$$E_{\text{bending}}^* = \frac{12 \overline{EI}}{bh^3} \quad (12)$$

according to Eq. (10).

In a more general case but with negligible twisting deformations, the normal and bending stiffnesses to be calculated are according to Eq. (4)

$$\int_A E_l(x,y) \begin{bmatrix} 1 & y & x \\ y & y^2 & xy \\ x & xy & x^2 \end{bmatrix} dA \quad (13)$$

The distribution of the longitudinal modulus of elasticity $E_l=E_l(x,y)$ over the cross section of the boards to be graded thus plays an essential role. In the following sections some results of measurements on spruce will therefore be presented with respect to the variation in space of E_l .

3 Variation of longitudinal modulus of elasticity

3.1 Introductory example

For simulations of stress-induced deformations in timber, a relevant description of the material parameters is very important, especially with respect to the longitudinal elasticity modulus and the spiral grain angle. These parameters strongly depend on growth characteristics and vary in space. In this section only some representative examples are selected to illustrate how the properties may vary from pith to bark in the radial direction, neglecting the variation in the longitudinal direction. A cross section of a board is shown in Fig. 3 (a). The conifer studied is spruce (*Picea abies*) with varying annual ring width. The associated distribution of the density over the cross section is given in Fig. 3 (b).

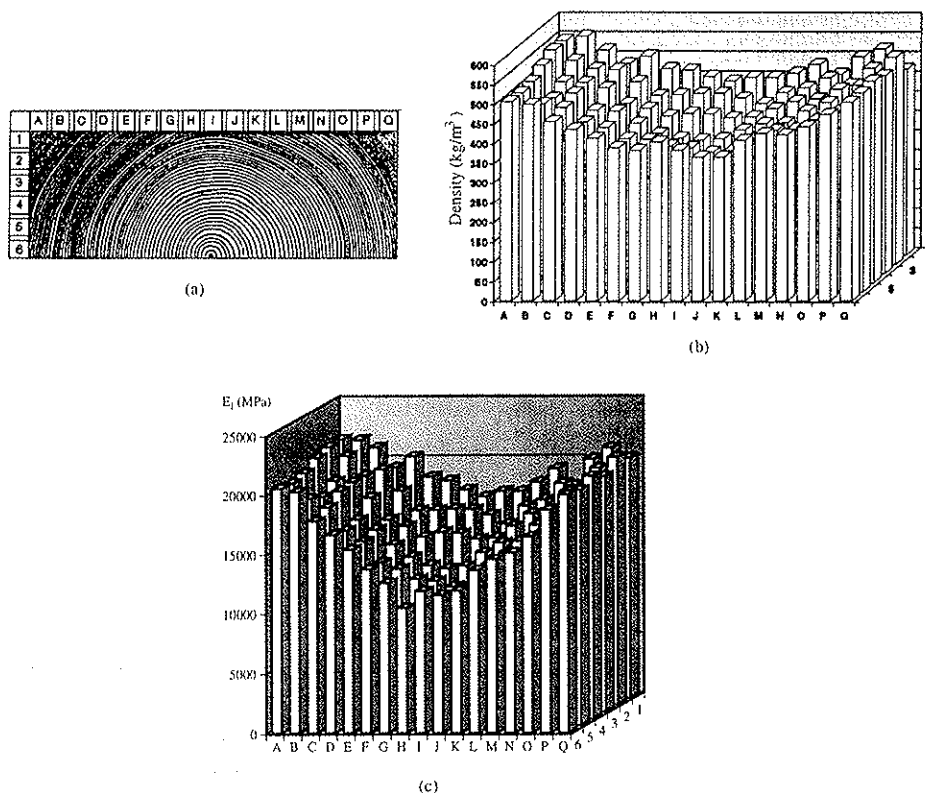
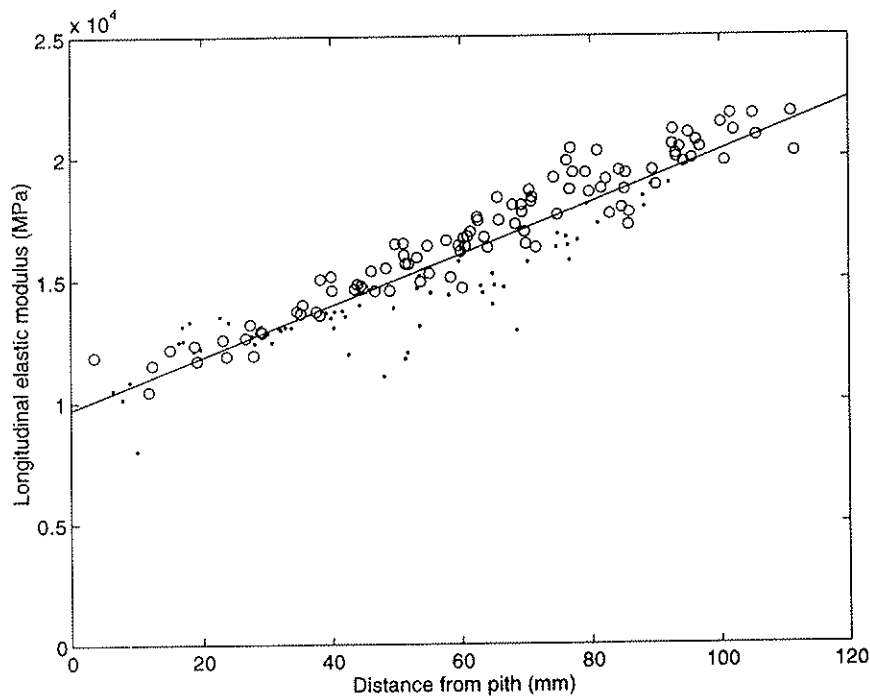
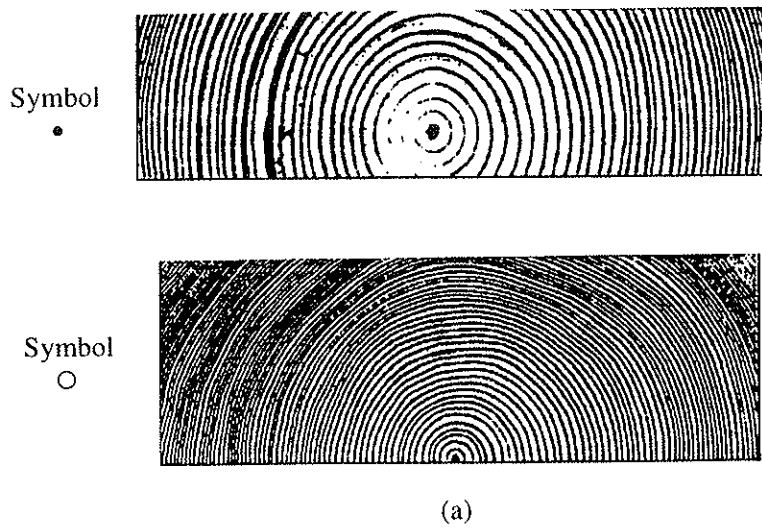


Figure 3. Property distributions over a cross section of a board.

- (a) Cross section
- (b) Density
- (c) Longitudinal elastic modulus, Wormuth (1993)



(b)
 Figure 4. Influence of distance from pith on longitudinal elastic modulus E_l .
 (a) Symbols for tested specimens.
 (b) E_l as a function of distance from pith.

A corresponding distribution of the longitudinal elastic modulus is illustrated in Fig. 3(c) and this distribution refers to the cross section in Fig. 3(a). The highest value of the elastic modulus is about twice as large as the lowest value. In Fig. 4(b) the values of Fig. 3(c), together with the values of another board shown in Fig. 4(a), are shown as a function of the distance from the pith. It can be observed that the distance from the pith has a very strong influence on the elastic modulus in the longitudinal direction. The relation between distance from pith and longitudinal elastic modulus for the two cross sections shown, can with good agreement be represented as $E_l = 9.7 \cdot 10^3 + 1.0 \cdot 10^5 r/r_r$ MPa, with $r_r = 1.0$ m. This relation is also shown in Fig. 4(b).

3.2 Boards with much compression wood

In one study (Ormarsson et al. 1998b) a number of boards with much compression wood and fibre misalignment were investigated. The measured parameters were density, spiral grain, conical shape, longitudinal modulus of elasticity and some shrinkage/swelling parameters. The boards were originally about 3000 mm long, and the size of the cross section was 120x48 mm. Special measurements on small specimens were made for the end regions of each board according to Fig. 5.

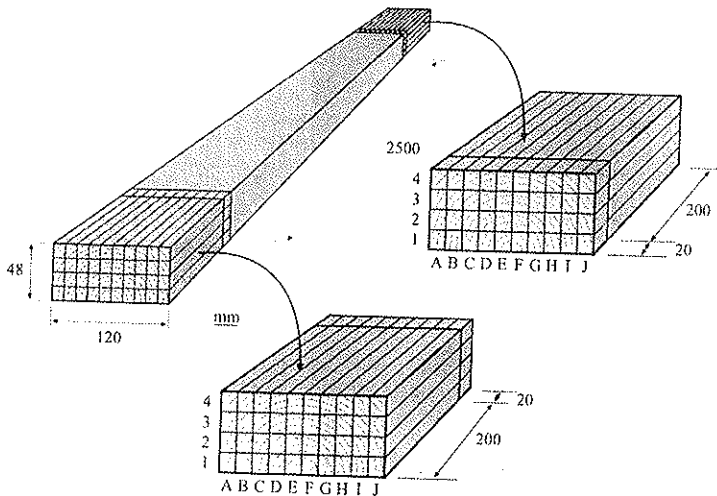


Figure 5. Geometry of the studs and small size specimens.

In Figures 6 and 7 the measured results for two boards from the same log are presented with respect to the density and the longitudinal modulus of elasticity E_l . The results show that very low values of E_l are obtained in case of compression wood, while the corresponding high density values indicate the opposite.

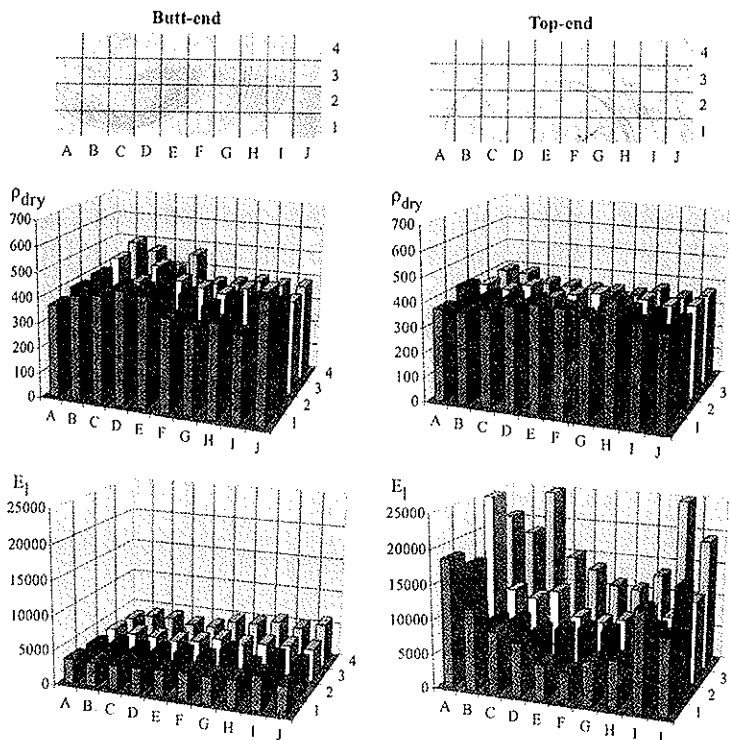


Figure 6. Distribution of density, and longitudinal elastic modulus for the board 27N.

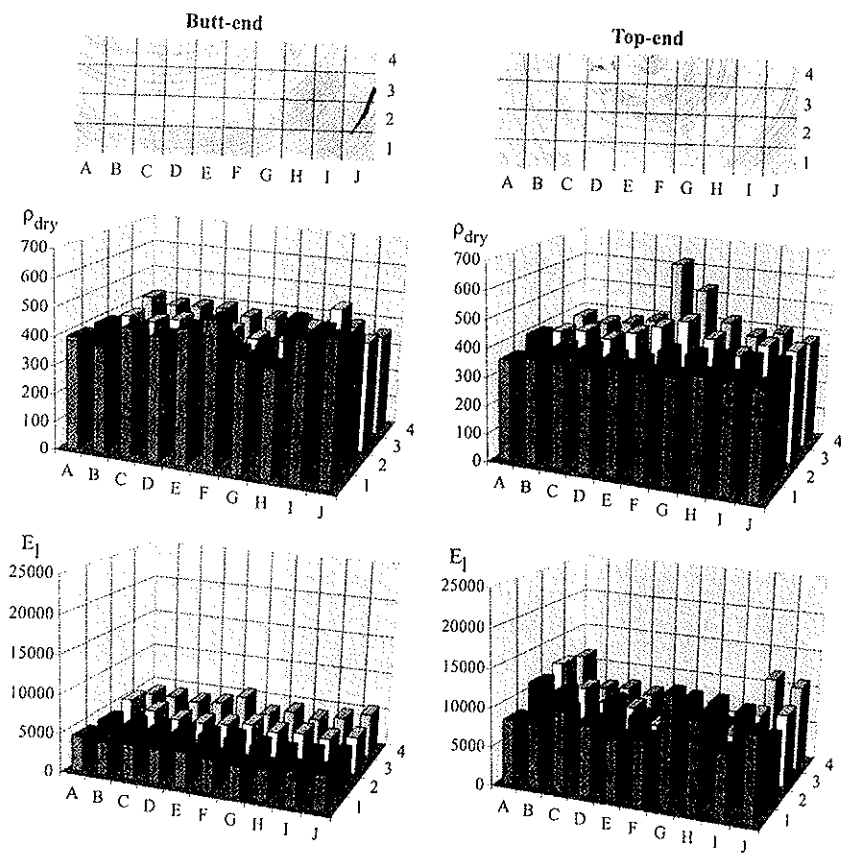


Figure 7. Distribution of density and longitudinal elastic modulus for the board 27U.

3.3 Spatial variations in trees of different social classes

Specimens from a total of 11 trees (Norway spruce) were sampled at four different sites of differing site quality classes in southern Sweden (Persson 1997). The height, type of crown, social class and individual position were determined for each of the standing trees. At each plot, samples were obtained from trees belonging to each of the social classes dominant, co-dominant and dominated, except for one plot where no dominated tree was found. Two discs were cut at three different heights from each tree as shown in Figure 8. Specimens for mechanical testing were taken from the discs labelled A and specimens for the experiments at the microstructural level from the discs labelled B.

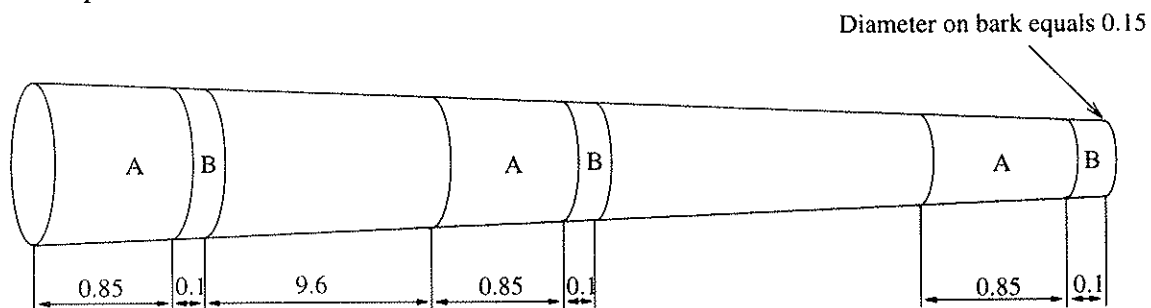


Figure 8. Cutting scheme for the stem. The discs labelled A were used for mechanical testing and the discs labelled B for microstructural measurements.

Specimens for clear-wood testing were taken from the discs labelled A in Figure 8. Specimens having a length of 300 mm and a cross section area of 10 by 10 mm were cut from north to south from all discs, Figure 9. Additional specimens were cut from some discs in a crossing pattern from east to west. For one of the trees the specimens were taken from eight different diameters that crossed each other at successive angles of 45 degrees. A total of about 700 specimens were used in the testing. The longitudinal modulus of elasticity, the coefficients of moisture induced shrinkage in the three main directions, and the density were determined. For each of the specimens, the angle between the fibre direction and the main longitudinal direction of the specimens was also measured. It was concluded that for most of the specimens this angle was less than 5 degrees and in most cases less than 2 degrees. The fibre deviation will therefore be neglected in the following presentation of results.

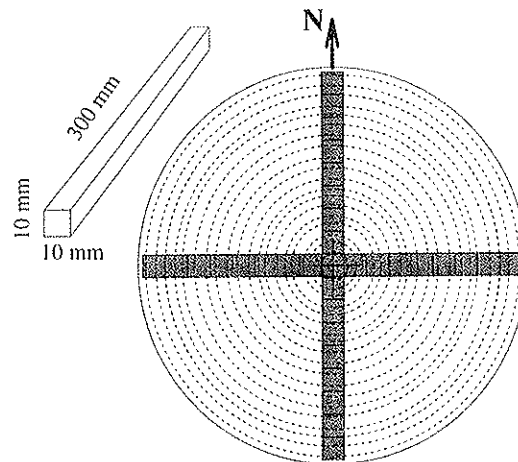


Figure 9. Cutting scheme and specimen used for clear-wood testing.

3.4 Density

Density measurements of 40 mm long samples cut from one end of the specimens shown in Figure 9 were made. This allows the average density and the longitudinal modulus of elasticity to be related to each other directly. The density measurements presented here relate to the dry weight divided by the volume in a dry condition. In Figure 10 the density measurements are shown from pith to bark for all trees and at all studied heights.

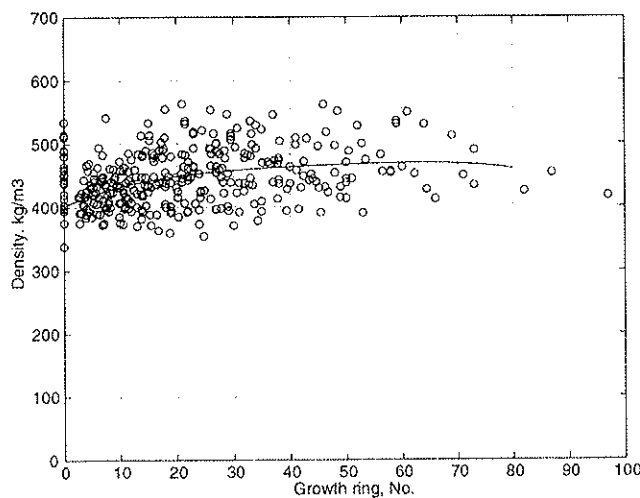


Figure 10. Density versus growth ring number for all the trees at all the three heights studied.

In the juvenile wood the density was low, increasing towards the bark. In most of the trees the local density in the pith seemed to be higher than in the surrounding wood. Since for many of the discs the density was found to decrease very abruptly just outside the pith, measurements for the pith specimen are excluded from the least square fits of density in Figure 10, resulting in a smoother fitting curve.

3.5 Stiffness properties

The longitudinal moduli of elasticity were determined for the specimens, see Figure 9, by applying a tensional load using an MTS testing machine. The force applied was measured by a load cell, whereas the displacements were determined by two 40 mm long strain gauges at the midpoint of the specimens. By using two strain gauges at opposite sides of the specimen, the strains due to curvature of the specimen were eliminated. The strains were determined from the mean elongation of the two strain gauges divided by the initial gauge length. The stresses were calculated as the applied load divided by the initial cross-sectional area of specimens. The moduli of elasticity were determined from the obtained stress-strain curves by determining the slope at the linear part of the curves. Prior to testing, the specimens were conditioned at 65% RH and 20⁰ C for about two weeks.

The results of the measurements indicate that the stiffness properties are strongly dependent upon the position in the stem, especially with respect to the radial direction. The stiffness is very low in the juvenile part but increases towards the bark. A stiffness up to four times as great was observed in the mature wood near the bark as in the juvenile wood. Since the differences in stiffness between the south and north directions were not found to be significant, the distinction concerning the side of the tree from which the specimens were sampled is neglected in the following, and only the distance from pith expressed by the growth ring number will be considered.

Figure 11 shows the longitudinal modulus of elasticity versus the growth ring number for different social classes together with fitted curves. For all three social classes, the modulus of elasticity is about 6000 MPa close to the pith. The increase along the radius from pith to bark for the co-dominant and dominated tree is similar, but the increase is less in the dominant trees. For the dominant trees there is a decrease of stiffness for higher growth ring numbers, but this result is probably due to the smaller amount of data obtained for this class.

Figure 12 shows the longitudinal modulus of elasticity versus the growth ring number for all trees for the three different heights together with fitted curves. For each of the heights, the stiffness is low near the pith and then increases towards the bark. The longitudinal modulus of elasticity is lower for the specimens taken from the bottom disc than for those taken from the middle and upper discs.

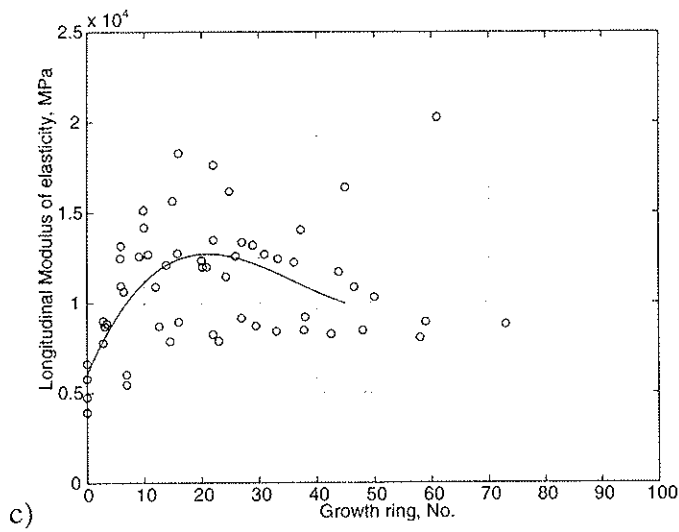
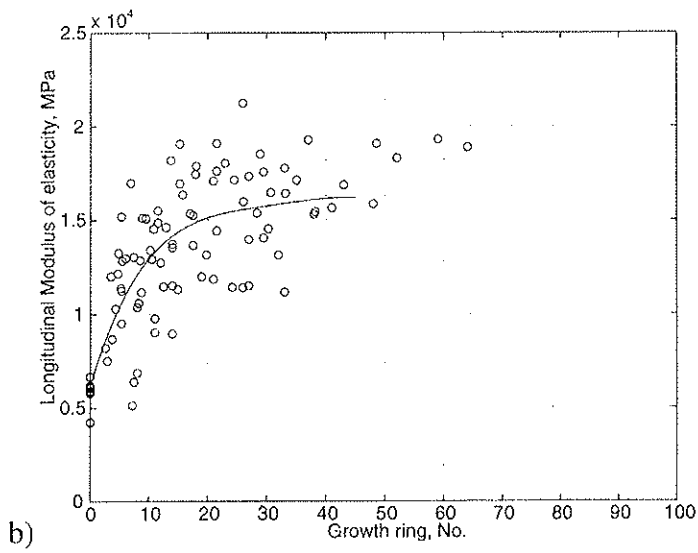
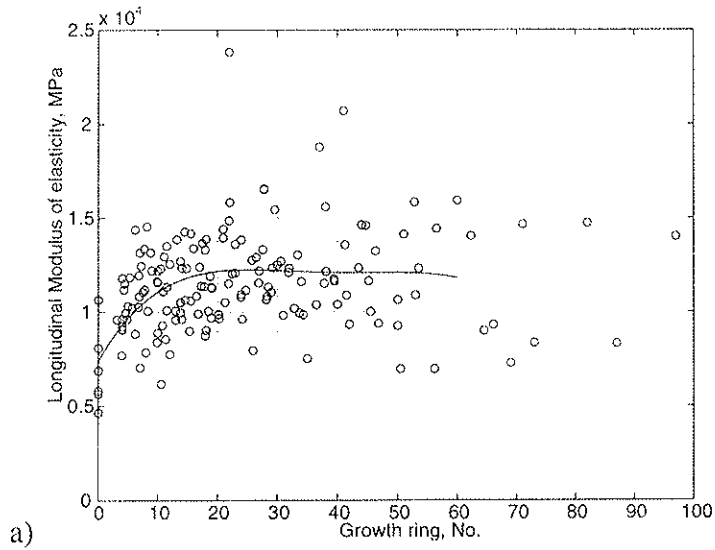


Figure 11. Longitudinal modulus of elasticity versus ring number for the different social classes. a) Dominant trees. b) Co-dominant trees. c) Dominated trees.

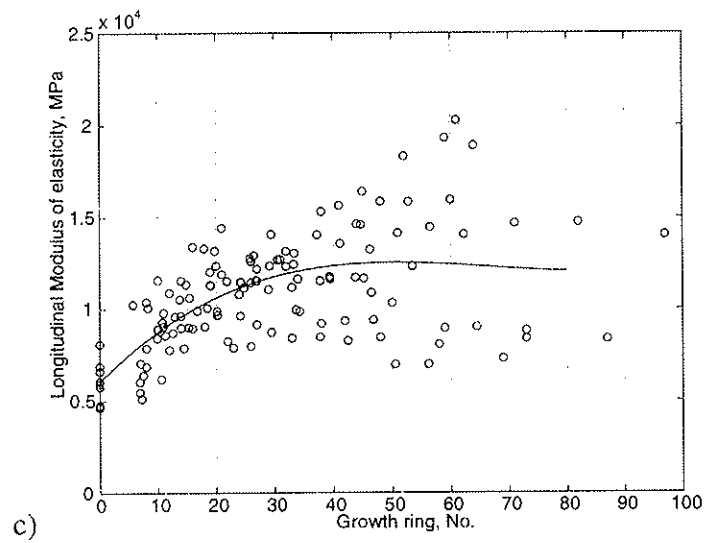
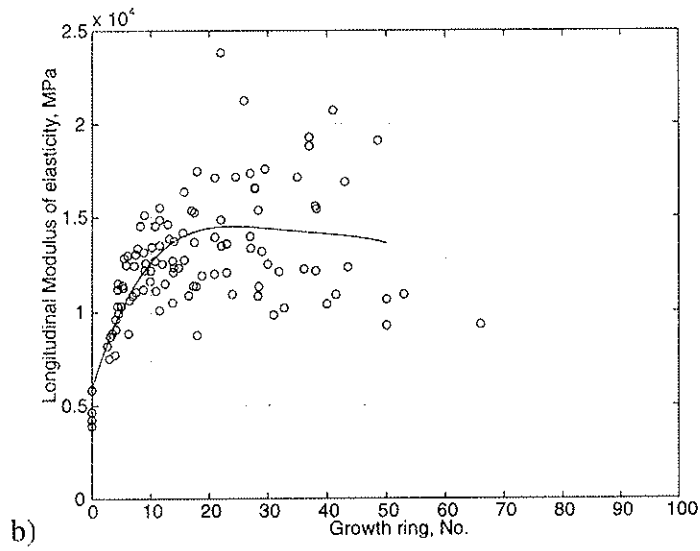
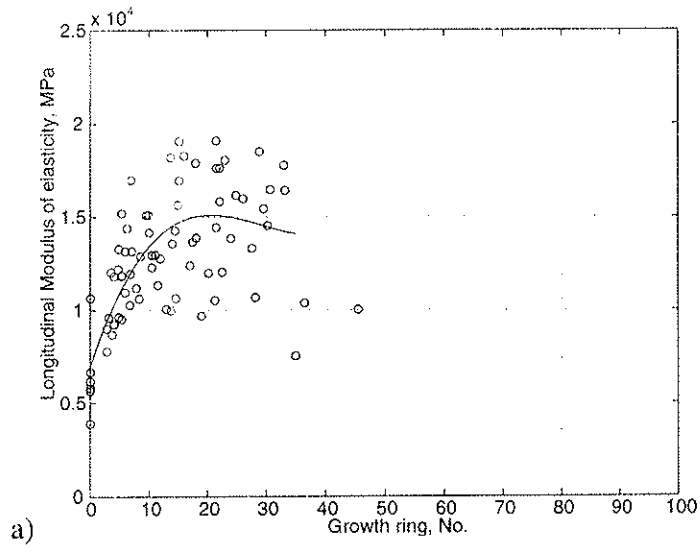


Figure 12. Longitudinal modulus of elasticity versus ring number at the three different heights. a) Top disc. b) Middle disc. c) Bottom disc.

4 Influence on stiffness of spiral grain and annual ring curvature

The fibre structure of wood makes the material properties strongly direction dependent. The fibre direction often deviates from the longitudinal direction of a studied tree and a studied board. This fibre deviation can be local effects around knots, but this type of local deviation was not of primary interest in this investigation which was focussed on fibre misalignments like spiral grain angle and conical angle. Spiral grain means that the fibres are oriented in a spiral manner in the log, see Fig 13. In addition to this, the fibres may have inclination due to the conical shape of the wooden stem. Such types of grain deviation may have a large influence on the properties of sawn timber.

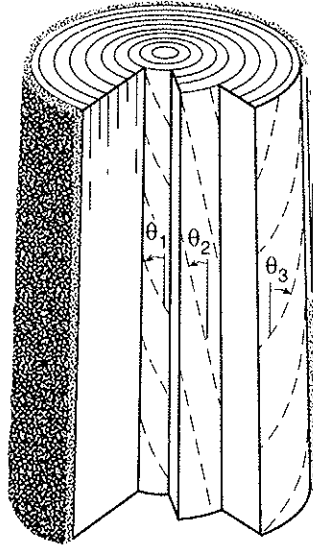


Figure 13. Illustration of spiral grain angle.

4.1 Equivalent modulus of elasticity

In order to describe the influence of spiral grain and ring curvature on the stiffnesses of a board, some of the formulations in Section 2 may be recalled. The stiffness formulations according to Eq. (2) may be rewritten as

$$\begin{bmatrix} S_{11} & S_{12} & S_{13} & S_{14} \\ S_{21} & S_{22} & S_{23} & S_{24} \\ S_{31} & S_{32} & S_{33} & S_{34} \\ S_{41} & S_{42} & S_{43} & S_{44} \end{bmatrix} \begin{bmatrix} n \\ m_x \\ m_y \\ \varphi \end{bmatrix} = \begin{bmatrix} N \\ M_x \\ M_y \\ T \end{bmatrix} \quad (13)$$

where $S_{ij} = S_{ji}$.

The stiffness parameters S_{ij} can be determined by studying four cases in which either the displacement variables or the associated forces are prescribed. Mixed combinations of prescribed quantities are also possible. In this paper the following four mixed cases are chosen.

	Case 1	Case 2	Case 3	Case 4
Prescribed	$n_1, m_{x1}=0, m_{y1}=0, T_1=0$	$n_2=0, m_{x2}, m_{y2}=0, T_2=0$	$n_3=0, m_{x3}=0, m_{y3}, T_3=0$	$N_4=0, M_{x4}=M_{y4}=0, \varphi_4$
Calculated	$N_1, M_{x1}, M_{y1}, \varphi_1$	$N_2, M_{x2}, M_{y2}, \varphi_2$	$N_3, M_{x3}, M_{y3}, \varphi_3$	n_4, m_{x4}, m_{y4}, T_4

This choice may be questioned, but has the advantage that the diagonal stiffnesses corresponding to tensioning and bending can be expressed simply as

$$S_{11} = \frac{N_1}{n_1} + \left(\frac{\varphi_1}{n_1} \right)^2 S_{44} \quad (14a)$$

$$S_{22} = \frac{M_{x2}}{m_{x2}} + \left(\frac{\varphi_2}{m_{x2}} \right)^2 S_{44} \quad (14b)$$

$$S_{33} = \frac{M_{y3}}{m_{y3}} + \left(\frac{\varphi_3}{m_{y3}} \right)^2 S_{44} \quad (14c)$$

and in most cases the influence of twist expressed by the rotation φ on S_{11} , S_{22} and S_{33} might be negligible. By accepting this we may introduce the following apparent moduli for the longitudinal stiffness (choosing our reference system in such a way that S_{12} , S_{13} and S_{23} are zero).

Effective MOE in tension.

$$E_{\text{equivalent}}^{\text{tension}} = \frac{N_1 L}{A n_1} \quad (15a)$$

where L is the length and A the area.
Effective MOE in edgewise bending

$$E_{\text{equivalent}}^{\text{bending edgewise}} = \frac{M_{x2} L}{I_y m_{x2}} \quad (15b)$$

where I_y is the moment of inertia for edgewise bending. Similarly, for flatwise bending we get

$$E_{\text{equivalent}}^{\text{bending flatwise}} = \frac{M_{y3} L}{I_x m_{y3}} \quad (15c)$$

These notations of affective MOE will be used in the following subsections.

4.2 Numerical simulations

The influence of spiral grain on tension, bending and torsional stiffness in sawn timber will be considered in the following, and some results from numerical simulations by FEM will be presented. The influence of varying stiffness parameters and the annual ring curvature is also investigated. The boards studied are 1.5 m long and 100 x 50 mm in cross section, and the pith is assumed to be parallel to the longitudinal direction of the board. The knowledge obtained can be used to show which of the material parameters are of importance for the stiffness grading process.

In Table 1.1 the material parameters used are shown. They are assumed to be representative for spruce (*Picea abies*). In order to eliminate the influence of radial variations of the material parameters and of the spiral grain angle on the effective timber stiffness, the parameters in this section are assumed to have a constant distribution over the cross section of the board.

Table 1.1 Material parameters used in the simulation.

Elastic strain parameters	$E_l = 9700$ MPa	$E_r = 400$ MPa	$E_t = 220$ MPa
	$G_{lr} = 400$ MPa	$G_{lt} = 250$ MPa	$G_{rt} = 25$ MPa
	$\nu_{lr} = 0.35$	$\nu_{lt} = 0.6$	$\nu_{rt} = 0.55$

4.3 Effective MOE in tension

To investigate the relationship between spiral grain angle and effective modulus of elasticity (MOE) in tension, a number of boards with different values of the spiral grain angle were studied. In the simulations the nodal displacements at the end cross sections of the boards were prescribed to a constant value in the longitudinal direction in order to obtain tensional stresses in the same direction. Three degrees of freedom at the mid-section of the board were prescribed to zero to avoid rigid body motions in the transversal directions of the board.

In Fig. 14 the influence of spiral grain angle on effective MOE in tension is shown for five boards with different distance from pith and thus different annual ring curvature. The results show that the MOE decreases rapidly with increasing spiral grain angle. It has been experimentally shown by (Dahlblom et al.) and (Harris) that the magnitude of the spiral grain angle normally varies between zero and say five degrees for Norway and Sitka spruce. For boards with spiral grain angle of about four degrees the effective MOE is 15% lower than for boards without spiral grain. In Fig 14 it is also indicated that a large annual ring curvature, corresponding to a small distance from pith, has an influence on MOE.

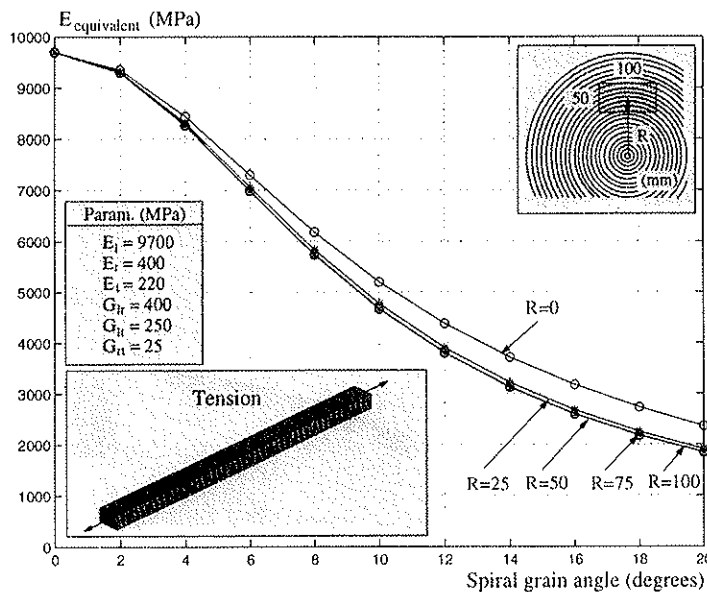


Figure 14 Influence of spiral grain angle on effective MOE in tension.

In order to study how some of the stiffness parameters affect the effective MOE in tension, a number of boards with different stiffness parameters were calculated for different spiral grain angles. In Fig. 15 is shown the influence on MOE of doubling one stiffness parameter at a time while the other stiffness parameters have the same values as in the reference case. The results show that only the two parameters E_l and G_{lt} have a substantial influence on the tension stiffness for the studied case of pith location. For a board without spiral grain the MOE increases as much as the longitudinal elastic modulus E_l . The curve $E_l = 2E_l^{ref}$ decreases much more rapidly than the reference curve. A board with spiral grain angle of about four degrees has 25% lower MOE than a board without spiral grain. It may be concluded that tension stiffness for boards with high ratios E_l/E_t are more sensitive to spiral grain deviation than boards with lower ratios.

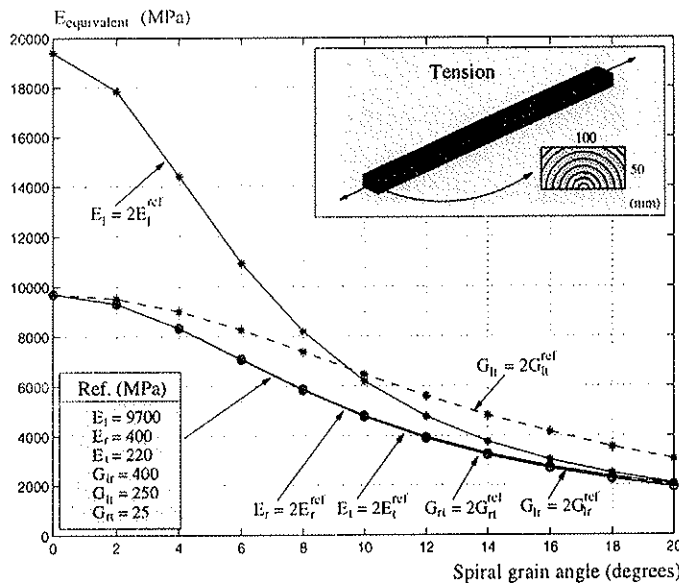


Figure 15. Influence of stiffness parameters on MOE in tension.

4.4 Effective MOE in bending

In this subsection some numerical simulations for predication of effective MOE in bending are presented. The influence of spiral grain angle and material parameters on effective MOE in bending is studied. Flatwise and edgewise bending are both regarded. In Fig. 16 the element mesh and prescribed nodal displacements in flatwise and edgewise bending are indicated. The board end surfaces are rotated by prescribing displacements on these surfaces.

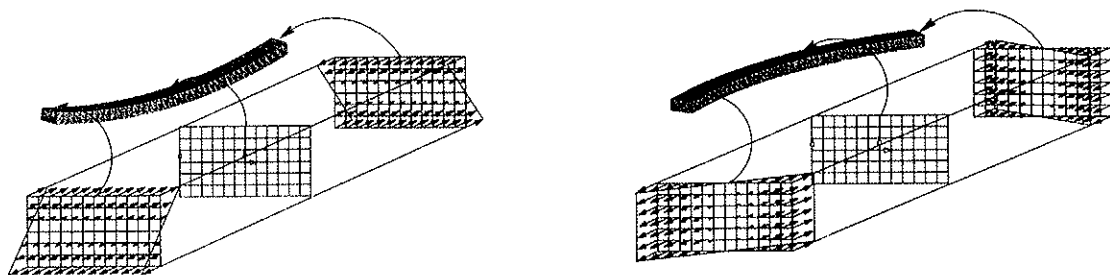


Figure 16. Prescribed displacements in numerical simulations.

- (a) Flatwise bending
- (b) Edgewise bending

The relationship between the spiral grain angle and the effective MOE in bending is shown in Fig 17. These results show very similar behaviour as was observed for tension loading. However, the distance from pith influencing the annual ring curvature has more influence on MOE in bending than in tension.

In Fig. 18 the influence of stiffness parameters on MOE in flat-ways bending is shown. As for tension loading, the parameters E_t and G_{lt} have a large influence on the MOE. The shear modulus G_{lr} has also some influence on the MOE.

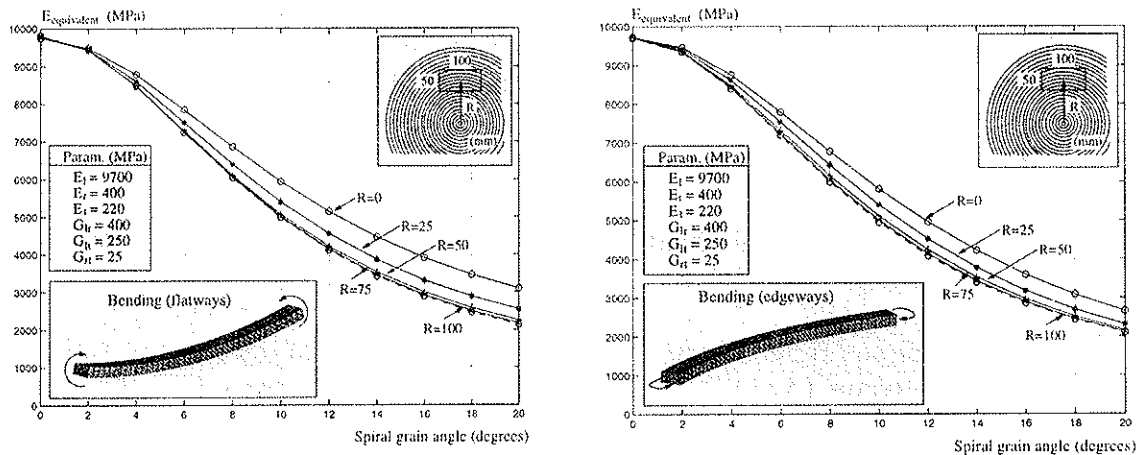


Figure 17. Influence of spiral grain angle on effective MOE
 (a) Flatwise bending
 (b) Edgewise bending

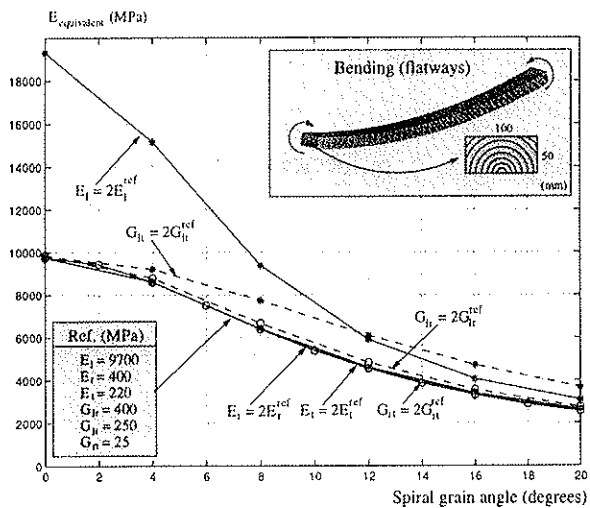


Figure 18. Influence of stiffness parameters on MOE in bending.

5 Some concluding remarks

The choice of proper stiffness parameters to be used in structural grading of timber is by no means a simple matter. Usually the coupling effects between tension, bending in two directions and twist are neglected. This may lead to a much too crude approach for grading of high quality timber and in the structural analysis of beam structures.

Due to strongly varying material properties, especially from pith to bark, it is often of great importance for the grading where in the log the sawn board comes from. This is today normally not considered in practice. The sawing pattern influences the positions of the boards to be sawn and might thus have a considerable influence on the strength and stiffness properties of the timber. Another phenomenon that must receive much more attention in grading of timber is the drastic reduction of strength and stiffness caused by compression wood.

Fibre misalignment, like spiral grain deviations, may have a considerable influence on the stiffness properties. It might substantially reduce the stiffness moduli for tension and bending and it must be considered properly in stiffness grading for high quality timber.

6 References

Boström L., Ormarsson S. and Dahlblom O. (1996): On determination of modulus of elasticity in bending. CIB-W18/29-10-3, Bordeaux/France.

Dahlblom O., Petersson H., et al.: Engineering properties of spruce - A study of variations from pith to bark, Report TVSM-7110, Division of Structural Mechanics, Lund University, in preparation.

Harris J. M. (1989): *Spiral Grain and Wave Phenomena in Wood Formation*, Springer-Verlag, Berlin Heidelberg.

Johansson C.J., Steffen A., and Wormuth E.-W. (1996): Relation of moduli of elasticity in flatwise and edgewise bending of solid timber. CIB-W18/29-10-4, Bordeaux/France.

Ormarsson S (1995): A finite element study of the shape stability of sawn timber subjected to moisture variations, Report TVSM-3017, Lund Institute of Technology, Division of Structural Mechanics, Lund, Sweden.

Ormarsson S., Dahlblom O., and Petersson H.(1998a): A numerical study of the shape stability of sawn timber subjected to moisture variation. Parts 1-3, Wood Science and Technology, 1998, in press.

Ormarsson S., Dahlblom O. and Petersson H. (1998b): Influence of compression wood on shape stability of timber, Report TVSM-3031, Lund Institute of Technology, Division of Structural Mechanics, Lund, Sweden.

Persson K., (1997): Modelling of Wood Properties by a Micromechanical Approach, Report TVSM-3020, Lund Institute of Technology, Division of Structural Mechanics, Lund, Sweden.

Wormuth E.-W.(1993): Study of the relation between flatwise and edgewise modulus of elasticity of sawn timber for the purpose of improving mechanical stress methods. Diploma work, University of Hamburg, Department of Wood Technology, Hamburg.

CIB-W18/31-5-2

**INTERNATIONAL COUNCIL FOR BUILDING RESEARCH STUDIES AND DOCUMENTATION
WORKING COMMISSION W18 - TIMBER STRUCTURES**

A COMPARISON OF IN-GRADE TEST PROCEDURES

by

R.H. Leicester
H. Breitingger
H. Fordham

CSIRO Building, Construction and Engineering
Melbourne

AUSTRALIA

MEETING THIRTY-ONE

SAVONLINNA

FINLAND

AUGUST 1998

A COMPARISON OF IN-GRADE TEST PROCEDURES

by

R.H. Leicester, H. Breitingger and H. Fordham
CSIRO Building, Construction and Engineering, Melbourne, Australia

ABSTRACT

The design properties derived for structural timber depend on the in-grade test procedures used to measure these properties. In this paper, the data obtained from a limited set of bending and tension tests undertaken according to European, North American and Australasian procedures is used. It was found that the European procedure can underestimate the in-service bending strength and stiffness and slightly overestimate the in-service tension strength.

1. INTRODUCTION

When performance based standards are applied, it is very useful to have in-grade test data for the design properties of structural timber. However, such data is expensive and time consuming to obtain. For example, to measure a full set of design properties of every commercial size/grade of a single species, something like 10,000 pieces of timber must be tested; the cost for this is about \$1 million (US) and the time required is about one year for a laboratory of reasonable size.

It is thus apparent that when different test procedures are used in various countries, it is highly desirable to avoid the necessity for retesting timber each time a new trading partnership is made. One method for doing this is to have some sort of procedure for equivalencing the data obtained between two different in-grade test methods. In a previous paper (Leicester *et al.*, 1996) a simple model was proposed for use in equivalencing procedures.

This paper presents data obtained from three sets of in-grade test methods. The data indicates the magnitude of the differences between the data obtained by the test methods, and also provides information for calibrating the proposed equivalencing models.

The three in-grade procedures compared are those given in European (European Committee of Standardisation, 1995a and b), North American (Green and Evans, 1987) and Australasian Standards (Standards Australia, 1992). These three in-grade procedures will be referred to as the CEN, USA and AS/NZS procedures.

2. TEST MATERIAL

The test material was kiln dried radiata pine, machine stress graded to F5 and F8 grades. The timber was graded and supplied in lengths of 4.8 m for 90 x 35 mm size timber, and in lengths of 5.4 m for 190 x 35 mm size timber. All timber was obtained from the same mill, but the 90 x 35 mm material and the 190 x 35 mm material was supplied one year apart.

A sample size of $N = 150$ was used for measuring each grade/size/property/procedure.

3. TEST METHODS

3.1 Bending Strength and Modulus of Elasticity

The details for the test configurations used for measuring the bending strength and modulus of elasticity are given in Figure 1 and Table 1. In addition, the procedure used for selecting the test specimens from the full lengths of graded timber were as follows:

- CEN method: worst defect to be found in the full-length of timber was located at mid span of the test specimens, with the tension edge chosen at random.
- USA method: worst defect to be found in the full-length timber was located somewhere within the test span, with the tension edge chosen at random.
- AS/NZS method: location of test specimen and tension edge chosen at random from full-lengths of timber.

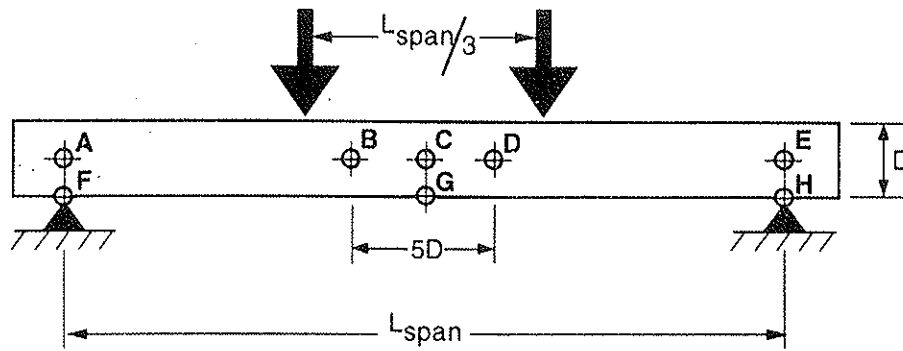


Figure 1. Schematic illustration of notation for bending test configuration.

Table 1.

Details of test configurations for bending strength and modulus of elasticity measurements

Procedure	Beam span (mm)		Deformation measurement locations (Figure 1).
	90 x 35	190 x 35	
CEN	1620	3420	C relative to B and D
USA	1530	3230	C relative to A and E
AS/NZS	1620	3420	G relative to F and H

3.2 Tension Strength

The details of the test configuration used for measuring the tension strength are given in Figure 2 and Table 2. In addition, the procedure used for selecting the test specimen from the full-lengths of graded timber were as follows:

- CEN method: worst defect to be found in the full-length of timber was located at mid span of the test specimen.
- USA method: worst defect to be found in the full-length of timber was to be located at a random location between the grips.
- AS/NZS method: test specimen chosen at random from the full lengths.

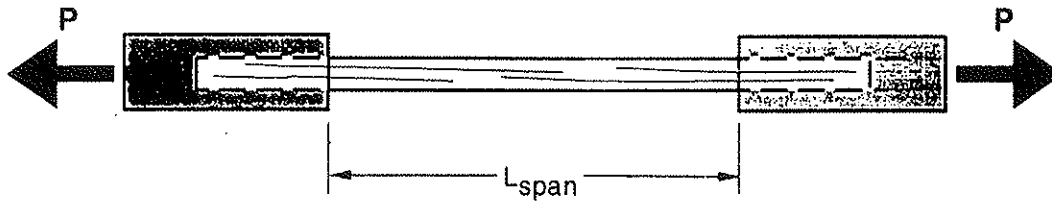


Figure 2. Configuration used for tension test.

Table 2.

Test configuration for tension strength test

Procedure	Clear distance between grips for 90 x 35 mm timber (mm)
CEN	810
USA	1080
AS/NZS	2700

4. TEST DATA

4.1 Modulus of Elasticity

The measured data for the modulus of elasticity is given in Table 3 and illustrated in Figures 3, 4 and 5. It is seen that for the smaller size, the CEN procedure gives a value of 20% less than the other methods and it is also associated with a larger coefficient of variation. This is to be expected as the CEN method measures the stiffness in the vicinity of a major defect rather than that of the total beam.

4.2 Bending Strength

The measured data for bending strength is given in Table 4 and illustrated in Figures 6, 7 and 8. The CEN values are expected to be the lowest because of the method of locating the worst defect. The measured values obtained from the CEN method are about 20% and 10% lower than those obtained by the AS/NZS method for the 90 x 35 mm and 190 x 35 mm pieces, respectively. As would be expected, the data obtained by the USA method lies between the other two.

The coefficients of variation is about the same for the data obtained by all the methods.

Table 3.

Comparison of measured modulus of elasticity

Structural parameter	90 x 35 mm		190 x 35 mm
	F5	F8	F8
Mean value (GPa)			
CEN	7.8	10.6	12.4
USA	9.8	12.2	12.5
AS/NZS	9.5	12.0	12.8
5-percentile value (GPa)			
CEN	4.4	5.9	7.7
USA	6.7	9.4	9.7
AS/NZS	6.1	9.0	10.5
Coefficient of variation			
CEN	0.30	0.30	0.21
USA	0.25	0.15	0.18
AS/NZS	0.26	0.16	0.14

Table 4.

Comparison of measured bending strength

Structural parameter	90 x 35 mm		190 x 35 mm
	F5	F8	F8
Mean value (MPa)			
CEN	31.1	43.7	41.7
USA	37.1	51.0	42.8
AS/NZS	38.5	53.2	46.4
5-percentile value (MPa)			
CEN	13.6	20.1	20.5
USA	14.7	23.8	20.3
AS/NZS	17.0	26.3	23.1
Coefficient of variation			
CEN	0.43	0.42	0.34
USA	0.47	0.37	0.36
AS/NZS	0.44	0.37	0.34

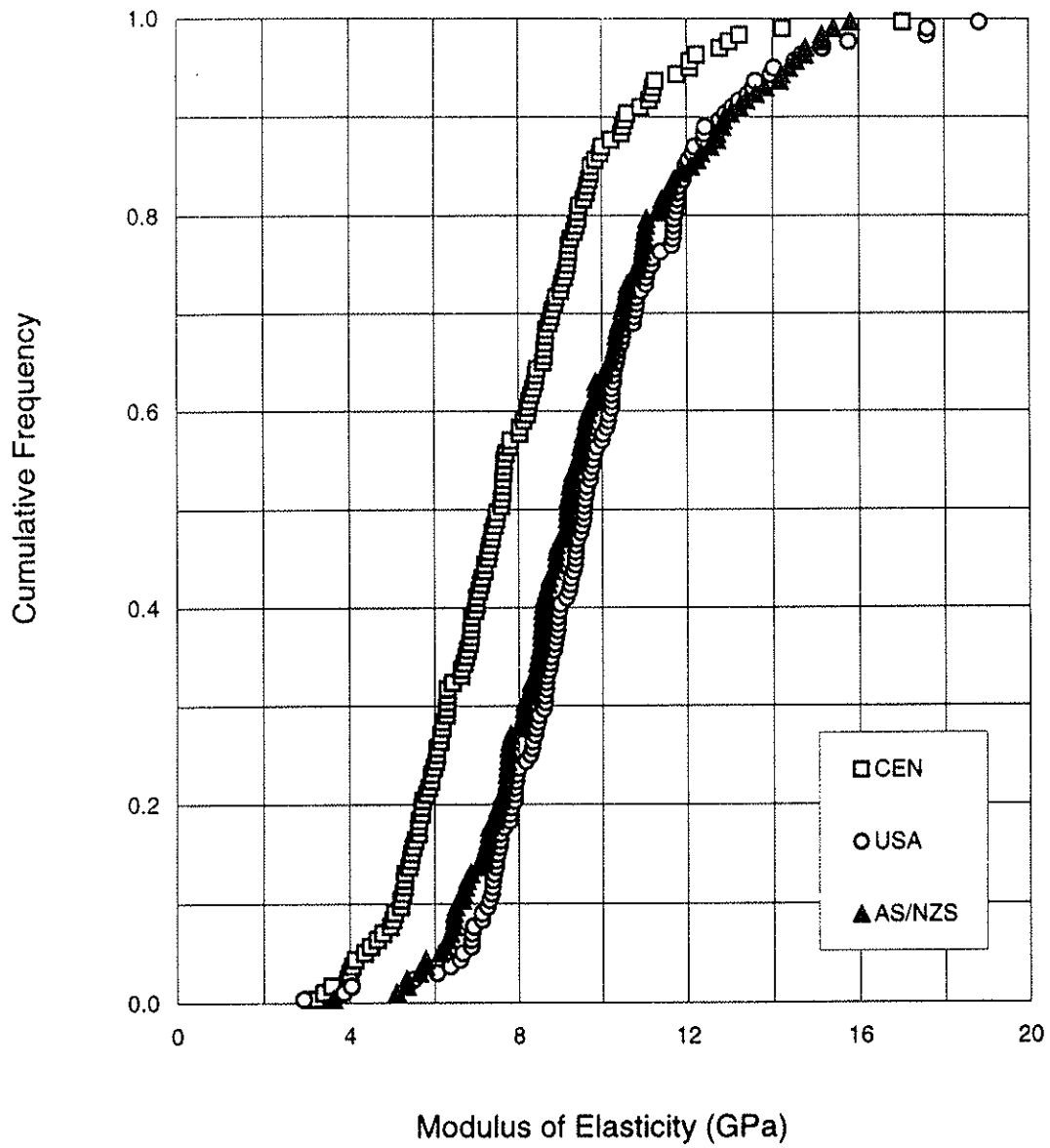


Figure 3. Measured modulus of elasticity for 90 x 35 mm timber, F5 material.

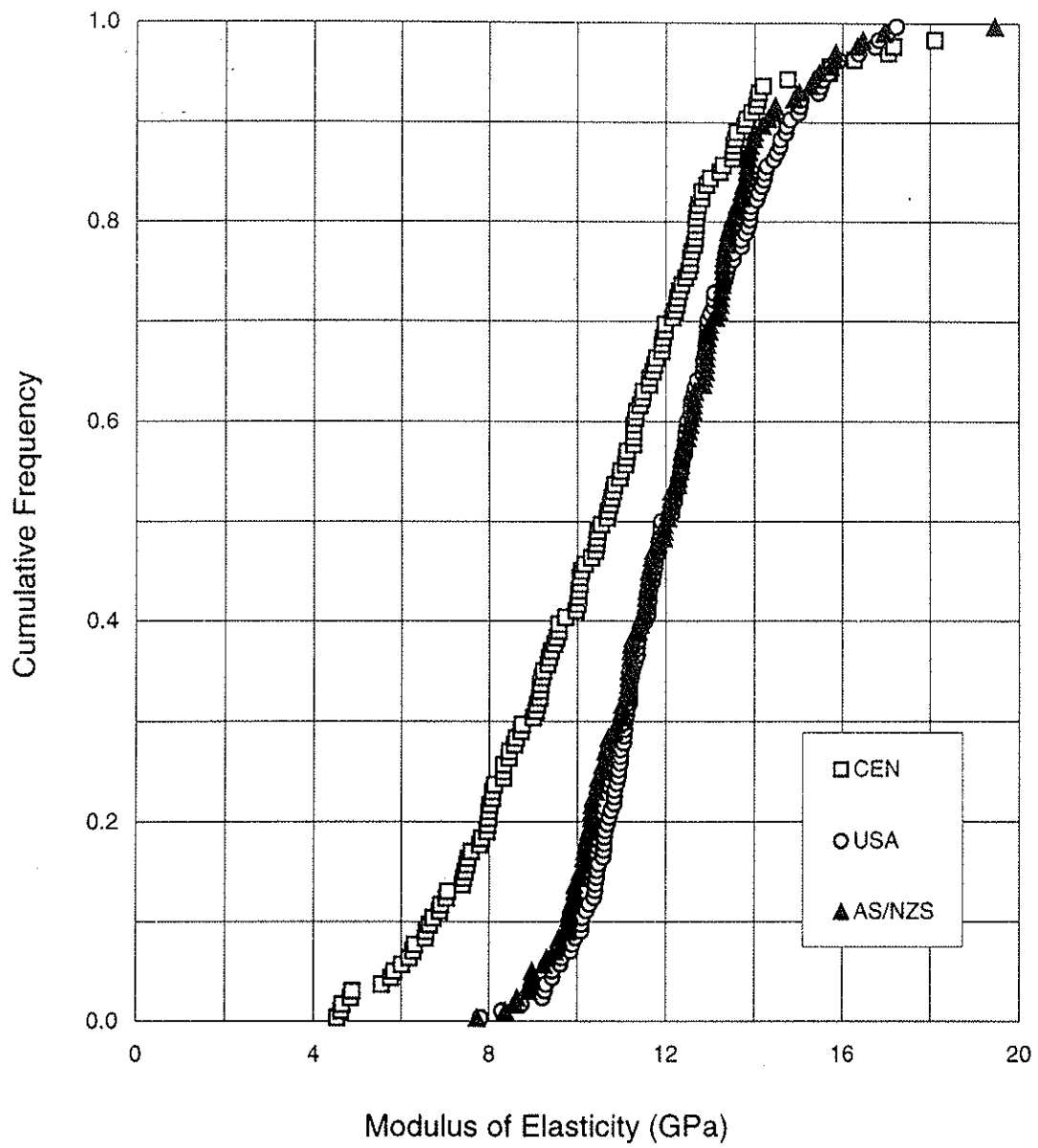


Figure 4. Measured modulus of elasticity for 90 x 35 mm timber, F8 material.

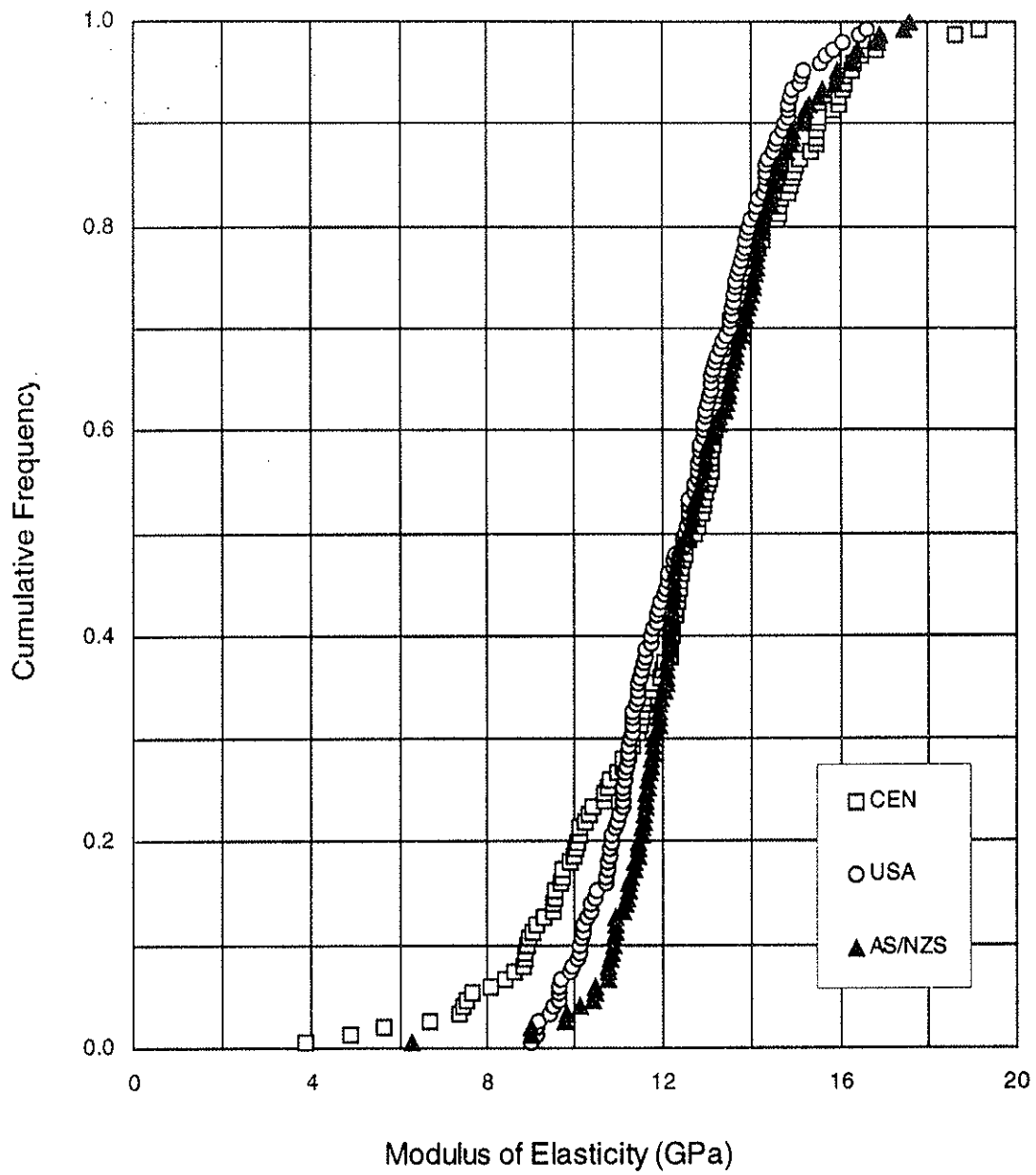


Figure 5. Measured modulus of elasticity for 190 x 35 mm timber, F8 material.

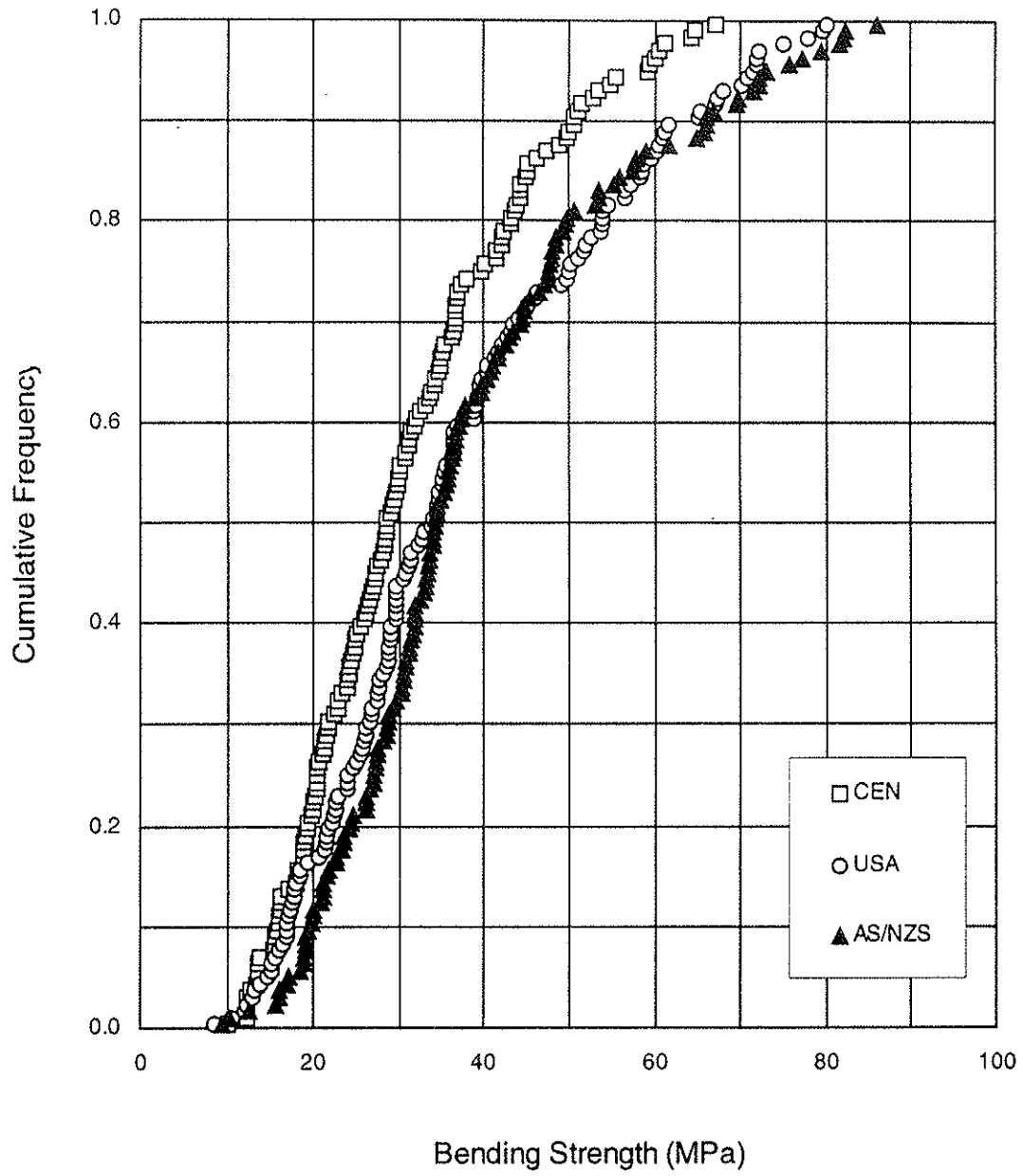


Figure 6. Measured bending strength for 90 x 35 mm timber, F5 material.

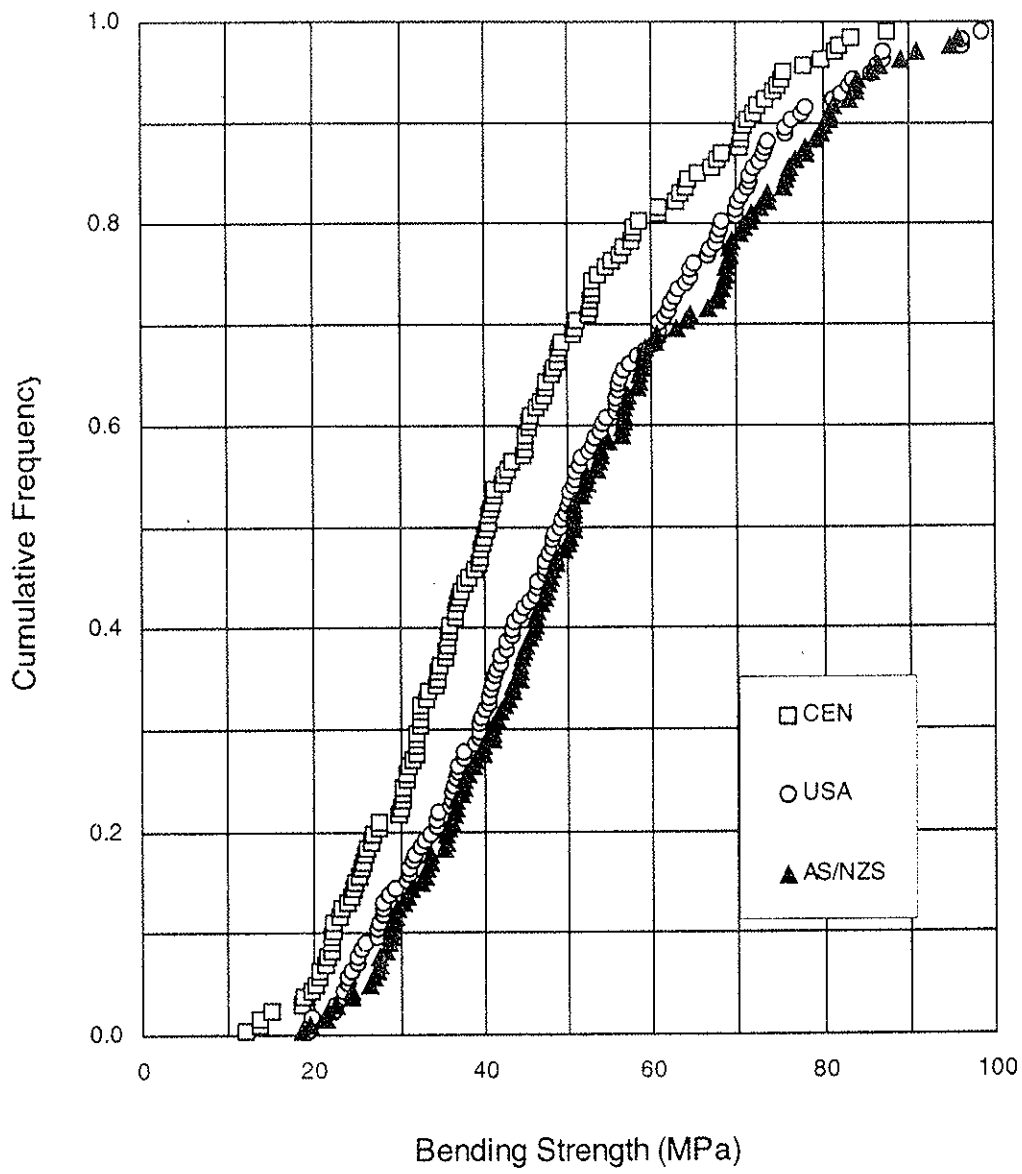


Figure 7. Measured bending strength for 90 x 35 mm timber, F8 material.

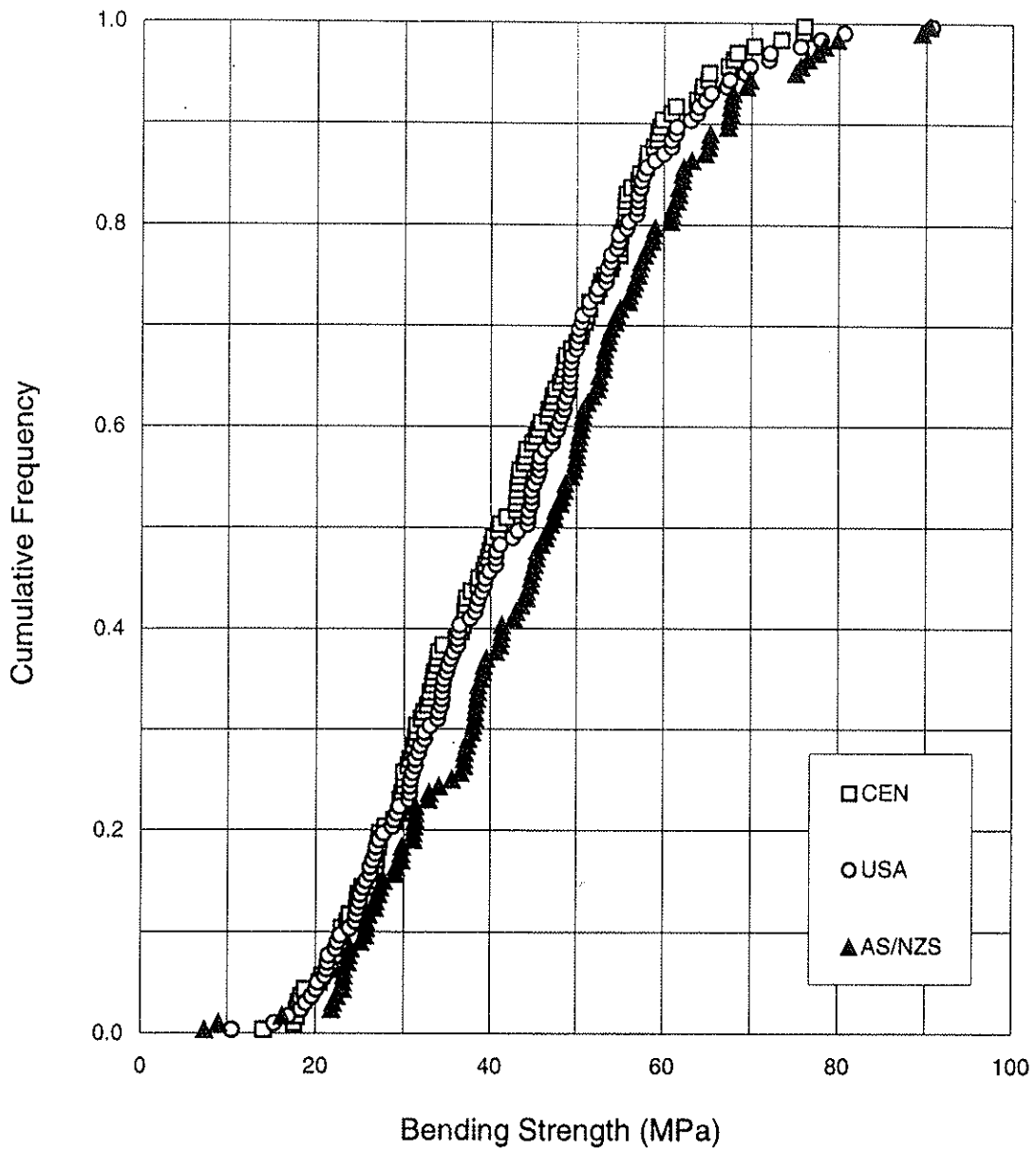


Figure 8. Measured bending strength for 190 x 35 mm timber, F8 material.

Table 5.

Comparison of measured tension strength

Structural parameter		90 x 35 mm
		F5
Mean value (MPa)	CEN	17.4
	USA	17.4
	AS/NZS	15.8
5-percentile value (MPa)	CEN	8.1
	USA	10.3
	AS/NZS	7.2
Coefficient of variation	CEN	0.42
	USA	0.42
	AS/NZS	0.38

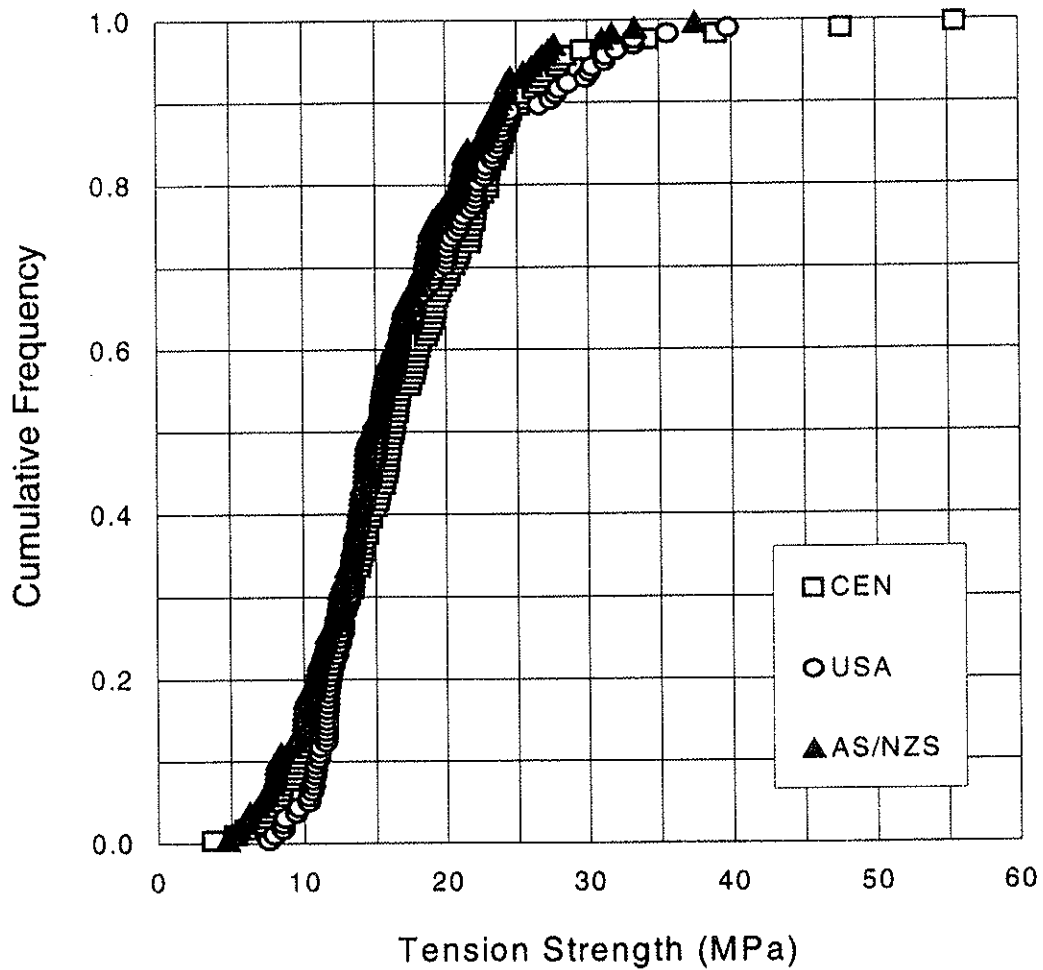


Figure 9. Measured tension strength for 90 x 35 mm timber, F5 material.

4.3 Tension Strength

The measured data for the tension strength is given in Table 5 and illustrated in Figure 9. It is interesting to note that the coefficient of variation is the same for all three procedures, but that contrary to the case for the bending strength tests, the AS/NZS procedure gives the lowest strength.

This observation would be consistent with the fact that the test operator, an experienced research engineer, was unable to correctly select the weakest defect in all cases for the CEN and USA tests. The average spacing of the defects in the 90 x 35 mm timber was about 1.2 m (Leicester *et al.*, 1996). Hence, typically there would be 2–3 defects within the AS/NZS test specimen. Thus, there is a reasonable chance that the AS/NZS test specimen will contain a weaker defect than that selected for the CEN and USA tests.

To obtain an idea of the chances of correctly choosing the weakest defect, three experienced laboratory personal were asked to predict the location of failure in the AS/NZS tension tests. On average each person chose the correct defect (where there was more than one) about 80% of the time. Hence, for almost 20% of the pieces, the AS/NZS procedure will produce a lower strength than the CEN procedure. A summary of the pooled prediction rates is given in Table 6.

Table 6.
Predicting of the weakest defect

Prediction success by 3 laboratory technicians	Occurrence %
3 out of 3 technicians correct	47
2 out of 3 technicians correct	19
1 out of 3 technicians correct	14
0 out of 3 technicians correct	7
Special cases (e.g. only one defect)	13

5. CONCLUSIONS

The data measured provides useful information on the differences that can be obtained between different in-grade test procedures. It also provides information for calibrating equivalencing models proposed in an earlier paper. The size and grade of timber used in this study probably provides the greatest differences likely to occur in practice.

Additionally, it is of interest to compare the data of the CEN and AS/NZS procedures. The AS/NZS procedure may be considered as an attempt to measure the properties of timber that would occur in-service. By comparison, the human bias applied in selecting the test specimens according to the CEN procedure leads to an underestimate of design bending strength and stiffness but (because it is imperfect) a small overestimate of tension strength.

6. REFERENCES

European Committee for Standardisation (1995a). EN 384: Structural Timber – Determination of Characteristic Values of Mechanical Properties and Density. Brussels, Belgium, February, 13 pages.

European Committee for Standardisation (1995b). EN 408: Timber Structures – Structural Timber and Glued Laminated Timber – Determination of Some Physical and Mechanical Properties.. Brussels, Belgium, 27 pages.

Green, D.W. and Evans, J.W. (1987). Mechanical Properties of Visually Graded Lumber, 1. A Summary. USDA Forest Products Laboratory, Madison, USA, 59 pages.

Leicester, R.H., Breiting, H.O. and Fordham, H. (1996). Equivalence of In-grade Testing Standards. *Proc. of CIB- W18 Meeting 29*, Bordeaux, France, August, Paper 29–6–20.

Standards Australia/Standards New Zealand. (1992). AS/NZS 4063: Timber–Stress-graded–In-grade Strength and Stiffness Evaluation. Sydney, Australia, 15 pages.

CIB-W18/31-6-1

**INTERNATIONAL COUNCIL FOR BUILDING RESEARCH STUDIES AND DOCUMENTATION
WORKING COMMISSION W18 - TIMBER STRUCTURES**

LENGTH AND MOMENT CONFIGURATION FACTORS

by

T Isaksson

Department of Structural Engineering
Lund University
SWEDEN

MEETING THIRTY-ONE

SAVONLINNA

FINLAND

AUGUST 1998

Length and Moment Configuration Factors

Tord Isaksson
Dept. of Structural Engineering
Lund University, Sweden

1 Abstract

The effect of length and load configuration on the load carrying capacity of a timber beam in the bending mode has been investigated using a model that takes into account the variation of bending strength both within and between timber members. The model is mainly based on two stochastic variables, the strength of a weak section and the distance between weak sections. The parameters of these two variables are determined by experimental tests.

Two different methods are used to quantify the effect of length and load configuration, both direct comparison of strengths at a given percentile and also a method that preserves the reliability index. The Weibull theory is also used to quantify the effects.

The strength in weak sections in a board was found to have a constant serial correlation, i.e. the correlation between the strength of two sections is not dependent on the distance between them.

The length effect according to comparison of percentiles was found to be lower than the one used in the Eurocode 5. The reliability index method results in a more or less non-existing length and load configuration effect. A doubling of length results in a 2 per cent lower load carrying capacity at the most. Changing from constant bending moment to a board with fixed supports and a uniformly distributed load, which is two extreme load cases, only results in a 6 per cent higher load carrying capacity.

2 Introduction

Due to the significant variability in material properties for structural timber, not only between members, but foremost within members it has been considered convenient to introduce various correction factors to account for this variability. In contrast to the variability within members, the between member variability is not unique for structural timber but is present for most structural materials and thus it is taken into account in the normal design procedure. The variability within members is the reason for a timber beam having an apparent strength that is dependent on length and type of loading.

Theoretical studies have been performed regarding the variability within members and the general conclusion seems to be that correction factors indeed are needed to account for this variability. The fundamental concept of these studies is the use of the weakest link theory in one shape or another, also known as the Weibull theory. Test results other than testing boards of different lengths is often in shortage. The outcome of the tests is dependent on species, grading methods and sawing patterns, just to name a few. Consequently the effect of length and load configuration is more or less pronounced in the different investigations.

In a research project at the department of Structural Engineering at Lund University the variability between and within timber members has been studied experimentally on Norway spruce grown in southern Sweden. The results are most likely valid for spruce grown in northern Europe.

The concept of the research is to establish a statistical model of the lengthwise variation of bending strength in a board. The model is schematically presented in *Figure 1* (Riberholt et al 1979). The distance between weak sections and strength of weak sections are the main stochastic variables and their parameters are determined through experimental work.

The method to determine strength in several weak sections within a board has been presented in Isaksson (1996). In *Figure 2* the test set-up is shown. The validity of the results from testing according to this method is checked with tests according to the EN 408 standard. The conclusion was that the new method did not significantly affect the results.

The distribution for distances between weak sections can be derived from knot measurements on boards in the sample tested according to the new method.

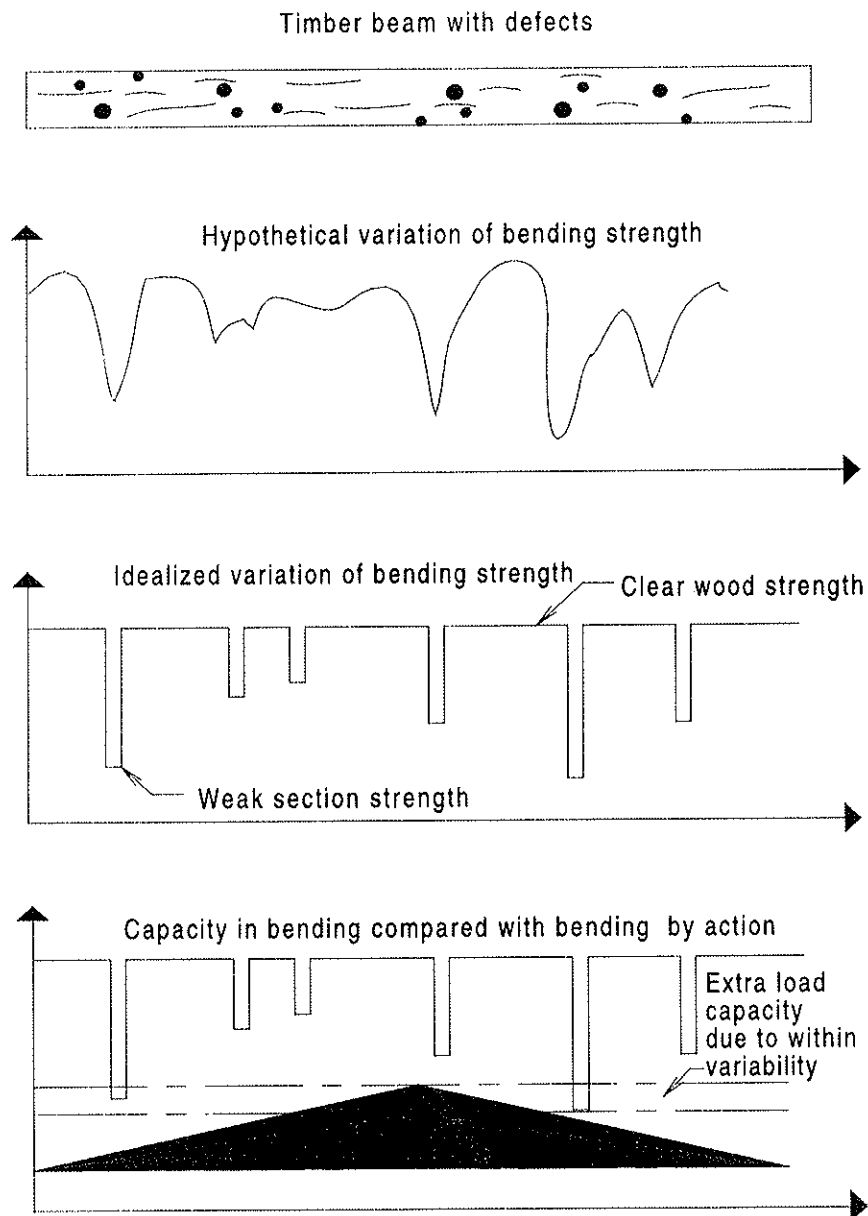


Figure 1. Modelling of lengthwise variation of bending strength in timber (Riberholt et al 1979).

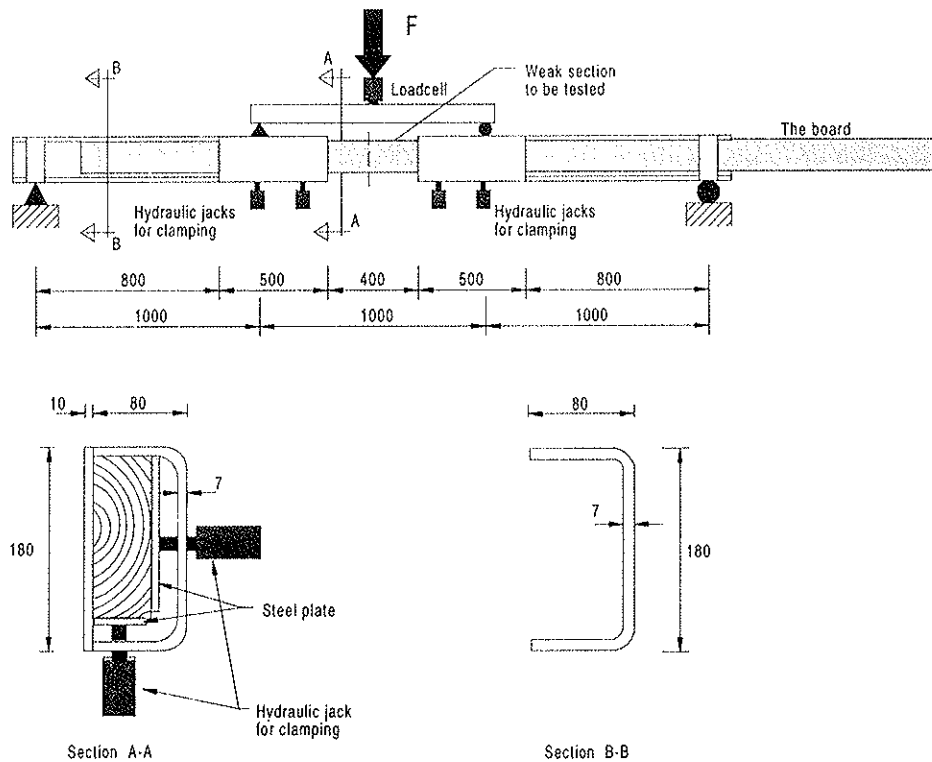


Figure 2. Arrangement for testing several weak sections within a board (Isaksson 1996).

Apart from the strength of weak sections and distance between weak sections, the strength between weak sections, i.e. more or less defect-free timber, is of interest. In Isaksson and Freysoldt (1997) the strength of weaker and stronger parts of a board was tested under a point load. The idea was both to compare strength in weak and strong parts of a board and to investigate the performance under a narrow moment peak caused by a point load. This is similar to the condition found at an inner support of a continuous beam. The results indicate a relatively small difference in strength between sections with defects and more or less defect-free sections. In boards of higher strength, sections selected as weak were sometimes stronger than defect-free ones. The importance of knowing the strength between weak sections is mainly connected to beams with varying moment distribution and narrow moment peaks, i.e. beams with fixed supports, continuous beams or subjected to point loads.

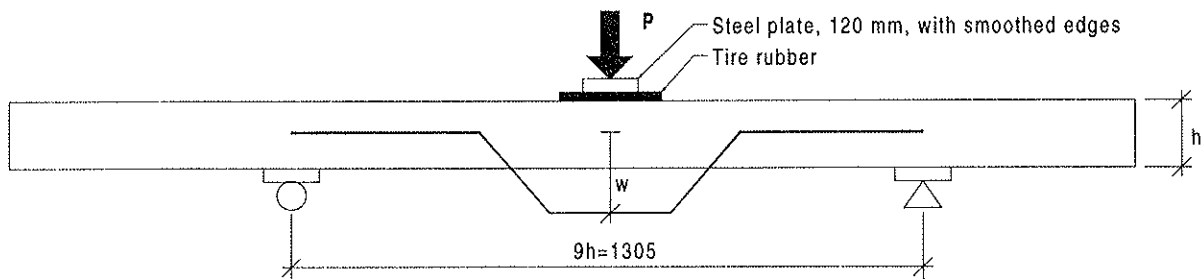


Figure 3. Test arrangement for determining bending strength of a board subjected to a point load.

3 Statistical model of lengthwise variation of bending strength

This section will describe how the different parameters in the model are derived. The model is built up by stochastic variables representing strength of weak section, strength between weak sections, distances between and width of weak sections.

3.1 Distance between weak sections

Based on data about position and size of all knots on all four faces of a board, different knot measures were calculated, see Isaksson 1996. As can be seen in *Table 1* the coefficient of correlation between these knot measures and the bending strength is about the same, 0.40.

Knot Measure	<i>TKAR</i>	<i>MKAR</i>	<i>CRATIO</i>	<i>NRATIO</i>	<i>W 0-1</i> <i>NRATIO P</i>	<i>W 1-2</i> <i>NRATIO P</i>	<i>W 2-1</i> <i>NRATIO P</i>
Correlation <i>r</i>	0.40	0.40	0.39	0.39	0.40	0.43	0.38

Table 1. Coefficient of correlation between bending strength and various knot measures.

Before any data can be extracted from the knot measures, the definition of a weak section has to be stated. First let us recall how the weak sections to be tested in the test set-up according to *Figure 2* were selected, see also Isaksson 1996. There were three grading parameters available for the boards, the Cook-Bolinder reading, the Finnograder reading and the visual *TKAR* measure. The procedure was:

1. First, minimum values from the three measurements must be represented, with the priority order *TKAR*, Finnograder and Cook-Bolinder. Now there are one, two or three sections selected, depending on whether they coincide or not.
2. Select as many more sections as possible, with regard to the restrictions of the test arrangement from the *TKAR* results, with priority given in order from the highest *TKAR*-value of the remaining sections. This procedure makes it possible to test 4-7 weak sections in each board. The boards had a length of 5.1 or 5.4 m.

The sections were thus selected mainly according to the *TKAR* reading. Therefore it is reasonable to base the stochastic variable *distance between weak sections* on the *TKAR* measure. *Table 1* does not contradict this. There was no limit as to how low the *TKAR* value of a section to be tested could be since as many sections as possible were tested and for stronger boards with fewer defects the *TKAR* readings were quite low. A low *TKAR* reading indicates a strong section. For weaker boards on the other hand, the knot measures could be high.

If a *TKAR* value is used to set a limit, above which sections are to be regarded as weak, then this limit should vary from board to board. It was decided to set the limit as a percentage of the maximum *TKAR* reading within each board. Two levels are used, 40 % and 50 % of the board-maximum *TKAR*. These gave a reasonable number of weak sections, having in mind that the mean distance between branches for Norway spruce is around 500 mm.

In *Figure 4*, three examples of the *TKAR* profiles and the two different limits are shown. Ranking the boards according to the strength of the weakest section according to the Cook-Bolinder and plotting the distances between weak sections for each board gives *Figure 5*. As can be seen the weak sections do not seem to be located further apart in stronger boards. Thus the distance *between weak sections* is assumed to be independent of the strength of the board. However, the distances would be dependent on strength if only one *TKARlimit* was used for all boards.

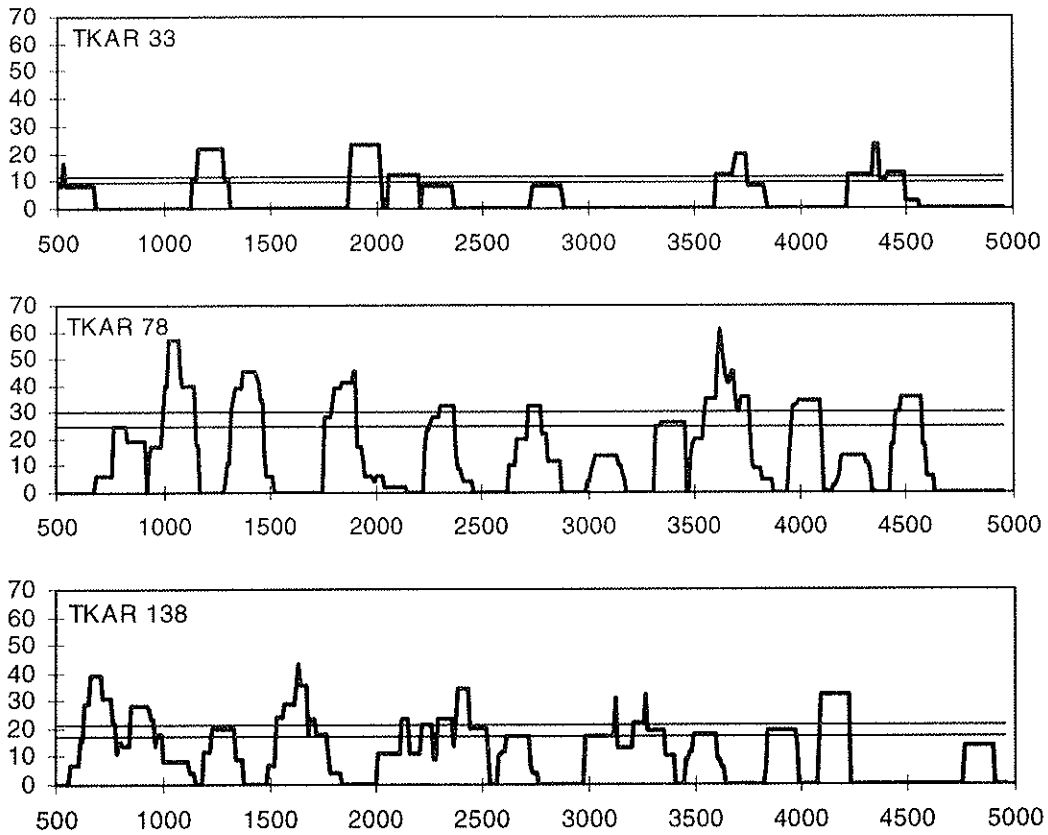


Figure 4. Three examples of TKAR profiles and the two limits of 40 and 50 per cent of maximum TKAR within each board.

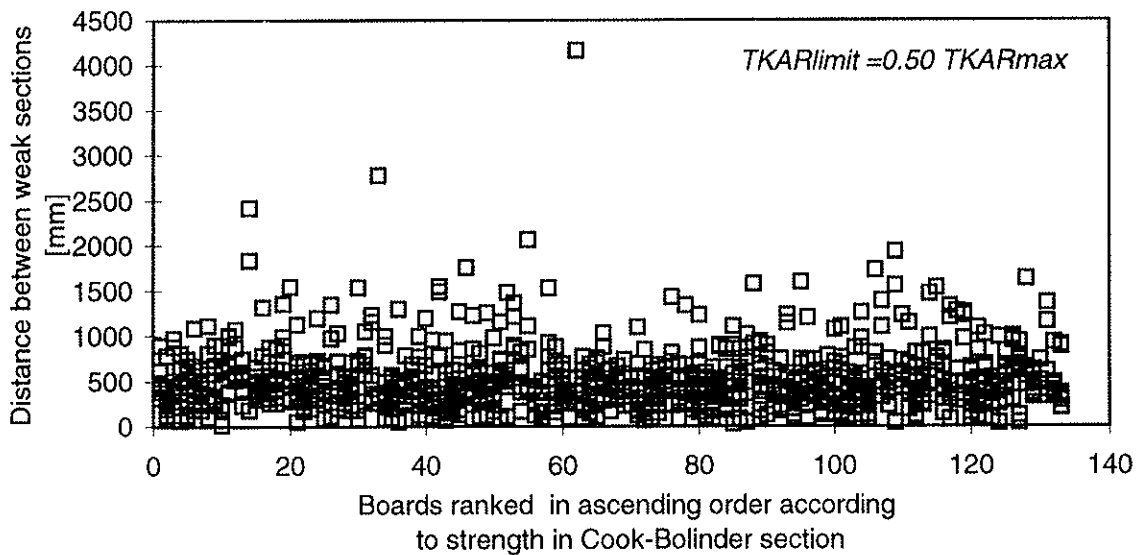


Figure 5. Distances for each board plotted against increasing strength in Cook-Bolinder section. Limit of 50 per cent of maximum TKAR value within each board.

As was concluded in Riberholt et al 1979, the number of weak sections in a board can be found to be exponentially distributed $\text{Exp}(1, 1/\lambda)$, which means that the distances will be gamma distributed $\Gamma(\eta, \lambda)$ with shape parameter η and scale parameter λ . In *Table 2* and *Table 3* below the results from fitting the normal, lognormal and gamma distributions to the two sets of distances are shown. None of the tests accept the hypothesis that the observations are from any of the suggested distributions. However, for large samples like these the tests often tend to reject the hypothesis. The gamma distribution is chosen to represent *distances between weak sections*. The mean distance between weak sections is 440 mm when *TKARlimit* is set to 40 per cent and 494 mm for 50 per cent.

Distribution	Parameters	Goodness of fit tests		
		Kolmogorov-Smirnov	Chi-square	Anderson-Darling
Normal	N(439.7, 269.6)	0.1054 *	0 *	31.275 *
Lognormal	log N(5.9098, 0.6245)	0.0801 *	0 *	10.316 *
Gamma	$\Gamma(2.9848, 147.31)$	0.0440 *	0.000255 *	3.434 *

*Table 2. Distribution fitting of distances between weak sections, TKAR limit 40%. 1189 observations. The hypothesis that the observations could be from either of the three is rejected in all tests. * denotes rejection of hypothesis.*

Distribution	Parameters	Goodness of fit tests		
		Kolmogorov-Smirnov	Chi-square	Anderson-Darling
Normal	N(493.9, 337.0)	0.1295 *	0 *	38.859 *
Lognormal	log N(5.9939, 0.6812)	0.0855 *	0 *	10.550 *
Gamma	$\Gamma(2.5445, 194.12)$	0.0497 *	0 *	4.458 *

*Table 3. Distribution fitting of distances between weak sections, TKAR limit 50%. 1035 observations. The hypothesis that the observations could be from either of the three is rejected in all tests. * denotes rejection of hypothesis.*

3.2 Width of weak sections

Based on the *TKAR* measure it is possible to estimate the width of the weak sections by recording the width of the *TKAR* reading at the limiting level, i.e. 40 or 50 per cent of the maximum board *TKAR*. The principle for determining the width is shown in *Figure 6*. The width of sections will be strongly influenced by the definition of *TKAR*, namely to add up knot areas within a length of 150 mm, Isaksson 1996. *Table 4* and *Table 5* summarise the results from fitting the normal, lognormal, beta and gamma distributions to the data. As can be seen none of the distributions fit to the data. This is due both to the large samples and to the nature of the data, i.e. adding knot areas within a fixed length. The widths are very concentrated around the 150-mm value. For the purpose of giving weak sections a stochastic width the beta distribution is selected. A constant width of 150 mm will also be used in the model.

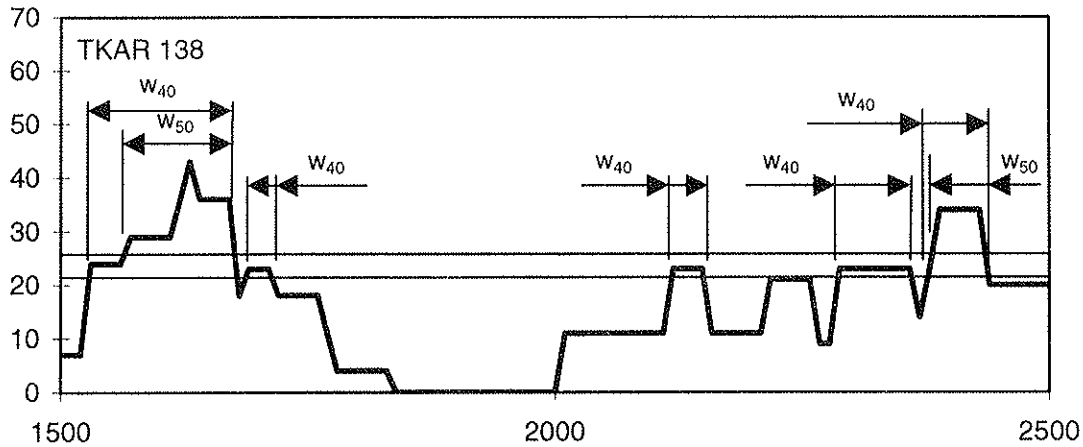


Figure 6. Example of determining width of weak sections. A part of board 138, previously shown in Figure 4. Index 40 and 50 refers to the TKARlimit.

Distribution	Parameters	Goodness of fit tests		
		Kolmogorov-Smirnov	Chi-square	Anderson-Darling
Normal	$N(134.5, 51.6)$	0.2336 *	0 *	83.219 *
Lognormal	$\log N(4.7829, 0.5830)$	0.2861 *	0 *	138.218 *
Beta	$\beta(3.5272, 6.9582)$	0.2401 *	0 *	144.810 *
Gamma	$\Gamma(4.3706, 30.7663)$	0.2686 *	0 *	116.054 *

Table 4. Distribution fitting of width of weak sections, TKARlimit 40%. 1189 observations. The hypothesis that the observations could be from either of the four is rejected in all tests. * denotes rejection of hypothesis.

Distribution	Parameters	Goodness of fit tests		
		Kolmogorov-Smirnov	Chi-square	Anderson-Darling
Normal	$N(121.9, 49.9)$	0.2274 *	0 *	77.602 *
Lognormal	$\log N(4.6504, 0.6699)$	0.2811 *	0 *	125.487 *
Beta	$\beta(3.100, 6.5985)$	0.2463 *	0 *	160.810 *
Gamma	$\Gamma(3.4254, 35.5767)$	0.2725 *	0 *	108.868 *

Table 5. Distribution fitting of distances between weak sections, TKARlimit 50%. 1035 observations. The hypothesis that the observations could be from either of the four is rejected in all tests. * denotes rejection of hypothesis.

3.3 Bending strength of weak sections

The first question is whether or not there is a stronger dependence between closely located sections than between sections located further apart, but still within the same board. A measure of the dependency is the serial lag- k correlation, i.e. the correlation between an observation from

one section and an observation from k previous sections. If $k=2$, it refers to the correlation between strengths of section 1 and 3 and section 2 and 4 and so on.

Based on the test results it is possible to determine up to lag-5 correlation. The results are shown in *Figure 7*. As can be seen the serial lag- k correlation is more or less 0.54 for all k -values. This simplifies things quite significantly. It means that the strength of a weak section is not more related to its neighbour section than to a section further away. The strength of a weak section can be modelled as a scatter around the board mean of weak sections. Källsner et al 1997 came to the same conclusion with a serial correlation of 0.55.

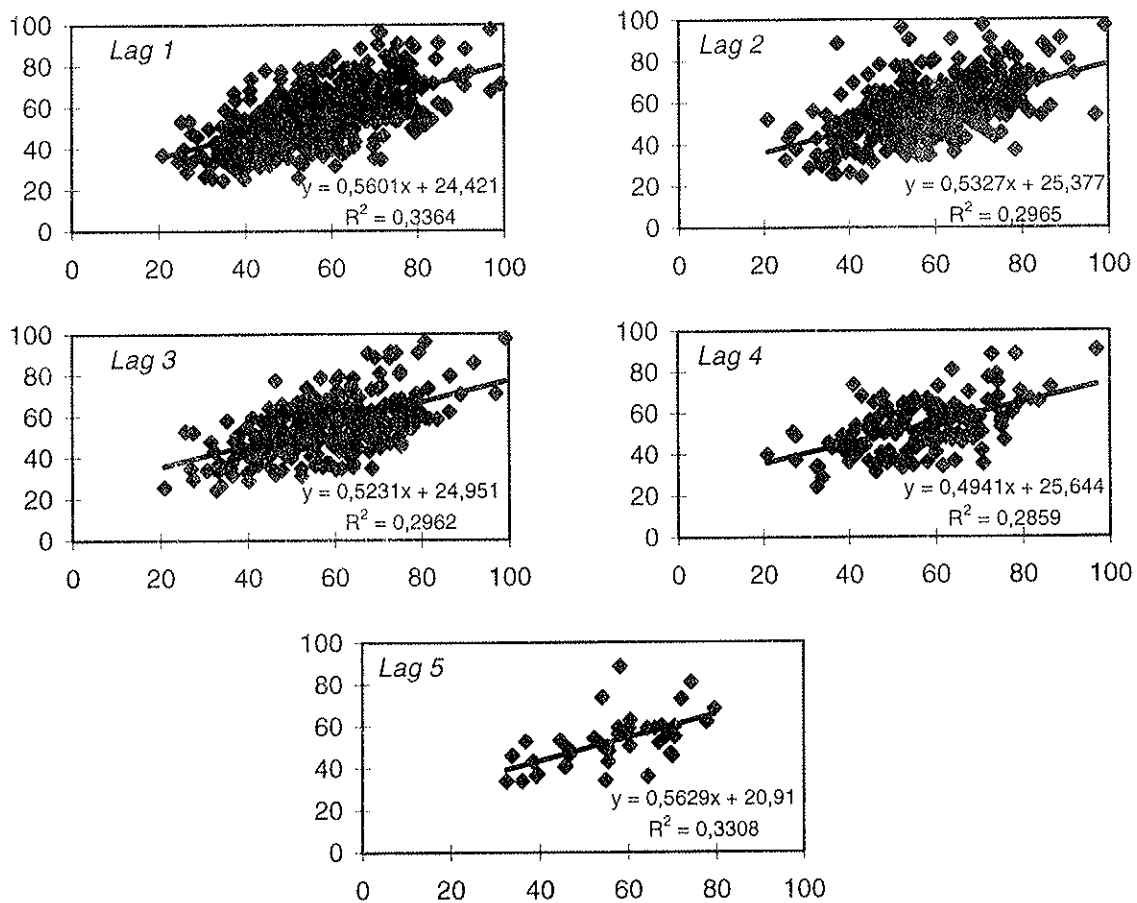


Figure 7. The serial lag- k correlation between bending strength of weak sections.

All in all there are 673 observed strengths distributed on 132 boards which gives an average of 5.1 tested sections per board. Half of the population of boards were 5.1 m long and the other half 5.4 m. The strengths were fitted to the usual suspects among statistical distributions and the results are shown in *Table 6*.

Distribution	Parameters	Goodness of fit tests		
		Kolmogorov-Smirnov	Chi-square	Anderson-Darling
Normal	N (57.334, 13.423)	0.0351	0.406	0.787
Lognormal	log N (4.01977, 0.247136)	0.0715 *	0.0001 *	4.067 *
Weibull 2	Weibull (62.588, 4.618)	0.0552 *	0.0021 *	2.522 *
Weibull 3	Weibull (41.219, 2.9370, 20.386)	0.06166 *	0 *	3538.2 *

Table 6. Distribution fitting of strength weak section, 673 observations. Only the normal distribution is accepted by the tests.

It seems that the normal distribution fits best to the data. However, using the normal distribution in the model will lead to occasional negative strengths. Thus, the log normal distribution seems to be more suitable.

From the serial lag- k correlation it was concluded that strengths of weak sections are equally correlated, i.e. independent of distance between them. Thus the standard deviation of bending strength in a weak section can be split up in a deviation σ_i around the overall mean of all weak sections in all boards μ , and σ_j around the mean of weak sections within a board ($\mu + \tau$), eq. (1)

$$\sigma_{ij} = \sqrt{\sigma_i^2 + \sigma_j^2} \quad (1)$$

The correlation coefficient becomes

$$\rho = \frac{\sigma_i^2}{\sigma_i^2 + \sigma_j^2} \quad (2)$$

The model can be written as in eq. (3) and visualised as in *Figure 8*.

$$f_{i,j} = \mu + \tau_i + \varepsilon_{ij} \quad (3)$$

where

- μ is the mean of all weak sections in all boards
- τ_i is the difference between the mean of weak sections within a board and μ .
Zero mean and standard deviation σ_i .
- ε_{ij} is the scatter around ($\mu + \tau_i$). Zero mean and standard deviation σ_j .
- i is the between board index
- j is the within board index

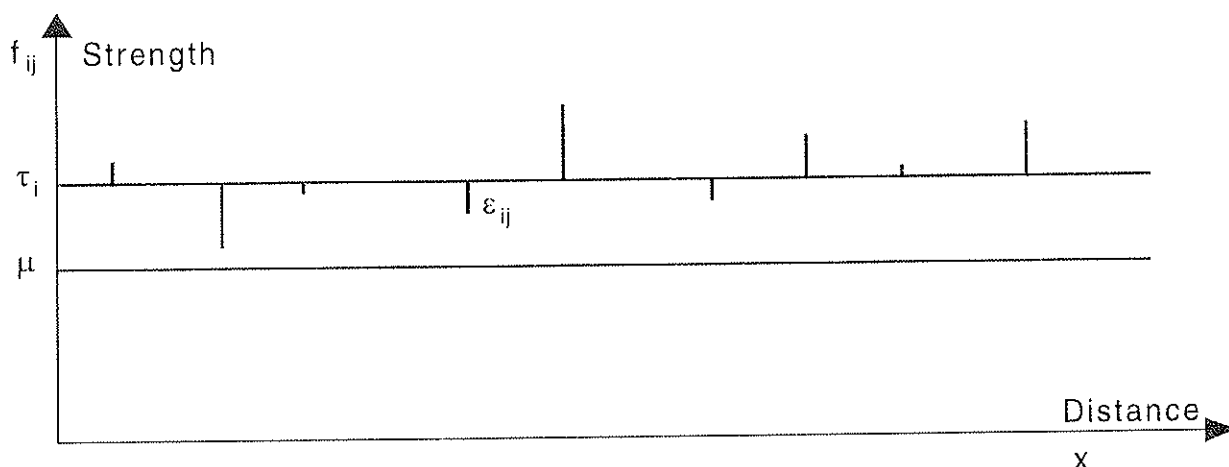


Figure 8. Statistical model of strength in weak sections.

In Table 7 the input to the model given in eq. (3) is presented for both normal and lognormal distributions. As mentioned before the lognormal distribution is the one to prefer since it only produces positive strengths.

Distribution	Number of observations	overall mean μ standard dev. σ_{ij}	$\tau_i : (0, \sigma_i)$ dev. around μ	$\varepsilon_{ij} : (0, \sigma_j)$ dev. around $\mu + \tau_i$
Normal	673	57.334 13.423	0 10.114	0 8.863
Lognormal	673	4.03038 0.24773	0 0.18747	0 0.16194

Table 7. Summary of the parameters in the model. Note that there is some minor discrepancy between parameters in this table and in Table 6 regarding the lognormal distribution.

3.4 Bending strength between weak sections

A model based on the principles shown in Figure 1 needs information about the strength between the weak sections. Test results presented in Isaksson and Freysoldt 1997 indicates a moderate difference between strength of weak sections and more or less defect-free parts of a board. There could be two ways of introducing this strength in the model:

1. Use regression analysis and predict the strength of stronger parts based on the strength of the weakest section from the model, eq. (3).
2. Simply use the strongest of the weakest sections given by eq. (3) and thus leave out the results from Isaksson and Freysoldt 1997.

3.5 Alternative model of lengthwise variation of bending strength

The problem of finding the strength between weak sections can be overcome by changing the model used so far. The principle of the model is shown in *Figure 9*. In this model there is no between-weak section strength. There are four reasons for using this model:

- The test results from Isaksson and Freysoldt 1997 showed quite moderate differences between strength of weak and strong sections.
- The testing of several weak sections also included quite strong sections, and thus they are already included in the model.
- The test set-up used for testing several weak sections gave the strength over a test length of 350 mm.
- The nature of the raw material. Norway spruce grown in northern Europe normally has quite closely spaced knot clusters. Even between the clusters there are defects. This more or less evens out the differences in strength.

The width of a section is given by the distribution for distances between weak sections, i.e. a gamma distribution according to section 3.1, *Table 2* and *Table 3*. The strength of a section is given by the lognormal distribution according to *Table 7* and eq. (3).

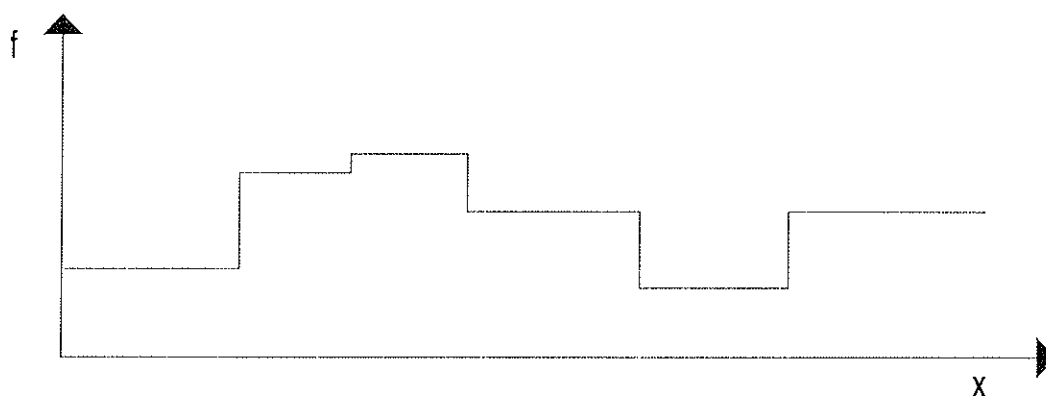


Figure 9. Modelling of lengthwise variation of bending strength using only weak section strengths.

3.6 Simulation study

Based on the previous sections it is possible to study the importance and sensitivity of the various parameters included in the model. However, in this paper only a few will be presented and used in the coming sections where the effects of length and load configuration on the load carrying capacity of a timber beam are studied. The seven load configurations are shown in *Figure 10*. *Table 8* gives the different inputs to the model. The LN50 and LN50step models will be the most used and the others are just compared with them in one figure.

Throughout the paper each sample consists of 10000 simulated boards. The shorter boards are cut out from a basic length of 5.5 m. This reduces the variability between samples when comparing strength of a board with different lengths.

Load configurations

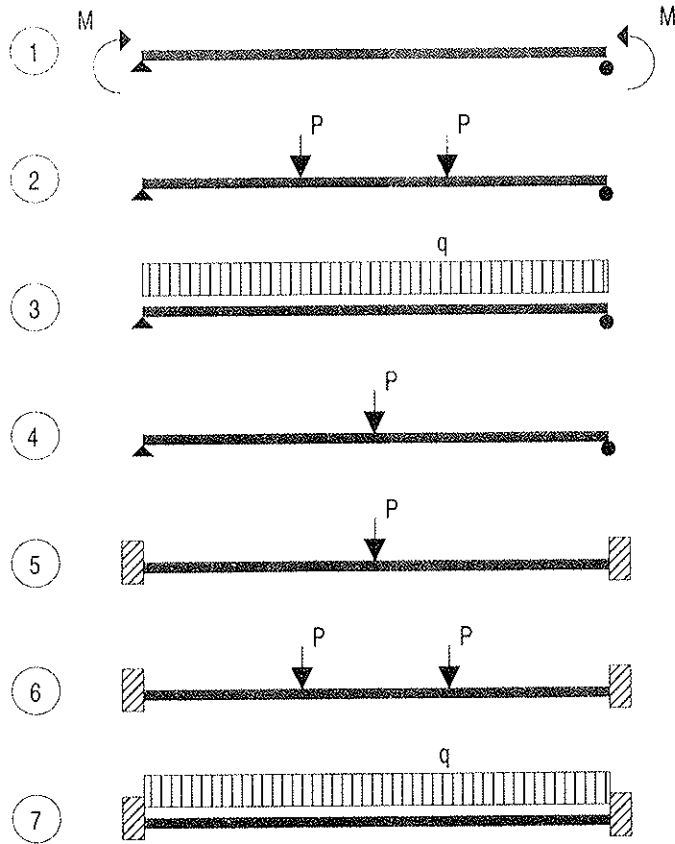


Figure 10. Seven different load configurations.

Model name	Distribution of strength	Distance between weak sections	Width of weak sections	Strength between weak sections
LN 40	LogN	TKARlimit 40	150 mm	Strongest weak section
LN 50	LogN	TKARlimit 50	150 mm	Strongest weak section
LN 50w	LogN	TKARlimit 50	TKARlimit 50	Strongest weak section
LN 502	LogN	TKARlimit 50	150 mm	Twice the strongest weak section
LN 40step	LogN	TKARlimit 40	weak sections are placed after each other width equals distance between sections	
LN 50step	LogN	TKARlimit 50		

Table 8. Different inputs to the statistical model.

4 Length and Moment Configuration Factors

4.1 Theories of length and load configuration effect

When the effect of length and load configuration on the load carrying capacity of a beam is studied, the Weibull theory is often adopted. The theory behind it has been presented extensively in the literature, see for example Madsen 1992. The length effect is written as eq. (4)

$$\frac{f_D}{f_R} = \left(\frac{L_R}{L_D} \right)^k \quad (4)$$

where f refers to strength and L to length. Index R refers to the reference length and D to the length of interest. The effect of different load configurations can be found in Johnson 1953 and Madsen 1992. Based on Weibull theory Johnson determined the probability of failure of a beam under different loading conditions and this gave correction factors for load configuration

Another way of determining correction factors is to use the definition of the reliability index. This method has also been used by Canisius 1994. The effect of length and load is analysed by preserving the probability of failure. In Eurocode 1, Basis of design and actions on structures, an indicative target reliability index in the ultimate limit state is given as 3.8, which corresponds to a probability of failure of less than 10^{-4} per year. Assuming log normally distributed resistance, R , and actions, S , leads to a simple expression of the probability of failure, eq. (5)

$$P_f = P(R < S) = P(\ln R - \ln S < 0) = \Phi\left(-\frac{\mu_R - \mu_S}{\sqrt{\sigma_R^2 + \sigma_S^2}}\right) = 1 - \Phi\left(\frac{\mu_R - \mu_S}{\sqrt{\sigma_R^2 + \sigma_S^2}}\right) \quad (5)$$

where $\ln R \in N(\mu_R, \sigma_R)$ and $\ln S \in N(\mu_S, \sigma_S)$.

Since the model of the variation of bending strength is based on the lognormal distribution, the results from simulation should be lognormally distributed. As for the actions, the lognormal distribution is chosen for the sake of simplicity.

Using the method of preserving the probability of failure for different lengths, as described above, means that either the resistance or action is multiplied with a correction factor to scale either of them up or down relative to the reference beam. If the factor k_S is applied to the action the probability of failure becomes

$$P_f = \Phi\left(-\frac{\mu_R - k_S \mu_S}{\sqrt{\sigma_R^2 + \sigma_S^2}}\right) \quad (6)$$

If the factor k_R is applied to the resistance variable the equation becomes

$$P_f = \Phi\left(-\frac{k_R \mu_R - \mu_S}{\sqrt{\sigma_R^2 + \sigma_S^2}}\right) \quad (7)$$

The resistance parameters μ_R and σ_R for each load configuration, see *Figure 10*, and length are estimated on a simulated sample of 10000 boards. A reference beam with a given load configuration and length is chosen. This beam should have the correction factor equal to 1. To be able to solve eq. (6) or (7) the coefficient of variation, COV_S , of the action has to be selected. Then σ_S can be written as eq. (8)

$$\sigma_S = COV_S \mu_S \quad (8)$$

and eq. (6) and (7) becomes

$$P_f = \Phi\left(-\frac{\mu_R - k_S \mu_S}{\sqrt{\sigma_R^2 + (COV_S k_S \mu_S)^2}}\right) \quad (9)$$

$$P_f = \Phi\left(-\frac{k_R \mu_R - \mu_S}{\sqrt{\sigma_R^2 + (COV_S \mu_S)^2}}\right) \quad (10)$$

μ_S is determined for the reference beam with $k_S = k_R = 1$. For a given probability of failure the remaining load configurations and lengths, eq. (9) and (10) are solved for k_S and k_R respectively.

Throughout this paper the COV_S is set to 25 per cent.

4.2 Length effect in Eurocode 5

Over the years a great number of experimental studies on length effect of structural timber has been carried out. There have been almost as many suggestions about the magnitude of the length effect as there has been investigations. This is due to several difficulties, for example in finding matched samples of different lengths or heights, different sawing patterns, grading methods and species.

If we focus on length effect and leave out the height and width effect, the length effect factor ranges from about 0.15 to 0.25, Barrett and Fewell 1990, Madsen 1992. This factor refers to k in eq. (4). Two investigations on the variation of bending strength within elements, Isaksson 1996 and Källsner et al 1997 gave a length effect factor of 0.10. These two investigations differ from the others by using results from testing the variability of the bending strength within members. Studying boards of different lengths cut from the same original board eliminates the variation between samples.

The length effect factor, or depth effect factors has found its way to the codes as well. The design of timber members in bending according to the Eurocode 5 includes a correction factor for depths h less than 150 mm given as:

$$k_h = \min\left\{\begin{array}{l} (150/h)^{0.2} \\ 1.3 \end{array}\right. \quad (11)$$

The factor is based on the exponent k in eq. (4) to be 0.20.

4.3 Length effect using the statistical model

Based on 10000 simulated boards, the length effect is studied. The model described in the previous chapter is used with six different inputs, see *Table 8*. The results are analysed using the two methods presented in section 4.1, namely comparison of percentiles (mean value) and preserving the reliability index. The first method is also compared to Weibull theory. The inputs named LN50 and LN50step are presented in detail and the others are only included in a comparison of sensitivity in the results to the inputs. Load configuration number two, see *Figure 10*, (third point loading) and a board length of 3 m is selected as reference beam. *Table 9* shows the comparison of means of the LN50 input to the model. For the reference load an increase in length from 2 m to 4 m results in a decrease in strength of 8 per cent. The other load configurations give about the same or less effect in length. As can be seen in *Table 10*, k according to eq. (4) is close to 0.10 for the tested material. For the first four load cases k is around 0.10 and then decreases to a minimum of 0.055 for load case seven. The length effect is thus lower for beams with fixed supports and a more varying moment distribution. In *Table 11* and *Table 12* the results from using LN50step as input are shown. In this case the length effect is even smaller, especially for the last three load cases. For the reference load an increase in length from 2 m to 4 m results in a decrease in strength of 6 per cent. The effect of load configuration will be discussed in the next section.

In

Figure 11 the length effect when comparing means of the two inputs LN50 and LN50step is shown together with the length effect when using Weibull for two different k . Again, the reference load is used. For this load and $k=0.1$ the Weibull theory seems to fit well. However, according to *Table 10* and *Table 12* k changes with load configuration.

Length (mm)	Load configuration according to <i>Figure 10</i>						
	1	2	3	4	5	6	7
1500	0.975	1.089	1.121	1.238	1.158	1.231	1.242
2000	0.945	1.051	1.085	1.206	1.136	1.213	1.228
2500	0.924	1.022	1.057	1.179	1.116	1.203	1.219
3000	0.908	1.000	1.036	1.158	1.099	1.187	1.204
3500	0.896	0.983	1.019	1.138	1.085	1.176	1.195
4000	0.886	0.970	1.005	1.122	1.072	1.162	1.182
4500	0.877	0.958	0.994	1.109	1.063	1.153	1.174
5000	0.869	0.948	0.984	1.098	1.056	1.145	1.167
5500	0.862	0.939	0.975	1.087	1.046	1.136	1.158

Table 9. Length and load configuration effect using the LN50 model. Comparison is made on the mean value.

Length (mm)	Load configuration according to <i>Figure 10</i>						
	1	2	3	4	5	6	7
2000	0.945	1.051	1.085	1.206	1.136	1.213	1.228
4000	0.886	0.970	1.005	1.122	1.072	1.162	1.182
k	0.093	0.116	0.110	0.104	0.084	0.062	0.055

Table 10. The exponent k according to eq. (4) for two lengths and the seven load configurations. Based on the LN50 model.

Length (mm)	Load configuration according to Figure 10						
	1	2	3	4	5	6	7
1500	0.976	1.062	1.100	1.224	1.039	1.051	1.052
2000	0.955	1.033	1.069	1.196	1.033	1.050	1.052
2500	0.938	1.014	1.048	1.170	1.024	1.045	1.048
3000	0.925	1.000	1.032	1.150	1.019	1.043	1.047
3500	0.914	0.987	1.019	1.131	1.015	1.042	1.046
4000	0.906	0.976	1.007	1.116	1.010	1.039	1.043
4500	0.898	0.967	0.998	1.103	1.006	1.038	1.042
5000	0.890	0.960	0.990	1.091	1.000	1.033	1.039
5500	0.884	0.953	0.983	1.082	0.998	1.033	1.038

Table 11. Length and load configuration effect using the LN50step model. Comparison is made on the mean value.

Length (mm)	Load configuration according to Figure 10						
	1	2	3	4	5	6	7
2000	0.955	1.033	1.069	1.196	1.033	1.050	1.052
4000	0.906	0.976	1.007	1.116	1.010	1.039	1.043
k	0.076	0.082	0.086	0.100	0.032	0.015	0.012

Table 12. . The exponent k according to eq. (4) for two lengths and the seven load configurations. Based on the LN50step model.

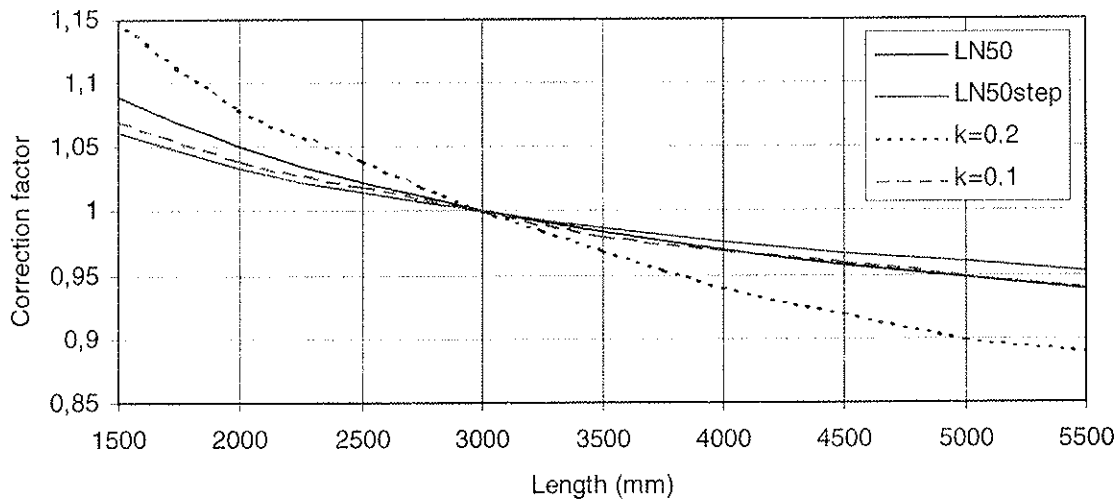


Figure 11. Length effect for the reference load. Two different inputs and two different k in eq.(4).

Figure 12 shows a comparison between the six different inputs to the model for the reference length and load. The results do not seem to be sensitive to the input to the model, at least not for simply supported beams.

If the length effect is determined by preserving the reliability index, the results for load case three (third point bending) are given in Table 13. The reference length is set to 3 m. The length effect has more or less disappeared compared to the results mentioned above. A 5.5-m long board has about 3 per cent less load carrying capacity than a 1.5-m long board, independent of reliability index. k_S and k_R refers to a correction factor on the action and resistance parameters

respectively. The *COV* of the load is set to 25 per cent. The factors are determined as described in section 4.1.

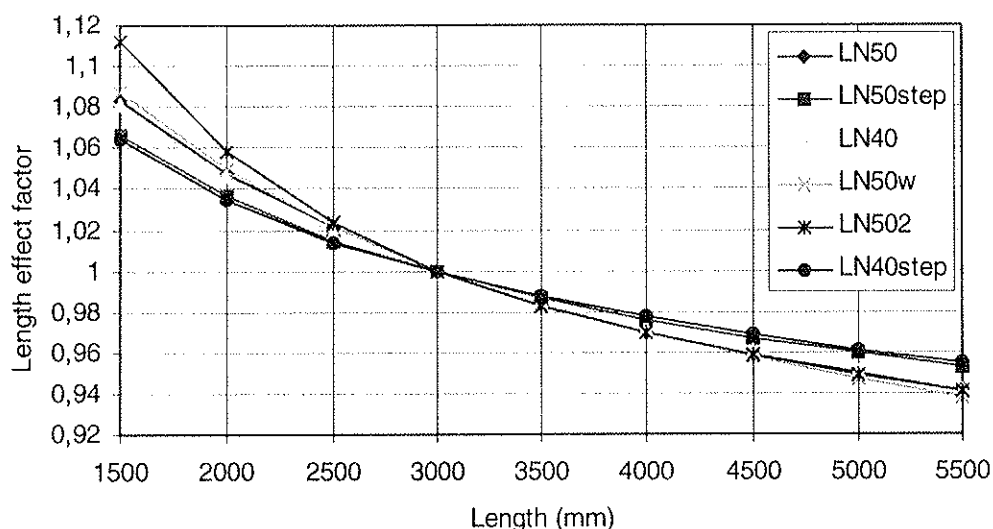


Figure 12. Comparison between the different models according to Table 8 for the reference load configuration (third point loading) and reference length of 3 m. The different inputs are compared to LN50.

Length (mm)	k_R				k_S			
	$P_I = 10^{-3}$	10^{-4}	10^{-5}	10^{-6}	$P_I = 10^{-3}$	10^{-4}	10^{-5}	10^{-6}
1500	0.985	0.987	0.988	0.990	1.016	1.015	1.014	1.012
2000	0.991	0.992	0.993	0.994	1.009	1.008	1.007	1.007
2500	0.996	0.997	0.997	0.998	1.004	1.003	1.003	1.002
3000	1	1	1	1	1	1	1	1
3500	1.003	1.003	1.003	1.002	0.996	0.997	0.997	0.997
4000	1.006	1.006	1.005	1.005	0.993	0.994	0.994	0.995
4500	1.008	1.008	1.007	1.006	0.991	0.992	0.992	0.993
5000	1.010	1.009	1.009	1.008	0.989	0.990	0.990	0.991
5500	1.012	1.011	1.01	1.009	0.987	0.988	0.989	0.990

Table 13. Length effect using reliability index. Load configuration two (third point loading). LN50 model.

4.4 Moment configuration factors using the statistical model

Using the same simulated boards as in the previous section the load configuration effect can be evaluated, both using a correction factor on a percentile (mean) and using the reliability index. Using the LN50 model the increase in load carrying capacity between the reference load configuration and beam with fixed supports and a uniformly distributed load is 20 per cent on the mean level, see Table 9. The other model, LN50step, gives very low load configuration effects for the beams with fixed supports, around 5 per cent, see Table 11. This is due to the absence of strong defect free sections. According to Table 10 and Table 12 it seems that k is dependent on type of load configuration. Also interesting to note is that when using Weibull theory the load configuration effect for load case four (simply supported with point load) and five (fixed supports

with point load) is equal, but the simulations show a significantly lower load configuration effect for load case five than case four, see *Table 9* and *Table 11*.

If the same loads are compared using the method of preserving the reliability index the effect is again, as with length effect, more or less gone. As shown in *Table 14* the maximum increase in load carrying capacity for the LN50 model is 6 per cent when comparing the extreme load cases one and seven, see *Figure 10*. The length of the board is 3 m. The correction factor on the action side, k_s , is shown in *Figure 13*, for different lengths and a given probability of failure. *Table 15* and *Figure 14* show the same but for the LN50step model. In this case the effect is as low as 3 per cent when comparing the same load cases as above.

Load configuration	k_R				k_S			
	$P_f = 10^{-3}$	10^{-4}	10^{-5}	10^{-6}	$P_f = 10^{-3}$	10^{-4}	10^{-5}	10^{-6}
1	1	1	1	1	1	1	1	1
2	0.9808	0.9821	0.9835	0.9847	1.0211	1.0201	1.0190	1.0179
3	0.9726	0.9740	0.9755	0.9768	1.0304	1.0294	1.0284	1.0274
4	0.9502	0.9528	0.9553	0.9576	1.0568	1.0551	1.0534	1.0517
5	0.9628	0.9655	0.9680	0.9704	1.0419	1.0399	1.0378	1.0357
6	0.9493	0.9531	0.9567	0.9602	1.0584	1.0553	1.0523	1.0492
7	0.9469	0.9509	0.9548	0.9585	1.0614	1.0582	1.0549	1.0516

Table 14. Load configuration effect, reference length 3 m. LN50.

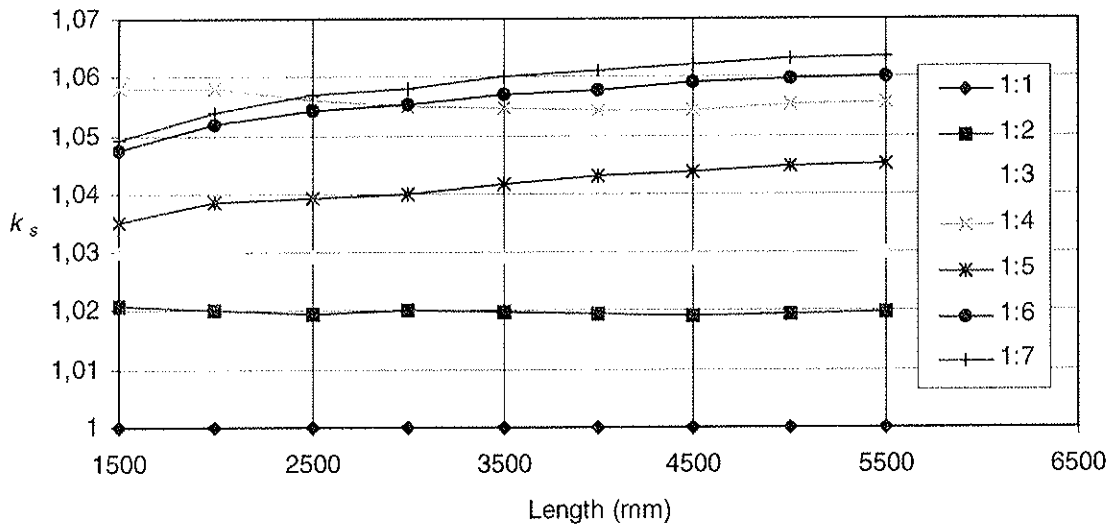


Figure 13. Load configuration factor k_s . LN50, $P_f = 10^{-4}$. Load case one is used as reference.

Load configuration	k_R				k_S			
	$P_f = 10^{-3}$	10^{-4}	10^{-5}	10^{-6}	$P_f = 10^{-3}$	10^{-4}	10^{-5}	10^{-6}
1	1	1	1	1	1	1	1	1
2	0.9835	0.9844	0.9853	0.9862	1.0180	1.0174	1.0167	1.0161
3	0.9760	0.9770	0.9780	0.9789	1.0264	1.0258	1.0253	1.0247
4	0.9533	0.9552	0.9570	0.9588	1.0529	1.0518	1.0508	1.0497
5	0.9782	0.9791	0.9798	0.9806	1.0238	1.0234	1.0230	1.0226
6	0.9737	0.9748	0.9759	0.9769	1.0290	1.0284	1.0278	1.0271
7	0.9731	0.9743	0.9754	0.9765	1.0297	1.0290	1.0283	1.0276

Table 15. Load configuration effect, reference length 3 m. LN50step.

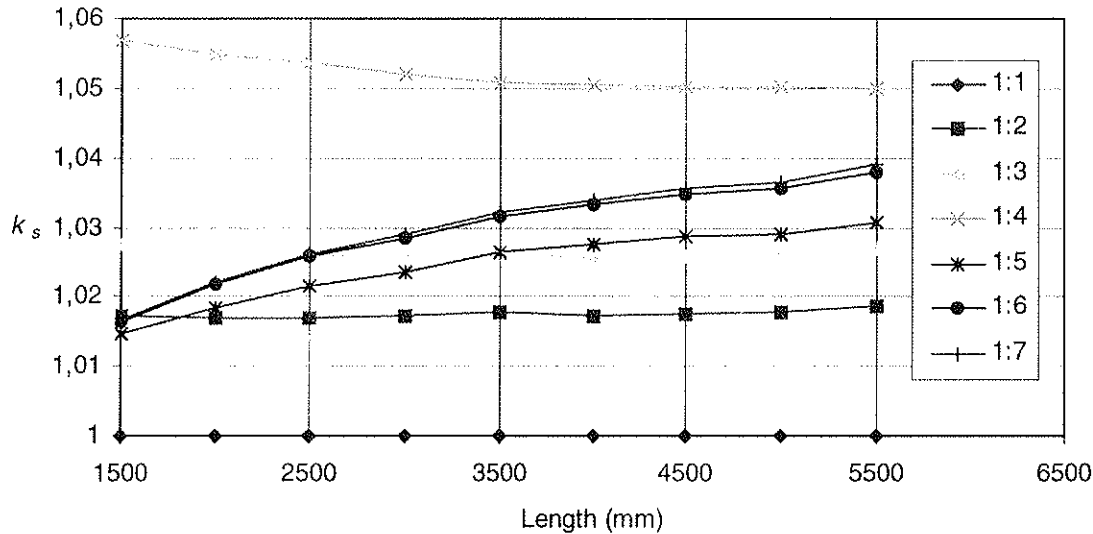


Figure 14. Load configuration factor k_s . LN50step, $P_f = 10^{-4}$. Load case one is used as reference.

4.5 Some remarks on the small length and load configuration effects

The results from the performed simulation studies in general show a significantly lower effect of length and load configuration than reported in for example Madsen 1992. Källsner et al 1997 also found the effect to be low. They had theories about a two-way effect, one purely statistical effect and one related to the actual testing. The latter can perhaps be explained by introducing fracture mechanics. However, the test results used in the presented model were compared with results from a matched sample tested according to the EN408 (third point loading), Isaksson 1996. It was found that the results did not differ significantly, i.e. the use of the test set-up according to *Figure 2* did not have any effect on the strength. This should be verified experimentally by testing boards of similar material with different lengths and load configurations.

5 Conclusions

Through experimental work it has been possible to determine the variation of bending strength both within and between members of structural timber. Based on the test results, a model of this variation has been developed. The basic input to the model is the two stochastic variables *strength of weak sections* and *distance between weak sections*.

Using this model, the effect of length and load configuration on the load carrying capacity of a beam has been investigated in a simulation study. The outcome of these simulations is analysed using two different methods of defining these effects. The first one is a comparison of percentiles (means) and the second one is referred to as the reliability index method. Most investigations on the length and load configuration effect have adopted the percentile method, which can be transformed to a Weibull effect.

CIB-W18/31-6-2

**INTERNATIONAL COUNCIL FOR BUILDING RESEARCH STUDIES AND DOCUMENTATION
WORKING COMMISSION W18 - TIMBER STRUCTURES**

TENSILE STRENGTH PERPENDICULAR TO GRAIN ACCORDING TO EN 1193

by

H J Blaß
M Schmid
University of Karlsruhe

GERMANY

MEETING THIRTY-ONE

SAVONLINNA

FINLAND

AUGUST 1998

Tensile Strength Perpendicular to Grain According to EN 1193

H.J. Blaß, M. Schmid
Lehrstuhl für Ingenieurholzbau und Baukonstruktionen
Universität Karlsruhe

1 Introduction

The tensile strength according to EN 384 is derived on the basis of a relationship between tensile strength perpendicular to grain and density:

$$f_{t,90,k} = 0,001 \rho \quad (1)$$

Equation (1) leads to higher characteristic tensile strength values for higher strength classes according to EN 338. In the German timber design code DIN 1052 the tensile strength perpendicular to grain is independent of the strength class. The same applies to the German National Application Document for EC5: a constant value of $f_{t,90,k} = 0,2 \text{ N/mm}^2$ for all classes is assumed (for the lowest class S7 $f_{t,90,k} = 0,0 \text{ N/mm}^2$). The National Design Specification (1991) of the USA specifies in 3.8.2 „... designs that induce tension stresses perpendicular to grain shall be avoided whenever possible. When tension stress perpendicular to grain cannot be avoided, mechanical reinforcement sufficient to resist all such stresses shall be considered ...“.

Ehlbeck and Kürth (1994) developed a test method later introduced in EN 1193. The corresponding test arrangement is shown in figure 1 and figure 2.

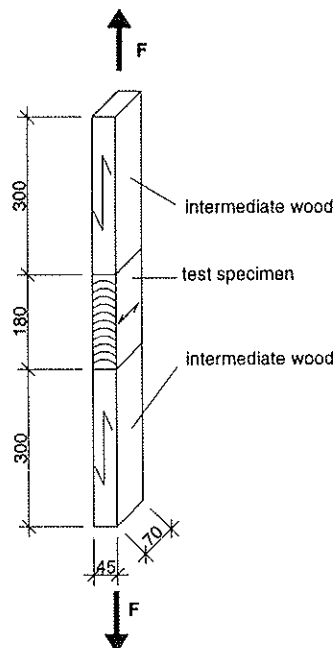


Figure 1: Test specimen for tensile strength perpendicular to grain

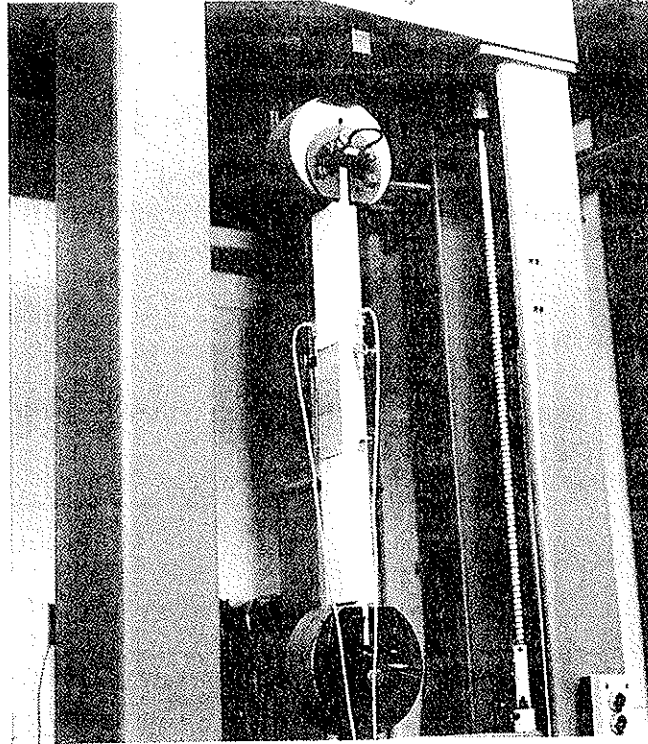


Figure 2: Test arrangement

The tested volume has a cross-section of 45 mm x 70 mm and a depth of 180 mm. Intermediate timbers stressed parallel to grain are bonded to the specimens. Two inductive measuring gauges are attached diagonally.

2 Material

187 tests according to EN 1193 were carried out at the University of Karlsruhe in 1997. The timber was taken from planks that were partly used in other test series for determining the edgewise bending strength and modulus of elasticity parallel to grain. The species was spruce (*picea abies*). Only for the specimens loaded mainly in tangential direction, bending strength and modulus of elasticity were known. Figure 3 shows the different orientations of the annual rings having a distinct influence on the tensile strength perpendicular to grain.

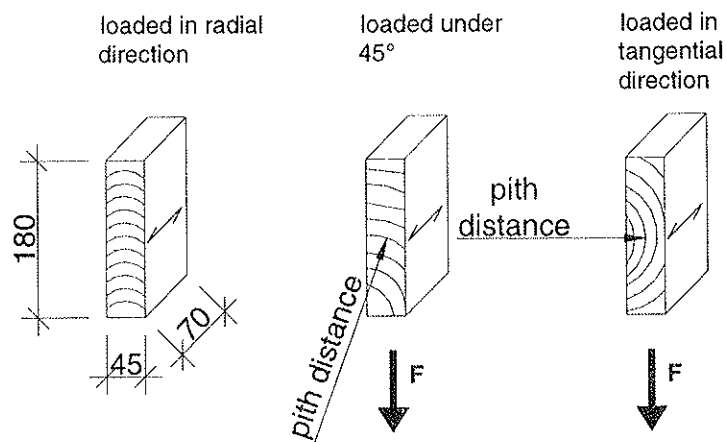


Figure 3: Orientation of annual rings within the specimens

Apart from the bending strength and the modulus of elasticity parallel to grain, the density, the annual ring width and the distance from the pith to the centre of the specimen were determined. For determining the pith distance copies of the test specimens were scanned by a CAD-system. Especially for the specimens loaded in radial direction these values were difficult to determine. For the different load directions the mean values of all parameters are given in the table 1.

Table 1: Parameter mean values

Orientation according to figure 3	number	density [kg/m ³]	bending strength [N/mm ²]	modulus of elasticity parallel to grain [N/mm ²]	annual ring width [mm]	pith distance [mm]
radial	24	477			3,5	138
45°	18	497			3,6	127
tangential	139	427	40,2	11686	3,2	63
including pith	6	423	41,5	11083	3,3	23
all	187	440	40,2	11673	3,3	77

Figure 4 shows a histogram of the density distribution with subgroups of annual ring orientation.

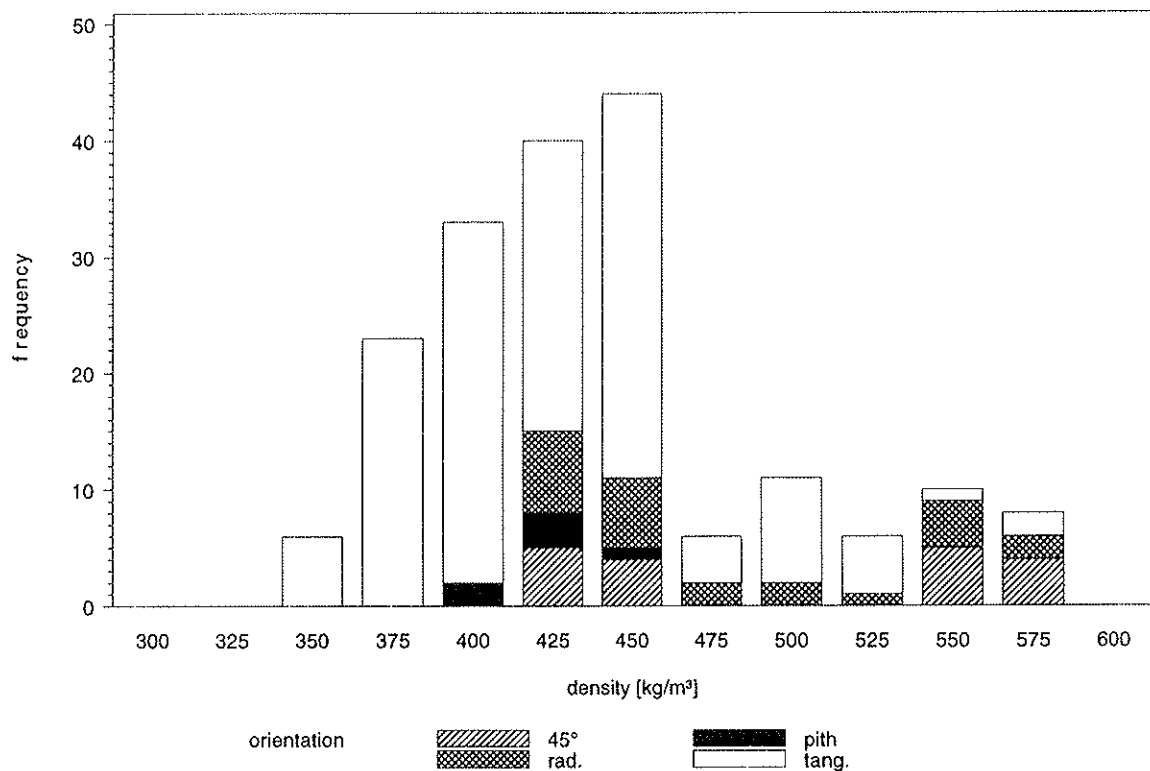


Figure 4: Distribution of density

Table 2 contains the correlation coefficients between the different parameters.

Table 2: Coefficients of correlation

	density	annual ring width	bending strength	modulus of elasticity parallel to grain	pith distance
density	-	-0,235	0,398	0,492	0,424
annual ring width	-0,235	-	-0,521	-0,516	-0,025
bending strength	0,398	-0,521	-	0,853	0,309
modulus of elasticity parallel to grain	0,492	-0,516	0,853	-	0,330
pith distance	0,439	-0,036	0,304	0,329	-

The material was sampled in order to achieve a representative sample for planks used for joists or trusses. It depends on the size of the tree and the way the timber is cut, if the orientation of the annual rings according to figure 3 is representative, too. One could expect that planks will be mostly cut as shown in figure 5. In the tests carried out in Karlsruhe these planks would be mainly stressed in tangential direction. Nevertheless the tests are evaluated separately for the different orientations.

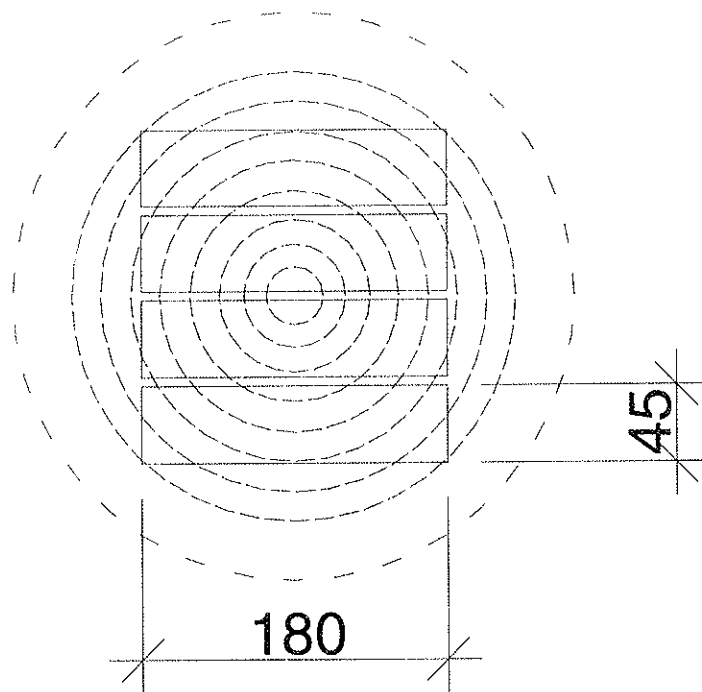


Figure 5: Cutting pattern

3 Results

53% of all specimens failed at the bonded joint between intermediate wood and test specimen. In table 3 mean values of tensile strength are given, depending on the location of rupture and the orientation of annual rings.

Table 3: Tensile strength

annual rings' orientation according to figure 3	fracture at joint		fracture in wood	
	$f_{t,90,mean}$ [N/mm ²]	number	$f_{t,90,mean}$ [N/mm ²]	number
radial	2,33	13	2,81	11
45°	1,92	15	2,64	3
tangential	1,94	71	1,65	68
including pith	-	-	1,02	6
all	1,99	99	1,79	88

It was assumed that the reason for the different failure behaviour and the different tensile strengths were caused by the different annual ring orientation, leading to anisotropic specimens. For every test specimen the difference between the two measured displacements was therefore evaluated. This was done in 10%-steps of the maximum force. Each point in figure 6 shows the mean value of these differences, again separated according to the orientation of annual rings.

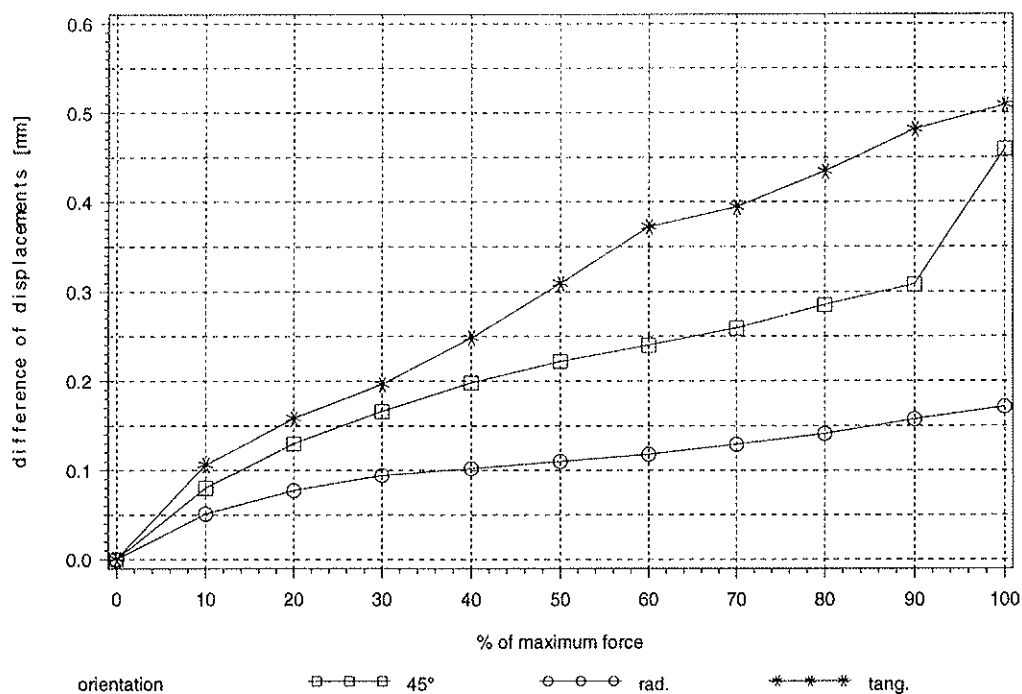


Figure 6: Differences of displacements between gauges versus parts of maximum force

Obviously the difference is greatest for specimens stressed in tangential direction, intermediate for specimens loaded under 45° and minor for specimens loaded in radial direction. The measured mean modulus of elasticity for the different orientations is given in table 4.

Table 4: Mean modulus of elasticity perpendicular to grain

	radial	45°	tangential	including pith
E_{90} [N/mm ²]	726	286	163	282

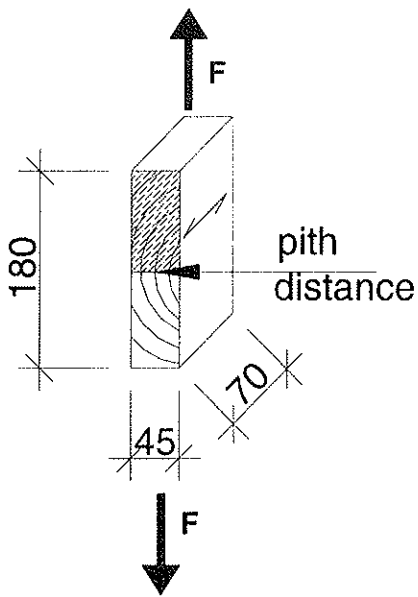
The large difference between radial and tangential modulus of elasticity leads to a non-uniform stress distribution. This is especially the case for the specimens loaded in tangential direction.

In order to assess the distribution of stress in the specimens a two-dimensional Finite Element calculation was performed. The stress-strain relationship used is given below. The first index marks the normal to the surface, the second the direction of stress or strain. 1 marks the radial, 2 the tangential and 3 the direction parallel to grain.

$$\begin{Bmatrix} \varepsilon_{11} \\ \varepsilon_{22} \\ \varepsilon_{33} \\ \gamma_{12} \\ \gamma_{13} \\ \gamma_{23} \end{Bmatrix} = \begin{bmatrix} a_{11} & a_{21} & a_{31} & 0 & 0 & 0 \\ a_{12} & a_{22} & a_{32} & 0 & 0 & 0 \\ a_{13} & a_{23} & a_{33} & 0 & 0 & 0 \\ 0 & 0 & 0 & a_{44} & 0 & 0 \\ 0 & 0 & 0 & 0 & a_{55} & 0 \\ 0 & 0 & 0 & 0 & 0 & a_{66} \end{bmatrix} \begin{Bmatrix} \sigma_{11} \\ \sigma_{22} \\ \sigma_{33} \\ \sigma_{12} \\ \sigma_{13} \\ \sigma_{23} \end{Bmatrix}$$

$$\begin{Bmatrix} \varepsilon_{11} \\ \varepsilon_{22} \\ \varepsilon_{33} \\ \gamma_{12} \\ \gamma_{13} \\ \gamma_{23} \end{Bmatrix} = \begin{bmatrix} 1,25 \cdot 10^{-3} & -750 \cdot 10^{-6} & -50,0 \cdot 10^{-6} & 0 & 0 & 0 \\ -750 \cdot 10^{-6} & 5,0 \cdot 10^{-3} & -75 \cdot 10^{-6} & 0 & 0 & 0 \\ -50,0 \cdot 10^{-6} & -75 \cdot 10^{-6} & 83,33 \cdot 10^{-6} & 0 & 0 & 0 \\ 0 & 0 & 0 & 25 \cdot 10^{-3} & 0 & 0 \\ 0 & 0 & 0 & 0 & 1,43 \cdot 10^{-3} & 0 \\ 0 & 0 & 0 & 0 & 0 & 1,43 \cdot 10^{-3} \end{bmatrix} \begin{Bmatrix} \sigma_{11} \\ \sigma_{22} \\ \sigma_{33} \\ \sigma_{12} \\ \sigma_{13} \\ \sigma_{23} \end{Bmatrix}$$

The values are taken from Neuhaus (1981). For $a_{22} = 1 / E_{22}$ Neuhaus recommends $1 / 420$ N/mm². a_{22} was assumed as $1 / 200$ N/mm² instead in order to reflect the measured values given in table 4 for tangential direction. Consequently the non-uniformity of the stress distribution is enlarged. In figure 9 the values calculated with $a_{22} = 1 / E_{22} = 1 / 420$ N/mm² are given in parentheses.



For the calculations a cylindrical coordinate system and plain strain condition was assumed. Figures 8 to 10 show the calculated stress distribution for half the cross section of specimens loaded in tangential direction with different pith distances. The applied load causes an average tensile stress of 1,8 N/mm², the mean strength of the specimens loaded in tangential direction.

Figure 7: Area shown in figures 8 to 10

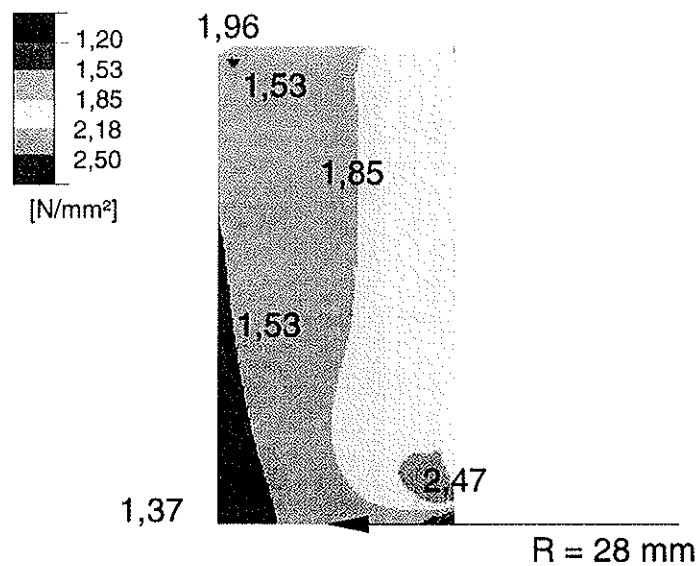


Figure 8: Perpendicular to grain stresses for a pith distance (radius) of 28 mm, the minimum radius of the tangential specimens

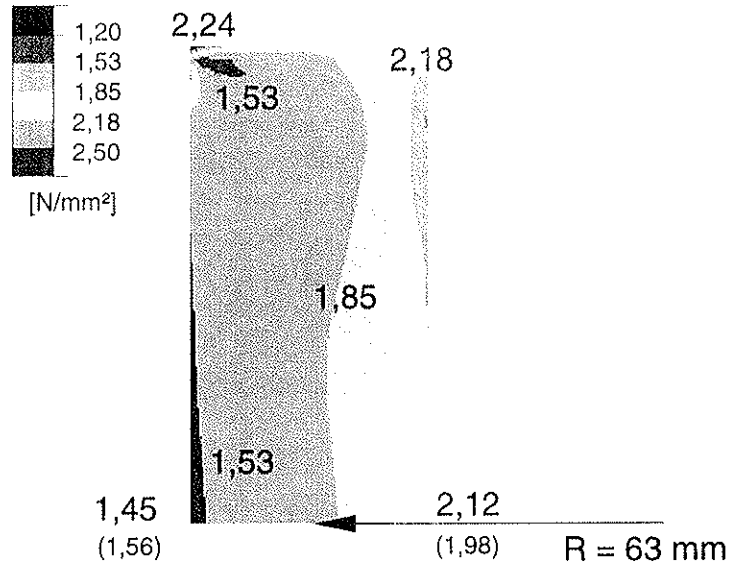


Figure 9: Perpendicular to grain stresses for a pith distance (radius) of 63 mm, the mean radius for tangential specimens

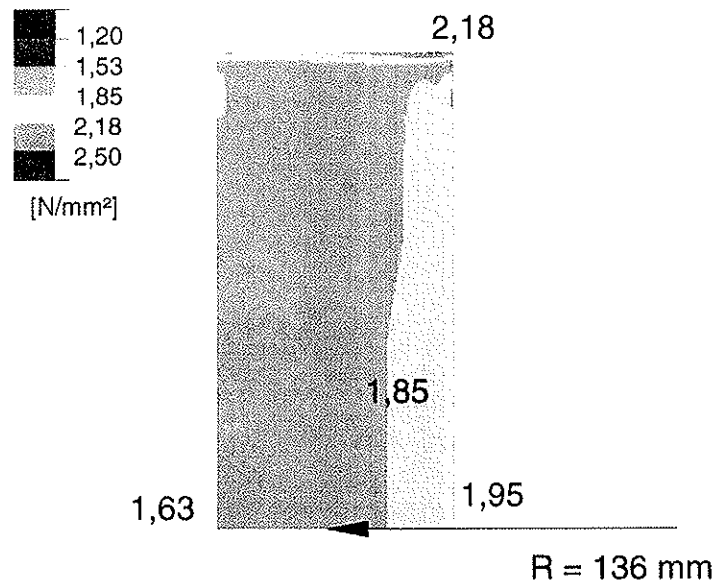


Figure 10: Perpendicular to grain stresses calculated for a pith distance (radius) of 136 mm, maximum radius of the tangential specimens

Figure 11 shows for comparison the calculated stresses for a radial specimen.

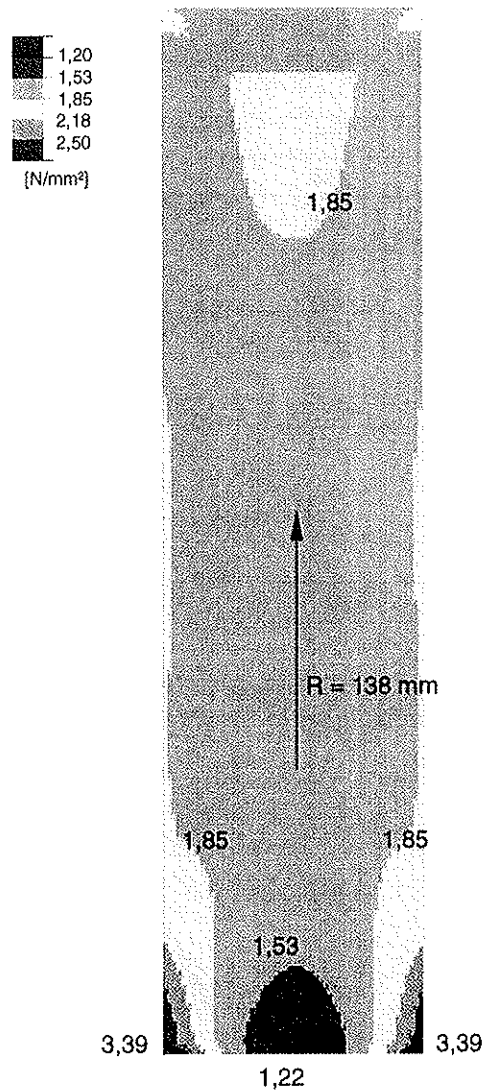


Figure 11: Perpendicular to grain stresses calculated for a pith distance (radius) of 138 mm, mean radius of the radial stressed specimens

9 out of 13 radial and 13 out of 15 45° specimens with a failure at the bond line broke at the side closer to the pith. For the 45° specimens both effects, stress peaks at the joint and non-uniform stress distribution in the wood seem to take effect. Only three specimens failed within the wood.

Table 5 contains the tensile strength values evaluated according to EN 1193, assuming a uniform stress distribution. The real non-uniform stress distribution will of course induce rupture at a lower force $F_{t,90,max}$ compared with a uniform stress distribution.

Table 5: Tensile strengths perpendicular to grain, separated by orientation

annual ring orientation	number	$f_{t,90,mean}$ [N/mm ²]	$f_{t,90,minimum}$ [N/mm ²]	$f_{t,90,maximum}$ [N/mm ²]	5% - fractile [N/mm ²]	standard-deviation [N/mm ²]
radial	24	2,55	1,84	3,19	1,84	0,485
45°	18	2,04	1,01	3,18	1,01	0,649
tangential rupture at bonded joint (density [kg/m ³])	71	1,94 (437)	0,57 (355)	2,77 (579)	1,41 (369)	0,382 (49,0)
tangential rupture in wood (density [kg/m ³])	68	1,65 (416)	0,70 (341)	2,77 (565)	0,92 (361)	0,418 (39,4)
tangential all (density [kg/m ³])	139	1,80 (427)	0,57 (341)	2,77 (579)	0,95 (364)	0,423 (45,7)
including pith	6	1,02	0,45	2,03	0,45	0,619
all	187	1,89	0,45	3,19	0,95	0,548

Figures 12 to 14 show the cumulative frequency distributions of the tensile strength perpendicular to grain of all specimens.

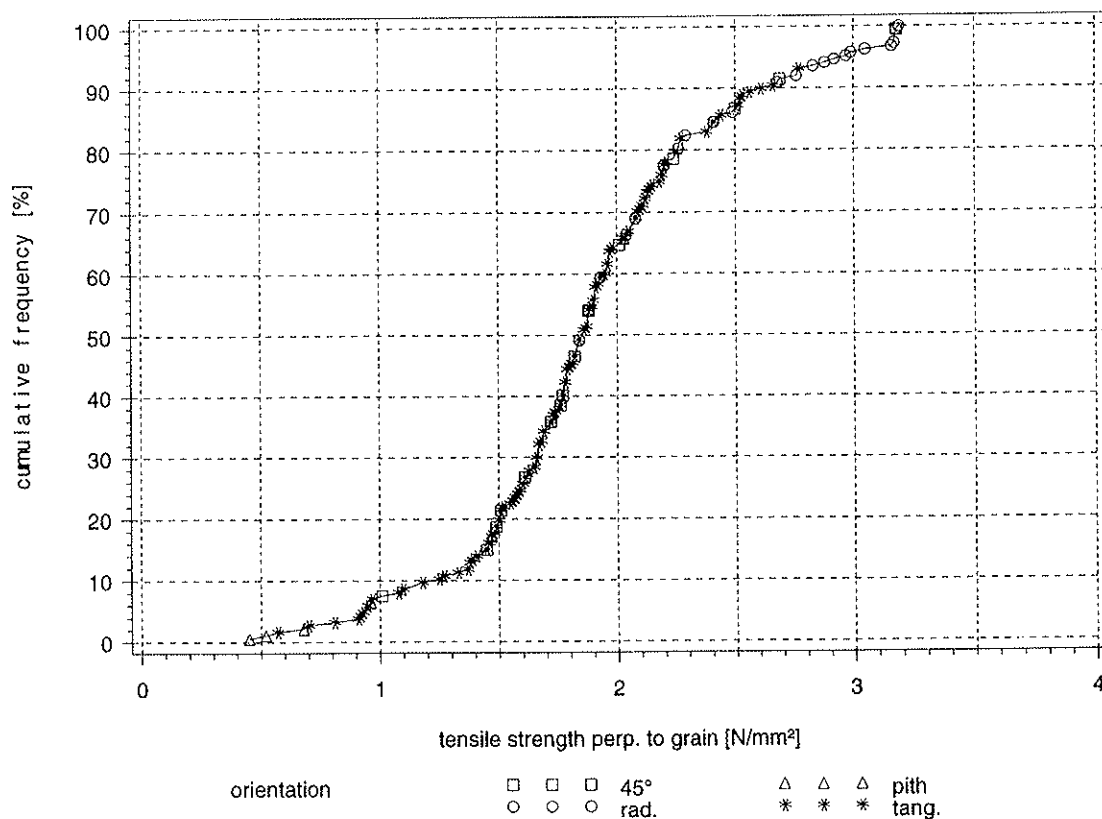


Figure 12: Cumulative frequency distribution of tensile strength perpendicular to grain

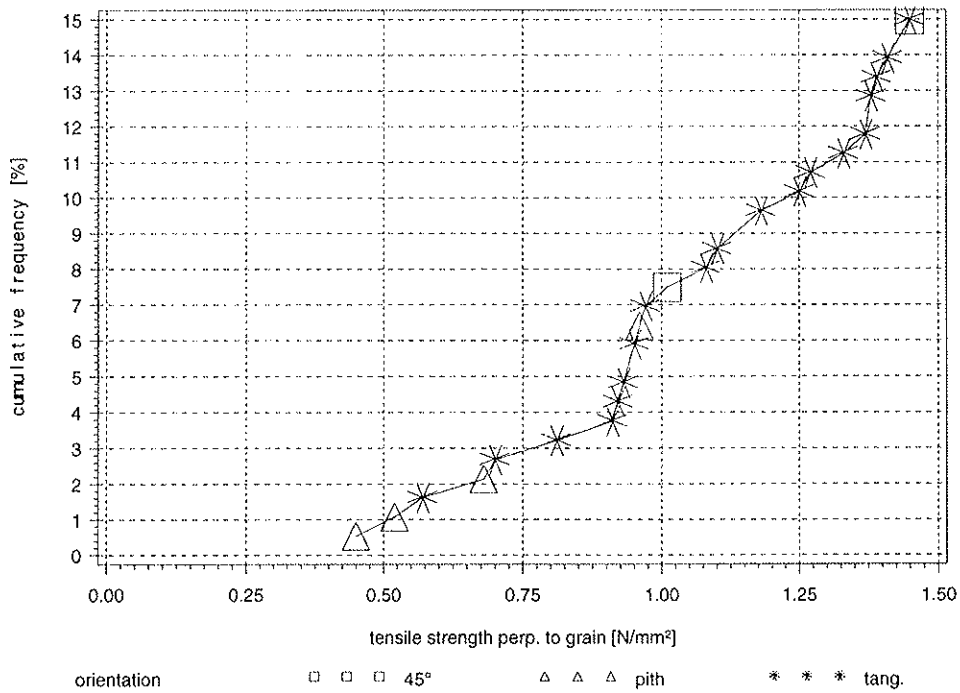


Figure 13: Lower 15% of cumulative frequency distribution of tensile strength perpendicular to grain

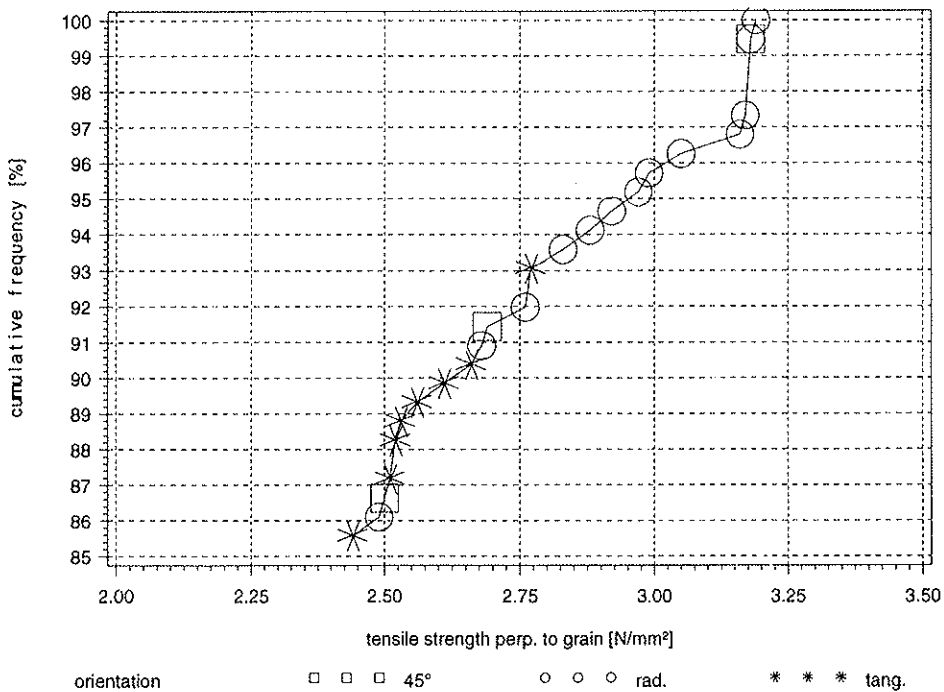


Figure 14: Upper 15% of cumulative frequency distribution of tensile strength perpendicular to grain

One important aim of the study was to check the correlation of tensile strength perpendicular to grain with other wood properties, especially the density. Table 6 contains the corresponding coefficients of correlation. Because of the different properties of the

groups (see table 1) and the different mechanical behaviour caused by the orientation, the values of the separated groups are more realistic than the overall values.

Table 6: Coefficients of correlation of tensile strength perpendicular to grain with the recorded parameters

Orientation	number	density	modulus of elasticity parallel to grain	bending strength	pith distance	annual ring width
radial	24	0,053	-	-	0,247	0,218
45°	18	-0,232	-	-	0,209	0,177
tangential rupture at bond line	71	0,577	0,322	0,300	0,046	-0,373
tangential rupture in wood	68	0,095	0,049	0,168	0,061	0,003
all tangential stressed	139	0,402	0,258	0,294	0,192	-0,250
pith	6	0,694	0,783	0,796	-0,789	-0,497
all	187	0,358	0,265	0,272	0,486	-0,088

Figure 15 shows the correlation with the density for the tangential specimens, separated by the location of rupture.

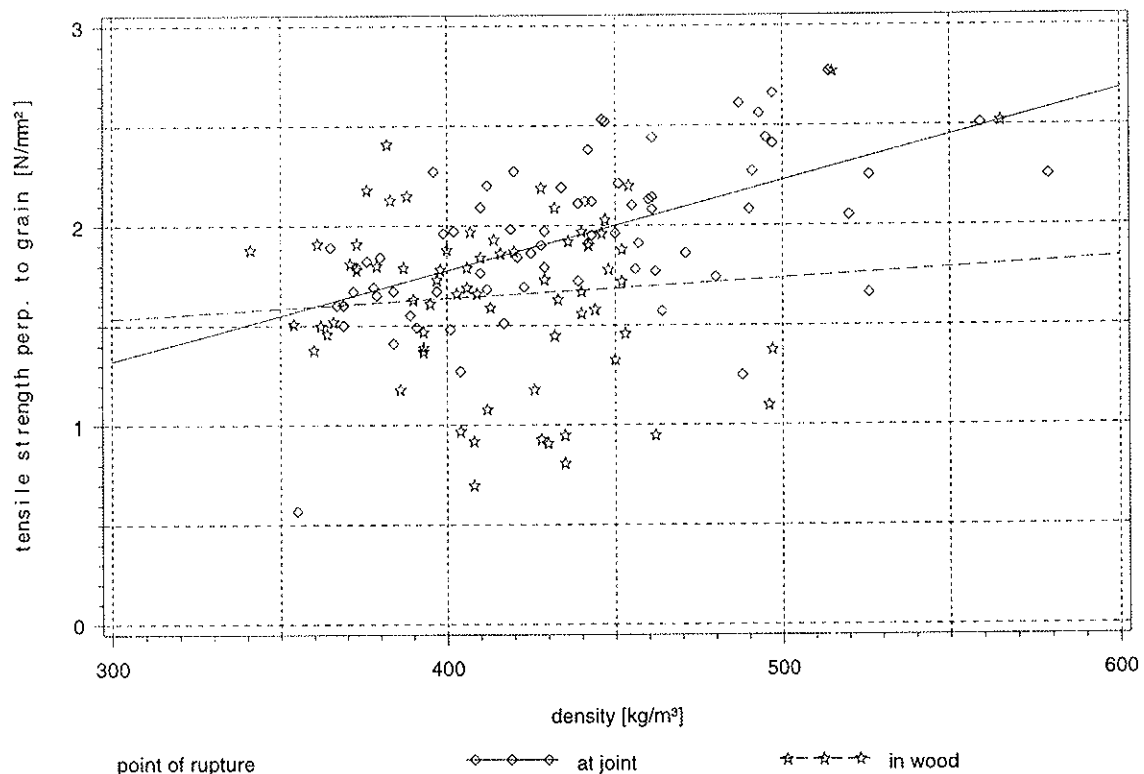


Figure 15: Tensile strength versus density for the tangential specimens
 Dashed line: rupture in wood: $f_{t,90} = 1,23 + 0,001 \cdot \rho$
 Solid line: rupture at joint: $f_{t,90} = -0,03 + 0,0045 \cdot \rho$

Figure 16 shows the correlation with the density for all specimens.

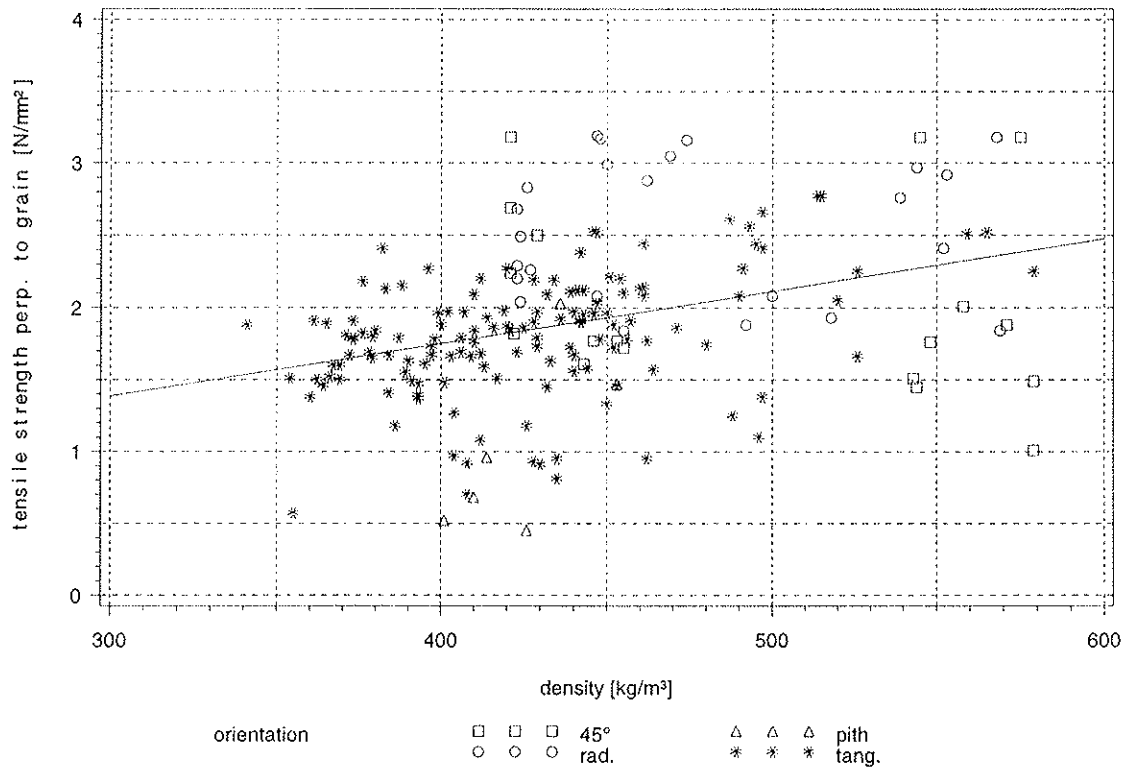


Figure 16: Tensile strength versus density for all specimens: $f_{t,90} = 0,298 + 0,0036 \cdot \rho$

The difference in coefficients of correlation between tensile strength and density for the tangential specimens with rupture at the bond line and rupture in wood, respectively, seems significant. The difference might be explained by Weibull's theory of rupture. Weibull (1939) assumes a random strength distribution within a volume. If stresses are varying, rupture not necessarily occurs at the point of maximum stresses, but starts where the ratio of stress to strength reaches a maximum.

Following Weibull's theory, rupture in wood might be caused by randomly distributed, microscopic, mechanical defects. A correlation of such defects with the density seems unlikely. A rupture at the bond line, however, takes place at a predetermined location, induced by stress peaks. In this case a correlation of tensile strength perpendicular to grain with density is shown by a coefficient of correlation of 0,577.

This assumption is confirmed by tests for determining the fracture energy of wood perpendicular to the grain, reported by Larsen and Gustafsson (1990). The crack in these tests is also induced at a predefined point. The following regression is given for the fracture energy G_{Ic} of European softwood : $G_{Ic} = - 146 + 1,04 \cdot \text{density}/(\text{kg}/\text{m}^3)$ [Nm/m²].

Figure 17 shows a Weibull distribution fitted to the tensile strength values of all specimens with rupture in the wood, ignoring the orientation of growth rings. If this distribution is tested with a chi-square test, an acceptance on the confidence level of 99,3% results, whereas the test for the specimens with rupture at the bond line is accepted on a confidence level of 92,2%.

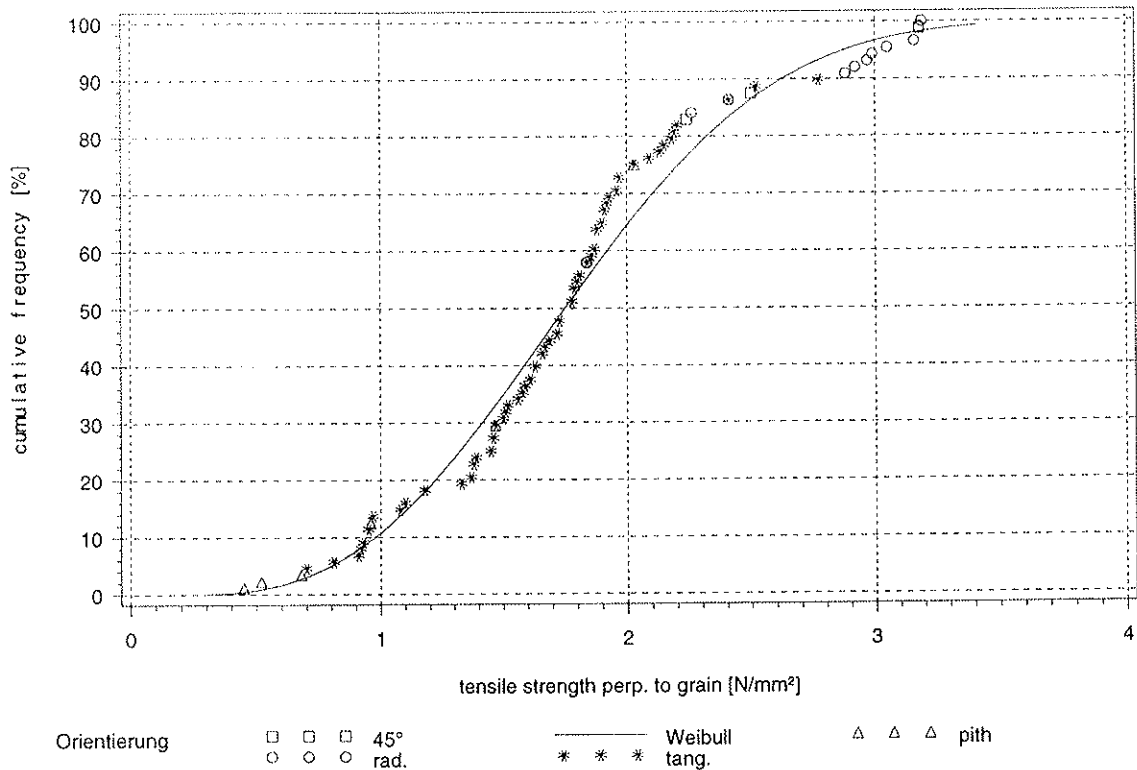


Figure 17: Weibull distribution fitted to the specimens with rupture in the wood:
 $S = 1 - \exp\left\{-\left(\frac{f_{t,90}-0,232}{1,746}\right)^{2,653}\right\}$

4 Summary

The tensile strength perpendicular to grain of 187 wood specimens was determined using the test arrangement of EN 1193 (see figures 1 and 2). 53 % of these specimens failed right at the bond line at the intermediate wood. By Finite Element calculations it was shown that stress intensities are evoked at the bond line and the stress distribution in the specimen is non-uniform.

An important aim of the project was to determine the correlation of tensile strength perpendicular to the grain with other properties, especially with the density. By separating the largest group of the tangential specimens by the location of rupture, the result was a comparatively high coefficient of correlation for specimens which failed at the joint and a very small coefficient of correlation for those with failure in the wood. One possible hypothesis for this result is based on Weibull's probabilistic fracture theory.

It has to be emphasised that the tests were done with nearly clear wood specimens without visible cracks or splits, which often occur in structural size timber. Especially because of cracks, the tensile strength perpendicular to grain in structural timber will be lower than the values given in table 5.

References

Ehlbeck, J. and Kürth, J. (1994). Ermittlung der Querkzugfestigkeit von Voll- und Brettschichtholz - Entwicklung eines Prüfverfahrens, Forschungsbericht der Versuchsanstalt für Stahl, Holz und Steine, Abteilung Ingenieurholzbau, Universität Karlsruhe (TH).

Larsen, H.J. and Gustafsson, P.J. (1990). The Fracture Energy of Wood in Tension Perpendicular to Grain. CIB-W18A/23-19-2

National Design Specification for Wood Construction (1991). American Forest Paper Association, Washington, D.C..

Commentary on the National Design Specification for Wood Construction (1993). American Forest Paper Association, Washington, D.C..

Neuhaus, F.-H. (1981). Elastizitätszahlen von Fichtenholz in Abhängigkeit von der Holzfeuchte, Mitteilung Nr. 81-8, Institut für konstruktiven Ingenieurbau Ruhr-Universität Bochum

Weibull, W. (1939). A statistical theory of the strength of materials. In: Royal Swedish Institute for Engineering Research, Proceedings, N. 141, S. 45

Weibull, W. (1939). The phenomenon of rupture in solids. In: Royal Swedish Institute for Engineering Research, Proceedings, N. 153, S. 55

**INTERNATIONAL COUNCIL FOR BUILDING RESEARCH STUDIES AND DOCUMENTATION
WORKING COMMISSION W18 - TIMBER STRUCTURES**

STRENGTH OF SMALL DIAMETER ROUND TIMBER

by

A Ranta-Maunus
U Saarelainen
VTT Building Technology

H Boren
Finnish Forest Research Institute

FINLAND

MEETING THIRTY-ONE

SAVONLINNA

FINLAND

AUGUST 1998

Strength of small diameter round timber

Alpo Ranta-Maunus and Urho Saarelainen, VTT Building Technology
Hannu Boren, Finnish Forest Research Institute, Finland

1 Introduction

In many European countries there is a surplus of small diameter (8-15 cm) round timber, which is harvested from forest thinnings. A joint European (FAIR) project was started 1996 in order to develop the use of small diameter round timber in construction. The overall objective of the research is to develop structural systems in which small diameter round timber can be used and thereby create a new market for small diameter roundwood. VTT is coordinating the project and the other participants are Agricultural Research Centre of Finland (MTT), Technological University Delft, University of Surrey from the UK, Lekopa Oy from Finland, Universität für Bodenkultur (BOKU) from Austria, and Centre Technique du Bois et de l'Ameublement (CTBA) from France.

The work includes the strength testing of the material, strength grading, and the development of structures. The aim is to facilitate international standardization in this area. As part of the initial market study, architects were asked to identify feasible types of structures in which round wood has a potential use, and several areas were established. A common factor in the different countries was: rural buildings and tourist industry buildings are likely to be appreciated when built of roundwood [5,6]. The results of the project, which will continue until the end of 1998, are summarised by Ranta-Maunus [1].

It is known that bending strength of round timber is fairly high. Some results of an old, unpublished Finnish research are shown in Fig. 1 indicating a clear dependence on knot size. In Finnish standards, a characteristic bending strength of 30 MPa has been adopted for pine and spruce round timber, if no other information is available. According to Fig. 1 this seems appropriate, when maximum knot diameter is not larger than 40 mm, or KAR (ratio of the sum of knot diameters to the circumference of the log) is less than 0.15.

Small diameter (80 to 150 mm) round wood could have lower strength than mature logs, because it is, to large extent, juvenile wood. On the other hand, the concept of size effect suggests that small diameter wood should have higher strength than large diameter timber. These conflicting arguments provide the background for the strength testing carried out in this project.

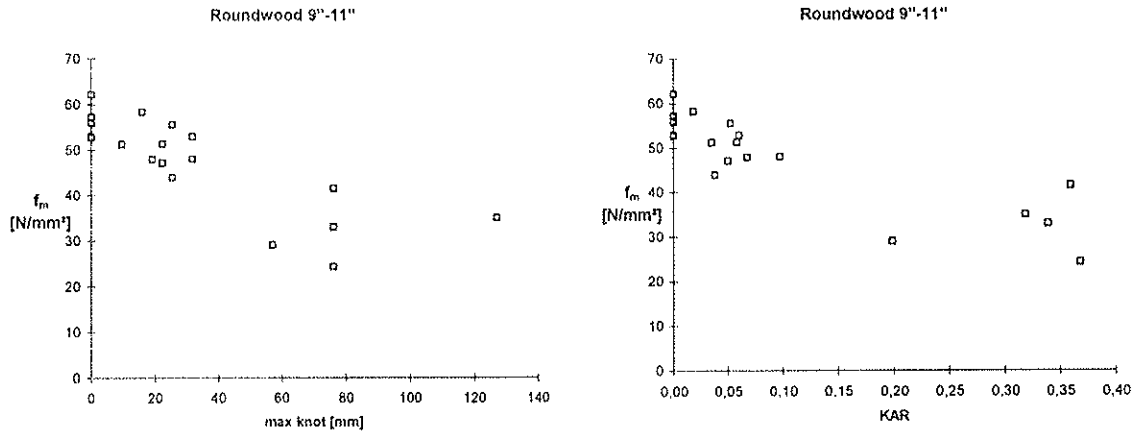


Figure 1 Bending strength of seasoned pine logs tested in 1950s.

2 Materials and methods

The total numbers of logs used for testing by various partners is given in Table 1. Same logs may have been used for different strength tests. This paper summarises the results of tests carried out in Finnish wood although some references are made to results obtained by other participants in the project.

Table 1 Number of stems harvested.

Species	Finland	Holland	UK	Austria	France
Scots pine	275		100		
Norway spruce	175			430	
Sitka spruce			100		
Japanese larch		200			
Douglas					780

The Finnish logs were dried to two target moisture contents: 18 and 12%. The objective in sampling was to use quality easily available in forest thinning when better logs are left to grow.

The quality of the timber has been studied considering several variables such as density, dimensions, curvature, growth ring width, knot sizes as well as stem curving and checking when drying. The average properties are summarized in Table 2. For comparison, the average basic density (ratio of oven-dry mass to green volume) of mature Norway spruce and Scots pine logs are 373 and 427 kg/m³ in South-Finland, respectively [8]. The average basic density of tested small diameter round Norway spruce and Scots pine were 385 and 395 kg/m³ (South-Finland), respectively. The average knot sum of tested round Norway spruce and Scots pine were 39 and 78 mm, respectively.

Bending testing was made using 4-point bending. Both the bending and compression testing method followed EN384 as closely as practical for round timber with conical shape and variable diameters.

Table 2 Average properties of the Finnish logs.

General average properties					
Species	Form	Annual increment cm	Annual ring width mm	Density at 12% MC kg/m ³	Gross grain mm/m
Scots pine	Round	41	3.4	471	24
	Partly sawn	39	3.2	482	26
	Squared sawn	38	5.0	422	49
Norway spruce	Round	27	1.7	459	12
	Squared sawn	28	2.3	432	27

		Diameter mm	KAR per circum, %	Max knot diameter, mm	Tapering mm/m
Scots pine	Round	125	20	20	4.0
	Partly sawn	148	16	21	4.2
	Sawn	101	26	27	0.0
Norway spruce	Round	109	11	11	3.8
	Sawn	101	13	14	0.0

3 Strength results

3.1 Bending

The bending results are given in Table 3 at testing conditions without any moisture adjustments. The 5th percentile values have been determined for each sample by using ranking method. These values show that the strength of small diameter round timber is fairly high, and a large proportion of the juvenile wood is not an obstacle for using this material in load bearing structures. The bending strength, in particular, is higher than would be obtained for sawn timber made from the same raw material [7]. This difference is caused partly by the cutting process in sawing, and partly by the round form. The latter causes a 10% difference in bending strength according to the Weibull theory ($k = 5$).

Table 3 Bending results for Finnish small diameter round timber at test conditions.

Sample identification	Sample size	Mean MC [%]	Mean density at 12%MC [kg/m ³]	Mean KAR [%]	$f_{m,mean}$ [N/mm ²]	$f_{m,05}$ [N/mm ²] by ranking	$E_{m,mean}$ [kN/mm ²]
pine 1+26+176	75	19.7	469	21.6	45.0	31.5	10.3
pine 51+76	50	13.4	455	20.1	49.1	34.8	11.3
pine 226	49	13.4	484	16.4	59.6	41.8	11.3
spruce 1+51	50	13.8	462	11.4	70.2	54.0	12.9
spruce 26+76	50	14.1	468	10.7	64.0	49.1	12.4
spruce 101+126	50	19.1	466	10.2	59.4	46.2	12.2

3.2 Compression

The results of the compression tests are given in Table 4. The ratio of compression to bending strength varies from 0.5 to 0.8 as obtained for different species by the different

Table 4 Compression results for Finnish small diameter round timber at test conditions.

Sample identification	Sample size	Mean MC [%]	Mean density at 12%MC [kg/m ³]	Mean KAR [%]	$f_{c,mean}$ [N/mm ²]	$f_{c,05}$ [N/mm ²] by ranking	$E_{c,mean}$ [kN/mm ²]
pine1+26+176	75	19.0	466	29.9	19.3	14.9	8.4
pine51+76	50	13.8	447	25.7	25.6	21.1	8.9
pine 226	50	10.8	506	8.3	37.3	30.0	11.5
spruce1+51	50	14.2	447	16.5	31.3	25.6	12.6
spruce26+76	50	14.2	453	12.3	32.7	28.1	12.7
spruce 101+126	50	18.7	453	13.2	26.3	21.3	12.2

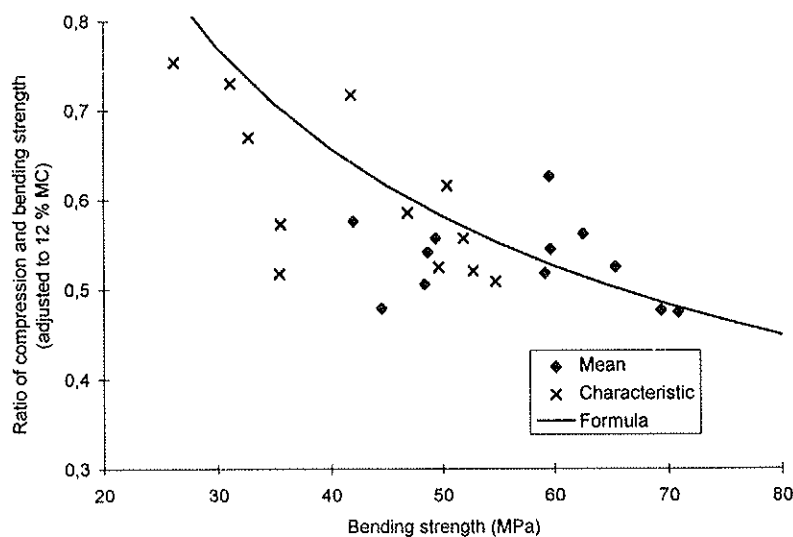


Figure 1 Ratio of compression and bending strength obtained by VTT. Points are mean and 5-percentile values for each sample of size 25. The formula refers to the ratio adopted in CEN standards for characteristic values of sawn timber $f_c = 5 f_m^{0.45}$.

participants in the project. For tested pine and spruce it is lower than for larch and Douglas fir. Finnish results are illustrated in Fig. 1. This variation may be influenced by the fact that experiments were made at different moisture contents (8-20 %), and the adjustment to 12% MC made according to CEN may be not adequate for compression. Also the quality of timber (density, KAR) in bending tests was slightly higher than the quality in compression tests except for one test series. It is concluded that the deviation of observations around the curve $f_c = 5 f_m^{0.45}$ is increased by the differences in the quality of compression and bending specimens. Detailed reports on strength values are given in several papers [2-4]. In order to avoid unsafe situations the values from the compression tests will also be used in strength grading.

3.3 Regression models

The effect of several variables on strength and stiffness has been studied using the multiple regression analysis. The results given in this paper are based on the combination of British and Finnish pine samples. A detailed analysis is reported in [3]. Several regression equations were determined and the significance of variables analyzed. In brief, the relations obtained are summarized as follows:

Stiffness in bending depends on knot sum (ks [mm]) and density [kg/m^3] as follows:

$$\text{LOG } E_m = 0.636 - 0.000803ks + 0.000998 \rho_{12} \quad \text{or} \quad (1)$$

$$E_m = 10^{0.636 - 0.000803ks + 0.000998 \rho_{12}}$$

For bending strength a linear relation to KAR, density, processing method ($p_2=0$ for machine debarking, 1 for barking iron) and tapering (t [mm/m]) was obtained:

$$f_m = 24.4 - 0.084ks/d + 0.0711 \rho_{12} + 5.5p_2 - 1.0t \quad (2)$$

For compression strength also a strong moisture (u [%]) dependence was obtained:

$$\text{LOG } f_{c,0} = 1.414 - 0.000945ks/d + 0.000825 \rho_{12} + 0.029 p_2 - 0.0217u \quad \text{or} \quad (3)$$

$$f_{c,0} = 10^{1.414 - 0.000945ks/d + 0.000825 \rho_{12} + 0.029 p_2 - 0.0217u}$$

3.3.1 Effect of knots

The effect of following knot parameters were analyzed: maximum diameter of knot, sum of knot diameters in a cross section and ratio of both to diameter / circumference of the pole. In most cases *KAR* appears to be as good as any other knot-related variable. In bending the best model gives knot size (ks) as the best indicator for stiffness instead of *KAR*. The effect of knot parameter is illustrated in Table 5, where density is 494 kg/m^3 and moisture content 17.6 %.

3.3.2 Effect of density

Density affected all measured strength and stiffness values. Table 6 gives the values calculated by using the obtained regression models. The knot sum is assumed to be 80 mm and the moisture content 17.6 %.

Table 5 The influence of the knot sum ks on E_m values and knot sum per diameter ks/d on $E_{c,0}$, $f_{c,0}$ and f_m .

ks mm	E_m	ks/d	$E_{c,0}$	$f_{c,0}$	f_m
0	13.5	0	11.6	27.6	55.0
20	13.0	20	11.1	26.4	53.3
40	12.5	40	10.6	25.3	51.7
60	12.0	60	10.1	24.2	50.0
80	11.6	80	9.7	23.2	48.3
100	11.2	100	9.3	22.2	46.6
120	10.8	120	8.9	21.2	44.9
140	10.4	140	8.5	20.3	43.3
160	10.0	160	8.1	19.5	41.6

Table 6 The influence of density ρ_{12} on $E_{c,0}$, E_m , $f_{c,0}$ and f_m .

ρ_{12}	$E_{c,0}$	E_m	$f_{c,0}$	f_m
300	5.9	7.6	16.5	35.7
350	6.8	8.6	18.2	39.2
400	7.8	9.6	20.0	42.8
450	8.9	10.8	22.0	46.4
500	10.2	12.1	24.2	49.9
550	11.6	13.5	26.6	53.5
600	13.3	15.2	29.2	57.0
650	15.2	17.0	32.1	60.6

3.3.3 Effect of woodworking

Some of the roundwood material was sawn partly (two opposite faces sawn). Another portion was sawn to squared form (100x100). Regression analysis was used to explain the effect of cross-section form [7]. To summarise, it can be concluded that round timber has higher stiffness and bending strength than sawn material. Partly sawn wood has the same values in edgewise and flatwise bending. When sawing timber, KAR is increasing which makes the difference bigger in practice than indicated here. The results are listed in Table 7 in form of relative values.

Table 7 Relative mean strength and stiffness of different shaped cross-sections [7].

	Bending		Compression	
	Strength	Stiffness	Strength	Stiffness
Sawn	1	1	1	1
Partly sawn	1.04	1.08	1	1
Round	1.14	1.08	1.05	1.13

3.3.4 Effect of moisture content

A statistical analysis gave a strong moisture dependence for compression strength and no dependence for bending strength or stiffness. Compression results are illustrated in Table 8. It has to be pointed out that larger diameter material had normally a little higher moisture content because the material was not perfectly conditioned. Therefore minor dependence on moisture and size are mixed and cannot be separated.

Table 8 The influence of moisture content on compression strength according to the EN 384 and the factor obtained from regression model: $f_{12} = f_u \cdot 10^{0.0217 \cdot (u - 12)}$. The numbers in bold are average test results for whole material.

u	EN 384	$f_{12} = f_u \cdot 10^{0.0217 \cdot (u - 12)}$
	$f_{c,0}$	$f_{c,0}$
12	28.7	32.2
13	27.9	30.6
14	27.2	29.1
15	26.4	27.7
16	25.7	26.3
17	24.9	25.0
17.2	24.8	24.8
18	24.2	23.8
19	23.5	22.7
20	22.7	21.6
21	22.0	20.5
22	21.2	19.5

3.3.5 Effect of diameter

The effect of diameter on strength was studied by statistical methods. No dependence was detected in the range of 80 to 150 mm analysed here. This is understandable, because juvenile wood makes timber with smaller diameter weaker, but the Weibull weakest link concept works in opposite direction. As a results, it is suggested that no size effect would be adopted for round timber.

3.4 Comparison to sawn timber

Spruce roundwood is compared to sawn timber (Norway spruce 42x145) as tested in a Nordic Industry funded project. Sample size is about 600 covering all Finland. For testing and analysis, EN 338, EN 384, EN 408 and EN 518 were applied. Cumulative distributions of bending strength, modulus of elasticity and density are given in Fig. 2. The 5th percentile value of bending strength of round spruce is double the value of sawn spruce even though the density distribution is fairly similar. The modulus of elasticity appears to be closely related to density, as expected. For pine, similar curves are given even though the sample is less representative, and density of round timber is considerably lower.

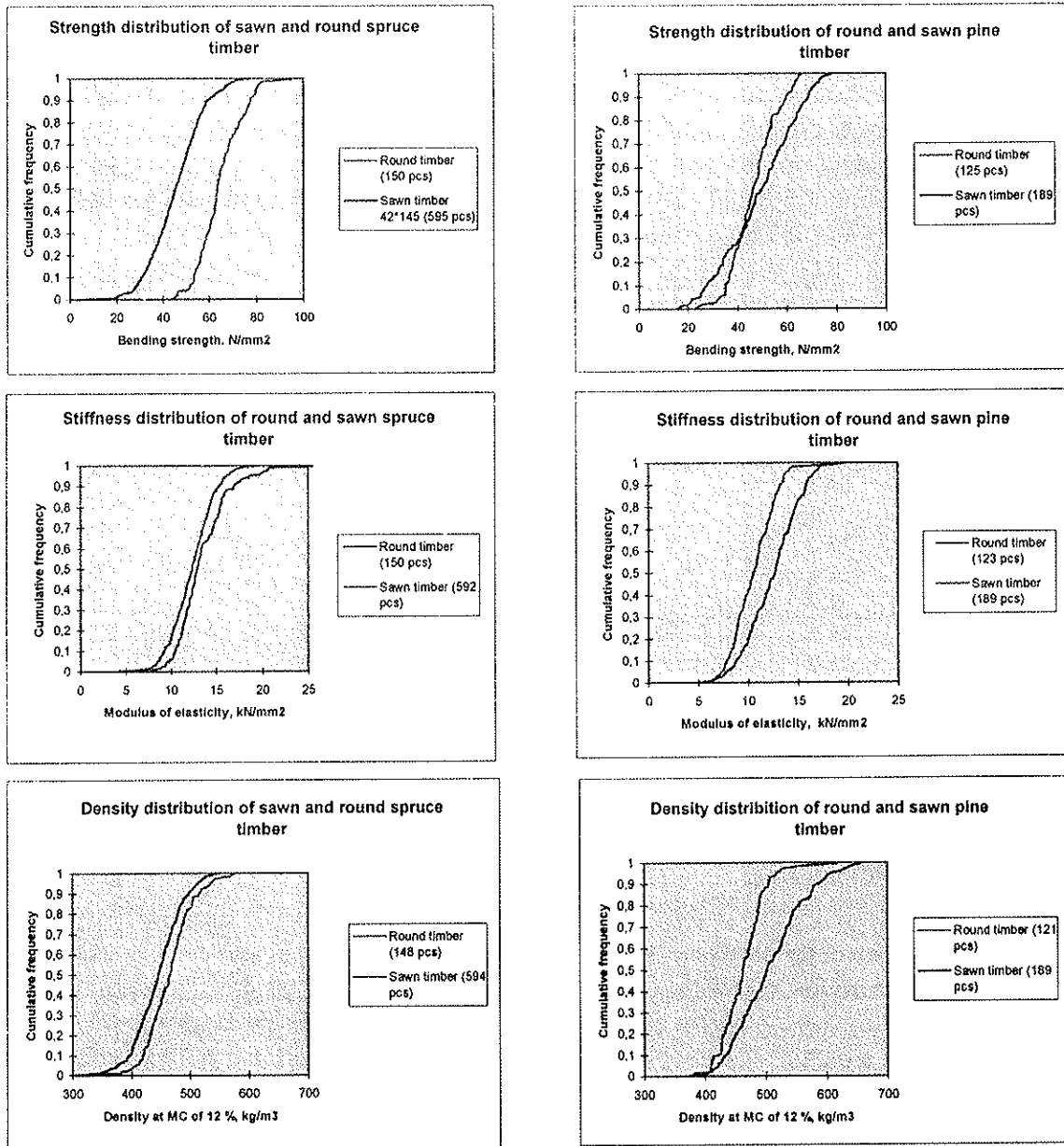


Figure 2 Comparison of bending strength, stiffness and density of round and sawn Finnish non-graded spruce and pine timber. Data for round pine does not include test series "pine 226".

4 Possible strength classes and grading

The development of strength grading methods and derivation of characteristic values will be carried out during the final year of the project. The preliminary results indicate that simple rules may be generated, based on knot diameters and annual growth, which will easily produce material up to strength class C30.

When the results of Tables 3 and 4 are adjusted to 12 % moisture content according to EN 384 (density : 0,5%/%, E : 2%/%, $f_{c,05}$: 3%/%) the values given in Table 9 are obtained.

Table 9 Characteristic values adjusted to 12 % MC in accordance with EN 384.

File	Sample size	Mean density [kg/m ³] (compression / bending)	Characteristic density (Mean - 1.65*st.d) (compression / bending)	$f_{m,05}$ [N/mm ²] by ranking	$f_{c,05}$ [N/mm ²] by ranking	$E_{m,mean}$ [kN/mm ²]
pine 1+26+176	75	466 / 469	410 / 405	31.5	18.0	11.9
pine 51+76	50	447 / 455	400 / 407	34.8	22.2	11.6
pine 226	50	506 / 484	435 / 414	41.8	28.9	11.6
spruce 1+51	50	447 / 462	394 / 390	54.0	27.3	13.4
spruce 26+76	50	453 / 468	377 / 397	49.1	30.0	12.9
spruce 101+126	50	453 / 466	394 / 409	46.2	25.6	13.9

While the variation in the knot sizes is greater for pine than for spruce, it is expected that the limitation of the knot size will increase the characteristic values from those uncensored values. The adjustment factor for the moisture content of the compression strength should be discussed.

5 Design aspects

Round timber has higher bending strength than sawn timber. In design of structures, however, this cannot be used to full benefit because the round form is far from optimum for flexural members. Round beams are flexible, and deflection is normally the critical factor. As a result, round beams have higher safety against ultimate limit state than required by design codes.

A round form of a member is well suited for columns and for tensile and compression members in trusses. In compression, buckling will be the dimensioning phenomenon, and in tensile members the capacity of joints is critical. This project will publish guidelines for design of engineered roundwood structures in the context of Eurocode 5 system.

Moisture dependence of compression strength was observed to be stronger than adopted in CEN standards. Therefore unsafe situations may occur, if bending testing at 12 % MC is used as basis for strength grading, and round timber is used under compression in service class 2. For this reason also compression information is planned to be used as a basis for strength grading of roundwood.

REFERENCES

- [1] Ranta-Maunus, A. "Small roundwood structures", *WCTE98* paper, 1998.
- [2] Barnard G., "Strength characteristics for small roundwood in bending and compression from a UK resource", *WCTE98*-paper.
- [3] Boren, H., Barnard G., "Analysis of small diameter round Scots pine strength and stiffness properties tested in bending and compression parallel to grain", Manuscript for Paper and Timber Journal, 1998.
- [4] De Vries, P.A., "Quality and Strength characterization of small diameter Larch (*larix kaempferi*)" C4-98-01. *Delft University of Technology*, 1998.
- [5] Perälä, A-L. (ed.), "Round small diameter timber for construction. Market summary". *VTT Research notes 1877*. Espoo 1997.
- [6] Huybers, P., "The Structural Application of Thin Roundwood Poles in Building", *Delft University of Technology*, 1996.
- [7] Boren, H., "The influence of processing methods on Timbers MOE and MOR in bending and compression parallel to grain", *WCTE98*-paper.
- [8] Kärkkäinen, M., "Puu, sen rakenne ja ominaisuudet", Helsinki, 1977.

CIB-W18/31-6-4

**INTERNATIONAL COUNCIL FOR BUILDING RESEARCH STUDIES AND DOCUMENTATION
WORKING COMMISSION W18 - TIMBER STRUCTURES**

**COMPRESSION STRENGTH PERPENDICULAR TO GRAIN OF
STRUCTURAL TIMBER AND GLULAM**

by

L Damkilde
P Hoffmeyer
T N Pedersen

Department of Structural Engineering and Materials
Technical University of Denmark

DENMARK

MEETING THIRTY-ONE

SAVONLINNA

FINLAND

AUGUST 1998

Compression strength perpendicular to grain of structural timber and glulam

Lars Damkilde, Preben Hoffmeyer, Torben N. Pedersen

Department of Structural Engineering and Materials
Technical University of Denmark, Building 118
DK-2800 Lyngby

Abstract

The characteristic strength values for compression perpendicular to grain as they appear in EN 338 (structural timber) and EN 1194 (glulam) are currently up for discussion. The present paper provides experimental results based on EN 1193 that may assist in the correct assignment of such strength values. The dominant failure mode of glulam specimens is shown to be fundamentally different from that of structural timber specimens. Glulam specimens often show tension perpendicular to grain failure before the compression strength value is reached. Such failure mode is not seen for structural timber. Nonetheless test results show that the levels of characteristic compression strength perpendicular to grain are of the same order for structural timber and glulam. The values are slightly lower than those appearing in EN 1194 and less than half of those appearing in EN 338. The paper presents a numerical analysis to prove the significant role of tension perpendicular to grain stresses in the failure mode of the glulam specimens.

1 Introduction

EN 1193 defines the experimental procedure to follow in assessing compression strength perpendicular to grain ($f_{c,90}$) for structural timber and glulam. Only limited research results based on this standard have been reported. The $f_{c,90}$ values as they appear in the strength classes of EN 338 (structural timber) and EN 1194 (glulam) therefore have a slender scientific basis. As a result of this uncertainty, the two strength classes were assigned very different $f_{c,90}$ values. However, there is no experimental evidence of such a difference.

Gehri [1997] discusses the current situation and provides an exhaustive review of previous research.

The scope of the present work is to provide adequate experimental evidence for the establishment of characteristic strength values for glulam and structural timber in compression perpendicular to grain in accordance with EN 1193.

2 Materials

2.1 Structural Timber

74 specimens were produced from cutoffs from the ordinary production of a major Danish producer of trusses. The cutoffs represented several weeks of production and included all dimensions (planed) in the range from 50 x 100 mm to 50 x 250 mm. The material represented a variety of Nordic sawmills and the quality is representative of normal Nordic structural timber.

The species was Norway spruce (*Picea abies*). Dimensions were 45 x 90 mm (planed). The specimens were conditioned to equilibrium at 20 °C and 65 % relative humidity

2.2 Glulam

120 specimens were produced from an equal number of cutoffs from the ordinary production of four different glulam manufacturers, one Swedish and three Danish. The cutoffs were sampled from many days of production and represented a variety of beam dimensions. The test material is representative of normal Nordic glulam quality.

In cases where cutoffs were taken from glulam including two strength grades, specimens were cut to include the representative mixture of both grades.

The species was Norway spruce (*Picea abies*). The height of the specimens was 200 mm. The width was varying and equal to the width of the cutoffs. The length was adjusted to produce a cross section of 25.000 mm². The specimens were conditioned to equilibrium at 20 °C and 65 % relative humidity.

3 Methods

3.1 Structural timber

Testing was carried out in accordance with EN 1193. Gauge length was 50 mm. The change of distance between crossheads was additionally measured for all specimens. In order to assess any influence of annual ring pattern on the mechanical properties the classification shown in Figure 1 was introduced.

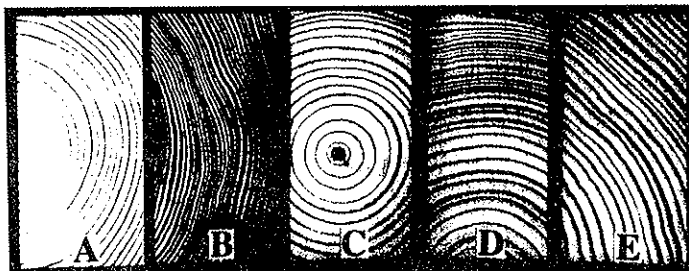


Figure 1 Classification of specimen type based on annual ring pattern

3.2 Glulam

Testing was carried out in accordance with EN 1193 except that deformations were predominantly measured as the change of distance between crossheads. For a small number of specimens additional measurements were taken by mounting extensometers onto the specimens. This was done in order to quantify any difference between the two methods. The gauge length of the extensometers was 100 mm.

4 Results and Discussion

A strength test of wood in compression perpendicular to grain does not produce a clear ultimate stress. The specimen shows a continuous growth of stress up to values of deformation which lies far beyond any practical use. Consequently, EN 1193 defines strength as the stress corresponding to a predefined strain (Figure 2). First, modulus of elasticity is calculated as the slope of the stress-strain curve defined by $\sigma = 0.1f_{c,90}$ and $\sigma = 0.4f_{c,90}$. Then a line of the same slope and passing through the point $(\sigma, \epsilon) = (0.0, 0.01)$ is produced. The stress corresponding to this line's intersection with the stress-strain curve defines the strength. It follows, that assessment of strength and elasticity according to EN 1193 is an iterative process.

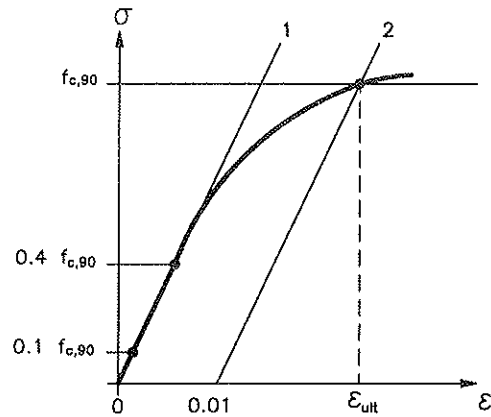


Figure 2 Definition of strength and modulus of elasticity perpendicular to grain according to EN 1193

4.1 Structural timber

A summary of results is shown in Table 1

Table 1 Structural timber – Modulus of elasticity ($E_{c,90}$), density (ρ_{12}), strength ($f_{c,90}$) and the strain (ϵ_{ult}) corresponding to the strength value

	$E_{c,90}$ (MPa)		ρ_{12} (kg/m ³)	$f_{c,90}$ (MPa)		ϵ_{ult} (%)	
gauge length (mm)	90	50		90	50	90	50
average	209	294	452	2.9	2.8	2.4	2.1
coeff. of variation (%)	31	34	9.6	13	13	12	13
5 th percentile			378	2.3	2.2		

4.1.1 Modulus of elasticity, $E_{c,90}$

Modulus of elasticity ($E_{c,90}$) is seen to depend strongly on gauge length. $E_{c,90}$ as calculated from the crosshead movements is only 69 % of that calculated from the 50 mm gauge length of the extensometers. Figure 3 shows evidence of a dependency of specimen type. This is to be expected since $E_{c,90}$ for spruce is known to be higher in the radial direction than in the tangential direction. Average values of $E_{c,90}$ (Table 2) for the five different specimen types confirm that modulus of elasticity is higher in the radial direction (type D) than in the tangential direction (type B). Types A, C and E constitute mixtures of radial and tangential directions, and modulus of elasticity values fall between those of types B and D. In the central part of the type E specimen the annual ring orientation is approximately 45 degrees to the radial or tangential directions. Such orientation should produce the lowest $E_{c,90}$ values, which is also seen to be the case.

Table 2 Mean values of $E_{c,90}$ and density as dependent on specimen type and gauge length

specimen type	A	B	C	D	E
$E_{c,90,mean}$ (MPa) (50 mm)	275	264	302	516	252
$E_{c,90,mean}$ (MPa) (90 mm)	187	171	254	339	241
$\rho_{12,mean}$ (kg/m ³)	458	444	454	447	446

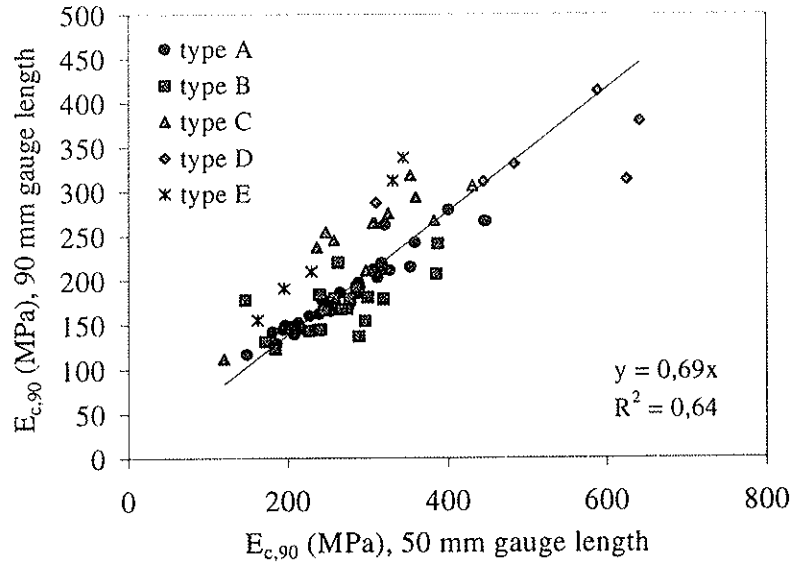


Figure 3 Relationship between modulus of elasticity, $E_{c,90}$, as calculated from crosshead movements and from the 50 mm gauge length of the extensometers.

4.1.2 Compression strength, $f_{c,90}$

The average compression strength perpendicular to grain of structural timber is 2.8 MPa for strain measured according to EN 1193 and 2.9 MPa for strain measured on the basis of crosshead movements. The relationship between the two sets of strength values is illustrated in Figure 4. The reason why both methods produce virtually the same strength values is that the lower values of modulus of elasticity are tied to higher values of ϵ_{ult} . Contrary to what was found for modulus of elasticity, strength does not appear to be much dependent on annual ring orientation (Table 3).

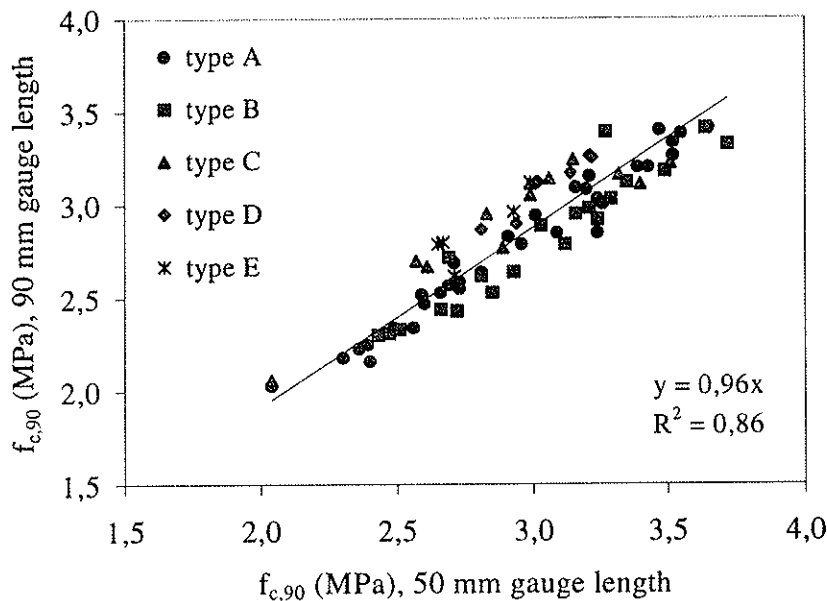


Figure 4 Relationship between compression strength $f_{c,90}$ as calculated from crosshead movements and from the 50 mm gauge length of the extensometers.

Table 3 Mean values of $f_{c,90}$ and density as dependent on specimen type and gauge length

specimen type	A	B	C	D	E
$f_{c,90,mean}$ (MPa) (50 mm)	2.9	3.0	3.0	3.1	2.8
$f_{c,90,mean}$ (MPa) (90 mm)	2.8	2.8	2.9	3.1	2.9
$\rho_{12,mean}$ (kg/m ³)	458	444	454	447	446

The characteristic value of strength, $f_{c,90,k}$, is 2.2 MPa. for the prescribed gauge length of 50 mm. For a 90 mm gauge length $f_{c,90,k}$ is 2.3 MPa.

4.1.3 Density, ρ_{12}

From Table 1 it appears that the coefficient of variation for density is 9.6 %, which is very close to the 10 % adopted by EN 338.

4.2 Glulam

A summary of results is shown in Table 4. The modulus of elasticity values are placed between brackets because the gauge length used for the tests do not permit a correct assessment. An estimate of the correct modulus of elasticity is carried out in Section 4.2.1

Table 4 Glulam – Modulus of elasticity ($E_{c,90}$), density (ρ_{12}), and strength ($f_{c,90}$) for 120 specimens. Gauge length is 200 mm

	$E_{c,90}$ (MPa)	ρ_{12} (kg/m ³)	$f_{c,90}$ (MPa)
average	(240)	466	2.9
coeff. of variation (%)	(24)	4.8	9.3
5 th percentile		433	2.4

4.2.1 Modulus of elasticity, $E_{c,90}$

For twelve specimens modulus of elasticity was assessed on the basis of two different deformation measurements. The results (Table 5) confirm what was found for structural timber with respect to the significant difference of modulus of elasticity at the same time that the strength values are almost identical. $E_{c,90}$ as calculated from the crosshead movements is only 75 % of that calculated from the 100 mm gauge length of the extensometers. The results for structural timber did not justify any conclusion regarding the influence of possible local stress concentrations at the crossheads. The reason is that the annual ring geometry most often is depending on gauge length (see Figure 1). The glulam specimens, however, have virtually the same annual ring orientation throughout the specimen height, and any systematic difference in modulus of elasticity therefore is very likely caused by the crossheads.

Table 5 Modulus of elasticity and strength $f_{c,90}$ as function of gauge length for 12 glulam specimens

	$E_{c,90}$ (MPa)	ρ_{12} (kg/m ³)	$f_{c,90}$ (MPa)
gauge length (mm)	200 100		200 100
average	274 367	478	3.0 2.9
coeff. of variation (%)	13 21	3.2	6.5 7.8

The average modulus of elasticity for the 120 glulam specimens is 240 MPa when based on strain values obtained from the movement of crossheads. From the test of twelve specimens including both types of deformation measurements the ratio between

corresponding moduli of elasticity may be obtained. This ratio is then used to estimate the correct average modulus of elasticity for the 120 glulam specimens to be $E_{c,90,mean} = 320$ MPa.

4.2.2 Compression strength, $f_{c,90}$

Because the strength values for both structural timber and glulam show no dependency of gauge length, it is concluded that the assessment of strength may be based on the cross head movements. This conclusion is confirmed by Figure 5 which shows that strength values based on the two different strain measurements are very close. Even a choice of a strain five times higher than the one percent strain prescribed by EN 1193 does not produce vastly different strength values.

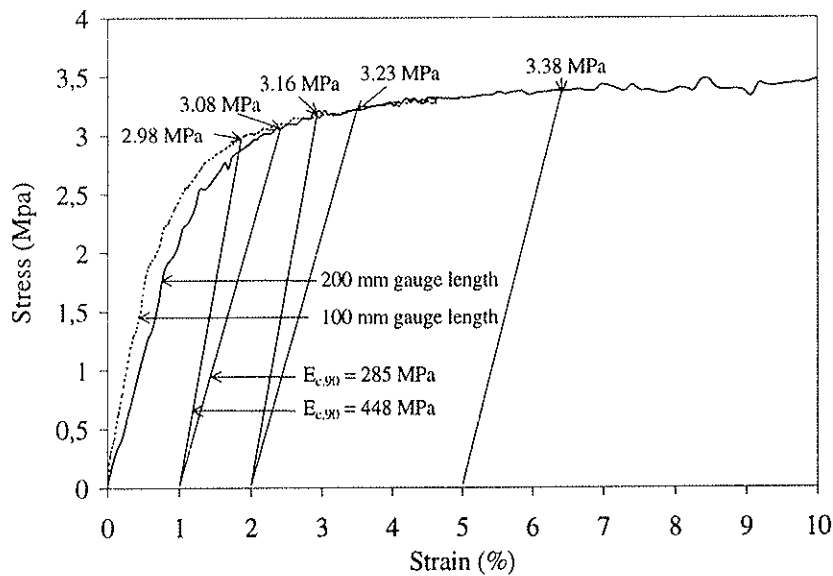


Figure 5 $f_{c,90}$ as dependent on gauge length and limiting strain (example)

The compression strength values for the four different samples representing four different manufacturers are shown in Table 6. A statistical analysis proves the mean strength values of all four samples to be equal at a 95 % significance level [Pedersen 1997]. In the present analysis, therefore, the four samples are treated as one large sample.

Table 6 Values of $f_{c,90}$ for samples from four manufacturers

Manufacturer	Number of specimens	Mean (MPa)	c.o.v. (%)	5-percentile (MPa)
A	12	2.89	11	2.38
B	64	2.89	10	2.47
C	29	2.88	7	2.55
D	15	2.78	8	2.37
All	120	2.87	9	2.44

The average compression strength perpendicular to grain of glulam is $f_{c,90,mean} = 2.9$ MPa (Table 4), which is identical to the average compression strength of structural timber. The characteristic value for glulam is $f_{c,90,k} = 2.4$ MPa, which is marginally higher than the value for structural timber. The difference reflects the lower coefficient of variation for glulam.

EN 384 prescribes the use of five samples of forty specimens each for the establishment of characteristic values. For less samples and/or specimens a penalty factor is introduced which is to take into account the uncertainty resulting from normal variability

of wood properties. As compression strength perpendicular to grain shows such very low variability within and between samples, EN 384 cannot be used.

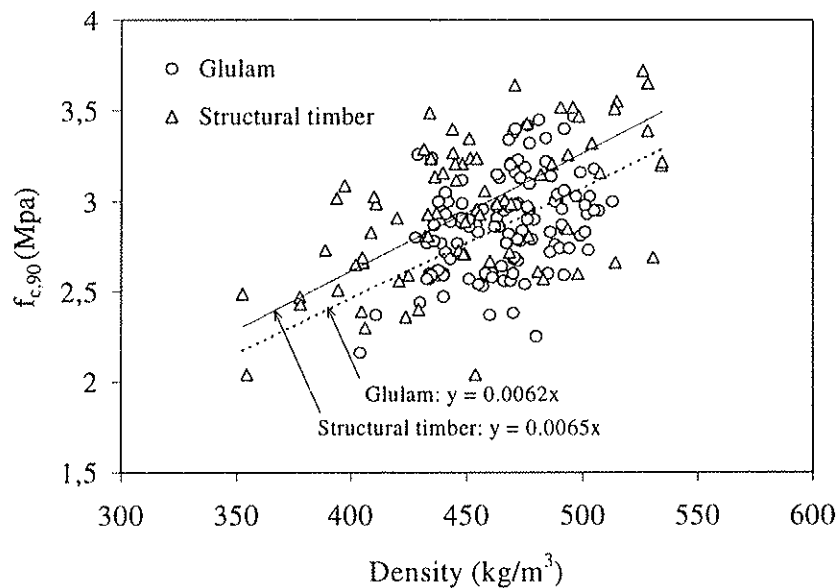


Figure 6 Compression strength $f_{c,90}$ as a function of density for glulam (circles) and structural timber (triangles)

The density strength relationship for glulam is shown in Figure 6. Superimposed are corresponding values for structural timber. The relationships are almost identical. Treating all results as one sample produces the regression equation: strength = 0,0063 density. As a rough estimate the following regression equation may be used for both average and 5-percentile values for both structural timber and glulam:

$$\text{STRENGTH (MPa)} = 0,006 \text{ DENSITY (kg/m}^3\text{)}$$

4.2.3 Density, ρ_{12}

From Table 4 it appears that the coefficient of variation for density is 4.8 %, which is half the value of that for structural timber. The small variability is a result of the lamination effect.

4.3 Failure patterns

All glulam specimens show crack development before the stress corresponding to $f_{c,90}$ is reached. The cracks develop due to tension perpendicular to grain failure and they run predominantly in the direction of the applied force (Figure 7). Such crack development may influence the level of compression strength perpendicular to grain. This problem is addressed in Section 5.

The failure patterns of the structural timber specimens were quite different from those of the glulam specimens. No specimens showed crack development before $f_{c,90}$ was reached. At large deformations cracks may eventually develop. For the predominant type A specimen, such cracks develop as a combined shear- and tension perpendicular to grain failure. The crack is oriented in the radial direction and located where the angle between the radial direction and the direction of the force is 45 degrees.

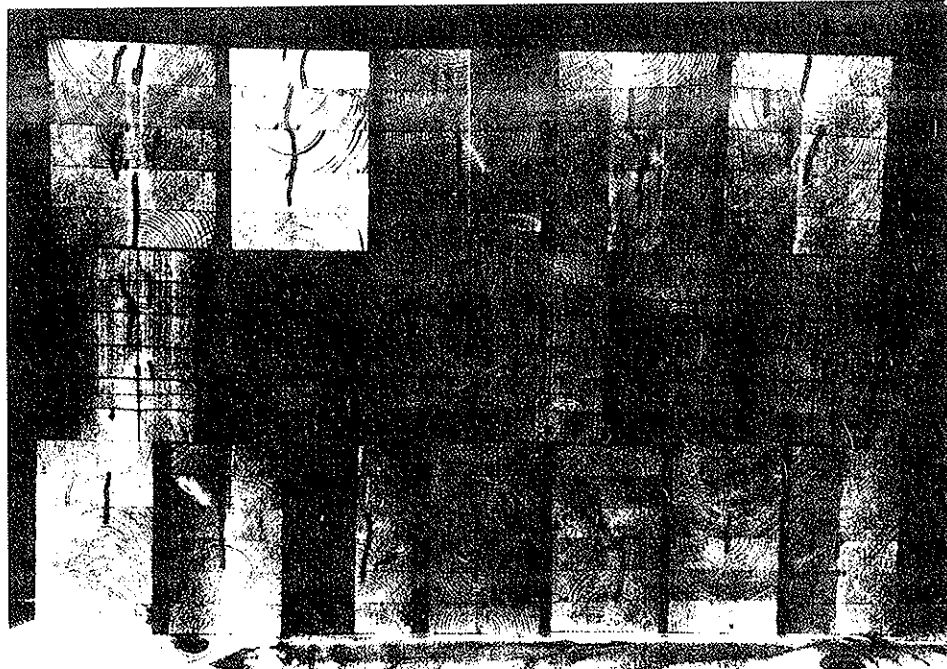


Figure 7 *Glulam specimens with marked cracks running in the direction of the applied force. The cracks appear before $f_{c,90}$ is reached. Specimens in the middle row have been taken to particularly high strains which makes the barrel form visible.*

5 Finite Element Modelling

The crack patterns of glulam illustrated in Figure 7 suggest the existence of tension stresses perpendicular to the loading direction. One explanation may be that differences in stiffness in radial and tangential directions cause a non-uniform stress state, which results in tension stresses leading to cracks.

In order to investigate whether the tension perpendicular to grain stresses are large enough to explain the crack pattern, a finite element analysis was carried out. The analysis is based on a linear elastic material behaviour. The results, therefore, are only indicative giving a rough idea of the stress level particularly for the tension perpendicular to grain stresses. A more detailed analysis should model the actual crack development process along with the associated redistribution of stresses.

The interesting stress distributions are in planes perpendicular to the grain. For an isotropic material the stress state would be uniaxial compression even though the stiff steel plates might introduce small stress concentrations at the corners. However, due to the cylindrical orthotropy of the timber non-uniform stresses build up independent of the loading arrangement. This has already been studied in a different context, see e.g. [Aicher and Dill-Langer 1997].

At the center of most of the glulam lamellas the annual rings run predominantly parallel to the wide face. However, moving towards the narrow face, the annual rings gradually change orientation and they may eventually become parallel to the narrow face. Because of this and because the radial stiffness is larger than the tangential stiffness (Table 2), the compressive stresses are concentrated in the middle of the glulam specimen. In order to establish this non-uniform stress state, shear stresses must develop. In combination with the Poisson effect tension stresses perpendicular to the load direction are then established. This effect is well-known even in isotropic materials. An example is cleavage tests of cylindrical specimens where compression in the radial direction creates tensile failure perpendicular to the direction of the applied load. In that case the non-uniform stress state is created by the geometrical shape of the specimen.

The glulam test specimen is modelled under an assumption of plane strain. This means that the stresses in the fiber direction are assumed negligible. This is reasonable

since the stiffness in the fiber direction is very much larger than in the transverse directions.

The calculations have been performed with the COSMOS system with eight noded isoparametric plane stress elements producing a linear stress variation within the element. The finite element mesh is a regular mesh, where each board has been modelled with sixteen elements in the height and fifty elements in the width. This very fine mesh is necessary in order to model the cylindrical orthotropy accurately.

The following elastic constants are assumed. The moduli of elasticity are rounded values of those presented in Table 2 (types B and D, 50 mm gauge length).

$$E_r = 500 \text{ MPa}$$

$$E_t = 275 \text{ MPa}$$

$$G_{rt} = 30 \text{ MPa}$$

$$\nu_{rt} = 0.31$$

Subscripts r and t refer to the radial and tangential direction respectively.

The particular glulam test specimen to be modelled consists of six boards with cross sectional dimensions 33.3 mm x 160 mm. All the five upper boards had the pith located below the board, whereas the last board had the pith located above the board. The location of the pith varies from board to board. However, in order to simplify the interpretation of the analysis all boards have been assigned an identical location of the pith. Based on average values of observed locations the pith is assumed located 20 mm below the bottom face for the upper five laminations and 20 mm above the top face for the lower lamination. Furthermore, the pith is assumed to lie on the line of symmetry, which eliminates any skewness in the stress pattern.

The load is transferred to the test specimen through very stiff steel plates, and the boundary condition therefore is modelled as a uniform displacement. The pressure is not uniform due to the differences in elastic moduli, but the total load on the steel plate defines an average compression level used in the comparison. The steel plate is assumed to restrict horizontal movements which then causes the observed barrel shape of the test specimens.

The results of the finite element modelling are illustrated in Figure 8 for the 'radial' stresses and in Figure 9 for the 'tangential' stresses.

The radial stresses (σ_{yy}) are in compression and the level in the middle are somewhat higher than at the sides as was assumed. Another interesting observation is that the level increases with depth towards the lower part of the specimen. This wedge shape form of carrying stresses is a result of the orientation of the annual rings of the laminations. The maximum compressive stress is about four times higher than the stress corresponding to a uniform distribution.

The tangential stress (σ_{xx}) distribution is somewhat more complicated and results in both compression and tension. High levels of tension stresses are found in many small areas, typically at the interface between boards where the E-moduli change discontinuously. The stress level is of the order 40% of the compression stress, which explains the fracture pattern.

In practice each lamination will have the pith placed differently and not necessarily in the plane of symmetry. One of the test specimens was measured in detail and each layer modelled according to the particular geometry of that specimen. This resulted in stress levels which were approximately 10 % larger. A more systematic study of the influence of geometrical differences would probably give results of the same order.

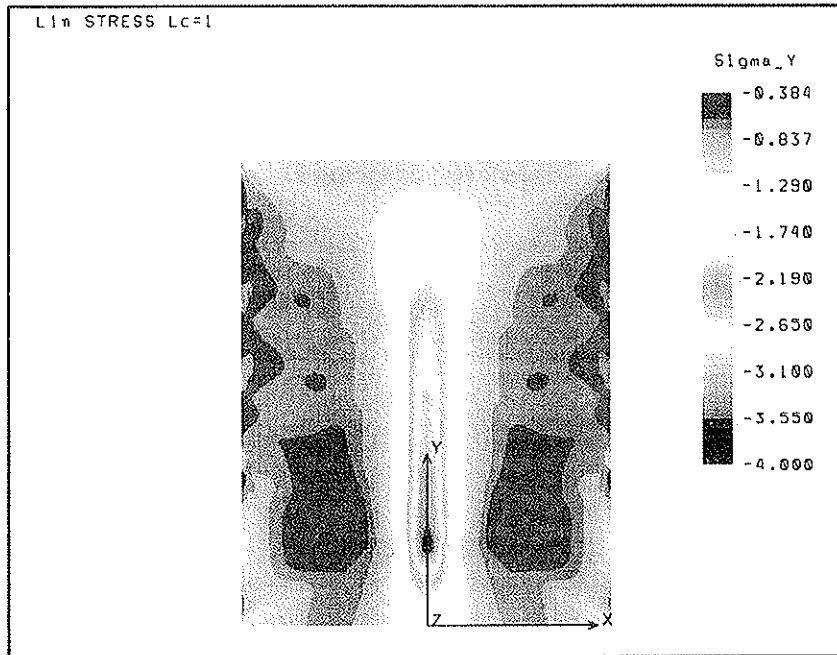


Figure 8 Distribution of radial stress (σ_{yy})

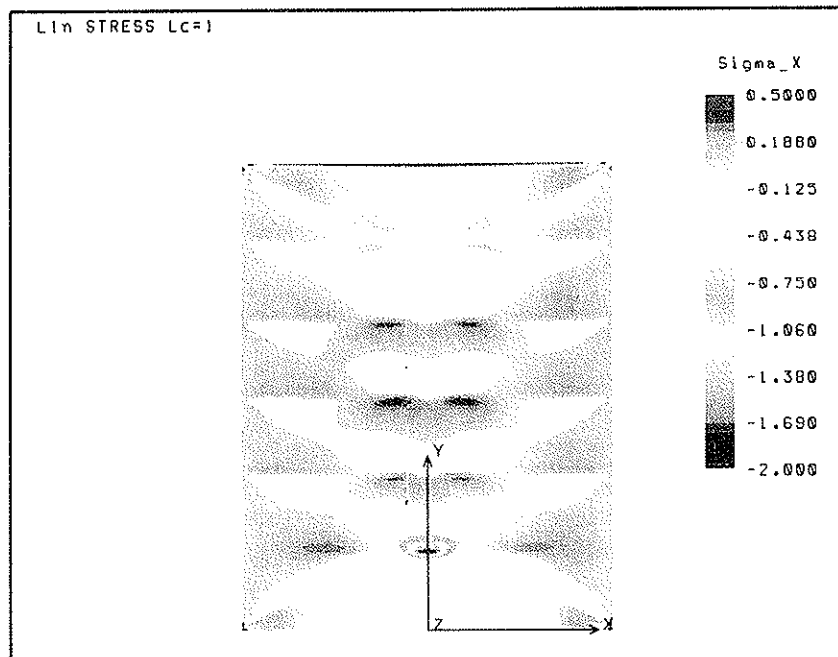


Figure 9 Distribution of tangential stress (σ_{xx})

6 Conclusions

- The compression strength of structural timber and glulam of Nordic origin and tested according to EN 1193 lies within the limits from 2.0 MPa to 4.0 MPa. The mean value for both structural timber and glulam is $f_{c,90,mean} = 2.9$ MPa. The 5-percentile values for both structural timber and glulam is $f_{c,90,k} = 2.3 - 2.4$ MPa.
- As a rough estimate of compression strength perpendicular to grain the following regression equation may be used for both average and 5-percentile values for both structural timber and glulam:

$$STRENGTH (MPa) = 0,006 DENSITY (kg/m^3)$$

- For the assessment of strength, the laborious measurement of strain prescribed by EN 1193 may be replaced with a measurement of the relative movements of the crossheads of the test machine. However, for the assessment of modulus of elasticity it is necessary to adhere to the prescriptions laid down by the standard.
- The average modulus of elasticity across the grain is of the order $E_{c,90,mean} \approx 300$ MPa for both structural timber and glulam.
- Finite element modelling proves that the inhomogeneous distribution of modulus of elasticity $E_{c,90}$ across a given specimen results in a complicated stress distribution.

The radial stresses (direction of applied force) are in compression and the level in the middle are higher than at the sides; the stress level increases with depth towards the lower part of the specimen. This wedge shape form of carrying stresses is a result of the annual ring orientation of the laminations. The maximum compressive stress is about four times that of the reference stress level.

The tangential stress distribution (transverse direction) is somewhat more complicated and results in both compression and tension. High levels of tension stresses are found in many small areas, typically in the bonds between boards where the E-moduli change discontinuously. The stress level is of the order 40% of the compression stress, which explains the fracture pattern.

7 Acknowledgements

Thanks are due to Limtræ Danmark A/S, Sections LNJ, Lilleheden and Øresø, Denmark and to Moelven Töreboda Limträ AB, Sweden, that delivered the glulam for the investigation.

8 References

Aicher, S; Dill-Langer G. 1997: "Climate Induced Stresses Perpendicular to the Grain in Glulam", Otto-Graf-Journal, Vol. 8., pp. 209-231

EN 338:1995: "Structural timber - Strength classes"

EN 1193:1997: "Structural timber - Structural and glued laminated timber - Determination of additional physical and mechanical properties"

EN 1194:1998: "Timber structures - Glued laminated timber - Strength classes and determination of characteristic values"

EN 384:1995: "Structural timber - Determination of characteristic values of mechanical properties and density"

Gehri, E. 1997: "Timber in compression perpendicular to grain". Proceedings of the International Conference of IUFRO S5.02 Timber Engineering, Department of Structural Engineering and Materials, Technical University of Denmark

Pedersen, T. N. 1997: "Compression strength perpendicular to grain". M.Sc. thesis (In Danish). Department of Structural Engineering and Materials, Technical University of Denmark.

INTERNATIONAL COUNCIL FOR BUILDING RESEARCH STUDIES AND DOCUMENTATION

WORKING COMMISSION W18 - TIMBER STRUCTURES

BEARING STRENGTH OF TIMBER BEAMS

by

R.H. Leicester

H. Fordham

H. Breitingner

CSIRO Building, Construction and Engineering
Melbourne

AUSTRALIA

MEETING THIRTY-ONE

SAVONLINNA

FINLAND

AUGUST 1998

BEARING STRENGTH OF TIMBER BEAMS

by

R.H. Leicester, H. Fordham, H. Breitingger
CSIRO Building, Construction and Engineering, Melbourne, Australia

ABSTRACT

In testing timber to determine design values for bearing pressures it is necessary to choose values for both strength and deformation limit states. This paper discusses various test configurations that may be used for in-grade measurements, and also discusses the question of applying a deformation limit in assessing strength properties.

The discussion is supplemented by test data from a project undertaken to develop an in-grade test to evaluate design bearing strengths for timber beams.

1. INTRODUCTION

The philosophy of in-grade testing refers to the measurement of the in-service structural properties of full-size, stress graded timber. Usually it is a simple matter to develop in-grade tests to measure most structural properties. However, for the case of the bearing strength of beams, there are several difficult decisions to be made before a suitable in-grade test for compression perpendicular to the grain can be chosen.

Some questions that must be decided are the following:

- What types of test configurations simulate in-service use?
- Is the relevant design property for bearing a strength or stiffness property or both?
- Should any deformation limit be applied when assessing strength?
- Should the length of the bearing area used be a fixed absolute value, or should it be a relative value that varies with the size of timber tested?
- Are the design bearing properties easily translated to a useful range of practical situations?

2. STRUCTURAL PARAMETERS

The schematic illustration of a typical load deformation graph is shown in Figure 1. The initial slope is obviously important for the derivation of a stiffness parameter to be used in serviceability computations.

Another parameter that is often used as a limit for serviceability is the proportional limit. This is difficult to evaluate experimentally and it is more convenient to use an intersection point with an offset line that runs parallel to the slope of the curve. In this study a 2 mm offset has been used.

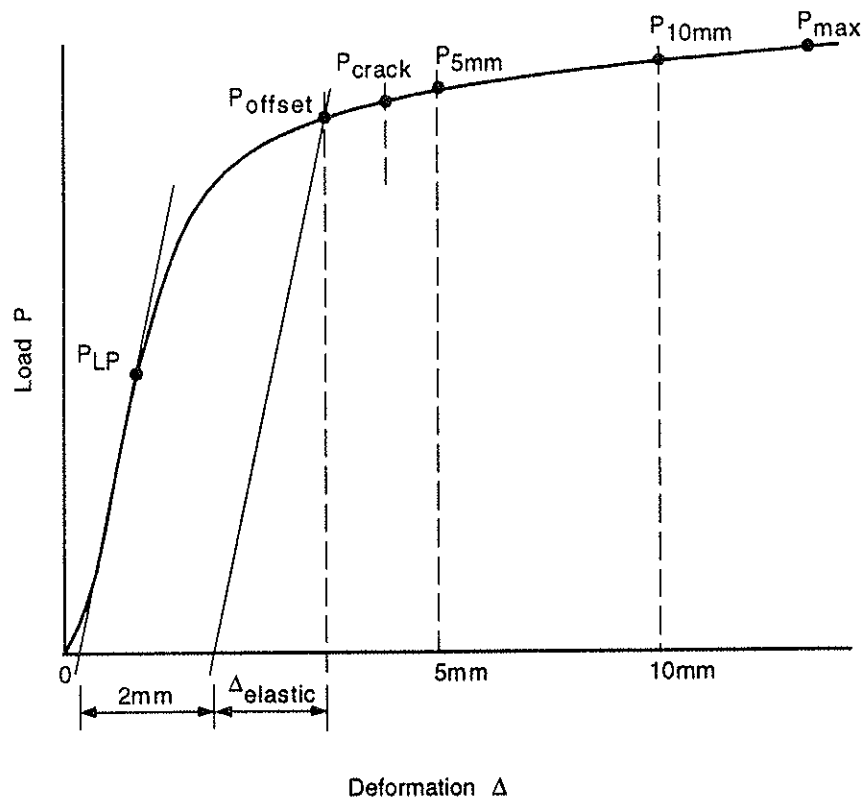


Figure 1. Example of a load deformation graph.

A third serviceability parameter that has been suggested is the occurrence of a loud audible crack. It is assumed that such cracking will lead to gradual deterioration of the beam.

For strength limit states, it was found not suitable to rely solely on the ultimate load, as this load capacity was strongly influenced by secondary matters (such as the rigidity of lateral supports) when the deformations were large. Thus a limiting deformation of some sort should be used in defining strength measured during a testing procedure.

In the following, the load on the bearing block is denoted by P and the deflection is denoted by Δ . In particular, the following notation is used for the recorded loads:

- P_{LP} = load at limit of proportionality
- P_{offset} = load at 2 mm offset
- P_{crack} = load at which an audible crack is heard
- $P_{5mm}, P_{10mm}, P_{20mm}, P_{40mm}$ = load at a deformation of 5, 10, 20 and 40 mm deformation
- P_{max} = load at failure of the test specimen.

During this project, computer records of all load deformation were stored in computer files. Hence, alternative parameters may be evaluated in the future if desired.

3. TEST CONFIGURATIONS

In testing small clear specimens, a standard test configuration as shown in Figure 2 was used.

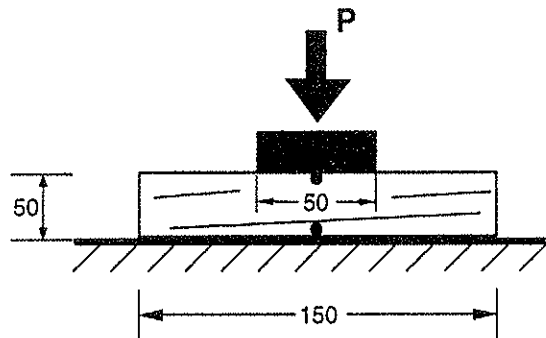
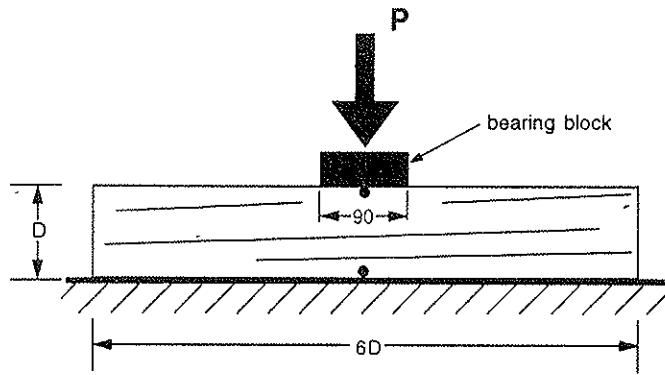
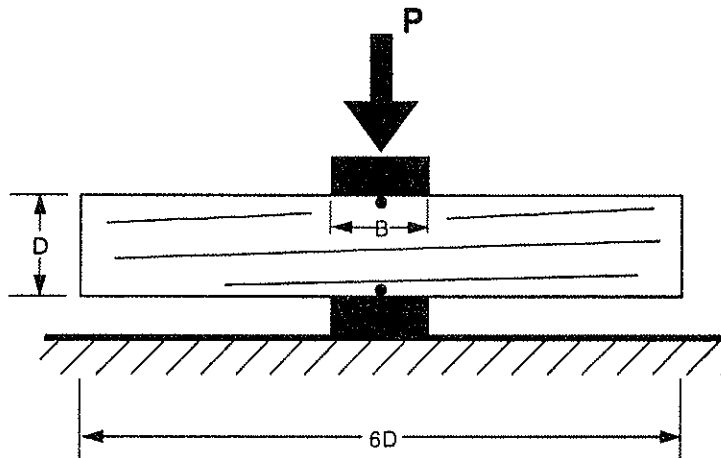


Figure 2. Configuration for testing small clear specimens.

For testing full size timber in-grade, the configurations shown in Figure 3 were used. The configuration shown in Configuration 'A' is the simplest test to undertake and may be recommended as an in-grade test if the stiffness and strength relate to test configurations that simulate in-service conditions. Configurations 'B' and 'C' are only slightly more difficult to undertake and they have the advantage that they do simulate in-service conditions, i.e. Configuration 'B' simulates a beam intersecting an interior column and Configuration 'C' simulates a beam intersecting an exterior column. At high stresses, Configuration 'C' was found to be prone to twisting distortions and to cracking. The test Configurations 'D' and 'E' are not suitable for in-grade tests, but are included to demonstrate the relationship between the in-grade tests and some other common in-service loading configurations.

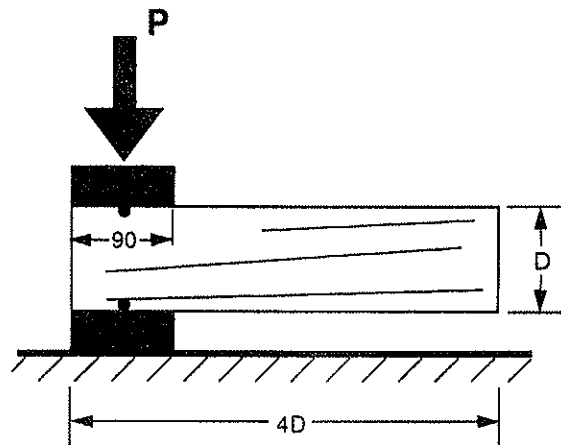


(a) Configuration 'A'



• reference points for deformation measurements

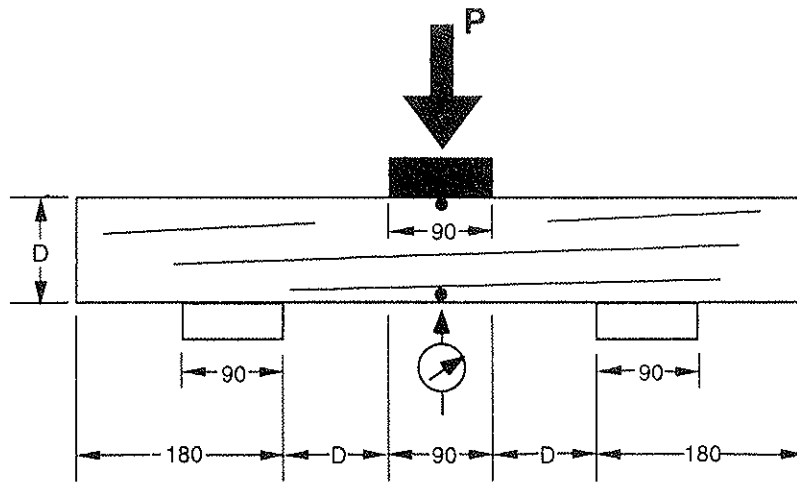
(b) Configuration 'B'



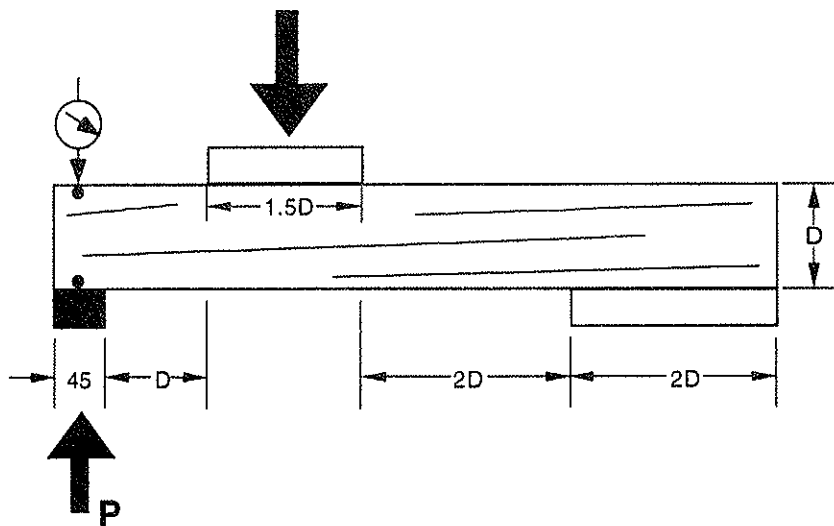
• reference points for deformation measurements

(c) Configuration 'C'

Figure 3. Configuration for testing structural size timber.



(d) Configuration 'D'



(e) configuration 'E'

Figure 3 cont.... Configuration for testing structural size timber.

Finally, it should be noted that an absolute rather than relative bearing length has been chosen. This is partly to match in-service practices and partly because in the initial stages at least, bearing is a local phenomenon and does not involve the full depth of a beam.

In Figures 2 and 3, the bearing blocks are shown in black and the deformation reported is the relative shortening of the timber between the two points indicated as circular black dots.

4. TEST MATERIAL

The test material used was cut from 4.2 metre lengths of kiln dried radiata pine. The timber sizes were 90 x 35 mm and 190 x 35 mm section. The timber was machine graded to Australian grades termed F5, F8 and F11. The threshold grading moduli used for those grades are 6.10, 8.59 and 11.59 GPa, respectively.

All the test material was obtained from a single mill. However, the material was obtained in five shipments over a period of two years. Because of possible changes in the resource, assessments of various parameters should be made with caution if these involve comparisons of specimens obtained from more than one shipment.

5. TEST PROCEDURES

The test specimens were selected from random locations within the timber supplied. The loads were applied so as to reach the 2 mm offset load in 2–3 minutes. The tests for the timber from shipments 1 and 2 were terminated after the deformation exceeded 10 mm. However, for material from the later shipments, the loads were taken to failure of the test specimens.

In attempting to take the loads to failure, it was found necessary to restrain the specimens, particularly the 190 x 35 mm specimens, against lateral distortion, buckling or rotational translation. Quite large forces were required for these rigid restraints. Such restraints would probably not occur in practical situations. If the test specimen were loaded to failure, the most common failure modes observed were:

- ring shear;
- lateral distortion/buckling;
- multiple horizontal cracks (particularly when using test Configuration 'C').

For test Configuration 'D', it was found that often failure was by bending rather than by bearing compression.

The sample size used for each test configuration, grade and size of timber was $N = 20$ for material from shipments 1 and 2 and $N = 10$ for all others.

6. TEST DATA

6.1 Notation and Definitions

The test results are reported in terms of a bearing stress f and stiffness k . The bearing stress is taken to be given by

$$f = \frac{P}{35 \times L_{\text{bear}}} \quad (1)$$

where L_{bear} denotes the length of the bearing area.

Using equation (1), the bearing stresses f_{LP} , f_{offset} , f_{crack} , $f_{5\text{mm}}$, $f_{10\text{mm}}$, $f_{20\text{mm}}$, $f_{40\text{mm}}$ and f_{max} are derived from P_{LP} , P_{offset} , P_{crack} , $P_{5\text{mm}}$, $P_{10\text{mm}}$, $P_{20\text{mm}}$, $P_{0\text{mm}}$ and P_{max} , respectively. For Configuration 'D', the value of P was taken to be 0.66 times the load applied by the testing machine.

The stiffness k is given by

$$k = f_{\text{offset}} / \Delta_{\text{elastic}} \quad (2)$$

where f_{offset} denotes the bearing stress corresponding to P_{offset} and Δ_{elastic} is the nominal elastic deformation corresponding to the offset load as shown in Figure 1.

6.2 Data from Testing Small Clears

Data of this type was used in early standards to derive design properties for bearing strength. Ten samples were taken for timber from each stress grade from shipment No. 5 and the overall average values obtained were as follows:

- density at 12% m.c. = 595 kg/m³
- f_{LP} = 8.5 MPa
- $f_{2.5\text{mm}}$ = 15.1 MPa.

In a previous study (Ditchburne *et al.*, 1975) the following data was obtained for small clears of kiln dried radiata pine:

- density @ 12% m.c. = 530 kg/m³
- $f_{LP} = 5.8$ MPa.

Based on a regression of the test data, it would appear that the current values of f_{LP} may be too high by about 20%, and the tests will need to be repeated.

6.3 Data from Testing Structural Size Timber

A brief summary of the data obtained is given in Tables 1 and 2. Average values of the properties indicated are shown. Values of f_{5mm} are shown for test configurations that result in load bearing on only one face of the timber and f_{10mm} for those that result in load bearing on two faces; these two figures are obviously directly comparable.

As a rough approximation it may be stated that Configuration 'A' is similar to the upper half of Configuration 'B' and Configuration 'C' is expected to behave as the right half of configuration 'B', i.e. all three configurations should be equivalent at least until gross distortions occur. This is consistent with the data obtained. The data from Configurations 'D' and 'E' are not entirely consistent and will need to be rechecked.

There is obviously an effect of machine grading on timber density and an effect of density on bearing strength and stiffness. The effect of bearing length can be obtained by comparing the data for configurations B1, B2 and B3.

The effect of deformation limit is shown in Table 3 for the case of 190 x 35 mm timber loaded in Configuration 'A'. Approximately half the specimens failed before a deformation limit of 40 mm was attained. It is seen that there is perhaps an additional 30% reserve strength after P_{offset} has been reached.

Table 4 illustrates the variability observed in the test data. The coefficient of variation lies in the range of 15–25% for bearing strength and 20–30% for stiffness. For density, it is about 10%.

For the material of shipments 3 and 4, a record was kept of the first clearly audible crack. It was found to occur at a load quite close to 2 mm offset load. This would tend to reinforce the concept of choosing the offset load for specifying characteristic values for serviceability limit states.

Table 1.
Average values of data for 90 x 35 mm timber

TEST	Shipment No.	Stress grade	Bearing length L_{bear} (mm)	Density at 12% m.c. (kg/m^3)	Bearing stiffness k (MPa/mm)	f_{offset} (MPa)	$f_{5\text{mm}}$ (MPa)	$f_{10\text{mm}}$ (MPa)
A	1	F5	90	504	9.1	11.2	12.1	
	1	F8	90	541	8.3	10.6	11.4	
	1	F11	90	613	9.0	12.4	13.1	
B-1	1	F5	45	485	7.64	11.9		14.9
	1	F8	45	534	6.8	11.2		14.8
	1	F11	45	602	7.0	13.6		17.8
B-2	1	F5	90	505	5.05	10		11.9
	1	F8	90	541	5.05	9.1		11.3
	1	F11	90	606	5.4	11		13.5
B-3	1	F5	180	512	4.5	8.5		9.5
	1	F8	180	545	4.4	8.4		9.5
	1	F11	180	593	4.6	9.2		10.5
C	1	F5	90	501	4.1	7.7		8.9
	1	F8	90	538	3.9	8.1		9.2
	1	F11	90	603	4.2	8.8		10.8
D	1	F5	90	488	10.5	9.6	9.7	
	1	F8	90	530	8.4	10.7	11.3	
	1	F11	90	600	8.5	12.2	12.9	
E	1	F5						
	1	F8	45	508	4.7	7.1	7.6	
	1	F11						

Table 2.
Average values of data for 190 x 35 mm timber

TEST	Shipment No.	Stress grade	Bearing length L_{bear} (mm)	Density at 12% m.c. (kg/m^3)	Bearing stiffness k (MPa/mm)	f_{offset} (MPa)	f_{5mm} (MPa)	f_{10mm} (MPa)
A	2	F5	90	526	6.2	10.6	11.2	
	2	F8	90	563	6.2	11.4	11.4	
	2	F11	90	601	5.8	12.2	12.4	
A	4	F5	90	487	3.6	9.5	9.6	
	3	F8	90	592	5.4	13.3	13.7	
	3	F11	90	586	4.6	11.8	12.1	
B-2	2	F5	90	538	3.9	9.4		11.3
	2	F8	90	555	4.0	9.7		11.8
	2	F11	90	584	3.8	9.6		11.7
B-2	4	F5	90	490	2.9	8.5		10.3
	3	F8	90	582	4.5	11.8		13.9
	3	F11	90	608	4.3	11.7		14.3
B-3	4	F5	180	478	2.4	7.0		8.1
	3	F8	180	581	3.9	10.4		11.2
	3	F11	180	537	3.7	9.4		11.2
C	2	F5	90	529	2.9	7.4		8.8
	2	F8	90	555	3.0	7.9		9.3
	2	F11	90	581	3.1	8.2		9.6
C	4	F5	90	476	1.9	6.7		7.6
	3	F8	90	593	2.7	9.8		11.2
	3	F11	90	591	2.5	9.0		10.2
D	2	F5	90	537	8.1	11.0	11.7	
	2	F8	90	557	8.4	11.8	12.6	
	2	F11	90	594	8.5	11.7	12.8	
E	2	F5	45	568	9.0	13.0	13.7	
	2	F8	45	568	8.4	12.7	13.4	
	2	F11	45	558	9.8	12.0	12.5	

Table 3.
Effect of deformation limit on load capacity
(Configuration 'A', 190 x 35 mm timber)

Stress grade	Density at 12% m.c. (kg/m ³)	Bearing pressure (MPa)			
		f_{offset}	$f_{5\text{mm}}$	$f_{10\text{mm}}$	$f_{20\text{mm}}$
F5	487	9.5	9.6	11.4	13.3
F8	592	13.3	13.7	16.5	17.2
F11	586	11.8	12.1	14.9	15.4

F5 – shipment 4

F8, F11 – shipment 3

Table 4.
Variability of bearing strength and stiffness
(Configuration 'A', 90 x 35 mm timber)

Stress grade	Coefficient of variation			
	Density at 12% m.c.	Stiffness k	f_{offset}	$f_{10\text{mm}}$
F5	0.10	0.29	0.24	0.24
F8	0.08	0.17	0.17	0.19
F11	0.12	0.31	0.19	0.19

7. CONCLUSIONS

In the selection of a configuration for a standard in-grade test, both Configurations 'A' and 'B', shown in Figure 3, are good candidates; the preference is probably for Configuration 'B' because it models a very practical in-service situation.

With respect to the data recorded, both the stiffness k and 2 mm offset stress, f_{offset} are useful parameters for the design of serviceability limit states.

For laboratory evaluations of characteristic values for strength limit states, it is suggested that some deformation limit be included. This is because at large deformations, very rigid restraints are required to prevent the test specimen from collapsing. For test configurations in which specimens experience local bearing pressures from only one side, such as Configuration 'A', the deformation limit should be 5 or 10 mm. For test configurations involving local bearing pressures from two sides, such as Configuration 'B', the limit may be doubled.

8. REFERENCES

Ditchburne, N., Kloot, N.H. and Rumball, B. (1975). The Mechanical Properties of Australian-grown *Pinus Radiata* D.Don. Division of Building Research Technical Paper (Second Series) No. 9, CSIRO, Australia.

CIB-W18/31-7-1

**INTERNATIONAL COUNCIL FOR BUILDING RESEARCH STUDIES AND DOCUMENTATION
WORKING COMMISSION W18 - TIMBER STRUCTURES**

**MECHANICAL PROPERTIES OF DOWEL TYPE JOINTS
UNDER REVERSED CYCLIC LATERAL LOADING**

by

M Yasumura

**Department of Forest Resources Science
Shizuoka University**

JAPAN

MEETING THIRTY-ONE

SAVONLINNA

FINLAND

AUGUST 1998

Mechanical Properties of Dowel Type Joints under Reversed Cyclic Lateral Loading

Motoi YASUMURA

Department of Forest Resources Science, Shizuoka University, Japan

Abstract : Timber joints connected with a bolt or a dowel were subjected to the monotonic and the reversed cyclic loading based on the protocols provided in CEN standard and ISO/TC165/WG7 draft, and the influence of the loading protocols and the reversed cyclic loading on the ultimate performance of joints was investigated. The specimen had the spruce glued-laminated timber and the steel plates of 12 mm thick connected with a bolt or a dowel of 16 mm diameter. The thickness of the timber was 2, 4, 8 and 12 times as large as the bolt diameter. The yield load obtained from the monotonic loading by CEN method showed comparatively good agreement with that by 5% off-set method. Although there were few differences in the ultimate strength between the monotonic and the reversed cyclic loading, considerable decrease of the ultimate displacement was observed in the reversed cyclic loading.

1 Introduction

Stiffness, load carrying capacity and the energy dissipation are the most important parameters to evaluate the seismic performance of the timber structures. Among these parameters, load carrying capacity and the energy dissipation shall be estimated by conducting the reversed cyclic loading test of the joints. The test method for determining the seismic performance of joints made with mechanical fasteners has been provided in CEN Standard [1] and also discussed in ISO/TC165/WG7 [2]. This standard and the draft provide different protocols for the reversed cyclic loading. The loading protocol of CEN Standard is based on the yield displacement corresponding to the yield load. That proposed in ISO/TC165/WG7 is based on the ultimate displacement corresponding to the failure load or 80% of the maximum load after the peak. Therefore, the reversed cyclic loading tests based on these loading protocols were conducted on the dowel type joints to investigate the influence of the loading protocols on the load carrying capacities and the ultimate displacement.

2 Specimens

Configurations of two groups of specimens are shown in Fig. 1. One was those having a main member of spruce glued-laminated timber and two steel side plates of 12 mm thickness connected with a single bolt of 16 mm diameter. The other was those having a main member of spruce glued-laminated timber and a steel center plate of 12 mm thickness inserted into a slit at the center of the main member and connected with a single dowel or a bolt of 16 mm diameter (d). End and edge distances of the bolt and dowel joints were respectively 114 mm (7d) and 48 mm (3d), and the thickness of the main members (L) was 32 mm (2d), 64 mm (4d) and 128 mm (8d) for the bolted joints with steel side plates, and 44 mm (2d), 76 mm (4d), 140 mm (8d) and 204 mm (12d) for the bolted or dowel joints with a steel center plate. The density of spruce glued-laminated timber was 410 kg/m³ in average, and the diameter of bolt holes was almost the same as the bolt and dowel diameter. The steel quality of the bolts and dowels was SS400.

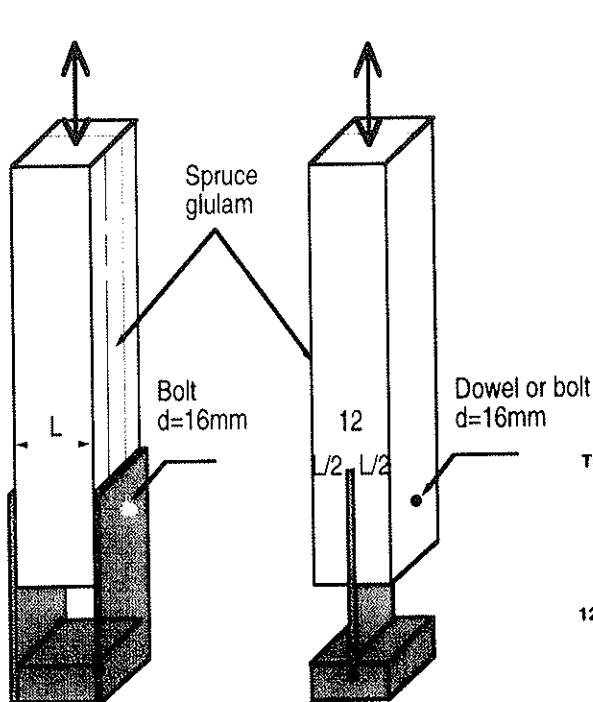


Fig.1 Configuration of specimens

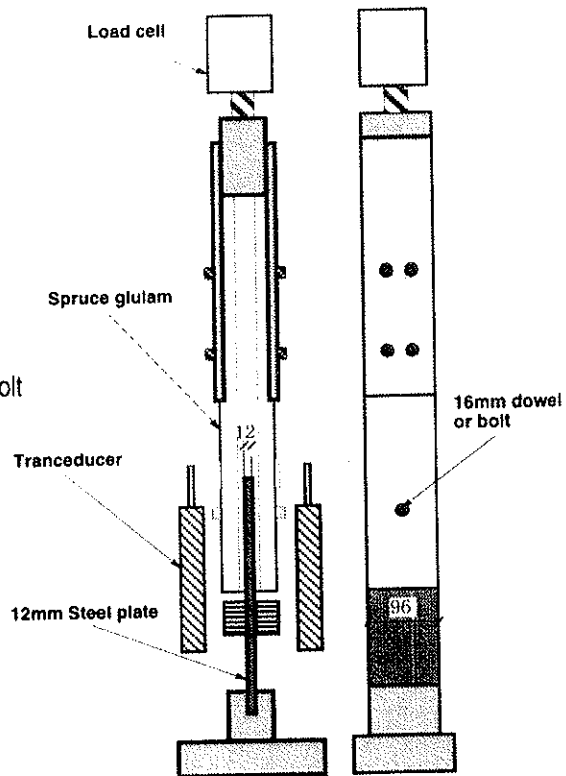


Fig 2 Test set-up

3 Test method

The upper part of the main member of the specimens were connected tightly to 100kN Tensilon through a load cell with two steel plates of 12 mm thickness with four high tensile bolts of 16mm diameter, and the steel plate(s) connected to the lower part of the main member with a bolt or a dowel was connected to the cross-head of Tensilon as shown in Fig. 2. Monotonic tensile loads were applied to three specimens of each type, and other six were subjected to the reversed cyclic loading. Both the protocol provided in prEN12512 and that proposed in ISO/TC165/WG7 were applied to the reversed cyclic loading tests. The yield displacement and ultimate displacement to determine the reversed cyclic protocols were obtained from the monotonic loading tests. The loading protocols in prEN12512 and ISO/TC165/WG7 draft are shown respectively in Figs. 3 and 4.

4 Results and Discussion

4.1 Yield load

Figs. 7 to 9 show the comparison of the yield loads in the monotonic loading test obtained from “1/6 method” and “5% off-set method” [3] with the calculated values by the yield theory[4]. The “1/6 method” is that provided in prEN12512 and defined by the intersection of two lines: the first line is determined by the drawn through the point on the load-slip curve corresponding to 0.1 Pmax (maximum load) and that corresponding to 0.4 Pmax, the other drawn as the tangent having an inclination of 1/6 of the first line. CEN standard as well as ISO/TC165/WG7 draft requires to determine the initial stiffness by two points corresponding to 0.1 Pmax and 0.4 Pmax. However, 0.6 Pmax was taken instead of 0.4 Pmax in this study as this area of 0.1 to 0.4 Pmax is sensible to the friction between the timber and steel plates,

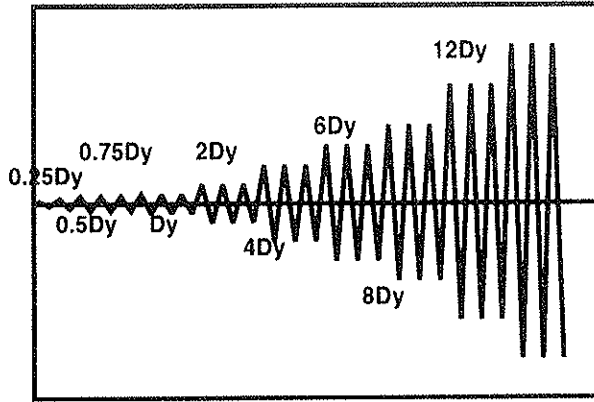


Fig. 3 Loading protocol by prEN12512 based on the yield displacement (D_y)

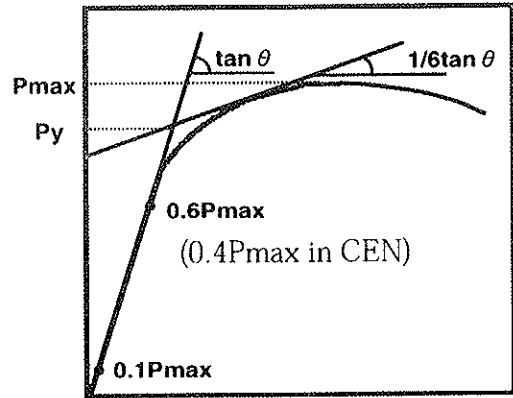


Fig. 5 Definition of the yield load by CEN

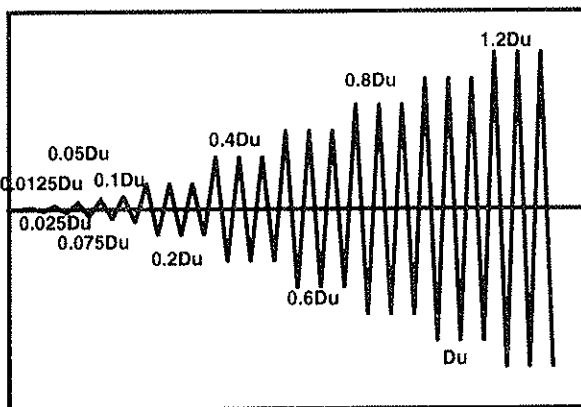


Fig. 4 Loading protocol by ISO/TC165/WG7 draft based on the ultimate displacement (D_u)

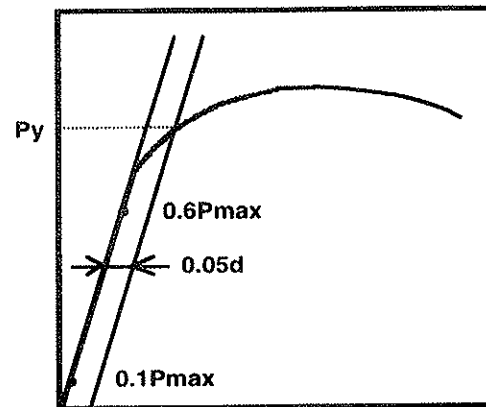


Fig. 6 Definition of the yield load by 5% off-set method

and it is preferable to take $0.6 P_{max}$ instead of $0.4 P_{max}$ to avoid this effect. As the inclination of $1/6$ of that of the first line is taken for the second line in CEN standard, the estimated yield load has the tendency to be dependent much upon the inclination of the first line. Therefore, the yield load obtained by “5% off-set method” was compared with those by “ $1/6$ method”. The yield load is defined by the intersection of the load-slip curves and the line which has the same inclination as that determined by the drawn through the point on the load-slip curve corresponding to $0.1 P_{max}$ and $0.6 P_{max}$ and off-set 0.05 times of the bolt diameter. The definition of the yield load by “ $1/6$ method” and “5% off-set method” are shown in Figs. 5 and 6, respectively. For the calculation of the yield load, the embedding strength of spruce and the yield moment of dowel were assumed to be 35.5 MPa and 490 MPa , respectively from the embedding test and the bending test of dowels.

These results indicates that the yield loads obtained by “ $1/6$ method” showed good agreement with those by “5% off-set method”, and they agreed also comparatively well with the calculated values by the yield theory in the bolted joints with steel side plates and a steel center plate. However, the experimental values showed approximately 30% smaller than the calculated values in the dowel joints with a steel center plate. This might be caused by the split of the slit at the center of main member. It is supposed that the slit of the main member was splitted due to the bending of the dowel, and the opening of the slit caused reducing the yield load. This failure did not happen in the bolted joints with a steel center plate.

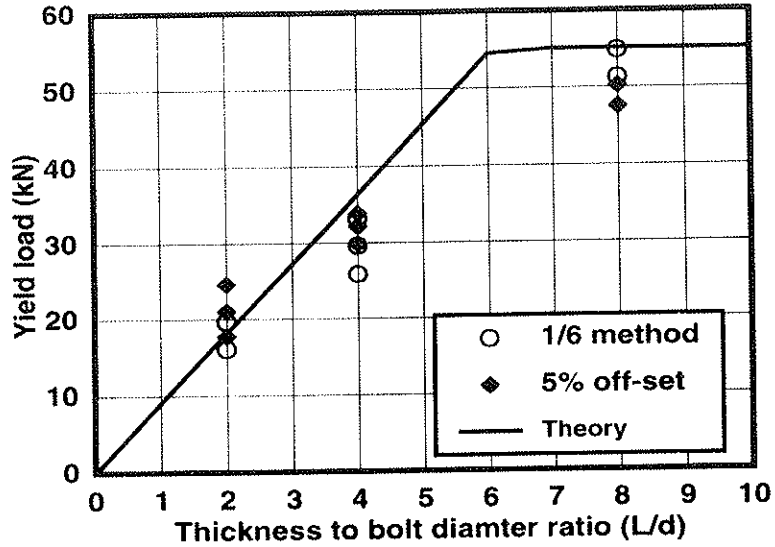


Fig. 7 Comparison of the yield loads with calculated values in the bolted joints with steel side plates

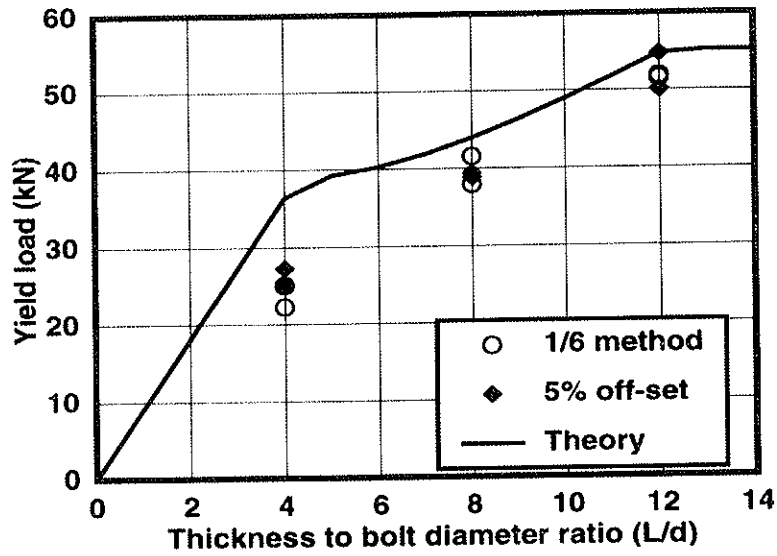


Fig. 8 Comparison of the yield loads with calculated values in the bolted joints with steel center plate

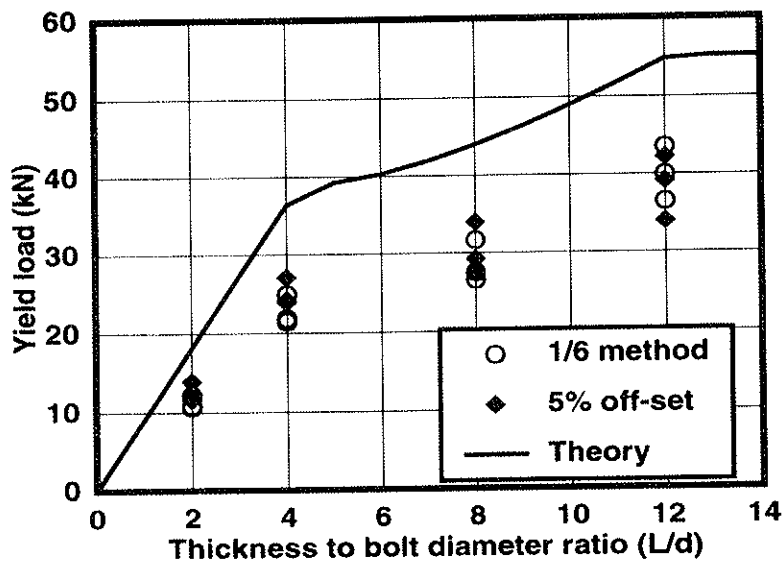


Fig. 9 Comparison of the yield loads with calculated values in the dowel joints with steel center plate

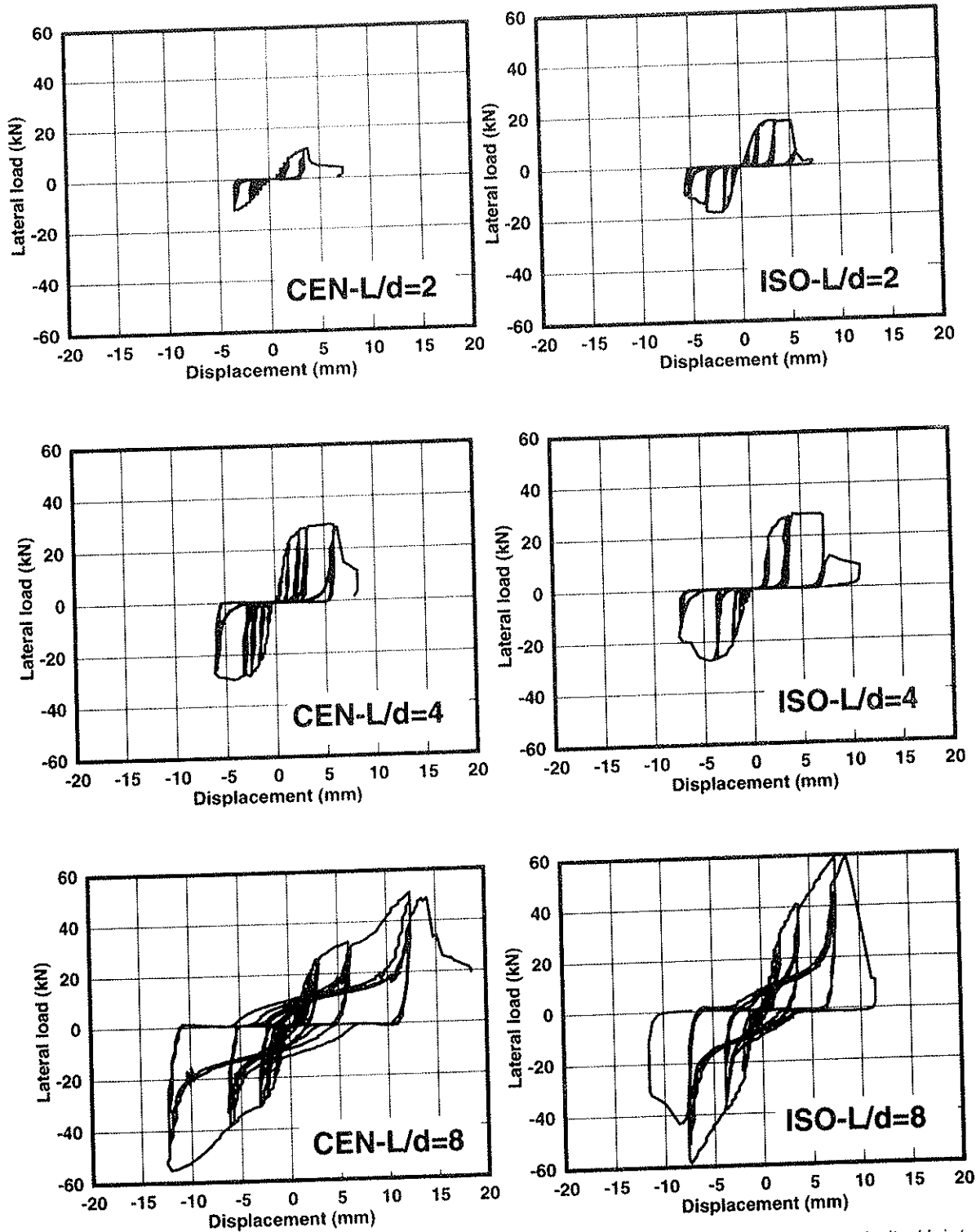


Fig.10 Load-slip relationship of the bolted joints with steel side plates by CEN protocol

Fig.11 Load-slip relationship of the bolted joints with steel side plates by ISO protocol

4.2 Load-slip relationship

Figs. 10 and 11 show the example of the load-slip relationships of the bolted joints with steel side plates in the reversed cyclic loading of prEN12512 and ISO/TC165/WG7 proposal, and Figs. 12 and 13 show those of the dowel joints with the steel center plate. It was shown that the hysteresis curves were well symmetrical in the positive and negative loading direction and contained slip behavior especially with the specimen whose thickness of main member

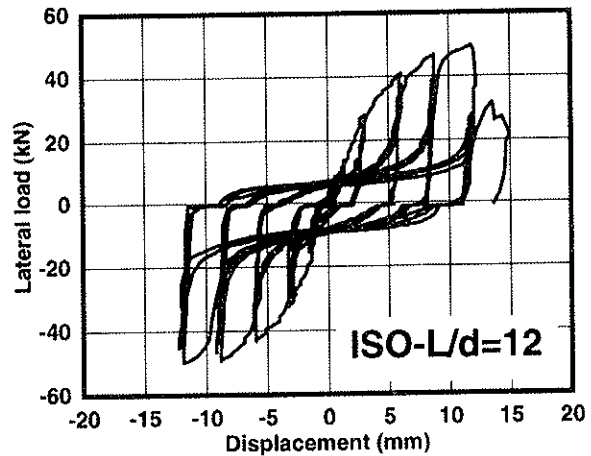
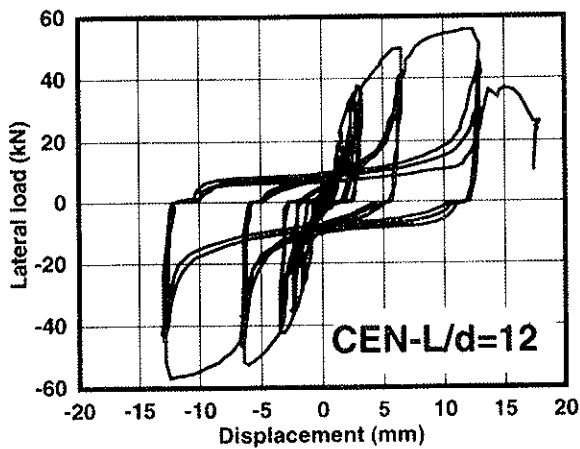
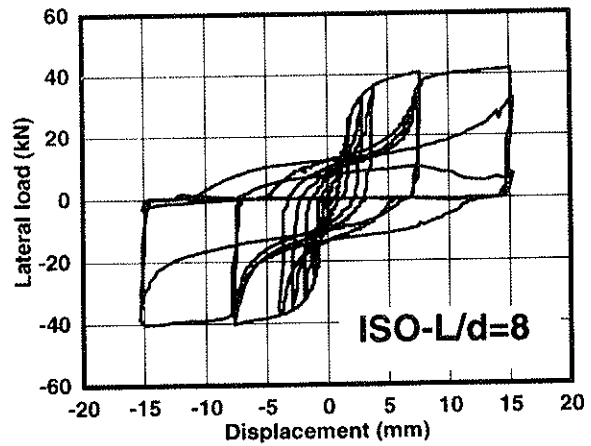
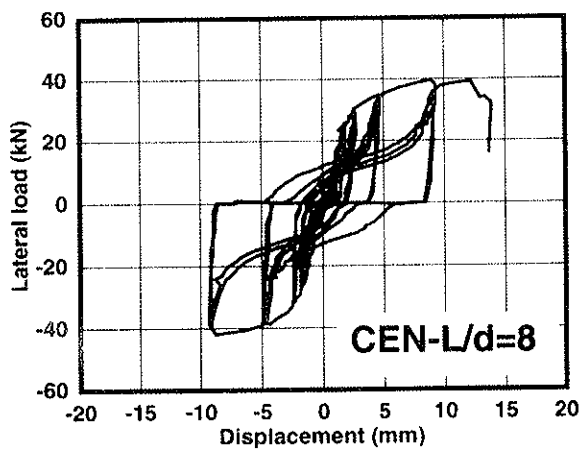
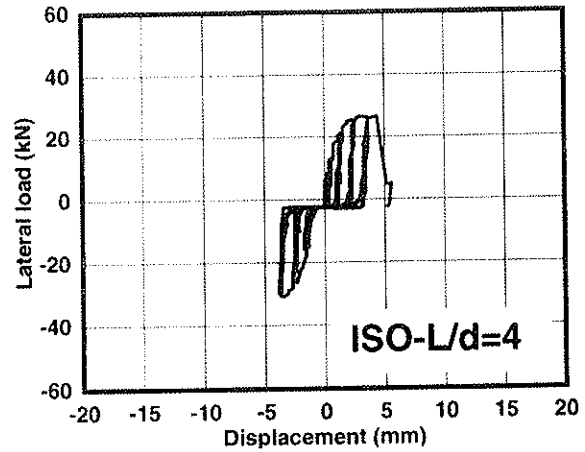
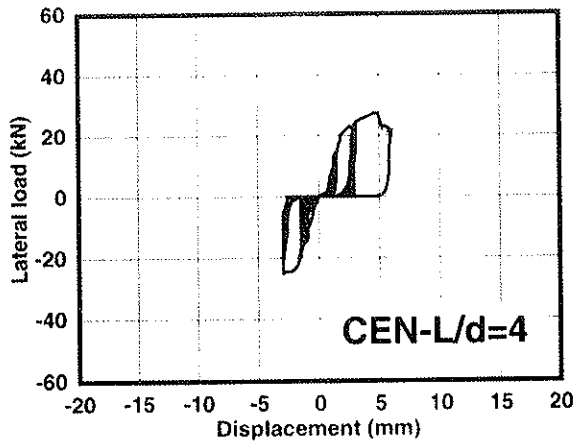


Fig.12 Load-slip relationship of the dowel joints with a steel center plates by CEN protocol

Fig.13 Load-slip relationship of the dowel joints with a steel center plates by ISO protocol

was small. They also demonstrate the differences of the load carrying capacity and the ductility in the specimens having the different member thickness.

4.3 Load Carrying capacity and ultimate displacement

Maximum loads of the bolted and dowel joints in the reversed cyclic loading with CEN and ISO draft protocols are compared with those in the monotonic loading test in Figs. 14 and 15.

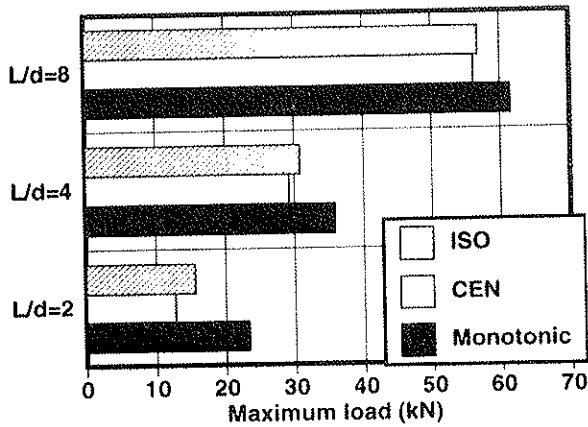


Fig. 14 Maximum load of the bolted joints with steel side plates

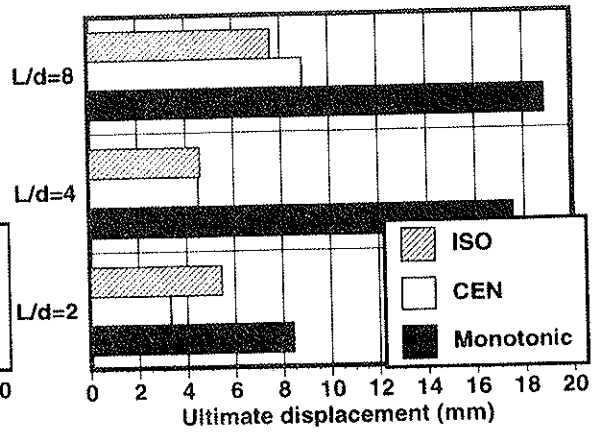


Fig. 16 Ultimate displacement of the bolted joints with steel side plates

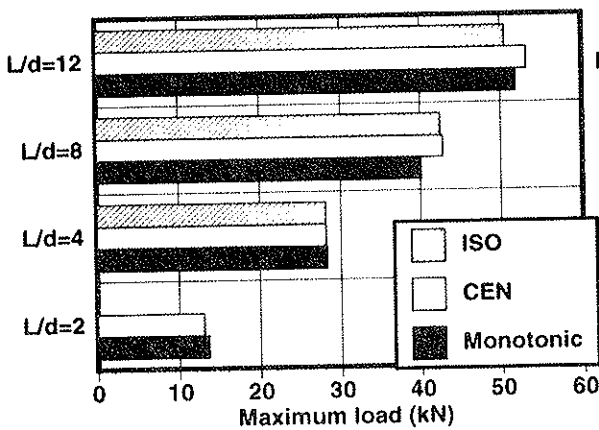


Fig. 15 Maximum load of the dowel joints with a steel center plate

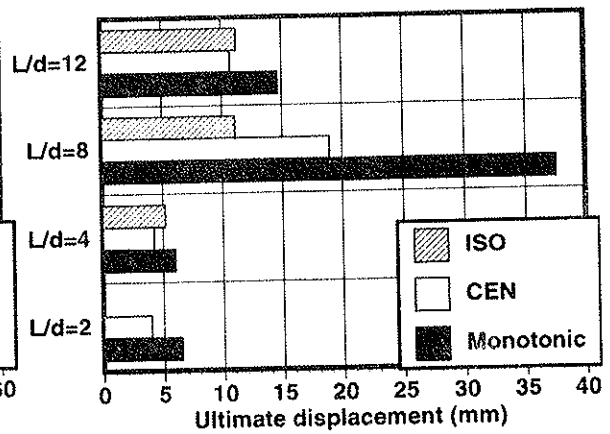


Fig. 17 Ultimate displacement of the dowel joints with a steel center plate

Ultimate displacement of the joints was obtained from the displacement corresponding to the smaller value between the failure load and 0.8 P_{max} after the peak. Most of the ultimate displacement was obtained from the failure load.

Quite few differences of the ultimate displacement was observed between CEN and ISO draft protocols. However, a significant decrease of the ultimate displacement due to the reversed cyclic loading was observed in both the specimens with steel side plates and a steel center plate. In the dowel joint with a steel center plate, the ultimate displacement of the specimen whose main member was twelve times as large as the bolt diameter was much smaller than those having the member thickness of eight times of the bolt diameter. This is caused by the fact that the split of the slit in the main member due to the bending deformation of a dowel was more significant in the joints having the member thickness of twelve times as large as the bolt diameter than those having the member thickness of eight times of the bolt diameter.

4.4 Equivalent viscous damping rate

Figs. 18 and 19 show the equivalent viscous damping rate in the specimen with steel side plates and a steel center plate. The equivalent viscous damping rate was obtained from the ratio of the potential energy at the peak of the hysteresis curves to the dissipated energy in a hysteresis cycle[5]. Only the equivalent viscous damping rate of the second and the third cycles is discussed in this paper, and those of the first cycle is not included in Fig. 18 and 19.

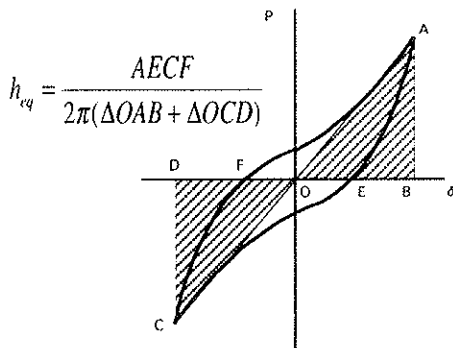
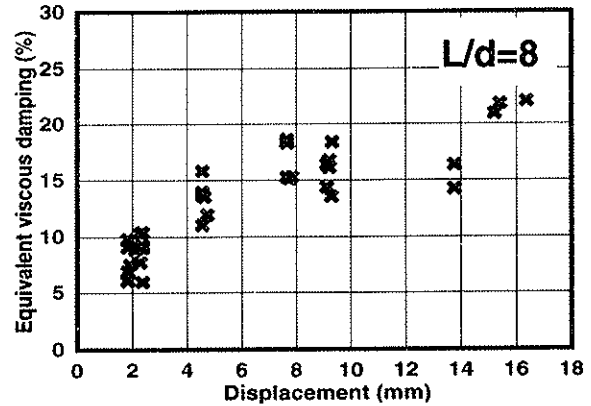
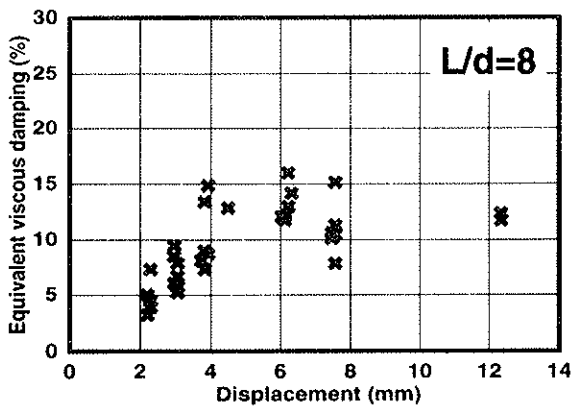
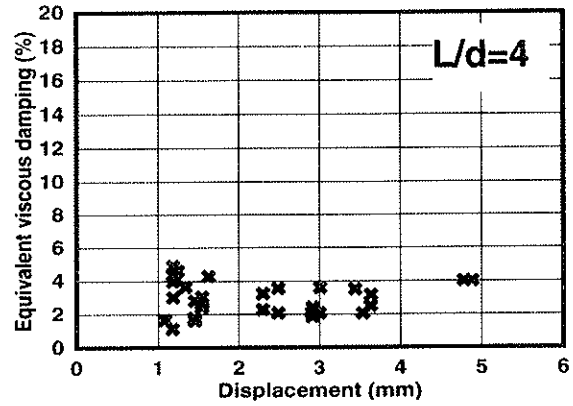
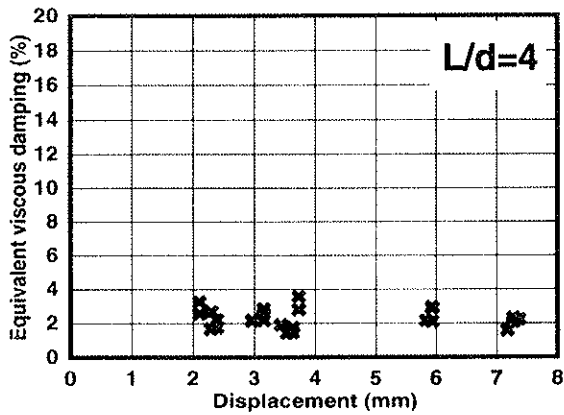
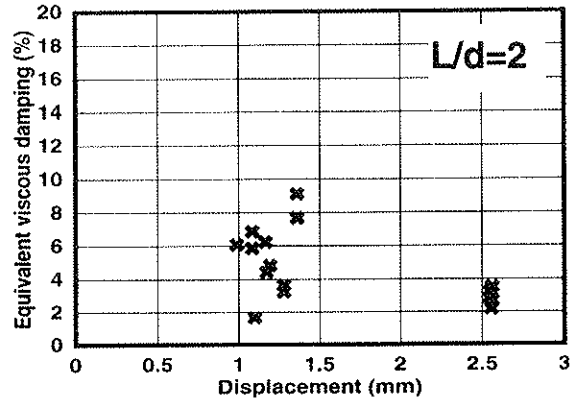
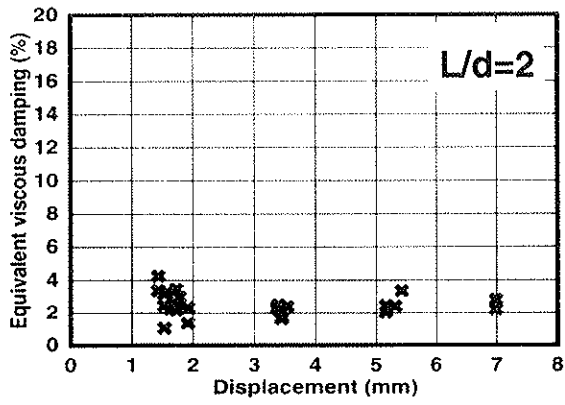


Fig.18 Equivalent viscous damping rate of the bolted joints with steel side plates

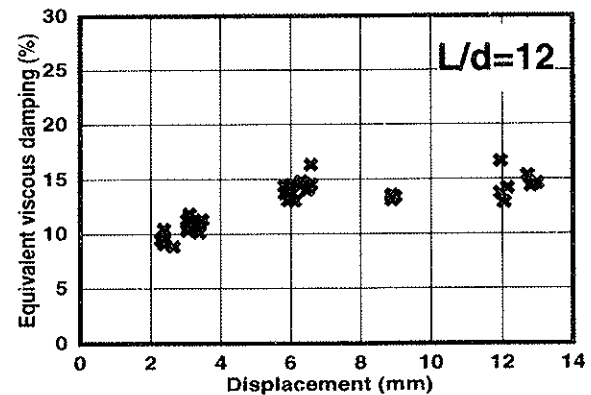


Fig.19 Equivalent viscous damping rate of the dowel joints with a steel center plate

It is shown from these figures that the equivalent viscous damping rate was almost constant and approximately 2 to 4% in the specimen whose member thickness was less than eight times of the bolt diameter. Equivalent viscous damping rate of the specimen whose member thickness was eight and twelve times of the bolt diameter varied 5 to 10% when the slip was 2 to 4 mm, and then it was almost constant and around 15% when the slip was larger than 4mm. This indicates that the joints having the member thickness of eight times of the bolt diameter shows higher energy dissipation than those having the smaller member thickness.

5 Conclusions

Summarizing the results mentioned above, the following conclusions are led;

- 1) Yield loads obtained by “1/6 method” showed good agreement with those by “5% offset method”, and they agreed also comparatively well with the calculated values by the yield theory in the bolted joints with steel side plates and a steel center plate.
- 2) Yield loads obtained from the experiments were approximately 30% smaller than the calculated values in the dowel joints with a steel center plate because of the split of the slit at the center of main member .
- 3) No significant difference of the maximum loads was observed between CEN and ISO draft loading protocols both in the specimens with steel side plate and a steel center plate.
- 4) Maximum load of the bolted joints with steel side plates in the reversed cyclic loading reduced 10 to 40% to that of the monotonic loading, however no significant reduction of the maximum load was observed in the dowel joints with a steel center plate.
- 5) Few differences of the ultimate displacement was observed between CEN and ISO draft protocols.
- 6) A significant decrease of the ultimate displacement due to the reversed cyclic loading was observed in both the specimens with steel side plates and a steel center plate.
- 7) In the dowel joint with a steel center plate, the ultimate displacement of the specimen whose main member was twelve times as large as the bolt diameter was much smaller than those having the member thickness of eight times of the bolt diameter because of the split of the slit in the main member due to the bending deformation of a dowel.
- 8) Joints having the member thickness of eight times of the bolt diameter shows higher energy dissipation than those having the smaller member thickness.

6 Acknowledgments

The author appreciates Mr. Shuto, graduate student of Shizuoka University, for conducting the testing of the joints.

7 References

1. CEN: “Timber structures - Test methods - Cyclic testing of joints made with mechanical fasteners”, prEN12512
2. ISO: “Timber structures - Joints made with mechanical fasteners - Quasi-static reversed-cyclic test method”, TC165/WG7 Draft, 1998
3. YASUMURA, M., “Evaluation of Wood Framed Shear Walls subjected to Lateral Load”, Proceedings of the 30th CIB-W18, paper 30-15-4, August 1997
4. YASUMURA, M., “Ultimate Properties of Bolted Joints in Glued-Laminated Timber”, Proceedings of the 20th CIB-W18, paper 30-7-3, September 1987
5. YASUMURA, M., “Evaluation of Seismic Performance of Timber Structures”, Proceedings of 1996 IWEC, Vol.1, October 1996

CIB-W18/31-7-2

INTERNATIONAL COUNCIL FOR BUILDING RESEARCH STUDIES AND DOCUMENTATION
WORKING COMMISSION W18 - TIMBER STRUCTURES

DESIGN OF JOINTS WITH LATERALLY LOADED DOWELS

by

A Mischler

Chair of Wood Technology
ETH Zürich
SWITZERLAND

MEETING THIRTY-ONE

SAVONLINNA

FINLAND

AUGUST 1998

Design of Joints with Laterally Loaded Dowels

Adrian Mischler

ETH Zurich, Wood Technology, Zurich, Switzerland

1 Introduction

The load-carrying capacity of joints with dowel type fasteners is in most codes based on the load-carrying capacity of the single fastener. Therefore it has been the aim of many researchers to determine the characteristic load-carrying capacities of single fasteners (Johansen [1949], Werner [1993]).

The following comparison between a multiple fastener connection and a single fastener may point out, that many factors which can strongly affect the load-carrying behavior of a multiple fastener joint are neglected in tests on single fasteners.

2 Differences between a single fastener and a multiple fastener joint

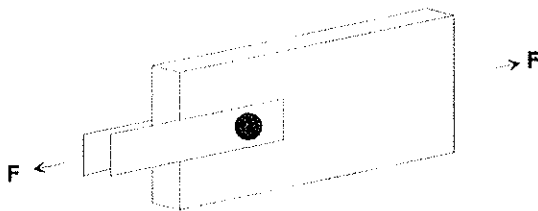


Figure 1a: Single fastener

- Low level of stress in timber
- No failure of the timber member
- Plastic behavior of embedment
- No influence of fabrication tolerances
- Hole force on one fastener

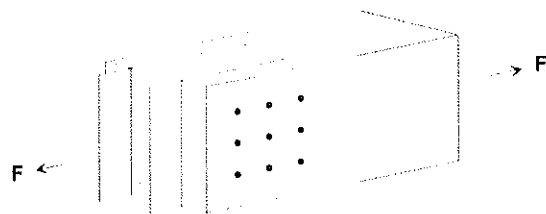


Figure 1b: Multiple fastener joint

- High level of stress in timber
- Often failure of the timber in the connection
- Brittle failure due to timber splitting along the grain
- Fabrication tolerances have an influence on load distribution among the fasteners
- Uneven distribution of loads among the fasteners

The ultimate resistance of a timber joint is not only limited by the resistance of the fasteners but also by the resistance of the timber. The European Yield Model deals only with the load-carrying capacity of fasteners based on the connector strength and the wood embedment resistance. It is assumed, that no brittle failure in the timber such as splitting, plug shear or tensile failure in the reduced cross section occurs before the fasteners reach their ultimate resistance. Such brittle failure modes should be prevented by prescribing end and edge distances, and fastener spacing. Recent research has shown that in multiple fastener connections, which are commonly used in timber structures, a failure of the timber parts is very often decisive. In these cases the failure loads are smaller than the load-carrying capacity predicted by the European Yield Model, since the connector interaction or group effect typically induces brittle failure modes due to stress concentrations in the timber.

3 Factors affecting the load-carrying capacity of multiple fastener joints

3.1 Influence of placement of fasteners

In mechanical timber joints the load in the timber member, which is distributed over the whole cross section has to be transformed to concentrated forces in the fasteners. The application of these concentrated forces creates high shear stresses and tensile stresses perpendicular to the grain in the timber along the rows of fasteners (Figure 2 and 3).

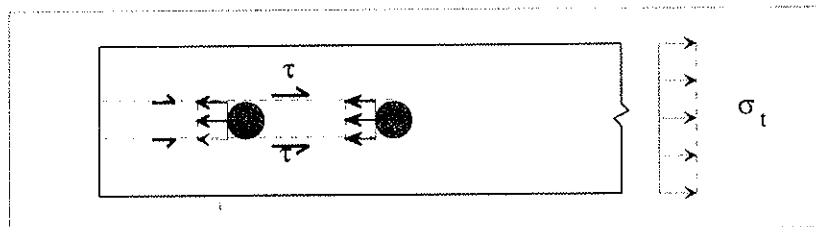


Figure 2: Load application in a mechanical timber joint.

As the timber is a non-isotropic material, concentrated forces, which are applied parallel to grain are poorly distributed throughout the cross-section. To reach a high degree of efficiency in a timber joint the fasteners have to be distributed over the entire section. The shear and tensile perpendicular to grain stresses are then governed by the dowel strength, the dowel diameter and the placement of the dowels. It has been found that the risk of failure in splitting and shear can be reduced by using small dowels. The load application of many slender dowels is typically more continuous and creates lower shear stresses than that of few larger dowels (Figure 3).

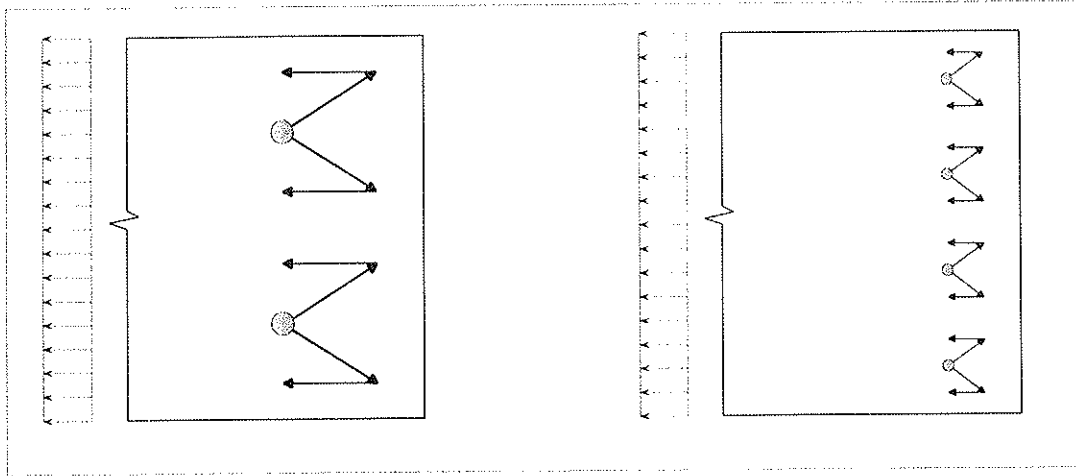


Figure 3: Forces in timber caused by dowels of different diameter.

The effect of local stress concentrations caused by an inadequate placement of fasteners can be shown by evaluating test results from a study by Masse, Salinas and Turnbull [1988]. The objective of this study was only to investigate the influence of the number of rows on the load-carrying capacity of bolted timber connections. They compared the failure load of connections with 4 dowels in line and 1 or 2 rows respectively (Figure 4). The failure loads are summarized in table 1.

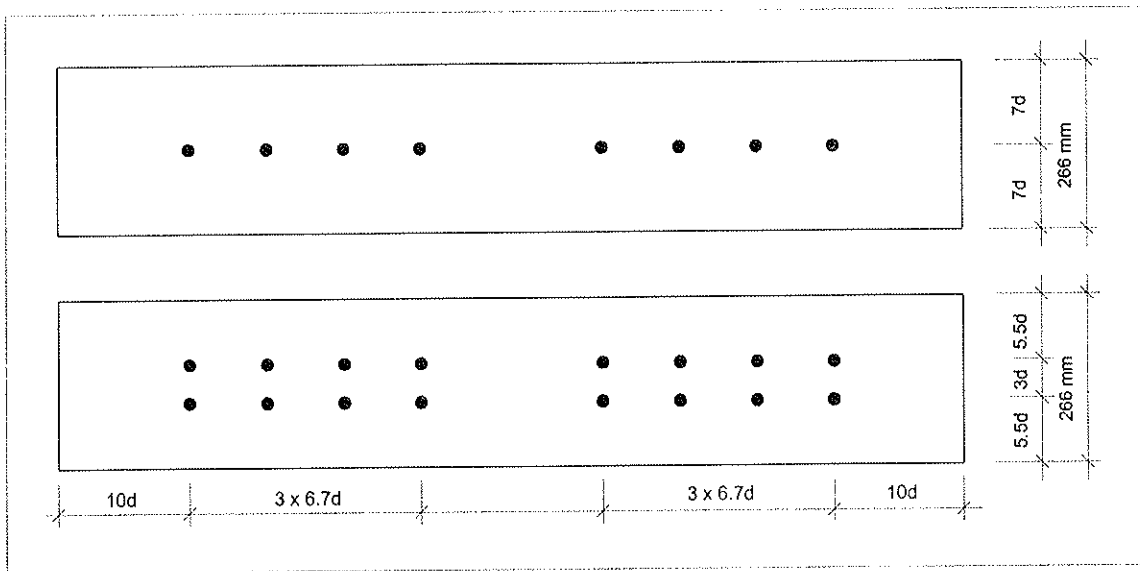


Figure 4: Specimen with 1 and 2 rows of bolts (bolt diameter = $\frac{3}{4}$ inch.)

Timber species	Connection with 1 row	Connection with 2 rows
Douglas Fir	61.9 kN	44.1 kN
Spruce	56.0 kN	33.8 kN

Table 1: Mean failure load per bolt according to Masse, Salinas and Turnbull [1988].

Based on these tests a reduction factor, depending on the number of rows, was introduced in the Canadian code CSA 086.1

By calculating the tensile stress in the reduced timber cross section under the assumption that the entire cross section is effective, no timber failure would be predicted. On the other hand by considering the local stress concentration between the two rows of dowels (Figure 5) it becomes more likely to encounter a wood failure before the bolts may reach their load-carrying capacity according to the tests with one row. In a simplified manner, the stress distribution across a bolt line may be approximated and the maximum stress calculated as shown in Figure 5.

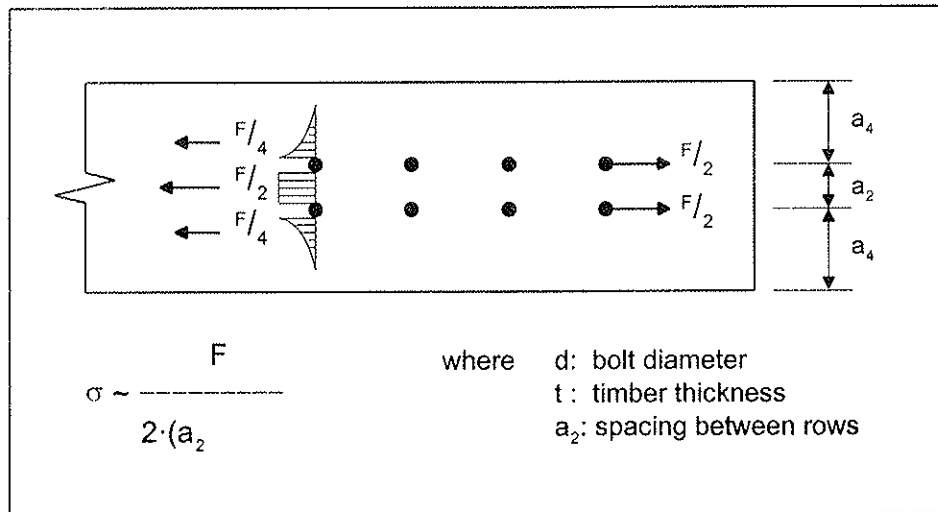


Figure 5: Stress distribution in the timber section.

Tensile stress in the timber between the 2 rows according to the failure loads of table 1:

Douglas-Fir	:	$\sigma = 35.7 \text{ N/mm}^2$
Spruce	:	$\sigma = 27.4 \text{ N/mm}^2$

The author believes that the failure of the connections with 2 rows is caused by these high stresses, which are dependent on the bolt and row spacing, as well as the bolt slenderness. Therefore, the results of these tests are not proof for a reduction in strength according to the number of rows alone. The connection resistance has to be calculated by taking into account the many factors that govern local stress concentrations. It was found, for example, that by distributing the dowels evenly over the whole width of the member, the stresses in the timber are distributed almost uniformly and no reduction is needed, even for 9 rows of fasteners (Mischler [1998]).

3.2 Influence of fabrication tolerances

For steel-to-timber connections the holes in the timber member and in the steel plates are usually drilled separately. If the distances between the holes in the different members of the joint are not exactly the same, an unequal load distribution among the fasteners occurs (Wilkinson [1986]). The influence of this unequal load distribution on the load-carrying capacity depends on the failure mode of the connection. When the connection fails in a brittle way after only small displacements between the timber and the steel plates, the fabrication tolerances strongly affect the strength of the connection. In the case of a ductile failure mode a certain amount of load redistribution is possible after larger deformations in the dowels.

The following connection tests on timber main members and steel side plates show the influence of fabrication tolerances on both the failure load and the stiffness. The specimens were made of LVL Kerto-S to reduce the variance of the material properties. The test set up is shown in Figure 6.

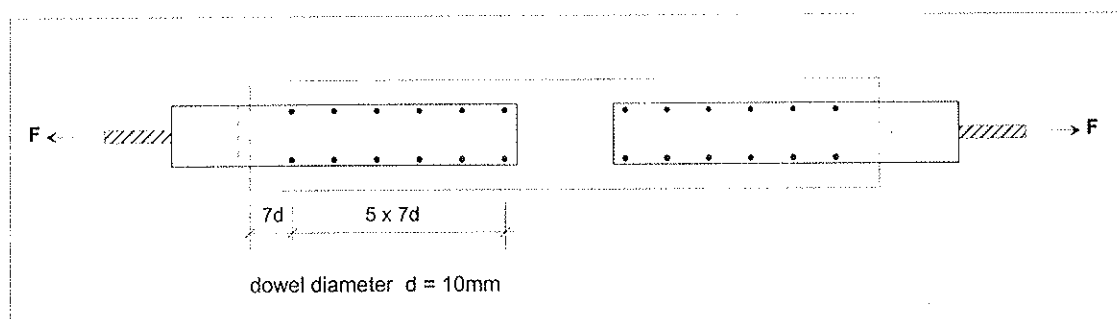


Figure 6: Test set up: Timber thickness = 32mm. \Rightarrow dowel slenderness ratio $\lambda = 3.2$

The holes in the timber were drilled with 3 different levels of fabrication accuracy. The measure of accuracy is the difference between the effective spacing between the holes and the nominal value of 70 mm. The same steel plates were used for all test series. The holes in the timber were drilled with a diameter of 10 mm and in the steel with a diameter of 12 mm. Tables 2 and 3 show the test results:

Precision of drilling	Smallest spacing	Largest spacing
+/- 0.05 mm	69.9 mm	70.1 mm
+/- 0.25 mm	69.5 mm	70.6 mm
+/- 2.00 mm	67.5 mm	72.6 mm

Table 2: Effective spacing between the dowels

Precision of drilling	Failure load	Stiffness
+/- 0.05 mm	127 kN = 100 %	128 kN/mm = 100 %
+/- 0.25 mm	93 kN = 73 %	81 kN/mm = 63 %
+/- 2.00 mm	80 kN = 62 %	35 kN/mm = 27 %

Table 3: Influence of fabrication tolerances in steel-to-timber joints with stocky dowels.

The failure in all tests was caused by splitting of the timber. Due to the small slenderness ratio of 3.2 the dowels were not bent.

These tests demonstrate that test results are only valid for connections, which are manufactured with the same accuracy as the test specimens. Therefore the precision of specimen manufacturing has to be reported in research reports, and rules concerning the fabrication tolerances have to be introduced in design codes.

4 Load-carrying capacity of laterally loaded dowels

4.1 Bending resistance of the dowel

The load-carrying capacity of laterally loaded dowels according to the European-Yield-Model is based on a plastic limit state model. Johansen [1949] who has first published this model assumed an ideal rigid-plastic behavior for both the timber and the steel dowel. Nevertheless, he determined the bending resistance of the dowel under the assumption of a fully elastic stress distribution, up to the plastic moment.

To accurately capture the resistance, however, a plastic design method has to be based on the plastic resistance of the materials. Therefore the plastic bending resistance and not the yield moment of the dowel has to be used to calculate the load-carrying capacity of laterally loaded dowels in timber joints. This plastic bending resistance of a steel dowel is not a constant value. It increases with larger deformations of the dowel because of strain hardening in the steel (Figure 7).

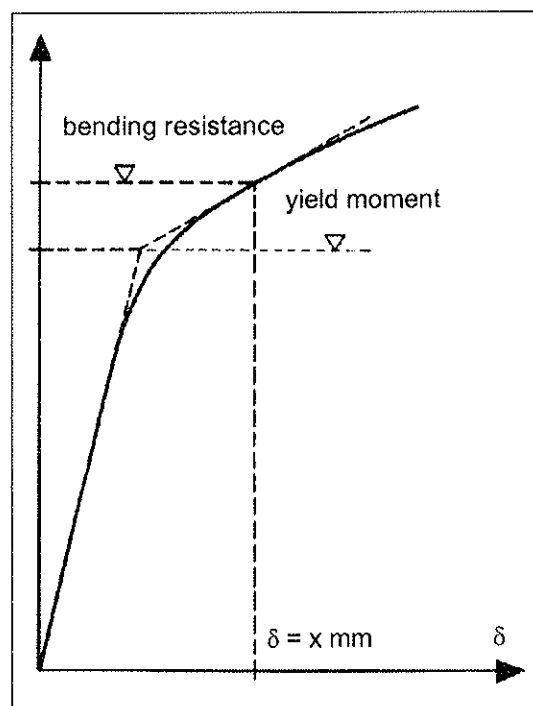


Figure 7: Bending behavior of a steel dowel according to Gehri and Fontana [1983]

When test results on doweled joints are used to validate a theoretical model, it is important, that the load-carrying capacities according to this model are calculated on the basis of effective material properties. Therefore the bending resistance of the dowel corresponding to the dowel deformation in the joint at maximum load has to be used in the theoretical model to determine the load-carrying capacity. This value is not only dependent on the properties of the dowel such as diameter and steel strength, but also on the ductility of the entire connection. If the maximum load in the joint is reached after large plastic deformation, the bending resistance of the dowel is higher than in a joint with brittle behavior.

4.2 Influence of timber properties

The embedding strength of timber, which is determined from tests on rigid single dowels is the only timber property used in the plastic model. However, the stress–distribution in the timber using a multiple–fastener joint is much more complicated than in a single–dowel–embedding test. Therefore, in tests on multiple–fastener joints the differences among the wood species are much more significant than in the normal embedding tests. The influence of the timber properties is demonstrated for two identical multiple shear connections, which were tested in specimen of softwood (spruce) and hardwood (beech). A typical load–deformation–plot of these tests is represented in Figure 8.

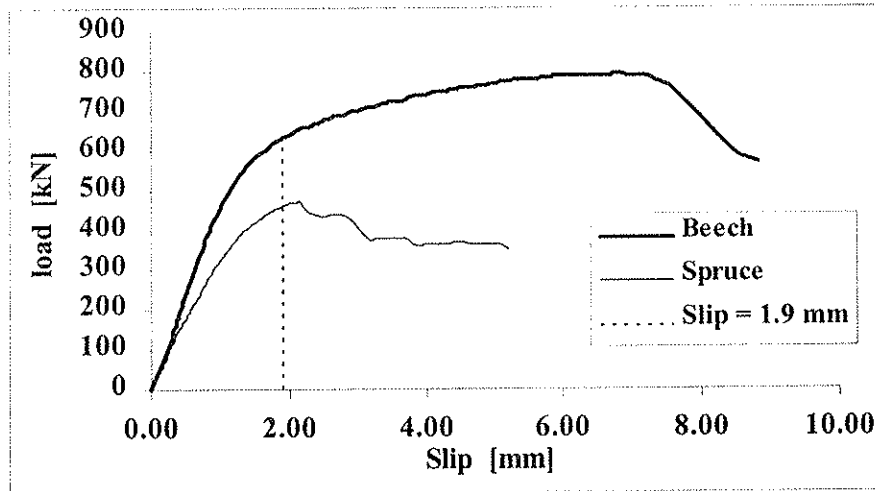


Figure 8: Typical load-slip-plot of identical joints in softwood and hardwood

The different ultimate resistance of the two joints is of course mainly caused by the higher embedding strength of the beech. The influence of the embedding strength becomes obvious when the resistance of the two joints are compared at the same deformation (Table 4). The tensile strength perpendicular to grain of the hardwood is much higher than that of the softwood. Therefore the hardwood joint reaches its maximum load after larger deformations than the softwood joint, which fails in splitting. This means that the bending resistance of the dowel is higher in the beech joint, even if in both joints the same dowel is used. Therefore, the ratio of failure load of the two compared joints is higher than the ratio of the loads at the same deformation level, which corresponds to the same bending resistance of the dowel.

Specimen	density	F ($\delta = 1.9$ mm)	F _{max}
Beech	647 kg/m ³	609 kN	777 kN
Spruce	480 kg/m ³	464 kN	491 kN
Ratio beech / spruce	1.35	1.31	1.58

Table 4: Resistance of the joints at the same deformation ($\delta = 1.9$ mm) and failure load (Mean values of 5 tests, according to Mischler [1998])

The efficiency of hardwood specimens in dowel joints is very high: The embedding strength in these hardwood specimens is higher than in softwood–specimens with the same density. The high increase of ductility and ultimate resistance using hardwoods can only be

observed when multiple fastener connections are tested. In connections with hardwood, no premature brittle failure occurs, due to the high strength in shear and tension perpendicular to the grain direction. Therefore doweled joints in hardwood can reach the full plastic load-carrying capacity. These tests with high ductility make it clear that the plastic bending resistance of the steel dowels is not a constant value, but increases with higher deformation of the dowel, because of strain hardening of the steel.

4.3 Influence of elastic deformations

In the European Yield Model it is assumed, that both materials the timber and the steel show an ideal rigid plastic load-deformation behavior. All elastic deformations are neglected.

In reality both the timber and the dowel are elastically deformed. Therefore, the embedding stress in the timber is not constant over the whole length of the dowel (Figure 9).

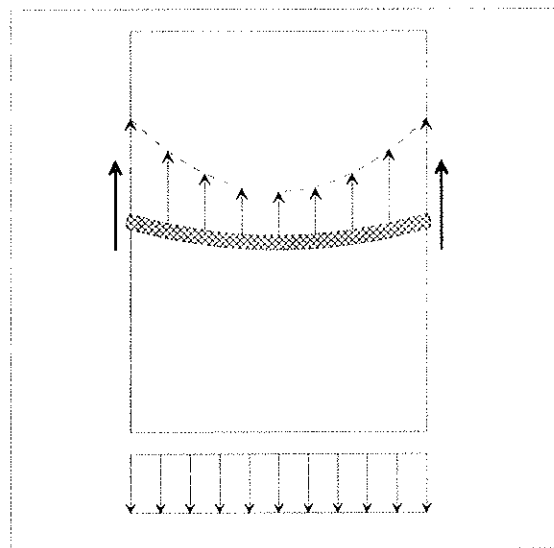


Figure 9: Embedding stress distribution along a deformed dowel.

The uneven load application of the bent dowel creates stress peaks, which may cause a premature splitting failure in the timber. As a result of these elastic deformations in the dowel, the theoretical limit slenderness ratio λ_y is in reality a range of slenderness $\lambda_{\text{optimal}} > \lambda_y$ (see Figure 10).

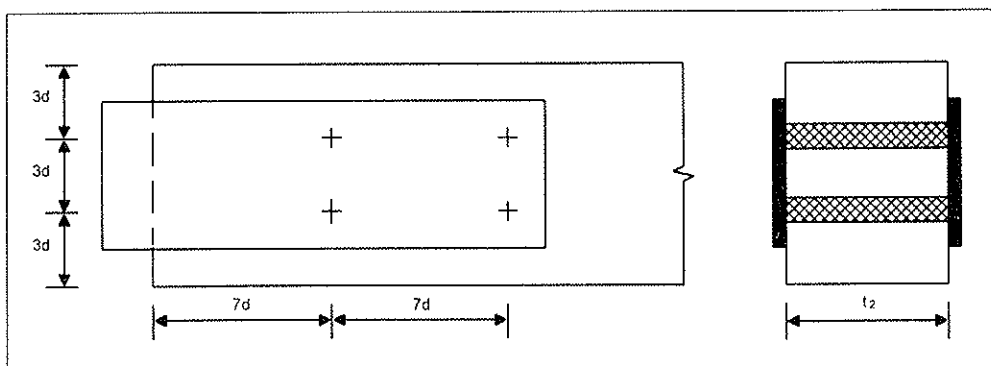


Figure 10a: Test set up.

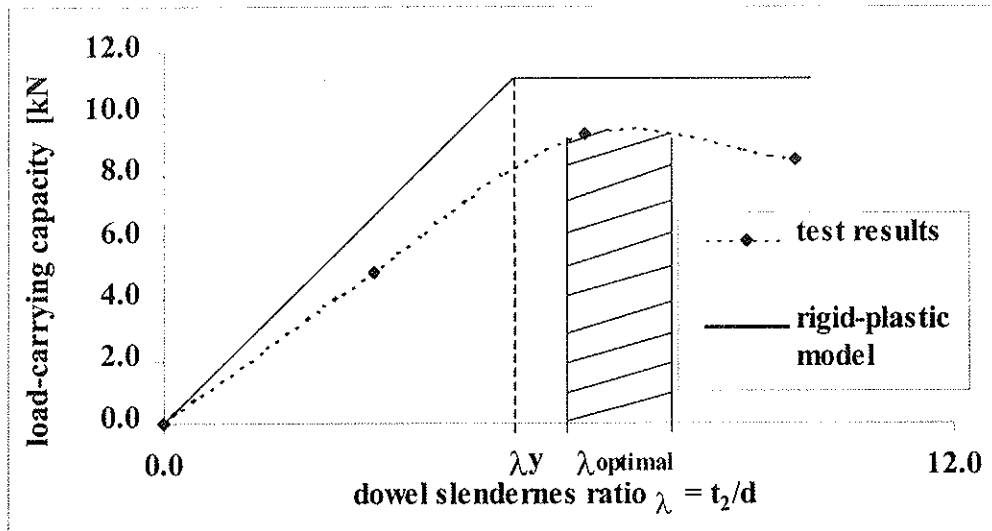


Figure 10b: Definition of limit slenderness ratio λ_y according to the rigid-plastic model and the slenderness range $\lambda_{\text{optimal}} > \lambda_y$ according to test results.

The load-deformation plot (Figure 11) of the joints with three different timber thickness shows that the connection with a timber thickness of 96 mm needs larger deformations to reach the maximum load than the joint with 64 mm timber thickness. After deformations of about 4 to 6 mm the timber fails in splitting. Therefore the ultimate resistance of doweled joints can decrease if the slenderness ratio of the dowel is much higher than the limit slenderness ratio λ_{optimal} as defined in Figure 10.

Connections with a dowel slenderness smaller than the limit slenderness ratio λ_y fail in splitting after even shorter deformations (Figure 11: timber thickness = 32 mm).

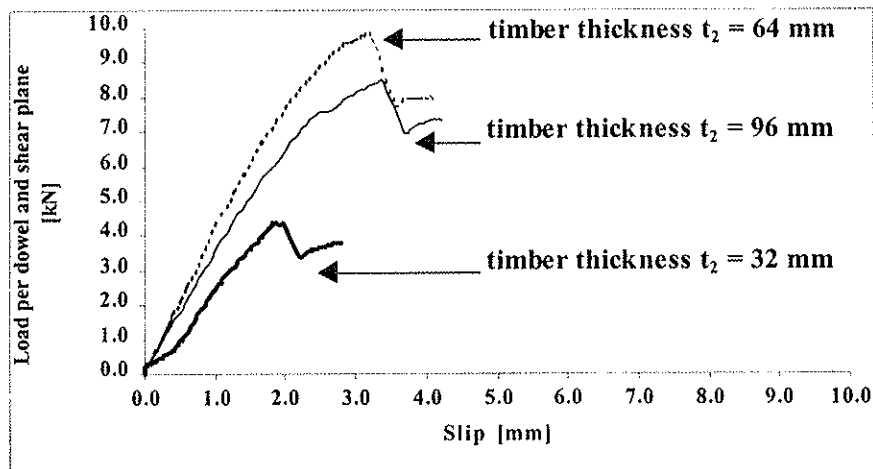


Figure 11: Load-deformation plot of doweled joints with different timber thickness (dowel diameter = 10 mm for each joint)

5 Principles for the design of connections

5.1 Principles

Timber connections have to be designed according to the following three main requirements :

- ultimate resistance
- stiffness
- ductile failure

In timber construction joints constitute the weakest points of the structure. Therefore joints should be designed of such a kind, that they develop plastic deformations before failure (i.e. a ductile failure mode).

The ductility of the connection has an important influence

- *on the load-carrying behavior of the whole structure:*
Even if the load-carrying capacity of the single joint is reduced by such a ductile design, the ultimate strength of the whole structure may increase, because a plastic redistribution of the internal forces becomes possible.
- *On the load-carrying capacity of the joint:*
The load-carrying capacity according to the European Yield Model can only be reached when no premature brittle failure in the timber occurs. In multiple fastener connections even small fabrication tolerances lead to an uneven load distribution among the fasteners. A certain balancing of these unequal forces is possible by plastic deformations in the joint.

For joints with multiple dowel type fasteners, ductile behavior is typically only possible if the failure occurs after significant plastic deformation of the steel dowels. This failure mode (Type III, according to the European Yield Model) can be reached when fasteners of effective slenderness ratio bigger than the limit slenderness ratio λ_y are used.

To reduce the risk of timber splitting the dowel strength and the spacing among the fasteners has to be adapted to the timber properties. The use of high strength dowels creates higher stresses in the timber. Therefore the spacing among the dowels has to be adapted also to the strength of the dowels. High strength dowels should generally not be used in timber of low tensile strength perpendicular to grain.

If the resistance of the fasteners is higher than the resistance of the timber in the net section, a brittle tensile failure occurs in the timber. Therefore an optimal adjustment of the number of fasteners on the tensile resistance of the timber in the net section is also necessary to avoid brittle failure.

To prevent a tensile failure the 5th percentile of timber strength should be bigger than the 95th percentile of the strength of the connection.

5.2 Verifications in joint design

The failure of a timber joint is often caused by the failure of the timber parts. Therefore two separate verifications have to be done in the design of timber joints:

- Resistance of the timber parts in the connection
- Resistance of the fasteners.

The verification of the timber should consider:

- the general stress distribution
- the local stress-peaks due to the load application by the fasteners
- the reduced cross-sectional timber area in the joint.

The load application by the fasteners creates additional shear and tension perpendicular to grain stresses in the joint. Two failures in plug shear are possible:

- shear failure of one row of dowels
- shear failure of a group of rows

To avoid the shear failure in one row the dowel strength and the spacing of the dowels has to be adapted to the shear strength of the timber.

A failure of a group of rows is possible by inadequate placing of the dowels (Figure 12). By applying a concentrated force parallel to grain only little distribution perpendicular to the grain direction is possible, due to the non-isotropic properties of timber. Therefore a reduced effective width has to be considered if the fasteners are not well distributed over the whole width of the timber.

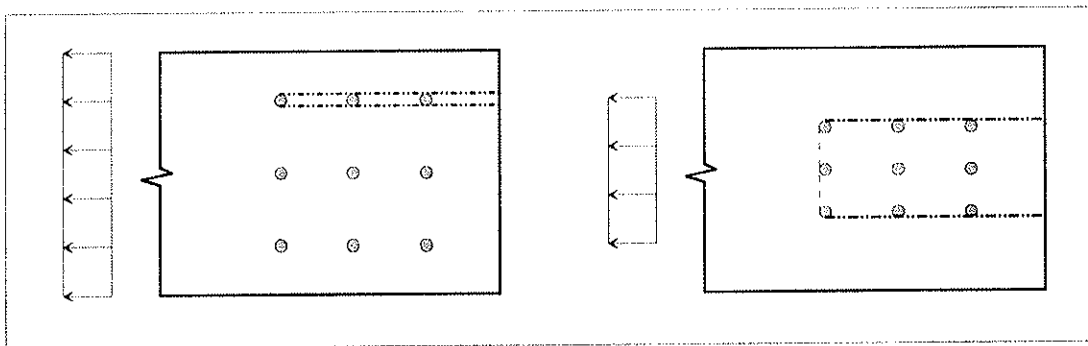


Figure 12: Shear failures of doweled connections and reduced effective width

6 References

- Gehri, E. , Fontana M. [1983]: Betrachtungen zum Tragverhalten von Passbolzen in Holz-Holz-Verbindungen, Baustatik und Stahlbau, Publ. Nr. 83-1, ETH Zürich, 1983.
- Gehri, E. [1992]: Eurocode 5, Part 1–1. Swiss proposals for new formulations and comments. 3rd November 1992.
- Gehri E. [1994]: Joints with dowel-type fasteners. A system factor or a systematic error? Paper prepared for the CIB-meeting in Sidney, 1994.
- Gehri, E. [1996]: Design of joints and frame corners using dowel-type fasteners. CIB-W18/29-7-6, Bordeaux, 1996.
- Gehri, E. [1997]: Einfluss der Lagerungsbedingungen auf das Tragverhalten einer Stahl-Holz-Bolzenverbindung, Professur für Holztechnologie, ETH Zürich, 1997.
- Johansen, K.W.[1949]: Theory of timber connections. IABSE, 98, 249-262, Zurich, 1949.
- Masse, D.I., Salinas, J.J., Turnbull, J.E. [1988]: Lateral Strength and Stiffness of Single and multiple Bolts in Glued-laminated Timber Loaded Parallel and Perpendicular to Grain. Unpublished contract, Eng. And Stat. Res. Centre, Research Branch, Agriculture Canada, Ottawa, ON, 1988.
- Mischler, A. [1998]: Bedeutung der Duktilität fuer das Tragverhalten von Stahl-Holz-Passbolzenverbindungen, Publ. Nr. 98-1 Professur für Holztechnologie, ETH Zürich, 1998
- Werner, H.[1993]: Tragfähigkeit von Holz-Verbindungen mit stiftförmigen Verbindungsmitteln unter Berücksichtigung streuender Einflussgrössen, 1993. Berichte der Versuchsanstalt für Stahl, Holz und Steine der Uni Karlsruhe, 4. Folge – Heft 28.
- Wilkinson, T.L. [1986]: Load distribution among bolts parallel to load. Journal of Structural Engineering, Vol. 112, No. 4, April 1986.

CIB-W18/31-7-3

INTERNATIONAL COUNCIL FOR BUILDING RESEARCH STUDIES AND DOCUMENTATION
WORKING COMMISSION W18 - TIMBER STRUCTURES

FLEXURAL BEHAVIOUR OF GLULAM BEAMS EDGE-JOINTED BY LAGSCREWS
WITH STEEL SPLICE PLATES

by

K Komatsu

Wood Research Institute
Kyoto University

JAPAN

MEETING THIRTY-ONE

SAVONLINNA

FINLAND

AUGUST 1998

Flexural Behavior of Glulam Beams Edge-Jointed by Lagscrews with Steel Splice Plates

Kohei Komatsu

Laboratory of Structural Function
Wood Research Institute, Kyoto University
Gokasyou, Uji-City, Kyoto-Prefecture, 611-0011, JAPAN

1 Introduction

Among various jointing technique for large cross-sectional glulam frame structures, lagscrew joint with steel splice plates shown in Fig.1 might be one of the most popular methods in Japan which is to be used on construction site for transmitting bending moment, axial force and shear force simultaneously.

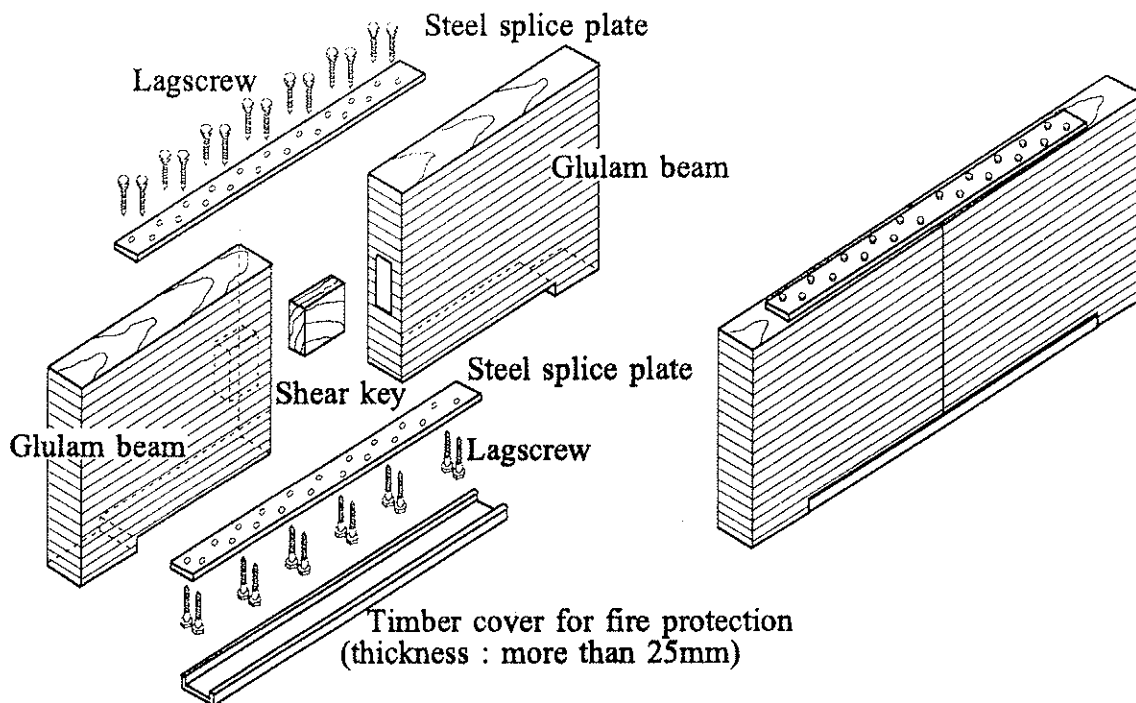


Fig.1 Lagscrew joint with steel splice plates

In practical design situation, transmission of stresses through the end-grain surfaces of glulam beams is usually ignored, and strength of this type of joint has been evaluated simply by assuming a coupling moment $M = gF$, where F is a pair of axial force acting in both steel splice plates at tensile side and compression side, and "g" is a distance between two splice plates. Moreover, effect of additional deflection due to slip of the joints has been ignored in most cases.

Contrary to this tradition, however, in this report a more precise calculation method for both stiffness and strength evaluation on this type of edge-joint will be proposed by taking the effect of following two conditions into consideration;

1. Compression stress transmission through the end-grain surfaces of glulam beams.
2. Existence of constant compression force

2 Theory

2.1 Determination of Neutral Axis

Fig.2
Model lagscrew joint for the analysis.

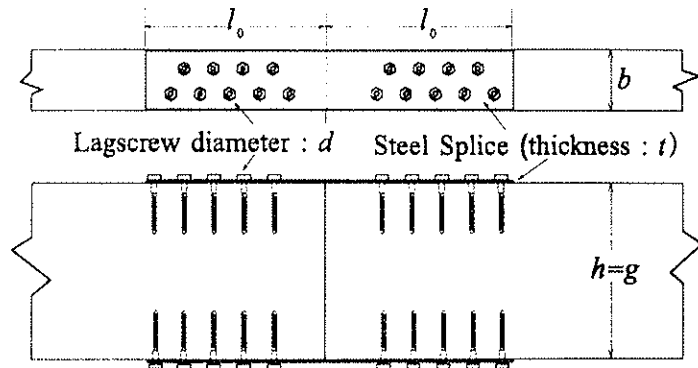


Fig.2 shows a model of lagscrew joint for the analysis. I assume that in compression side, stress can be transmitted through the end-grain surfaces of glulam beam, while in tensile side, it can be transmitted through steel splice plate as shown in Fig.3-b).

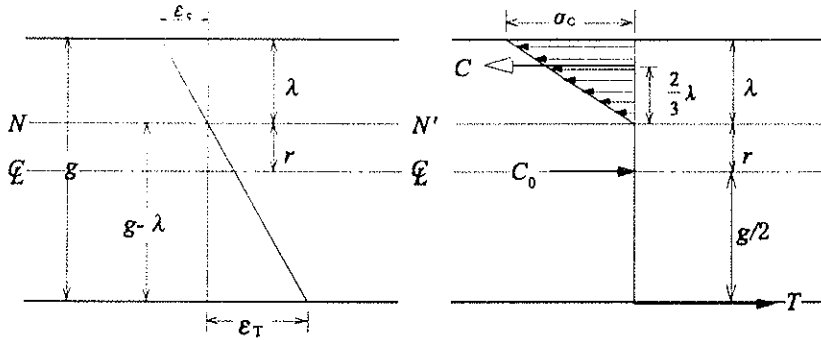


Fig.3
Assumption of stresses and strain distribution in the model lagscrew joint.

a) Strain distribution

b) Stress distribution

On the basis of the assumption that the strain distributes linearly as shown in Fig.3-a), the tensile strain ϵ_T is expressed by means of compression strain ϵ_c as;

$$\epsilon_T = \epsilon_c \left(\frac{g-\lambda}{\lambda} \right) \quad \dots 1)$$

where,

λ : distance from outer compression surface to the neutral axis.

g : effective depth of beam.

The corresponding stresses components are;

$$\sigma_c = E_w \epsilon_c \quad \dots 2) \quad \sigma_T = E_s \epsilon_T = E_s \epsilon_c \left(\frac{g-\lambda}{\lambda} \right) \quad \dots 3)$$

where,

E_w : Modulus of elasticity of glulam beam.

E_s : "Apparent" modulus of elasticity of steel plate.

The resultant compression force C is;

$$C = b \int_0^\lambda \sigma_c \frac{y}{\lambda} dy = b \int_0^\lambda \frac{E_w \epsilon_c}{\lambda} y dy = \frac{b E_w \epsilon_c}{\lambda} \int_0^\lambda y dy = \frac{b E_w \epsilon_c \lambda}{2} \quad \dots 4)$$

where,

b : width of glulam beam

While, the resultant tensile force T acting in a steel splice plate is;

$$T = \sigma_T A_s = E_s \varepsilon_c \left(\frac{g-\lambda}{\lambda} \right) A_s \quad \dots 5)$$

where,

A_s : cross sectional area of the steel splice plate.

An equilibrium equation among the tensile force T , the compression force C and the constant compression force C_0 is;

$$C_0 = C - T \quad \dots 6)$$

Substituting equations 4) and 5) into 6), compression strain ε_c is expressed as;

$$\varepsilon_c = \frac{C_0}{\frac{E_w b \lambda}{2} - E_s A_s \left(\frac{g-\lambda}{\lambda} \right)} \quad \dots 7)$$

Another equilibrium condition on the moment around geometrical center is;

$$M = C \left(\frac{2\lambda}{3} + r \right) + T \frac{g}{2} \quad \dots 8)$$

where,

M : moment due to external force.

r : distance from geometrical center to the neutral axis (refer to Fig.3).

Substituting equations 4) and 5) into 8), compression strain ε_c is also expressed as;

$$\varepsilon_c = \frac{M}{\left(\frac{E_w b \lambda}{2} \right) \left(\frac{g}{2} - \frac{\lambda}{3} \right) + \frac{E_s A_s g (g-\lambda)}{2\lambda}} \quad \dots 9)$$

Putting equations 7) and 9) as equivalent, an important equation 10) can be obtained as;

$$C_0 \left\{ E_w b \lambda^2 \left(\frac{g}{2} - \frac{\lambda}{3} \right) + E_s A_s g (g-\lambda) \right\} = M (E_w b \lambda^2 - 2 E_s A_s (g-\lambda)) \quad \dots 10)$$

If there is no constant compression force C_0 , left-hand side of the equation 10) becomes zero, thus location of the neutral axis λ can be derived from right-hand side of the equation 10) independent from moment M as ;

$$\lambda^2 + 2 \frac{E_s A_s}{E_w b} \lambda - 2 \frac{E_s A_s}{E_w b} g = 0 \quad \dots 11)$$

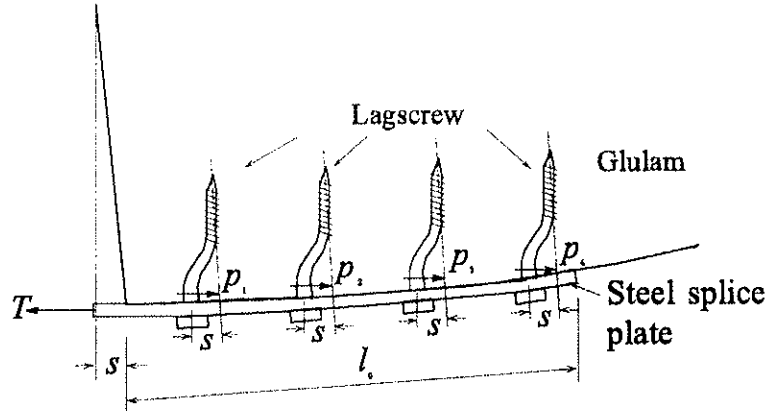
On the other hand, if $C_0 > 0$, then location of the neutral axis λ must be determined by solving cubic equation 12) as the function of both C_0 and moment M ;

$$\lambda^3 - 3\left(\frac{g}{2} - \frac{M}{C_0}\right)\lambda^2 + 6\frac{E_s A_s}{E_w b}\left(\frac{g}{2} + \frac{M}{C_0}\right)\lambda - 6\frac{E_s A_s}{E_w b}\left(\frac{g}{2} + \frac{M}{C_0}\right)g = 0 \quad \dots 12)$$

2.2 Consideration of Slip Displacement of Lagscrews

Up to here, analysis has been executed by considering tensile strain ϵ_T as "apparent strain in the steel splice plate". In fact, however, the actual tensile elongation at the part of end-grain is mostly caused by slip displacement S of the lagscrews as illustrated in Fig.4. Thus, the apparent tensile strain ϵ_T should be replaced by that which involves actual displacement due to slip S of the lagscrews.

Fig.4
Slip displacement S of lagscrew due to tensile force T



In this report, tensile strain ϵ_T was assumed as a "mean strain" caused by the slip displacement S of lagscrew within an "effective length l_0 " as shown in Fig.4. Hence, tensile stress σ_T , tensile strain ϵ_T and relationship between tensile force T and slip displacement S were defined as;

$$\sigma_T = \frac{T}{A_s}, \quad \epsilon_T \doteq \frac{S}{l_0}, \quad T = \sum p_i = \sum K_{s,i} S \quad \dots 13)$$

where,

l_0 : effective length of steel splice plate (refer to Fig.4)

p_i : force acting on each lagscrew (refer to Fig.4)

$K_{s,i}$: slip modulus of each lagscrew

S : slip displacement of lagscrew (assumed as equal for all lagscrew based on "rigid floor assumption". Refer to Fig.4)

Therefore, equivalent tensile rigidity of steel splice plate can be expressed as;

$$E_s \doteq \left(\frac{\sum K_{s,i} l_0}{A_s} \right) \text{ or } E_s A_s \doteq l_0 \sum K_{s,i} \quad \dots 14)$$

Consequently, location of the neutral axis λ might be determined by solving cubic equation 15) using appropriate numerical calculation technique.

$$\lambda^3 - 3\left(\frac{g}{2} - \frac{M}{C_0}\right)\lambda^2 + 6\beta\left(\frac{g}{2} + \frac{M}{C_0}\right)\lambda - 6\beta\left(\frac{g}{2} + \frac{M}{C_0}\right)g = 0 \quad \dots 15)$$

where,

$$\beta = \frac{I_0 \sum K_{s,i}}{bE_w} \quad \dots 16)$$

2.3 Rotational Rigidity of the Joint

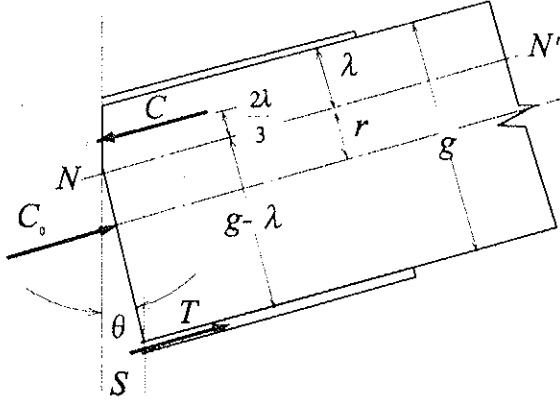


Fig.5

Rotation θ or opening S at the part of mid-span along the end-grain surface

By referring the schematic model for the end-grain opening shown in Fig.5, the half rotation angle θ at the part of joint can be approximately defined as;

$$\theta = \frac{S}{g-\lambda} \quad \dots 17)$$

Considering again an equilibrium condition among C , T , and C_0 as well as that of moment M around the geometrical center, following relationship between moment M due to external force and the half rotation angle θ is obtained;

$$M = \left\{ \sum K_{s,i} (g-\lambda) \left(g - \frac{\lambda}{3} \right) \frac{(2\lambda^3 - 3g\lambda^2 + 6\beta g\lambda - 6\beta g^2)}{4\beta(6g\lambda - 6g^2 - \lambda^2)} \right\} \theta \quad \dots 18)$$

Thus, the rotational rigidity R_J of half side of the joint in GLT beam is defined as;

$$R_J = \left\{ \sum K_{s,i} (g-\lambda) \left(g - \frac{\lambda}{3} \right) \frac{(2\lambda^3 - 3g\lambda^2 + 6\beta g\lambda - 6\beta g^2)}{4\beta(6g\lambda - 6g^2 - \lambda^2)} \right\} \quad \dots 19)$$

From equation 18) or 19), it can be seen that moment-rotation relationship is also dependent on moment M and constant compression force C_0 , thus the flexural behaviour of lagscrew jointed GLT-beam is expected to be non-linear even if a linear slip modulus K_s for lagscrew joints is used.

2.4 Mid-Span Deflection of Edge-Jointed GLT Beam

According to the virtual work theory, mid-span deflection δ of an edge-jointed GLT beam subjected to a four pints bending load as shown in Fig. 8 can be estimated as;

$$\delta = \frac{P(3I_s L^2 - 4I_s^3)}{48EI} + \frac{\kappa P I_s}{2GA} + \frac{P I_s L}{4R_J} \quad \dots 20)$$

where,

l : shear span defined in Fig.6. L : bending span length of the beam.
 EI : flexural rigidity of GLT beam. GA : shear rigidity of GLT beam.
 κ : coefficient for shear deformation (=1.2 for rectangular cross section).
 R : half rotational rigidity of lagscrew joint defined in eq.19).

2.5 Calculation Method

2.5.1 Initial compression force C_0 and tensile force T in a steel splice plate

When a constant compression force C_0 is applied, a part of axial force flows into two steel splice plates. So, in the tensile splice plate, until tensile force T becomes larger than this initial compression force C_{0j} , no slip between GLT member and steel splice plate nor end-grain opening occur. Thus, before starting calculation, it is important to evaluate this initial compression force C_{0j} in tensile side steel plate.

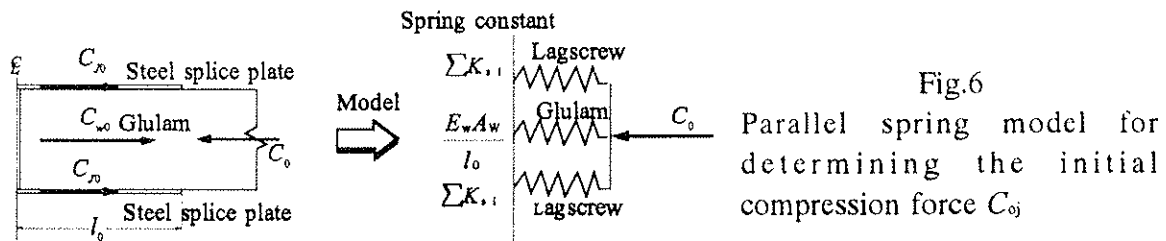


Fig.6

Parallel spring model for determining the initial compression force C_{0j}

By assuming three parallel springs model shown in Fig.6, the initial compression force C_{0j} in steel splice plate is obtained as;

$$C_{j0} = \frac{\sum K_{s,i}}{2\sum K_{s,i} + \frac{E_w A_w}{l_0}} C_0 \quad \dots 21)$$

While, tensile force T acting in a tensile splice plate is;

$$T = \frac{M - C_0 \left(\frac{g}{2} - \frac{\lambda}{3} \right)}{\left(g - \frac{\lambda}{3} \right)} \quad \dots 22)$$

In an actual numerical calculation program, only when T is larger than C_{0j} , additional deflection due to slip displacement of lagscrews should be accounted and should be added to. Fig.7 shows a flow-chart of an actual numerical calculation method.

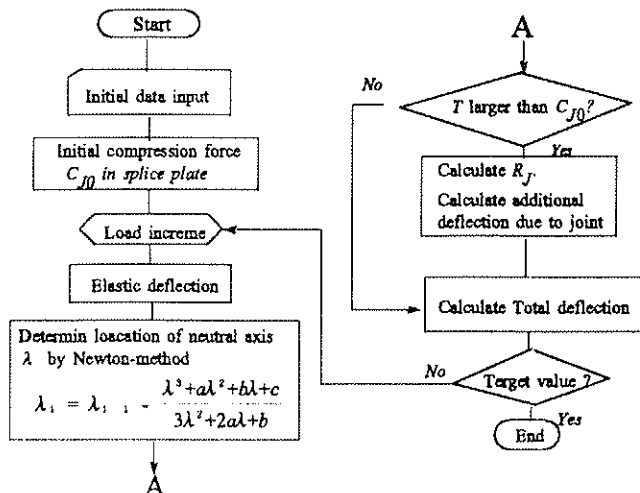


Fig.7

Flow-chart of an actual numerical calculation method

3 Experiments

3.1 Test Specimens

Four joint specimens were prepared using Douglas-fir (*Pseudotsuga menziesii*) GLT beams in accordance with axial compression level. Table 1 shows specifications for test specimens.

Code name of specimen	Fastener	Steel splice plate	Axial constant force C_0
LAGC00	8 lagscrews whose diameter $d=16\text{mm}$ and length $l=160\text{mm}$ were used per splice plate	SS400 steel plate of thickness 11mm	0 tonf
LAGC33			6.5 tonf
LAGC66			13.3 tonf
LAGC100			20 tonf
Properties of Douglas fir glulam beams used			
Production SD.	JAS E105-f300 Mean MOE assumed = 125000kgf/cm^2		
Cross section	$b = 150\text{mm}$	$h = 464\text{mm}$	$L = 3000\text{mm}$
Timber density TD	$TD\text{-mean} = 527\text{kg/m}^3$	S.D. = 9kg/m^3	$n=11$
Moisture content MC	$MC\text{-mean} = 12\%$	S.D. = 12%	$n=11$

Table 1 Specifications for test specimens.

3.2 Bending Test Method

Fig.8 shows a four points bending test set-up for joint specimens.

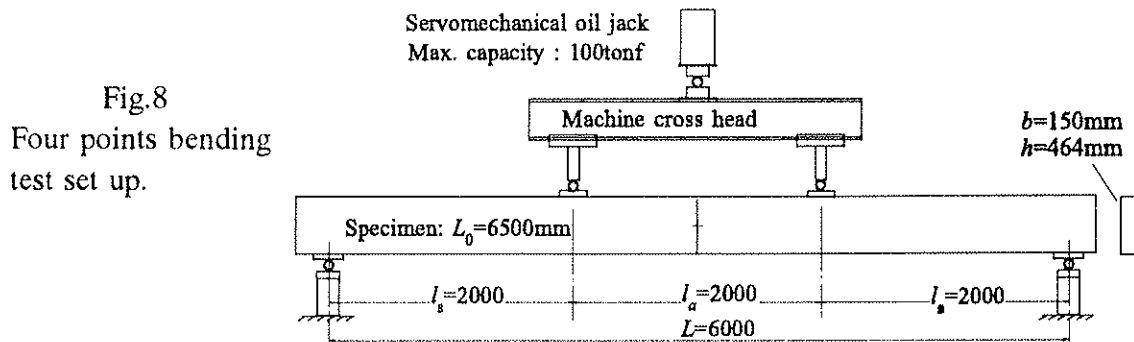


Fig.8
Four points bending test set up.

Fig.9 shows a details of lagscrew joint.

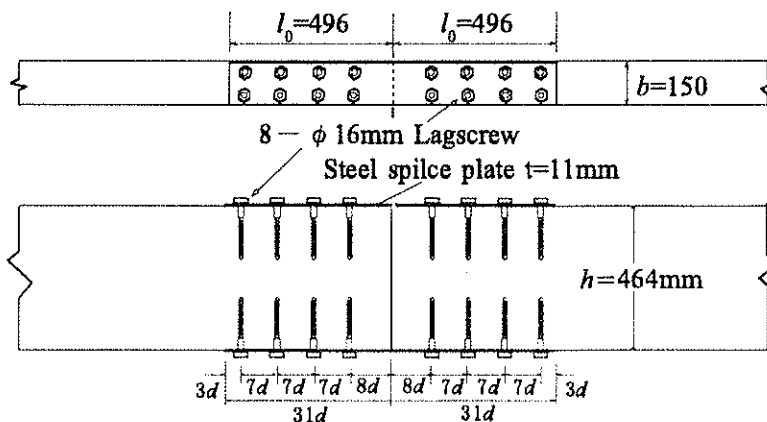
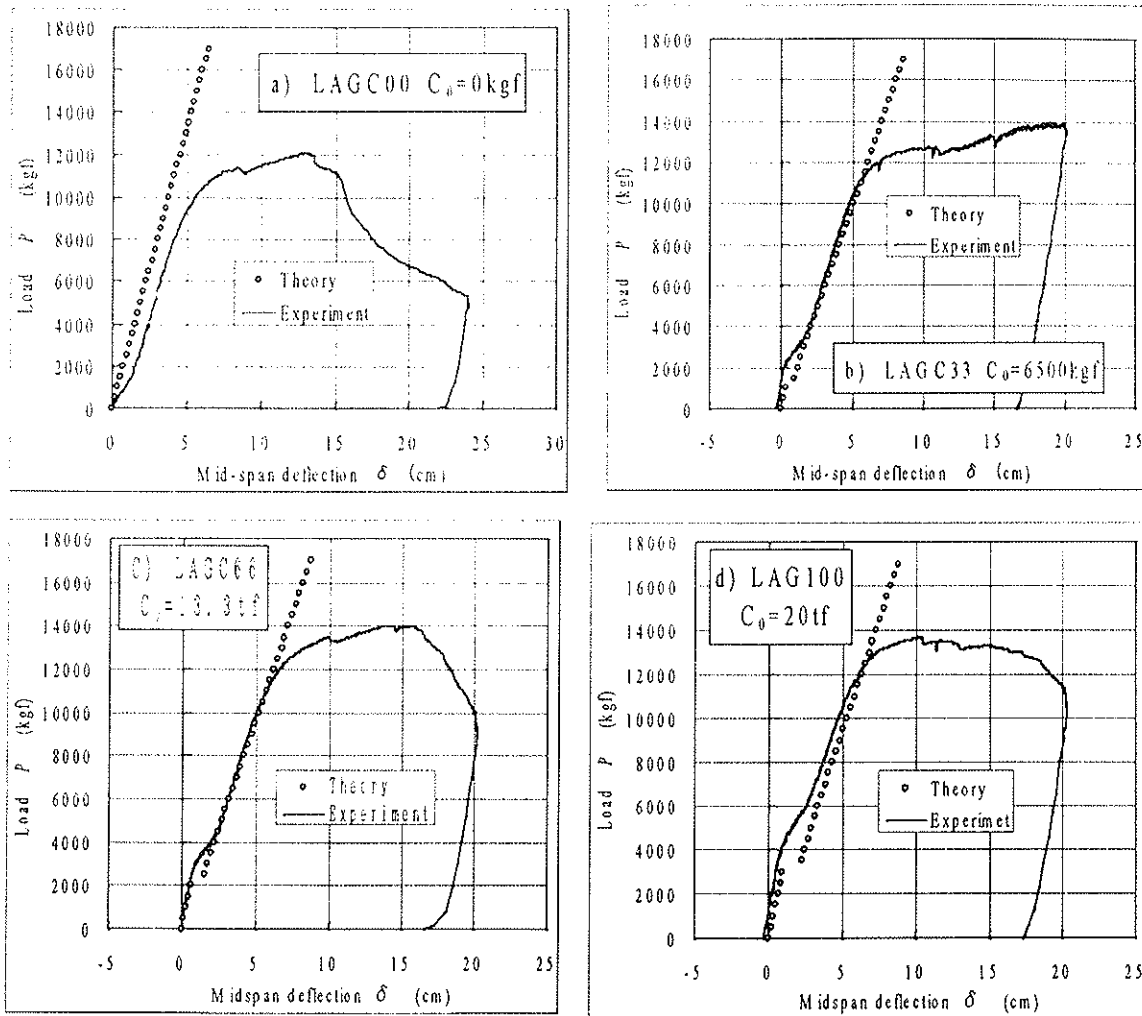


Fig.9
Details of lagscrew joint.

4 Results and Discussion

Figs.10-a), b), c) and d) shows comparisons between observed load (P) - midspan deflection(δ). In these calculations, slip modulus of $K_s=62000\text{kgf/cm}$, which was approximately determined by a non-linear FEM analysis using a drift-pin model with

same size as lagscrew used in the experiments, was used constantly up to the end of calculation.



Figs.10 -a),b),c),d) comparisons between load (P) - deflection(δ) relationship observed and calculated ones.

Theoretical model proposed in this report could predict well about the "special behaviour at the initial loading stage" where the effect of initial compression force on the stiffness of jointed beam was dominant. Therefore, good agreements between theoretical calculation and experimental observations were obtained especially for the specimens having a constant axial compression forces.

For further research needs, proposal of practical design equations based on this kind of theoretical study will be required.

Acknowledgements

This research is a part of a big research project directed by HOWTEC (Japan Housing and Wood Technology Center).

The author would like to thank to the financial support from HOWTEC as well as to Mr. Kotsuka from Takenaka Co. Ltd. for his contribution to the theoretical support and also to Mr. Suzuki from Saito Timber Industry for his technical advice on production of test specimens.

**INTERNATIONAL COUNCIL FOR BUILDING RESEARCH STUDIES AND DOCUMENTATION
WORKING COMMISSION W18 - TIMBER STRUCTURES**

DESIGN ON TIMBER CAPACITY IN NAILED STEEL-TO-TIMBER JOINTS

by

J Kangas
VTT Building Technology

J Vesa
Helsinki University of Technology

FINLAND

MEETING THIRTY-ONE

SAVONLINNA

FINLAND

AUGUST 1998

Design on Timber Capacity in nailed Steel-to-Timber Joints

by
Jorma Kangas
VTT Building Technology,
Janne Vesa
Helsinki University of Technology (HUT)
Finland

1 Introduction

In design codes, nail spacings are mainly used to avoid splitting during nailing. In the case of predrilled holes and steel-to-timber connections increased nail density is allowed. This may lead to the exceeding of the timber capacity in the joint area, and to the unfavourable brittle block tearing failure with reduced capacity of the joint.

Block tearing failure mode has been found in the testing of nailed steel-to-timber joints with small nail spacings. The capacity of the nailed connection with given spacings depends on the nail capacity up to a certain joint length, after which the block tearing failure may occur, i.e., a block of timber will be cut out from the joint.

The failure mode was first found, when MNC-connector was tested with KertoS-LVL. More test series with different timber materials, annular ringed shank nails, spacings and end distances were carried out to verify the model generally. Additional test series were conducted recently where the timber capacity was near the nail capacity of the connection.

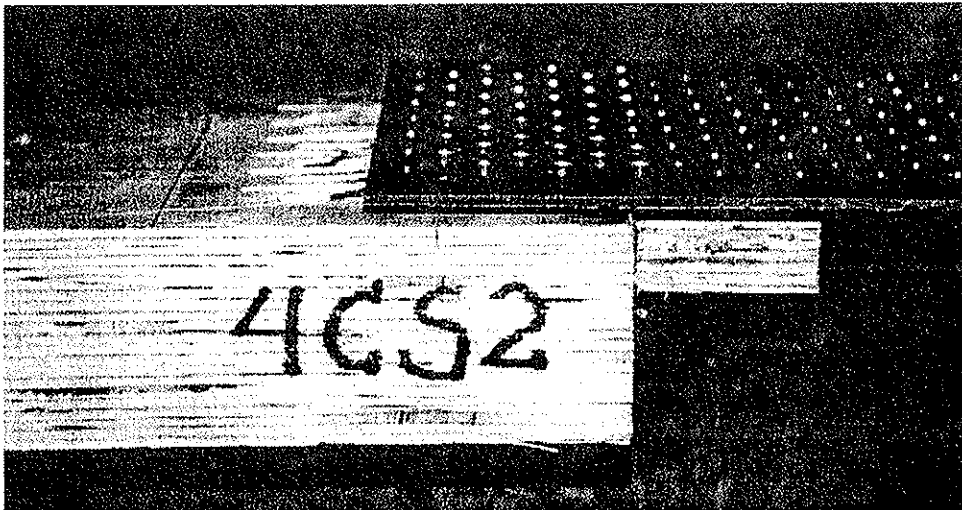


Figure 1 - Block tearing failure in steel-to-Kerto-S-LVL joint with dense nailing.

This paper presents a simple method to design the timber capacity in nailed thick steel-to-timber connections. The capacity is limited by the sum of the tensile and shear capacities of timber in the effective timber area of the connection. It will also be proved that the proposed model explains the test results of glulam rivet connections much better than does the model of three different failure modes, which has been presented earlier.

2 Tensile Test Series

2.1 Joints with MNC-Connectors

Multiple Nail Connectors (MNC) are originally created for long-span trusses made of Kerto-LVL. The connector consists of a 10 mm thick steel plate with 50 mm long flat cone nails. The nails are rectangular in shape ($d_1 \times d_2 = 3 \times 4 \text{ mm}^2$) and welded perpendicularly on both sides of the plate. Each nail has a 4 mm long cone in the base to increase its effective length, and the longer sides of nails are profiled to increase the anchorage strength.

Nail spacings are 40 mm ($10d_2$) parallel to the grain (a_1) and 12 mm ($4d_1$) perpendicular to the grain (a_2) in a staggered arrangement. The mean nail area ($a_1 \cdot a_2$) is 9% larger than the minimum value given in codes for nailed thick steel-to-timber connections (single reduction of spacing).

MNC-connector was tested with KertoS-LVL and glulam for German approval. Since 1984, during 12 years, numerous test series have been carried out with MNC-connectors in Helsinki University of Technology and in the University of Karlsruhe. Length, width and end distances have varied widely. The number of nails in the grain direction (n_1) has varied between 1,5...21 and the number of nails perpendicular to the grain (n_2) in the range of 5...30. The end distance (a_3) used in most cases has been 60 mm. End distances of 107 mm and 200 mm have also been used. These test results have been published and used to model the block tearing failure mode of steel-to-timber joints in tension [1].

2.2 Joints with dense Nailing

In the test series conducted at VTT in the spring of 1997, the steel plates used were made of plain structural steel (Fe 52 D) and of two thicknesses: 4 mm and 6 mm depending on the nails chosen. The nails were BMF 4,0×40 mm and BMF 6,0×60 mm annular ringed shank nails with penetration lengths of 36 mm and 54 mm, respectively. The diameter and depth of predrilled holes in timber were 3,5 mm and 30 mm for 4,0×40 nails, and 5,0 mm and 50 mm for 6,0×60 nails. The diameter of predrilled holes in steel plates was 4,3 mm and 6,5 mm, respectively.

Altogether 21 test series of three parallel test pieces were conducted, 14 of which were done with 4 mm nails and seven with 6 mm nails. Kerto-S-LVL (figure 1) and Kerto-Q-LVL were both used in six series and sawn timber (spruce) in nine series (figure 2). Test series were labelled as series A, B, C and D according to the joint type. Joint lengths in Series A and C were short with three nails in line and correspondingly series B and D were long (6 - 7 nails).

Nail spacings were chosen according to Eurocode 5, resulting in staggered nail rows. In the test series A and D, the nail spacings of a timber-to-timber joint were reduced by a factor of 0.7 corresponding to either predrilling of timber or steel-to-timber connection, and referred to here as a **single reduction**. In the test series B and C, a **double reduction** of $0,7 \times 0,7$ was used corresponding to both predrilling and a steel-to-timber connection. Minimum nail spacing a_1 parallel to the grain was $5d$ (20 mm and 30 mm) and correspondingly a_2 perpendicular to the grain 9 mm and 13 mm.



Figure 2 - Block tearing failure in steel-to-sawn timber joint with dense nailing.

Since the steel plates were perforated according to one pattern only (minimum nail density), appropriate nail arrangements were achieved by leaving some of the nail rows and lines unnailed. The average nail spacings corresponded, however, to the nail density desired. These test results were reported in CIB-meeting in Vancouver [2].

2.3 Joints with near balanced Capacities

In the test series conducted at VTT in the beginning of 1998, the perforated steel plates and the nails used were the same as in the test series described in chapter 2.2 above. Nail spacings and end distances were chosen to achieve near balanced nail- and timber capacities in the joint area. Kerto-S-LVL and sawn timber (spruce) were both used. Altogether 37 nailed test pieces were loaded, 17 of which were done with 4 mm nails and 20 with 6 mm nails.

Test series were divided in two groups. Relatively small test pieces were used to achieve reasonable load levels also for the duration of load testing (DOL). Their maximum load was about 50 kN. The maximum load in the other group was about 100 kN. Detailed results of these test series will be published this year [3].

2.4 Joints with Glulam Rivets

Glulam Rivet is a flat nail ($d_1 \times d_2 = 3 \times 6 \text{ mm}^2$) with low-gradient cone head in order to fasten tightly into the holes in the steel plates. Information about the test pieces is from Foschi [4]. Steel plates are fastened by glulam rivets to the sides of glulam beams made of Douglas-fir, 24f grade. The given symbols with their numeric values in the test pieces were:

- penetration h : 3 in
- number of nails perpendicular to the grain NR: 8...12
- number of nails parallel to the grain NC: 6...12
- spacing of nails parallel to the grain e_x : 1...2 in
- spacing of nails perpendicular to the grain e_y : 0.5...1 in
- end distance d_x : 2...20,5 in

3 Load-Carrying Capacity of Nailed Steel-to-Timber Joints

3.1 Basic Parameters

3.1.1 Embedding Strength

The embedding strength ($f_{h,k}$) can be calculated by equations (1) and (2) based on Johansen's theory as given in Eurocode 5 (6.3.1.2a 6.3.1.2b). Parameters affecting this material property are the nail diameter (d) and timber density (ρ_k in kg/m^3). Predrilled holes were made for the round nails (4 mm and 6 mm), while the flat nails ($3 \times 4 \text{ mm}^2$ and $3 \times 6 \text{ mm}^2$) were without predrilling.

$$\text{without predrilled holes} \quad f_{h,k} = 0,082 \rho_k d^{-0,3} \text{ N/mm}^2. \quad (1)$$

$$\text{with predrilled holes} \quad f_{h,k} = 0,082(1-0,01d) \rho_k \text{ N/mm}^2. \quad (2)$$

3.1.2 Yield Moment

The yield moment ($M_{y,k}$) of rectangular nails with a minimum tensile strength 600 N/mm^2 of the wire can be calculated by equation (3) presented in Eurocode 5 (6.3.1.2d). It has been applied here for flat ($d_1 \times d_2$) nails by formula (4). The yield moment of annular ringed shank nails has been calculated by the formula (5), given by the manufacturer of BMF nails.

$$\text{for square nails} \quad M_{y,k} = 270 d^{2,6} \text{ Nmm}. \quad (3)$$

$$\text{for flat square nails} \quad M_{y,k} = 270 \cdot d_1 \cdot d_2^{1,6} \text{ Nmm}. \quad (4)$$

$$\text{for threaded nails} \quad M_{y,k} \geq 6.7 \cdot (20-d) \cdot d^3 \text{ Nmm}. \quad (5)$$

3.1.2 Effective Thickness

Effective thickness of timber member in the nailed joint area t_{ef} is an important parameter in calculating the timber capacity. It can be calculated by formula (6). Its function is as follows. In a nailed thick steel-to-timber joint the nails are rigidly in steel. A typical yield mechanism of such a joint is one with two plastic hinges - one at the interface of the steel and timber and the other at a distance t_{ef} from this interface. A free-body diagram of a nail in single shear is shown in Figure 3.

$$t_{ef} = 2 \{M_{y,k} / (f_{h,k} d)\}^{1/2} \quad (6)$$

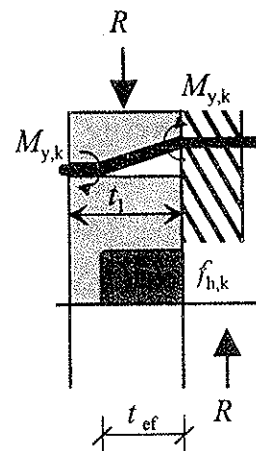


Figure 3 - A free-body diagram of a nail with two plastic hinges.

According to Johansen's theory of dowel-type fasteners the embedding stresses are constant from the surface as far as the second plastic hinge. Its distance t_{ef} , effective thickness in the block tearing model, can be solved by the equilibrium condition of the forces in figure 3.

3.2 Modelling of the Block Tearing

Shear force from the steel plate transfers to the timber member by embedding capacity of the fasteners. It is logical to think that the force in timber is transferred by the tensile stresses in the beginning of the joint and by the shear stresses along the joint surface. Due to the plasticity the stresses in the effective areas can be assumed to be constant and in the failure to be equal to the material capacities.

In the block tearing failure of a steel-to-timber joint, a block of timber is torn off from the timber member. The width of this block corresponds to the width of the nailed joint, and the depth in the area of highest tensile stresses to the distance of the second plastic hinge from the timber surface. The total capacity is limited by the sum of the nail capacities (R_N) and by the sum of the tensile and shear capacities of the timber member with the reduced dimensions, as presented in formula (7):

$$R = \min \left\{ \begin{array}{l} n_b n_l R_N \\ b_{ef} t_{ef} f_{t,0} + b_{ef} l_j f_{v,90} \end{array} \right. \quad (7)$$

where n	is the total number of nails
n_b	is the number of nails perpendicular to the grain
n_l	is the number of nails parallel to the grain
R_N	is the nail capacity
b_{ef}	is the effective width of the nailed area $\{=b_N+(4 - n_b) d\}$
b_N	is the width of the nailed area
t_{ef}	is the effective thickness of the nailed area
l_j	is the length of the joint $(=l_N+a_3)$
l_N	is the length of the nailed area
a_3	is the end distance of the timber member
$f_{t,0}$	is the tensile strength of timber in the grain direction
$f_{v,90}$	is the flatwise shear strength of Kerto-S-LVL, or the rolling shear strength of Kerto-Q-LVL, or the shear strength of sawn timber.

3.3 Effective Width

Effective width of the nailed area (b_{ef}) is used in formula (7) to reduce the stressed area both in tension and in shear. Formula (7) was first developed to explain the failure mechanism in the joints of MNC-connectors and to fit the test results to the model. It has already been presented by Kangas 1996 [1]. Width b of the joint was taken as $b = n_b \cdot a_2$, where a_2 was $4d$ or $b = b_N + 4d$. The predrilling of holes and the penetrating of threaded nails cuts the grains of timber. Therefore the width of the joint shall be reduced by the sum of the thickness of the nails to achieve the effective width b_{ef} of the nailed area, formula (8). Also the stress distribution in shear will not be quite even, so b_{ef} is applied to the area in shear too.

$$b_{ef} = b_N + (4 - n_b) \cdot d \quad (8)$$

Formula (8) is valid only for such materials that are homogeneous in the grain direction, e.g. sawn timber and Kerto-S-LVL. For Kerto-Q-LVL and plywood, the effect of cross veneers can be taken into account by increasing the effective width (b_{ef}) in shear by a factor of $2b_{ad}$, where b_{ad} is the additional width of a timber block, due to the edgewise shear capacity of cross veneers. Thus, the increased width (b_{ef}') of the area under shear stresses of Kerto-Q-LVL members equals the following:

$$b_{ef}' = b_{ef} + 2b_{ad}, \quad (9)$$

where $b_{ad} \leq a_4 - 2d$

a_4 is the edge distance of the outermost nail lines.

4 Test Results

4.1 Properties of Timber Material and Nails

When calculating the joint capacities by the proposed model the characteristic material properties of table 1 have been used. Values of characteristic density (ρ_k) are used to calculate the embedding strength ($f_{h,k}$) of timber, which in turn is used with the yield moment ($M_{y,k}$) of the nails to calculate the effective thickness (t_{ef}) of timber members. Characteristic tensile ($f_{t,k}$) and shear ($f_{v,k}$) strength values of timber are also given in table 1. Characteristic tensile strength in bending ($f_{m,k}$) is used with materials of large variation in tensile strength properties (due to knots in timber).

Table 1 - The properties of timber material and nails, which are needed in calculating timber capacity in the joint: density (ρ_k), tensile ($f_{t(m),k}$), shear ($f_{v,k}$) and embedding strength ($f_{h,k}$), yield moment ($M_{y,k}$) and effective thickness (t_{ef}).

Material	Nail mm	ρ_k kg/m ³	$f_{t(m),k}$ N/mm ²	$f_{v,k}$ N/mm ²	$f_{h,k}$ N/mm ²	$M_{y,k}$ Nmm	t_{ef} mm
Kerto-S-LVL	3x4	480	38	3	28,3	7400	18,7
	4	480	38	3	37,8	6900	13,5
	6	480	38	3	37,0	20300	19,1
Kerto-Q-LVL	4	480	27	1,5	37,8	6900	13,5
Kerto-Q-LVL	6	480	27	1,5	37,0	20300	19,1
Timber	3x4	380	30	3	22,4	7400	21,0
	4	380	30	3	29,9	6900	15,1
	6	380	30	3	29,3	20300	21,5
	3x6	380	30	3	22,4	14200	29,1

4.2 MNC Tests

A reduction method, similar to the method presented in EC5 for bolted joints, has been given in German approval to calculate the capacities of more than six MNC nails in line with the load direction. The load-carrying capacity of the additional nails has been reduced by 60 % resulting in the effective number (n_{ef}) of nails. This method corresponds well to the test results obtained with Kerto-S-LVL. However, such a reduction can be used only for the above-mentioned nail spacings and the end distance of 60 mm.

The mean load-carrying nail capacity obtained for Kerto-LVL in tests was 2.8 kN and 2.5 kN for glulam. Figure 4 presents the mean values of test series with Kerto-S-LVL (five parallel test pieces) and the curves calculated by formula (7) using the values from table 1.

Since the spacing of MNC-connector is constant, it was natural also to consider the capacity of the joint as a function of number of nails in line in load direction. Due to that the curves had to be calculated and drawn for each three end distances a_3 separately in figure 4.

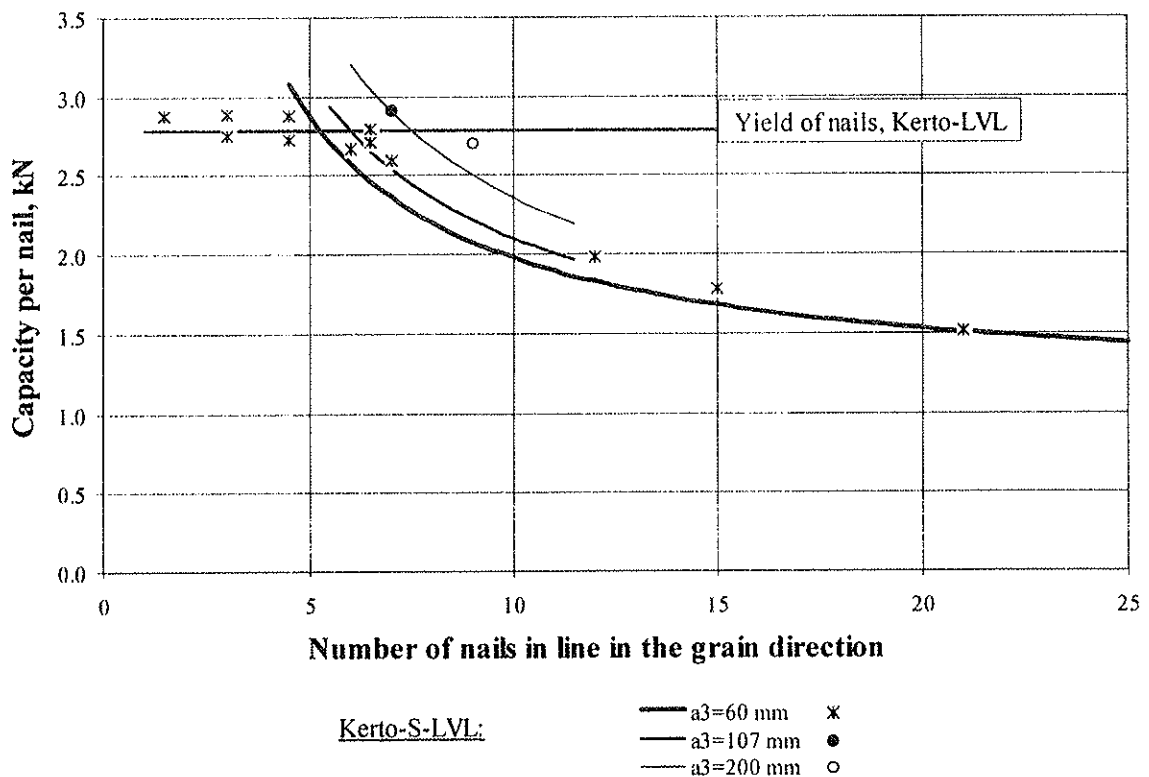


Figure 4 - Mean values per nail of test series with five parallel test pieces of Kerto-S-LVL joints with MNC connectors and the corresponding curves according to the model.

The same test results are shown as a function of the length of the joint in figure 5, which expresses clearly the combined effect of tensile and shear capacities of timber in the joint area. Test results of long glulam joints are fitted in the same graph.

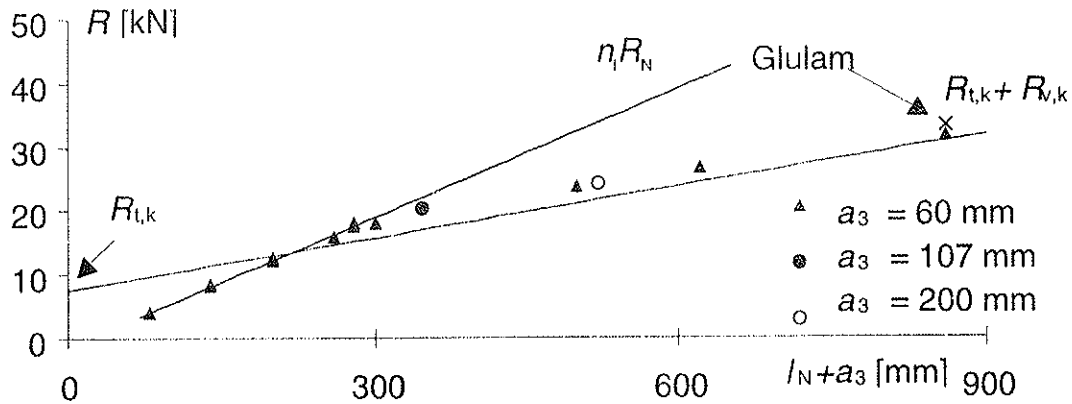


Figure 5 - Mean capacities of five test pieces of joints with MNC-connectors as a function of the joint length divided by the number of the nail rows in line with the load direction and the lines of the calculated capacities. $n_1 \cdot R_N$ is the nail capacity, $R_{t,k}$ is the tensile and $R_{v,k}$ is the shear capacity of timber.

4.3 Tests with nailed Joints

The tests with series A resulted in clear yield of nails regardless of the material used as timber members. Test series B and C of double reduction in spacing resulted in clear block tearing failure with joint slip less than 2 mm. In test series D of single reduction, the dominant failure mode was block tearing. With the test pieces of sawn timber, this was accompanied with the yielding of nails and therefore with larger joint slips.

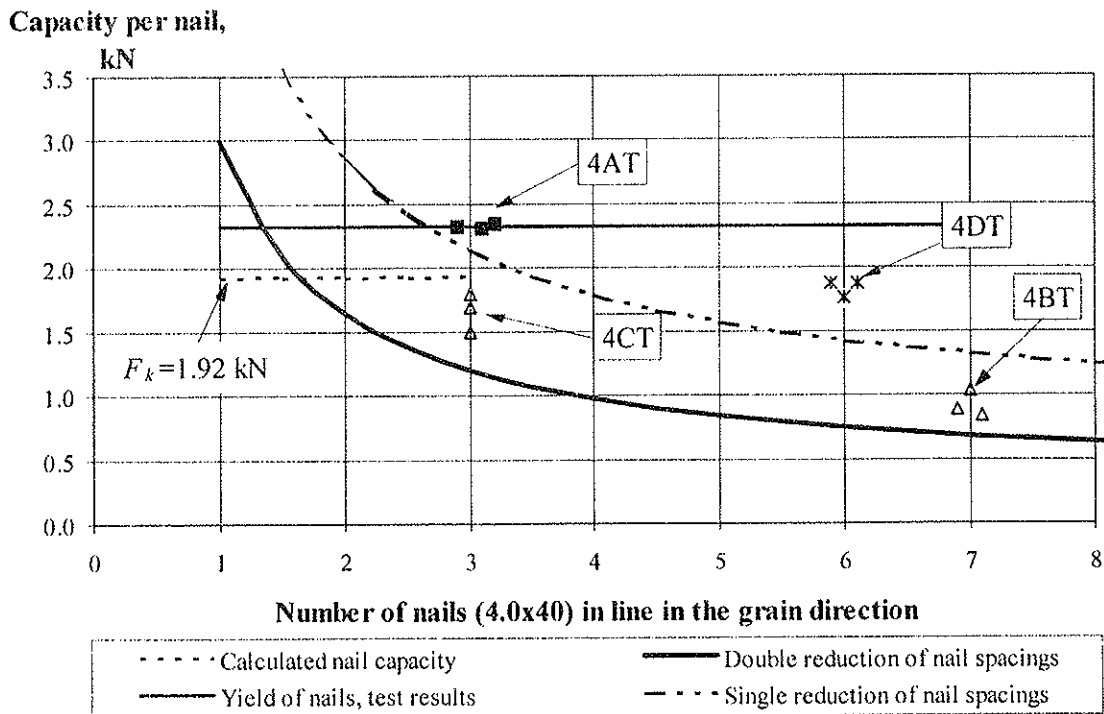


Figure 6 - Shear capacity per nail of thick steel-to-timber joints and calculated timber capacity. BMF 4.0×40 mm nails are used in sawn timber (C30).

The strength values and the calculated location of the plastic hinge (l_{ef}) used in the modelling are presented in Table 1. Figure 6 presents the individual test results for sawn timber and 4 mm nails and the calculated capacities with single and double reduction of spacing as a function of number of nails in line in load direction. It is easy to see the amount of reduction of capacities with allowed densities of nailing.

Figure 7 presents all individual test results of nailed joints with different timber materials and 6 mm nails tested in VTT as a function of the length of the joint and divided by the effective width. The lines of timber capacities are calculated by the material values given in table 1.

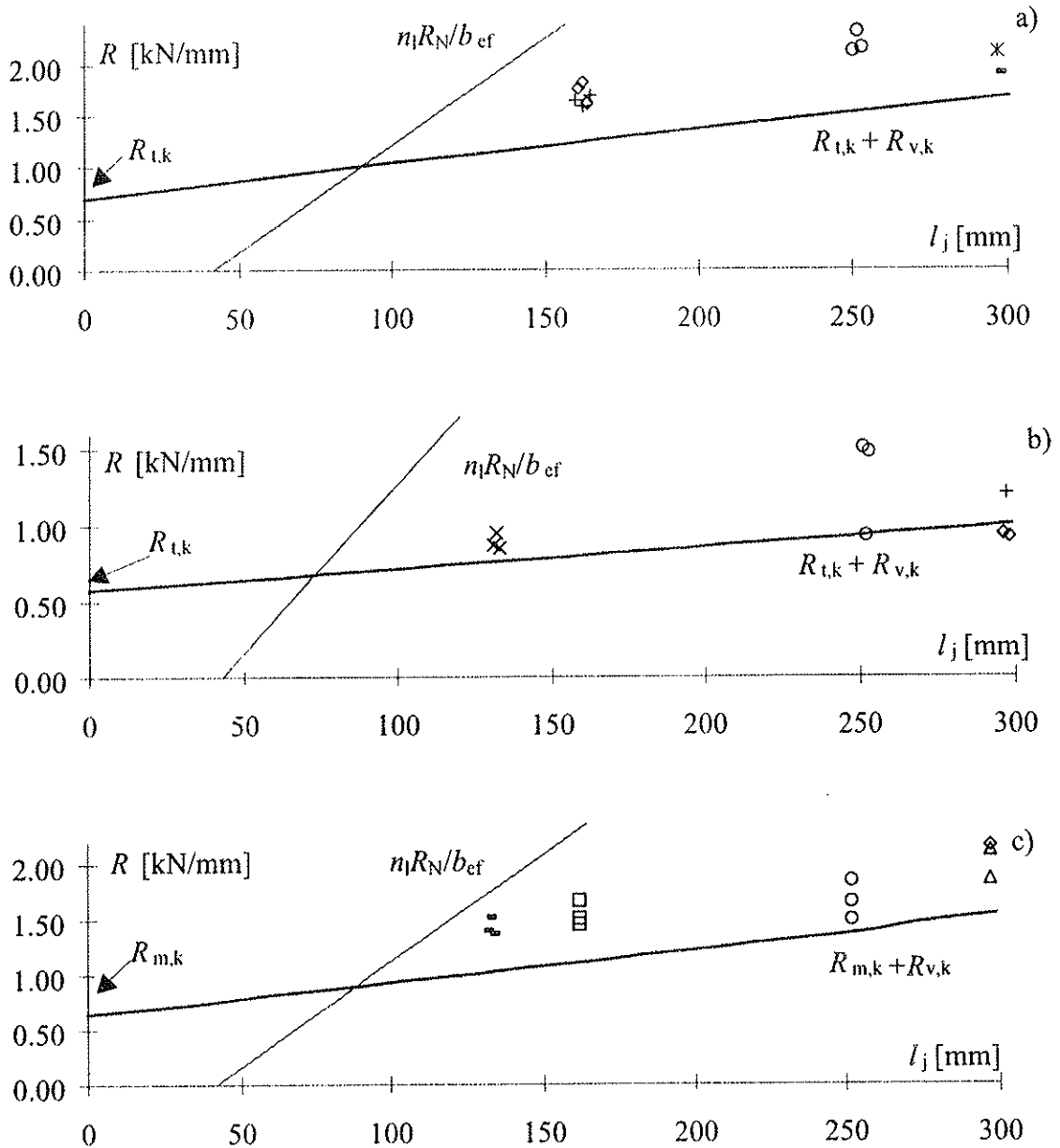


Figure 7 - Shear capacity per b_{ef} of nailed thick steel-to-timber joints and lines of nail capacity (notation $n_1 R_N$) and timber capacity according to the model. BMF 6.0×60 mm nails are used in (a) Kerto-S-LVL, (b) Kerto-Q-LVL and c) sawn timber (C30).

4.4 Tests with Glulam Rivet Connections

Test results given by Foschi [4] were from the test series conducted at the University of Alberta (UA) and by Littleford (L). Number of the similar test pieces in the reported test series varied from 1 to 6. The nail capacity P^* 1.3 kips/rivet, tensile strength of timber f_t 5600 psi and shear strength of timber f_v 650 psi were used in calculations by Foschi.

Test results, calculated tensile (R_t), shear (R_v) and nail (R_N) capacities by Foschi and timber capacities $R_T (=R_t+R_v)$ by Kangas are shown in table 2. The tensile capacity of timber was not decisive in any test series in calculations by Foschi - only shear capacity of timber and nail capacity. While in the model of Kangas all tensile capacity of timber in effective joint area took always part of the load. That explains the large difference between the calculated timber capacities in column $(R_v-R_T)/R_T$.

Table 2 - Test results (in kips) of glulam rivet joints and calculated capacities by the models of Foschi and Kangas. The decisive failure modes by Foschi are underlined. Relative difference between the calculated timber capacities (R_v-R_T)/ R_T (in%) are given.

Test series	Tested				Foschi			Kangas	$R_v - R_T$
	R_1	R_2	R_3	R_{mean}	R_t	R_v	R_N	R_T	R_T
UA1	11,4	21,0	23,2	18,5	37,8	<u>15,8</u>	32,5	14,2	11
UA2	36,4	30,1	38,1	34,9	67,4	<u>27,7</u>	32,5	32,4	-15
UA3	21,7	22,1	25,7	23,2	56,9	<u>27,6</u>	65,0	18,2	52
UA4	69,3	62,3	58,9	63,5	101,7	<u>51,3</u>	65,0	44,9	14
UA5	35,5	39,4	45,3	40,1	95,7	<u>57,2</u>	130,0	36,5	57
UA6	102,5		145,1	123,8	199,4	152,1	<u>130,0</u>	95,5	59
UA7	54,1	39,6	44,4	46,0	132,1	<u>82,5</u>	195,0	54,7	51
UA8	165,5	162,0		163,8	287,2	270,4	<u>195,0</u>	146,1	85
UA9	52,1	67,1	59,6	59,6	132,1	<u>82,5</u>	195,0	86,5	-5
UA10	210,0			210,0	287,2	270,4	<u>195,0</u>	216,6	25
L1	120,0	133,0		126,5	153,7	<u>99,4</u>	249,6	111,8	-11
L2	67,0	76,0	72,0	71,7	123,2	<u>80,5</u>	187,2	47,7	69
L3	76,0	80,0	69,0	75,0	123,2	<u>80,5</u>	187,2	47,7	69
L4	70,0	67,0	79,0	72,0	98,8	<u>57,6</u>	140,4	57,8	0
L5	71,0	64,0		67,5	98,8	<u>57,6</u>	140,4	57,8	0
L6	130,0			130,0	156,3	<u>75,6</u>	124,8	107,4	-30
L7	90,0			90,0	142,6	<u>61,3</u>	62,4	104,6	-41

The mean values of the test results in different test series and theoretical failure loads by the model of Foschi are plotted in figure 8 (open symbols). The capacities of timber in the joint area (black symbols) calculated by the model of Kangas have also been plotted.

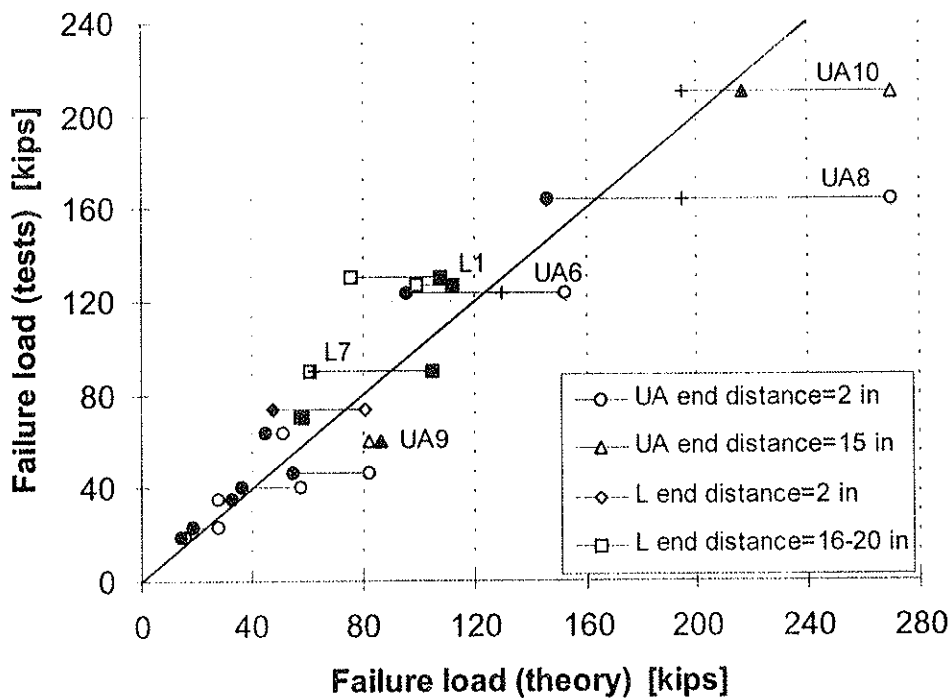


Figure 8 - The mean values of failure loads of the glulam rivet joints compared with the theoretical capacities by the models of Foschi (open symbols) and of Kangas (black symbols). Calculated timber capacities are also given, when the nail capacity was limiting (notation +).

Calculated timber capacities are also given, when the nail capacity was limiting (test series UA6 and UA8) and when the test joint reached the nail capacity (UA10 and L7). In test series UA6 one test joint had timber failure and the other reached the nail capacity, in test series UA8 both test joints had timber failure. In both cases the model of Foschi gave timber capacity far on the unsafe side, while the capacity in the proposed model was on the safe side. In test series UA10 the test joint reached the nail capacity. Timber had a little capacity left according to the proposed model, while Foschi got a lot more. In test series L7 the test joint reached the nail capacity and timber capacity were a little lower by Foschi, while timber had much capacity left according to the proposed model.

In many cases the timber capacity is overestimated and in some cases underestimated by the model of Foschi. In seven of 17 test series overestimation of timber capacity was more than 50%, if the model of Kangas is giving the right values as the writers believe.

Test series UA9 was the only case, where the model of Kangas matched a little worse on unsafe side with the test results than that of Foschi. On the other hand test series UA9 is like the test series L1, where the spacing is similar, but the number of nails in both directions and the end distance were a little bigger. Its capacity was 2,1-fold but theoretically only 1,2-fold, so its relative strength was 1,75-fold. In the test arrangements or in reporting of test series UA9 must have been something wrong.

In seven of 17 test series end distance a_3 was between 380...520 mm. Only in test series UA9 the calculated timber capacity was more than test result and that is explained in the previous paragraph. It proves that end distance a_3 can be as long as 0,5 m and can be calculated to transfer its share of the load in the proposed model.

5 Design of Timber Capacity

Procedure of designing the timber capacity in the joint area of nailed steel-to-timber joints can be done as follows, when load F , timber material, its properties and dimensions are known.

- the nail type and size are chosen,
- effective thickness t_{ef} is calculated by formula (6),
- number of nails perpendicular to the grain n_b is chosen,
- effective width of the nailed area b_{ef} is calculated by formula (8),
- tensile capacity of timber is calculated by $R_{t,k} = t_{ef} \cdot b_{ef} \cdot f_{t,k}$,
- wanted shear capacity is calculated: $R_{v,k} = F - R_{t,k}$,
- minimum length l_j of the joint is calculated by $l_j = R_{v,k} / (b_{ef} \cdot f_{v,k})$
- timber capacity is $R_{T,k} = R_{t,k} + R_{v,k}$,
- nail capacity $R_{N,k}$ is calculated by formula (10).

For thick steel-to-thick timber joints, the nail capacity applying Eurocode 5 is

$$R_{N,k} = 1,5(2M_{y,k} \cdot f_{h,k} \cdot d)^{1/2} \quad (10)$$

For plastic mode of failure nail capacity R_N shall be less than timber capacity R_T . If the calculated length of the joint is too long, the value of the tensile capacity of timber R_t ought to be increased or broader timber to be used. R_t can be increased by fewer number n_b of nails perpendicular to the grain and by increasing the value of effective thickness t_{ef} . That can be made simply by choosing bigger nails or quite other type of nails (like glulam rivets).

Figure 9 shows in principle the effect of different strength values on the timber capacity in the joint area of different lengths. The tensile capacity R_t can be affected by the selecting of the size and type of the nail.

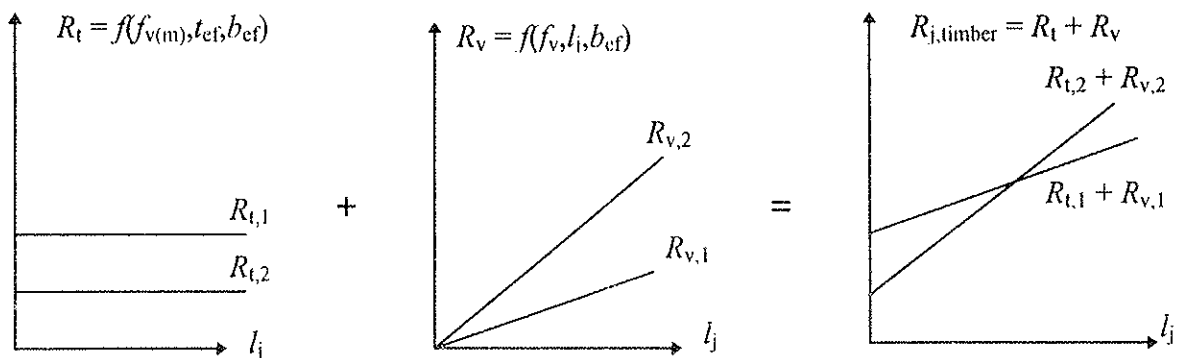


Figure 9 - Illustrative diagram about the design of timber capacity in the joint area of two cases with different materials.

6 Concluding Remarks

In nailed timber connections, nail spacings are mainly given to avoid splitting during nailing. In the case of predrilled holes and steel-to-timber connections increased nail density is allowed by design codes. This leads to the exceeding of the tensile and shear capacity of the timber member in the joint area, and the unfavourable brittle mode of failure with reduced capacity of the joint.

The allowable nail spacings of EC5 are, therefore, found too small for nailed steel-to-timber connections, since the reduction in nail spacings due to both predrilling and steel connectors is not acceptable. In long timber joints, no reduction should be allowed at all. The increase in the end distance a_3 or in the joint length, however, could allow dense nailing patterns.

Design method of timber capacity for steel-to-timber connection with cluster of nails has been presented. The main task is to calculate the timber capacity in the joint. This method allows a simple design procedure for this type of connection. The procedure is advantageous, in that it permits to optimize the connection in the sense that premature wood failures are controlled and full use is made of the load-carrying capacity of the nails.

Failure loads predicted by the model compare well with those obtained in tests carried on with different timber materials, types and sizes of nails, sizes of the nailed area and end distances up to half a meter. Thus design recommendations presented here can be used in all nailed thick steel-to-timber connections.

References

- [1] Kangas, J. & Väänänen, H. 1996. The Capacity of Multiple-Nail-Connector/Kerto-LVL Joints. In: Proceedings of the International Wood Engineering Conference (IWEC), Volume 3. p. 279-282. New Orleans, Louisiana, USA.
- [2] Kangas, J., Aalto, K., Kevarinmäki, A. 1997. Modelling of the block tearing failure in nailed steel-to-timber joints. *CIB-W18 meeting 30*, CIB-W18/30-7-2, Vancouver, British Columbia, Canada.
- [3] Vesa, J., Kangas, J., 1998. Block tearing tests near the balanced timber and nail capacities of nailed Steel-to-Timber Joints, Publication 83. Helsinki University of Technology. Laboratory of Structural Engineering and Building Physics. Espoo, Finland.
- [4] Foschi, R., 1973. Stress analysis and design of glulam rivet connections for parallel-to-grain loading of wood. Information report VP-X-116, Department of the Environment Canadian Forestry Service Western Forest Products Laboratory, Vancouver, British Columbia.
- [5] Hilson, B. O. 1995. Joints with dowel-type fasteners - Theory. In: Blass, H. J. & al. Timber Engineering STEP 1, lecture C3. Centrum Hout, The Netherlands.
- [6] Eurocode 5. 1993. Design of timber structures - Part 1-1: General rules and rules for buildings. ENV 1995-1-1:1993: European Committee for Standardization. Brussels, Belgium. 110 p.

CIB-W18/31-7-5

**INTERNATIONAL COUNCIL FOR BUILDING RESEARCH STUDIES AND DOCUMENTATION
WORKING COMMISSION W18 - TIMBER STRUCTURES**

TIMBER CONTACT IN CHORD SPLICES OF NAIL PLATE STRUCTURES

by

Ari Kevarinmäki
Technical Research Centre of Finland (VTT)
FINLAND

MEETING THIRTY-ONE

SAVONLINNA

FINLAND

AUGUST 1998

Timber contact in chord splices of nail plate structures

Ari Kevarinmäki

Technical Research Centre of Finland VTT, Finland

1 Introduction

In Eurocode 5 (ENV 1995-1-1 1993) the contact pressure between timber members may be taken into account to reduce the joint force, F_A , in compression provided that the gap between the members has an average value not greater than 1 mm and a maximum value of 2 mm. In such cases the joint should be designed for a minimum compression force of $F_A/2$. However, EC 5 does not give any rules for utilization of the timber contact in the bending of chord splices.

In Nordic the countries the moment capacity of nail plate joints of chord splices with utilization of the timber contact has been used in practical design since the 1970s. The method was developed experimentally by Gunnar Edlund (1971, 1973). In compression the design value of the joint normal force is 1/3 of the applied normal force of the chord (N_d), i.e. the timber contact reduction is 2/3. The design equations are based on the force couples: the moment, M_d , is analyzed as a tension force of the plate and a compression force of the timber contact located at a distance of $h/6$ from the chord edge. The interaction between the normal force and the moment is taken into account by the bi-linear capacity curve. Theoretically the design method is clearly on the unsafe side with a big tension force, because when the whole cross-section of the timber member is in tension there is no joint contact and no force couple for the moment.

The aim of this study was to develop new design equations suitable for use with EC5 for the chord splices with symmetrically placed nail plates, when the main direction of the nail plate is combined with the grain direction. The work may be done by theoretical calculations using previously developed models of the moment capacity and rotational stiffness of nail plate joints (Kangas & Kevarinmäki 1995, Kevarinmäki & Kangas 1995, Kevarinmäki 1996). The proposals for utilization of the timber contact in the chord splices are verified with bending and eccentric tension tests on different kinds of nail plate joints.

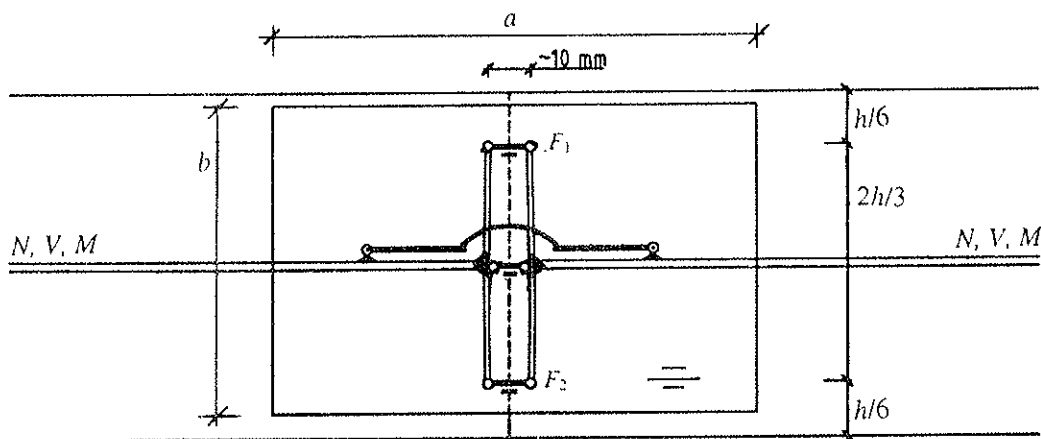
2 Analysis model

The simplified Equations (1) - (13) are based on theoretical calculations in which the stiffness in anchorage (the bi-linear model), the plate stiffness in the joint line and the contact stresses of the timber have been taken into account. The calculations have been made using different nail plate size and chord height combinations with several nail plate types. The gap between the timber members has been taken into account and the simplified governing conditions have been fixed so that they are on the safe side, when the value of the gap between the timber members on the compression side is 1 mm.

The calculation model is presented in Figure 1. The plate force F_A and the plate moment M_A for the anchorage and the joint line design are half of those force and moment values acting on the beam element connecting the anchorage areas to each others (half because there are plates on both sides). The capacity of this beam element has been determined by the plastic joint line and anchorage design methods proposed for Eurocode 5 by Kangas & Kevarinmäki (1995).

The calculation model fulfills the conditions of equilibrium, strength and compatibility non-linearly by the following stiffness models and values of the elements:

- Joint gap: there is no contact stiffness before closure of the joint gap (Figure 2a).
- Linear translational anchorage stiffness in semi-rigid node-points: $k_F = 2K_{F,u,u}A_{ef}$.
- Bi-linear rotational anchorage stiffness ($2K_r$) in semi-rigid node points according to Figure 3 (Kevarinmäki 1996).
- Plastification of steel: rigid-plastic stress-strain model for the beam element that connects the anchorage areas (Figure 2b); when the compression strength of the plate, $f_{c,\alpha=0}$, is achieved on the edge of the plate, the gap closes and the contact element begins to function.
- Plastification of wood: rigid-plastic force-compression model for the contact elements (Figure 2a); the maximum compression force of a contact element is limited to the compression strength of wood achieved on the whole timber cross-section described by the actual contact element ($f_{c,0} t h/3$).



— Stiff beam element

— Beam element with steel properties

⊥ Rigidly fixed

○ Pure hinge

— Compression member (contact) element with wood properties

• Semi-rigid node point:
$$K_r = \begin{cases} K_{\phi,u} I_F & \text{when } \tau_{M,el} \leq f_{a,0,0} \\ K_{\phi,u,p} I_P & \text{when } \tau_{M,el} > f_{a,0,0} \end{cases}$$

Figure 1 Calculation model for splice joint analysis. Semi-rigid node points are located on the centroid of the effective anchorage area.

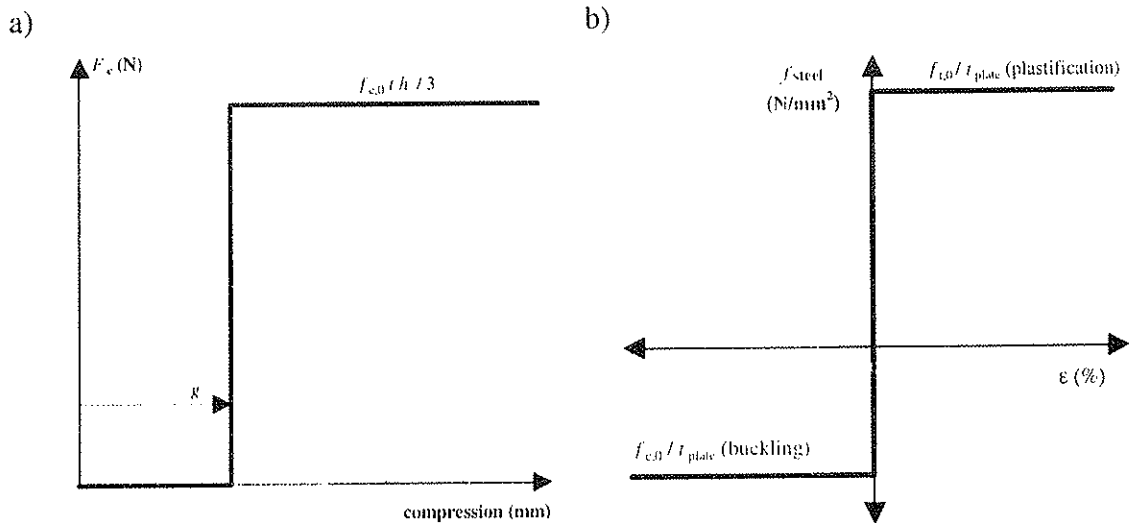


Figure 2 Simplified wood and steel properties used in analysis: a) force-compression dependence of the contact element and b) stress-strain model for the beam element that connects the semi-rigid node points to each other (the height of the beam element is b and the thickness $= 2t_{plate}$).

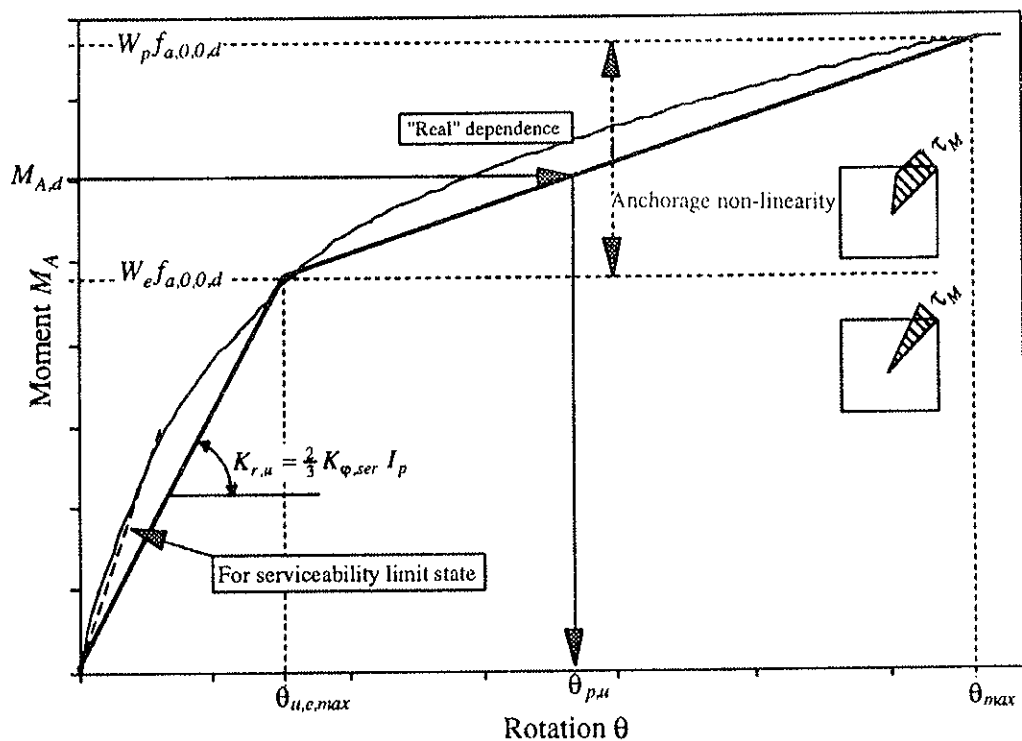


Figure 3 Bi-linear moment-rotation dependence in anchorage of nail plate joint (Kevarinmäki 1996).

The theoretical analysis has been made with the mean strength and stiffness values of the materials defined by the standard tests for W and FIX nail plates. The thickness of these plates is 1.3 mm, the length of the teeth 13..15 mm and the strength classes of the steel S350GD+Z (FIX) and S400GD+Z (W). For the compression strength of wood the characteristic value of strength class C40 (26 N/mm^2) has been used and the chord thickness t was 42 mm. The capacity calculations of example joints have been done iteratively in a stepwise manner with checking of the strength and compatibility conditions at every value of the load.

3 Pure bending moment

3.1 Simplified equations for plate moment and plate force

The theoretical moment capacities of example splice joints of FIX and W nail plates were calculated with different combinations of plate sizes and chord heights and with different values of joint gaps by the analysis model presented in Chapter 2. The relation of the sum of plate moments M_A to the chord moment M was solved in all the cases. It may be safely concluded that the value of this relation ($2M_A/M$) is generally at most $\frac{1}{2}$. Then the following very simple equations may be written for the values of plate moment M_A and plate tension force F_A in the case of an symmetrical splice joint which transfers only a bending moment M of chord:

$$M_A = \frac{1}{4} M \quad (1)$$

$$F_A = \frac{3M}{4h} \quad (2)$$

where h is the height of the chord.

The equations are based on the assumption that 50 % of the bending moment of the joint goes through the contact couple and 50 % by the moment stresses of the nail plate. The contact point is assumed to be at a distance of $h/6$ from the compression side of the chord.

3.2 Effects of joint gap, plate length and chord height

The theoretical calculations were made both with a joint gap value of zero and 1.667 mm. The latter is the maximum gap value allowed according to Eurocode 5 for the compression joints at the point of $h/6$ from the edge of the member when the timber contact is utilized. This corresponds to a situation in which the edge gap of compression side is 2 mm and the tension side is in contact, when the average value of the gap is 1 mm on the centerline of the member.

Generally the effect of the joint gap on the total bending capacity of the joint was quite small, as shown in the example of Figure 4, where the capacity of FIX nail plate 100x160 with a chord height of 122 mm was calculated with different gap values. The joint gap has a bigger impact on the internal joint force and moment combination: with a gap value more than 1 mm the plate moment M_A obtains in certain cases a clearly higher value than $M/4$: with a maximum gap value at about $M/3$. However, then the tension force of the plate F_A has a smaller value than is given in Equation (2), which gives the joint a higher plate moment capacity reserve. The total theoretical bending capacity of the joint was in all calculated cases with the maximum gap value at least 95 % of the joint capacity calculated according to the simplified Equations (1) and (2).

The effect of the joint gap with different plate length values is seen in examples presented in Figure 5. There are no joint gap effects on the joint capacity nor on the internal plate moment values in the case of a long nail plate, where the critical factor is the plate joint line capacity. After joint line buckling of the compression side, the gap closes and the force couple develops as in the case of a contact joint.

With the maximum joint gap the value of the plate moment (M_A) becomes even smaller, and the failure mode changes from the anchorage to the plate even though the external moment (M) increases. This is due to the rigid joint line: the rotations develop in the anchorage without timber contact before the moment is so high that it leads to clear

anchorage plastification, as may be seen in Figures 5b, 6 and 7 by the plastification factor of the moment anchorage $k = \tau_{M,e}/f_{a,0,0}$. Without non-linearity of the moment anchorage, no timber contact would normally appear by the bending moment in the anchorage-critical splice joint in the case of the maximum allowed joint gap.

The plate height - chord height relationship affects the effectiveness of the timber contact, as may be seen by the comparison of the calculation results presented in Figures 6 and 7. The simplified Equations (1) and (2) have been fixed for the case where the height of the nail plate (b) is equal to the chord height (h) (Figure 6). If the nail plate is narrower than the chord, the simplified equations are on the safe side, because then the corresponding part of the chord, the simplified equations are on the safe side, because then the corresponding part of the plate moment (M_A) starts to decline and the tension force (F_A) of the plate starts to rise.

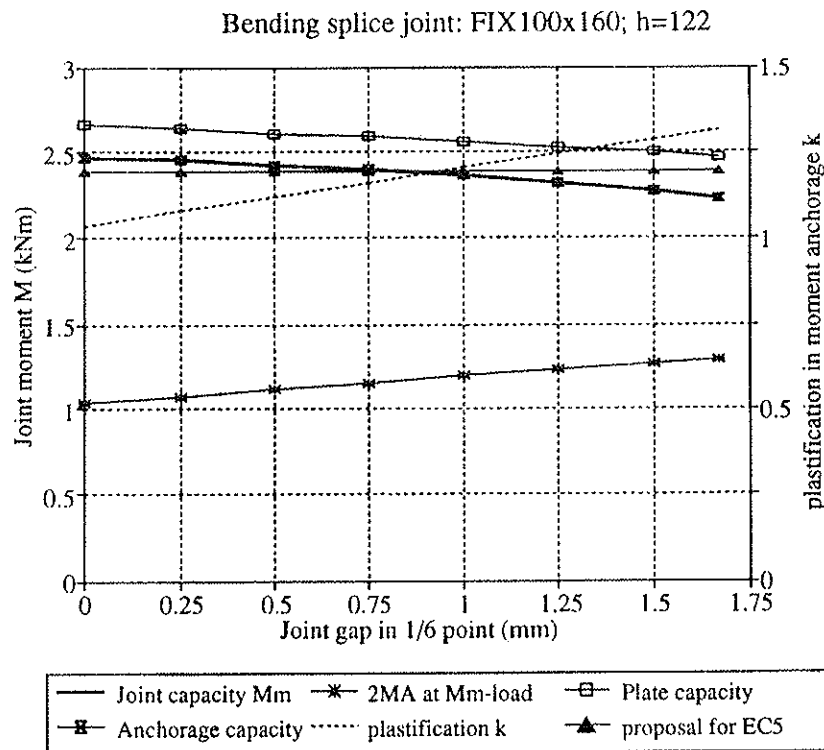


Figure 4 Calculated bending capacities of a FIX -nail plate splice joint with different joint gap values. "Proposal for EC5" corresponds with Equations (1) and (2).

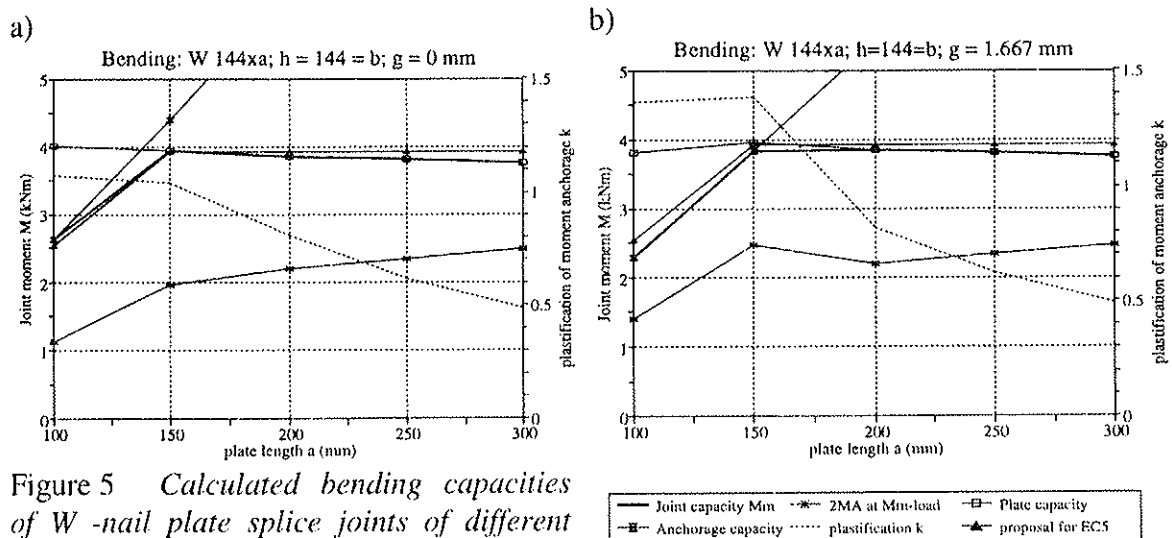


Figure 5 Calculated bending capacities of W -nail plate splice joints of different plate lengths a) with no joint gap and b) with a joint gap of 1.667 mm.

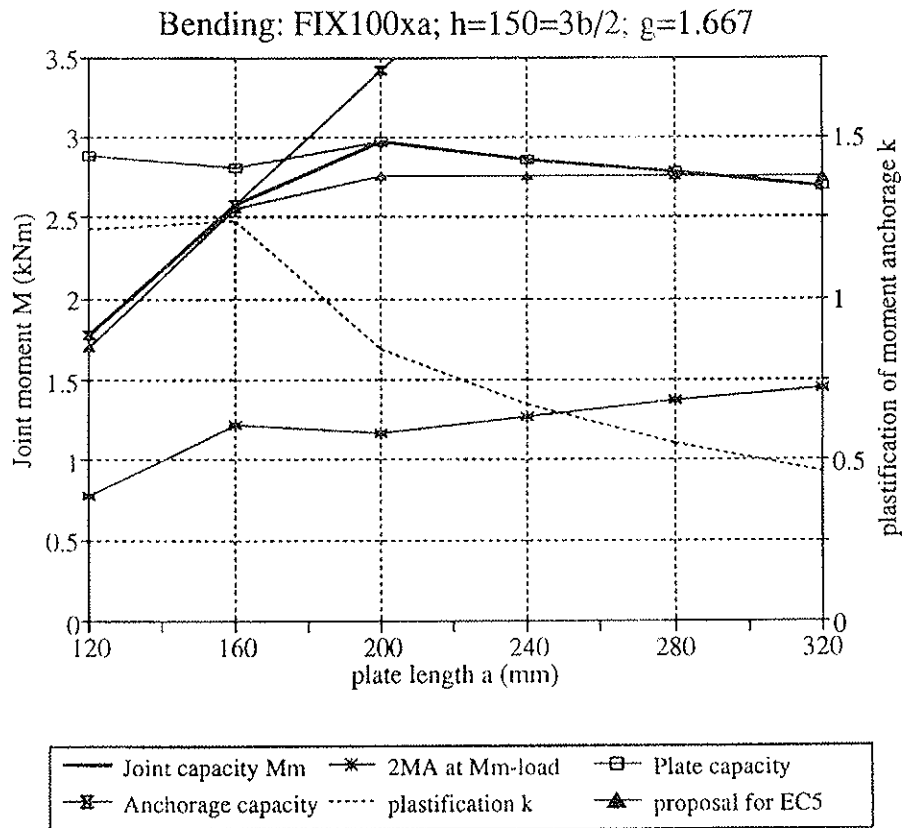


Figure 6 Calculated bending capacities of FIX -nail plate splice joints of different plate lengths with a joint gap of 1.667 mm and a plate height of $\frac{2}{3}h$.

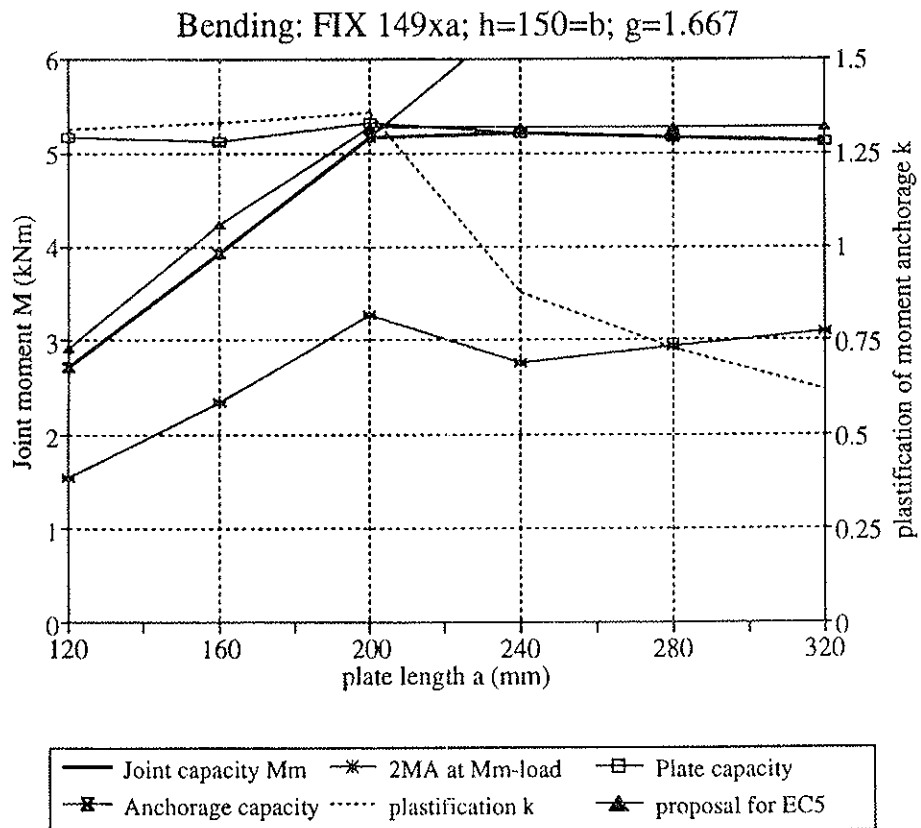


Figure 7 Calculated bending capacities of FIX -nail plate splice joints of different plate lengths with a joint gap of 1.667 mm and a plate height $b = h$.

4 Tension splices

4.1 Simplified equations for plate moment and plate force

An acceptable approximation of the theoretical calculations presented in Paragraph 4.2 may be written as follows: when the applied tension force causes anchorage stresses which are higher than half of the anchorage strength and the value of the joint gap is 1 mm, the whole moment goes through the nail plate (Figure 8). With smaller tension forces there is contact pressure on the compression side of timber members in failure of combined moment-tension loading. The effect of tension force, N , on the value of the plate force and moment may be then taken into account as follows:

$$F_A = \sqrt{\left(\frac{N}{2} + \frac{3|M_s|(1-\mu_t)}{4h}\right)^2 + \left(\frac{V}{2}\right)^2} \quad (3)$$

$$M_A = \frac{1}{4}(1 + \mu_t)M_s \quad (4)$$

$$\mu_t = \frac{N}{f_{a,0,0} A_{ef}} \leq 1 \quad (5)$$

where V is the shear force of the chord and

M_s is the chord moment increased by the joint eccentricity of the shear force:

$$M_s = M + V e \quad (6)$$

where e is the distance from the centroid of the effective area to the joint line.

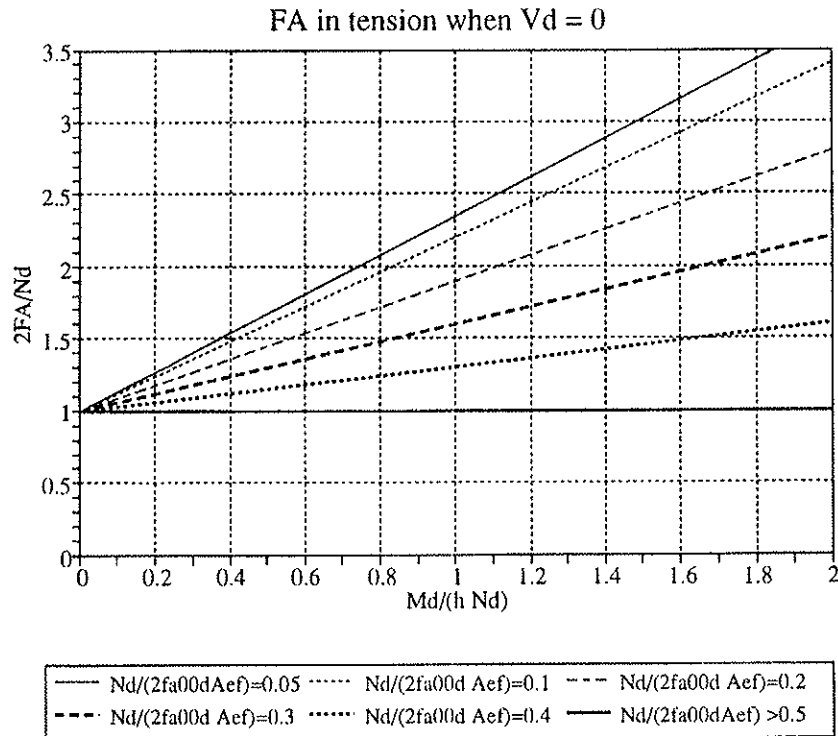


Figure 8 The relationship between the tension force acting on the nail plates, $2F_A$, and the tension force affecting on the chord, N_d , in proportion to the relative chord moment, $M_d/(hN_d)$, solved by the simplified Equations (3)-(5).

4.2 Comparison calculations

The joint gap of tension splices is increased by the tension force and also by the moment if there is contact pressure on the compression side of the joint. The value of the tension force-moment relationship for the point where the contact pressure disappears depends on the actual joint geometry (plate geometry and size and chord dimensions), on the anchorage stiffness of the nail plate, on the compression strength of the plate and on the initial value of the joint gap.

The moment capacity calculations were made as a tension force function for example joints of FIX and W nail plates with plate lengths of 150 and 160 mm, so that the plate capacity of the joint line and the anchorage capacity would be near each other. The plate size, chord height and joint gap were the variables. The joint capacities were calculated also by the present Eurocode, by Edlund's method (Finnish Code: PLY 1983) and by the simplified Equations (3) - (5) presented as a "proposal for EC5". Some of these calculation results are presented in Figures 9 - 11. The tension force area where no contact pressure would appear on the joint line by the moment is shown in the figures by a note $F_1 = 0$.

From the results of calculations presented in Figures 9 - 11 it may be seen that when there is no more contact pressure, the anchorage capacity curve changes from a straight line to a curve, which corresponds with the interaction curves of the plastic anchorage capacity (Kevarinmäki 1996). Also the plate capacity of the joint line has a linear dependence ($M_s(N)$) on the timber contact, as presented in Figures 9 and 11. The failure value of the plate moment M_A is constant with all tension force values, when the timber contact is acting, as shown in Figure 10. This means that the plate-chord moment relationship M_A/M_s depends linearly on the tension force when there is contact pressure as assumed in Eq. (10).

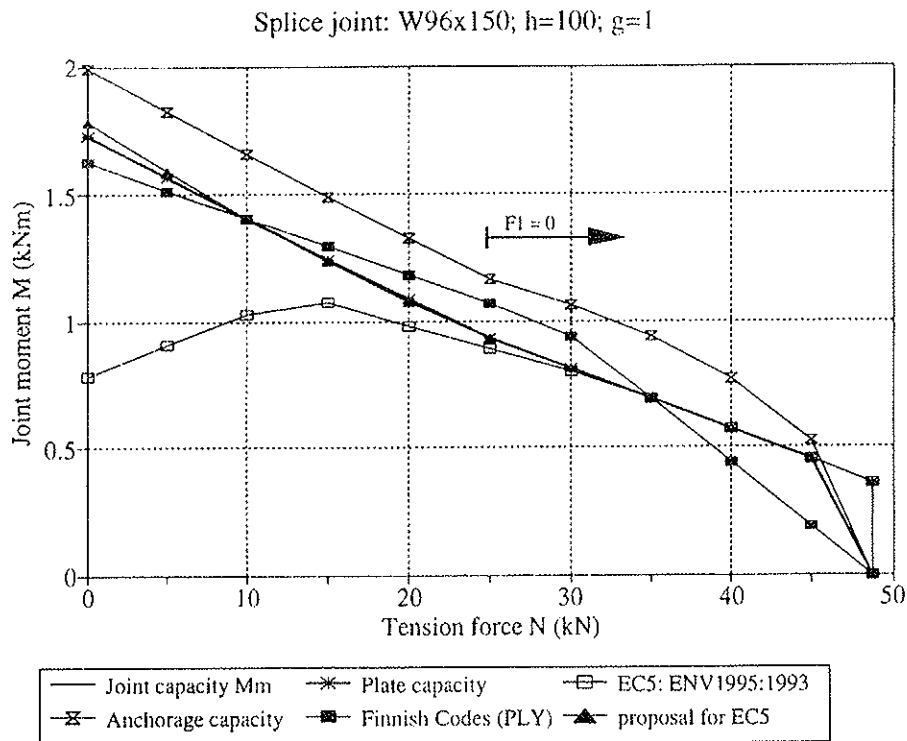


Figure 9 *Tension-bending interaction capacity curves of a W nail plate (96x150) splice joint for a chord height of 100 mm with a joint gap of 1 mm calculated by the mean strength values. The joint is critically governed by the plate capacity of the joint line, except in a pure tension case where the anchorage is the governing condition. At tension load level >25 kN there is no contact pressure in bending failure.*

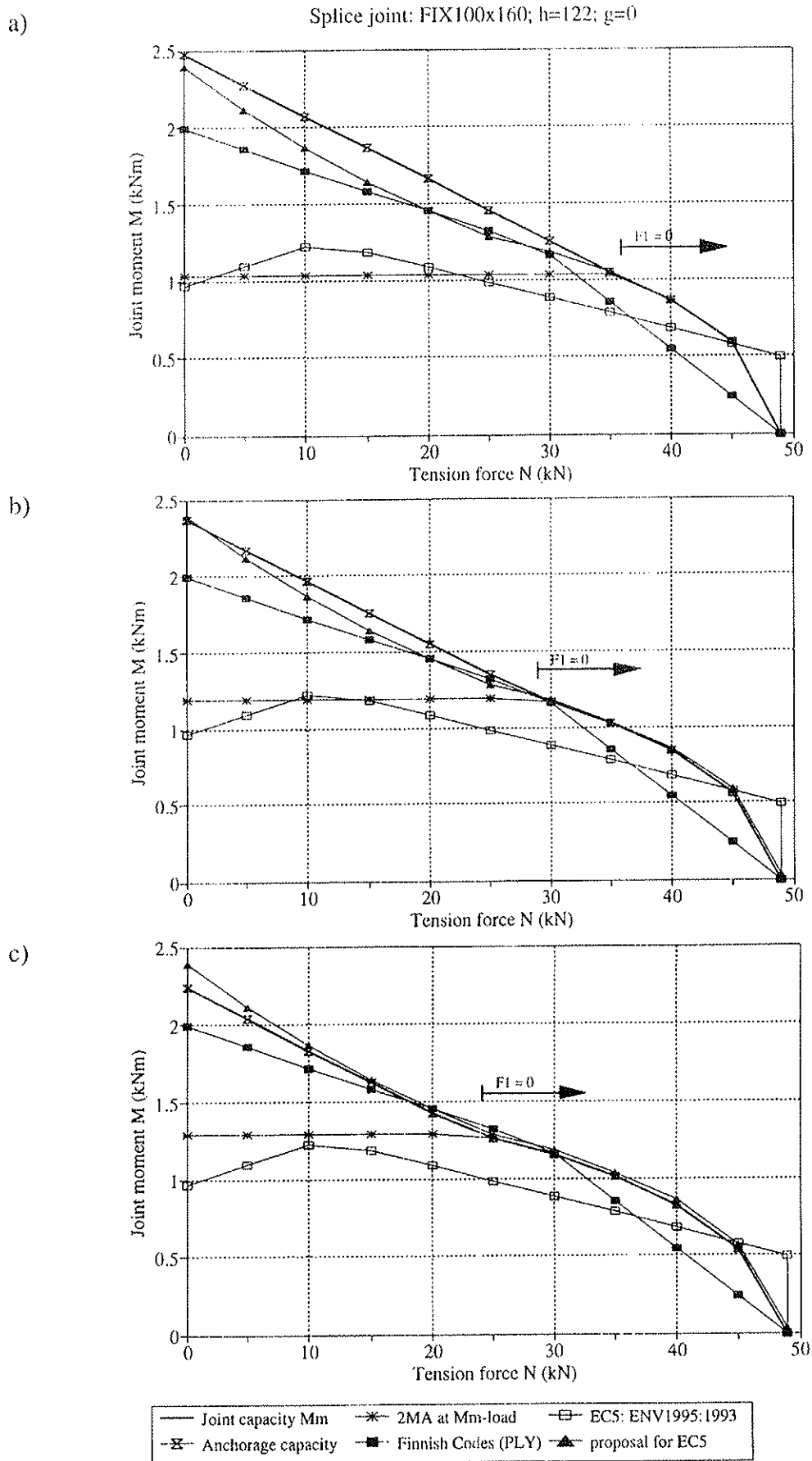


Figure 10 Calculated tension-bending interaction capacity curves of a FIX -nail plate splice joint with a joint gap value of a) 0, b) 1 and c) 1.667 mm.

The maximum value of the tension load, which still leads to the contact pressure of joint line in combined tension-bending failure, depends, in addition to joint gap, on the relationship between the heights of the plate and the chord. If the nail plate is as high as the chord and the initial value of the joint gap is 1 mm, the failure contact disappears at a tension load level of about 50 % of the anchorage tension capacity, as shown in Figure 9. The smaller the height relationship between the plate and chord, the higher the tension load level may be with the joint contact in the combined tension-bending failure, as can be seen by comparing Figures 9, 10 b) and 11. In the example of Figure 11 the relationship between the plate and chord heights is 2/3, and the maximum tension load level with contact pressure is about 65 %.

The simplified Equations (3)-(5) have been defined for the case of the plate width equal to the chord height, as may be seen Figure 9: the capacity line of the simplified method combined almost exactly with the theoretical curve. In the case of Figure 11 ($b = 2h/3$), the simplified method is on the safe side: the biggest difference appears at a tension load level of 27 %, where the simplified method gives about 82 % of the theoretical moment capacity. With the maximum joint gap value of 1.667 mm at the $h/6$ point, the simplified Equations are still at an acceptable level, so long as the nail plate width is at most 80 % of the chord height (Figure 10 c)).

The present Eurocode method (EC5 1993) is generally very conservative in combined tension-bending loading of chord splices, especially in the cases of big moments. In a pure bending case the joint capacity calculated according to EC5 may be less than 40 % of the theoretical capacity, when the same mean values for the strength properties are used in both calculations (see Figure 11). The low bending capacity is due to the governing condition of the plate buckling in the joint line, which is not allowed by EC5. With higher tension forces and no timber contact, the results of the EC5 method differs from the theoretically calculated anchorage capacity due to the different anchorage design criteria.

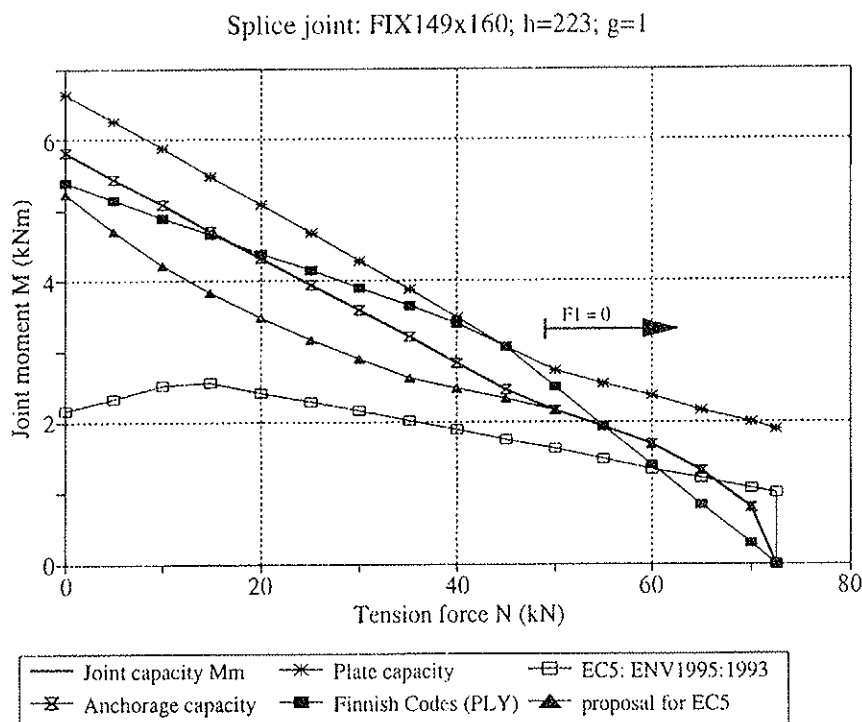


Figure 11 Tension-bending interaction capacity curves of a FIX nail plate (149x160) splice joint for a chord height of 223 mm with a joint gap of 1 mm calculated by the mean strength values.

The moment capacities of example joints were also calculated by Edlund's method according to the old Finnish Code (PLY 1983). Generally these formulae give a result that is quite close to that calculated theoretically, although Edlund's method is based, in the case of a big tension force, on the impossible concept of a contact compression and plate tension force couple. However, the experimentally determined reduction factor, $\frac{2}{3}$, is on the right level also by these calculated examples. The pure moment capacity of Edlund's method is slightly conservative: in the calculated cases it was at most about 15 % below the theoretical moment capacity.

The tension-bending interaction capacity of Edlund's method may be on the unsafe side in the case of a plate capacity critical joint (Figure 9) or in the case of the narrow nail plate compared to the chord height (Figure 11). In these cases the biggest differences appeared in the area where the tension load level from the pure tension capacity was 50.65 %. There the theoretical moment capacity was exceeded at most by 20 % .

5 Compression splices

5.1 Simplified methods

According to Eurocode 5 (1993), half of the compression force may be transferred by the timber contact. If this assumption is connected to the simplified Equations (1) and (2) defined for a pure bending case, the compression force per plate is calculated as:

$$F_A = \frac{N}{4} - \frac{3M}{4h} \quad (7)$$

and the bending moment M_A by Equation (1). This simplification means that, when the moment is high enough ($M > Nh/3$), the plate force will be in tension at joint failure. This leads to totally different plate force and plate moment values to those presently given in Eurocode 5, as shown in Figure 12.

According to the theoretical calculations the assumption (7 & 1) is conservative, especially with high compression force values. A more accurate result would be obtained by the following simplified equations, where the effectiveness of the timber contact depends on the relationship between the chord's compression force, N , and the anchorage capacity and the compression capacity of timber (F_c):

When $N \leq \frac{1}{3} F_c = \frac{1}{3} f_{c,0} t h$:

$$F_A = \sqrt{\left(\frac{\eta N}{4} - \frac{3 |M_s| (1 + \mu_c)}{4 h} \right)^2 + \left(\frac{V}{2} \right)^2} \quad (8)$$

$$M_A = \frac{1}{4} (1 - \mu_c) M_s \quad (9)$$

where $\eta = \left(\frac{3 f_{a,0,0} A_{ef}}{2 N} \right)^2 \leq 1$ and $\mu_c = \frac{N}{4 f_{a,0,0} A_{ef}} \leq 0.5$ (10, 11)

When $N > \frac{1}{3} F_c = \frac{1}{3} f_{c,0} t h$:

$$F_A = \sqrt{\left(\frac{N}{20} \left(\frac{3 N}{f_{c,0} t h} + 1 \right) \right)^2 + \left(\frac{V}{2} \right)^2} \quad \text{and} \quad M_A = \frac{1}{8} M_s \quad (12, 13)$$

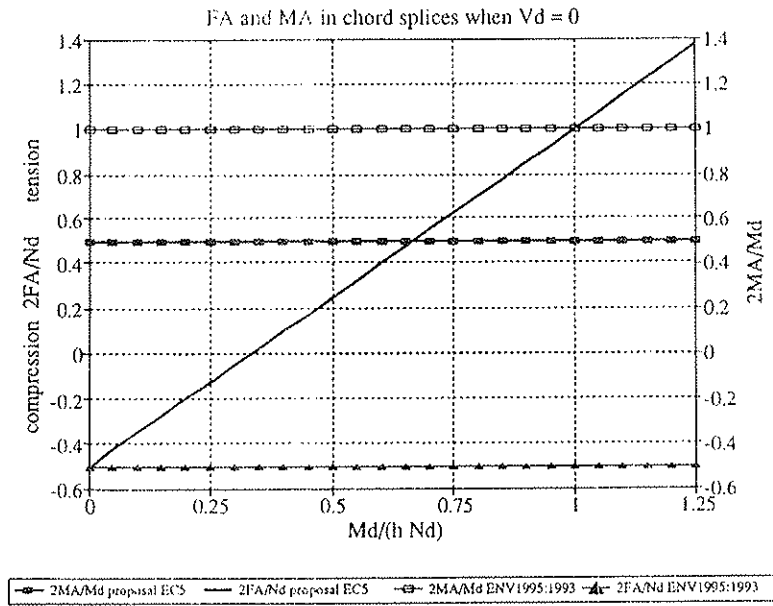


Figure 12
 The relative plate force and plate moment values in compression splices solved by Equations (1) and (7) ("proposal EC5") and according to Eurocode 5.

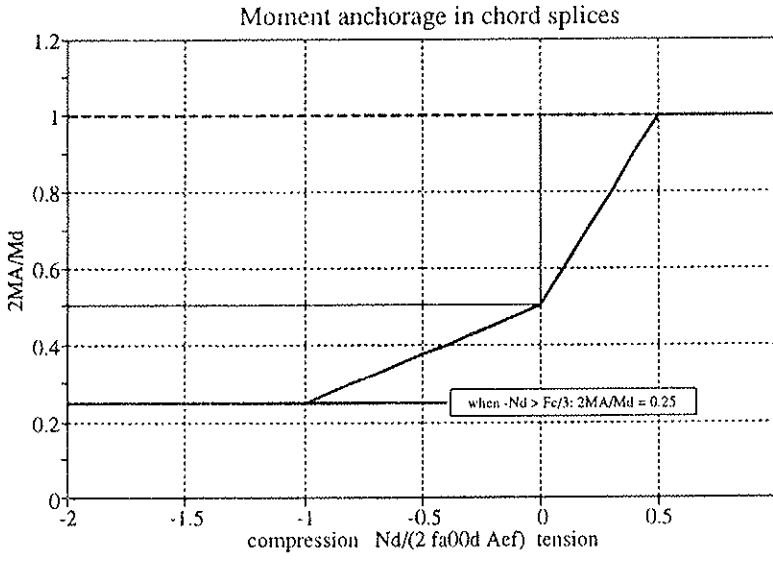


Figure 13
 The relationship between the moment acting on the nail plates, $2M_A$, and the moment acting on the chord, M_d , in proportion to the utilization level of the joint's normal force anchorage capacity solved by the derived simplified Equations (4), (9) and (13) (thick solid line), by the more simplified Equation (1) of compression area (solid line) and by EC5 (thick dashed line).

5.2 Comparison calculations

The theoretical calculations for the moment capacity of the example joints were made with a compression force (N) step of 5 kN. The following four different types of the joint behavior may be observed in combined compression-moment failure, depending on the value of the compression force:

1. The compression force is so small that the compression capacity of the wood has not been achieved on the contact side ($F_1 < F_c$). The plate force (F_A) is in tension and the critical factor is the anchorage or the plate tension capacity in the joint line.
2. The compression strength of the wood has been achieved on the contact side to a chord height of $h/3$ ($F_1 = F_c$). However, there is still axial tension force in the nail plates ($F_A > 0$). The failure criteria are the anchorage or the plate's joint line capacity. On the joint line there may be tension failure or the compression capacity of the plates is exceeded on the contact side due to the high moment (denoted in the figures by "plate plastification").

- The external axial force is already so high that also the normal force of the plate is in compression ($F_A < 0$). The height of the contact zone is, however, less than $2/3h$, so there is no force in the lower contact element of Figure 1 ($F_2 = 0$). The critical factor is the compression capacity of the plates.
- The external normal force is so high, and, on the other hand, the moment is so small, that the height of the joint's contact zone is greater than $2/3h$ (denoted in figures by " F_2 compression"). When the normal force is high enough, the whole cross section of the timber is in compression, and theoretically then there is no need for any nail plates in pure interaction of the force and moment. This is possible when $M \leq Nh/6$. In such a case, the joint would not limit the capacity of the timber member if no nail plates were used. To prevent this, the analysis model was corrected in this region so that the plate moment (M_A) obtains a constant value corresponding to the plate moment calculated in the failure with the external normal force value which gives the joints a contact zone height of $2/3h$. In that region the failure load depends on the compression capacity of the plates or on the timber member's capacity in combined compression and bending.

The simplified Equations (8) - (13) have been defined by taken these different joint behaviors into account. The comparisons between the theoretical results and the calculated simplified capacities of some examples are shown in Figures 14 - 16. The factors η and μ_c of the simplified Equations are fixed so that the normal force-moment capacity curve are always on the safe side when the nail plate height is less than 90 % of the chord height and the maximum joint gap is less than 1 mm. The simplified method is clearly on the safe side with narrower nail plates (lower b/h relation), as may be seen in Figure 15. When the nail plate height is equal to the chord height, the simplified method may, within a certain range, give higher moment capacities than the theoretical model. However, this difference is insignificant (Figure 16). Also the impact of the joint gap on the joint capacity is insignificant in the joint behavior regions 2, 3 and 4, where the contact side of the joint is plastified. With lower compression force values the effectiveness of the joint gap is smaller than in the pure bending case (Figure 14).

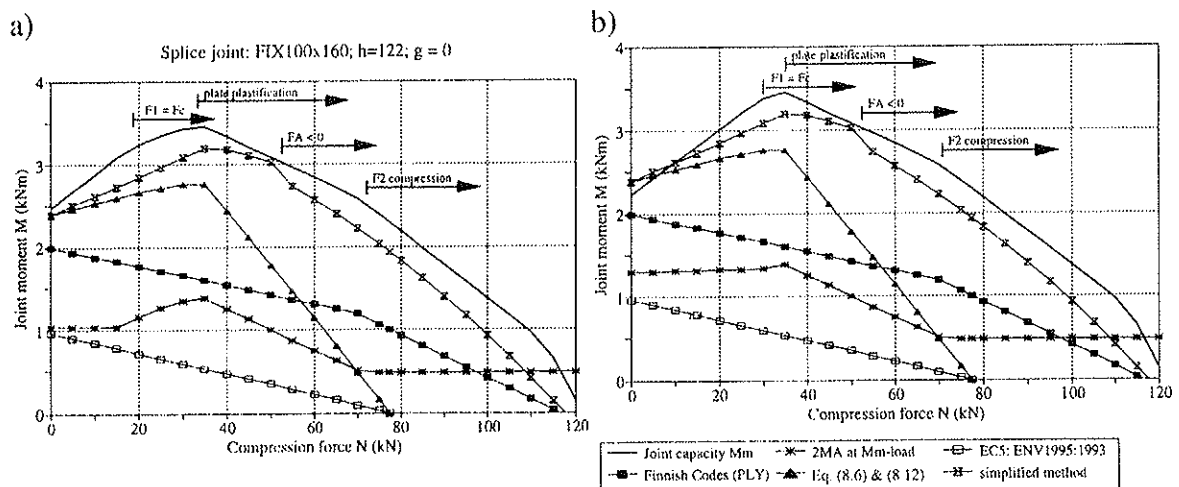


Figure 14 Calculated compression-bending interaction capacity curves of a FIX nail plate splice joint with joint gap values of a) 0 and b) 1.67 mm.

The use of more simplified Equations (1) and (7) with the assumption that half of the compression force is transferred by the timber contact leads to a conservative result, especially with high normal force values. However, it gives much better results than the present Eurocode 5 method. The moment capacity of the compressed splice joint is really low when calculated according to the EC5, as is shown in Figures 14 - 16. The theoretically

calculated maximum moment capacity is normally achieved at the point where failures of the plate on the tension and compression sides are equally critical factors. At this optimum point the moment capacity calculated by EC5 is in all cases less than 20 % of the theoretical maximum moment value, because the bending capacity of EC5 decreases linearly as the compression force increases. The conservatism of the EC5 method is emphasized with the narrow nail plates, as is shown in Figure 15. Also the compression-bending interaction capacity of Edlund's method (the same as the Finnish Code: PLY 1983) is clearly conservative, although it gives much higher capacities than the EC5 method.

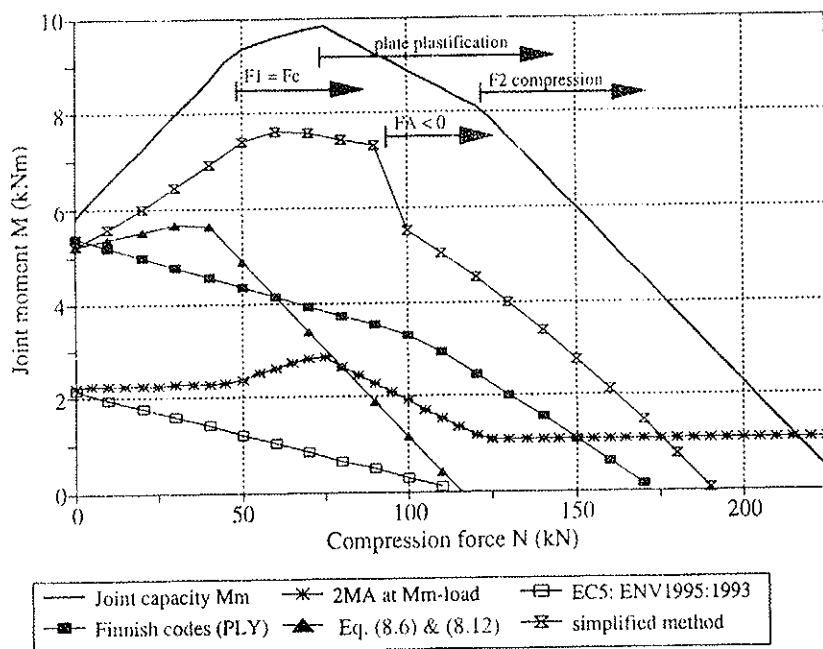


Figure 15 *Compression-bending interaction capacity curves of a FIX nail plate (149x160) splice joint for a chord height of 223 mm with a joint gap of 1 mm calculated by the mean strength values.*

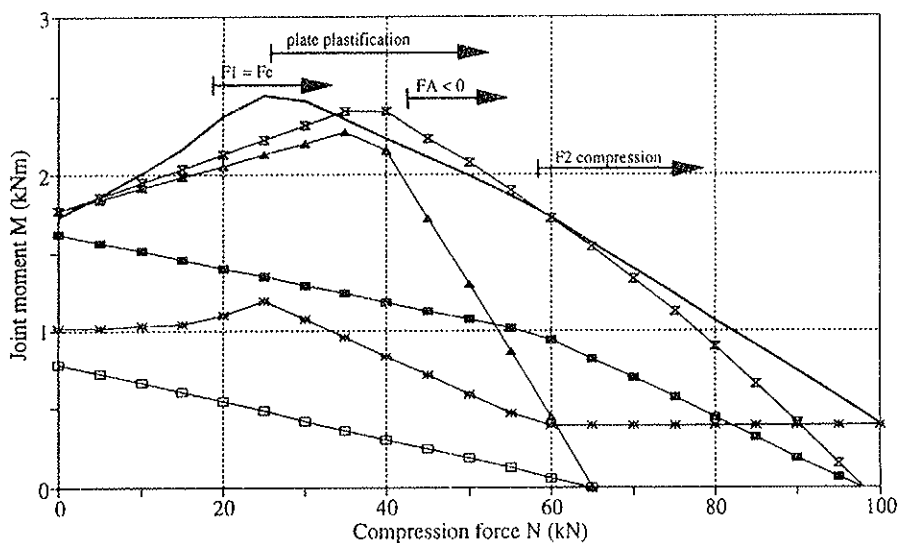


Figure 16 *Compression-bending interaction capacity curves of a W nail plate (96x150) splice joint for a chord height of 100 mm with a joint gap of 1 mm calculated by the mean strength values. The plate capacity of the joint line is the governing condition: by tension capacity when the compression force $N \leq 25$ kN, and otherwise by the plate compression capacity. At load level $N < 42$ kN, the plate normal force F_A is in tension.*

6 Comparison with test results

6.1 Bending tests of FIX nail plate joints

The bending tests of FIX nail plate joints reported here were carried out at Helsinki University of Technology in 1995 by the author. The dimensions of the test specimens and load arrangements are shown in Figure 17. The wood material was Finnish spruce (*Picea Abies*). The densities and the moisture contents of the wood were measured and the mean values are presented in Table 1. Each test series contained five similar test specimens. The test variable was the initial value of the joint gap fixed as follows:

- test series number 0: no gap,
- test series number 1: straight joint gap of 1 mm from edge to edge, and
- test series number 2: diagonal gap of 2 mm on the compression side (Figure 18).

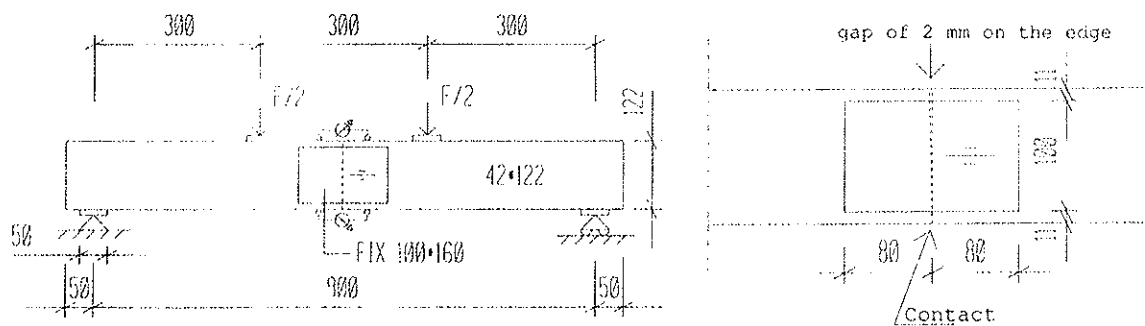


Figure 17 The dimensions of the test specimens and loading arrangements used in the FIX -nail plate bending tests. Figure 18 The joint gap in test series number 2.

The reason for failure in all the tests was anchorage. The timber contact was developed to the compression side in all the tests. In test series number 2 the nail plates buckled on the compression side before the timber contact was achieved. The buckling load was between 7,5 and 9,0 kN. In tests series 0 and 1 no nail plate buckling was observed. The test results and the failure moments adjusted to a moisture content of 15 weight-% and a density of 360 kg/m³ are shown in Table 1. The comparison between the test results and the calculated mean capacities according to the theoretical model, the simplified method, Eurocode 5 and Edlund's method (PLY 1983) are shown.

The comparison presented in Table 1 shows that the theoretically calculated mean capacities have a good agreement with the test results. However, in the tests the effect of the joint gap was not so significant as the theoretical calculations show. The simplified method corresponded well with the test results. The failure mode of the tests (anchorage) was same as was calculated theoretically and with the simplified method.

Table 1 Bending test results and comparisons with the calculated capacities.

Test series	$\rho_{0,m}$ (kg/m ³)	ω (%)	M_{max} (kNm)	M_{mod} (kNm)	Theory M_{mod}/M_{cal}	Simplified M_{mod}/M_{cal}	EC5 -93 M_{mod}/M_{cal}	PLY -83 M_{mod}/M_{cal}
0	370	12,9	2,575	2,383	0,963	0,996	2,461	1,196
1	383	13,1	2,588	2,365	0,998	0,989	2,442	1,187
2	371	13,3	2,428	2,270	1,016	0,949	2,344	1,139
Mean M_{mod}/M_{cal}					0,992	0,978	2,416	1,174

Edlund's compression contact - tension plate force model (PLY 1983) gives smaller capacities, but the difference is not great: the tests results were only 8.22 % higher. The critical factor of PLY's method was the anchorage in tension. The EC5 method was really conservative: the calculated capacities were exceeded on average by a factor of 2.4. The governing condition of EC5 was plate buckling on the compression side of the joint line.

6.2 Bending tests by Leivo (1991)

Mika Leivo tested 150 nail plate joint specimens in his doctoral thesis (1991). The results of the contact test specimens have been analyzed here. In the other bending tests the joint gap was 3 mm, i.e. higher than allowed when the contact is utilized. The W nail plate, size 60x150, was used and the dimensions of the chord members were 45x95 mm². The test results and the comparisons with the theories are shown in Table 2.

The failure mode of the contact test specimens was anchorage, although all the calculations showed that there should be plate tension failure, except in the case of EC5, where buckling failure on the compression side was the critical factor. The theoretical anchorage capacity was a mean value of 8 % higher than the average test result, as shown in Table 2 ("Theory anc."). The lower anchorage capacity may be due to the long-term loading histories of the nail plate joints prior to their failure loading.

The theoretical model ("Theory 1/6") and the simplified method were conservative: the average failure load was about 1.4 times higher than calculated. When the calculations were done on the assumption that the contact point had been sited on the chord edge, they corresponded well with the test results ("Theory 0"). The assumption that the contact point concentrates at a distance of $h/6$ from the chord edge is conservative due to the narrow nail plate ($b/h = 0.63$). However, according to EC5, this joint is not valid for a splice joint, because the b/h relationship should be at least $2/3$. So the presented simplified method is not so conservative in cases of practical splice joints.

Edlund's method (PLY 1983) is in quite good agreement with the test results in this case, because in bending of the narrow nail plate joint the behavior of the joint is close to that in the force-couple model. The Eurocode method is really conservative, because the contact is not utilized in pure bending. The calculated buckling capacity of the nail plates was exceeded in the tests on average by a factor of 3.25.

Table 2 *The moment capacities of Leivo's contact test specimens and the calculated capacities.*

Test series	<i>n</i>	M_{max} (kNm)	M_{mod} (kNm)	Theory 1/6 M_{mod}/M_{cat}	Theory 0 M_{mod}/M_{cat}	Theory anc. M_{mod}/M_{cat}	Simplified M_{mod}/M_{cat}	EC5 -93 M_{mod}/M_{cat}	PLY -83 M_{mod}/M_{cat}
A5a	8	1,197	1,105	1,341	0,953	0,885	1,364	3,130	1,066
A5b	8	1,324	1,232	1,495	1,062	0,986	1,521	3,490	1,188
A6a	8	1,125	1,030	1,250	0,888	0,825	1,272	2,918	0,993
A6b	8	1,344	1,231	1,494	1,061	0,986	1,520	3,487	1,187
C5a	4	1,263	1,160	1,408	1,000	0,929	1,432	3,286	1,119
C5b	4	1,194	1,096	1,330	0,945	0,878	1,353	3,105	1,057
C6a	4	1,285	1,170	1,420	1,009	0,937	1,444	3,314	1,128
C6b	4	1,253	1,140	1,383	0,983	0,913	1,407	3,229	1,099
F5a	9	1,250	1,071	1,300	0,923	0,857	1,322	3,034	1,033
F5b	9	1,444	1,237	1,501	1,066	0,990	1,527	3,504	1,193
Mean M_{mod}/M_{cat}				1,394	0,990	0,920	1,418	3,254	1,108

6.3 Bending tests by Nielsen (1996)

Jacob Nielsen examined bending test splices in his doctoral thesis (1996). The nail plate used was from Gang-Nail Systems, type GNA 20S, with a plate thickness of 1 mm and a tooth length of 8 mm. The dimensions and loading arrangements of test specimens are presented in Figure 19. The timber was Swedish spruce (*Picea abies*) of strength class K-24 according to DS 413. The moisture content of the conditioned wood was about 13 %. The bending tests were performed with three different plate sizes with symmetric and eccentric plate locations. Only the results of the symmetrically jointed test specimens have been analyzed here. The gap size was also a variable in Nielsen's test series BE6, BE7 and BE8, being 0, 0.5 and 0.7 mm, respectively. However, the real gap sizes were measured before the start of the test and they were clearly higher: the average values were 0.5 mm (BE6), 1.0 mm (BE7) and 1.2 mm (BE8), respectively.

The strength and stiffness values of the GNA 20S nail plates have been calculated for the analysis by the author from the tension test results of the GNA 20S plate presented by Nielsen & Rathkjen (1994). The following values were determined: the tension strength of plate $f_{t,0,m} = 263 \text{ N/mm}$, the anchorage strength in the main direction $f_{a,0,0,m} = 3.66 \text{ N/mm}^2$ and in the weakest direction $f_{a,90,0,m} = 1.95 \text{ N/mm}^2$, the translational stiffness modulus in the main direction $K_{F,0,0,ser} = 7.57 \text{ N/mm}^3$, the rotational stiffness modulus as an average value of translational stiffness of the different directions $K_{\phi,ser} = 9.35 \text{ N/mm}^3$ and the ultimate anchorage slip $\delta_u = 1.36 \text{ mm}$. The compression strength value used for the GNA 20S plate, $f_{c,0,m} = 110 \text{ N/mm}$, is estimated from nail plates of the same type.

The bending test results and the comparisons with the theories are shown in Table 3. The failure type was tensile rupture of the plates in each test. The plate buckling was observed during the test in all other cases expect in eight tests of series BE6-8. The initial value of the joint gap of those test specimens was less than 1.1 mm.

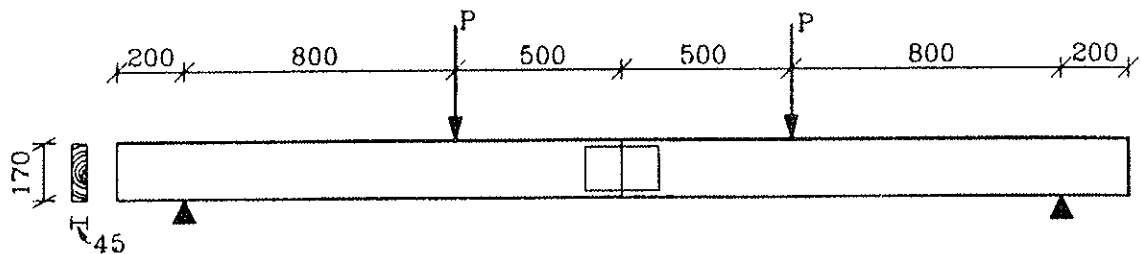


Figure 19 Dimensions of test specimens and loading arrangements (Nielsen 1996).

Table 3 The moment capacities of Nielsen's bending test specimens and the calculated capacities.

Test series	plate size	n	joint gap (mm)	M_{max} (kNm)	M_m (kNm)	Theory M_m/M_{cal}	Simplified M_m/M_{cal}	EC5 -93 M_m/M_{cal}	PLY -83 M_m/M_{cal}
BE1	76x159	5	0,0↔1,3	1,60↔1,84	1,688	1,119	1,482	5,308	0,771
BE3	130x317	5	0,1↔1,0	3,00↔3,32	3,172	1,156	1,123	3,413	0,819
BE6-8	103x159	15	0,0↔1,6	2,28↔3,08	2,619	1,191	1,365	4,488	0,882
Mean M_m/M_{cal}						1,155	1,323	4,403	0,824

The theoretical capacities of the different test series were determined with the measured average joint gap size. The governing condition in the calculations was the plate tension capacity expect with the EC5 method, where the compression strength of the plate was the critical factor. The high conservatism of EC5 is emphasized with the narrow nail plates,

where the buckling capacity of the plates is achieved with a small moment, because the contact pressure is not utilized at all. The comparison presented in Table 3 shows that the theoretical model and the simplified method suits well also for a thin nail plate with the short teeth. The simplified method is more on the safe side with the narrower nail plates, as was also showed theoretically before. However, Edlund's method (PLY) leads to a solution on the unsafe side in all these analyzed cases of the thin nail plate.

6.4 Combined bending and tension tests by Wolfe (1990)

Ronald W. Wolfe has published a study about the load capacity of nail plate joints under combined bending and axial loads (1990). The tests series included a series of pure bending tests (B-series), eccentric tension tests with three different eccentricity levels (C-series) and also a series of centric tension tests (A-series). The original test data files have been available to the author. The detailed test setups are presented by Wolfe, Hall and Lyles (1991). Some strength and stiffness properties of the nail plates used have been determined for the analysis from the tests reported in Stahl, Wolfe, Cramer and McDonald (1994).

The nail plate used was "a 3 by 5.25 inch 20-gauge plate with a tooth density of 9 teeth per square inch" and "the wood used was a medium density southern pine" (Wolfe 1990). The thickness of 20-gauge plate is 0.91 mm, the tooth length is 7.62 mm and there is one tooth per 71.7 mm². Twenty-four teeth had been removed around the center line of each plate. The plate size was 76x133 mm² and the effective plate area A_{ef} was 4300 mm². The test joints had been fabricated using 2 by 4 standard lumber, i.e. the cross section was 38 x 89 mm². The pieces had been tightly butted and held in alignment to produce test specimens that were straight with no gap.

In the axial tension tests (A-series) there were 20 parallel test specimens; 8 of them failed due to yielding of the steel, and the rest failed due to the anchorage. According to the these tests the mean value of the tension strength of 20-gauge plate $f_{t,0,m}$ is 208 N/mm and the anchorage strength $f_{a,0,0,m} = 3.32$ N/mm². The compression strength of the plate, $f_{c,0,m} = 93$ N/mm used in analysis, is calculated from the compression test results of 20-gauge plate with a gap size of 6.35 mm obtained by Stahl & al. (1994).

The force-slip dependence of 20-gauges plate may be presented according to the Foschi's (1977) equation:

$$F = (P_0 + P_1 \delta)(1 - e^{-K\delta/P_0}) \quad (14)$$

The values of constants K , P_0 and P_1 for different loading direction combinations are presented in Stahl & al. (1994) so that they are the best fit between standard test results. The following mean values of strength and stiffness properties of 20-gauge plate used in the calculations have been determined using these values: $f_{a,90,90,m} = 2.30$ N/mm², $K_{F,0,scr} = 12.6$ N/mm³ and $K_{\phi,scr} = 9.5$ N/mm³.

The bending and eccentric tension test results and the comparisons with the theories are shown in Table 4 and graphically in Figure 20. The failure type of all these tests was tensile rupture of the plates. In bending tests, the compression edge strands buckled before the tension edge stands were strained to failure. The theoretical calculations were made also on the assumption that the contact point had been sited on the chord edge (denoted as "Theory 0" in Table 4). They corresponded better with the test results than the calculations made on the assumption that the contact point concentrates at a distance of $h/6$ from the chord edge ("Theory 1/6"). However, the conservatism of the theoretical model, and of the simplified method, seems to result from the higher plastified steel stresses, acting on the joint line in

combined tension and bending, than in the tension strength tests. This is possible because in straight tension, the failure occurs after rupture of the weakest plate strand. In combined - and more over in pure - bending, the probability that the weakest strand locates on the fully plastified area is smaller. This is also the reason why, in this case, PLY's method is in such good accordance with the test result, although theoretically it should be clearly on the unsafe side in combined tension and bending. The situation would probably be different if the anchorage were the critical factor.

The weakness of the EC5 method also in the cases of tension splices with high moments may be seen in Figure 20. The capacity curve of EC5 combined to the simplified method, when the tension force is so high that there is no joint contact according to Equation (5) ($N \geq f_{a,0,0}A_{ef}$). This point of the test joints corresponds with the value of eccentricity $e = M/N = 49,9$ mm.

Table 4 *The results of Wolfe's combined bending and tension tests and the calculated capacities.*

Test series	n	$e = M/F$ (mm)	M_m (kNm)	Theory 1/6 M_m/M_{cal}	Theory 0 M_m/M_{cal}	Simplified M_m/M_{cal}	EC5 -93 M_m/M_{cal}	PLY -83 M_m/M_{cal}
B	10	∞	0,981	1,271	0,902	1,333	3,633	1,158
CH	12	192	0,803	1,191	0,898	1,279	2,677	1,046
CM	10	61,1	0,687	1,294	1,057	1,402	1,753	1,078
CL	10	17,6	0,376	1,241	1,129	1,297	1,297	1,042
Mean M_m/M_{cal}				1,249	0,996	1,328	2,340	1,081

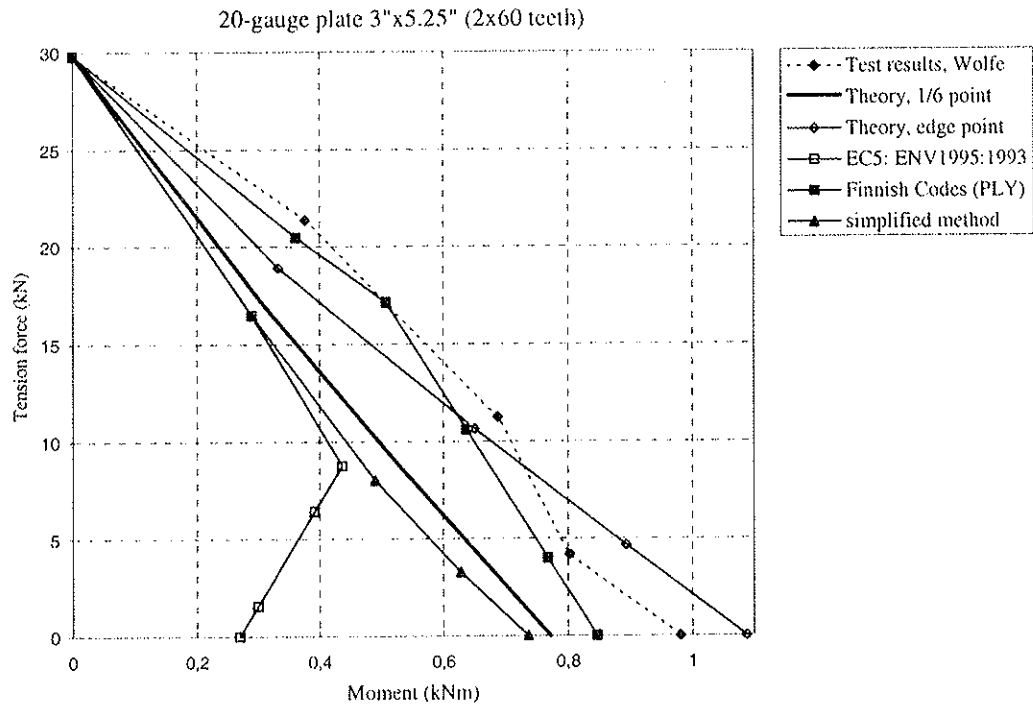


Figure 20 *Combined force-moment capacities by tests and calculations.*

7 Conclusions

In addition of the semi-rigid anchorage stiffness, also the stiffness of the plate in the joint line (plastification), the timber contact and the effect of joint gap on them could be taken into account already in the determination of the member forces and moments of the nail

plate structure. However, this would lead to a heavy iterative design procedure and the influence of these factors on the member forces and moments would not be significant. But very big differences would be observed in the force and moment values acting on the plate if the analysis were done without taking account of the timber contact and the plate plastification (allowed buckling). The effects of these factors may be calculated theoretically with general plate and wood properties and with certain allowed joint gaps. Based on the results of the theoretical calculations it is possible to derive simplified equations for the determination of plate forces and moments.

The results of the analysis of the effect of the timber-to-timber contact in chord splices is shown and the general simplified method of determining the force and moment components acting on the plate in both tension and compression loaded chord splices with the bending moment has been derived. The simplified design method developed was verified with the altogether 148 bending and eccentric tension tests of different kinds of nail plate joints. The simplified method corresponds well with the test results of anchorage failure, and it is on the safe side when the plate capacity of the joint line is the critical factor. The conservatism of the calculation method is due to the higher plate tension stresses developed in bending than determined in axial tension tests.

Eurocode 5 (1993) does not give any rules for the utilization of the timber contact in bending and, together with the weak compression strength of nail plates, this leads to a very conservative design results in bending joints. The failure loads of the bending tests were 2,4..5,3 times higher than the capacities calculated by EC5 with the mean strength values, and the difference is further emphasized in combined compression and bending. The very simple assumption that 50 % of the bending moment of joint transfers through the contact couple and 50 % by the moment stresses of the nail plate, solved with the compression splices (Equations (1&7)), leads to much better results, as shown in the example of Figure 21. However, EC5 is conservative also in combined tension and bending, if the bending moment is so high that there is contact pressure on the compression side of the joint, which has been shown also by the analysis of the eccentric tension test results of Wolfe (1990).

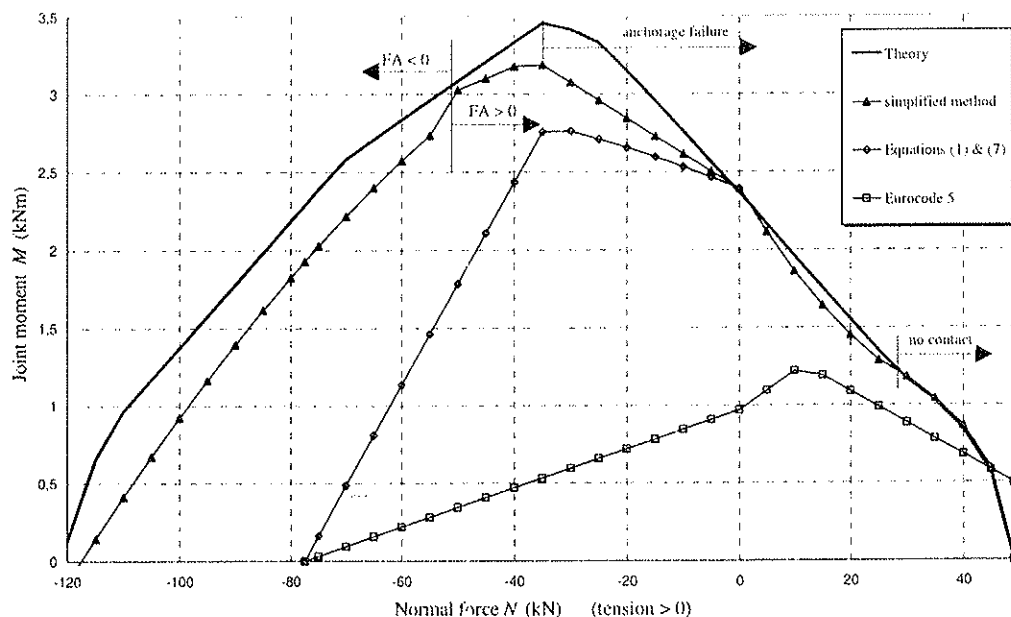


Figure 21 *Moment-normal force capacity curves with different calculation methods for a FIX100x160 splice joint with a 122 mm chord height and a 1 mm joint gap. The calculations have been made with the mean strength values.*

The simplified Equations (1) - (13) presented here are included in the new Finnish Design Code for Nail Plate Structures (RTL 1998), which was accepted and taken into use on May 6, 1998. The new Finnish design rules are based on Eurocode 5, and we hope that the rules of splice joint design will be improved also in the conversion to the official EN standard of ENV 1995-1-1.

References

- Edlund, G., 1971, Längdskarning av träbalkar med spikplätsförband. Statens institut för byggnadsforskningen. Rapport R40. Stockholm. 236 p.
- Edlund, G., 1973, Spikplåtar som förbindare i träfackverk. Statens institut för byggnadsforskningen. Rapport R52. Stockholm. 326 p.
- ENV 1995-1-1, 1993, Eurocode 5 - Design of Timber Structures - Part 1-1: General Rules for Buildings. CEN Brussels. 110 p.
- Foschi R., 1977, Analysis of Wood Diaphragms and Trusses. Canadian Journal of Civil Engineering, 4(3) 345 - 362.
- Kangas, J. & Kevarinmäki, A., 1995, Joints with punched metal-plate fasteners. In: Blass, H. J., Görlacher, R., Steck, G., eds. Holzbauwerke: STEP 3. Arbeitsgemeinschaft Holz e.V., Düsseldorf, Germany. pp. 10/1-10/31.
- Kevarinmäki, A., 1996, Moment Capacity and Stiffness of Punched Metal Plate Fastener Joints. Proceedings of the International Wood Engineering Conference 1996. New Orleans, Louisiana, USA. pp. 1:385-392.
- Kevarinmäki, A. & Kangas, J., 1995, Moment capacity and rotational stiffness of punched metal plate fastener joints. Proceedings of the fifth international symposium: Wood in Engineering Structures. Kocovce, Slovak. Republic. pp. 207 -224.
- Leivo, M., 1991, On the Stiffness Changes in Nail Plate Trusses. VTT Publications 80. Espoo, Finland. 192 p.
- Nielsen, J., 1996, Stiffness analysis of nail-plate joints subjected to short-term loads. Structural design paper no. 2. Institut for Bygningsteknik, Depart. of Building Technology and Structural Engineering, Aalborg Universitetscenter. Aalborg, Denmark. 173 p.
- Nielsen, J. & Rathkjen, 1994, Laterally loaded nail-plates. Structural design paper no. 1. Institut for Bygningsteknik, Depart. of Building Technology and Structural Engineering, Aalborg Universitetscenter. Aalborg, Denmark. 41 p.
- Puurakenteiden laadunvalvontayhdistys PLY ry [The Quality Control Association for Timber Structures], 1983, Naulalevyrakenteiden suunnitteluohjeet [Design Rules for Nail Plate Structures]. NR-toimikunta, Espoo, Finland. 22 p.
- Rakennustuotteiden laatu RTL ry [The Association of Building Materials Quality RTL], 1998, Naulalevyrakenteiden suunnitteluohjeet [Design Rules for Nail Plate Structures]. 6.5.1998, Helsinki, Finland. 50 p.
- Stahl, D., Wolfe, R., Cramer, S. & McDonald, D., 1994, Strength and Stiffness of Large-Gap Metal-plate Wood Connections. Forest Products Laboratory, Research Paper FPL-RL-535. Madison, USA. 9 p.
- Wolfe R., 1990, Metal-plate connections loaded in combined bending and tension. Forest Products Journal, vol. 40, No. 9. pp. 17-23.
- Wolfe, R., Hall, M. & Lyles, D., 1991, Test Apparatus for Simulating Interactive Loads on Metal Plate Wood Connections. Journal of testing and evaluation, vol. 19, No. 6. pp. 421-428.

CIB-W18/31-7-6

**INTERNATIONAL COUNCIL FOR BUILDING RESEARCH STUDIES AND DOCUMENTATION
WORKING COMMISSION W18 - TIMBER STRUCTURES**

THE FASTENER YIELD STRENGTH IN BENDING

by

A Jorissen
Delft University of Technology

THE NETHERLANDS

H J Blaß
University of Karlsruhe

GERMANY

MEETING THIRTY-ONE

SAVONLINNA

FINLAND

AUGUST 1998

The fastener Yield Strength in Bending

A. Jorissen

Delft University of Technology, The Netherlands

H.J. Blass

University of Karlsruhe, Germany

Introduction

The strength of single fastener connections with dowel type fasteners is, in Europe, determined according to the Yield Model, first presented by K.W. Johansen (1949). The fastener's yield capacity and the embedment strength are both governing material properties.

The fastener's yield capacity in bending is often determined according to prEN 409 (1994). Although the method, described in this standard, is meant for nails with a diameter < 8 mm, it is also used for other dowel type fasteners, e.g. bolts. It is discussed whether using this method for diameters > 8 mm is recommendable or not.

ENV 1995-1-1: 1993 (Eurocode 5)

For round steel bolts ENV 1995-1-1:1993 (Eurocode 5, 1994) requires that the characteristic value for the yield moment $M_{y,k}$ is calculated according to equation (1).

$$M_{y,k} = \frac{0.8 f_{u,k} d^3}{6} \quad (1)$$

Where: $f_{u,k}$ the characteristic tensile strength.

Apparently, the fastener yield strength in bending is assumed as $f_y = 0.8 f_u$, which is shown in figure 1.

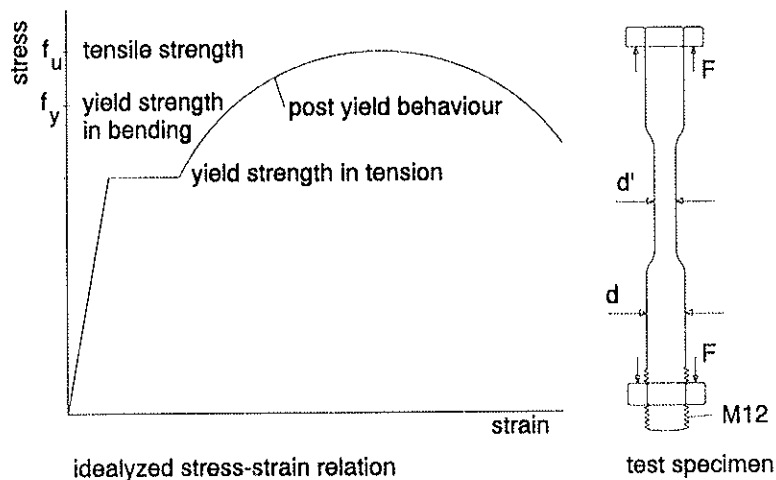


Figure 1: Idealized stress-strain relation for mild steel bolts in tension and the test specimen used to determine this relation.

The idealized stress-strain relation as shown in figure 1 is obtained with tension tests. The test specimens used in the research described in this paper are also shown in figure 1.

The fastener yield strength in bending is calculated according to equation (3).

$$f_u = \frac{4 F_{\max}}{\pi (d')^2} \quad (2)$$

$$f_y = 0.8 f_u \quad (3)$$

prEN 409: 1993

The bolt yield strength in bending is frequently determined according to prEN 409: 1993 (1994), although the method described in this standard is only meant for nails with a diameter < 8 mm. According to prEN 409 the yield capacity in bending is defined as: "bending moment at the maximum load sustained by a nail under test, or the bending moment at which the nail has deformed through an angle of 45°, whichever is the lesser".

Several bolt bending tests according to prEN 409 were carried out at the University Fridericiana in Karlsruhe. The moment-bending angle relations for all tests are similar and shown in figure 2.

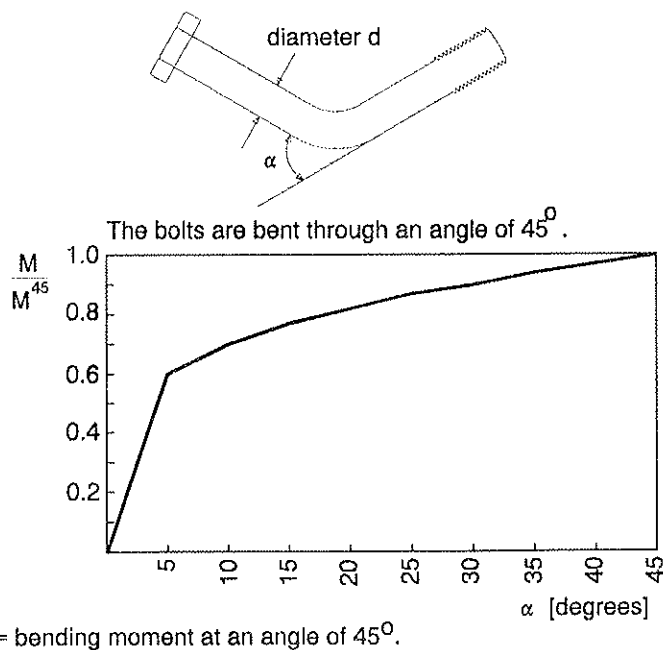


Figure 2: Bolts tested to determine the yield capacity in bending according to prEN 409.

When bolted connections ($d > 8$ mm) are tested to failure, an angle of 45° is not reached, even not when slender bolts are used. Especially in multiple fastener connections, the angle at failure load is much lower (see table 2). Consider, for

example, an angle of 15° at failure load. According to the moment-angle graph shown in figure 2, about 75% of $M^{45} = M_y$, where M_y is the full plastic bending moment, is reached. For failure mode 3 according to the Johansen's Yield Model (1949), the load carrying capacity is reduced most compared to the value determined with full plastic bending capacity ($= M_y$), see figure 3. For failure mode 2, the reduction in load carrying capacity is less. The bending capacity does not affect the load carrying capacity of connections with rigid fasteners (failure mode 1). The failure deformations of bolts at different failure modes are shown in figure 5. The yield capacity in bending is determined according to equation (4).

$$f_y = \frac{6 M_y}{d^3} \quad (4)$$

Influence of the bending angle on the load carrying capacity

Since the fastener bending moment increases with the bending angle, the failure load and the failure mode are both affected by this angle: failure mode 3 at low angles ('low' load) and failure mode 2 at high angles ('high' load), which is shown by the slenderness ratio obtained with equation (5). An example is given in figure 3.

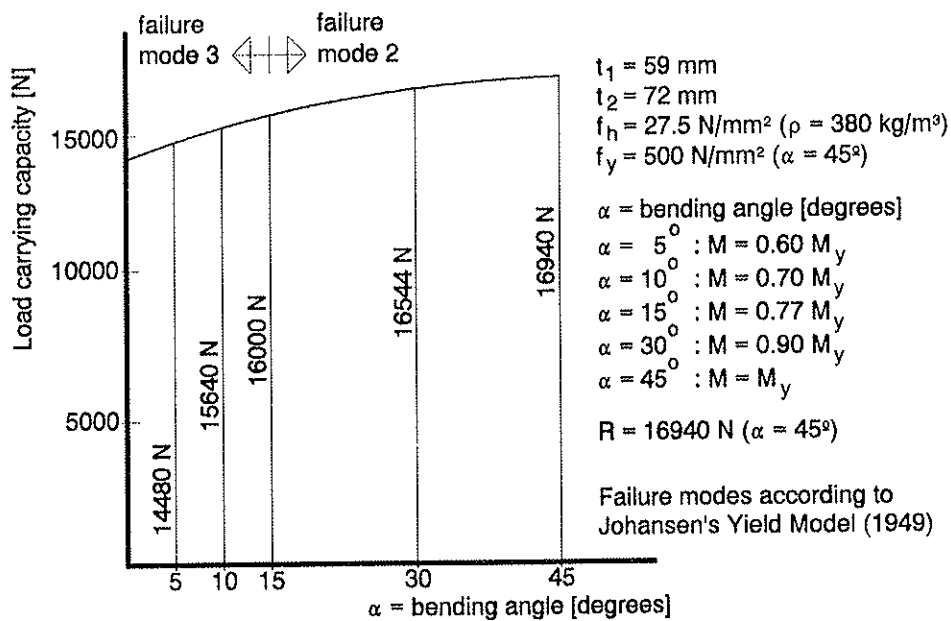


Figure 3: Influence of the bending angle.

Figure 3 shows that for $\alpha = 5^\circ$ the load carrying capacity is reduced to 87% of the calculated capacity according to the Yield Model with full plastic bending capacity.

For slenderness ratio's smaller than obtained with equation (5), failure mode 2 is governing (rigid fasteners i.e. failure mode 1 is not considered), otherwise failure mode 3 is governing.

$$\lambda = 1.39 \sqrt{\frac{f_y}{f_h}} \quad (5)$$

It is assumed that the embedment strength is always reached for $\alpha > 0^\circ$. Consequently, for lower values of f_y , i.e. for lower bending angles, failure mode 3 is reached at a lower slenderness ratio. The example given in figure 3 shows that with the given timber sizes and bolt diameter (given slenderness ratio) failure mode 2 is expected if the full bending moment M_y can be obtained, failure mode 3 is obtained at smaller moments, i.e. smaller bending angles.

The yield capacity in bending

Both methods for the determination of the yield capacity in bending (Eurocode 5 and prEN 409), equations (3) and (4), are used. Only bolts M12 were tested. The results are given in table 1.

d mm	length mm	mark on bolt head	f_y				$\frac{Eq. (4)}{Eq. (3)}$
			prEN 409 equation (4)		Eurocode 5 equation (3)		
			mean N/mm ²	c.o.v. %	mean N/mm ²	c.o.v. %	
10.65	130	4.6 z	552	0.2	330	6	1.67
	140	-	631	0.7	466	2	1.35
	160	-	625	0.2			
11.75	120	6.8 gfd	680	20	420	4	1.62
	220	4.6	514	7			

Table 1: Yield capacity in bending according to equations (3) and (4).

The yield capacity in bending according to prEN 409 (equation (4)) is considerably higher than obtained with the tension test according to figure 1 (equation (3)), which partly can be explained by the post yielding behaviour: while testing in bending, the cross section is partly loaded beyond the yield strength. Therefore, Eurocode 5 assumes $f_y = 0.8 f_u$, which is higher than the yield strength in tension.

Furthermore, the cross section reduces during the tension test when it is loaded beyond the yield strength. Since the tension strength according to equation (2) is calculated using the original bolt diameter d' , the actual tension strength is higher than calculated. Based on these considerations, it can be concluded that the determination of the yield capacity in bending with a bending test, i.e. prEN 409, is closer to reality than based on a tension test.

Bending angles recorded

The bending angles presented in table 2 are obtained from about 950 tests on symmetrical timber-to-timber connections with one to nine bolts M12.

The deformation of a dowel type fastener depends on the fastener slenderness, which is, for the timber middle member, shown in figure 4, i.e. (a) low slenderness (rigid) results in hardly any deformation and (c) high slenderness results in high deformation.

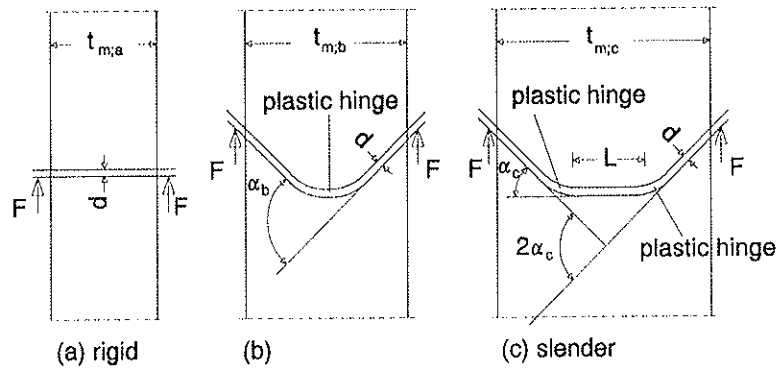


Figure 4: Deformation of a dowel type fastener in the middle member depending on the fastener slenderness.

Figure 2 shows the deformed shape of the dowel type fastener (bolt) after testing according to prEN 409, which equals the deformed shape of the fastener shown in figure 4 (b): angle = α_b . Figure 4 (b) can be considered as figure 4 (c) with $L = 0$, which results in $\alpha_b = 2\alpha_c$. Consequently, to determine the fastener yield capacity in bending the angle shown in figure 2 must be divided by two.

The bolts in the symmetrical connections deform in three different ways with shapes shown in figure 5 and defined by Johansen (1949).

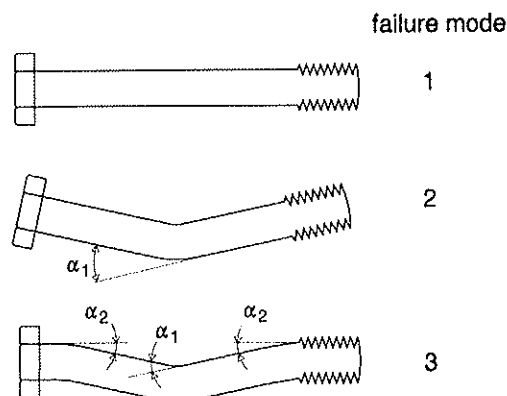


Figure 5: Bolt (dowel) deformation observed at the three different failure modes.

To obtain the yield moment determined by the bending angle α_1 , $\frac{1}{2}\alpha_1$ must be taken in stead of α_1 , as discussed in relation to figure 4.

The scatter in bending angles recorded is large, see table 2, which can be explained by the scatter in timber properties and by the low size and strength requirements for the M12 bolts.

d mm	t ₁ mm	t ₂ mm	n	a ₁ mm	a ₃ mm	angle		
						$\frac{1}{2}\alpha_1$ °		α_2 °
						mean°	c.o.v. %	
10.65	24	48	1		84	14	29	10
11.25	24	48	3	60	60	12	49	
			3	60	84	13	62	
			3	84	84	12	20	
			3	132	84	18	26	
11.75	24	48	5	60	84	10	51	
			9	60	84	4	48	
			9	84	84	9	36	
			9	132	84	5	79	
			9	60	60	0		
			9	84	60	5	89	
10.65	59	72	3	60	60	7	35	
			3	60	84	9	19	
			3	84	84	14	29	
11.75	59	72	1		84	24	12	
			5	36	84	3	73	
			5	60	84	8	19	
			5	84	84	5	66	
			5	60	60	11	13	
			5	84	60	11	20	
			9	60	84	5	44	
			9	84	84	7	27	
			9	132	84	9	33	
			9	60	60	5	39	
			9	84	60	8	27	

Table 2: Bending angles recorded.

Table 2 shows that, even for single fastener connections, an angle of 45° is never reached. Consequently, the fastener yield capacity in bending reached in tests on double shear connections is less than determined according to prEN 409. For multiple fastener connections table 2 shows that the average bending angle ($= \frac{1}{2}\alpha_1$) does not exceed 5° to 10°. The fastener yield capacity in bending considered for Johansen's Yield Model is only 60% to 70% of the value determined according to prEN 409, see figure 2, which

results in equation (6).

$$M_y < 0.70 M^{45} \quad (6)$$

Consequently, prEN 409 can only be applied to large diameter dowel type fastener for low bending angles.

For $M_y = 0.70 M^{45}$, table 2 changes in table 3.

Table 3: Yield capacity in bending according to equations (3) and (4).

d mm	length mm	mark on bolt head	f_y			
			prEN 409 equation (4)		Eurocode 5 equation (3)	
			mean N/mm ²	c.o.v. %	mean N/mm ²	c.o.v. %
10.65	130	4.6 z	386	0.2	330	6
	140	-	442	0.7	466	2
	160	-	438	0.2		
11.75	120	6.8 gfd	476	20	420	4
	220	4.6	360	7		

Note: in equation (4) $M_y = 0.70 M^{45}$.

Table 3 shows that the values based on the bending test described in prEN 409 [3] (equation (4)) and the values determined with a tension test and Eurocode 5 [2] (equation (3)) do reasonably agree with each other.

Summary and conclusion

In this paper the determination of the fasteners yield strength in bending for large diameter dowel type fasteners is discussed. ENV 1995-1-1: 1993 (1994) requires a tension test. A bending test for small diameters, (nails) is described in prEN 409: 1993 (1994), which is also frequently used for large diameters.

Since dowel type fasteners are loaded in bending, a bending test prevails for large diameter dowels also. However, since the bending angle required in prEN 409 (= 45°) is never reached for large diameters, this required angle should be reduced (e.g. 10°).

The factor 0.8 in equations (1) and (3) given in Eurocode 5 seems to reflect bending angles reached at failure load reasonable well.

Symbols

Main symbols:

t_1	thickness of the timber side members
t_2	thickness of the timber middle member
F	load
M	bending moment
R	resistance
f	strength
d	diameter
n	number of fasteners in the row in the load direction (parallel to the grain)
a_1	spacing
a_3	end distance
α	angle
ρ	density

Subscripts:

h	embedment
u	ultimate
y	yield
k	characteristic

Acknowledgements

This research is supported by the Dutch Technology Foundation (STW).

References

Johansen, K.W. *Theory of timber connections*. International Association of Bridge and Structural Engineering, Publication 9:249-262, 1949.

ENV 1995-1: 1993 (Eurocode 5). *Design of timber structures. Part 1-1: General rules and rules for buildings*. Comité Européen de Normalisation, Brussels, Belgium, 1994.

prEN 409: 1993. *Timber structures - Test methods - Determination of the yield moment of dowel type fasteners - Nails*. Comité Européen de Normalisation, Brussels, Belgium, 1994.

CIB-W18/31-7-7

**INTERNATIONAL COUNCIL FOR BUILDING RESEARCH STUDIES AND DOCUMENTATION
WORKING COMMISSION W18 - TIMBER STRUCTURES**

**A PROPOSAL FOR SIMPLIFICATION OF JOHANSEN'S FORMULAE,
DEALING WITH THE DESIGN OF DOWELLED-TYPE FASTENERS**

by

F Rouger

CTBA

FRANCE

MEETING THIRTY-ONE

SAVONLINNA

FINLAND

AUGUST 1998

A proposal for simplification of Johansen's formulae, dealing with the design of dowelled-type fasteners

by Frédéric ROUGER¹

Abstract.

In Eurocode 5, design equations of dowel-type fasteners are based on the theory of plasticity. Experiments have shown that these equations are well calibrated for single fasteners, but unsafe for multiple fasteners, especially in the case of timber failures. One idea to compensate this problem is to tend to more ductile fasteners, involving more plasticity. This paper proposes a simplification of design equations, especially in the case of mixed modes of failure. This approach is based on numerical methods, and therefore quite different from the original mechanical model. The proposed equations are easy to use, but contain an additional safety margin due to the approximations which are made. This safety can be further calibrated by adjusting the design equations for multiple fasteners.

Introduction.

In the design of connections, equations have been formulated by Johansen [1] on the basis of plasticity. They are incorporated in Eurocode 5 [2]. These equations have shown to be efficient for single fasteners, but difficult to handle. Different researchers have tried to simplify the approach ([3], [4]). This paper presents a new way of simplification, efficient but conservative for failure modes involving timber. At the present stage, the analysis was done for single and double shear connections. It will be easy to extend it for other cases.

1. Double shear connections.

1.1. Design equations according to Eurocode 5.

In Eurocode 5, the design equation for a double shear connection is given by :

$$R_d = \min \left\{ \begin{array}{l} 1, 1 \frac{f_{h,1,d} t_1 d}{2 + \beta} \left[\sqrt{2\beta(1 + \beta) + \frac{0.5 f_{h,1,d} t_2 d \beta}{f_{h,1,d} d t_1^2}} \frac{f_{h,1,d} t_1 d}{0.5 f_{h,1,d} t_2 d \beta} - \beta \right] \\ 1, 1 \sqrt{\frac{2\beta}{1 + \beta}} \sqrt{2 M_{y,d} f_{h,1,d} d} \end{array} \right. \quad (1)$$

where $f_{h,1,d}$ is the design embedding strength of lateral elements,
 $f_{h,2,d}$ is the design embedding strength of the central element,
 d is the fastener diameter,
 t_1 and t_2 are the thicknesses of lateral and central elements,
 $M_{y,d}$ is the design yield moment of the fastener,

¹ Centre Technique du Bois et de l'Ameublement, Pôle Construction, Unité Etudes et Recherche
Laboratoire de Rhéologie du Bois de Bordeaux (INRA, CNRS, Université Bordeaux I), DRA CNRS

$$\beta = f_{h,2,d} / f_{h,1,d}$$

The four equations represent failure modes **g**, **h**, **j** & **k** (see Figure 1)

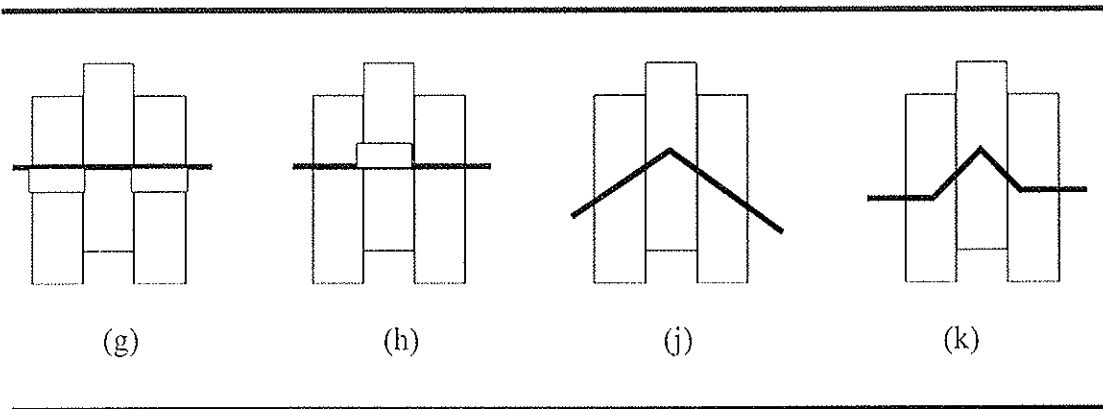


Figure 1 : Failure modes of a double shear connection

1.2. The Möller approach [5]

We can consider as a first step that modes **g** and **h** are strictly symmetrical, by replacing t_1 by $t_2/2$. We will consider in the following modes **g**, **j** & **k**. According to Möller, these equations can be represented graphically, by changing definitions :

$$k_1 = \frac{t_1 \sqrt{f_{h,1,d}}}{\sqrt{M_{y,d} / d}} \quad (2)$$

and

$$R_d = k_2 \sqrt{M_{y,d} f_{h,1,d} d} \quad (3)$$

In this case, k_2 is a function of k_1 , according to :

$$k_2 = \min(A(k_1, \beta)) \quad (4)$$

and

$$A(k_1, \beta) = \frac{k_1}{2 \cdot \beta} \cdot \frac{2 \cdot \beta \cdot (1 - \beta) \cdot k_1^2 + 4 \cdot \beta \cdot (2 - \beta) \cdot \beta}{k_1^2 + 1 - \beta} \quad (5)$$

Figure 2 shows $k_2 = f(k_1)$ for $\beta = 1.0$

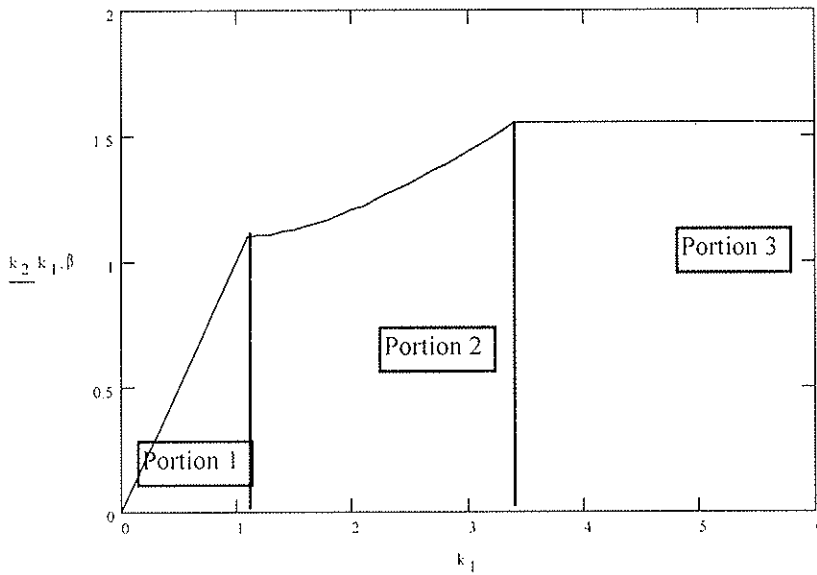


Figure 2 : Möller curve

1.3. Numerical approach for simplification of the equations.

Experimental investigations have shown that the equations which are described above work well for single fasteners, but not for multiple fasteners, especially in the case of timber failures. One idea to compensate this problem is to tend to more ductile fasteners, involving more plasticity. If we are also concerned with simplification of the equations, one come to the following proposal : the first two portions of the curve (corresponding to brittle and mixed failure) could be replaced by a straight line starting from the origin and ending at the beginning of portion 3 (corresponding to ductile failure). To know this point, we have to calculate this intersection point between portions 2 & 3, which is given by :

$$f(k_1, \beta) = 1.1 \cdot \frac{k_1}{2 \cdot \beta} - 2 \cdot \beta \cdot (1 - \beta) - \frac{4 \cdot \beta \cdot (2 - \beta)}{k_1^2} - \beta = 0 \quad (6)$$

The equation $f(k_1, \beta) = 0$ will give the value of k_1 corresponding to the intersection. As we see, the solution will be a function of β , and is not obvious to find. Therefore, we have to fix an interval for β . As β reflects the ratio between the embedding strengths of lateral and central elements, we can assume that it varies between 0.3 and 3.0. Therefore, we have varied β between 0.1 and 5.0 (these values can be changed easily) and solved equation (6) on this interval. The solution is noted $k_{1, \text{sol}}$. The variation of $k_{1, \text{sol}}$ as a function of β is shown in Figure 3.

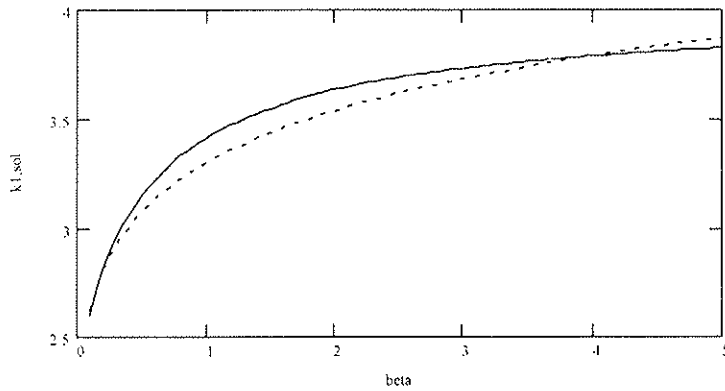


Figure 3 : $k_{1,sol} = f(\beta)$

It seems obvious that k_1 is a power function of β . Therefore, we have fitted a function of this form :

$$k_1(\beta) = u_0 \beta^{\frac{1}{u_1}} \quad (7)$$

The result of this fit (dashed line in Figure 3) is given below :

$$u_0 = 3.3 \quad u_1 = 10$$

According to this solution, we have a new Möller curve, which for $\beta = 1.0$, is illustrated in Figure 4. The variable k_3 represents the simplified model made with two straight lines. The variation of this model with β is illustrated in Figure 5.

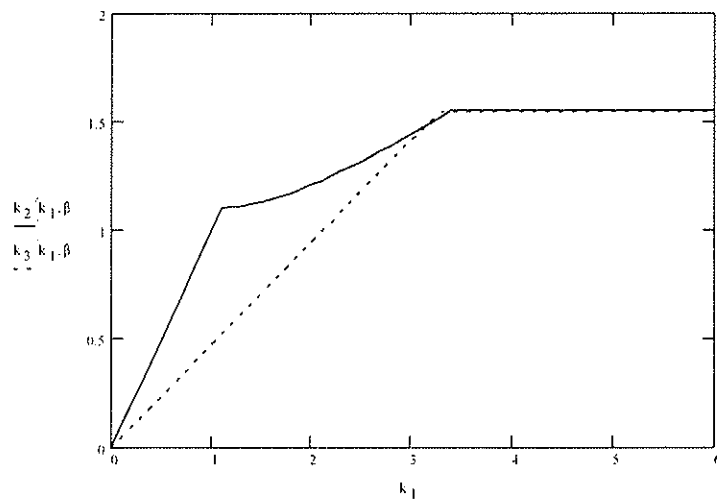


Figure 4 : Modified Möller curve.

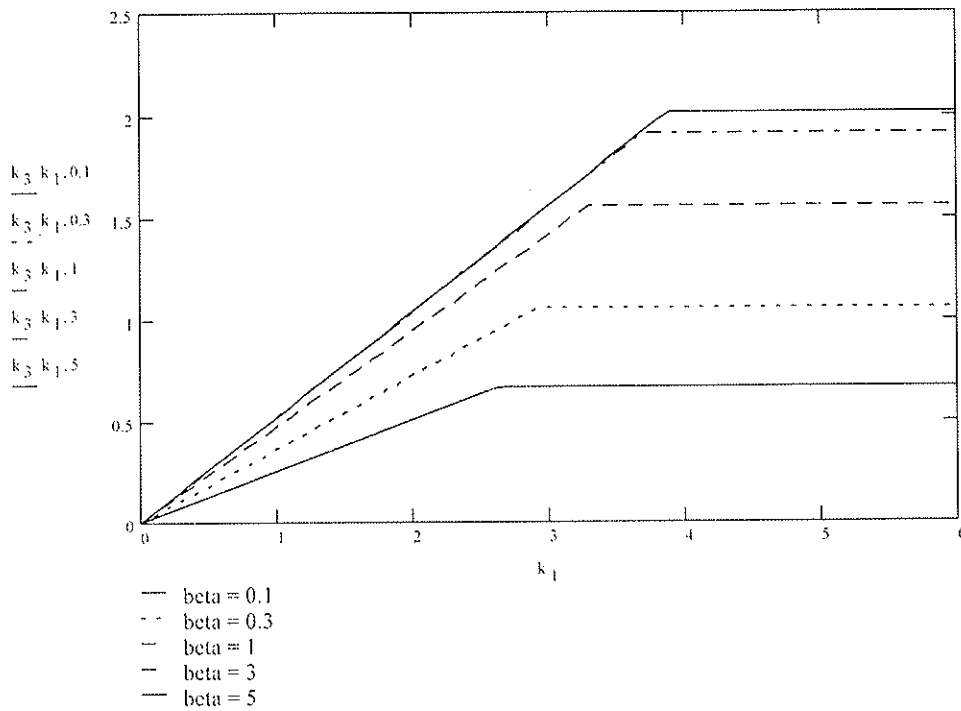


Figure 5 : Simplified model as a function of β

In order to evaluate the simplification, we can calculate the minimum ratio between the simplified model and the initial one. In the case of double shear, this ratio is a function of β , illustrated in Figure 6.

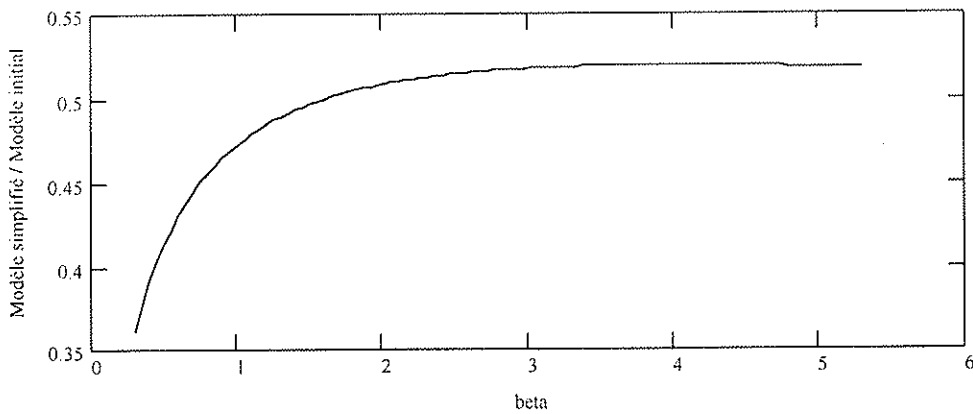


Figure 6 : Minimum ratio between simplified and initial models, double shear.

Note : Further investigation shows that equation (7) can be replaced by an exact solution which is given by :

$$k_1(\beta) = 2 \left(1 + \sqrt{\frac{\beta}{1+\beta}} \right)$$

1.4. Simplified design equations in Eurocode 5.

According to this assumption, the new design equations for double shear connections would be :

$$R_d = \sqrt{\frac{4\beta}{1+\beta}} \min \left\{ \begin{array}{l} \frac{1}{3} \beta^{-0.1} t_1 d f_{h,1,d} \\ \frac{1}{6} \beta^{-0.1} t_2 d f_{h,2,d} \\ 1,1 \sqrt{M_{y,d} f_{h,1,d} d} \end{array} \right. \quad (8)$$

We will note for this equation and in the following modes **a'**, **b'**, **c'**, each of these modes representing the following simplifications :

- Mode a' : simplification of modes g & j
- Mode b' : simplification of modes h & j,
- Mode c' : Mode k

2. Single shear connections.

2.1. Design equations according to Eurocode 5.

In Eurocode 5, the design equation for a single shear connection is given by :

$$R_d = \left\{ \begin{array}{l} \frac{f_{h,1,d} t_1 d}{1+\beta} \left[\sqrt{\beta + 2\beta^2 \left[1 + \frac{t_2}{t_1} + \left(\frac{t_2}{t_1} \right)^2 \right] + \beta^3 \left(\frac{t_2}{t_1} \right)^2} - \beta \left(1 + \frac{t_2}{t_1} \right) \right] \\ 1,1 \frac{f_{h,1,d} t_1 d}{2+\beta} \left[\sqrt{2\beta(1+\beta) + \frac{4\beta(2+\beta) M_{y,d}}{f_{h,1,d} d t_1^2}} - \beta \right] \\ 1,1 \frac{f_{h,1,d} t_2 d}{1+2\beta} \left[\sqrt{2\beta^2(1+\beta) + \frac{4\beta(1+2\beta) M_{y,d}}{f_{h,1,d} d t_2^2}} - \beta \right] \\ 1,1 \sqrt{\frac{2\beta}{1+\beta}} \sqrt{2 M_{y,d} f_{h,1,d} d} \end{array} \right. \quad (9)$$

where the six equations represent different modes of failure, i.e. **a**, **b**, **c**, **d**, **e** & **f**. (see Figure 7)

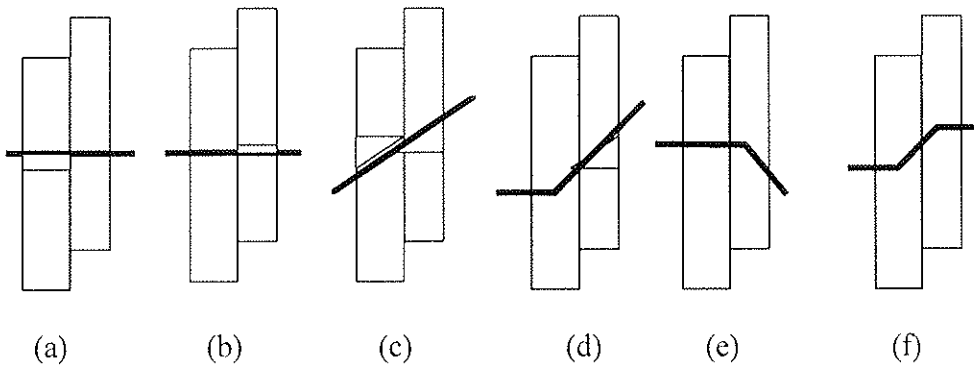


Figure 7 : Failure modes for a single shear connection

2.2. Consideration of mode c.

If we use the approximations which have been made for double shear connections, we can notice the following

- Modes **a** & **d** are replaced by mode **a'**
- Modes **b** & **e** are replaced by mode **b'** (for mode **b'**, we replace $t_2/2$ by t_2)
- Mode **f** is replaced by mode **c'**

The only mode we have to investigate is mode **c**, which, in the Möller diagramme, can also be represented by a straight line starting from the origin. If we want to use only the equations corresponding to double shear, we have to know if the slope of mode **c** is lower than the one of modes **a'** & **b'** (in this case, mode **c** would become the governing mode). As we saw previously, modes **a'** & **b'** are identical, excepting a subscript permutation. Therefore, we can investigate modes **a'** et **c**. The slope ratio between modes **c** & **a'** is given by :

$$f(\alpha, \beta) = \frac{1 - \beta}{1 + \beta} \cdot \frac{1 - \beta \cdot 2 \cdot \beta^2 \cdot 1 - \alpha + \alpha^2 + \beta^3 \cdot \alpha^2}{1 + \beta} \cdot \beta \cdot (1 - \alpha) \quad (10)$$

where $\alpha = t_2/t_1$ and $\beta = f_{h,2,d} / f_{h,1,d}$

As we consider that mode **a'** is governing mode **b'**, we have :

$$f_{h,1,d} t_1 \leq f_{h,2,d} t_2 \quad (11)$$

or :

$$\beta > 1/\alpha$$

So, when we fix a value for α , we can vary β from $1/\alpha$ to a given value. Two examples ($\alpha = 1.0$ and $\alpha = 0.298$) are given in Figure 8 and Figure 9. We see that the values of β for which

the slope ratio is less than 1 are very few. Therefore, we can think about detecting the minimum value of f , as a function of α . The result is illustrated in Figure 10.

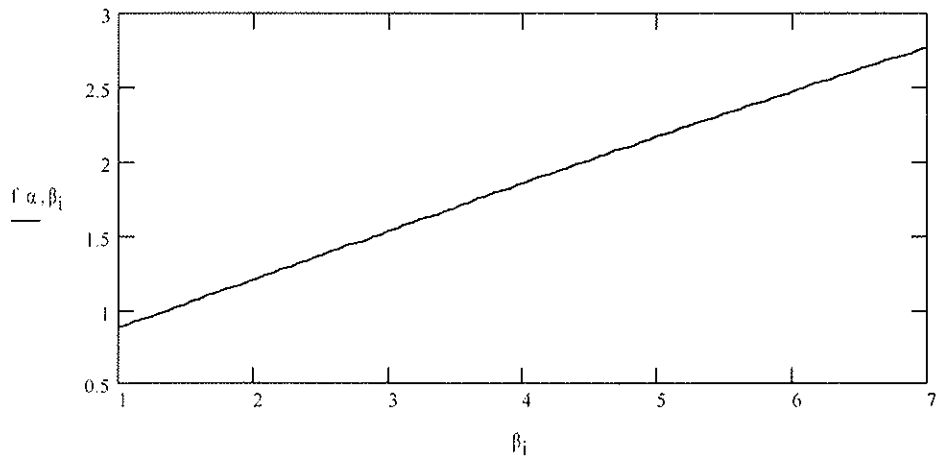


Figure 8 : Slope ratio for $\alpha = 1.0$

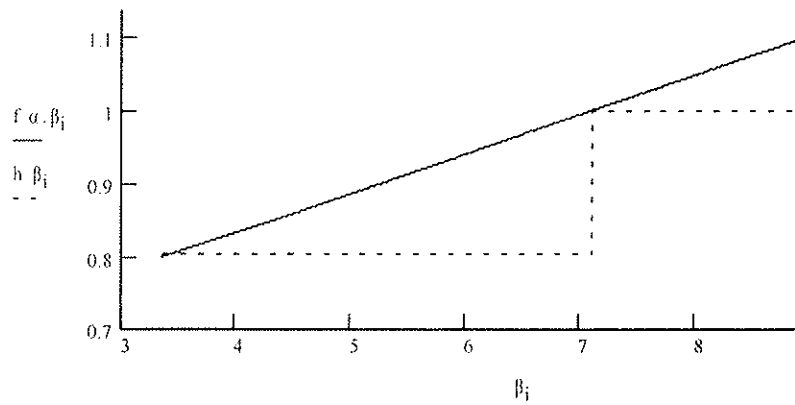


Figure 9 : Slope ratio for $\alpha = 0.298$ (dashed line corresponds to equation (15))

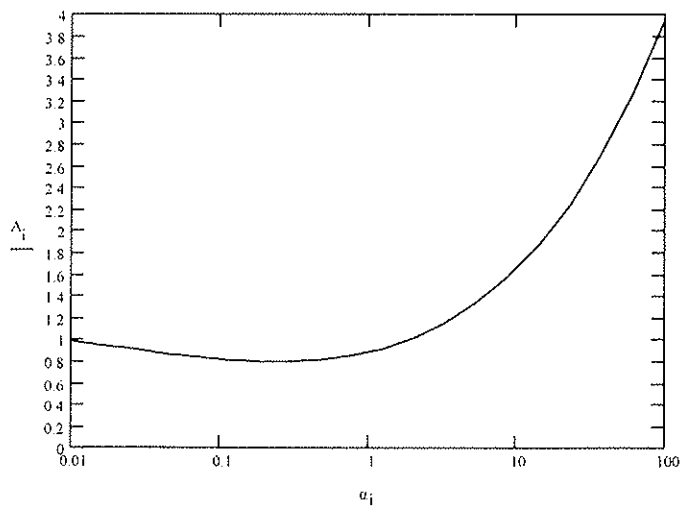


Figure 10 : Minimum slope ratio (Min $f(\alpha)$)

The absolute minimum is $f(0.298) = 0.799$

2.3. Simplified design equations for Eurocode 5.

Therefore, we can omit mode **c** if we apply a coefficient of 0.8 to modes **a'** and **b'**. The resulting design equation in Eurocode 5 would be :

$$R_d = \sqrt{\frac{4\beta}{1+\beta}} \min \begin{cases} \frac{0.8}{3} \beta^{-0.1} t_1 df_{h,1,d} \\ \frac{0.8}{3} \beta^{-0.1} t_2 df_{h,2,d} \\ 1,1 \sqrt{M_{y,d} f_{h,1,d} d} \end{cases} \quad (12)$$

This design equation is represented in the Möller coordinates for $\beta = 1.0$ (see Figure 11).

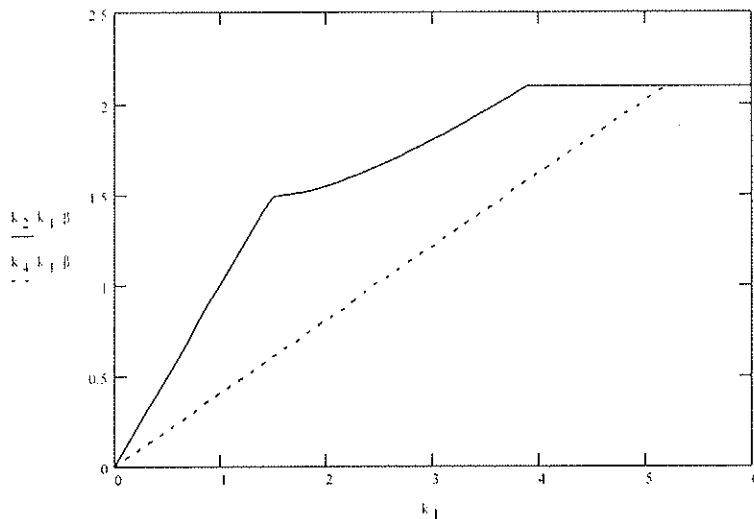


Figure 11 : Design equations for single shear connections

This approach seems very conservative, since there is a wide interval of α for which the slope ratio is larger than 1.0. Therefore, we can also refine this approach. If we zoom on Figure 10, the portion of the curve for which the slope ratio is less than 1.0, we obtain the following figure :

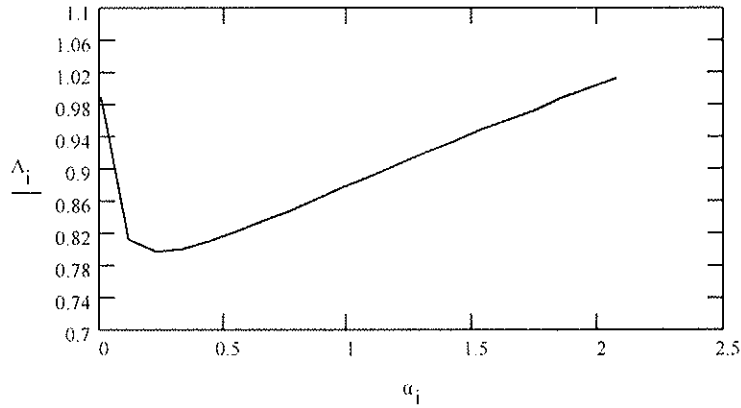


Figure 12 : Zoom on Figure 10 for slope ratio less than 1

On this curve, we can fit an equation of this form :

$$f(x) = S_0 \cdot x + S_1 \frac{S_2}{x} \quad (13)$$

The exact result of the fit is :

$$S = \begin{matrix} 0.123 & & 0.12 \\ 0.756 & \text{which we can approximate as } S & 0.76 \\ 2.335 \cdot 10^{-3} & & 2 \cdot 10^{-3} \end{matrix}$$

This fit is illustrated in Figure 13.

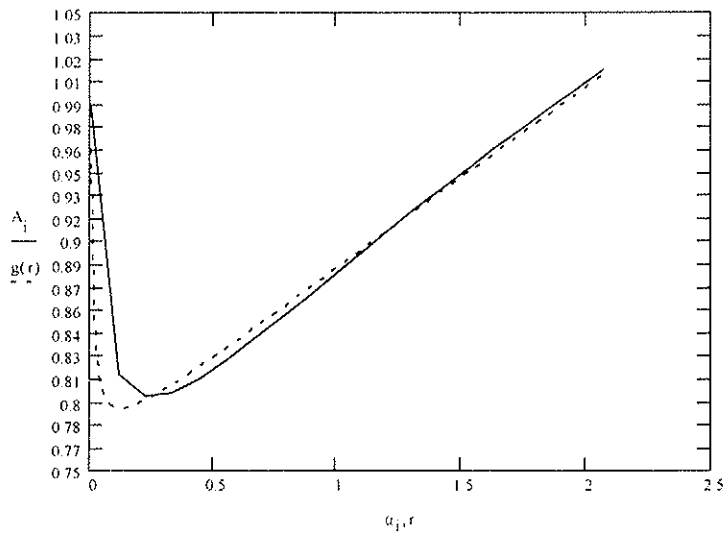


Figure 13 : Fitted function for the slope ratio

In this case, the design equations should be :

$$R_d = \sqrt{\frac{4\beta}{1+\beta}} \min \left\{ \begin{array}{l} \frac{\xi}{3} \beta^{-0.1} t_1 df_{h,1,d} \\ \frac{\xi}{3} \beta^{-0.1} t_2 df_{h,2,d} \\ 1,1 \sqrt{M_{y,d} f_{h,1,d} d} \end{array} \right. \quad (14)$$

with

$$\xi = \min \left\{ 1.0, 0.76 + 0.12 \frac{t_2}{t_1} + 2.10^{-3} \frac{t_1}{t_2} \right\} \quad (15)$$

The following figures (Figure 14, Figure 15, Figure 16) illustrate the design equations for $\beta = 1.0$ and $\alpha = 0.1, 1.0, 10.0$. $k_2(k_1, \beta)$ corresponds to equation (4), $k_4(k_1, \beta)$ corresponds to equation (12), $k_5(k_1, \beta)$ corresponds to equation (14).

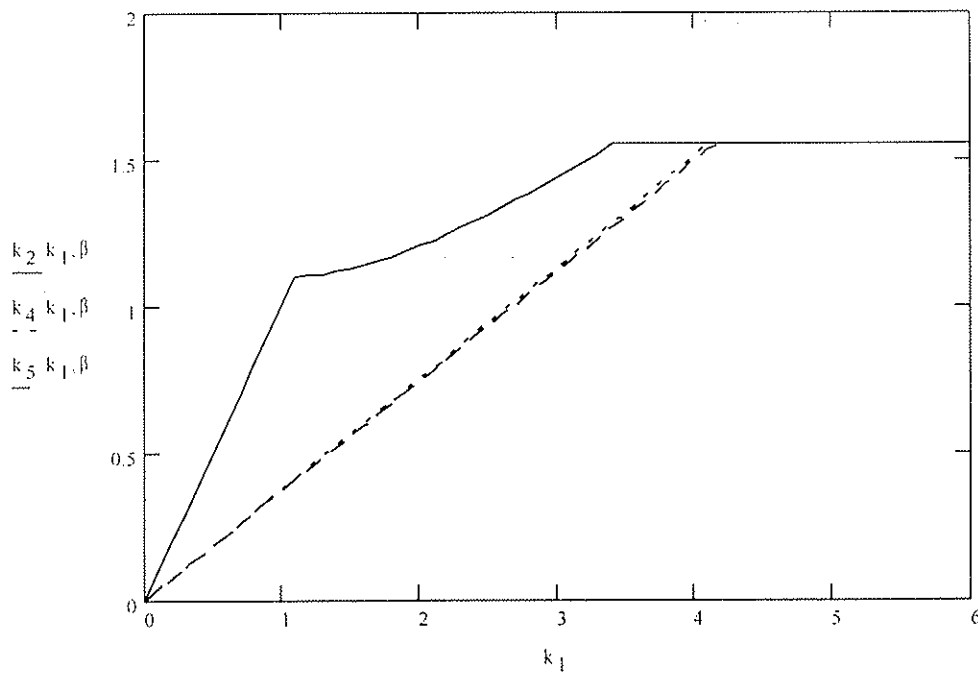


Figure 14 : Simplified design equation, $\alpha = 0.1$

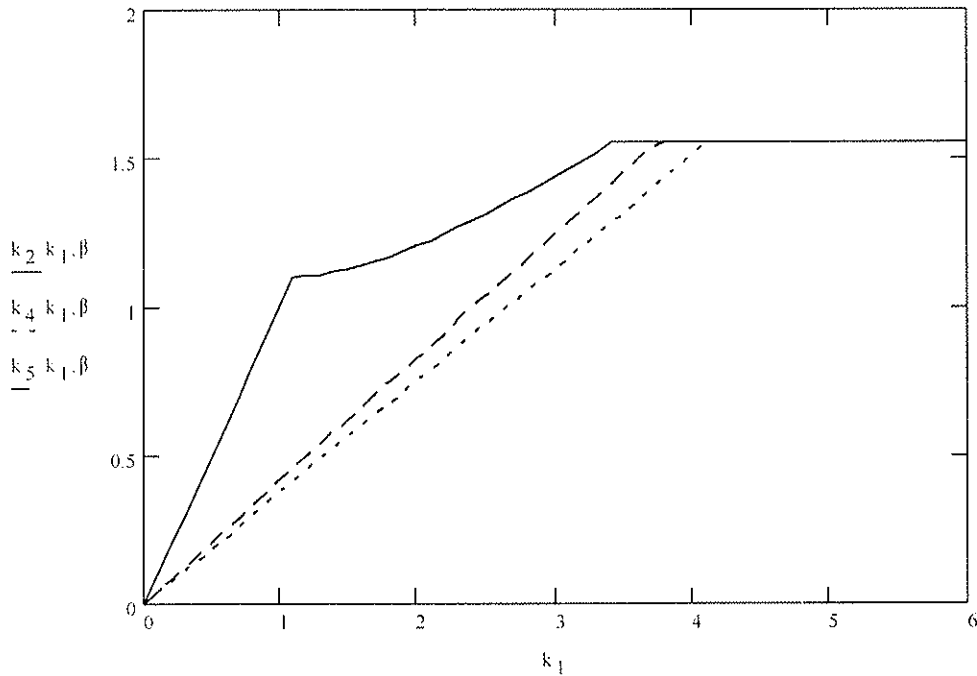


Figure 15 : Simplified design equation, $\alpha = 1$

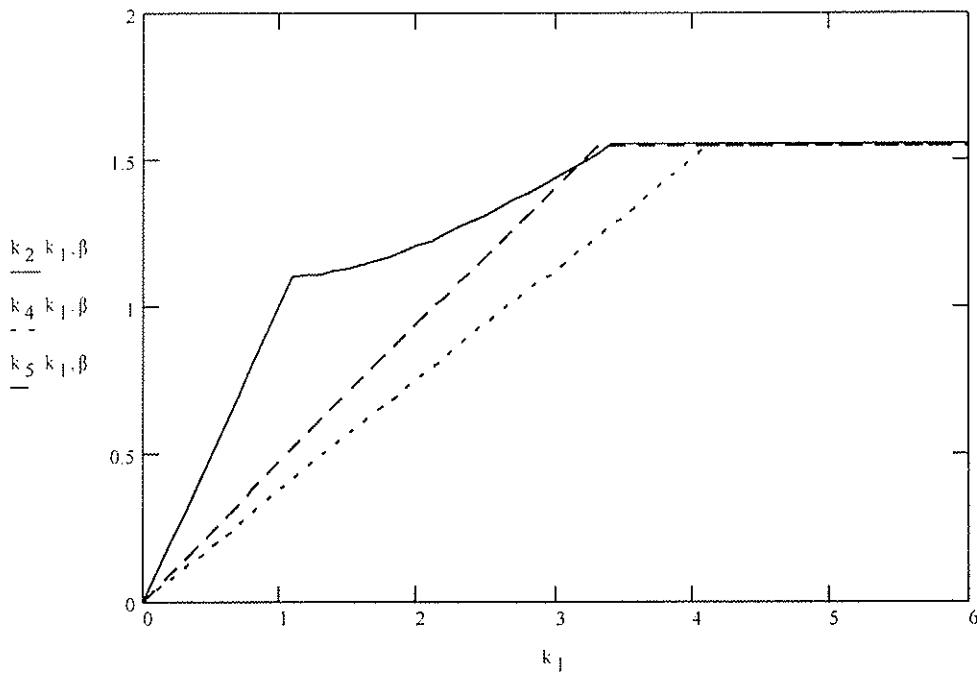


Figure 16 : Simplified design equation, $\alpha = 10$

One can see that this approach, more refined, does not affect very much the design.

Conclusions.

This approach gives much simpler equations, but seems to be very safe for a single fastener (up to 60% reduction, but for a very narrow zone). It could be compensated by the formula for the effective number of fasteners. It could be also calibrated by changing the slope of the first line in the simplified equations for single and double shear connections. Before incorporating

this approach in Eurocode 5, further calibrations and discussions are needed. But we should keep in mind that simple design rules make timber design more understandable for engineers.

Références

[1] Johansen, K.W. (1949). Theory of timber connections. International Association of Bridge and Structural Engineering. Publication n. 9:249-262. Bern

[2] ENV 1995-1:1. (1993) Eurocode 5. Design of timber structures. Part 1-1 : General.

[3] Hilson, B.O. (1995). Joints with dowel-type fasteners - Theory. in Timber Engineering STEP 1 by H.J. Blass & al., Centrum Hout, The Netherlands

[4] Kangas J. and Kurkela J. (1996). A simple method for lateral load-carrying capacity of dowel-type fasteners. Paper 29-7-1, 29th CIBW18 Meeting, Bordeaux, France

[5] Möller, T. (1951). En ny method för beräkning av spikförband. Report n. 117. Chalmers University of Technology, Sweden

CIB-W18/31-7-8

**INTERNATIONAL COUNCIL FOR BUILDING RESEARCH STUDIES AND DOCUMENTATION
WORKING COMMISSION W18 - TIMBER STRUCTURES**

SIMPLIFIED DESIGN OF CONNECTIONS WITH DOWEL-TYPE FASTENERS

by

H J Blaß
J Ehlbeck
University of Karlsruhe

GERMANY

MEETING THIRTY-ONE

SAVONLINNA

FINLAND

AUGUST 1998

Simplified design of connections with dowel-type fasteners

HANS JOACHIM BLASS

JÜRGEN EHLBECK

UNIVERSITÄT KARLSRUHE, GERMANY

1 Introduction

The present design equations for connections with dowel-type fasteners according to Eurocode 5 should be revised. Reasons for this are:

- The equations based on Johansen's theory are unwieldy and therefore are not readily accepted by practising engineers. It is also very difficult to present load-carrying capacities in tables because e.g. the design values are calculated by modifying the embedding strength differently from the fastener yield moment and many parameters would have to be considered. Kangas and Kurkela (1996) therefore made a proposal to simplify the design of the lateral load-carrying capacity of dowel-type fasteners. However, their proposal relies on diagrams.
- Recent research results as well as ongoing research projects show that in many cases the load-carrying capacity calculated on the basis of Johansen's theory is not reached in multiple-fastener-joints. This is especially the case if stout fasteners are used, i.e. if the ratio of embedded length to fastener diameter (fastener slenderness ratio) is small. In these cases the failure mode often is splitting of the timber, a mode not considered in the Johansen theory. Therefore, the practising engineers should be encouraged to design joints with high fastener slenderness ratios.

Johansen's theory on the other hand presents a method generally applicable and based on a simple mechanical model to determine the load-carrying capacity of connections with dowel-type fasteners. Numerous test results have shown that Johansen's theory allows accurate prediction of the load-carrying capacity, if timber splitting can be excluded as a failure mode.

Therefore it is proposed to include the equations based on Johansen's theory in an Annex of Eurocode 5. This would allow engineers to use Johansen's theory in those cases, where timber splitting can be excluded, e.g. by reinforcing the joint area. A simplified design method should be incorporated in the main text of Eurocode 5 for those engineers who do not deal with timber structures on a daily basis. This simplified design method presented below would, however, in some cases lead to conservative results.

2 Simplified design method

The tendency for splitting in timber connections decreases with increasing fastener slenderness. Consequently, slender fasteners should be used leading to failure modes with two plastic hinges per shear plane. This failure mode - called failure mode 3 in Hilson (1995) - is shown in figure 1. Only

for steel-to-timber connections with thin outer steel members, mode 3 is not possible. In this case the preferable failure mode is mode 2 (see figure 1).

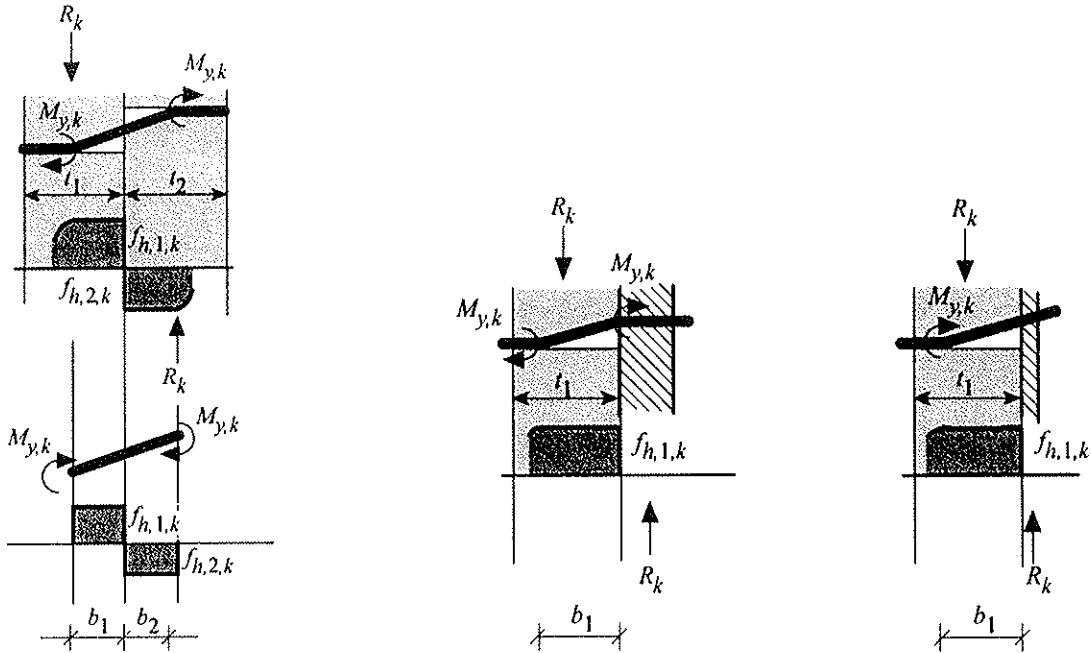


Fig. 1 Failure mode 3 according to Johansen for timber-to-timber connections (left), for steel-to-timber-connections (middle) and failure mode 2 for steel-to-timber-connections with thin outer steel members.

Failure mode 3 is characterised by two plastic hinges in the dowel-type fastener per shear plane. The characteristic value of the load-carrying capacity per fastener per shear plane for this failure mode is (failure mode 2 for steel-to-timber-connections with thin outer steel members):

Timber-to-timber and panel-to-timber joints with fasteners in single or double shear:

$$R_k = \sqrt{\frac{2\beta}{1+\beta}} \sqrt{2M_{y,k} f_{h,1,k} d} \quad (1)$$

Steel-to-timber joints with inner thin or thick steel plates or with outer thick steel plates:

$$R_k = \sqrt{2} \sqrt{2M_{y,k} f_{h,1,k} d} \quad (2)$$

Steel-to-timber joints with outer thin steel plates:

$$R_k = \sqrt{2M_{y,k} f_{h,1,k} d} \quad (3)$$

The use of equations (1) to (3) is significantly easier than the use of the equations in paragraph 6.2 of Eurocode 5. However, equations (1) to (3) only apply, if requirements concerning minimum embedded lengths are met. Only then the preferred failure modes can be expected. In the following, the necessary embedded lengths are derived by equalling the load-carrying capacities of failure modes 2 and 3, respectively (2 and 1 for thin outer steel plates).

Timber-to-timber and panel-to-timber joints with fasteners in single or double shear

The required minimum embedded length t_1 for side member 1 results from equalling equations (5) and (7) of STEP lecture C3 by Hilson:

$$t_1 \geq \left(2\sqrt{\frac{\beta}{1+\beta}} + 2 \right) \sqrt{\frac{M_{y,k}}{f_{h,1,k} d}} \quad (4)$$

Similarly, the minimum embedded length t_2 for member 2 of a single shear joint follows from equalling equations (6) and (7) of STEP/C3:

$$t_2 \geq \left(2 \frac{1}{\sqrt{1+\beta}} + 2 \right) \sqrt{\frac{M_{y,k}}{f_{h,2,k} d}} \quad (5)$$

The minimum embedded length t_2 for the middle member of a double shear connection follows likewise from equations (9) and (11) of STEP/C3:

$$t_2 \geq \left(\frac{4}{\sqrt{1+\beta}} \right) \sqrt{\frac{M_{y,k}}{f_{h,2,k} d}} \quad (6)$$

Steel-to-timber joints with inner thick or thin steel plates or with outer thick steel plates

The minimum penetration t for fasteners in single and double shear results from equalling equations (12) and (13), or (13) and (14), respectively of STEP lecture C3:

$$t \geq 2 \sqrt{\frac{M_{y,k}}{f_{h,k} d}} \text{ for fasteners in double shear in middle members} \quad (7)$$

$$t \geq 4 \sqrt{\frac{M_{y,k}}{f_{h,k} d}} \text{ for all other cases} \quad (8)$$

Steel-to-timber joints with outer thin steel plates

Similarly, the minimum embedded length t for connections in single and double shear follows as:

$$t \geq (2\sqrt{2}) \sqrt{\frac{M_{y,k}}{f_{h,k} d}} \text{ for fasteners in double shear in middle members} \quad (9)$$

$$t \geq (2 + \sqrt{2}) \sqrt{\frac{M_{y,k}}{f_{h,k} d}} \text{ for all other cases} \quad (10)$$

Since in practice there will be cases where the minimum embedded length given above is not appropriate, there should be an allowance for smaller embedded lengths. It is proposed to decrease the load-carrying capacity according to equations (1) to (3) in these cases with the ratio of actual to minimum embedded length. This simplified proposal is shown in figure 2.

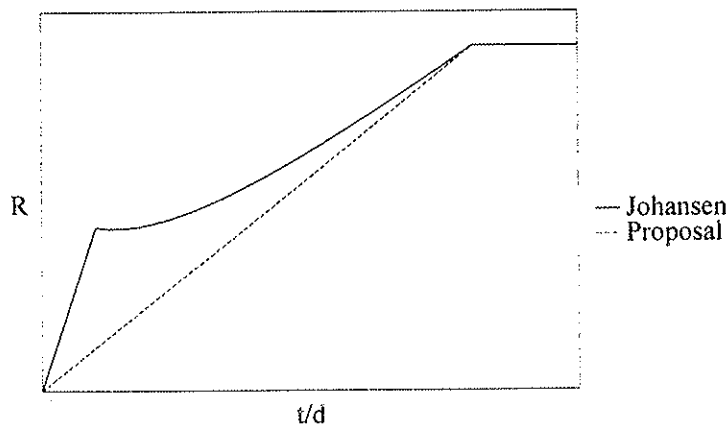


Fig. 2 Load-carrying capacity of a dowel-type fastener depending on fastener slenderness ratio t/d according to Johansen and the simplified proposal.

3 Partial safety coefficients

The design load-carrying capacities in the present version of Eurocode 5 are calculated by modifying the embedding strength of the timber and the fastener yield moment. In equations (1) to (3), both, the embedding strength and the yield moment, for which different partial safety coefficients apply, are under the square root. Since only the embedding strength is to be modified by k_{mod} , using the partial safety coefficient γ_M for timber as well as k_{mod} to modify the characteristic load-carrying capacity R_k would be too conservative.

The application of Eurocode 5 would nevertheless be easier if the *characteristic* load-carrying capacity R_k is determined first and then the corresponding design value. This procedure is also necessary, if characteristic values are determined through tests. In the following, the necessary partial coefficient for the connection is derived if k_{mod} is applied to the characteristic load-carrying capacity R_k of the connection.

According to the present version of Eurocode 5 the design value of the load-carrying capacity for timber-to-timber joints with $\beta = 1$ is determined as:

$$R_d = \sqrt{2M_{y,d} f_{h,1,d} d} \quad (11)$$

where

$$M_{y,d} = \frac{M_{y,k}}{\gamma_M} \quad (12)$$

$$f_{h,1,d} = \frac{f_{h,1,k} \cdot k_{mod}}{\gamma_M} \quad (13)$$

If the partial safety coefficients and k_{mod} are put before the square root, R_d follows as:

$$R_d = \sqrt{\frac{k_{mod}}{\gamma_{M,Steel} \cdot \gamma_{M,Timber}}} \sqrt{2M_{y,k} f_{h,1,k} d} = \sqrt{\frac{k_{mod}}{\gamma_{M,Steel} \cdot \gamma_{M,Timber}}} R_k \quad (14)$$

If a design procedure is preferred, where the characteristic load-carrying capacity is modified by k_{mod} and γ_M , equation (15) follows:

$$R_d = \frac{k_{mod} R_k}{\gamma_{M,Connection}} \quad (15)$$

If equations (14) and (15) should lead to the same result, $\gamma_{M,Connection}$ follows as:

$$\gamma_{M,Connection} = \sqrt{k_{mod} \gamma_{M,Steel} \gamma_{M,Timber}} \quad (16)$$

Using $\gamma_M = 1,1$ for steel and $\gamma_M = 1,3$ for timber, the values for $\gamma_{M,Connection}$ range between 1,00 to 1,13 for $k_{mod} = 0,7$ to $k_{mod} = 0,9$. Therefore, a value of $\gamma_{M,Connection} = 1,1$ is proposed.

4 Conclusion

Using the ideal-plastic approach by Johansen as a basis, simplified design equations are proposed for connections with dowel-type fasteners. Only the failure mode with two plastic hinges per shear plane is used for timber-to-timber and steel-to-timber connections with inner thin or thick steel plates or with outer thick steel plates. For steel-to-timber joints with outer thin steel plates the failure mode with one plastic hinge per shear plane serves as a basis. Minimum embedded lengths are required to guarantee these failure modes.

If the specified minimum embedded lengths of the fasteners are used, the load carrying capacity of the connection reaches a maximum value and the behaviour is more ductile compared with stout fasteners. For cases, where the minimum embedded lengths are not reached, a proportional decrease in the calculated load-carrying capacity of the connection is proposed.

In order to further simplify the design of connections with dowel-type fasteners, a partial safety coefficient for the connection, $\gamma_{M,Connection} = 1,1$, is proposed. In this case, the design value of the load-carrying capacity of the connection has to be modified using the appropriate k_{mod} -value as well.

5 References

Kangas, J. and Kurkela, J. 1996: A simple method for lateral load-carrying capacity of Dowel-Type fasteners. Proceedings, CIB-W18 Timber Structures, Meeting 29, Bordeaux, France, ISSN 0945-6996

Hilson, B.O. 1995: Joints with dowel-type fasteners - theory. Timber Engineering STEP 1, First Edition, Centrum Hout, The Netherlands, ISBN 90-5645-001-8

CIB-W18/31-9-1

INTERNATIONAL COUNCIL FOR BUILDING RESEARCH STUDIES AND DOCUMENTATION
WORKING COMMISSION W18 - TIMBER STRUCTURES

DURATION OF LOAD EFFECT IN TENSION PERPENDICULAR TO GRAIN
IN CURVED GLULAM

by

A Ranta-Maunus
VTT Building Technology

FINLAND

MEETING THIRTY-ONE

SAVONLINNA

FINLAND

AUGUST 1998

Duration of load effect in tension perpendicular to grain in curved glulam

Alpo Ranta-Maunus
VTT Building Technology, Finland

1 Introduction

The strength of timber depends on its moisture content and the duration of load, which has been commonly known for a long time. Strength reduction is accelerated by moisture variation as has been observed under bending load as well as under tension perpendicular to grain. In the latter case, moisture gradients tend to cause local swelling or shrinkage, which changes the stress distribution and has an impact on load bearing capacity.

This paper concentrates on cases where a failure of curved glued laminated timber beam is caused by tensile stresses perpendicular to grain. The theoretical focus of this research is on stress distribution through thickness. During this research period the focus has been shifting: at the beginning it was believed that creep, especially mechano-sorptive creep, will change the stress distribution and consequently impair the load bearing capacity [1]. This being still true, another factor seems to be more important: moisture induced stresses in internal parts of the beam during wetting can easily exceed all other effects. Accordingly, duration of load effect is partly being replaced by “maximum moisture gradient during the life time-effect”.

The reasons why the observed strength under long-term loading is lower than that obtained in short term testing at a constant moisture content are defined in this paper as follows:

- material is weakened by accumulating damage due to a constantly high stress level and duration of the stress. The factor to take this reduction into account is denoted by k_t .
- stress distribution: load bearing capacity of the member is lowered by changes in stress distribution caused by creep and hygro expansion. The factor used to take this reduction into account is denoted by k_σ .

This paper summarises the experimental and calculation results. The total effect of load duration combined with moisture effects is calculated by

$$k_{DotL} = k_\sigma k_t \quad (1)$$

Firstly, k_t is calculated based on experiments carried out under constant humidity conditions, and finally k_σ can be determined from cyclic humidity tests.

2 Experiments

Two different programs have been implemented to determine the duration of load effect on tension strength perpendicular to grain in different sized curved beams exposed to cyclically varying humidity. The earlier project (VTT) was carried out 1991-1993 [2,3]. The later, more comprehensive project (EU/AIR) was completed in 1997 [4,5]. As part of the AIR-project tensile tests with specimen volumes of 0.01 and 0.03 m³ were made by FMFA in Germany [6]. The curved beam test series are summarised in Table 1. Loading configuration is illustrated in Fig. 1. The distance between loads, l , is given in Table 1 as a characteristic dimension with regard to the length effect. The radius of curvature at VTT tests was about 3 m and at AIR tests 5.7 m.

Spruce material used in tensile experiments was the same as in curved beams (AIR). One difference in long term experiments was that the tensile specimens were conditioned at 65 % RH before experiments whereas curved beams were conditioned at the average humidity of anticipated cyclic conditions. In tensile experiments and in earlier VTT tests, the long term load was applied by hanging loads (lever arms) whereas in the later tests (AIR) on curved beams the load was applied by a spring system.

All experiments were carried out under a stepwise increasing load, one step being 28 days. It was assumed that medium term load duration is most relevant for timber structures. For roof structures, the snow load is dimensioning in northern countries. Even if the cumulative action of snow load is a much longer duration, the design loads are based on maximum snow load over 50 years, and 4 weeks is a reasonable estimate for the time the load exceeds 90 % of the design value.

The results of the experiments carried out at VTT and FMFA are summarised in Table 2 and discussed in [7]. Experimental conclusions are presented in Chapters 3 through 5.

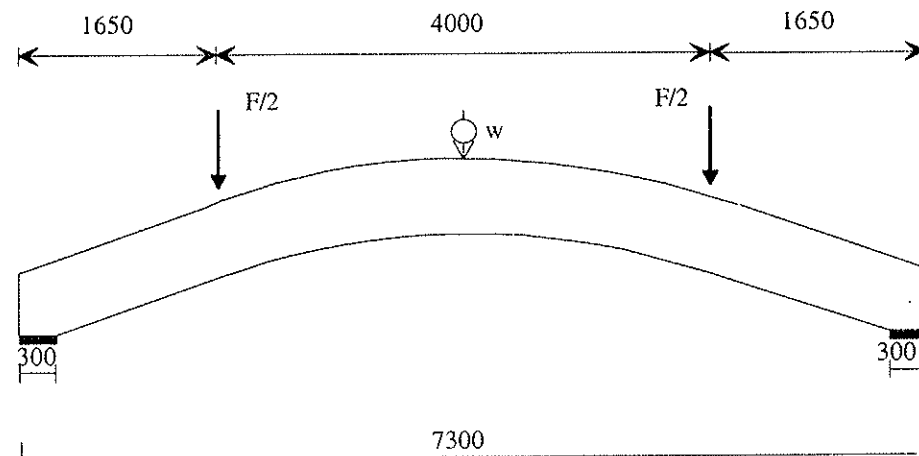


Figure 1 Schematic of loading and supporting positions.

Table 1 Dimensions of curved glulam test specimens.

Test series	Specimen dimensions (mm)	l (mm)	Loading type	Conditions
VTT S1+S3	90 x 400 x 4300	1000	short term + step wise long term	cyclic RH 40<->85%
VTT S2	90 x 400 x 4300	1000	step wise long term	cyclic RH painted
AIR S1	90 x 600 x 5400	2000	short term	65% RH
AIR S2	90 x 600 x 5400	2000	step wise long term	cyclic RH 55<->90%
AIR S3	90 x 600 x 7400	4000	short term	65% RH
AIR S4	90 x 600 x 7400	4000	step wise long term	85% RH
AIR S5a	140 x 600 x 7400	4000	short term	65% RH
AIR S5b	140 x 600 x 7400	4000	short term	85% RH
AIR S6	140 x 600 x 7400	4000	step wise long term	cyclic RH 55<->90%
AIR S8	140 x 600 x 7400	4000	step wise long term	85% RH

3 Effect of loading time at constant humidity

The results obtained at constant humidity were used to calculate the pure time factor k_t . The time to failure at final load level of the “average” specimen closest to the 50 percentile level was used in the analysis, and the calculation of relative stress level the short term strength at the same fractile level was used. The test results are given in Table 2 and illustrated in Fig. 2. k_t extrapolated to 6 months load duration range from 0.64 to 0.82 being similar to the values obtained under bending with the exception that tension strength perpendicular to grain was as high at 85 % as at 65 % RH. 3 test series of 5 give practically the same behaviour. The result of series AIR S8 was adopted as representative behaviour at a constant moisture content when calculating the extent of additional moisture effect in next chapter.

Table 2 Compilation of major ramp and DOL test results on tension strength perpendicular to the grain of glulam obtained with curved beams and structural sized tension specimens [7].

Test and specimen configurations		Units	Results of different test series at VTT and FMFA					
			tension specimens		curved beams			
			AIR 01a-d	AIR 03a-d	VTTS1/2/3 ¹⁾	AIR S1/2	AIR S3/4	AIR S5/8/6
Specimen characteristics	(Apex) volume	V	0,01	0,03	0,036	0,108	0,216	0,336
	lamella thickness	d	33	33	16	33	33	33
	lamella width	b	90	140	90	90	90	140
	mean density	ρ_{mean}	530	493	470	496	503	493
Ramp load results	test series		AIR 01a	AIR 03a	S1	AIR S1	AIR S3	AIR S5
	sample size		44	44	12	8	8	16
	mean moisture content	%	12	12	12,3	11,6	11,4	12-15
	$f_{t, 90, mean}$	N/mm ²	0,89	0,67	1,21	0,85	0,71	0,61
$f_{t, 90, 05}$	N/mm ²	0,74	0,55	0,95	0,72	0,59	0,46	
Duration of load results Constant climate	test series		AIR 01b	AIR 03b	S2		AIR S4	AIR S8
	relative humidity	%	65	65	40-85 ²⁾		85	85
	mean moisture content	%	12	12	11-12 ²⁾		18	18
	sample size	-	15	15	6		8	8
	$k_{DOL, mean}$	-	0,70	0,75	0,76		0,87	0,77
	time to failure for sample mean	t _{f, mean}	22	24	13		4	14
	$k_{DOL, mean, extrapolated for 6 months test duration}$	-	0,64	0,70	0,70		0,82	0,71
Cyclic climate	test series		AIR 01c	AIR 03c	S3	AIR S2		AIR S6
	relative humidity span (RH)	%	55-90	55-90	40-85	55-90		55-90
	cycle length	d	28	28	28	28		28
	conditioning before cycling (RH)	%	65	65	70	75		75
	sample size	-	15	15	12	8		8
	$k_{DOL, mean}$	-	0,45	0,50	0,55	0,60		0,66
time to failure	t _{f, mean}	17,5	18,5	20	28		15	
Natural sheltered outdoor climate	test series		AIR 01d	AIR 03d				
	relative humidity span (RH)	%	35-95	45-90				
	temperature span	°C	-5-22	2-22				
	conditioning before loading (RH)	%	65	65				
	sample size	-	15	15				
$k_{DOL, mean}$	-	0,60	0,65					
time to failure	t _{f, mean}	2,6	24,5					

¹⁾ Different material tested in earlier test series preceding AIR project

²⁾ Beams coated with alkyd paint

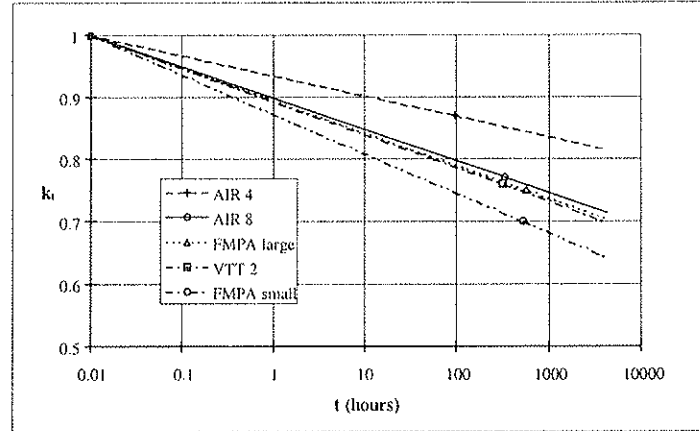


Figure 2 Stress level vs. log time to failure. The observation points show when the “average” beam closest to 50 percentile failed.

4 Effect of cyclically changing humidity

The results obtained under changing humidity conditions are also shown in Table 2. The effect of moisture variation on strength is expressed in terms of factor k_{σ} as defined in eqn. (1), and these factors are compiled in Table 3. The pure time effect, k_t is estimated based on the test series AIR S8 which was adopted as average behaviour at constant humidity. Total k_{DOL} is determined for the average beam for tests in variable humidity. Slightly different values of k_{σ} were obtained when k_t was estimated separately for each test series based on an identical test at constant humidity [6]. The results reveal that the moisture cycles used will roughly double the effect of load duration in a few weeks. Wider cross-sections are less sensitive to moisture cycling than narrow ones. Effective protection against changing moisture appears to be provided by normal surface treatment with alkyd paint. It overcomes most of the effect of moisture cycling with a cycle length of 4 weeks.

Table 3 Comparison of DOL factors obtained in cyclic humidity tests.

	VTT S2 painted curved beams	VTT S1&3 curved beams	AIR S2 curved beams	AIR S6 curved beams	FMPA small tensile	FMPA large tensile
Conditioning RH (%)	70	70	75	75	65	65
RH cycle (%)	40<->85	40<->85	55<->90	55<->90	55<->90	55<->90
Width (mm)	90	90	90	140	90	140
Time to failure (days)	13	20	28	17	18	19
Estimated k_t	0.77	0.76	0.75	0.77	0.76	0.76
Observed k_{pol}	0.76	0.55	0.60	0.66	0.45	0.50
$k_{\sigma} = \frac{k_{DOL}}{k_t}$	0.99	0.72	0.79	0.86	0.59	0.66

5 Volume effect

The results show a clear volume effect: tensile strength perpendicular to grain depends on the width and length of the curved beam, as explained in the test reports. The volume effect is stronger in short term ramp loading than in long term loading. When the results for tensile specimens are compared to curved beams, it is observed that beams are stronger than can be predicted based on tensile experiments: a curved beam has the same strength as a tensile specimen if the volume of constant moment span is about 9 times the volume of the tensile specimen. Based on a parabolic vertical stress distribution in beams, we would expect that the beam volume being nearly 3 times the volume of the tension specimen, strength would be equal. The other way of adjusting beam values for compatibility with tensile test is to divide stresses by factor k_{dis} , as has been done in Eurocode 5. In Figure 3 failure stresses of beams have been divided by factor $k_{dis} = 1.85$, which together with the volume effect exponent of 0.2 gives a good fit of tensile and beam results obtained in long term testing at constant humidity. Cyclic moisture content results are not exactly comparable, because tensile tests were subjected to a stronger moisture change. Short term loading results for curved beams show a larger volume effect with exponent 0.3.

The great difference in strengths between curved beams and tensile specimens cannot be fully explained. Compression stresses perpendicular to grain in areas subjected to load will decrease the volume where tensile stresses perpendicular to grain are close to nominal value. However, this effect alone is not assumed to explain the difference.

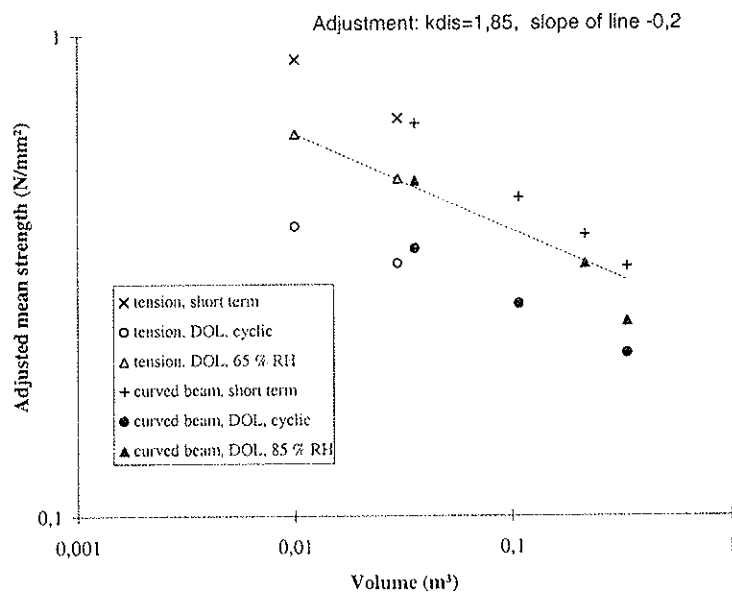


Figure 3 Strength perpendicular to grain vs. volume on double logarithmic scale. Curved beam strength is divided by 1.85. Slope of line corresponds to a volume effect exponent 0.2.

6 Calculation of moisture load

6.1 Description of the method

Factor k_{σ} in eqn. (1) understands changing moisture content as a reduction in the strength of the material. Another approach is to consider moisture effect as an additional load. Therefore refined methods of structural analysis have been developed that include moisture transport analysis and stress calculation. A few slightly different methods have been applied in numerical calculation. For moisture computation, both one-dimensional [8] and two-dimensional [9] methods have been used. For structural analysis a two-dimensional FEM was used [10], but for more complex moisture histories a one-dimensional approximation was adopted for practical reasons [5]. The method described below has been used by Hukka for wood drying applications [8].

6.1.1 Mathematical formulation

The mathematical model is based on the use of calculated moisture distribution in the wood as input data for a stress model, which is then used to predict the expected surface checking in wood drying applications, and the load bearing capacity of curved beams.

Moisture and energy transport

Moisture transport inside wood is calculated using a simple diffusion equation with an effective diffusion coefficient. The equations of moisture and energy transport in wood are formulated in a conservative integral form in one dimension. Moisture is governed by

$$\frac{\partial}{\partial t} \int_V u dV = \oint_{\partial V} D_{eff} \frac{\partial u}{\partial x} dS \quad (2)$$

The effective diffusion coefficient is of the form

$$D_{eff} = \exp(a_0 + a_1 u) \quad (3)$$

Energy transport in wood obeys Fourier's heat conduction law, which can be expressed in integral form as

$$\frac{\partial}{\partial t} \int_V c \rho T dV = \oint_{\partial V} \lambda \frac{\partial T}{\partial x} dS \quad (4)$$

The heat equation is related to the moisture equation only through the boundary conditions at the surface of the wood. The mass flux density at the boundary is calculated using an analogy between heat and mass transfer given by the boundary-layer theory:

$$F_u = k_{paint} \beta_l (p_v^* - p_v) \frac{\beta_w}{\beta_l} \quad (5)$$

where k_{paint} is the resistance caused by surface coating (where applicable), β_l mass is the transfer coefficient from liquid water. The vapour pressure at the wood surface p_v^* is characterised by the sorption curve. The last correction term is the difference between

vapour emission from wood and liquid water surfaces and is a function of the moisture content of the wood surface.

The energy flux density entering the wood is the convective heat-transfer rate reduced by the portion that is consumed by the evaporation of water at the surface:

$$F_e = \alpha(T - T^*) - h_v F_u \quad (6)$$

The heat-transfer coefficient is a function of air velocity, here taken $\alpha = 3 \frac{W}{m^2 K}$.

Stress Model

The calculation of stress is based on a deformation model including shrinkage, elastic, viscoelastic and mechano-sorptive strain components [11]:

$$\epsilon_{tot} = J_0 \cdot \sigma + \epsilon_{ve}(\sigma) + \epsilon_{ms}(\sigma) + \epsilon_s \quad (7)$$

The viscoelastic behaviour has been modelled using the generalised Kelvin material model with seven Kelvin-units in series, and the elastic response is included within the viscoelastic effect. Time-moisture content equivalence and a shift factor is used in modelling the dependency of creep rate on moisture content. Mechano-sorptive creep is also modelled using four Kelvin units in series, whose deformation depends on the absolute value of the moisture content change but not of time.

Two boundary conditions are applied:

- condition of equilibrium reveals:

$$\int_A \sigma dx = \frac{3M}{2Rh} \quad (8)$$

where A is area of through cross-section with unit length, M is the bending moment acting on the curved beam, R is the mean radius of curvature and h is the height of the beam.

- as condition of compatibility total strain is assumed to be constant throughout the cross-section.

6.1.2 Numerical method

The moisture and energy equations (2) and (4) are formulated in a conservative form and are thus ready to be used for calculation employing the control-volume method [12,13]. The computational area is divided into discrete finite volumes according to Fig. 4.

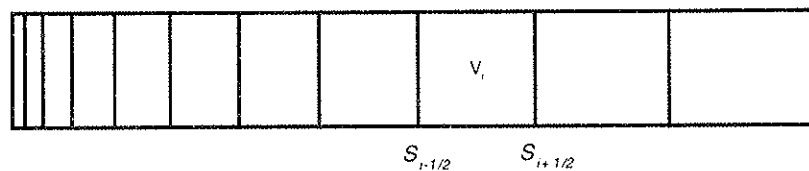


Figure 4 A one-dimensional computational grid using the control volume method.

The moisture equation is integrated over one control volume and the temporal derivative is discretised using a fully implicit method. The result is

$$\Delta u_i = -\frac{\Delta t}{V_i} \left(F_{i+1/2}^{n+1} - F_{i-1/2}^{n+1} \right) \quad (9)$$

This equation still includes the flux terms at the unknown new time-step. To calculate them a method called flux linearisation is used:

$$F_{i+1/2}^{n+1} = F_{i+1/2}^n + \frac{\partial F_{i+1/2}}{\partial u_{i+1}} \Delta u_{i+1} + \frac{\partial F_{i+1/2}}{\partial u_i} \Delta u_i \quad (10)$$

These partial derivatives are easily calculated. The method yields a tridiagonal matrix equation which is straightforward to solve. No iteration is necessary.

As the moisture and energy equations are only coupled through the boundary conditions, they may be solved separately. The time step in temporal integration is chosen to keep the maximum moisture change within a time-step under a pre-defined limit. Previous local moisture changes are utilised to predict the optimal step.

The calculation being one-dimensional with respect to wood, the stresses are calculated in one direction with a changing angle between tangential and radial directions. Symmetry of the analysed cross-section is used and the numerical formulation is based on the total strain being constant through the cross-section. As a condition of equilibrium the integrated stress is constant depending on mechanical load as given in eqn (8). The integration with respect to time is made using a fully implicit method, which gives the following equation for total strain:

$$\varepsilon_{tot} \cdot \int \frac{dx}{A(x)} = \int \frac{B(x)}{A(x)} dx \quad (11)$$

The functions $A(x)$ and $B(x)$ include the individual components of strain. As the total strain is known, the stress can be solved from eq. (7).

The hypothesis for the analysis is that Weibull theory can be used to predict the strength when stress distribution is uneven, also in the direction through thickness. The effective Weibull stress caused by external mechanical loads (σ_L) and moisture effects (σ_M) is calculated as

$$(\sigma_L + \sigma_M)_{eff, .90} = \left(\frac{1}{V_{ref}} \int_V \sigma_{i,90}^k dV \right)^{1/k} \quad (12)$$

Equivalent stress calculated by eqn.(12) gives the value of constant stress in the reference volume V_{ref} causing the same probability of failure as the actual stress distribution in the actual volume V , according to the Weibull theory. Depending on value of V_{ref} used in calculation, the volume effect can be incorporated or left out ($V_{ref} = V$). More details on the calculation are reported in other papers [5,7].

6.2 Analysis of experiments

Tests in the AIR-S2 series having 90 mm thick beams have been simulated by the calculation method. Moisture content at surface varies between 11 and 18 %, and in the middle it remains close to 15 %. The stress distribution through thickness of the beam is shown after a dry period (126 days) and after the following wet period (140 days) when the average stress is 0.5 MPa (Fig. 3). Calculated Weibull stresses at the same times are 0.6 and 1.4 MPa, respectively, when no volume effect is incorporated. This is a typical situation in cyclic tests showing that wet periods are more likely to cause damage than dry periods.

An important factor when calculating stresses is the orientation of annual rings in the lamellae of glulam. The usual build-up of glulam results in a situation in which stress perpendicular to grain peaks in the middle of beams [10]. This is the basic reason why moisture gradients with wet surface are more likely to cause failure than equal gradients with dry surface.

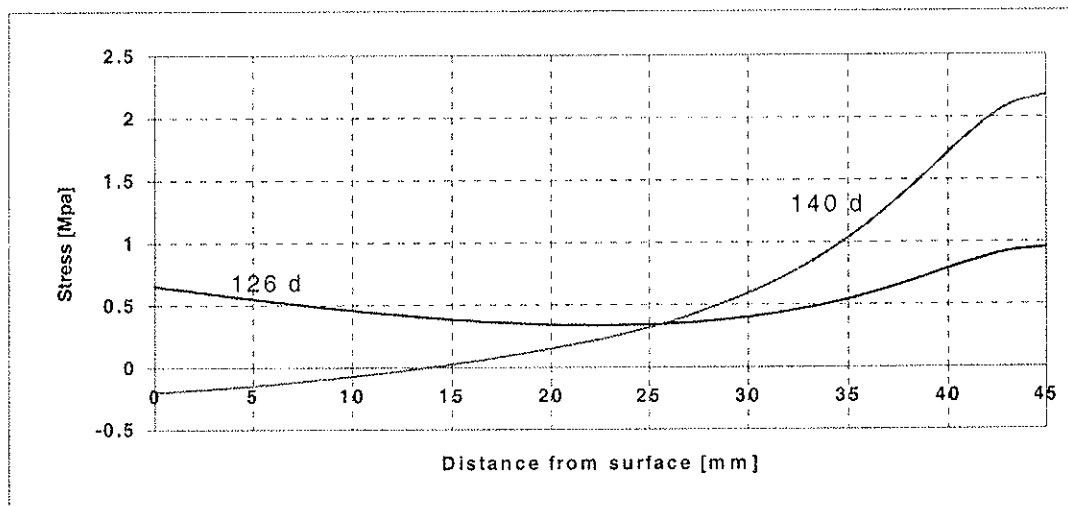


Figure 5 Calculated stress distribution for half thickness of beam in test series AIR-S2 after dry period (126 d) and wet period (140 d).

6.3 Equivalent stresses

The effect of moisture cycles is compared to the effect of mechanical loading at constant humidity by computing the value of mechanical load which causes the same Weibull stress as a combination of mechanical and moisture load. The results are given in Table 4. Test cycles and single humidity changes have been analysed. Moisture load corresponds to an extra load of 0.15 to 0.35 MPa when acting simultaneously with a mechanical load of 0.2 MPa, when the beam is not surface coated. A good surface coating (vapour barrier) will decrease the moisture load in an example from 0.15 to 0.05 MPa. A single fast change from 65 % RH to 90 % RH seems to be more effective than the test cycles analysed. The conclusion is that fast changes of climate from a dry to a wet season with a duration of several weeks are the most harmful for structures subjected to tension stress perpendicular to grain.

Table 4 Calculated equivalent (mean) stresses $\sigma_{t,90}$ for combinations of moisture cycling and load.

Width (mm)	RH cycle	Equivalent load (MPa) for combined effect when external load is 0.2 MPa	Equivalent load (MPa) for combined effect when external load is 0.5 MPa
90	55%<->90% ¹	0.45	0.81
140	55%<->90% ¹	0.36	0.73
90	40%<->85% ²	0.35	0.71
90	40%<->85% ² painted	0.25	0.57
90	76%>-90% ³	0.40	0.73
90	65%>-90% ³	0.52	0.87
140	76%>-90% ³	0.41	0.75
140	65%>-90% ³	0.55	0.90

1) Test cycle in AIR experiments at FMPA and VTT [5], [6]

2) Test cycle in earlier VTT study [3]

3) Single fast change from equilibrium, lasting for 4 weeks.

7 Conclusions

Tensile stresses perpendicular to grain in curved and tapered beams, and in tension specimens cut from glulam, are found to be higher in the middle section, in the plane where the pith is located, and much lower over the rest of the cross-section. The same is true also during moisture cycling in long term loading. Thus, failure will start when stresses in the middle exceed the strength. In practical situations, maximal stresses are obtained when a dry period is followed by a humid period, and both periods are long.

When the effect of moisture changes is compared to the effect of mechanical loading, we can conclude that the moisture load caused by the analysed cycles corresponds to an extra load of 0.15 to 0.35 MPa when acting simultaneously with a mechanical load causing stress of 0.2 MPa, when the beam is not surface coated. A good coating will decrease the moisture load by 70 %. A single fast change from 65 % RH to 90 % RH seems to be more effective than the test cycles analysed.

While moisture gradients proved to be more important than realised in advance, some other factors appeared to be less important: creep after several moisture cycles seems not to change the level of stresses from that of the first cycle. Accordingly, for the analysis of the duration of load behaviour under tensile stress perpendicular to grain, it is of great importance to consider the largest moisture cycle or change. All other duration of load effects are of much less importance and can well be estimated on the basis of the traditional stress ratio vs. log time to failure graph based on ideal constant humidity experiments. Under ideal constant conditions duration of load effect in tension perpendicular to grain is slightly less severe than suggested by the Madison curve.

Volume effect during long term loading is found to be of the same order than adopted in Eurocode 5. The strength of a curved beam in comparison to a tensile specimen is higher than expected justifying the use of a higher k_{dis} value, 1.85 for curved beams. On the other hand k_{mod} factors should be lower, about 0.5 for medium and long term loads, or an additional moisture load should be calculated, depending on the surface coating or impregnation of curved beams.

Acknowledgements

This work is part of the project "Duration of load effect on different sized timber beams" (EC contract AIR2-CT94-1057) coordinated by professor P. Morlier. The work is also supported by VTT Building Technology, Academy of Finland, The Technology Development Centre of Finland, and Late-Rakenteet Oy. The help of these organisations is gratefully acknowledged.

References

- [1] Ranta-Maunus, A., "Impact of mechano-sorptive creep to the long-term strength of timber", *Holz als Roh- und Werkstoff*, vol 48, p. 67-71, 1990.
- [2] Gowda, S., Ranta-Maunus, A. "Curved and cambered glulam beams. Part 1. Short term load tests", *VTT Research Notes* 1500, Espoo, 96 p. + app. 39 p., 1993.
- [3] Ranta-Maunus, A., Gowda, S. S., "Curved and cambered glulam beams. Part 2. Long term load tests under cyclically varying humidity", *VTT Publications* 171, Espoo, 36 p. + app. 18 p. 1994.
- [4] Gowda, S., Ranta-Maunus, A., "Duration of load effect on curved glulam beams. Part 1. Short term reference tests", *VTT Research Notes* 1741. Espoo, 66 p.+ app. 11 p. 1996.
- [5] Gowda, S., Korttesmaa, M., Ranta-Maunus, A., "Duration of load effect on curved glulam beams. Part 2. Long term load tests and analysis", *VTT Publications* 334, Espoo, 1998.
- [6] Aicher, S., Dill-Langer, G., "Duration of load effect for glulam in tension perpendicular to the grain", *Research Report, FMPA – Otto-Graf-Institute –*, Stuttgart, 1998.
- [7] Aicher, S., Dill-Langer, G., Ranta-Maunus, A., "Duration of load effect in tension perpendicular to the grain of glulam in different climates", *Holz als Roh- und Werkstoff*, 1998.
- [8] Hukka A., "Mathematical modelling of the industrial timber drying process", Doctoral Thesis. To be published in VTT Publications. 1998.
- [9] Hanhijärvi, A., "Modelling of creep deformation mechanisms in wood", *VTT Publications* 231, Espoo, 143 p. + app. 3p., 1995.
- [10] Hanhijärvi, A., Ranta-Maunus, A., "Computational analysis of the effect of transverse anisotropy and annual ring pattern in cross-sections of curved glulam beams on the size effect of strength. *European Workshop on Application of Statistics and Probabilities in Wood Mechanics* (in press), Bordeaux, 12 p. 1996.
- [11] Hanhijärvi A. "Perpendicular-to-Grain Creep of Finnish Softwoods in High Temperature Drying Conditions - Experiments and Modelling in Temperature Range 95-125 °C", *VTT Publications* 301, Espoo, 94 p. + app. 176 p, 1997.
- [12] Patankar S. V., "Numerical Heat Transfer and Fluid Flow". Hemisphere, Washington, New York, London. 197 p. 1980.
- [13] Strang, G., "Introduction to Applied Mathematics". Wellesley-Cambridge Press. 758 p. 1986.

INTERNATIONAL COUNCIL FOR BUILDING RESEARCH STUDIES AND DOCUMENTATION

WORKING COMMISSION W18 - TIMBER STRUCTURES

**DEPTH FACTOR FOR GLUED LAMINATED TIMBER
DISCUSSION OF THE EUROCODE 5 APPROACH**

by

B Källsner

Träteknik, Swedish Institute for Wood Technology Research

O Carling

Uppsala

C J Johansson

SP, Swedish National Testing and Research Institute

SWEDEN

MEETING THIRTY-ONE

SAVONLINNA

FINLAND

AUGUST 1998

Depth factor for glued laminated timber

Discussion of the Eurocode 5 approach

B. Källsner¹, O. Carling² and C.J. Johansson³

¹Trätec - Swedish Institute for Wood Technology Research, bo.kallsner@tratek.se

²Bjerkning Ingenjörbyrå, Uppsala, Sweden, olle.carling@bjerkning.se

³SP Swedish National Testing and Research Institute, cajo@sp.se

1 Abstract

In Eurocode 5 the bending strength of glued laminated timber depends on the depth of the beam. This paper gives comments on some European investigations of glued laminated timber of spruce (*Picea Abies*) where the influence of depth has been studied. The test results indicate that the depth factor k_h based on 5-percentiles should be lower than given in Eurocode 5. Further, there is a tendency of lower coefficient of variation in the bending strength of deep beams than of shallow beams. This has an effect on the partial safety factor which could be handled by reducing k_h . Based on this it could be argued that the depth factor k_h should be removed from Eurocode 5.

2 Introduction

It is well-known that the bending strength of glued laminated timber (glulam) depends on the size of the beam and the load configuration. In EC5 (Eurocode 5) this is taken into account by the factor k_h . For depths in bending or widths in tension less than 600 mm the characteristic values for the bending and the tension strength according to prEN 1194 may be increased by the factor k_h , where

$$k_h = \min \begin{cases} (600/h)^{0,2} \\ 1,15 \end{cases} \quad (1)$$

with h in mm. The handling of the size effect in EC5 is very simplified. Thus it is understood that the length to depth ratio is close to the ratio given in the test standard.

In connection with the conversion of EC5 from a prestandard to an EN, the project team responsible for the conversion has asked for further national comments in order to facilitate the redrafting of the code. One issue that has been commented on by Sweden is the depth factor for glulam. The Swedish proposal is that the depth factor for glulam in bending should be removed from EC5. The two main arguments for this proposal are:

- the depth factor, given in EC5, may be correct when the mean strength of glulam beams is considered but seems to be too high when the 5-percentile is considered.

- the lower coefficient of variation for the bending strength of deep glulam beams than for shallow ones motivates a lower partial safety factor for deep beams. This could be considered as a compensation for the depth effect noted for the 5-percentile strength.

This paper is presented in order to obtain a broader discussion on the Swedish proposal.

3 European test results

3.1 General

In this chapter the results from an Austrian /1/ and a Norwegian investigation /2/ are presented and compared with the results from three minor Swedish investigations /3/-/5/. Only test series containing beams of different depths are presented. All the tests have in principle been performed according to the European standard EN 408 (similar to ISO 8375).

All pieces of timber used for the test specimens has been European grown spruce (*Picea Abies*). When sawing the logs a sawing pattern of similar kind has been used. The quality of the structural timber used for the beams has varied. The pieces of timber have been graded visually or by machine. The thickness of the laminations was 33 mm in the Austrian and the Norwegian investigations and 45 mm in the Swedish investigations.

The results of the beam tests are summarised in table 1 and table 2. In table 1 the mean value and the characteristic value of the bending strength f_m together with its coefficient of variation (COV) are presented. The characteristic values represent 5-percentiles calculated at a confidence level of 50 %. In table 2 calculated values on the factor k_h are presented. The value on the factor k_h that is given in EC5 is mainly based on mean values but should be based on 5-percentile values. In table 2 both values are given.

Comments on the test results of each investigation are given in sections 3.2 - 3.4.

3.2 Austria

A summary of an extensive Austrian investigation of glulam beams is given in /1/. In order to obtain a representative sample of Austrian timber, the timber was taken from 18 Austrian sawmills. Four pieces of timber was sawn from each log (4 EX log). The timber was machine graded in an Eurogrecomat machine. In this machine the local modulus of elasticity is determined by flatwise bending, while density, size and position of knots are determined by X-rays. The timber was graded into the Austrian and German strength classes MS10, MS13 and MS17. The characteristic bending strength of a sample of the timber belonging to the different strength classes was obtained to respectively 19,3, 24,4 and 31,1 N/mm².

It should be noted that the span of the deep beams was 16h instead of the preferred value 18h given in the test standard. This means that the bending strength values for the deep beams in table 1 should be reduced by about 1 % and the k_h values in table 2 increased by about 1 %.

Table 1 Results from bending tests of glulam beams.

Project	Quality of lamination	Dimension of beam mm ²	Number of beams	Beam bending strength f_m			Failure in finger joints %
				Mean N/mm ²	COV	Characteristic N/mm ²	
Austria /1/	MS10	160 x 297	23	27,9	0,12	22,4 (N)	9
	MS10	160 x 594	10	25,3	0,09	21,5 (N)	5
	MS17	160 x 297	20	43,0	0,15	32,5 (N)	39
	MS17	160 x 594	18	39,4	0,13	31,2 (N)	24
Norway /2/	T30M	90 x 300	24	44,0	0,15	34,1 (W) 32,8 (N)	25
	T30M	90 x 600	20	39,4	0,10	32,0 (W) 32,7 (N)	30
Sweden /3/	LT30	113 x 315	4	42,4	0,11	34,7 (N)	25
	LT30	113 x 495	4	38,9	0,12	31,3 (N)	25
	LT30	113 x 315	4	44,2	0,06	39,9 (N)	50
	LT30	113 x 495	4	31,9	0,09	27,2 (N)	0
	LT30	113 x 315	4	41,6	0,06	37,4 (N)	50
	LT30	113 x 495	4	41,5	0,18	28,9 (N)	75
	LT30	113 x 315	All	42,7	0,08	37,3 (N)	42
	LT30	113 x 495	All	37,4	0,17	26,8 (N)	33
Sweden /4/	LT30-C35	115 x 270	5	38,5	0,08	33,6 (N)	0
	LT30-C35	115 x 540	5	38,2	0,06	34,5 (N)	20
Sweden /5/	LT30	115 x 270	10	43,2	0,18	30,5 (N)	No information
	LT30	115 x 540	10	37,5	0,12	30,1 (N)	

(N) = Normal distribution

(W) = Weibull distribution

Table 2 Calculated values of the factor k_{11} from the different investigations.

Project	k_{11} based on	
	mean values	5-percentiles
Austria /1/: MS10	1,10	1,04 (N)
MS17	1,10	1,05 (N)
Norway /2/	1,12	1,07 (W) 1,00 (N)
Sweden /3/ All	1,15	(1,39 (N))
Sweden /4/	1,01	0,97 (N)
Sweden /5/	1,15	1,01-1,15 (N)

(N) = Normal distribution

(W) = Weibull distribution

For both the low quality (MS10) and the high quality timber (MS17) the coefficient of variation for the beam bending strength is lower for the deep beams than for the shallow beams. The test results do not indicate that the k_{11} factor varies with respect to the quality of the timber.

3.3 Norway

A Norwegian study of the depth factor has been reported in /2/. The timber was graded by a Computermatic grading machine to the Norwegian strength class T30M (characteristic bending strength of 30 N/mm²).

On calculating the characteristic bending strength of the beams both normal and three-parameter Weibull distributions were used. The latter best fitted the data. These values are very close to the Austrian values. If the test data are instead assumed to be of normal distribution the k_n values become lower. This illustrates how sensitive the characteristic value is to the choice of distribution function. The characteristic bending strength values based on the normal distribution in /2/ were calculated under the assumption of a confidence level of 75 %. The values in table 1 were calculated at a confidence level of 50 %.

The mean value and the 5-percentile of the bending strength for the beams of 300 mm depth are in very good agreement with the previous Norwegian results presented in /6/.

3.4 Sweden

3.4.1 Tests of standard beams

The purpose of this investigation was to study the strength and stiffness variation of standard glulam beams in Sweden taken from normal production. See reference /3/. The beams were bought from three glulam factories. The quality of the timber was supposed to be LT30 which is the highest visual grade for glulam laminations in Sweden. In 11 of the 24 beams the knots in the outer laminations did not fulfil the requirements of the grade.

It is seen from table 1 that the coefficient of variation is fairly low in all but one test series. Further it is seen that the mean strength of the deep beams from the second factory is considerably lower than for the other factories. Since it could be expected that the quality of the laminations was not the same in the shallow and the deep beams it is difficult to compare the influence of beam depth on the bending strength. With the depth ratio 495/315 = 1,57 equation (1) gives $k_n = 1,09$ which value should be compared with 1,15 found in table 2 for the quotient between the mean values.

3.4.2 Tests of beams with special lamination lay-up

The intended approach in this project /4/ was to test two different sizes of beams in short and long term loading in order to compare the size effect. For economic reasons the number of tests was limited and therefore it was decided to manufacture beams with less strength variation than in standard beams. The timber selected was visually graded LT30 of normal quality taken from one glulam factory. After the visual grading all pieces of timber were graded in a Cook-Bolinder grading machine. All pieces of timber with an expected bending strength less than 35 N/mm², corresponding to the European strength class C35, were rejected (3 %). The rest of the pieces of timber were ranked with respect to the lowest bending stiffness along each piece. The pieces of timber were numbered in ascending order with the lowest number for the piece with the lowest stiffness. The glulam beams were systematically built up starting with the lowest number in the tension zone and the highest number in the compression zone. The laminations in the tension zone of all beams can be

characterised by having low between-lamination strength variation, but the within-lamination variation due to knots and finger joints was probably substantial.

The results of the short term tests show that the mean of the bending strength values are almost the same for the two beam depths. This indicates that the larger number of weak zones, in the form of knots and finger joints, occurring in the deep beams is fully compensated for by the laminating effect.

Since the bending strength of glulam beams is mainly determined by the strength of the laminations on the tension side, and the laminations in this investigation have been very well-matched, it seems reasonable to believe that the factor k_{11} decreases with improved grading.

3.4.3 Medium-term tests of standard beams

The purpose of this project was to find out if there is a significant size effect under medium-term loading. See reference /5/. The timber for the laminations was visually graded LT30. The beams were part of the normal production, with the supplementary request that all pieces of timber should be of the same origin.

The beams were loaded in a procedure simulating an increasing snow load. After approximately four months with constant load, the load was increased stepwise every second week until failure occurred. The factor k_{11} in table 2 based on the mean values is 1,15. The corresponding factor based on the 5-percentiles is 1,01. The latter value was obtained assuming normal distribution. Since one of the values, in the test series with deep beams, is much higher than the others, it is reasonable to reject this value when the 5-percentile is calculated. In that case the factor k_{11} becomes equal to 1,15.

4 Partial safety factor for glued laminated timber

In connection with calibration of partial coefficients in Sweden /7/ the influence of the coefficient of variation on the partial safety factor for different wood-based materials was investigated. The result of the calculations is shown for glulam beams in table 3. In the bending strength data of table 1 it can be seen that there is a tendency towards a lower coefficient of variation for the deep beams than for the shallow beams. In the Austrian and the Norwegian investigations the coefficient of variation changes from about 0,14 (shallow beam) to 0,11 (deep beam). This change corresponds to a change of the partial safety factor of about 3 %. However, it is not reasonable to have different safety factors for different beam depths. An easier way of acting is to compensate for this by omitting the correction for depth.

Table 3 Influence of coefficient of variation on partial safety factor for glulam.

Coefficient of variation	Partial safety factor
0,15	1,40
0,12	1,35
0,07	1,30

5 Conclusion

The Austrian and the Norwegian investigations indicate that the depth factor k_h based on 5-percentiles should be about 1,06. In both investigations machine graded timber was used.

A Swedish investigation with well-matched laminations on the tension side of the beams indicate that k_h may be even lower when there is a low variation in the strength of the laminations. This means on the other hand that k_h may be somewhat higher for visually graded timber where there is a somewhat higher variation in the strength of the timber.

There is a tendency towards a lower coefficient of variation in the bending strength for deep beams than for shallow ones. This has an effect on the partial safety factor which could be handled by reducing k_h by about 3 %.

Based on the discussion above it is proposed that the depth factor k_h should be removed from EC5.

For other wood species than spruce (*Picea Abies*) where other sawing patterns are used and where large single traversing knots appear in the laminations, it cannot be excluded that the depth factor k_h is different.

References

- [1] Schickhofer G. 1996: Development of efficient glued laminated timber, *CIB-W18 Meeting*, Paper 29-12-1, Bordeaux, France.
- [2] Aasheim, E.; Solli, K. H. 1995: Size factor of Norwegian glued laminated beams, *CIB-W18 Meeting*, Paper 28-12-2, Copenhagen, Denmark.
- [3] Johansson, C. J.; Anneling, R. 1987: *Testing of glued laminated timber beams* (in Swedish), SP - Swedish National Testing Institute, Report 86B2,1036, Borås, Sweden.
- [4] Carling, O.; Johansson, C. J. 1997: *Bending strength of glued laminated timber beams - The size effect - A question of grading* (in Swedish), Under preparation, Bjerking Ingenjörbyrå AB, Uppsala, Sweden.
- [5] Carling, O. 1997: *Bending strength of glued laminated timber beams - Size effect at simulated snow load - Experimental investigation* (in Swedish), preliminary version 1997-10-14, Bjerking Ingenjörbyrå AB, Uppsala, Sweden.
- [6] Falk, R. H.; Solli, K. H.; Aasheim, E. 1992: *The performance of glued laminated beams manufactured from machine stress graded Norwegian spruce*, The Norwegian Institute of Wood Technology, Meddelelse 77, Oslo, Norway.
- [7] Albrektsson, L. 1996: *Determination of partial safety factors for timber structures* (in Swedish), National Board of Housing, Building and Planning, Rapport 1996:11, Karlskrona, Sweden.

CIB-W18/31-15-1

INTERNATIONAL COUNCIL FOR BUILDING RESEARCH STUDIES AND DOCUMENTATION
WORKING COMMISSION W18 - TIMBER STRUCTURES

SEISMIC PERFORMANCE TESTING ON WOOD FRAMED SHEAR WALL

by

N Kawai

Codes and Evaluation Research Centre
Building Research Institute

JAPAN

MEETING THIRTY-ONE

SAVONLINNA

FINLAND

AUGUST 1998

Seismic Performance Testing on Wood Framed Shear Wall

Naohito Kawai
Codes and Evaluation Research Center
Building Research Institute, Japan

1. Abstract

To investigate the seismic performance of a shear wall used in wood frame construction and to confirm the adequacy of the response prediction based on the static loading test, a series of tests, which consists of static loading test, pseudo-dynamic test and shaking table test, was executed. The plywood sheathed shear wall of the specimen in each test was assembled with the same specification. The results of the pseudo-dynamic test and the shaking table test were compared with the result of response analysis using the load-displacement hysteresis model based on the static cyclic test result. The analytical result agreed well with the test results when the hysteresis models are used with considering the influence of the damage in one side to the opposite side.

2. Introduction

The prediction of response against the strong ground motion is the basis of seismic performance evaluation of buildings. There are several convenient methods proposed to predict the maximum response displacement, for example, application of property of energy conservation and equivalent linear analysis (or Capacity Spectrum Method (CSM)). The former is often used as the basis of modification factors to reduce the seismic force considering non-linear response, for example, q in European Standard and D_s in Building Standard Law (BSL) of Japan. The latter is now discussed in Japan to be applied in the BSL enforcement order as a new evaluation method of seismic performance of buildings.

Concerning timber structures, the adequacy of applying the CSM method has not been discussed enough. It is need to compare the results between time history analysis and CSM to confirm the applicability and to develop the details of application method. Before these woks, it is important to confirm the adequacy of the hysteresis models used in the time history analysis.

First in this paper, the results of shaking table test, pseudo-dynamic test and static loading test on a shear wall used in wood frame construction are summarized. Next, the result of the time history analysis based on the static cyclic loading test is discussed compared with the results of shaking table test and pseudo-dynamic test.

Several types of hysteresis model have been proposed for wood framed shear walls. The combination of bi-linear model and slip model is proposed as one of the models which agree well with result of static tests or pseudo-dynamic tests[1][2]. In this paper, the combination model is used with a modification considering the influence of large displacement in one side to the behavior in the opposite side.

3. Testing Methods

3.1 Static cyclic loading test

Fig. 1 shows schematic diagram of the specimen and loading method in the static loading test. One specimen of wood framed shear wall sheathed with plywood on one side was tested. The species and the grade of the framing members are S-P-F, JAS Standard and the sectional size is 38 mm × 89 mm. The grade of the plywood is JAS No.2 (conifer plywood) with a thickness of 9.5 mm. Nails of JIS CN50, 50 mm in length and 2.87 mm in diameter, are used with the spacing of 100 mm along four edges and 150 mm along the center stud. At the end of the wall, double studs are used connected to the steel base with a hold down connector and a bolt. The length of the wall is 910 mm between the center of outside studs at the end of the wall, and the height is 2450 mm. Lateral load was applied to the top of the wall through the loading beam using the loading protocol shown in Fig.2 which is similar to that provided in CEN standard[3]. The yield displacement D_y was determined based on the result of monotonic loading test by the protocol proposed by Yasumura and Kawai[4].

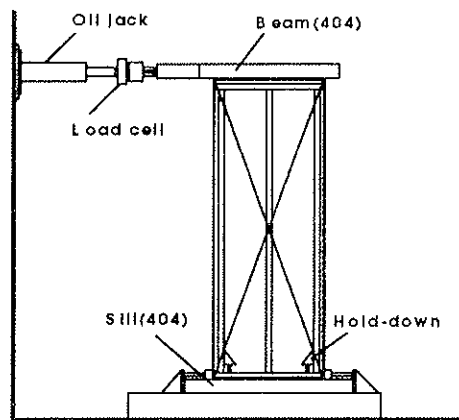


Fig. 1 Static loading test apparatus

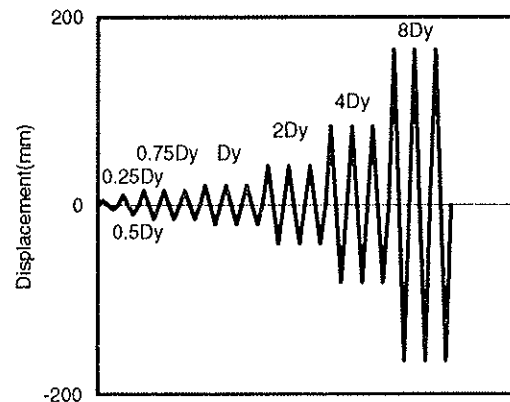


Fig. 2 Loading protocol

3.2 Shaking table test

Fig. 3 shows the schematic diagrams of the specimen and the measuring method in the shaking table test. One box-shaped specimen with two shear walls arranged parallel in both sides was tested. The specification of the shear wall was same as that used in the static cyclic loading test except that triple studs are used at the end of the shear wall. The mass of 4284 kg is put on the ceiling. The target value of the mass (m) was determined according to Eq. 1. This value corresponds to the 80 % of the upper limit in seismic design against the

strong ground motion as 1 g is the standard elastic response acceleration in Japan.

$$D_s m g = 0.8 Q_u \quad (\text{Eq.1})$$

Here, D_s = structural characteristics factor (= 0.3) (which corresponds to the reciprocal number of the European behavior factor q), m = the mass, g = gravity acceleration, Q_u = ultimate shear strength of the shear wall (= 15.6 kN for two walls of 910 mm in length). D_s and Q_u were determined according to the structural design manual in Japan [5].

The earthquake wave used was the north-south component of the Kobe earthquake (1995) recorded in Kobe Marine Meteorological Observatory with reduction to about 60 %, the target maximum velocity of which is 55 cm/sec while the maximum velocity of original wave is 90.2 cm/sec. The acceleration record with a sampling frequency of 50 Hz was used. Absolute acceleration and relative displacement are measured in some points of specimen as shown in Fig. 3 with a sampling frequency of 200 Hz.

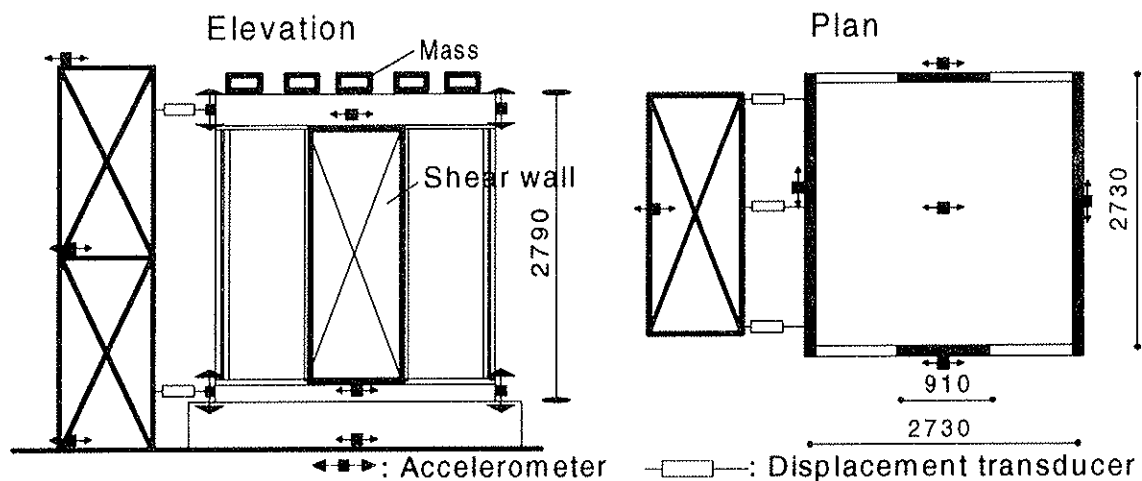


Fig. 3 Schematic diagrams of shaking table test

3.3 Pseudo-dynamic test

After the shaking table test, pseudo-dynamic test on the shear wall with the same specification was performed using the acceleration record measured on the table in the shaking table test as the input wave with a sampling frequency of 100 Hz. Fig. 4 shows the schematic diagrams of the specimen and the loading and measuring method. The shape and the dimension of the specimen were almost same as those used in shaking table test. Differences between the specimens are only for the convenience of the loading. The height of the ceiling beams was a little higher than shaking table test and the width between the shear walls was 2.1 m while it was 2.73 m in the shaking table test.

Newmark's β method with zero substituted for β was used to calculate the target displacement of each loading step. The same value of mass used in shaking table test, 4284

kg, was also assumed in the calculation part of the pseudo-dynamic test. However, no actual mass was put on the specimen. The value of coefficient of viscous damping (C) was assumed to be constant during the response, and was determined to be $2.94 \text{ kN}\cdot\text{sec/m}$ using the damping factor (h) assumed to be 2 % and initial stiffness based on the free vibration test on the specimen of the shaking table test.

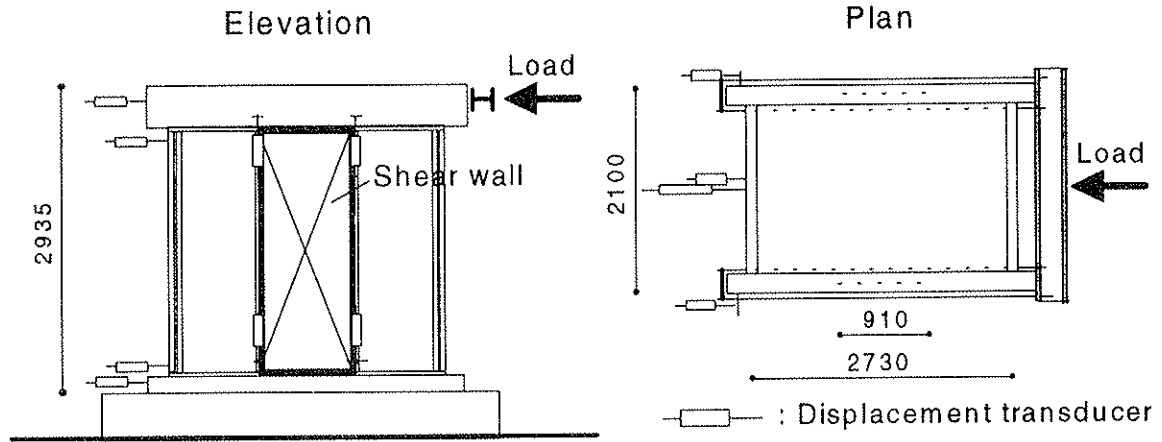


Fig. 4 Schematic diagrams of pseudo-dynamic test

4. Test results

4.1 Static cyclic loading test

Result of the static cyclic loading test is mentioned in the sections 4 and 5 related to the time history analysis.

4.2 Shaking table test

Fig. 5 shows the time history waves observed in the shaking table test, which are waves of input acceleration, response absolute acceleration, relative velocity and relative displacement at the top of the specimen. The response relative velocity is obtained by the integral calculus of relative acceleration. Fig. 6 shows the relationship between load and displacement. The value of load is calculated as the product of mass and absolute acceleration as shown in Eq. 2, that means it consists of restoring force and effect of damping.

$$Q = -m(\ddot{y}_0 + \ddot{y}) = C\dot{y} + Ky \quad (\text{Eq.2})$$

4.3 Pseudo-dynamic test

Fig. 7 shows the time history waves and Fig. 8 shows the relationship between load and displacement observed in the pseudo-dynamic test. These values are measured or calculated in each step of loading during the test. In Fig. 8, solid line means the relationship using the load applied by the jack and dotted line means that using the load calculated by Eq. 2.

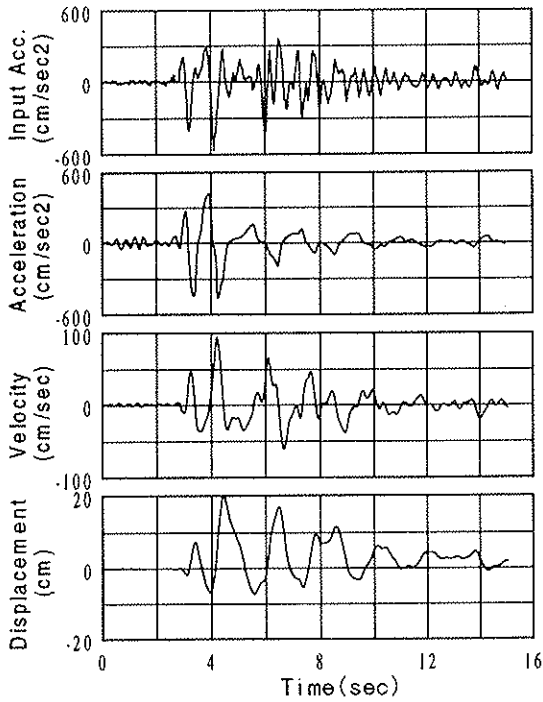


Fig.5 Time history waves observed in shaking table test

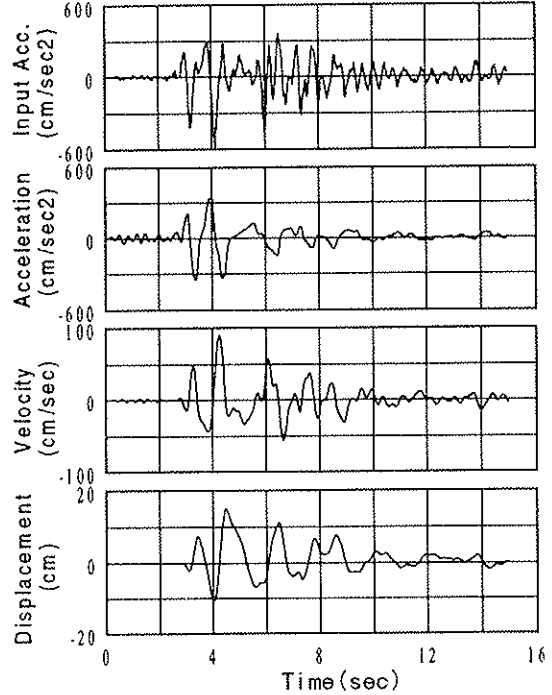


Fig. 7 Time history waves observed in pseudo-dynamic test

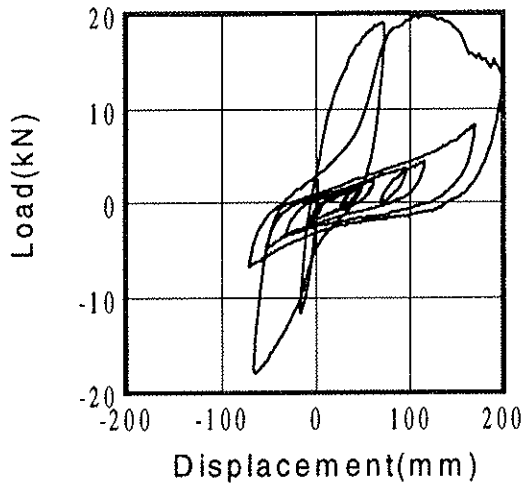


Fig. 6 Load-displacement curve observed in shaking table test

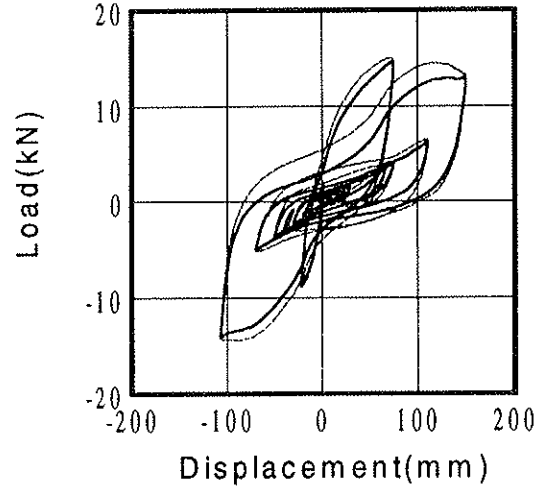


Fig. 8 Load-displacement curve observed in pseudo-dynamic test

5. Time history analysis

5.1 Analysis method

Time history response analysis was executed using a load-displacement hysteresis model based on the result of static cyclic loading test. Fig. 9 shows the combination model of bi-linear and slip, and Table 1 shows the parameters of the model which are determined so that the load-displacement relationships agree well with the static test result. Fig. 10 shows the comparison of load-displacement relationship between the model and the test result.

In the analysis, the experienced maximum displacement in one side (e.g. in positive displacement side) is used also in the opposite side (in negative displacement side), if it is over the displacement at the maximum strength. This assumption is based on the behavior observed in shaking table test and pseudo-dynamic test. The damage of nailed joints at large displacement in one side, such as punched out or withdrawal, apparently influences the following behavior not only in the same side but also in the opposite side.

The response analysis method used was linear acceleration method (or Newmark's β method with $1/6$ substituted for β). Values of mass and coefficient of viscous damping assumed and input acceleration wave used in the analysis were same as those used in the pseudo-dynamic test.

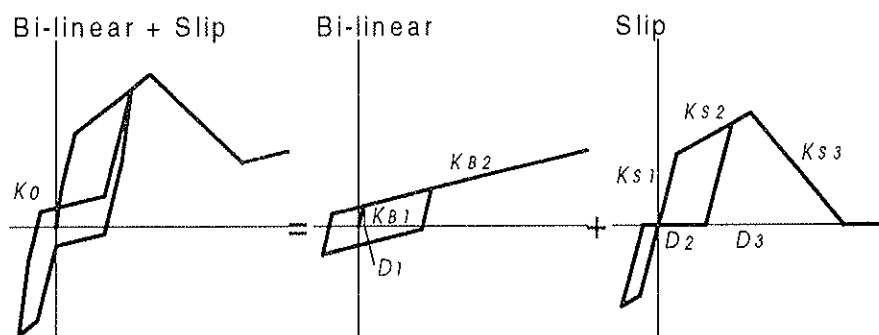


Fig. 9 Hysteresis model used in the time history analysis

Table 1 Parameters used in the analysis

K_0 (kN/cm)	K_{B1}/K_0	K_{B2}/K_0	K_{S1}/K_0	K_{S2}/K_0	K_{S3}/K_0	D_1 (mm)	D_2 (mm)	D_3 (mm)
11.77	0.58	0.02	0.42	0.04	-0.06	4	20	70

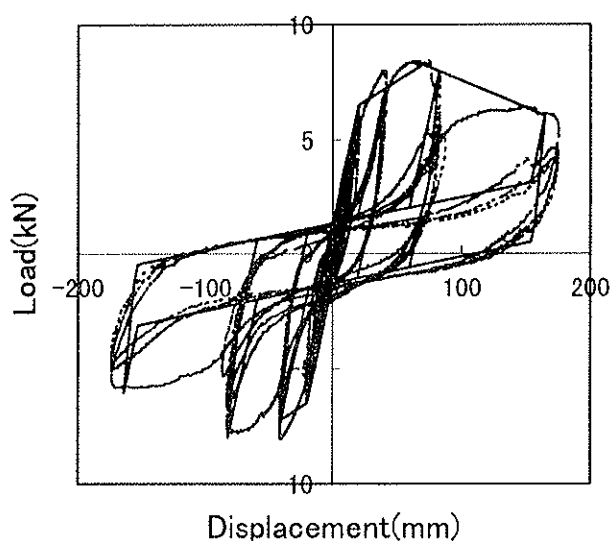


Fig. 10 Comparison of load-displacement relationship between the result of static loading test and the model

5.2 Analysis result

Fig. 11 shows the time history waves and Fig. 12 shows the relationship between load and displacement obtained by the analysis.

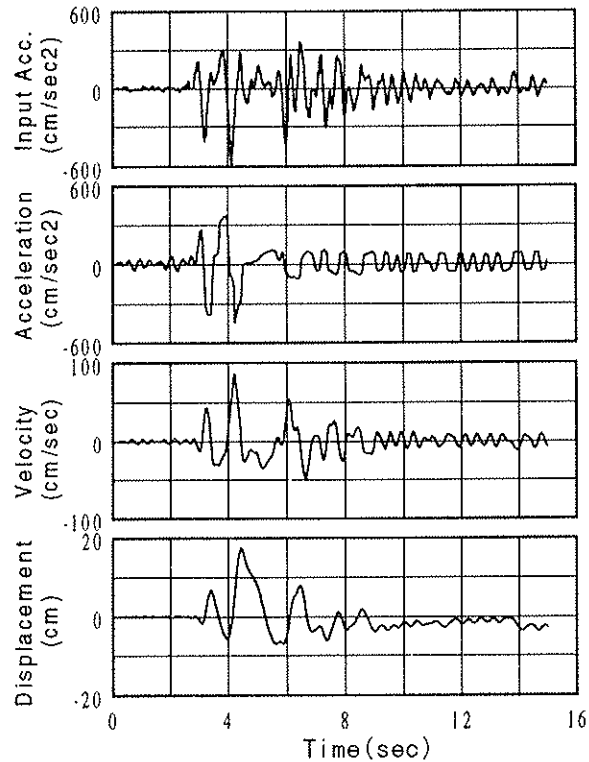


Fig. 11 Time history waves by the analysis

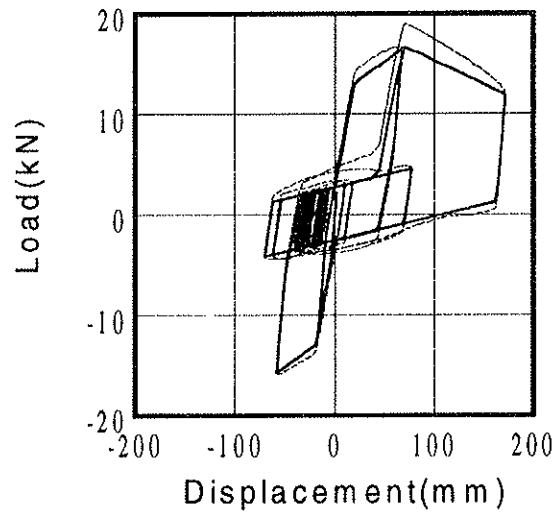


Fig. 12 Load-displacement relationships by the analysis

6. Discussions

6.1 Comparison of the results

Comparing the time history waves and load-displacement relationships shown in Fig. 5 to 8, 11 and 12, we see that the response in the shaking table test is simulated well in the

pseudo-dynamic test as well as in the time history analysis. Especially, the analysis result agreed well with the result of the shaking table test.

However, there are small differences among them. Table 2 shows the comparison of maximum (and minimum in the negative side) response values obtained by the tests and the analysis. Maximum response values of absolute acceleration, relative velocity and relative displacement observed in shaking table test are almost larger than those in pseudo-dynamic test. And the values obtained by the time history analysis come between them and nearer to those in shaking table test.

It is likely that the variety of shear strength of the specimens caused the difference. Comparing the load-displacement curves in Fig. 6 and 12, the load in the pseudo-dynamic test is lower than the model based on the static loading test though both specimens are loaded statically.

Table 2 Comparison of maximum response values

	AA max (cm/sec ²)	AA min (cm/sec ²)	RV max (cm/sec)	RV min (cm/sec)	RD max (cm)	RD min (cm)
Shaking table test	420	-461	94.0	-60.7	19.9	-7.1
Pseudo-dynamic test	337	-350	89.9	-55.0	14.9	-10.6
Analysis	370	-444	85.1	-48.1	17.2	-7.0

6.2 Damping factor

In the convenient method of response prediction called as CSM, one of the most important problem is the assumption of the damping factor h in the equivalent linear response. To investigate the appropriate value of h , the substitute damping h_s is often used[6], which is defined by Eq. 3.

$$h_s = \frac{-\int_0^t \ddot{y}_0 \dot{y} dt}{\omega_e \int_0^t \dot{y}^2 dt} \quad (\text{Eq. 3})$$

Here, ω_e means the natural circular frequency of the equivalent linear response calculated with using the maximum response displacement and the load at the point. The values of h_s calculated from the result of the shaking table test and the pseudo-dynamic test during the time from 0 to 15 seconds are 29.6 % and 27.1 %, respectively. While, h_s calculated from analytical result is 44.4 %, which is approximately 1.5 times of the test results. It suggest that the hysteresis model based on the static loading test should be improved from the view point of damping.

Fig. 13 shows the equivalent viscous damping factor (h_{eq}) obtained by static cyclic loading test and the hysteresis model. The value of h_{eq} depends on the loading history, and tends to increase according to the displacement. In the large displacement area, h_{eq} becomes almost

constant to 20 % to 25 % for the first loop and 15 % to 20 % for the second and third loops. While, the value of viscous damping (h') calculated by Eq. 4 using the assumption and the result of pseudo-dynamic test was 7.6 %. Here, h' is the viscous damping factor modified using ω_e of the equivalent linear response.

$$h' = \frac{C}{2m\omega_e} \quad (\text{Eq. 4})$$

Therefore, h_s is approximately equal to the summation of h_{eq} for the first loop and h' at least in the result of the pseudo-dynamic test.

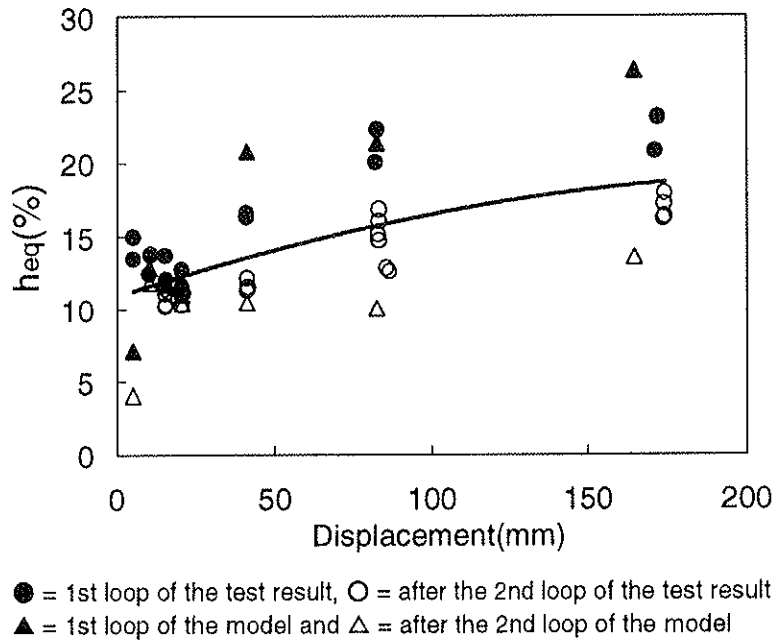


Fig. 13 Equivalent viscous damping factor h_{eq} obtained by static loading test and the hysteresis model

7. Conclusions

The earthquake response of a wood framed shear wall was obtained by shaking table test and pseudo-dynamic test. The result of the time history analysis using the hysteresis model of bi-linear and slip based on the static cyclic loading test, agreed well with the results of shaking table test and pseudo-dynamic test when the influence of large displacement in one side to the behavior in the opposite side is considered. However, the comparison of substitute damping h_s suggests that it is necessary to improve the hysteresis model based on the static test result. And the value of h_s obtained by the pseudo-dynamic test was approximately equal to the summation of equivalent viscous damping h_{eq} and modified viscous damping h' .

8. Acknowledgment

These tests were executed as a part of collaborative research of Building Research Institute with Japan Two-by-four Home Builders Association. Author would like to thank Mr. Sakabe of the Association and the other participants of the collaborative research as well as Mr. Okabe of Center for Better Living for execution of the tests.

9. References

- [1] Sakamoto, I., Y. Ohashi, and M. Shibata: Theoretical analysis of seismic response of wooden dwellings in Japan, Proceedings of Pacific Timber Engineering Conference, 1984.
- [2] Tarabia, A. and F. Kamiya: Analytical seismic response of wood shear walls using hysteresis models of nailed joints, Journal of the Japan Wood Research Society, Vol.42, No.11,1996.
- [3] CEN: EN TC 124. 117, May 1994
- [4] Yasumura, M. and N. Kawai,: Evaluation of Wood Framed Shear Walls subjected to Lateral Load, CIB-W18/30-15-4,1997
- [5] Japan Two-by-four Home Builders Association: Structural calculation manual for buildings of wood frame construction, 1992.
- [6] Shibata, A. and M.A. Sozen: Substituted Structure Method for Seismic Design in R/C, Proceedings of ASCE, Vol. 102, No. ST1, 1976.

**INTERNATIONAL COUNCIL FOR BUILDING RESEARCH STUDIES AND DOCUMENTATION
WORKING COMMISSION W18 - TIMBER STRUCTURES**

**ROBUSTNESS PRINCIPLES IN THE DESIGN OF MEDIUM-RISE
TIMBER-FRAMED BUILDINGS**

by

C J Mettem
M W Milner
R J Bainbridge

TRADA Technology

V Enjily

BRE Ltd

UNITED KINGDOM

MEETING THIRTY-ONE

SAVONLINNA

FINLAND

AUGUST 1998

Robustness Principles in the Design of Medium-Rise Timber-Framed Buildings

By: **C.J. Mettem, M.W. Milner & R.J. Bainbridge**, TRADA Technology, UK
V. Enjily, BRE Ltd., UK

Abstract

One of the general principles for the structural design of buildings, which is almost universally accepted, is that exceptional conditions should be considered. For example, ENV 1991-1 has the fundamental requirement that a structure shall be designed & executed in such a way that it will not be damaged by events such as fire, explosion, impact or consequences of human errors, to an extent disproportionate to the original cause. In terms of exceptional events other than fire, this is often termed the "Robustness Requirement".

For residential timber-framed construction in the low-rise (1 to 3 storey) category, good robustness has been well established by experience, & has also been demonstrated by test. Such buildings are, by their very nature, cellular, lightweight, tied together & constructed using materials with broadly a good response to many of the forms of accidental event which are of a brief duration.

To address the concerns of the industry & regulatory authorities that better guidance is now required on what is to be expected in terms of robustness for medium-rise timber-frame, & how it can be demonstrated, a pre-feasibility study, & a Stage 1 Project was carried out. This led to the planning of a programme of physical tests on a six-storey structure, the aims of which are described in this paper.

1. INTRODUCTION

Timber-frame construction is ideally suited to the need for reliable, fast-built, high quality medium-rise accommodation [1]. However, to compete against alternative materials, especially structural masonry, costs need to be kept under constant review. This entails eliminating unnecessary expense, & especially in the instance of this paper, getting rid of inessential structural details which do not enhance performance.

Building regulations in the UK [2,3,4] contain specific requirements for resistance to accidental damage. The avoidance of collapse which is disproportionate to the cause, is a fundamental principle amongst these. No fully agreed application rules yet exist for medium-rise timber-frame, & this situation has led to the inclusion of a number of typical details which may in fact be unnecessary. Leading developers consider that the inherent robustness of panellised construction, with well-fixed connections & composite tying, via diaphragm floors to suitable foundation anchorages, provides adequate robustness in itself, rendering special measures redundant.

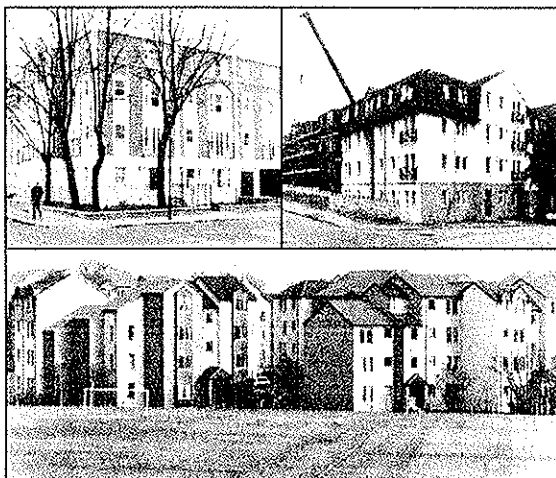


Figure 1 *Some Examples of Existing Medium-Rise Timber-Framed Buildings*



Figure 2 *Five Storey Timber-Framed Apartments in South Wales*

Figure 1 illustrates examples of modern medium-rise timber-framed buildings in the UK. Typically, & until recently, such buildings have consisted of four timber-frame storeys, usually clad in masonry, the styles of which vary somewhat according to the region. Commencing with four storeys of timber-frame erected on

basements, or on a fully-masonry ground floor, developments have led to actual structures in commercial practice, such as that shown in Figure 2, with five fully timber-framed storeys.

A feasibility study was jointly undertaken by TRADA Technology & BRE in 1994 [5], to review & summarise construction requirements & research needs relating to this subject. A programme of component testing & full-scale building tests was developed. The ultimate aim of this work is to draw up & publish an authoritative national Guidance Document. This will link in turn to codes & standards coming into force, in particular Eurocode 5: Part 1-1 [6] & certain parts of Eurocode 1 [7].

This paper considers the current requirements for resistance to accidental damage as they relate to medium-rise timber-frame. It also provides a preliminary overview of the testing for robustness of a building which omits all deliberate & additional strengthening measures above those inherent in normal platform frame timber buildings.

2. ROBUSTNESS - THE RESISTANCE TO ACCIDENTAL DAMAGE

2.1 The General Requirement For Robustness In Buildings

Robustness in buildings is required to provide protection for both the occupants, & for those in the surrounding vicinity, in the face of various forms of accidental event. Ever since the collapse of the Ronan Point pre-fabricated concrete panel high-rise tower block in 1968 (see Figure 3) [8], due to a relatively minor gas explosion, there have been strict regulatory requirements throughout the UK, with respect to resistance to accidental damage.

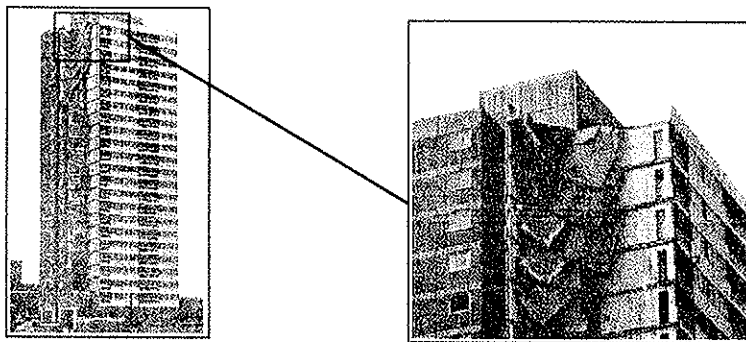


Figure 3 Ronan Point, Newham, London - May 1968

Comparable events elsewhere have also influenced both professional & public opinions on a wider scale. For example, the investigations following a bombing incident in The Murrah Federal Building, Oklahoma concluded that the collapse was disproportionate to the region of the structure directly affected by the blast, & was progressive [9]. This led to new design recommendations for reinforced concrete structures in North America, drawing upon seismic design knowledge. It is of importance to note that seismic design is not a normal consideration in a number of European member states, including the UK. Therefore, whilst it is recognised that knowledge in relation to this subject may prove to be of use if enhancement measures are required to meet disproportionate collapse requirements, it is known that there is a sizeable degree of inherent robustness in the current form of timber construction due to system effects & in-built safety factors under design situations other than accidental.

The importance of ensuring that structures are designed in such a manner as to achieve efficiency whilst retaining robustness is recognised in a recent report by the UK Standing Committee On Structural Safety (SCOSS), a joint body of the professional institutions of Civil & Structural Engineers [10]. This concluded that, 'Attempting to protect buildings fully from damage by massive explosions is not realistic, but aiming to achieve robust structures, i.e. structures resistant to disproportionate collapse, may give a degree of explosion resistance'.

In the UK, therefore, in addition to the normal vertical & lateral resistance calculations, additional formal calculations are required for larger structures to prove that the building will remain stable & will not experience "Disproportionate Collapse" in the event of an accident. Such calculations may derive from one of several alternative philosophies & consequent assumptions. The regulations are deliberately couched in such a manner that the nature of the "accident" itself is undefined. For calculation purposes, the "accident" is normally translated to the non-existence of some specific load-bearing element.

2.2 The Eurocodes Approach

The safety format of the Eurocodes, in formally recognising accidental actions as being associated with factors different from normal design, is undoubtedly one of the major areas of improvement, in comparison with older national codes. In EC5: Part 1.1 for example, the design values of accidental actions are defined formally in Table 2.3.2.2 & its associated clauses.

As a fundamental design requirement for all structures [7], a design must not suffer disproportionate damage through accidental events, & EC1: Part 1 goes as far as defining appropriate methods to limit or avoid such risks (2.2.(4)P), as described in Table 1.

Avoiding, eliminating or reducing the hazards which the structure may sustain
Selecting a structural form which has low sensitivity to the hazards considered
Selecting a structural form & design that can survive adequately the accident removal of an individual element or a limited part of a structure, or the occurrence of acceptable localised damage
Avoiding as far as possible structural systems which may collapse without warning
Tying the structure together

Table 1 *Measures to satisfy EC1 Robustness Requirements*

In codes such as EC1, some hazards giving rise to exceptional conditions are defined, whereas others, such as sabotage, warfare & falling rocks, are deliberately excluded [7,14]. Risk is expressed in terms of the probability & consequences of such undesirable events. A residual risk is acknowledged, & its acceptability is supposed to be determined from the costs of safety measures, & from conceivable public reaction after an accident.

Although failures of an accidental nature, whatever their cause, should have collapse consequences which are of as controlled & non-catastrophic a nature as possible, such types of failure are, by their very definition, “extremely rare” & it is recognised that nothing can be guaranteed to be absolutely safe. Qualification of exactly how safe a building may be under such circumstances is a challenge to reliability theoreticians which is not yet solved [11,12].

In order to replace the desired reliability (& hence robustness) in context, it is necessary to consider the place of design in relation to the goals. The design process must be carried through in such a way as to promote a safe, & economical solution. The pressures of economic delivery of structures can be seen to act as a device to discourage “over-design”.

A recent assessment of the concept of over-design [13] identified the prime objective of an engineer as production of “*a robust solution, without risk of catastrophic failure, but in the most economic & practical way possible*”. The dilemma was identified & it was thus observed that “*there must inevitably be an element of over-design*”. This of course has implications essentially involving safety criteria. As identified by Schneider [11], “*it is not the structure as such that is designated safe, but rather the people in its area of influence*”.

In the context of very large structures, further consideration may be justified, beyond the primary considerations of safety. For example the cost implications associated with redress of damage & restoration of acceptable performance in parts of the structure adjacent to the collapsed region. However, in general serviceability criteria, which if exceeded may lead to complaints from building users, have little direct connection with design for robustness. Nevertheless when a large building structure, such as a medium-rise timber-frame, is formally “designed” to ensure robustness, then the design process should also entail checking the implications of the necessary design features upon the global performance of the structure, including the various serviceability limit state aspects.

2.3 Definition of Collapse

Whilst the true definition of “collapse” is related to the sudden loss of strength resulting in failure of elements (i.e. ULS limits), in a structural context it can be argued that excessive irreversible deflection in a structural system as the direct result of an accidental event may be an equally justified practical limit for design purposes. A point to note is that in order to conform, the building does not have to be usable with normal “comfort” levels directly after the event.

For these purposes, the masonry cladding in timber-frame buildings is not at present deemed “structural”, although it is considered to shield the timber structure from a proportion of the wind load in the normal calculations. Hence failure in the masonry is not considered in relation to compliance of the timber structure. However, there is clearly a realistic limit to the extent of masonry collapse which will be acceptable, & it is an important function of the full-scale building tests to help to identify this.

2.4 Definitions & Limitations For Structural Compliance

To satisfy building regulation requirements, it is necessary to ensure that the safe egress of people can be achieved when a building has a structural problem which is not disproportionate to the cause. For example, an event that causes only the removal of localised supports, which for timber-frame may be considered as the denial of a principal load bearing wall, would be expected to be followed by safe egress with an absolute minimum of one hour duration.

A secondary principle has been identified, which is to ensure that the building provides safe access for emergency services, so that temporary propping can be inserted, to re-establish stability. Under such conditions, it is considered necessary to resist further “disproportionate collapse” for between 1 & 5 days. This requirement falls outside the building regulations requirements, & magnifies the subjective aspects of the disproportionate collapse assessment. Since timber structures are known to be sensitive to time dependant loading, this introduces additional technical complexities.

2.5 Compliance With Disproportionate Collapse Requirements

Because of the relatively low numbers of medium-rise buildings at present (compared with the millions of low-rise timber-framed buildings in Europe), & due to the limited experience of their performance to date, design procedures to ensure robustness follow formalistic measures.

Demonstration of compliance is at present achieved, by checking that upon notional removal of each support member under consideration, one at a time in each storey in turn, the area of collapse of the structure within the storey & the immediately adjacent storeys is limited to the lesser of 15% of the floor area of the storey or 70m², as identified in Figure 4.

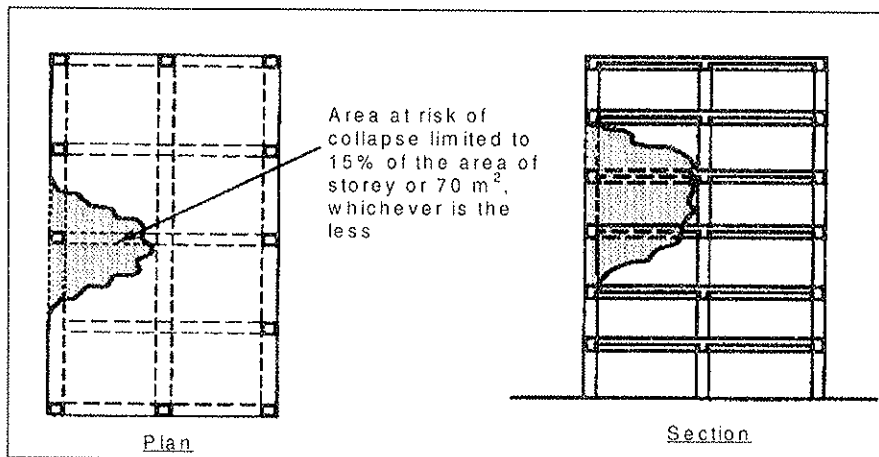


Figure 4 Graphical Definition of Collapse Area

For residential timber-framed construction in the low-rise (1 to 3 storey) category, good robustness has been well established by experience [15], & has been demonstrated to a certain extent by test [16], as shown in Figure 5.



Figure 5 Robustness of Low-Rise Timber Construction [16]

3. EXPERIMENTATION BASIS

As explained above, the feasibility study [5] cited the need for a full-scale test programme. In conjunction with the more recent regulatory & code developments described above, this led to a final experimental plan, which is currently in progress at the time of writing.

These physical tests involve the removal of panels along one external wall, & one internal load-bearing wall of a six-storey test building, shown in Figure 6.

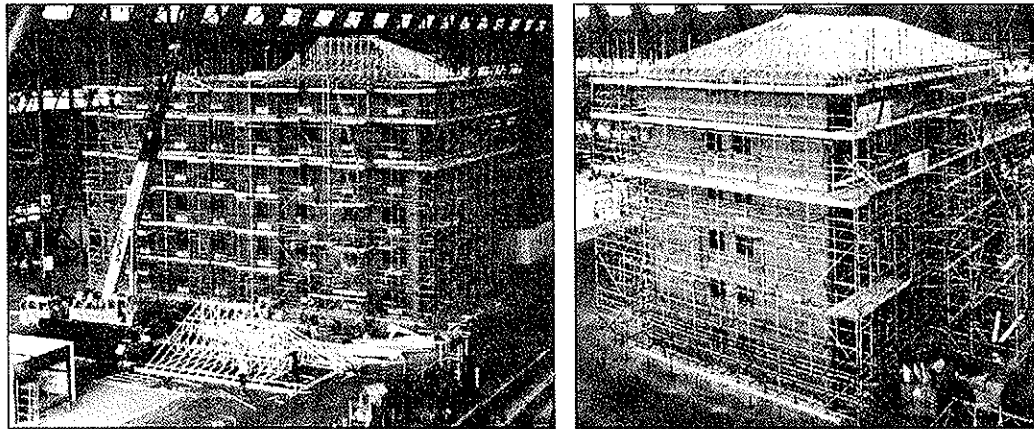


Figure 6 Prototype Test Building During Construction

Clearly, before these walls are experimentally removed, & analysis of the entire building has been necessary, to predict its likely behaviour. Whole building behaviour is complex, & only approximate predictions of likely “post-event” behaviour have been possible so far. The approach to date has simply been to treat the building as a series of two dimensional assemblages. Clearly, more effort is required to improve upon this approach in the future, & whole-building modelling could be a realistically achievable aim.

Predictions of the behaviour of the structure when selected load bearing walls are removed, are shown in the sketch drawings contained in Figure 7.

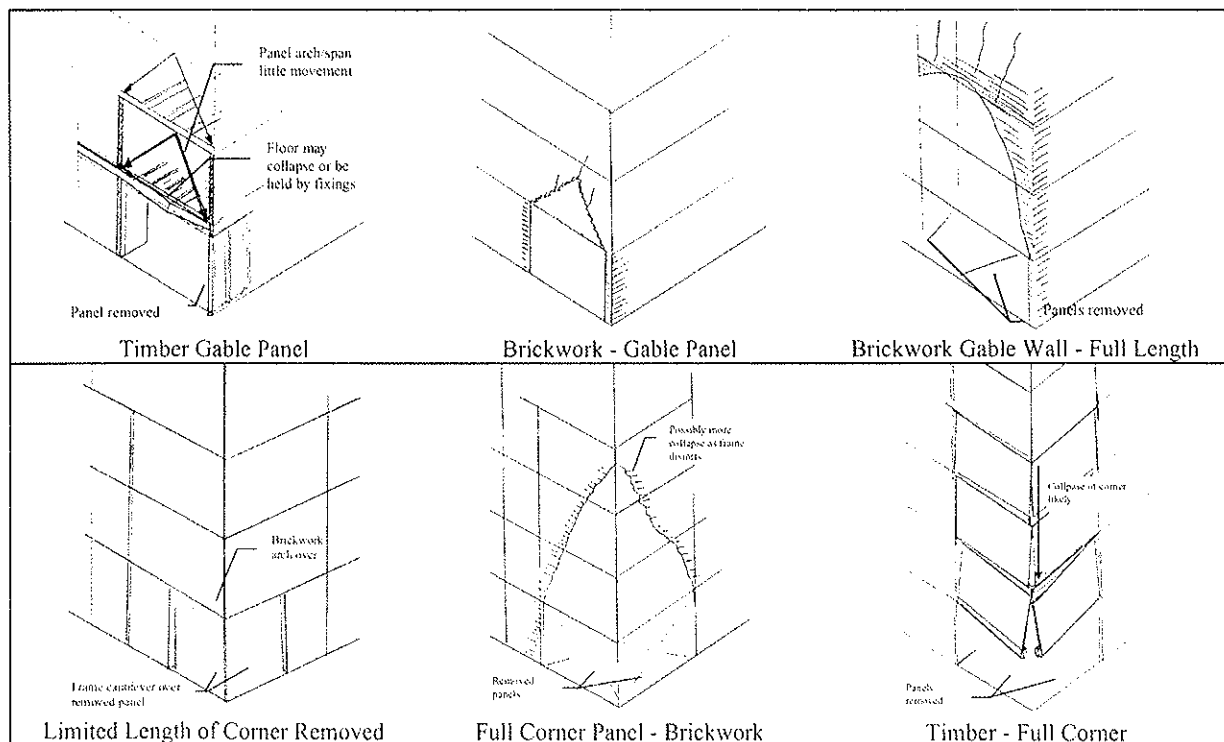


Figure 7 Sketches of Predicated Partial Collapse Mode from Test

To reflect the design calculations necessary for assessment of an accidental situation, the loading conditions applied to the residual structure after removal of lengths of wall were as presented in Table 2. These

may also be further explored in future calculations, where action combinations relating to accidental damage in the Eurocodes can be brought into play.

Load Component	Magnitude of Action
Full dead load	Full in-service dead load, including all finishes
1/3 floor imposed load	0.5 kN/m ² for flats (not reduced for number of storeys).
1/3 roof imposed load	Snow & storage
Wind load	No wind load conditions are included

Table 2 Loading Conditions Assumed During Accidental Damage Predictive Calculations

4. CONCLUSIONS

Tests currently in progress will permit an evaluation of the actual behaviour of a typical six storey medium-rise timber-framed structure when selected vertical load bearing wall panels are removed. It is hoped that this will verify that the inherent stiffness of cellular platform timber-frame construction can provide robustness, so that in the event of an accident, such buildings will not suffer collapse to an extent disproportionate to the cause.

This research will develop a basis for design guidance on the theoretical procedures required in the future. It is however recognised, that although these whole building tests will produce useful results, they will in some ways be restricted to buildings of a form similar to the test prototype. Therefore, if comprehensive authoritative guidance is to be produced, from which other buildings could be designed/checked against disproportionate collapse, then other tests may be required. These tests would address issues not covered in the current research, such as the comparative effects of removal of internal walls with doors & external walls with openings. Further studies to identify the strength of deep OSB & plasterboard sheathed panels would also be beneficial.

The wider-reaching impacts of such research include not only the permeation of information into codes, standards & regulations, but also enhancement of the fundamental appreciation of this form of structure that will be beneficial to future investigations of full structure & component behaviour, whether through physical test methods & procedures, or as a tool for representative numerical modelling or reliability based studies.

This subject not only has implications for design under accidental situations, but also for appreciation & quantification of material interaction & structural system effects which are applicable to development & refinement of many aspects of limit states design for timber structures as a whole.

REFERENCES

- [1] METTEM, C.J., BAINBRIDGE, R.J., PITTS, G.C. & ENJILY, V., (1998). Timber Frame Construction For Medium Rise Buildings. Progress in Structural Engineering & Materials, Volume 1, Issue 3, Timber Construction, Construction Research Communications Ltd., UK.
- [2] HMSO, (1991). The Building Regulations 1991. Department of the Environment & Welsh Office, London.
- [3] HMSO, (1990). The Building Standards (Scottish) Regulations. The Scottish Office, Edinburgh, 1990.
- [4] HMSO, (1994). The Building Regulations (Northern Ireland). Department of the Environment for Northern Ireland, Belfast.
- [5] METTEM, C.J., PITTS, G.C., STEER, P.J., & ENJILY, V., (1996). Current developments in Medium-Rise Timber Frame Buildings in the UK. CIB-W18/29-15-4. CIB-W18 Meeting Twenty-Nine, Bordeaux, France.
- [6] BSI, (1994). DD ENV 1995-1-1:1994. Eurocode 5: Design of Timber Structures : Part 1.1: General Rules, & Rules for Buildings. BSI, London.
- [7] BSI, (1996). DD ENV 1991-1-1:1996. Eurocode 1 - Basis of Design & Actions on Structures - Part 1: Basis of Design. BSI, London.
- [8] SCOTT, G., (1976). Building Disasters & Failures - A Practical Report. The Construction Press Ltd., Lancaster, UK.
- [9] CORELY, W.G., (1997). Evaluating Structural Damage Caused By Oklahoma City Bombing. Model Analysis As A Design Tool, IStructE Informal Study Group Newsletter No. 79, June 1997, Taywood Engineering, Southall, Middlesex, England.
- [10] SCOSS, (1997) Structural Safety 1994-96: Eleventh Report of SCOSS. Structural Engineering International, Volume 7, Number 2. IABSE, Zurich.
- [11] SCHNEIDER, J. (1997). Introduction To Safety & Reliability of Structure. Structural Engineering Document 5, IABSE, Zurich, Switzerland.

- [12] BAINBRIDGE, R.J. & METTEM, C.J., (1997). Reliability Based Design In Relation to the Performance of Timber Structural Systems. Proceedings of Reliability Based Design of Timber Structures Seminar, CTBA, Paris.
- [13] AUSTIN, J.A., (1998). Over-design: Fact or Fiction? The Structural Engineer, Volume 76, No. 2. IStructE, London.
- [14] GULVANESSIAN, H. & HOLICKY, M., (1996). Designers' Handbook to Eurocode 1. Thomas Telford, London.
- [15] METTEM, C.J. & MARCROFT, J.P., (1990). Disproportionate Collapse of Timber Structures. CIB-W18/23-15-6, CIB-W18 Meeting Twenty-Three, Lisbon, Portugal.
- [16] METTEM, C.J. & MARCROFT, J.P., (1993). Simulated Accidental Events on a Trussed Rafter Roofed Building. CIB-W18/26-14-6, CIB-W18 Meeting Twenty-Six, Athens, Georgia, USA.

**INTERNATIONAL COUNCIL FOR BUILDING RESEARCH STUDIES AND DOCUMENTATION
WORKING COMMISSION W18 - TIMBER STRUCTURES**

**NUMERICAL SIMULATION OF PSEUDO-DYNAMIC TESTS
PERFORMED TO SHEAR WALLS**

by

L Daudeville

L Davenne

N Richard

Laboratoire de Mécanique et Technologie
Cachan

FRANCE

N Kawai

Building Research Institute
Tsukuba, Ibaraki

M Yasumura

Shizuoka University

JAPAN

MEETING THIRTY-ONE

SAVONLINNA

FINLAND

AUGUST 1998

Numerical simulation of pseudo-dynamic tests performed to shear walls

Laurent Daudeville, Luc Davenne, Nicolas Richard

Laboratoire de Mécanique et Technologie, ENS Cachan /CNRS / Univ. Paris 6

61, avenue du Président Wilson, F- 94235 Cachan, France

E-mail Laurent.Daudeville@lmt.ens-cachan.fr

Naohito Kawai

Building Research Institute, 1 Tatehara, Tsukuba, Ibaraki 305, Japan

Motoï Yasumura

Department of Forest Resources Science, Faculty of Agriculture, Shizuoka University

836 Ohya, Shizuoka 422, Japan

1. Introduction

Timber structures have satisfactory performances due to the high strength-to-weight ratio of wood and due to the unit actions of diaphragms and shear walls whose seismic behaviour is governed by fasteners (Soltis 1984, Turner et al. 1990).

However, considerable damage has been reported to light-frame wood buildings in earthquakes like the 1995 Hyogo-Ken Nanbu's one. The presence of large openings, the simplified design methods may explain it.

A cooperative research is developed in Japan for the analysis of structural performances of timber shear walls under seismic loading. The project includes a series of full scale Pseudo-Dynamic (PSD) and shaking table tests of shear walls made of posts, beams and sheathing panels. Rigid walls prevent the structure from vibrations in the directions perpendicular to the motion. The program will be finalised with a series of dynamic, pseudo-dynamic and static tests of two storey buildings with asymmetrical shear wall composition which are

supposed to produce more complicated vibration modes such as torsion and three dimensional movements.

The “Laboratoire de Mécanique et Technologie”, Cachan France, is involved in this project in the Finite Element (FE) modelling.

This modelling work is aimed at providing a numerical method for the analysis of dynamic performances of timber structures. This tool can help to reduce costly experimental programs, as a development tool to assist researchers in the formulation of seismic design procedures, as a predictive tool to study various factors affecting the structural response and to interpret experimental data, and as an analysis tool in the design of structures in earthquake-prone regions.

Many experimental programs have been conducted over full scale shear walls either under static, cyclic or dynamic loading (Stewart 1987, Kamiya 1988, Dolan 1989, Lam et al 1996). A common observation from these tests is that the hysteresis trace of a wood subsystem or subassembly is governed by the hysteretic characteristics of its primary connection. Thus, it is only necessary to characterise the hysteretic behaviour of wood joints to characterise the behaviour of wood structures and structural systems. Dowrick (1986) noticed similarities in the hysteresis shapes of the dowel type fasteners (nails and bolts).

Some authors worked on the modelling of joints for the simulation of the response of such shear walls under static loading (Gupta & Kuo 1985, Schmidt & Moody 1989, Falk & Itani 1989, Dolan & Foschi 1991) or under cyclic or dynamic loading (Kivell et al 1981, Kazal et al. 1994, Tarabia & Kamiya 1996, Tarabia & Itani 1997).

Some important phenomena, especially in the cyclic models, were not taken into account in the literature. For example, for several cycles at the same imposed displacement, the strength degradation between the first cycle (loading cycle) and the other cycles (stabilised cycles) were not modelled. An other experimentally observed phenomenon is the difference between the monotonic curve and the peaks envelope of the loading cycles, a strength degradation occurs gradually as the number of cycles increases. In both cases, the dissipated energy is affected and the behaviour of the wall under seismic loading may be very different.

The current models available in the literature are sometimes inappropriate for joints with different configurations and material components. A model is proposed in this paper that

takes into account the general hysteretic features of wood joints. This model is simple and easy to identify.

Comparisons between numerical and experimental responses of shear walls with plywood sheathings nailed on timber frames tested in pseudo-dynamic conditions are given. All the tests presented in this paper were performed at the Building Research Institute, Tsukuba Japan.

2. Pseudo-dynamic tests

The PSD test method is a hybrid testing method combining the numerical integration of the motion of a complex structure, condensed on a reduced number of degrees-of-freedom (DOF), here one, and the experimental measurement of the restoring force which results from this motion. The numerical simulation of the inertial force allows performing a dynamical test in a dilated time scale and thus to use a reduced hydraulic power. The use of an explicit time integration scheme is the most immediate for PSD testing. Knowing all the relevant quantities at any time level (n), it is possible to compute and impose the displacement at the next time level ($n+1$) to the structure, to measure the resulting restoring forces and then to proceed further. The Newmark's β scheme is here used with $\beta = 0$ and $\alpha = 0.5$. The acceleration (A_{n+1}), the velocity (V_{n+1}), and the displacement (D_{n+1}) at time ($n+1$) are calculated with the restoring force (R_{n+1}), the lumped structure mass (M), the damping coefficient (C) and the ground acceleration (A_{n+1}^g). The assumed mass of each wall is determined so that the mass times ($0.3 \times 9.81 \text{ ms}^{-2}$) equals the horizontal design strength. That force is obtained for an horizontal displacement equal to 1/120 of the wall height. The mass (fictitious for the PSD tests) is the one used in the shaking table tests. The viscous dumping coefficient is constant and calculated with a dumping ratio of 2%, the mass and the initial stiffness. Equations (1), (2) and (3) show the iterative scheme:

$$A_{n+1} = - \frac{\left[C \left(V_n + \frac{\Delta t}{2} A_n \right) + R_{n+1} + M A_{n+1}^g \right]}{\left(M + C \frac{\Delta t}{2} \right)} \quad (1)$$

$$V_{n+1} = V_n + \frac{\Delta t}{2} (A_{n+1} + A_n) \quad (2)$$

$$D_{n+1} = D_n + V_n \Delta t + \frac{\Delta t^2}{2} A_n \quad (3)$$

This simple one DOF model that consists in lumping the mass at the top of the wall is correct for the seismic analysis of timber frame structures because of the low mass of the structure compared to the floor or roof mass.

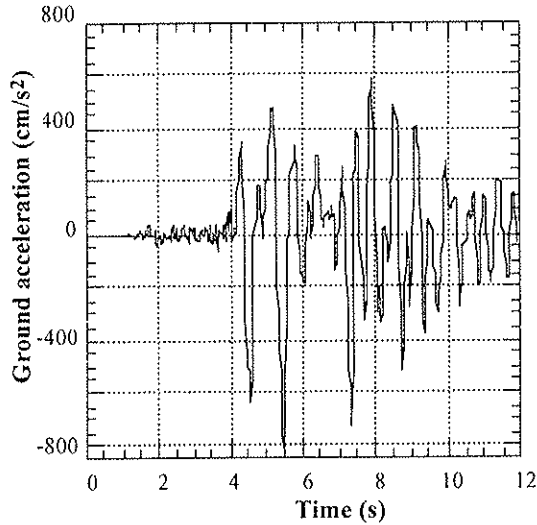


Figure 1. Ground acceleration (1995 Hyogo-Ken Nanbu earthquake)

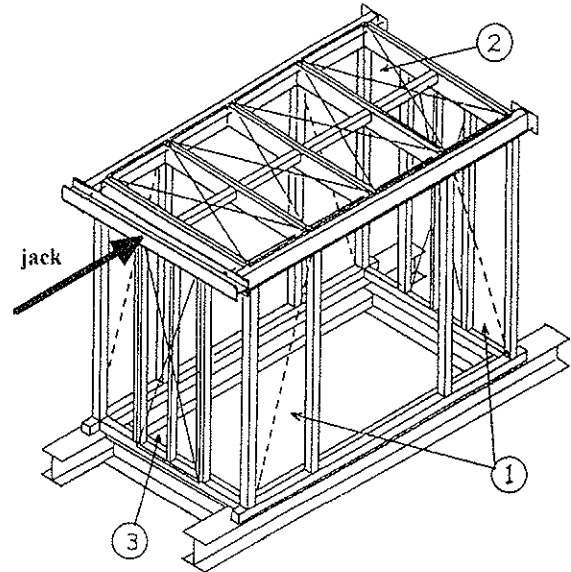


Figure 2. Perspective view of the PSD set-up of wall P1 (opening)

The ground acceleration evolution used during the tests is shown on Figure 1. Three walls (P1, P2 and P3) made of plywood panels nailed to lumber frames were tested. Figure 2 gives a perspective view of the experimental set-up for the wall P1. Two parallel and identical shear walls are connected by rigid walls (② and ③). The plywood panels ① are nailed to lumber frames. The two other tested shear walls are presented on Figures 3 and 4. The spacing of the nails (50 mm long) is 150 mm. The connection between the vertical and horizontal framing members is prevented completely from separation during the testing, for instance hold-downs are used at each corner of walls and openings. The wood member species is Douglas-fir (120x180 horizontal members) and Hem-fir (other members), the plywood thickness is 9 mm

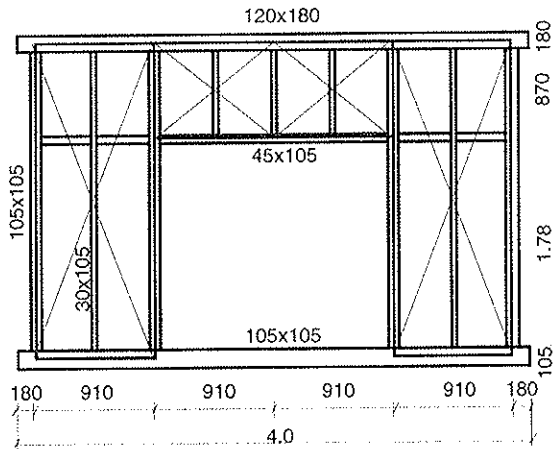


Figure 3. Shear wall P2 (door)

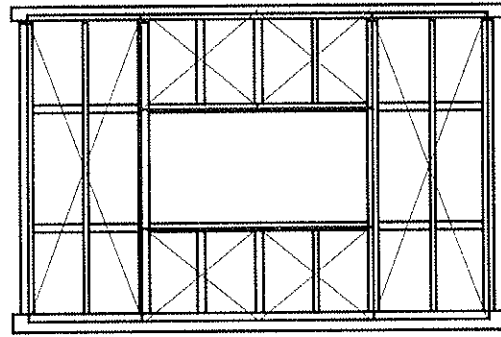


Figure 4. Shear wall P3 (window)

3. Hysteretic behaviour of nailed joints and shear walls

Figure 5 shows the experimental set-up for the determination of the individual behaviour of the nailed plywood-to-lumber connection. Four nails are tested to ensure conditions of symmetry, the individual nail response is assumed to be the quarter of the whole one. Monotonic and cyclic displacements were prescribed. The cyclic loading protocol is the European standard CEN TC 124.117 (three reversed cycles for each level of increasing displacement).

The typical load-slip responses of a nailed plywood-to-lumber connection under monotonic and reversed cyclic displacement are shown on Figure 6. These curves are the average response from six monotonic and six cyclic tests. The characteristic features of the hysteretic behaviour can be noted from this figure:

- non-linear inelastic load-displacement relationship without a distinct yield point;
- degradation of strength when cyclically loaded (the cyclic strength is lower than the monotonic one);
- degradation of strength when cyclically loaded to the same displacement (the second cycle strength is lower than the first cycle one);
- pinched hysteresis loops (i.e., thinner loops in the middle than near extreme ends).

Foliente (1995) added to the previous features the stiffness degradation. According to the tests performed to the nailed plywood-to-lumber connections, the stiffness degradation during cycles (i.e. the unloading slope variation) is insignificant. Nevertheless a general model should take a possible stiffness degradation into account. Lam et al. (1996) noted

some fatigue breakage of nails during cyclic tests of walls. This failure mode did not occur during the presented tests but must be taken into account in a general model.

According to Kamiya et al. (1997) experimental studies, there is no loading rate effect on strength of nailed plywood-to-lumber joints for slip rates varying from 1 to 3000 mm/min.

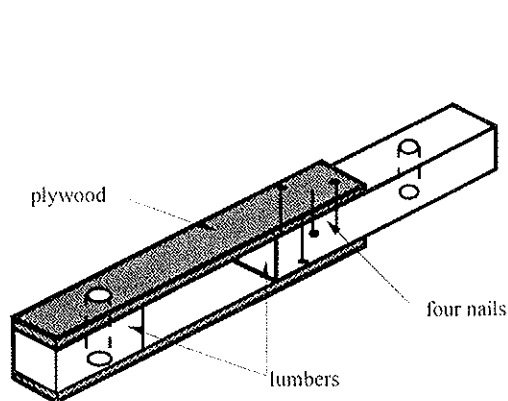


Figure 5. Nail testing set-up

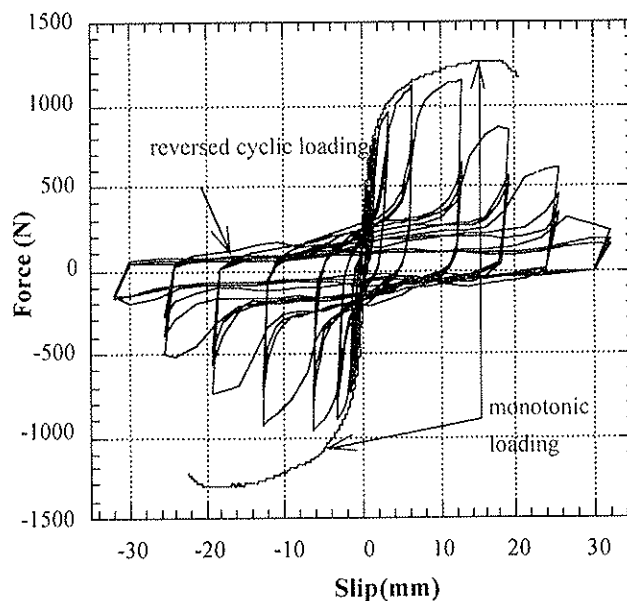


Figure 6. Monotonic and cyclic load-slip curves of individual nailed plywood-to-lumber connection

Figure 7 gives the load-displacement response of the wall P2 subjected to both monotonic and reversed cyclic loading (same loading protocol as before). It can be verified that the nailed sheathing behaviour governs the whole hysteretic behaviour of the shear wall.

Note this paper does not deal with walls subjected to monotonic and reversed cycles. Numerical and experimental results of the three walls under such loadings were presented in (Davenne et al. 1997).

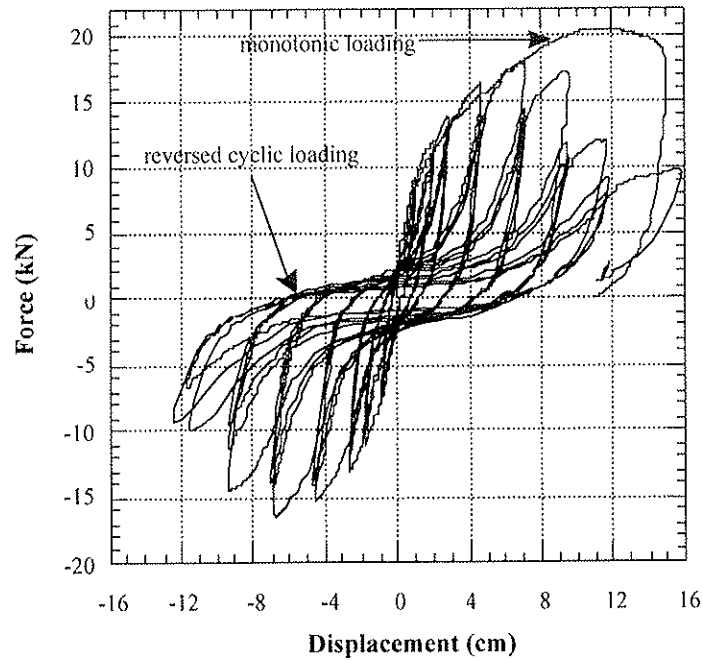


Figure 7. Wall P2: Load-displacement curves under monotonic and cyclic loading

4. Modelling

4.1 FE modelling

All the non-linear phenomena are assumed to be concentrated in dowel-type fasteners. The computation is carried out in plane stress in the plane of the wall. The lumber frames are modelled with 2D beam elements (elastic, isotropic). The connection between two beams is modelled as an hinge with a rotational spring whose stiffness is given between zero (free relative rotation) and infinity (clamped). The plywood sheathing plates are modelled with 2D plane stress elements (elastic, orthotropic). The fasteners between the beams and the plates are modelled with a two perpendicular spring system (Figure 8). The beam node and the plate node have the same coordinates. The stiffness matrix of the nailed joint element which relates the nodal forces to nodal displacements is implemented in the FE code.

In order to reduce the number of DOF, it is possible to consider some groups of nails and to use a lumping technique to obtain the stiffness matrix of the equivalent element. This technique is not used in the presented calculations, each nailed connection is described to evaluate the quality of the nailed connection modelling.

Some constraints between DOF are introduced to prevent the sheathing elements from overlapping. These constraints are satisfied by means of Lagrange multipliers.

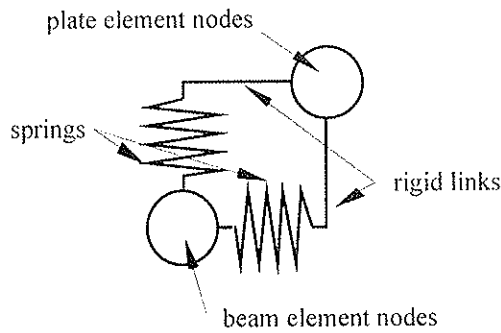


Figure 8. Spring model of fasteners

4.2 Nailed joint modelling

The main features noted by observing the hysteretic behaviour of a dowel-type fastener are taken into account in the proposed modelling that was first presented in (Davenne et al. 1997). Figure 9 shows the force-slip curve under reversed cyclic displacement (0,1,...,17 path loading). This model needs six parameters to describe the nailed joint constitutive behaviour under monotonic loading and four more parameters to describe any reversed loading.

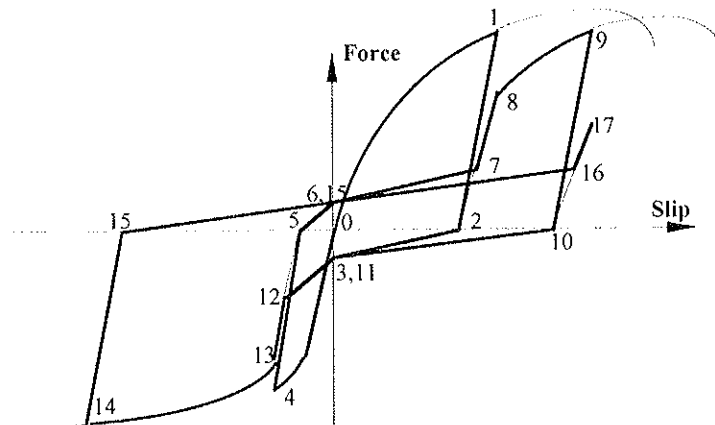


Figure 9. Hysteretic modelling of the nailed plywood-to-lumber connection

The different stages of the path correspond to yielding of wood, yielding of the nail, formation of gaps, friction and nail withdrawal.

This model was identified with experimental results of Figure 6. Note that no rate effect is taken into account in the modelling.

The constitutive relation relates the relative displacement between the lumber and the sheathing to the force between these two elements. It is assumed that the force direction (local, at the joint level) doesn't change a lot during the loading of the wall (global, at the

wall level). Even with a radial loading path, this assumption may be violated if there are force redistributions. However, in the walls tested here, this assumption has been checked and can be kept. In the future, the constitutive relations will be written in two dimensions with coupling between the directions.

5. Numerical simulation of PSD tests

The aim of that paper is not the comparison of PSD and shaking table tests and the discussion of the validity of PSD test results but the validation of the proposed FE approach. Thus the following results were obtained with static analyses (like tests).

Because of the lack of information, some coarse assumptions are chosen:

- the hold-downs are not modelled, presented calculations are carried out with a zero stiffness between beams;
- elastic properties of lumber frames and plywood are chosen equal to:

$$E_L = 15 \text{ GPa} ; E_T = E_R = 0.6 \text{ GPa} ; G_{LT} = G_{LR} = 0.7 \text{ GPa} ; \nu_{LT} = \nu_{LR} = 0.5 \quad (4)$$

The experimental top wall displacement is prescribed to walls P1, P2 and P3. Figure 10, 11 and 12 give the comparison between experimental (solid line) and calculated (dashed line) restoring forces versus displacement for each wall.

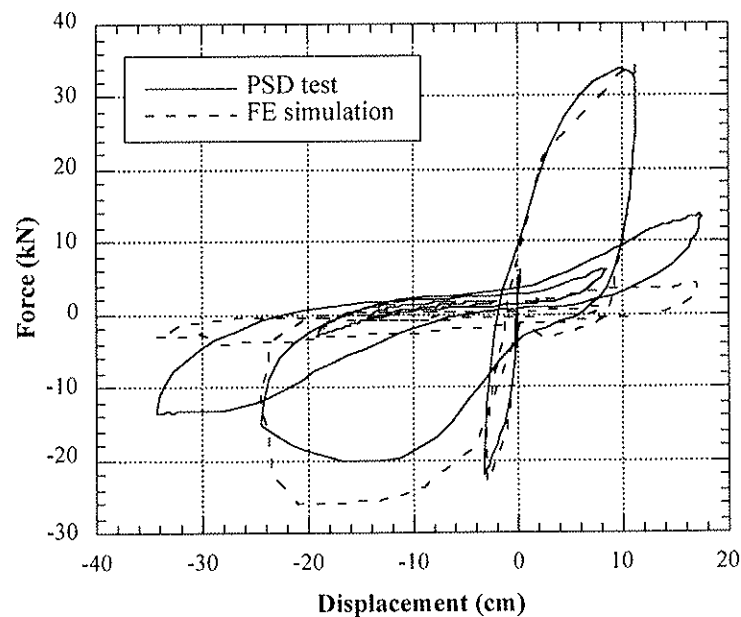


Figure 10. PSD response of wall P1

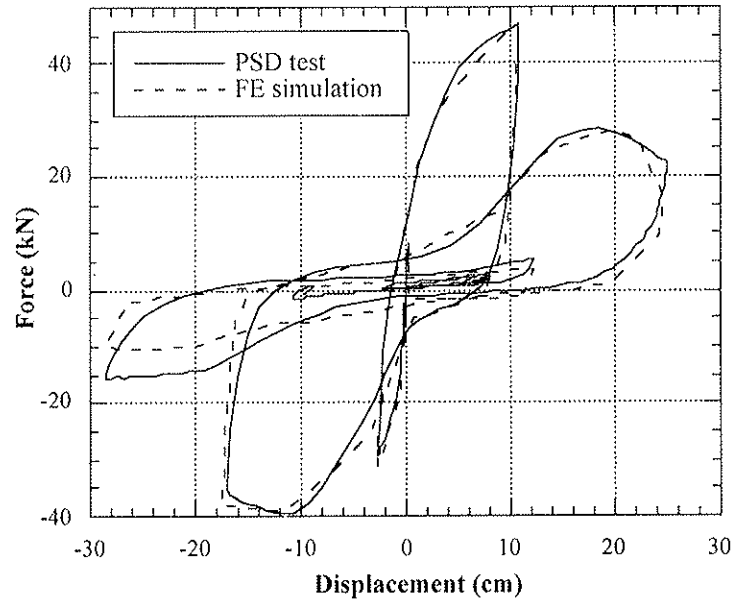


Figure 11. PSD response of wall P2

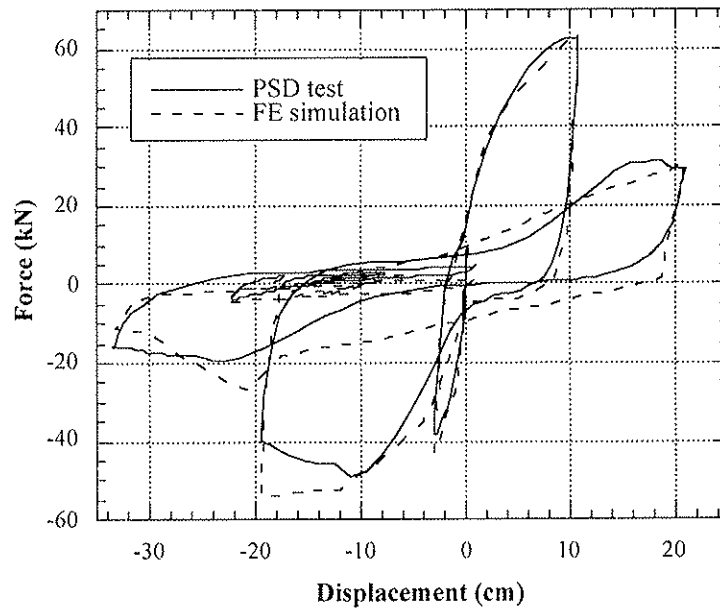


Figure 12. PSD response of wall P3

Figures 10-12 show a good agreement between numerical and experimental results for the three walls. Nevertheless last loops are not well described. After the first loops in which the maximum restoring forces are reached, the model predicts strengths lower than the experimental ones. A possible explanation is that the model does not account the non nailed connections (hold-downs, connections between lumbers). These connections have no influence as long as the nailed connections are not damaged but contribute towards strength as soon as some nails are severely damaged.

6. Conclusion

A simplified FE analysis of timber structures under severe loading is presented. All the degradation phenomena are assumed to occur in joints. According to literature, dowel type joints exhibit the same load-slip behaviour under monotonic or reversed cyclic loading. The main features of this typical behaviour were characterised from tests on nailed plywood-to-lumber connections and a model that relates the force in the connection to the relative displacement between wooden members is proposed.

This model was implemented in a FE code for the simulation of the PSD load-displacement response of three shear walls with plywood sheathing.

Despite of coarse assumptions concerning the elastic properties of materials or the non nailed joints, the experimental and numerical results fit quite nicely.

Some shaking table tests were carried out to walls in Japan. At the time this paper is written, the results are not available yet.

The simulation of the dynamic tests will allow to validate completely the proposed model.

ACKNOWLEDGEMENTS

The authors would like to thank the STA (Science and Technology Agency), Japan, for financial support and Dr. K. Watanabe, Manager of this collaborative research for advice.

REFERENCES

- CEN TC124.117. 1994. Timber structures - Test methods - Cyclic testing of joints made with mechanical fasteners. CEN, Brussels Belgium.
- Davenne, L. Daudeville, L. Kawai, N. & Yasumura, M. 1997. A numerical analysis of shear walls structural performances. Proceedings of the 30th CIB-W18 Meeting, Vancouver Canada: paper 30-15-2.
- Dolan, J.D. 1989. The dynamic response of timber shear walls. Ph. D. Dissertation. Dept. of Civil Engineering, UBC, Vancouver Canada.
- Dolan, J.D. & Foschi, R.O. 1991. Struct. analysis for static loads on timber shear walls. *J. of Struct. Engrg.* 117(3): 851-861.
- Dowrick, D.J. 1986. Hysteresis loops for timber structures. *Bull. of New-Zealand Nat. Soc. of Earthquake Engrg.* 19(20): 143-152.

- Falk, R.H. & Itani, R.Y. 1989. Finite element modeling of wood diaphragms. *J. of Struct. Engrg.* 115(3): 543-559.
- Foliente, G.C. 1995. Hysteresis modeling of wood joints and structural systems. *J. of Struct. Engrg.* 121(6): 1013-1022.
- Foschi, R. 1977. Analysis of wood diaphragms and trusses, Part I: diaphragms. *Canadian J. of Civil Engrg.* 17: 345-352.
- Gupta, A.K. & Kuo, G.P. 1985. Behavior of wood-framed shear walls. *J. of Struct. Engrg.* 111(8): 1722-1733.
- Kamiya, F. Sugimote, K. & Mii, N. 1997. Hysteretic lateral resistance of plywood-lumber nailed joints. *J. of Japan Wood Res. Soc.* 43(6): 474-481.
- Kazal, B. Leichti, R.J. & Itani, R.Y. 1994. Nonlinear finite-element model of complete light-frame wood structures. *J. of Struct. Engrg.* 120(1): 100-119.
- Kivell, B.T. Moss, P.J. & Carr, A.J. 1981. Hysteretic modeling of moment resisting nailed timber joints. *Bull. of New-Zealand Nat. Soc. of Earthquake Engrg.* 14(4): 233-245.
- Lam, F. Prion, H.G.L. & He M. 1996. Lateral resistance of wood based shear walls panels with oversized sheathing panels. Proceedings of the 29th CIB-W18 Meeting, Bordeaux France: paper 29-15-1.
- Newmark, N.M. 1959. A method of computation for structural dynamics. *J. of Engrg. Mech.* 85:67-94.
- Schmidt, R.J. & Moody, R.C. 1989. Modeling laterally loaded light-frame buildings. *J. of Struct. Engrg.* 115(1): 201-217.
- Soltis, L.A. 1984. Low-rise timber buildings subjected to seismic, wind and snow loads. *J. of Struct. Eng.* 110(4): 744-753.
- Tarabia, A.M. & Itani, R.Y. 1997. Static and dynamic modeling of light-frame wood buildings. *Comp. and Struct.* 63(2): 319-334.
- Tarabia, A.M. & Kamiya, F. 1996. Analytical seismic response of wood shear walls using hysteresis models of nailed joints. *J. of Japan Wood Res. Soc.* 42(11): 1064-1071.
- Turner, L.S. Stewart, F. & Cheung, K.C. 1990. Performance of wood structures: Loma Prieta earthquake aftermath. *Wood Des. Focus* 1(4):14-16.

**INTERNATIONAL COUNCIL FOR BUILDING RESEARCH STUDIES AND DOCUMENTATION
WORKING COMMISSION W18 - TIMBER STRUCTURES**

FORCE MODIFICATION FACTORS FOR BRACED TIMBER FRAMES

by

H G L Prion
M Popovski
Department of Wood Science
University of British Columbia

E Karacabeyli
Forintek Canada Corp.

CANADA

MEETING THIRTY-ONE

SAVONLINNA

FINLAND

AUGUST 1998

Force modification factors for braced timber frames

Helmut G. L. Prion, Assistant Professor, Department of Civil Engineering, University of British Columbia, Vancouver, Canada

Marjan Popovski, Ph.D. Candidate, Department of Civil Engineering, University of British Columbia, Vancouver, Canada

Erol Karacabeyli, Senior wood scientist, Forintek Canada Corp., Western Laboratory, Vancouver, Canada

1 Introduction

Braced frames are very often the simplest and most economical structural systems used in timber construction to resist lateral loads. This type of system is often used in glued-laminated timber construction and in heavy post and beam construction. Bracing essentially provides triangulation by means of diagonal members inserted in the rectangular bays of the frame. In concentrically braced frames, there is essentially no eccentricity in the joints and the lateral forces are resisted by almost pure axial loads in the braces. Diagonal braces, however, have the disadvantage of obstructing movement of people and goods and are usually located in the plane of the wall.

Timber structures are generally recognized to perform well when subjected to earthquake ground motion. This is attributed largely to wood's high specific strength (strength-to-weight ratio) and its enhanced strength under short term loading. Traditional timber systems also have a high degree of redundancy as well as sufficient ductility and energy absorption capacity. Favorable system geometry, e.g. symmetrical plan and elevation, also contributed to its performance. Regardless of the demonstrated satisfactory performance, however, it was shown that timber construction in itself is not a guarantee for adequate structural performance during an earthquake. This was particularly evident during some of the recent strong earthquakes such as Northridge, California (1994) and especially Kobe, Japan (1995). During these earthquakes, many timber buildings collapsed causing extensive damage and human loss. The lessons learned from Kobe are of particular interest for the performance of braced timber systems. A majority of the buildings that collapsed were of the post and beam construction type, which is essentially a braced framing system. While many factors contributed to the poor performance, the lack of an adequate bracing system was the main reason for collapse (Popovski, 1996).

The seismic response of a braced timber structure in general is a complex issue, involving many different interacting factors, which need to be understood and quantified. One of the most important considerations is to provide a system that can absorb large amounts of energy and thus lower the earthquake-induced forces, while maintaining adequate stiffness to avoid excessive deformations. To satisfy these requirements, the seismic design process must include a careful balance of strength, stiffness and ductility. In braced timber frames significant deflection of the frame is dependent on the joint deformations. The stiffer nature of the braced frames represents an advantage in the case of low to medium intensity

earthquakes, because less movement causes less damage to non-structural elements and serviceability requirements are easily met. On the other hand, it often also means less potential for energy absorption, leading to higher forces and lower system redundancy.

2 Quasi-static connection tests

Based on results from previous studies (Buchanan, 1989, Yasumura, 1990), it was evident that further research is needed in the field of seismic resistance of braced timber frames. Currently, a research project on braced timber frames is underway at the University of British Columbia (UBC) in collaboration with researchers at Forintek Canada Corp. The main objectives of the research are to: (i) develop an understanding and determine the factors that influence the seismic behavior of braced timber frames with different connection details; (ii) develop an analytical procedure to obtain corresponding force reduction factors for braced timber frames with different connection details; and (iii) provide designers and code officials with relevant information about design details needed to obtain the corresponding force modification factors.

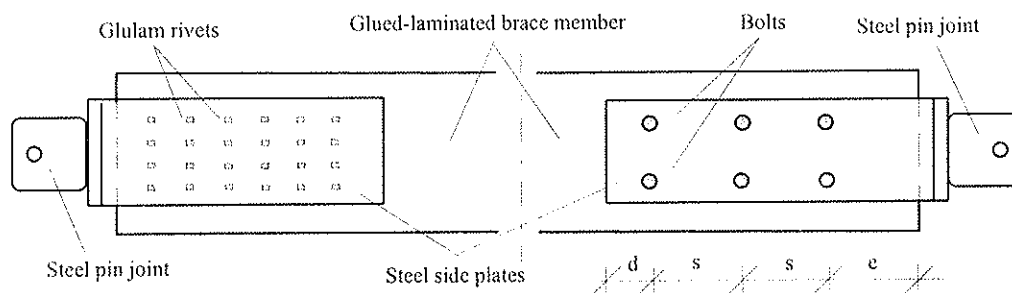


Figure 1. Typical details of riveted and bolted braced frame connections.

As it was expected that the seismic response of braced timber frames would largely depend on the connections, a significant part of the experimental program was focused on the behavior of different connection details. Displacement controlled monotonic and cyclic tests were conducted on different connections to determine their adequacy in resisting reversing loads such as experienced in seismic events. Two different connector types, namely mild steel bolts and glulam rivets (also known as griplam nails) were considered. Glulam rivets are high-strength oval-shaped nails with a tapered head and maximum shank diameter of 6.4 mm (1/4 in). The flat cross-section of the shank prevents splitting of the wood while the tapered head, after being driven into a 6.4 mm (1/4 in) round hole in the steel plate, provides fixity. This also ensures the formation of a plastic hinge at the head of the rivet under large deformations. Glulam rivets have proven to be very efficient connectors for the transfer of large loads in heavy timber construction.

The test specimens were chosen to represent typical connection details used in braced timber frames (Figure 1), consisting of wood brace member, connectors (bolts or rivets) and steel plates on both sides. The brace member consisted of grade C, Spruce-Pine-Fir (SPF) glued-laminated timber, 130 x 152 mm (5 x 6 in) in cross section. Steel plates for bolted connections were 12.7 mm (1/2 in) thick, while riveted connections were built using 6.4 mm (1/4 in) plates. Mild steel ASTM A307 bolts were used with three different diameters: 9.5 mm (3/8 in), 12.7 mm (1/2 in) and 19 mm (3/4 in). The member thickness to bolt diameter ratio (bolt slenderness l/d) was 13.3, 10.0 and 6.7 respectively. For the riveted connections, 65 mm (2.5 in) long rivets were used. Three replicates were tested

from each connection in both static and cyclic tests. Table 1 summarizes some of the facts for the connections that have been tested.

Table 1. Connections used in quasi-static tests.

Fastener type Test group	9.5 mm Bolts		12.7 mm Bolts		19 mm Bolts		Rivets	
	I	II	I	II	I	I	II	
Total connectors	10	3	6	2	2	48*	18*	
Rows	2	1	2	1	1	4	3	
Connectors in row	5	3	3	2	2	6	3	
End distance (mm)	114		152		228		75	
Spacing (mm)	40		51		76		25	
Design load (kN)	64.4	24.2	67.6	28.1	56.9	90.7	34.0	

* Number of rivets on both sides, i.e. half of that number is on one side.

The end distance e was 12 times the bolt diameter ($12d$), which is larger than the minimum proposed distance of $10d$ according to the Canadian Timber Design Code (CSA-086.1). The spacing s between bolts in the row was $4d$, which is the minimum requirement. The

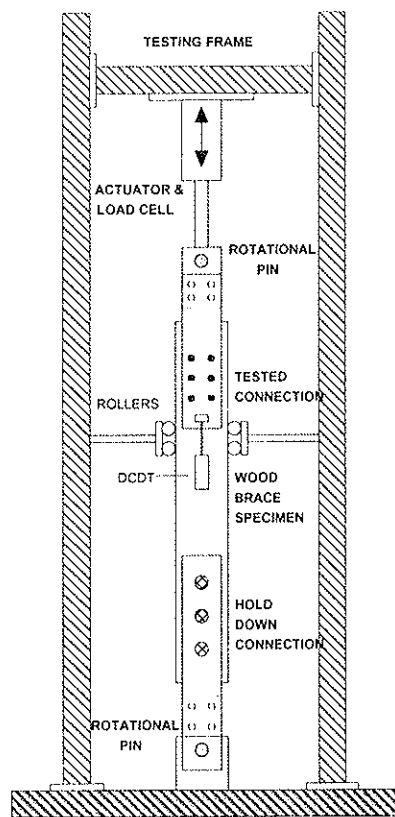


Figure 2. Quasi-static test setup.

spacing between rivets in the riveted connections was 25 mm (1 in) in all directions, while the end distance e was 75 mm (3 in). The wood was conditioned in a laboratory environment at a temperature of $20 \pm 3^\circ\text{C}$ and relative humidity of $50 \pm 10\%$ for six months, which adequately represents dry service conditions.

Two types of quasi-static tests were conducted: monotonic and cyclic. All tests were conducted under displacement control in the Wood Engineering Laboratory at Forintek Canada Corp. in Vancouver. A simplified scheme of the connection test setup is shown in Figure 2. The glulam brace specimens with length of approximately 1.5 m (5 ft) were held in place by an over-designed hold-down connection at the bottom, while the connection to be tested was at the top. Active members of the tested connections were the steel side plates, held by a bolted fixture attached to the load cell and the actuator. The bolted connections were thus loaded in double shear, while rivets were loaded in single shear. To ensure a pure axial state of loading on the specimen, two rotational hinges at the top and at the bottom were used. A pair of rollers prevented the specimens from lateral movement. Connection slip was measured using two displacement transducers (DCDT), one on each side of the specimen. The load was measured using the load cell attached to the MTS actuator.

2.1 Results and discussion

Monotonic tests were conducted by applying tension load to the connection with a displacement rate of 5 mm (0.2 inches) per minute. Properties such as initial stiffness, ultimate load, yield load, ultimate displacement and ductility were determined from these

tests. The average yield displacement was one of the most important properties determined, because the cyclic testing protocol was defined in terms of this value.

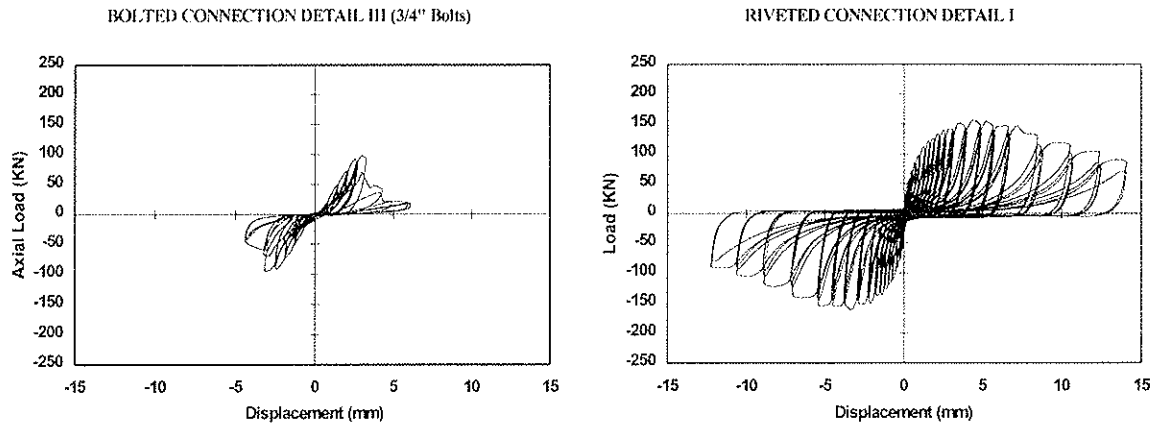


Figure 3. Typical hysteresis loops from cyclic connection tests - first test group.

The connections in both monotonic and cyclic tests always failed in tension. The glulam rivets and bolts yielded in a ductile single shear and double shear mode respectively. It was found, however, that yield modes and failure modes for the same connection type could vary considerably. For glulam riveted connections, the early behavior was almost completely governed by yielding of the fasteners, while the failure mode was fastener pullout from the wood. In the case of bolted connections, a double-shear-yielding mode was noticed with extensive wood crushing, but the failure mode was always splitting of the wood member. Splitting of the wood always occurred at the maximum load. However, most of the connections were able to carry a significant percentage of the maximum load for some time after splitting had occurred. Typical load-deformation relationships of the bolted and riveted connection from the first test group are shown in Figure 3.

It is evident that significant pinching of the hysteresis curves occurred, which is common for connections in timber structures. The pinching effect results in thinner loops in the

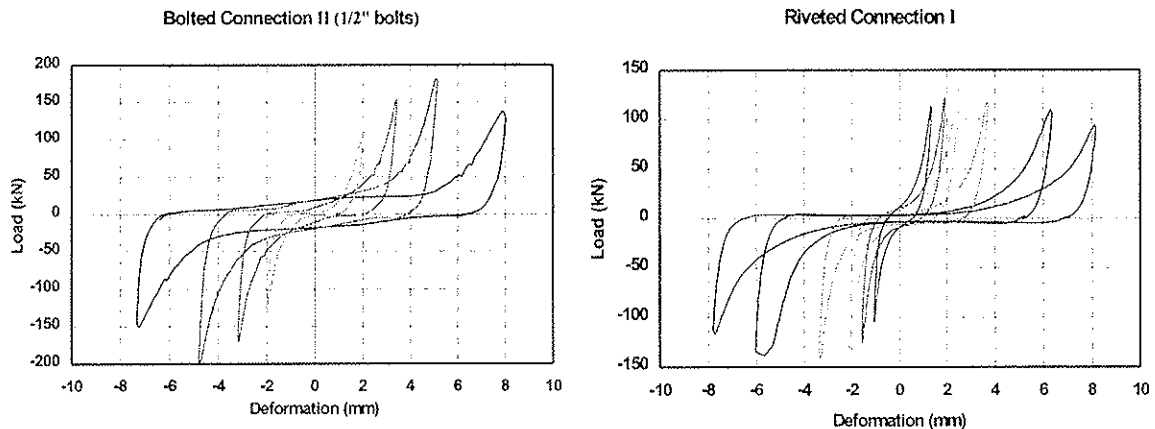


Figure 4. Single hysteresis loops of bolted and riveted connection at different deformation levels.

middle compared to near the ends, which is typical for hysteresis loops where connector yielding and wood crushing occurs, forming a gap during the process. This is illustrated in Figure 4, which shows the stabilized (third) loop for each group of three cycles, at different deformation levels. The initial cycle, which follows the envelope curve, is thus not shown.

It was found that in bolted connections the pinching effect was most significant at low deformation levels, while the hysteresis loops were getting thicker as the deformation increased. The opposite was found to hold for the riveted connections. Since the area inside the hysteresis loop for each cycle represents the amount of energy dissipated during that cycle, pinching in timber braced frames reduces the hysteretic damping of the structure. Recent test results have shown, however, that the shape of the hysteresis loop (pinching) is not so important for timber structures in general, whereas the ability of sustaining large deformations without significant deterioration in strength, is much more significant (Buchanan, 1988).

Although the relatively small number of replicates tested prevents any statistically supported conclusions to be drawn, some definite trends could be observed. A brief summary of some of the average connection properties obtained from cyclic tests is given in Table 2. All the properties were based on non-stabilized (first cycle) envelopes, using the European CEN Standard.

Table 2. Average connection properties obtained from cyclic tests.

Fastener	9.5 mm Bolts		12.7mm Bolts		19 mm Bolts	Rivets	
	I	II	I	II	I	I	II
Yield load (kN)	136.7	40.5	141.5	51.4	79.8	82.5	34.9
Yield displ. (mm)	2.07	1.90	2.76	2.78	1.80	0.62	0.74
Ultimate load (kN)	164.5	54.2	188.0	68.1	105.0	153.6	63.5
Displ. at capacity	3.5	3.85	5.56	6.3	3.25	4.33	5.71
Ultimate displ.	5.53	5.18	7.57	8.59	3.90	9.54	13.32
Initial stiffness	72.8	27.5	68.5	22.1	58.8	154.6	48.33
Ductility	2.67	2.72	2.74	3.09	2.17	15.4	18.0
Safety factor	2.55	2.23	2.78	2.42	1.84	1.69	1.86

The obtained ultimate load for all connections was significantly higher than the design load (between 1.7 to 2.8 times). It appears that the connections with large diameter bolts have a smaller safety factor, according to the current Canadian Timber Design Code. Connections with two rows of bolts (group I) showed a higher safety factor than the connections with one row of bolts (group II). This could mean that the existing row factor (0.8 for two rows) in the Canadian design equations might be too severe. Generally, riveted connections showed a lower safety factor than bolted connections, but higher consistency. It was also noticed that the capacity per rivet of the connections of the first test group (3.2 kN/rivet) was lower than the corresponding capacity (3.5 kN/rivet) of the connections of the second test group. This is a very interesting finding which suggest that there might be a certain "size effect" or "group effect" in case of riveted connections as well.

In general, glulam riveted connections showed superior performance in terms of ductility compared to the bolted connections for similar design load levels. They exhibited a capability of resisting many load reversals without significant strength deterioration. Under reversed cyclic loading, riveted connections developed some slackness and finally complete pullout, which resulted in very pinched hysteresis loops. Overall, large displacements were typically possible before failure, which permits ample warning before structural failure. In bolted connections with lower slenderness ratios (3/4 in bolts) rigidity of the bolts lead to more uniformly distributed bearing stresses in the wood member, which resulted in abrupt wood splitting and sudden loss of bearing capacity. Connections with

higher slenderness ratios (smaller diameter bolts) exhibited more desirable behavior, although wood splitting was consistently the failure mechanism for all bolted connections tested.

3 Single brace shake table tests

In the second phase of the experimental part, single brace shake table tests were conducted on a number of test specimens. The tests were conducted in the Earthquake Engineering Laboratory in the Department of Civil Engineering, University of British Columbia in Vancouver. The main objectives of this part were: (i) to determine the influence of dynamic rate of loading on connection behavior; (ii) compare the dynamic connection behavior and properties with results from quasi-static tests and (iii) verify the analytical connection and frame models developed on the basis of static tests.

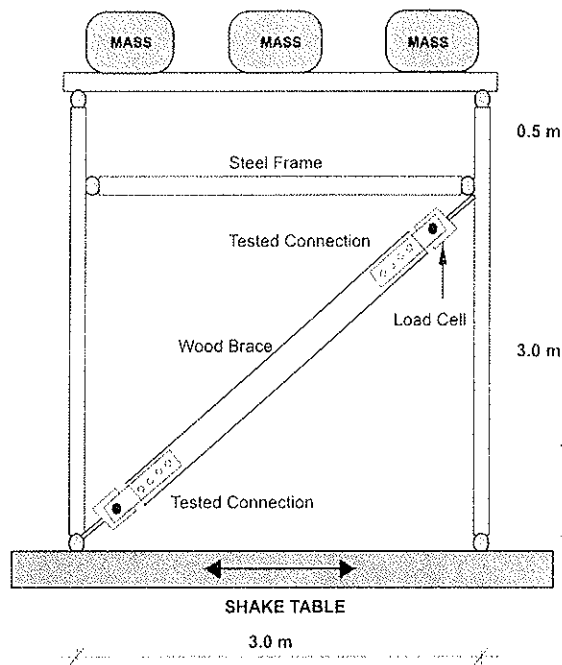


Figure 5. Shake table testing frame setup.

other system. Secondly, only the braces are expected to exhibit non-linear behavior, while all other members are typically designed to remain in the linear elastic range. Regardless of the material of all the other elements, the non-linear behavior of the brace would govern the system response.

A total of eight braces (frames) were tested, utilizing four of the connections that were previously tested quasi-statically, i.e. all three from the second test group plus the 19 mm bolted connection. The axial load in the brace was measured directly from the installed load cell at the top end of the brace, while the connection slip was obtained from the displacement transducers mounted at both connections. To ensure a pure axial load state in the brace, pinned connections were introduced at the top and at the bottom of the brace. The frame was loaded with a total mass of 4,500 kg (10,000 lbs.) on the top. The fundamental period of the system experimentally determined with a calibrated hammer test technique, was found to be 0.25 sec. (4 Hz) for all specimens. The Joshua Tree Station acceleration record (E-W direction) from the 1992 Landers, California earthquake, was used as the input ground motion scaled to different peak acceleration levels. During the

shake table tests it was not always possible to obtain ultimate deformation in the brace, even though a record with peak acceleration of 0.53g was used, the highest possible acceleration that the test frame could safely be used for.

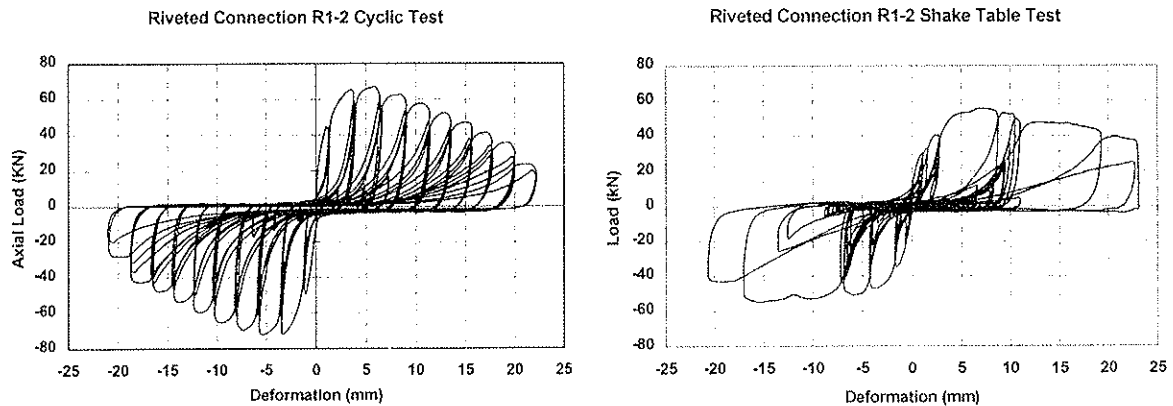


Figure 6. Comparison of cyclic versus shake table results for riveted connection detail.

The shake table test results showed that average maximum load for all connections was from 10 to 13 % lower than the corresponding load obtained from the quasi-static cyclic tests. Although this is within the expected variability for wood structures, this finding is in contradiction with the fact that wood as a material and thus the wood joints have enhanced strength under short-term loading. It appears that obtaining lower loads in shake table tests might be among other reasons due to loosening and impact effects during the shaking. In addition, a significant vertical component of motion noticed during the tests, might contributed as well. Since only two replicates from each connection were tested, however, no statistically supported conclusions can be drawn at this point. The initial stiffness for bolted connections obtained from shake table tests was found to be higher than the corresponding one obtained from cyclic tests. The opposite was found to hold for riveted connections. It was also noticed that the ductility for all bolted connections was higher in case of shake table tests than that in case of cyclic tests. Riveted connections again, showed lower ductility during shake table tests. Some comparisons between the results obtained from cyclic and shake table tests on riveted connections are shown in Figure 6.

4 Analytical studies

Based on the results obtained from the cyclic and shaking table tests, non-linear mathematical models for all tested connections were defined. It appeared that the stabilized (third cycle) envelope from the cyclic tests most adequately represented the estimated fifth percentile of the connection resistance, so this envelope was taken as a basis for defining the mathematical connection models. From several mathematical models available for the modeling of timber joints, the so-called “Florence” non-linear model, developed by Dr. Ario Ceccotti and his collaborators from The University of Florence, Italy, was found to be most suitable (Ceccotti, 1992). The model (Figure 7) is defined by a total of nine parameters: six stiffness parameters ($K1$ to $K6$), two displacement parameters ($U1$ and $U2$), and one force parameter - F_0 .

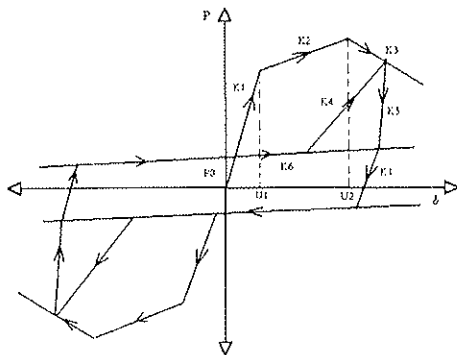


Figure 7. Mathematical model for connection behavior used in dynamic analyses.

The mathematical model was incorporated into the well-known computer program DRAIN 2DX (Powell, 1993) for non-linear static and dynamic analysis of structures. Modeling of the connection behavior in each case was done not only in terms of strength and stiffness, but also in terms of energy dissipation. Model parameters were chosen so that the hysteretic energy (area within the hysteresis loop) calculated from the analytical response matches the hysteretic energy dissipated during the cyclic test. These mathematical connection models were incorporated in a non-linear analytical model of a whole braced timber frame. Using DRAIN 2DX, a series of non-linear static and time history dynamic analyses were performed to determine the seismic performance of this type of structural system.

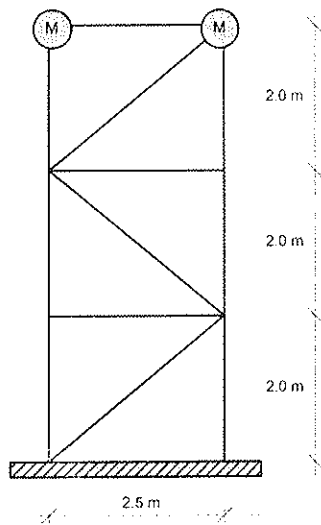


Figure 8. Analytical braced frame model.

A simple braced timber frame model, that represents the lateral load resisting system of a laboratory or warehouse type structure, was chosen as a basic model for analysis (Fig. 8). All connections in the model were assumed to be pinned, with horizontal and vertical members assumed to be linearly elastic. The mass of the structure was assumed to be concentrated at the roof level only. Dynamic time history analyses were conducted using five different acceleration records from previous earthquakes around the world (Table 3). Records were chosen to satisfy the seismic zonal parameters from The National Building Code of Canada (NBCC) for a locality such as Vancouver, with peak horizontal ground velocity of 0.21 m/sec and peak horizontal ground acceleration of 0.23g, with probability of exceedance of 10% in 50 years. They also represent earthquakes with different frequency characteristics throughout the spectrum. The damping value used in analyses was 3% of critical damping for all cases.

Table 3. Main characteristics of the acceleration records used in analyses.

Record Name	Velocity (m/s)	Acceleration (g)	A/V ratio	Event	Magnitude
VAN-29	0.213	0.23	1.08	San Fernando 1971	6.4
VAN-48	0.235	0.23	0.98	San Fernando 1971	6.4
VAN-68	0.245	0.23	0.94	Montenegro 1979	6.4
VAN-72	0.193	0.23	1.19	Montenegro 1979	7.0
VAN-83	0.227	0.23	1.01	Loma Prieta 1989	7.1

The main emphasis of the analyses was on evaluating the force modification factor (R-factor) in NBCC. For braced timber frames, when built with “ductile connections”, the assigned R-factor is 2.0, while other braced timber frames are assigned an R-factor of 1.5. Results from the non-linear dynamic analyses can be summarized in graphs such as those shown in Figure 9. Each graph presents analysis results for a frame that utilizes certain connection detail. For example, Figure 10 shows results for frames that have connections with 9.5 mm bolts (3/8 in) and glulam rivets both from the second testing group. Each line on the graph represents a deformation demand (Y-axis) of the lowest brace of a braced frame structure designed with a certain R-factor (X-axis) according to NBCC, for each of the five different earthquakes. The two horizontal lines represent the yield deformation and the ultimate deformation capacity of the brace, respectively. Because braced timber frames as a system typically have a low degree of redundancy, failure of the structure was

assumed when the deformation demand of one or more earthquakes exceeded the deformation capacity of the structure.

As shown in the figure, the braced frame model with 9.5 mm (3/8 in) bolted connections would survive all five earthquakes if designed with an R-factor lower than 1.75. On the

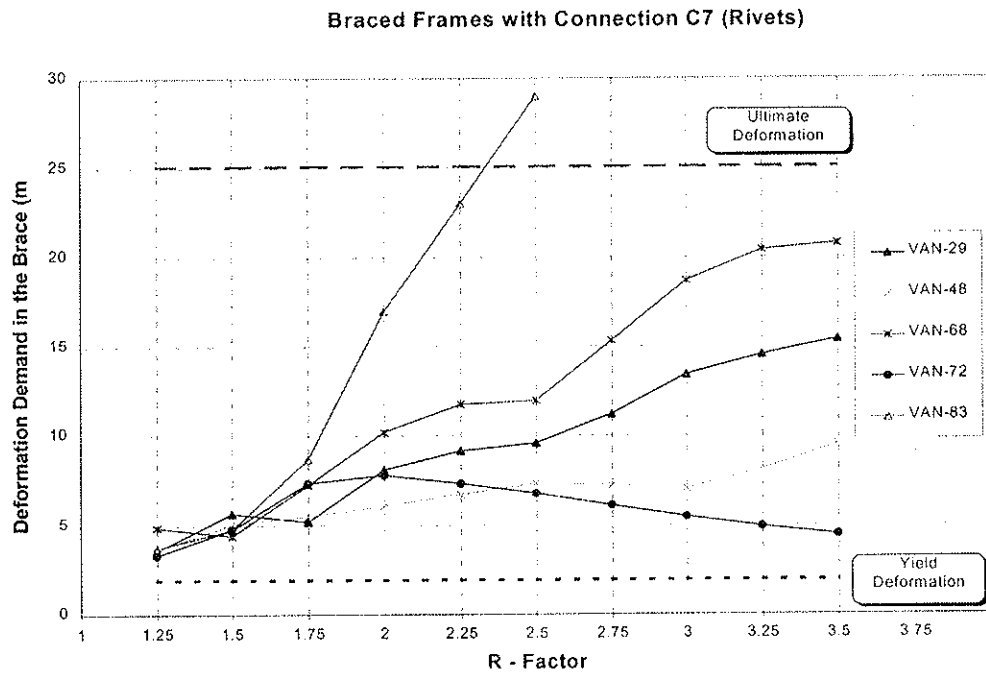
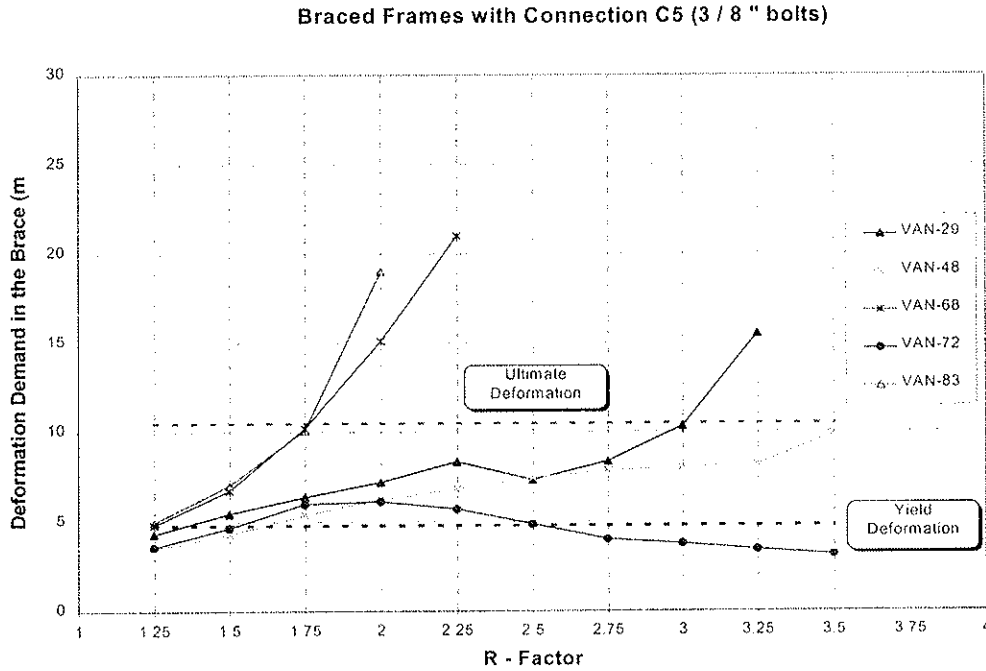


Figure 9. Deformation demand on a braced timber frames with bolted and riveted connections.

other hand, the same frame, when built with riveted connections, could survive all the earthquakes if designed with R-factor lower than 2.25. Similar analyses were done for frames with all other connections from both test groups. Values for R-factors obtained from analyses of the braced frames with all seven different connection details from both test groups are summarized in Table 4. Two different values of R-factors are presented in

Table 4 for bolted connections. The difference occurs if different failure criteria for connections are used. According to CEN Standard, the ultimate displacement capacity of all connections can be determined at a point where the load drops to an 80% level of the maximum load. Tests showed that in bolted connections splitting always began at the maximum load, so the displacement at this point can also be defined as the ultimate displacement. If this failure criterion is used, then the maximum R-factors for which the structure will survive all earthquakes are given in the last row of Table 4. This criterion was not applied to the riveted connections because they do not experience any splitting effects.

Table 4. Maximum R-factors for braced timber frames with different connections.

Fastener	9.5 mm Bolts		12.7mm Bolts		19 mm Bolts		Rivets	
	I	II	I	II	I	I	II	
R-factor (at 80 %)	2.0	1.75	2.0	2.0	1.5	2.0	2.25	
R-factor (max load)	1.75	1.5	1.75	1.75	1.5	-	-	

As it can be seen from Figure 9, the earthquake record VAN-83 was critical for both cases. It was found that this earthquake was actually critical for all seven different cases of braced frames. The influence of this record on the response of the frames was significant because of the high spectral amplitudes in its response spectrum for longer periods (Figure 10). Those amplitudes are much higher than the amplitudes given in the NBCC design spectrum for a site such as Vancouver. This long period range (from 0.5 to 1.2 sec) corresponds to the range of natural periods of timber braced frames with different

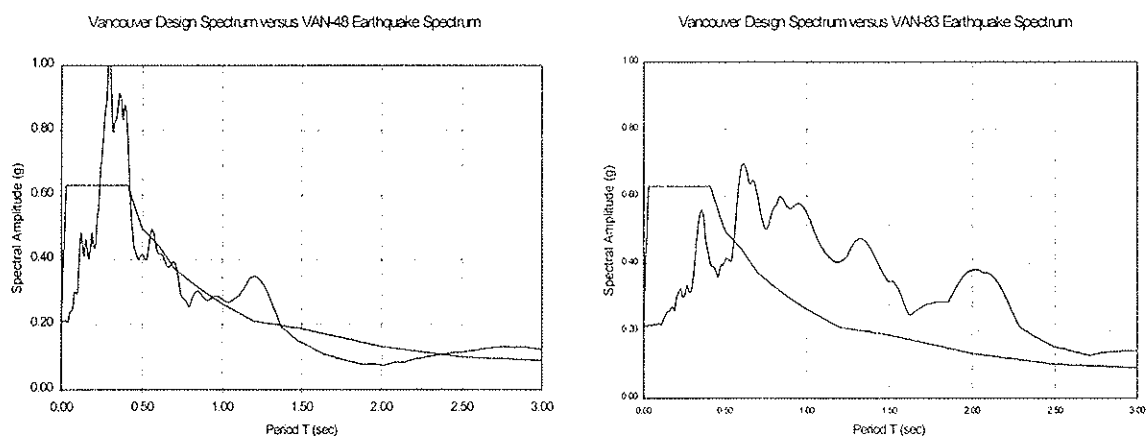


Figure 10. Response spectra for two of the earthquake records used in the analyses.

connections during shaking. Contrary to common belief that braced timber frames are quite stiff structures, their initial natural periods were found to be from 0.4 to 0.85 sec., depending on the connection and the R-factor used for design. For example, a frame designed with an R-factor of 2.0 had a period from 0.49 to 0.64 sec., depending on the connection. These initial periods are significantly prolonged during the actual seismic event, because of the loosening of the connections after the first few larger cycles of motion.

5 Concluding remarks and recommendations

Braced timber frames can be used as efficient lateral load resistance systems in buildings. Because energy absorption capacity and overall ductility of these frames is typically influenced by the connections used, adequate connection design is of particular interest when these frames are used in high-risk earthquake zones. Results from current research on seismic performance and force modification factors for braced timber frames are presented in this paper. Static and dynamic tests were conducted on a several connection details with different diameter bolts and high strength glulam rivets, with steel side plates. The resulting hysteresis loops were used to develop non-linear mathematical models on a connection and frame level. The models were then used in numerous non-linear time history dynamic analyses, from which it was possible to determine the influence of different connection details on seismic response of braced timber frames.

From the presented results, it is evident that the seismic response of braced timber frames is heavily influenced by the behavior of the connections. The results suggest that braced frames with different connections should not be assigned the same R-factor. Braced timber frames with mild steel (ASTM A-307) bolted connections, with slenderness ratios (l/d) of 10 or higher showed far more adequate seismic performance than those frames that utilized bolts with lower slenderness ratios. Further research is needed, however, to study the effects of other parameters such as end distance, spacing, number of rows number of bolts in a row etc., for the development of general recommendations that will ensure ductile behavior of braced frames with bolted connections. Until such re-search is undertaken, an R-factor of 1.5 appears to be reasonable for braced timber frames with slender bolts.

On the other hand, glulam riveted connections showed promising results when used for braced timber frames. They were the only connections tested that consistently showed non-brittle deformations in the wood along with yielding of the connectors even at large displacement levels. In addition, riveted connections do not have as many parameters that influence their cyclic behavior, other than those implemented in the CSAO86.1-94 design guidelines. Braced frames with glulam riveted connections designed in rivet yielding mode may be assigned an R factor of 2.0, in recognition of their higher and more consistent ductility capacity.

Acknowledgments

The authors gratefully acknowledge financial and in-kind support for this project from The Science Council of British Columbia, Forintek Canada Corp. and The University of British Columbia. Technical help from staff at Forintek and The Department of Civil Engineering at UBC is also acknowledged. Finally, the authors acknowledge the interest and very useful comments by Dr. Ario Ceccotti from the University of Florence in Italy, during his stay at Forintek.

References

Buchanan, A. H. Practical Design of Timber Structures to Resist Earthquakes. Proceedings of The International Timber Engineering Conference, 813-822. Seattle, Washington, 1988.

CEN. Comite' Europeen de Normalisation. Timber structures test methods - cyclic testing of joints with mechanical fasteners. EN TC 124.117, European Committee for Standardization, Brussels, Belgium, 1995.

Ceccotti, A. & Vignoli, A. Numerical Modeling of Timber Semirigid Joints for Structural Analysis under Dynamic Loading. Proceedings COST C1 Workshop, ENSAIS, 1: 240-249. Strasbourg, France, 1992.

CSA. Canadian Standards Association O86.1-94. Engineering Design in Wood (Limit States Design). CSA, Etobicoke, Ontario, Canada.

Karacabeyli, E. & Stieda, C. K. A. Lateral resistance of engineered wood structures to seismic and wind loads. Science Report 1 project No. 1565K242, Forintek Canada Corp. 1994.

Madsen, B. Structural Behaviour of Timber. North Vancouver: Timber Engineering Ltd. 1992.

NBCC. National Building Code of Canada. Canadian Commission on Building and Fire Codes, National Research Council of Canada, 1995.

Popovski, M., Prion, H., & Karacabeyli E. Seismic performance of braced timber frames. Proceedings of Fourth International Wood Engineering Conference. 1: 323-330. New Orleans, Louisiana, 1996.

Powell, G. H. Drain-2DX Base Program Description and User Guide. Report No. UCB/SEMM - 93/17, Berkeley, California, 1993.

Prion, H. G. L. & Foschi, R. Cyclic behavior of dowel type connections. Proceedings of Pacific Timber Engineering Conference. 2 : 19. Gold Coast, Australia 1994.

Williams G. & Karacabeyli, E. Glulam Rivet Connections in Wood Construction. Proceedings of Fourth International Wood Engineering Conference. 4: 347-354. New Orleans, Louisiana, 1996.

Yasumura, M. Seismic behavior of arched frames and braced frames. Proceedings of International Timber Engineering Conference. p. 863. Tokyo, Japan, 1990.

Yasumura, M. Seismic behavior of braced frames in timber construction. Proceedings of meeting twenty-three, The International Council for Building Research Studies and Documentation, Working Commission W18 - Timber Structures. Paper (23-15-4). Lisbon, Portugal, 1990.

**INTERNATIONAL COUNCIL FOR BUILDING RESEARCH STUDIES AND DOCUMENTATION
WORKING COMMISSION W18 - TIMBER STRUCTURES**

**REVISION OF ENV 1995-1-2: CHARRING AND DEGRADATION OF
STRENGTH AND STIFFNESS**

by

J König

Trätec

Swedish Institute for Wood Technology Research
SWEDEN

MEETING THIRTY-ONE

SAVONLINNA

FINLAND

AUGUST 1998

Revision of ENV 1995-1-2: Charring and degradation of strength and stiffness

Jürgen König

Trätec - Swedish Institute for Wood Technology Research, Sweden

Summary

Calculating the load-carrying capacity of fire exposed timber members, the designer needs information on, firstly, charring depths in order to determine the cross-sectional properties of the residual cross section, and secondly, the degradation of strength and stiffness. In the present Fire Part of Eurocode 5, charring is dealt with in a crude way. Especially, it is not possible to consider charring of protected timber surfaces in a rational way. The present model may lead to unsafe, or in other cases unduly conservative results. According to the proposed model, charring is properly defined, and a distinction is made with regard to different charring and protection phases.

For parametric fire exposure, the present method is not operational. Reviewing the background papers and extending the method for determination of strength and stiffness degradation according to annex A of ENV 1995-1-2, a revised model is proposed for the determination of relationships between load-carrying capacity and time.

1 Introduction

ENV 1995-1-2, the Fire Part of Eurocode 5¹ was published by CEN in November 1994. This European pre-standard and the Fire Parts of the other Eurocodes have now (April 1998), somewhat delayed, passed the stage of Two-year enquiry. CEN Member Bodies, i.e. the National Standards Organisations were asked to submit comments on this European pre-standard (ENV) to be considered during the redrafting for conversion to a European Standard (EN). The result of this enquiry was that a majority voted for redrafting and conversion to EN of all Fire Parts.

The intention of the Two-year enquiry was to collect National comments based on the experiences from experimental application during the first two years after the publication of the pre-standard. Due to considerable delay in introducing the Fire Part of Eurocode 5 (and the other Fire Parts) as National Pre-standards for experimental use, however, only very few comments were submitted expressing the views of designers working in the field.

This paper discusses the two properties of timber that are most essential with respect to the load-carrying performance of timber structures in the event of fire: The charring of the timber member giving rise to a reduction of the cross section of the member, and the

degradation of strength and stiffness (modulus of elasticity) of the residual cross section due to the influence of temperature and moisture. It is stressed that the format should be simple, although it should open up for extended application using data not given in the Fire Part or not yet available.

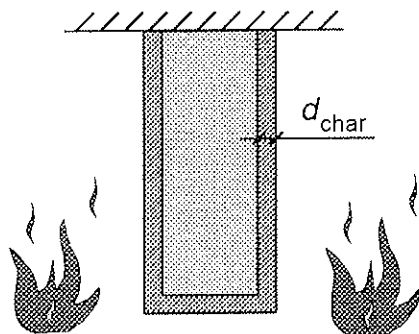


Figure 1: Glued laminated beam fire exposed on three sides

For the determination of the load-carrying capacity of timber members, the application rules of the Fire Part refer to simple rectangular cross sections that are exposed to fire on three or four sides, see figure 1, showing a glued laminated beam where the upper side is protected by another structural member, e.g. a floor slab, or figure 2, showing a light timber frame wall assembly without cavity insulation. Using the application rules of the Fire Part, it is easy to determine the thickness of the charred layer and to determine the bending strength of the residual cross section. However,

when the cavity of the wall assembly is filled with insulation material, e.g. bat-type glass or rock fibre, see figure 3, the application rules would give unsafe results.

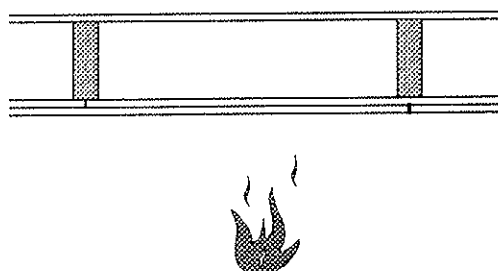


Figure 2: Light timber frame wall assembly with void cavity

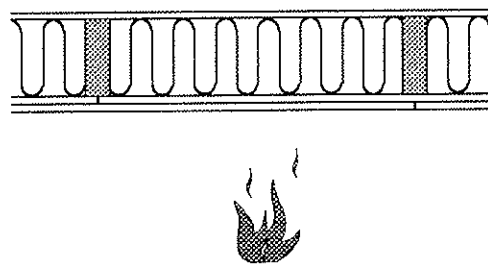


Figure 3: Light timber frame wall assembly with cavity insulation

2 Charring rates and charring depths

2.1 General

In ENV 1995-1-2 charring of wood and wood-based panels is considered in a non-consistent and confusing way. Due to the lack of a test standard for the determination of charring rates, the charring rate was not properly defined. Meanwhile, however, the widely accepted definition of the charring depth as being the position of the 300-degree isotherm has been adopted in Draft ENV YYY5 Part 7².

Information on charring rates at standard fire can be found at several places of the Fire Part i.e. both in clause 3.1 Charring depths, and annex A Reduced strength and stiffness method for standard fire. For clarity, all basic information should be found in clause 3.1 and rearranged in a logic way. Since charring of timber, among other things, is influenced by the shape of the cross section, this influence should be excluded in the definition of charring as a material property. In the design, the influence of the cross section should be taken into

account by applying relevant radii of arris roundings, or, for simplicity, by application of notional charring rates where the effect of increased charring at arrises is assumed to be included.

The following distinction should be made:

- The **basic charring rate** β_0 is the charring rate at one-dimensional heat flux at standard fire exposure, i.e. the charring rate obtained in fire tests on wide members remote from arrises (in ENV 1995-1-2 this is denoted as β) with fire exposure on one side. A test standard should be developed for the determination of the basic charring rate of wood and wood-based panels, prescribing the minimum thickness of the test piece such that the thickness does not influence the charring rate ("thermally thick" test pieces, exposed on one side). When this charring rate is used for the determination of the residual cross section of members, the corner radii at arrises shall be taken into account separately. In design by calculation, for simplicity, the charring depth should be assumed to increase at a constant rate, even though this is not true in reality, see test results shown in figure 4. We can see that charring does not start at the time $t = 0$, and that the charring rate is decreasing after some time since the char layer of increasing thickness provides better and better insulation

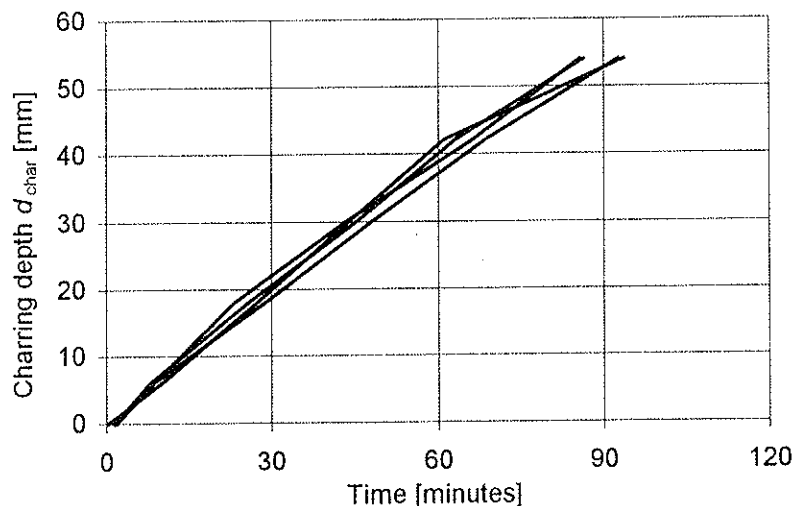


Figure 4: Test results of charring depth versus time at one-dimensional heat transfer (standard fire exposure)

to the residual cross section. Therefore, the charring rate should be related to a specified time, e.g. 30 minutes, or a specified charring depth, e.g. 30 mm.

- The **notional charring rate** β_n is a charring rate that may be used when the increased charring at arrises is not taken into account separately (the subscript n was used in the CIB-code³, while in ENV 1995-1-2 the notional charring rate is denoted as β_0). The notional charring rate should also include the effect of fissures where relevant, i.e. normally only in large cross sections of solid timber.

- The **real charring rate** β is the charring rate at one or two-dimensional heat transfer to be used in more general modelling, e.g. in small cross sections as shown in figure 3.

EN 1995-1-2 should contain only values of basic and notional charring rates.

2.2 Protected timber members

In ENV 1995-1-2, a fire protective cladding is assumed to delay the start of charring by the time period t_{pr} . For simplicity, for surfaces protected by fire protective claddings, it is anticipated that the charring rate is the same, irrespective of whether charring is considered of initially unprotected or protected surfaces. This assumption may, however, lead to unsafe or unduly conservative solutions, since the charring behaviour deviates considerably from this assumption. In reality, the charring rate is dependent on the gas temperature in the fire compartment. When the fire protective cladding falls off, at standard fire exposure, the charring rate is generally higher compared to charring of initially unprotected surfaces, see figure 5. Again, for simplicity, it should be tried to apply a linear approximation, such as shown in figure 6, preferably by relating the charring rate to a specified depth.

The effect of fire protective claddings depends on its ability to provide thermal insulation by

- low thermal conductivity
- remaining coherent (stickability), and
- remaining fixed to the member.

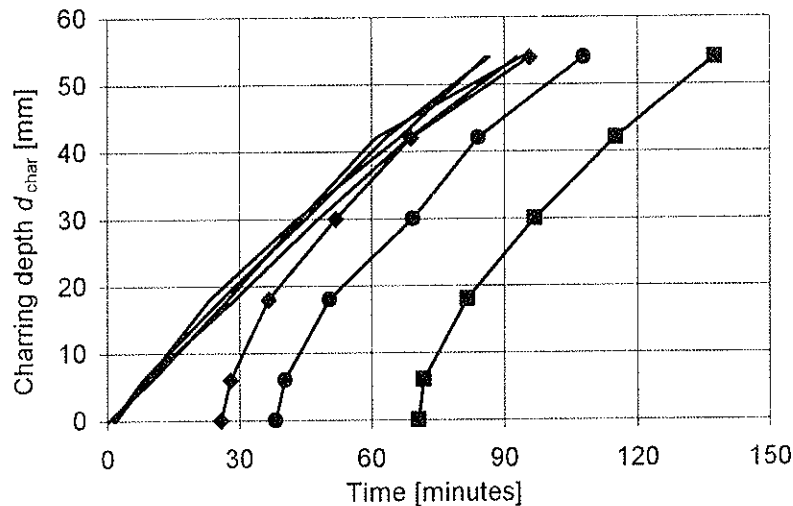


Figure 5: Test results of charring depths versus time - effect of delay of start of charring (standard fire exposure)

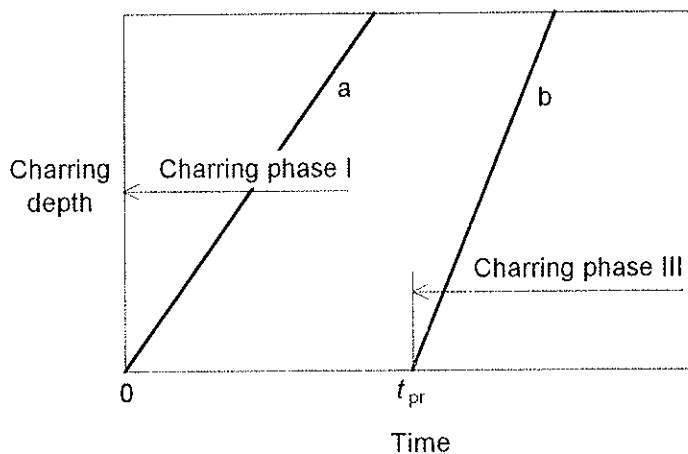


Figure 6: Charring depth of initially unprotected (a) and protected (b) members

In some materials, such as gypsum plasterboards, a considerable amount of heat is dissipated by chemical processes, such as the calcination of the gypsum.

In general, the charring behaviour of protected members can be described by figure 7. Where the fire protection (cladding) is made of incombustible boards (see figure 7a), the first part of the protection phase is characterized by charring being completely prevented as long as the temperature of the surface of the wood members does not reach 300 °C. Provided that the cladding remains coherent and fixed to the member, this is followed by the transition to charring phase II at time t_{pr} , characterized by the wood surface temperature reaching 300 °C. Due to the thermal insulation provided by the cladding, however, in this stage the charring rate is normally smaller than in wood members which are unprotected right from the beginning of the fire exposure. The transition from charring phase II to charring phase III is characterized by the failure of the cladding, i.e. they fall off and leave the timber frame completely unprotected against the fire in the compartment. In this stage, in general, as shown above, the charring rate is different from the charring rate of wood members that are unprotected right from the beginning (charring phase I).

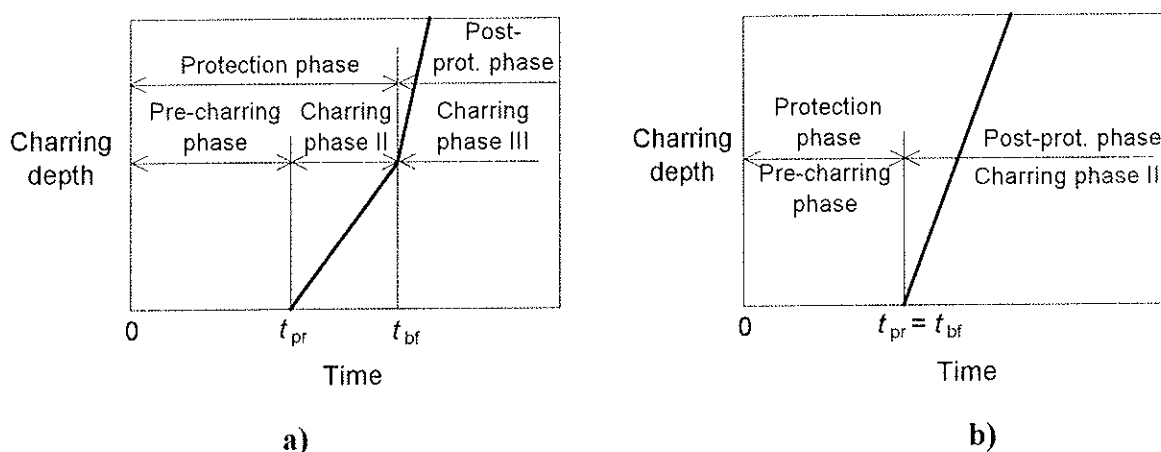


Figure 7: Charring phases of protected members: a) Non-combustible protection, b) Combustible protection

When the cladding consists of wood-based panels, the pre-charring phase changes immediately to the post-charring phase since the boards are burned when charring starts in the timber member, see figure 7b.

The possibility of considering different charring rates during the different phases of protection is taken into account in Draft ENV YYY5 Part 7.

2.3 Proposed change of wording

Clause 3.1 (Charring depths) should be changed to:

”(1)P Charring of wood shall be taken into account for all surfaces directly exposed to fire, or, where relevant, for protected surfaces, where charring of the wood is possible during the relevant time of fire exposure.

(2)P The charring depth shall be calculated taking into account the time of fire exposure and the relevant charring rate. The charring depth may be taken either as the position of the char-line or as a notional charring depth.

- (3) The position of the char-line should be taken as the position of the 300-degree isotherm.
 Note: This assumption is valid for most softwoods and hardwoods
- (4) For standard fire exposure the charring rate may be taken as constant with time.
- (5) For parametric fire exposure, design charring rates are given in annex ...
- (6) For initially unprotected surfaces of timber ..., for standard fire exposure, design charring rates β_0 and β_n are given in table
- (7) For wood-based panels ..., for standard fire exposure, the following design charring rates should be applied: ...
- (8) When surfaces of members are covered by fire protective claddings or are aligned with other structural members with a failure time that is smaller than the required fire resistance time $t_{fi,req}$, charring of the member starts at the failure time t_{pr} of the cladding or the aligned protecting structural member.
- (9) It should be taken into account that the charring rates are different during the protection phase and post-protection phase of initially fire protected surfaces”

3 Structural fire design of members - load-bearing capacity

The load-bearing capacity of a timber member is affected by the charring of the wood, causing a reduction of the original cross section and of the degradation of strength and stiffness properties. The design actions may be reduced compared to the design actions in ”cold design”, since there is only a small probability that a fire occurs at the same time that the structure is loaded by maximum mechanical actions. Hence the design of a timber member for a required fire resistance, e.g. a beam or a column, comprises the following steps:

- Determination of thermal and reduced mechanical actions
- Determination of the residual cross-section (consideration of char-layer)
- Determination of reduced material strength (due to temperature and moisture)
- Calculation of load-bearing capacity using input parameters from above.

3.1 Residual cross-section

The residual cross section is the initial cross section of the member reduced by the char layer of depth d_{char} . Two options are given for the determination of the charring depth, with the notations of ENV 1995-1-2:

$$d_{char} = \beta_0 t \quad (1)$$

or
$$d_{char} = \beta t \quad (2)$$

where t is the time of fire exposure and β and β_0 are charring rates according the following: When the charring rate β is used the corner roundings should be taken into account separately, while β_0 is a notional charring rate which is assumed to include the effects of corner roundings in an approximate way.

The charring rates given for softwoods (solid timber and glued laminated timber) within the European strength class system⁴ are assumed to be independent of density. For timber with lower characteristic density than 290 kg/m³ an extrapolation formula is given.

3.2 Determination of reduced material strength

For load-bearing verification the design strength and stiffness properties shall be determined as

$$f_{fi,d} = k_{mod,fi} k_{fi} \frac{f_k}{\gamma_{M,fi}} \quad (3)$$

$$E_{fi,d} = k_{mod,fi} k_{fi} \frac{E_{k,05}}{\gamma_{M,fi}} \quad (4)$$

with

$$\begin{aligned} k_{fi} &= 1,25 && \text{for solid timber} \\ k_{fi} &= 1,15 && \text{for glued laminated timber} \\ \gamma_{M,fi} &= 1,0 \end{aligned}$$

where

$f_{fi,d}$	is the design value of strength (modulus of rupture) in the case of fire
$E_{fi,d}$	is the design value of modulus of elasticity in the case of fire
f_k	is the characteristic strength (modulus of rupture) at normal temperature
$E_{k,05}$	is the characteristic modulus of elasticity (five percentile)
$k_{mod,fi}$	is the modification factor for fire, taking into account the effects of temperature and moisture
$\gamma_{M,fi}$	is the partial safety factor for material in the case of fire
k_{fi}	is a coefficient, see below.

The technical committee responsible for the drafting of all Eurocodes, CEN/TC 250, had decided that for structural fire design the partial safety factors for all materials should be put equal to one. Therefore, it was necessary to introduce the coefficient k_{fi} and calibrate it such that the well-known values according to national design codes would be obtained. The values of $k_{fi} f_k$ and $k_{fi} E_{k,05}$ correspond approximately to twenty percentiles, while f_k and $E_{k,05}$ are five percentile values. It is intended to avoid the introduction of k_{fi} into the future EN version by permitting partial safety values smaller than unity, e.g. $\gamma_{M,fi} = 0,8$ for solid timber.

For consideration of the degradation of strength, two alternatives are given. Some CEN Members required to give the option of a simplified method. The strength is then formally not reduced, this is however compensated for by reducing the residual cross section (obtained by reducing the initial cross section by the char layer according to expression (2)), by further 7 mm. As a simplification, no distinction is made to consider whether the member is in tension, compression or bending.

A higher degree of accuracy is achieved by using the alternative method. The value of $k_{mod,fi}$ is determined according to figure 8 where p/A_r is a measure of the heating of the residual cross section (where p is the perimeter of the fire exposed cross section in metres and A_r is the area of the residual cross section in m^2). The diagram shows linear relationships, indicating that they are rather approximate. There have been made only very few tests in the past where the properties of each specimen were well-defined. Thus the curves are calibrated to existing design rules rather than based on new results. The format, however, allows to improve the method when more knowledge is available.

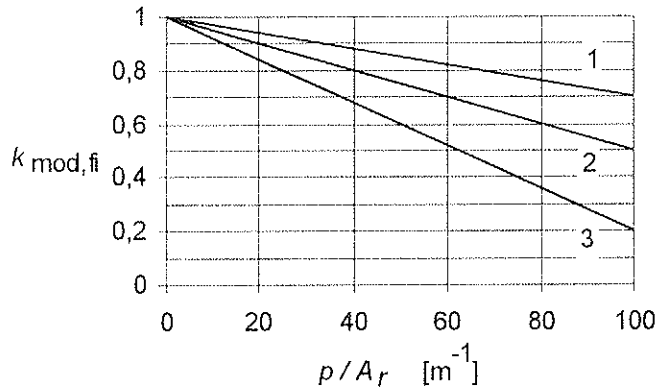


Figure 8: Determination of modification factor for fire.
1: MOR for tension and MOE
2: MOR for bending
3: MOR for compression

Comparing these two methods, it is obvious that the application of the so-called simplified method does not lead to a considerably smaller amount of design work, which would be the main reason for using a simplified method. On the other hand, the alternative method allows for consideration of the type of action effect. Another advantage is that it is easier to extend its application to constructions not yet included in Eurocode 5.

3.3 Example: Glulam and solid beam exposed to standard fire on three sides

For two timber cross sections, a glulam beam of dimension 170 mm × 400 mm and a light solid beam of dimension 45 mm × 145 mm, both exposed to standard fire on three sides, in figure 9 is shown the variation with time of the section modulus W_{fi} , the modification factor for fire $k_{mod,fi}$ and the resulting bending moment capacity $R_{M,fi}$. The section modulus and bending moment capacity are shown in relation to their initial values at ambient temperature ("cold" design). We can see that the effect of the strength degradation of the residual cross section of the glulam beam is small, while it is much greater in the case of light cross sections.

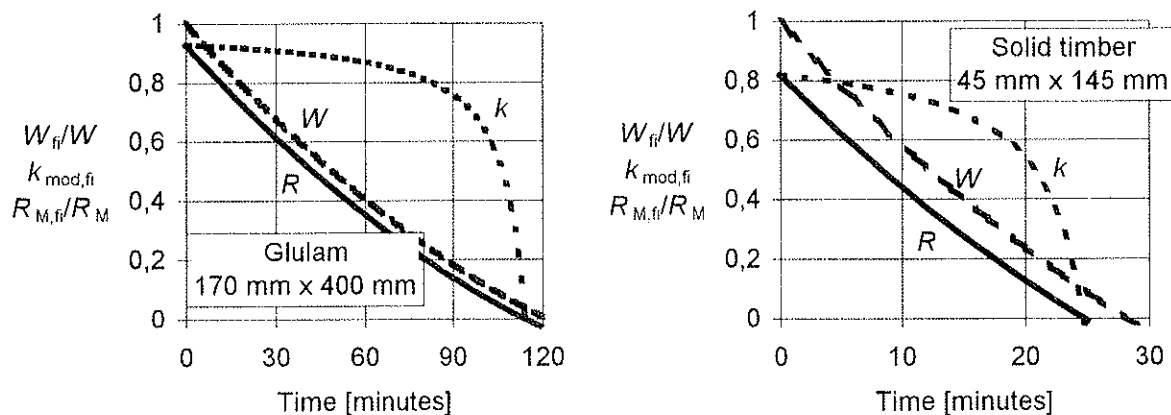


Figure 9: Examples of glulam beam (left) and light solid beam (right) exposed to standard fire on three sides. Variation of section modulus, modification factor for fire and bending moment capacity with time

3.4 Natural fire scenarios: parametric fire exposure

In an informative annex, a design method is given for glued laminated beams in edgewise bending exposed to parametric fires. The fire curves are determined according to the energy balance method⁵ where the temperature is dependant on the fire load density and the properties of the enclosure of the fire compartment with respect to openings and thermal properties. The method given is still incomplete and should be improved in the EN version of the code.

The fire scenario is described in time steps of t_0 in minutes with

$$t_0 = 0,006 \frac{q_{td}}{F} \quad (5)$$

where q_{td} is the design fire load density related to the total area of the compartment boundary in MJ/m² and F is the opening factor in m^{0.5}, see ENV 1995-1-2 annex D for more details.

The method implies that the charring rate is constant during the initial phase of length t_0 and decreases then linearly with time to zero during the following time period of length $2 t_0$. After this time period the char layer does not increase any more, however both strength (MOR) and stiffness (MOE) continue to decrease. The code gives the following expression⁷ for the determination of modification factor for fire:

$$k_{\text{mod,fi}} = 1,0 - 3,2 \frac{d_{\text{char}}}{b} \quad (6)$$

where b is the initial width of the beam and d_{char} is the charring depth. From the underlying test report⁸ can be seen that this expression gives the load bearing capacity at the time of $5 t_0$. In order to make this method complete, i.e. to give the designer a tool for determining a complete relationship between load-bearing capacity and time, the following is proposed to be included during the redrafting of the code:

During the time period until $t = 3 t_0$ the modification factor for fire is determined according to figure 3, for $t = 5 t_0$ it is calculated according to expression (6) and for the time period between $3 t_0$ and $5 t_0$ linear interpolation may be applied. No test results are available for times beyond this stage. Figure 10 illustrates how this method should be applied. The example shows the variation of the parameters for the glulam beam from figure 7 (left). The fire load of 170 MJ/m² and the opening factor of 0,04 m^{0.5} is representative for residential buildings. The glulam beam is assumed to be in a "stone" building (concrete, masonry), i.e. the thermal inertia of the heavy compartment boundary is high.

From the diagram we can see that the beam, e.g. when designed for a fire resistance of 60 minutes, would fail first after 90 minutes in the natural fire scenario used here. Contrary to the fire scenario of standard fire exposure, the natural fire scenario describes the load-bearing behaviour of the structure in a real time scale.

This allows the regulators to define appropriate requirements with respect to local conditions - the type of building and measures of active fire suppression - either by fire resistance times in a real time scale or time equivalents in terms of standard fire exposure.

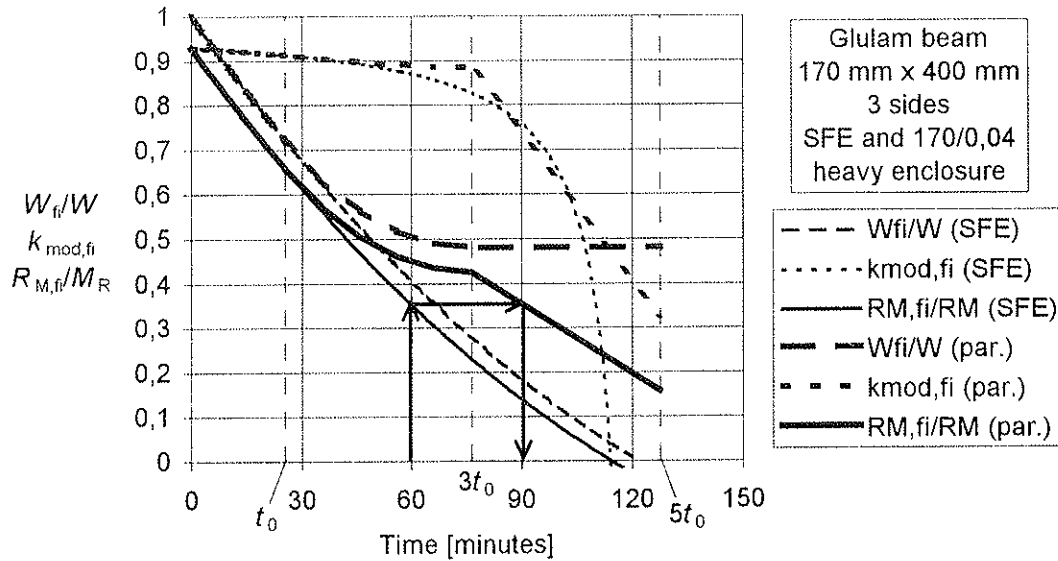


Figure 10: Illustration of glulam beam in standard fire (SFE) and parametric fire exposure

4 References

- ¹ ENV 1995-1-2:1994, Eurocode 5 - Design of timber structures, Part 1-2 - Structural fire design, Brussels, 1994
- ² Draft ENV YYY5 Part 7 Fire tests on elements of building construction: Test method for determining the contribution to the fire resistance of structural members: By applied protection to timber members. CEN/TC 127, 1997
- ³ CIB Structural Timber Design Code. CIB, Publication 66, 1983
- ⁴ EN 338 Structural Timber - Strength classes, CEN, Brussels, 1995
- ⁵ Magnusson, S E & Thelandersson, S, Temperature-time curves of complete process of fire development. Acta Polytechnica Scandinavica, Stockholm 1970
- ⁶ Bolonius Olesen, F & König, J, Tests on glued-laminated beams in bending exposed to natural fires. CIB W18, Meeting Twenty-five in Åhus, Paper 25-16-2, 1992
- ⁷ Toft Hansen, F & Bolonius Olesen, F, Full-scale tests on loaded glulam beams exposed to natural fires. Aalborg University, Aalborg, 1992

CIB-W18/31-21-1

INTERNATIONAL COUNCIL FOR BUILDING RESEARCH STUDIES AND DOCUMENTATION
WORKING COMMISSION W18 - TIMBER STRUCTURES

DEVELOPMENT OF AN OPTIMISED TEST CONFIGURATION TO DETERMINE
SHEAR STRENGTH OF GLUED LAMINATED TIMBER

by

G Schickhofer
B Obermayr
Department of Timber Engineering
Technical University of Graz

AUSTRIA

MEETING THIRTY-ONE

SAVONLINNA

FINLAND

AUGUST 1998

Development of an optimised test configuration to determine shear strength of glued laminated timber

G. Schickhofer
B. Obermayr
Technical University of Graz
Department of Timber Engineering
AUSTRIA

Abstract

Based on international known research projects on the determination of shear strength of timber we try to define an optimised test configuration for GLT. Research on this field restricts to solid timber cross-sections of small dimension. There is a lack of vast research on cross-sections of bigger dimension and hence a secure determination of characteristic shear strength values for GLT can not be provided. Additional to the ordinary influences on the specimen the respective test configuration exercises an very important influence on the determination of shear strength in a test. Literature mentions various configurations in this field. Moreover we have to face the problem of the combination of shear, bending and compression (also tension) perpendicular to grain stresses. All these influences lead to a reduction of the percentage of specimens failed in shear and require therefore a higher test effort (enlarged number of specimens).

To avoid that fact we examine one test configuration - the I-cross-section form. Additional to two test series (2*6=12 specimens) with different depths (h=608mm and h=320mm) we do finite element analysis for the respective test configuration to find out the distribution of shear stress and of compression stress perpendicular to grain within the range of support. This proceeding is necessary since some of the specimens did not show a clear failure in shear as reason for fracture. As a result of our work, referring to compression perpendicular to grain within the range of support, we present an optimised I-cross-section and a rectangular cross-section with reinforced flanges. The depth of reference amounted to h=608mm and h=592mm. The relation of span L to depth H of this three point bending test configuration was 5 : 1. Three more series (3+3+6=12 beams) with the respective dimensions of reference were tested, to verify the optimised results of the series 1 and 2.

1 Introduction

The tables 1 and 2 of the prEN 1194:1998 specify the relevant characteristic shear strength values for the respective GLT strength classes. These values can also be confirmed according to the relation $f_{v,g,k}=0,32*f_{t,0,l,k}^{0,8}$ normatively defined in annex A/table A.1. This formal correlation of the characteristic shear strength $f_{v,g,k}$ of a GLT beam and the characteristic tension strength $f_{t,0,l,k}$ of a lamination was derived from actual shear stress values, used in the existing design codes. We can not unequivocally duplicate this function.

It is true that prEN1194:1998 refers to EN 408 and also to prEN 1193, but the test configuration there only considers the determination of shear strength values of small specimens for solid timber and boards used for the production of GLT. We could not find any definition of a test configuration to determine the shear strength of GLT in consequence of beam bending, neither in EN 408 nor in prEN 1193. It seemed necessary to define a test configuration by which shear strength values can be made comprehensible respectively can be found out, since there scarcely exist results on bigger dimensioned pieces of GLT.

2 Background

A work conducted by F. Lam, H. Yee and J.D. Barrett pointed out that the actual test situation does not correspond to the demands of stress, since - based on shear block tests performed according to ASTM D143 - a modification factor of 4.1 leads to the conclusion of a design value for large sized structural timber components. The influence of cracks gets taken into consideration by means of an additional factor. During this actual piece of research two test configurations have been examined, which are used at the US Forest Laboratory and at the CSIRO, Australia, as well. There we find a two span five point bending test configuration with a relation span to depth of L:H=5:1 and L:H=6:1. They tested structural timber with a cross-sectional dimension of 38/185mm. Each of the three tested kinds of timber (DF, HF, SPF) was represented by 100 pieces of specimen. The overhang, measured from the point of support to the edge of the beam, amounted at 185mm. As an important result they found out that only about 40% failure in shear could be reached. That output of failure in shear seems rather unacceptable, if we just consider the costs of such tests. Based on the test configuration L:H=5:1 the test configuration L:H=6:1 brought out the reasonable result of about 10% to 30% lower average shear strength values for the quoted kind of timber (effect of volume).

When we take a closer look at the two span five point bending test configuration L:H=5:1 we notice clearly that because of the geometrical conditions and because of the situation of the loading plate no distinct shear stress field can develop (the loading fields influence on each other). Additional to the conditions of symmetry in the middle support (automatically horizontal prevention of deformation) this might be also a reason for the determination made in a contribution of R.H. Leicester and F.G. Young, where they found out the difference of 40% between a single span shear test configuration with 3 point load support and a two span configuration with 5 point load support.

Another very interesting test program of D.R. Rammer and D.I. McLean tested 1279 solid timber specimens, which were exposed to different kinds of boundary conditions. The test configurations were a two span 5:1 configuration with 5 point load support and a single span 5:1 configuration with 3 point load support. Based on the tested cross-section dimensions 51/102mm to 102/356mm the relatively strong influence of volume within those small dimensions could be made obvious. This influence decreases with an increase of volume. Moreover the influence of moisture is shown, which might be less important at the GLT because of the rather constant and smaller difference between initial moisture content and equal moisture content.

Some existing vast test programs, which mostly concern solid timber, can not be used in full compliance with GLT. That fact was the reason for our effort. We wanted to establish a

commonly valid test configuration, at least for European needs, and searched for a technical clarification of the formal dependence quoted in the prEN 1194:1998 $f_{v,g,k}=0,32*f_{t,0,i,k}^{0,8}$. In this piece of our work, different from a two span five point bending test configuration, we propose a single span three point bending test configuration. The cross-section shape of the series 1, 2 and 5 is an I-cross-section. The series 3 and 4 show a rectangular cross-section reinforced by flanges. We aim at the establishment of comparable test results, based on generally accepted configurations, to reach by that means reliable values for a normative work.

3 Preliminary Tests

3.1 Test configuration

Our preliminary tests consisted of two series (serie 1 and serie 2), which differentiated in the dimensions of the specimens, the which aimed at the determination of the influence of the volume on the shear strength. The depth of the beams in serie 1 was fixed with reference to prEN 1194:1998 at 608mm. In serie 2 the depth of the beams was frankly picked out at 320mm. To avoid an reciprocal influence of support and loading point the span was fixed, according to the knowledge we had got from literature, at the quintuple of the depth of the beam (L:H=5:1). The design of flanges and those of webs rose from the need for a maximum of bending stiffness in comparison to the shear stiffness. The bottom chord was made up of not finger jointed laminations, so that the tension zone was not weakened superfluously.

The exact configuration of the test you take from figure 3.1.

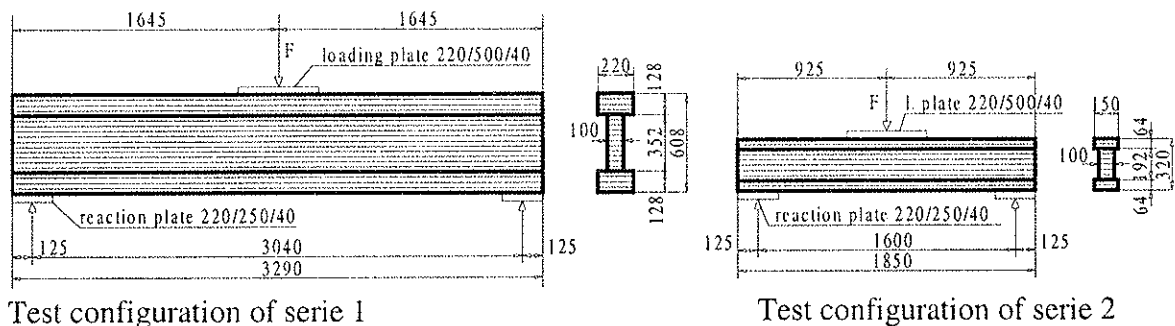


Figure 3.1: Test configuration of the preliminary test

The kind of timber we used was visually graded spruce timber (S13 according to DIN 4074 →BS14 comparable to GL28 according to prEN1194:1998). We tested 6 beams per serie and by that we were able to estimate the test configuration itself, but only in a very restricted way we could state something about the reached strengths.

3.2 Results of the tests

The suitability of the test configuration was estimated on base of the pictures of fracture, which you find in annex B for all specimens. We found out that by choosing the I cross-section the bending failure could almost be avoided. So only one of twelve beams broke because of bending. Looking at the fractures more closely, we notice that the specimens

quite often failed in the zone between the bottom chord and the web. The characteristics of that failures are, that on the one hand the cracks follow the annual rings within the cross-section and on the other they started from the edge between the bottom chord and the web. An following FE-analysis, we comment it in chapter 3.3, brought up that within this zone the stress of the compression perpendicular to grain reached -6 N/mm^2 , which can lead to such shear failures following the annual rings. That is why those cracks can not be necessarily explained by failure in shear.

The grades of strength we reached are of course only in a relative way representative, nevertheless they show clearly the influence of volume on the shear strength. In serie 1 the average stress of shear in the middle of the beam at the moment of crack amounted to 4.18 N/mm^2 in serie 2 however to 4.94 N/mm^2 . This means a difference of 18% (see also annex A).

3.3 Finite element analysis

To receive more knowledge about the behaviour of cracks within the test configuration an FE-analysis was applied. The most important thing was to find out why many of the specimens failed within the transition zone between bottom chord and web. For that means we created a three-dimensional net in the FE-program Abaqus 5.6. 3-d because we wanted to observe also eventual effects of notch between flange and web. To simplify the modelling we presumed orthotrope material. We fixed the load at 400 kN.

The most important result of the FE-calculation was the existence of a very elevated stress of compression perpendicular to grain within the zone of support. Figure 3.2 represents on the one hand the compression perpendicular to grain in the edge cross-section, on the other hand we see the distribution of stresses perpendicular to grain between bottom chord and web in the cross-sectional axle longitudinal to the beam.

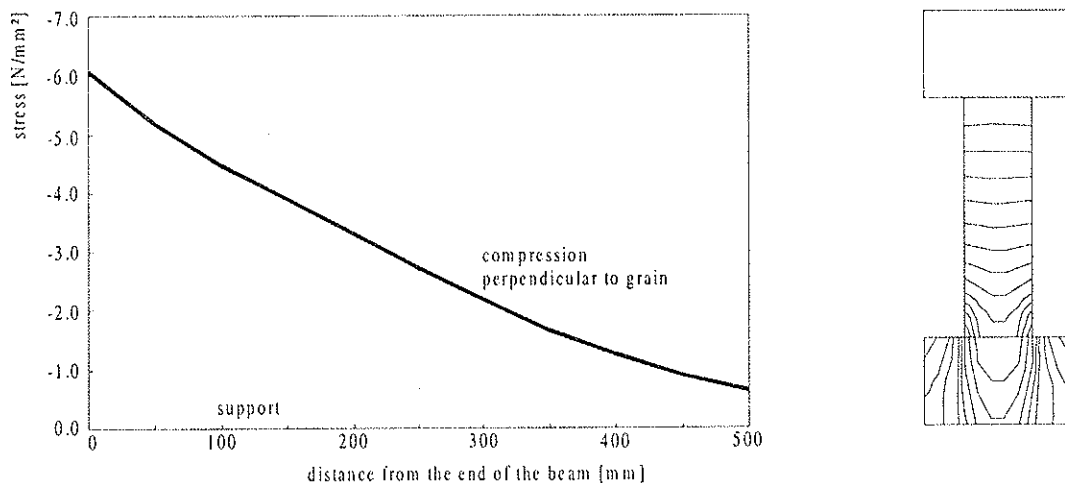


Figure 3.2: stress perpendicular to grain in the zone of support

By another FE-analysis is shown how compression perpendicular to grain cause cracks. For this we examine only the second laminations of the web. We created a 2-dimensional FE model, approximating the structure of the annual rings by means of concentric circles. The load corresponds to the compression perpendicular to grain between the first and the second web lamination resulting from the previous FE analysis.

Figure 3.4 shows the deformed shape of the lamination. You notice, that the annual rings have a need to straighten. This fact causes shear stresses from 3.5 to 4.0 N/mm², which can be the reason for a failure (slide) following the annual rings. Since the material values for early wood and late wood are missing, we can not make any well-founded examination. Nevertheless we can come to the conclusion that compression perpendicular to grain can be decisive for failure within the transition zone between bottom chord and web. Followingly a failure within this zone can not be clearly defined, which leads to problems as far as the evaluation of the tests is concerned.

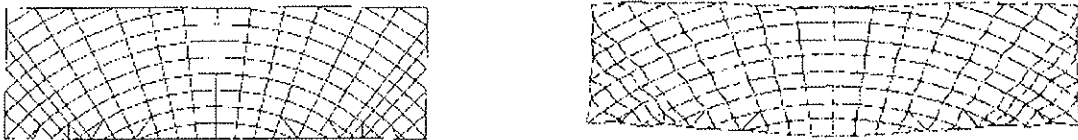


Figure 3.4: FE-net and deformed shape of the lamination

4 Optimised test configuration

4.1 Modified configuration

As we mentioned in chapter 3.3 there are concentrations of compression perpendicular to grain in the support zone within the configuration of the preliminary tests, the which can lead to a premature failure of the test beam. A very problematical fact is, that those cracks can not be distinguished from shear cracks. That is why we modified the configuration of serie 1, so that above the support a rather constant distribution of compression stress perpendicular to grain longitudinal to the beam was settled.

Another FE-analysis made clear that the missing overhang was the reason for this concentration of stress. Since an overhang rises the shear strength at the edge of the beam we can not intend it without limitations. So additional to the arrangement of 5cm overhang the support plate was lengthened 10 cm and the point of support was transferred towards the interior part. As you see in figure 4.1 we proved a balanced distribution of stresses perpendicular to grain longitudinal to the beam. The maximal compression perpendicular to grain at a load of 400kN now amounts to -3.0 N/mm² in stead of former -6.0 N/mm².

We could not expunge the concentrations of compression perpendicular to grain at the angles between bottom chord and web, since they are conditioned by cross-section. How that fact influences on the crack behaviour we discuss in detail looking at another serie of tests.

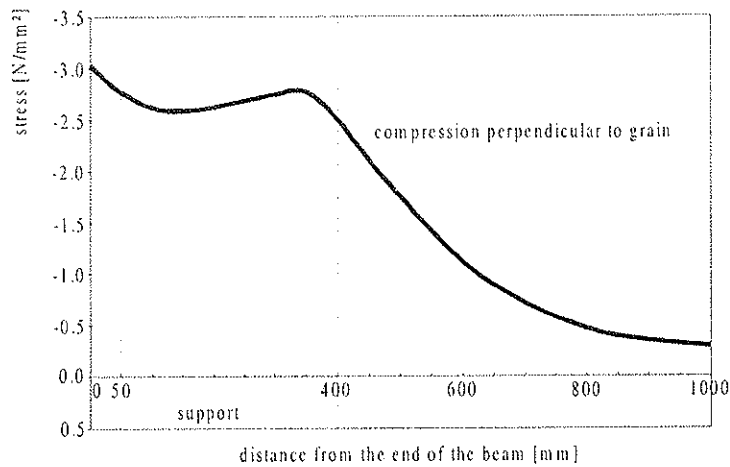


Figure 4.1: distribution of compression stresses perpendicular to grain longitudinal to the beam

Take test configuration from figure 4.2.

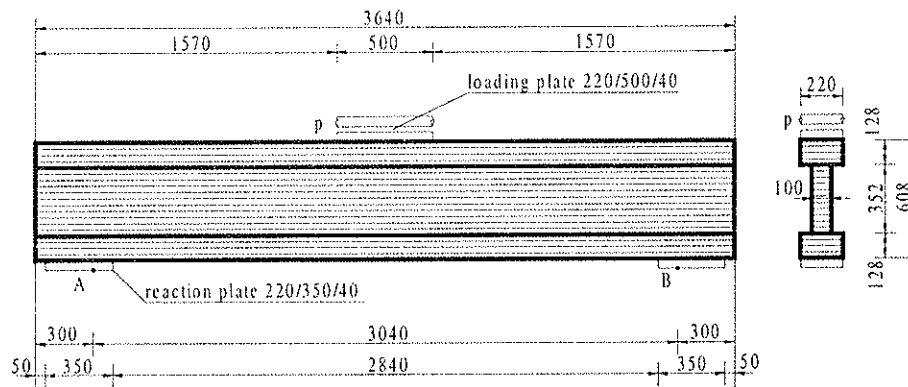


Figure 4.2: modified test configuration of serie 1 (see serie 5)

4.2 Test configuration with rectangular cross-section

From the preliminary tests (see chapter 3) we knew that an I cross-section is problematical as far as the effect of notch between bottom chord and web is concerned. That is why we developed a test beam with rectangular cross-section.

To reach a sufficient bending strength it was necessary to glue materials of superior quality. First of all those materials had to meet the demands of high tension strength and high compression strength perpendicular to grain. The later is necessary to minimise the dimensions of the loading plate. Another task of the reinforced flanges is to provide a sufficient load allocating effect, which diminishes the compression perpendicular to grain of the GLT innerzone. Materials corresponding to these demands are f. e. hardwood or Kerto.

Of course also at the rectangular cross-section we meet the problem of a superior compression perpendicular to grain at the end of the beam, so that the shape of support introduced in chapter 4.1 is applied.

Figure 4.3 shows the test configuration with rectangular cross-section. As in serie 1 we fixed the depth of the beam with reference to prEN 1194:1998. The relation from span to depth again amounts at 5:1. The strength of the flange of 120mm provides a sufficient allocating effect.

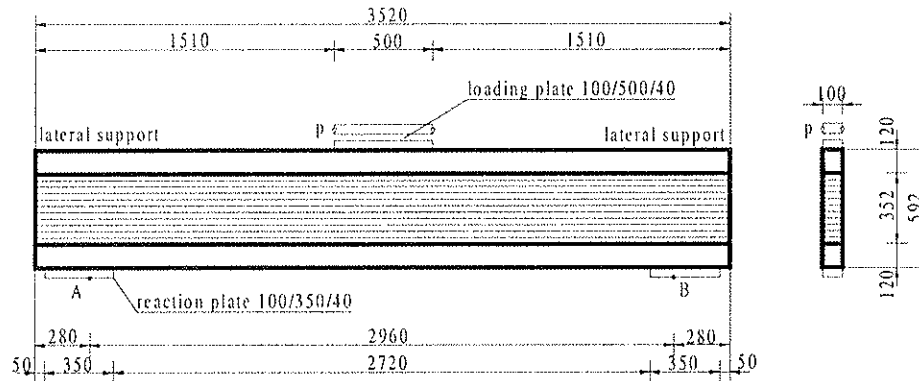


Figure 4.3: Test configuration with a rectangular cross-section (see series 3 and 4)

5 Tests to check the optimised test configurations

5.1 Rectangular cross-section

To comprehend the influence of the mechanical properties of the material used to reinforce the flanges we tested 3 beams with Kerto-S-flanges (in serie 3) and 3 beams with flanges of robinia (in serie 4). We directed our attention first of all at the E-modulus. Kerto-S showed almost the same E-modulus as GLT, while that of robinia is extremely superior (see annex A). From that we conclude that beams reinforced with Kerto-S react like GLT beams with rectangular cross-section, those reinforced with robinia, however, react like GLT beams with an I-cross-section. The relevant test configuration please take from figure 4.3.

The tests revealed that the very problem is not represented by the compression perpendicular to grain above the support but by those within the range of the loading plate. In serie 3 Kerto-S failed in one case. In serie 4 we had one failure in compression perpendicular to grain of the GLT innerzone beyond the loading plate, a fact we attribute to the high stress (426 kN) which could not be sufficiently allocated by the flange reinforced with robinia. Nevertheless two of three beams failed because of shear, as you can see from the figures of crack in annex C. Please note the evident differences between the strength values we reached in both of the series (serie 3: $f_{v,m}=3.90 \text{ N/mm}^2$, serie 4: $f_{v,m}=4.84 \text{ N/mm}^2$).

5.2 Modified configuration of serie 1

To comment on the modified configuration of serie 1 we tested 6 beams (serie 5). The exact test configuration take from figure 4.2.

The figures of cracks you see in annex C make clear that four of six beams show a shear fracture, which occurred independent of the problematic compression perpendicular to grain above the support. The other two beams failed at the supreme lamination of the bottom chord. From this fact we can conclude, that it has to be influenced in spite of a reduced compression perpendicular to grain at the edge of the beam. In both cases a slide,

starting from the bottom chord to the web, following the annual rings, was the reason for the failure.

Further tests should take care of the fact that the right side of the supreme bottom chord lamination should always be down below. By that a formation of a slide can be excluded within both beams of the series.

6 Conclusions

By doing this tests we aimed at the development of a test configuration which had structural size and reached a high number of failures in shear (21 of 24 specimens: 87.5%). When we chose the I-cross section we were able to fulfil both requests.

The depth of reference of 608 mm, the test beams had, corresponded to prEN 1194 of 600mm for test of accordance as far as grading is concerned based on the characteristic values of bending strength.

Failures in bending could be almost excluded by the use of an I-cross-section. The problem of this configuration is represented by the concentrations of compression perpendicular to grain between bottom chord and web. Those concentrations are not the only reason for a failure, but they cause a premature failure in shear. The tests pointed out that first of all the supreme bottom chord is concerned. The problem, however, can be reduced by arranging the annual rings in the right way (right side down). Another but more laborious way is to round the edges between bottom chord and web, so that the effect of notch can be reduced. We adopt this method mainly for solid timber, since in that case I-cross-section is milled out.

Moreover we favourite the system of single span three point bending with a relation between span and depth of 5:1. The advantage of that system compared to the two span five point bending test configuration is that the problem of the compression perpendicular to grain can be obviously reduced by means of supporting rolls. Moreover the test is not handicapped by a failure at the edge of the beam. Tests made by R.H. Leicester and F.G. Young prove that the system of two span five point bending test configuration show elevated values because of a restrained failure in shear. Their tests on failures in shear of laminated veneer lumber had examined both systems. According to their results the two span five point bending configuration reached a shear strength of 40% superior to that one of the single span three point bending test configuration.

The configuration can be used for solid timber and GLT of any size, as well, so that an influence of volume gets realisable.

The following relations are indicatives for the determination of test beams:

- $H/L: 5:1$
- $H/H_F: 5:1$
- $W_F/W_W: 2:1$

The single span three point bending test configuration with rectangular cross-section and reinforced chord represents possibly an alternative to the I-cross-section. Mainly there doesn't rise any problem of compression perpendicular to grain between bottom chord and web. The problem of compression perpendicular to the grain in the range of the loading

plate can be solved by lengthening the loading plate. More information has to be gathered, however, on how the mechanical properties of the material used to reinforce the flange influence on the strength values, which had been quite various at the tests.

7 Acknowledgments

We appreciate the Technical Commission of the Austrian GLT Association and first of all the European President of GLT Association Mr H. Stingl, since they enabled us to do this piece of work. Moreover we want to give our thanks also to the Experimental Laboratory for Structural Engineerings of the TU Graz, above all K. Kernbichler and J. Linder, since they assisted our project decisively. Discussion with E. Gehri from the ETH Zurich helped us a lot on our way. Of course we want to thank everybody for the interest taken in our work.

8 Literature

CODES, STANDARDS

prEN 1193: 'Holzbauwerke Bauholz für tragende Zwecke und Brettschichtholz Bestimmung der Scherfestigkeit und der mechanischen Eigenschaften rechtwinkelig zur Faserichtung', 6/1997

prEN 1194: 'Timber structures glued laminated timber strength classes and determination of characteristic values', 2/1998

Z-9.1-100: 'Allgemeine bauaufsichtliche Zulassung für KERTO-Furnierschichtholz', Deutsches Institut für Bautechnik, 11/1997

PAPERS

Korin, U.: 'determination of the shear strength of timbers'

Proceedings of the International Wood Engineering Conference, Volume 2, New Orleans, USA, 10/1996

Lam, F.; Yee, H.; Barret, J.D.: 'shear strength of Canadian softwood structural lumber'

Proceedings CIB-W18, meeting twenty-eight, Copenhagen, Denmark, 4/1995

Leicester, R.H.; Young, F.G.: 'shear strength of continuous beams'

Proceedings CIB-W18, meeting twenty-four, Oxford, UK, 9/1991

Madsen, B.: 'shear strength of Douglas fir timbers'

Proceedings CIB-W18, meeting twenty-eight, Copenhagen, Denmark, 4/1995

Rammer, R.d.: 'recent research on the shear strength of wood beams'

Proceedings of the International Wood Engineering Conference, Volume 2, New Orleans, USA, 10/1996

DIPLOMA THESIS

Jauernig, H.: 'Untersuchungen über die Verklebung von Robinie bei höheren Holzfeuchten' Universität Hamburg, Fachbereich Biologie, 3/1997

ANNEX A

Evaluation of the test results

S1	ALL SPECIMENS	SPECIMENS FAILED IN SHEAR	
	middle	middle	point of failure
NUMBER:	6	5	5
$f_{v,g,50}$ [N/mm ²]	4,18	4,10	3,53
COV [%]	15	15	15
$f_{v,g,05}$ [N/mm ²]	3,14	3,08	2,65

S2	ALL SPECIMENS	SPECIMENS FAILED IN SHEAR	
	middle	middle	point of failure
NUMBER:	6	6	6
$f_{v,g,50}$ [N/mm ²]	4,94	4,94	4,38
COV [%]	15	15	15
$f_{v,g,05}$ [N/mm ²]	3,71	3,71	3,29

S3	ALL SPECIMENS	SPECIMENS FAILED IN SHEAR	
	middle	middle	point of failure
NUMBER:	3	2	2
$f_{v,g,50}$ [N/mm ²]	3,90	3,90	3,61
COV [%]	-	-	-
$f_{v,g,05}$ [N/mm ²]	-	-	-

S4	ALL SPECIMENS	SPECIMENS FAILED IN SHEAR	
	middle	middle	point of failure
NUMBER:	3	2	2
$f_{v,g,50}$ [N/mm ²]	4,84	4,80	4,75
COV [%]	-	-	-
$f_{v,g,05}$ [N/mm ²]	-	-	-

S5	ALL SPECIMENS	SPECIMENS FAILED IN SHEAR	
	middle	middle	point of failure
NUMBER:	6	6	6
$f_{v,g,50}$ [N/mm ²]	4,33	4,33	3,92
COV [%]	15	15	15
$f_{v,g,05}$ [N/mm ²]	3,25	3,25	2,94

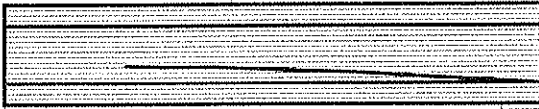
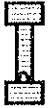
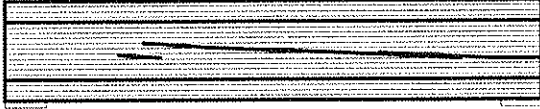


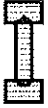

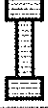


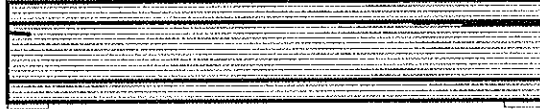
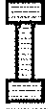
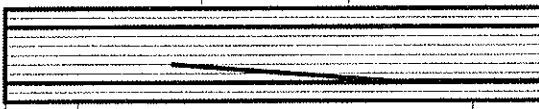







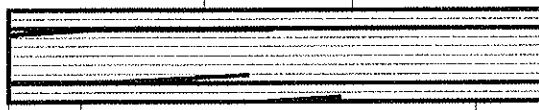

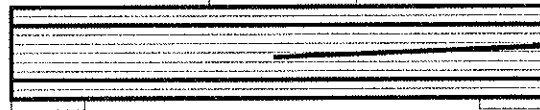

ANNOTATIONS

middle..... shear stress in the middle of the beam at the moment of crack
 point of fail....shear stress at the point of failure because of shear
 COV=15%.... assumed because of the small number of specimens

Mechanical properties of GL28, Kerto-S and Robinia

		GL 28h			KERTO-S	ROBINIA
$E_{0,g,mean}$	[N/mm ²]:	12600	$E_{0,l,mean}$	[N/mm ²]:	13000	18000
$G_{g,mean}$	[N/mm ²]:	780	G_{mean}	[N/mm ²]:	600	1100
$f_{m,g,k}$	[N/mm ²]:	28.0	$f_{t,0,1,05/50,(k)*}$	[N/mm ²]:	38.0*/-	36.8/83.1
$f_{c,90,g,k}$	[N/mm ²]:	3.0	$f_{c,90,k}$	[N/mm ²]:	5.0-7.0	-

ANNEX B: Pictures of fracture of the preliminary tests

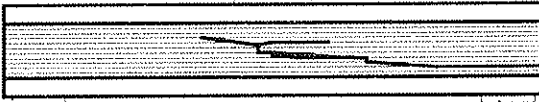



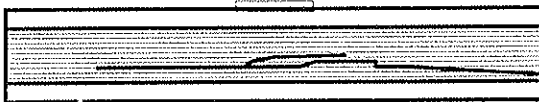





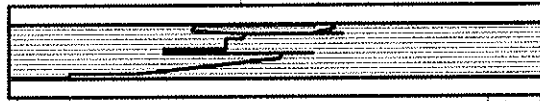




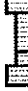
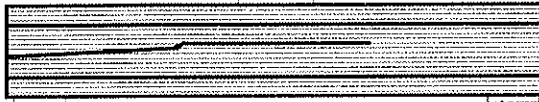



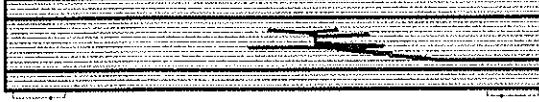

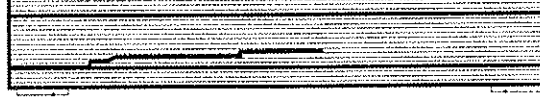

<p>S1B1 failure load $F=370\text{kN}$</p>   <p>$f_v = 4.17 \text{ N/mm}^2$ mode = FS</p>	<p>S1B2 failure load $F=345\text{kN}$</p>   <p>$f_v = 3.89 \text{ N/mm}^2$ mode = FS</p>
<p>S1B3 failure load $F=360\text{kN}$</p>   <p>$f_v = 4.06 \text{ N/mm}^2$ mode = FS</p>	<p>S1B4 failure load $F=405\text{kN}$</p>   <p>$f_v = 4.57 \text{ N/mm}^2$ mode = FB</p>
<p>S1B5 failure load $F=370\text{kN}$</p>   <p>$f_v = 4.17 \text{ N/mm}^2$ mode = FS</p>	<p>S1B6 failure load $F=374\text{kN}$</p>   <p>$f_v = 4.22 \text{ N/mm}^2$ mode = FS</p>
<p>S2B1 failure load $F=222\text{kN}$</p>   <p>$f_v = 4.93 \text{ N/mm}^2$ mode = FS</p>	<p>S2B2 failure load $F=206\text{kN}$</p>   <p>$f_v = 4.58 \text{ N/mm}^2$ mode = FS</p>
<p>S2B3 failure load $F=246\text{kN}$</p>   <p>$f_v = 5.47 \text{ N/mm}^2$ mode = FS</p>	<p>S2B4 failure load $F=218\text{kN}$</p>   <p>$f_v = 4.85 \text{ N/mm}^2$ mode = FS</p>
<p>S2B5 failure load $F=200\text{kN}$</p>   <p>$f_v = 4.45 \text{ N/mm}^2$ mode = FS</p>	<p>S2B6 failure load $F=242\text{kN}$</p>   <p>$f_v = 5.38 \text{ N/mm}^2$ mode = FS</p>

FB.....failure in bending

FC.....failure in compression perpendicular to grain

FS.....failure in shear

ANNEX C: Pictures of fracture of the tests to check the optimised configurations

<p>S3B1 failure load F=338kN</p>   <p>$f_v = 4.23 \text{ N/mm}^2$ mode = FS</p>	<p>S3B2 failure load F=285kN</p>   <p>$f_v = 3.57 \text{ N/mm}^2$ mode = FS</p>
<p>S3B3 failure load F=312kN</p>   <p>$f_v = 3.91 \text{ N/mm}^2$ mode = FC</p>	<p>S4B1 failure load F=432kN</p>   <p>$f_v = 4.98 \text{ N/mm}^2$ mode = FS</p>
<p>S4B2 failure load F=401kN</p>   <p>$f_v = 4.62 \text{ N/mm}^2$ mode = FS</p>	<p>S4B3 failure load F=426kN</p>   <p>$f_v = 4.91 \text{ N/mm}^2$ mode = FC</p>
<p>S5B1 failure load F=405kN</p>   <p>$f_v = 4.57 \text{ N/mm}^2$ mode = FS</p>	<p>S5B2 failure load F=358kN</p>   <p>$f_v = 4.04 \text{ N/mm}^2$ mode = FS</p>
<p>S5B3 failure load F=404kN</p>   <p>$f_v = 4.55 \text{ N/mm}^2$ mode = FS</p>	<p>S5B4 failure load F=364kN</p>   <p>$f_v = 4.10 \text{ N/mm}^2$ mode = FS</p>
<p>S5B5 failure load F=426kN</p>   <p>$f_v = 4.80 \text{ N/mm}^2$ mode = FS</p>	<p>S5B6 failure load F=346kN</p>   <p>$f_v = 3.90 \text{ N/mm}^2$ mode = FS</p>

FB.....failure in bending

FC.....failure in compression perpendicular to grain

FS.....failure in shear

CIB-W18/31-21-2

INTERNATIONAL COUNCIL FOR BUILDING RESEARCH STUDIES AND DOCUMENTATION
WORKING COMMISSION W18 - TIMBER STRUCTURES

**AN IMPACT STRENGTH TEST METHOD FOR STRUCTURAL TIMBER:
THE THEORY AND A PRELIMINARY STUDY**

by

T D G Canisius
British Research Establishment Ltd.

UNITED KINGDOM

MEETING THIRTY-ONE

SAVONLINNA

FINLAND

AUGUST 1998

An Impact Strength Test Method for Structural Timber: The Theory and a Preliminary Study

T.D.G. Canisius

Building Research Establishment Ltd., The United Kingdom

1 Introduction

Structural timber strengths for design purposes are obtained from standard strength tests where failures are achieved in 5 ± 2 minutes. Tests indicate that under shorter times-to-failure wood is stronger than under longer times-to-failure. Thus, in Codes, for design of timber under short term loads, strength enhancement factors seemingly based on small clear specimens, and to be applied to the standard test strengths (or derived 'long term' strengths), are available.

Research at The University of British Columbia has shown that the small clear specimen behaviour need not represent the impact strength properties of structural timber. These tests where a heavy mass was dropped on simply supported specimens have shown either no enhancement or even a strength reduction under impact [Madsen, 1992]. In this case, as the failure loads were of very short durations of only a few milliseconds and the beams were stiff, the initiation of failure could have been different from what may be observed under much longer duration loadings, for example in the region of 0.1 sec under human jump loads (see Figure 1 and Canisius *et.al.*[1997, 1998]). Also, it is not known whether the impact behaviour of 'joists' is different from that of more flexible 'planks' such as scaffold boards.

The fact that the behaviour of structural timber under fast rates of loading applied by test machines is different from clear specimen behaviour has been noted by Karacabeyli and Barret [1993] who also described the past work in this area. They made a combined analysis of various published and unpublished data from 'joist' tests and produced a formula which provides the strength under different times to failure.

Due to the above there exists some uncertainty on the applicability of impact strength enhancement factors in Codes and the literature, especially to scaffold boards. However, so far it seems to have been not possible to investigate it because of the difficulty of applying impact loads in a controlled manner.

A method to determine impact strength of structural timber is presented in this paper. Monte Carlo simulations of two series of tests, which demonstrate the appropriateness and robustness of the method, are presented. The success of the test method would allow a cheaper and controlled way of testing timber for impact strength. Of course, the principles enunciated here can be used to impact test any other material in a controlled manner.

2 Basis of the proposed test method

The test method is proposed on the following premises.

- A mass dropped from a height can be used to break a piece of simply supported timber.
- If the mass first falls on to a spring placed on the timber, then the impact duration will be less than otherwise.
- The compression or extension (depending on the test rig detail) of a linear elastic spring, or a system of springs, presents a way of measuring the load applied to the specimen at a given time.

In the past, as reported by Madsen [1992], the dropping of a heavy mass from a height had been used to obtain the impact strength of structural timber. This principle had been used in more advanced forms by dropping the mass on to a soft material during testing concrete anchors at the Ruhr-University Bochum [see Kratzig and Niemann, 1996] and by using a designed pack of timber during the testing of masonry walls by Gilbert *et. al.* [1998]. However, these have not addressed the high variability in properties to be found, for example, in timber. Hence, the method proposed here is a considerable advancement over the current state of the art.

3 The fundamental theory

Consider a simply supported massless beam supporting a massless spring of stiffness k_0 . A mass M is to be dropped on to the spring from a height h above it (Figure 2). The assumption of a massless beam is a reasonable approximation with respect to a timber beam subject to high impact loads from large masses. Of course, if deemed necessary due to its weight, it is possible to consider the mass of the spring system to be used.

Figure 2 shows the system, both before the start and at a time t after impact, but before reaching the maximum response. Here, δ_0 is the contraction (or, dependent on the detail, the expansion) of the spring, and δ_B is the generalised displacement of the beam measured at its mid-span. The generalised (dynamic) stiffness of the beam, obtainable in terms of its (dynamic) flexural rigidity and span, is denoted here by k_B . The beam is assumed to be symmetrical about its centre line.

The differential equation of motion of the mass M , after impacting the spring, can be written as

$$k_0 \delta_0(t) + M \left[\ddot{\delta}_0(t) + \ddot{\delta}_B(t) \right] - Mg = 0 \quad (1)$$

where g is the acceleration due to gravity. Here a dot over a letter denotes a velocity while two dots denote an acceleration. The initial conditions are given by

$$\delta_0(0) = 0 \quad ; \quad \dot{\delta}_0(0) = \sqrt{2gh} \quad (2)$$

As the beam is assumed massless, its equation of motion simplifies to

$$k_0 \ddot{\delta}_0(t) = k_B \ddot{\delta}_B(t) \quad (3)$$

Equations 1 and 3 can be combined to provide the differential equation of motion of the system, in terms of the spring compression $\delta_0(t)$, as

$$M \left[1 + \frac{k_0}{k_B} \right] \ddot{\delta}_0(t) + k_0 \delta_0(t) = Mg \quad (4)$$

with the initial conditions given by Equation 2. The solution to Equation 4 provides the spring deformation as

$$\delta_0(t) = \sqrt{\frac{2Mgh}{\bar{k}}} \sin \sqrt{\frac{\bar{k}}{M}} t - \frac{Mg}{k_0} \cos \sqrt{\frac{\bar{k}}{M}} t + \frac{Mg}{k_0} \quad (5)$$

Here the effective stiffness, \bar{k} , of the beam-spring combination has been expressed by

$$\bar{k} = \frac{k_0 k_B}{k_0 + k_B} \quad (6)$$

On obtaining the time derivative of Equation 5,

$$\dot{\delta}_0(t) = \sqrt{2gh} \cos \sqrt{\frac{\bar{k}}{M}} t + \frac{g}{k_0} \sqrt{M\bar{k}} \sin \sqrt{\frac{\bar{k}}{M}} t \quad (7)$$

At time T , when the maximum displacement of the spring occurs,

$$\dot{\delta}_0(T) = 0 \quad (8)$$

Equation 8 provides the instance of the 'first' maximum spring force (assuming no beam failure).

On solving Equations 7 and 8,

$$T = \sqrt{\frac{M}{\bar{k}}} \tan^{-1} \left[-\sqrt{\frac{2hk_0(k_0 + k_B)}{gMk_B}} \right] \quad (9)$$

The maximum spring force, F_{max} , is given by

$$F_{max} = k_0 \delta_0(T) \quad (10)$$

and can be found using Equations 5 and 9.

Ideally, during an impact test, the time T should be equal to the target time to failure T_i , and F_{max} should be just higher than the strength of the beam. In practice, for a given beam the maximum load may be smaller than the beam strength, thus, providing only a proof load test. Similarly, a low strength beam may fail much earlier than the target time. In such a case the result would be acceptable if the time to failure is not far off from that intended.

4 Behaviour during a test

Consider a programme of tests on a sample for which the spring stiffness k_0 and the drop mass M have been chosen (see Section 5). Let a particular specimen (beam) have a generalised strength S . Then, if the developed maximum spring force F_{max} is greater than S , the beam fails as desired. Let the actual time to failure of the specimen, assuming failure occurs, be t_{act} . Then,

$$\delta_0(t_{act}) = \frac{S}{k_0} \quad (11)$$

Using Equation 5, Equation 11 can be rearranged to give

$$t_{act} = \sqrt{\frac{M}{\bar{k}}} \left[\tan^{-1} \sqrt{\frac{k_B Mg}{2k_B h(k_0 + k_B)}} + \sin^{-1} \left(\frac{S - Mg}{\sqrt{C}} \right) \right] \quad (12)$$

where

$$C = \frac{2Mghk_0^2}{\bar{k}} + (Mg)^2 \quad (13)$$

Then, for the considered beam, the drop height of the mass M can be obtained from

$$\sqrt{\frac{2Mgh}{\bar{k}}} = \frac{S - Mg}{k_0 \sin \sqrt{\frac{\bar{k}}{M}} T_i} + \frac{Mg}{k_0} \tan \sqrt{\frac{\bar{k}}{M}} T_i \quad (14)$$

Equation 14 has been obtained by rearranging Equation 12, and then substituting T_i for T_{act} . As the actual strength S of the beam is not known, the drop height needs to be calculated using a predicted strength. As this prediction is based on statistical relations, the actual strength may sometimes be higher than that predicted. Thus, in practice, in order to guarantee failure, it will be necessary to boost the drop height by a selected fraction (see Section 6.2).

5 Theoretical considerations for design of a test rig

Ideally, depending on the beam stiffness and its expected strength, different test rig design parameters (k_0 and M) and drop heights (h) need to be considered before testing each specimen. Although this would provide the optimum test conditions, it is impractical. A good compromise is to select a drop mass and a spring stiffness to be used with (at least) a particular sample of specimens. The drop height may then be varied according to the specimen to be tested. This approach, which is followed here, is detailed below.

Let the generalised dynamic stiffness of a beam be known from prior tests. Then, the spring stiffness, the drop mass and the drop height should be such that the following relations are satisfied:

$$\begin{aligned} F_{max} &> \text{expected impact strength, and} \\ T_{act} &\approx \text{target rise time (time-to-failure) } T_t . \end{aligned}$$

As an additional condition, a 'desirable' spring deformation δ_d can be introduced. It is considered as that to be expected from a beam with a strength correlated to a given fractile of the beam stiffness (see Section 6.3). Then, if this condition is applied as $\delta_0(T_{act}) < \delta_d$, and the estimated impact strength of this beam is F_{maxM} , the required spring stiffness is given by

$$k_0 > \frac{F_{maxM}}{\delta_d} \quad (15)$$

Of course, beams stronger than the selected percentile would need a higher spring deformation before failure. That is, the above is only a design criterion. The actual practical limit of the spring deformation may be made higher than this 'desirable' value. If the practical limit is smaller than that required by the stronger beams, then they would not fail. In such a case a truncated statistical distribution can be fitted to the failed specimen strengths.

For a particular series of tests, several drop masses can be considered so that the optimum mass may be selected with the help of computer simulations described below. On having the drop mass, it is possible to obtain the drop height for each test specimen.

6 Computer Simulation of a Test Series

In order to investigate the feasibility of the proposed test method, a comprehensive series of Monte Carlo simulations of test conditions and tests was initiated. The simulations were carried out to investigate the following aspects of the test conditions:

- the value of the drop mass,
- the 'desired' spring response assumed in the design, and
- the accuracy of the estimation of the dynamic strength.

Some initial results, including a study of the sensitivity of the method to errors in the estimated strength, are presented in this paper. Due to the lack of space, only the results for a single drop mass are presented here.

The spring design was based on the mean static strength related to the 25th percentile of the beam stiffness distribution. Considering that the problem at hand is the performance of scaffold boards under human jump conditions, a time to failure of 0.1 seconds was used.

6.1 The sample of timber

The Monte Carlo simulations were conducted with respect to the sample of scaffold boards from the BRE databank referred to in Canisius *et.al.* [1998]. As an approximation, the grading machine-based stiffness was considered as the dynamic (impact) stiffness of the boards. The boards of 225mmX38mm cross section and 1.2m length were assumed to be simply supported at their two ends. The beam stiffnesses and strengths were considered to have Normal distributions.

6.2 Simulation procedure

The following are the main steps relevant to the presented results. The stiffness and strength referred to below are the generalised values at the mid span of the beam, and were obtained from the corresponding basic 'stress' values.

Stage 1: Preliminary items and spring design for a test sample

1. Specify the target time to failure and select a drop mass. Select a 'desirable' spring deformation, to be based on the mean strength related to the selected stiffness percentile (Here the 25th percentile).
2. Select an actual impact strength enhancement (or reduction), which can be either constant, or vary linearly or parabolically as a function of the beam stiffness or static strength percentile.
3. Using the standard strength-stiffness correlation, find the average static strength correlated to the above stiffness percentile. Boost this value by an enhancement factor to account for the statistical variation of strength about its mean at the given stiffness. To consider the impact strength, further boost it by a factor which depends on an assumed enhancement over the static strength.
4. Determine spring stiffness based on the boosted strength and the 'desirable' spring deformation.

Stage 2: Simulation of tests

5. Generate a random value of the dynamic stiffness. Obtain the correlated mean static strength for this stiffness. Generate a random static strength by considering a normal distribution centred at this mean strength. Determine the impact strength. These are considered as the actual properties of a specimen.
6. To simulate an actual test, determine the drop height based on the mean strength correlated to the measured stiffness. Boost it by a fraction to account for the unknown (in a test) statistical variation of strength and the dynamic strength 'enhancement'.
7. Simulate a test. Determine the maximum force applied. Check whether the specimen fails. If it fails, determine the time to failure.
8. Repeat Steps 5 to 7 for each simulation.

It needs to be mentioned here that the failure checks in the computer simulations are carried out using the impact strength for target time to failure, instead of that at the actual time to failure. However, when the calculated times to failures are close to the target, as occurred in the simulated tests, the error due to this is negligible.

6.3 Results

The following presents some results from two sets of simulations. The target time to failure was 0.1 seconds. To allow better comparisons, the simulations for each test series were carried out by initialising the random number generators identically. The test rig design and test drop heights were based on an assumed enhancement of 20% over the static strength. One set of simulations was carried out to study the results when this design assumption was correct: *i.e.* an actual constant strength enhancement of 1.2 times the static strength exists. The other set was carried out to test the results when this assumption was grossly incorrect, *viz.* when the actual strength change under impact was a reduction of 10% from the standard value.

As an example, the results from a series of tests which correctly assumed the strength enhancement of 20% are shown in Figure 3. The shown results are for the case of 0.25m 'desirable' spring deformation and a drop mass of 300kg. The simulation numbers have been plotted in the abscissa. The spring stiffness required for this case was 30.9kN/m. In this case the times to failure are very close to the 0.1 second target and, they are generally within the band formed by 0.03 and 0.20 seconds. Here 'closeness' implies a time-to-failure which gives rise to a negligible change in strength when compared to that at the target time to failure. Zero times to failure has been used in the graph to indicate the 9 strong specimens which did not fail during the tests. The drop heights also form a reasonable and practical set. The distribution of dynamic strengths obtained from the simulations can be seen in Figure 3. These have a pattern similar to the linear elastic spring response as its deformations are directly related to the beam strength. During these tests, 272 of the 500 specimens failed with deformations smaller than the 'desirable' value while 219 failed with deformations larger than that.

The simulation results for the above example, but when the actual strength change due to impact was a 10% reduction from the standard test values, are shown in Figure 4. In this case the spring design and drop height calculations were based on the assumed strength enhancement of 20% over the standard strength. As the drop heights also were calculated assuming this strength enhancement, they are the same as that for the previous test series. As to be expected, due to low impact strengths, the spring deformations at failure are less than those for the previous test series. In addition, similarly, the times to failure are smaller than the corresponding values for the previous case. However, these times are still generally within the band formed by 0.02 and 0.14 seconds, *i.e.* within 0.2 and 1.4 times the target time, and are reasonable. In this case, 432 specimens failed with spring deformations smaller than the 'desirable' value while the remaining 68 failed with larger spring deformations. In this way, this example has shown the robustness of the test method and its insensitivity to a gross error in the assumption on strength changes under impact.

7 Discussion

The presented results have shown that the proposed test method is able to provide times to failure closer to the target. During tests, it will generally be not possible to obtain the exact designed time to failure as the strength of a specimen is not known beforehand. This is true even in the case of standard testing where a tolerance $\pm 40\%$ of the desired time is allowed. In the proposed method, the tolerance required will depend on the test rig parameters chosen. Simple calculations have indicated that the strength error due to the achieved distributions

in times to failure are small as to be negligible. Some scatter in tests is even acceptable as for a given family of loads, for example the human jump loads, the time to peak load need not be constant but may have a random distribution. Thus, the times-to-failure provided by the proposed tests, when proper rig parameters and drop heights are chosen, can be considered acceptable. By designing the test rig and choosing rig parameters such that only the lower tail of the strength distribution is obtained (*i.e.* failed during testing), it should be possible to obtain a much smaller scatter in the times-to-failure.

The results presented for the case where the test rig was designed with and without a fair idea of the impact strength changes have indicated the robustness of the test method. The 'incorrectly assumed strength' case used the same drop heights as for the 'correctly assumed strength' case due to the wrong assumption on impact strength. As these drop heights were larger than required for the actual strengths, the former, as to be expected, provided slightly lower times to failure. However, even in this case, the times to failure were sufficiently close to the target as to make the results acceptable.

In addition to the above provision of the desired time to failure, major advantages of the proposed test method are its relatively small cost compared to a complex test machine and the provision of the load time history through the spring deformation-time history.

In a future paper it is intended to present a study on the selection of optimum test rig parameters (spring and drop mass) In addition, the effects of the following simplifications of the test method, are expected to be presented:

- the use of a single drop height or a limited number of drop heights for a given sample,
- the use of different factors to boost the strength and drop height during spring design and drop height calculations,
- the use of different drop masses,
- the use of different stiffness percentiles in the design of the spring system (currently the 25th percentile), especially in reducing the scatter in times to failure, and
- the use of static beam stiffness in the test rig design and drop height calculation (in the present case, grading machine-based stiffness was used as the dynamic stiffness).

In addition, if deemed required, the effect of the mass of the spring system will be investigated. The ultimate aim is to design the system such that only a single drop height can be used to obtain the lower tail of the strength distribution.

Of course, the practical implementation of the method would present its own challenges, *e.g.* deviations from assumed linear behaviour and the determination of a suitable loading area, that need to be addressed.

8 Conclusion

This paper presented the theory for a new test method to determine the impact strength of structural timber under a controlled time-to-failure. Monte-Carlo simulations carried out on a sample of scaffold boards have shown the appropriateness and robustness of the test method. However, further theoretical studies are needed to make the procedure simple and optimal.

References

Canisius, T.D.G., Bougard, A.J. and Ellis, B.R. (1997); *Human impact loads on timber scaffold boards*, Proc. of Seminar 'Working at Height', Maitra, A. (Editor), Thomas Telford, London, 1997.

Canisius, T.D.G., Bougard, A.J. and Ellis, B.R. (1987); *Performance of timber scaffold boards under human impact loads*, BRE Publication Draft PD 19/98 (Submitted to Proc. Inst. Civil Engrs. : Structures and Buildings).

Gilbert M., Hobbs B., Molyneaux T.C.K., Melbourne C. and Watson A.J. (1998); *Laboratory Impact Testing of Free Standing Masonry Walls*, Masonry International, **11**(3), pp. 71-79.

Karacabeyli E. and Barret J.D. (1993); *Rate of loading effects on strength of lumber*, Forest Prod. J., **43**(5), pp. 28-36.

Kratzig, W.B. and Niemann, H-J. (1966); *Dynamics of Civil Engineering Structures*, A.A. Balkema, Rotterdam, The Netherlands.

Madsen, B. (1992); *Structural Behaviour of Timber*, Timber Engineering Ltd., North Vancouver, Canada.

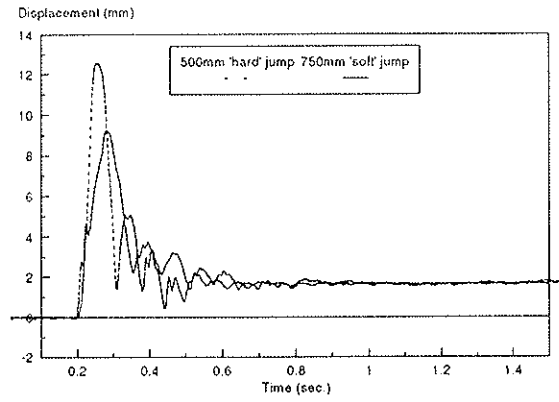


Figure 1. Typical Board Deflection vs. Time curves for human jump load test on simply supported scaffold boards.

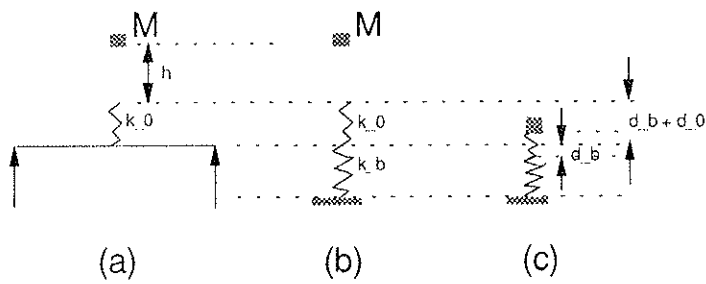


Figure 2. (a) The beam-spring-mass system; (b) The idealisation, and (c) The system at time t after impact.

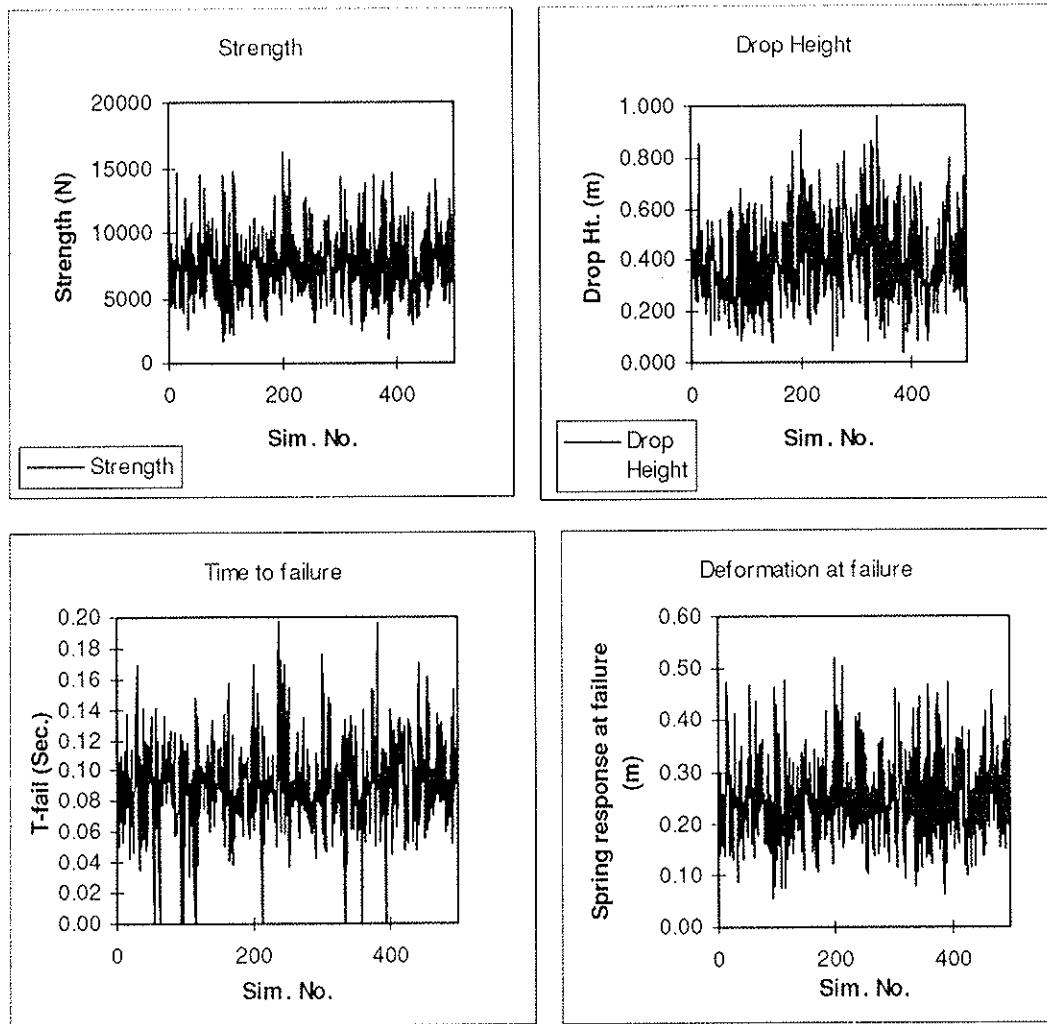


Figure 3. Impact test simulation for $\delta_d = 0.25\text{m}$, $M=300\text{kg}$ and Correct Strength Assumption.

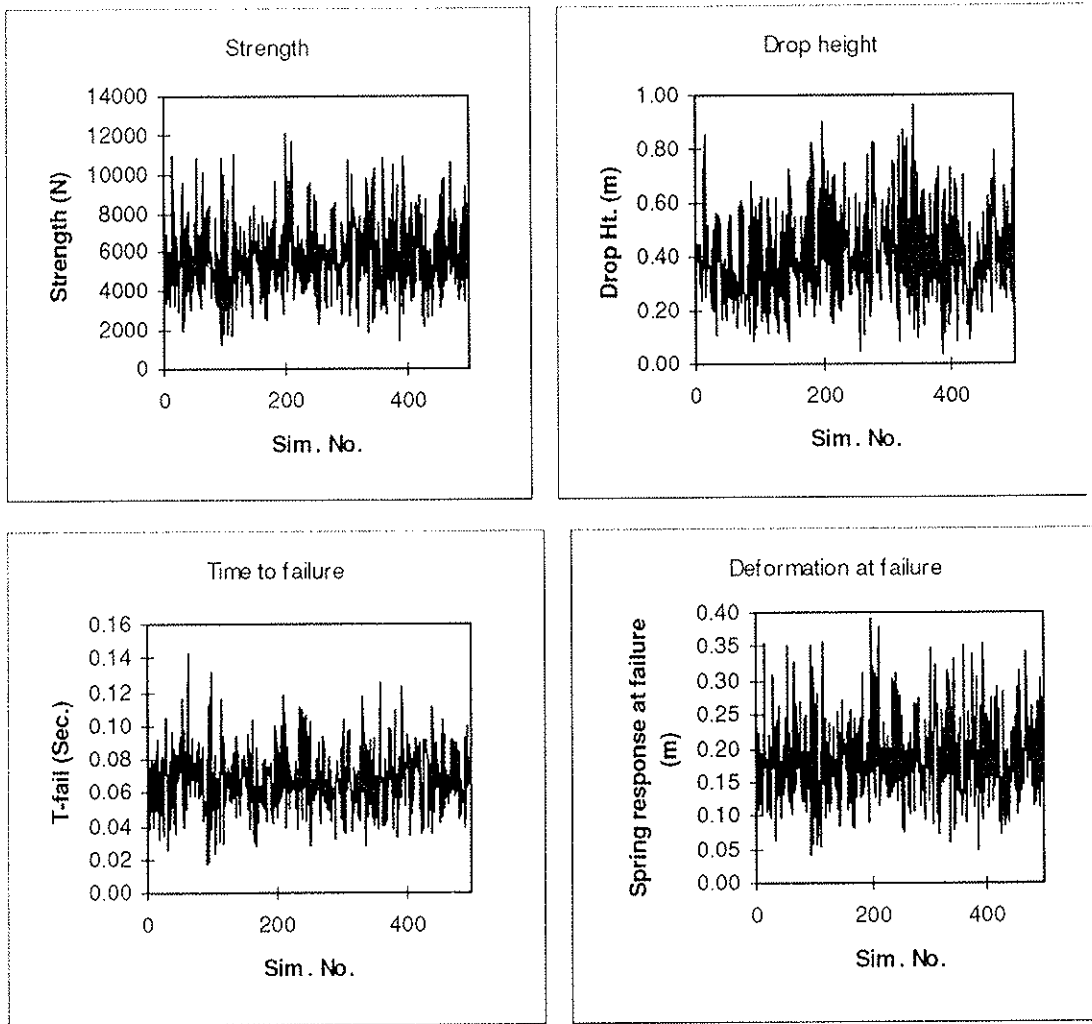


Figure 4. Impact test simulation for $\delta_d = 0.25\text{m}$, $M=300\text{kg}$ and Incorrect Strength Assumption.